Intramolecular Singlet Fission in Acenes

Samuel Nathan Sanders

Submitted in partial fulfillment of the

requirements for the degree of Doctor of Philosophy

in the Graduate School or Arts and Sciences

COLUMBIA UNIVERSITY

2018

ABSTRACT

Intramolecular Singlet Fission in Acenes

Samuel Nathan Sanders

In 2017, 98 gigawatts of solar capacity were added globally, outpacing new contributions from coal, gas and nuclear plants combined, based on 161 billion dollars of investment. Solar is the leading contributor to the clean energy revolution and continues to grow in market share and drop in price every year as economy of scale advances the technology. Within this market, silicon and cadmium telluride solar cells dominate nearly all of market share, converting roughly 20% of incident solar power into electricity. It is worth noting that the gains from a 1% increase in power conversion efficiency of the typical 20% solar cell to 21% would be measured, annually, in billions of dollars. If the solar cells installed last year had 1% more power conversion efficiency and the power displaced coal power generation, this enhancement in efficiency would now save roughly 8,000,000 pounds of carbon dioxide emission *per hour* every hour for the ~220,000-hour (~25 year) lifetime of the solar cells.

Within this context, enhancing the power conversion efficiency of solar cells is crucial economically and environmentally. Because sunlight is incident on the earth as a broad spectrum of different colors, the energy of the photons spans a wide range. Unfortunately, the spectral range limits power conversion efficiency. For example, solar cells are transparent to photons with insufficient energy, while photons with excess energy relax to the band edge of the solar material, losing the excess energy as heat. This thesis focuses on improving the utilization of high energy photons currently lost to this thermalization process.

In Chapter 1, we introduce the photophysical process of singlet exciton fission and give an overview of the field, with a focus on its potential for incorporation into photovoltaic devices. In Chapter 2-8, we discuss our results realizing singlet exciton fission in molecular systems, specifically bipentacenes. This chapter includes the synthesis of these materials, theoretical calculations predicting and rationalizing their photophysical behavior, and the spectroscopic characterization used to demonstrate the singlet fission process. In Chapter 3, we detail a modular synthetic approach to oligomers and even the first polymer of pentacene. We also discuss some basic properties of these materials using techniques such as linear absorption, cyclic voltammetry, and grazing incidence wide angle X-ray scattering spectroscopy. In Chapter 4, we investigate the photophysics of these materials. Photoluminescence upconversion spectroscopy reveals the decay of the singlet exciton on ultrafast timescales, while transient absorption spectroscopy is used to assign the singlet fission timescale, as well as to characterize the triplet absorption spectra.

Chapter 5 discusses the synthesis and photophysics of homoconjugated and non-conjugated pentacene dimers, where singlet fission occurs through sigma bonds. Again, transient absorption spectroscopy is crucial to the assignment of the photophysics at play, but continuous wave time resolved electron spin resonance measurements yield additional insights into interaction between the resulting triplet pair excitons. Chapter 6 provides further detail into the formation of strongly exchange coupled triplet pair states. Continuous wave time resolved electron spin resonance spectroscopy is used to determine the quintet character of these states, and pulsed electron spin resonance measurements nutate the spin of these states to confirm this assignment. Chapter 7 provides the first demonstration that singlet exciton fission is also possible in heterodimer systems. Finally, Chapter 8 delves more deeply into the exciton correlations in these materials with a special focus on the pentacene-tetracene dimer system.

Table of Contents

List of Figures

List of Tables

Acknowledgements

I am deeply grateful to many people who have helped me along my path to completing this thesis. Some people have contributed scientifically, others have helped with motivation and focus, and equally as important, others have helped me maintain sanity throughout graduate school. While it is almost impossible to create an exhaustive list, I will mention a few of those people here. I am thankful to Natalia Lebedeva who taught me at UNC Chapel Hill with incredible patience how to conduct research, and to Sergei Sheiko for taking me in his lab. I am grateful to Helen Tran, who was my earliest mentor in graduate school, and while my project diverged from her areas of study, her training on laboratory techniques, how to craft a presentation, as well as how to handle collaborators, graduate school, chemicals, etc… were essential during my formative graduate school years. I am very thankful for mentorship and advice from Mike Steigerwald, who is a treasure of the Columbia chemistry department. His advice, incredible chemical intuition, and interesting ideas were crucial to the inception and success of my research projects, and his support during difficult times was essential and greatly appreciated. Every chemistry department should have their own Mike Steigerwald. Unfortunately, there is only one Mike, and we are lucky to have him at Columbia. I am extremely grateful to Elango Kumarasamy, a postdoc who joined my project as it became clear I was better at spectroscopy than synthetic chemistry. I am grateful to him for his patience and his positive attitude, as well as all the molecules he made that were crucial to our

success. Still more important, I am grateful that outside of science we became great friends. I am thankful for younger graduate students such as Andrew Pun, Lauren Yablon and most recently Kaia Parenti who joined the singlet fission projects. Andrew has branched out in new and exciting ways since then, and Kaia and Lauren continue to make great strides on singlet fission research. I can't wait to see what they come up with over the next couple years. In addition to being great collaborators, they are excellent coworkers and friends and it has been a pleasure to share projects and lab space with all three of them. I have learned a lot from them, and I hope I've been able to pass along a bit of scientific or professional wisdom to them as well. I am also grateful for JLow, Spencer, Jessica, Isaac, Anastasia, Rachel, Jianlong, etc… who I have not collaborated with as extensively but who have made the lab such a pleasant place to come to work.

I am thankful to everyone in my second home at the University of New South Wales, particularly Dane, Amir and Jo, who welcomed me into their lab and country like family. I took awesome trips to Jenolan caves and to see kangaroos with Jo and learned as much ESR as I could from Dane, Amir and Murad. Seeing Amir and Sahar's kittens and horses were a particular highlight!

I am thankful to Luis for taking me into his lab despite my apprehension about synthetic chemistry, and for his faith in me to take my projects in a direction far outside the usual wheelhouse of our lab and the freedom to pursue different ideas. I am thankful for his guidance and mentorship, but it was not all science and we had some fun times, too! I would like to thank Matt Sfeir at Brookhaven National Lab who taught me everything I know about spectroscopy. Matt is an outstanding scientist, mentor, and friend. We have spent so much time working together on data or manuscripts the past few years, it will frankly be weird doing science in the future without his input on anything and everything, and his excellent intuition and insights into every detail,

technical or strategic. It has been a ton of fun working with him and learning physical chemistry, as well as getting his hot takes on the NBA, Kanye West, and internet personalities, and I will miss our collaboration greatly.

I have to thank Bonnie's parents for taking good care of us the past years. It has been a great comfort having them just across the way in New Jersey, and they have always been very supportive in driving to bring us home to NJ or dropping off food and just being there for us while we struggled through graduate school. I have to give a huge thanks to my parents for their support the past five years, and prior. The values they instilled in me were essential to my early interest in alternative energy research, and while neither of them are scientists, they have displayed endless patience in listening and trying to understand the intracacies of my early research on microbubbles, or my more recent work on downconverting high energy light. The may find these topics impenetrable but have always been a great source of support, career advice and a willing ear.

Most of all I have to thank Bonnie Choi, who is my favorite person and my wife by the time of this publication, who has been my rock (and even occasional crystallographer!) these past ten years or so. I would not be where I am today without you, and I cannot imagine life without you. We have survived the struggles and enjoyed the good times of grad school together, and I would not have it any other way. I am so excited to see where life takes us in our next chapter.

To Bonnie, Mom, Dad

1 Singlet Fission: Progress and Prospects in Solar Cells

1.1 Preface

This chapter is based on a manuscript entitled "Singlet Fission: Progress and Prospects in Solar Cells" by Jianlong Xia, Samuel N. Sanders, Wei Cheng, Jonathan Z. Low, Jinping Liu, Luis M. Campos, and Taolei Sun published in *Advanced Materials*.

1.2 Introduction

Converting solar energy into electricity with photovoltaic (PV) cells is a renewable and clean way to tackle global energy and environmental challenges. Intensive research is directed toward reducing fabrication costs as well as improving power conversion efficiency (PCE).[1] However, progress in this area is fundamentally constrained by the thermodynamic limit of ~33% PCE for single-junction solar cells, known as the Shockley-Queisser limit.[2] Multiple exciton generation (MEG), a process of producing multiple electron-hole pairs after the absorption of a single photon, represents a promising route to overcome this barrier.[3,4] Singlet exciton fission, also referred to as singlet fission (SF, Figure 1.1), is an efficient MEG process in organic semiconductors, by which a photoexcited high-energy singlet exciton is converted into a pair of low-energy triplet excitons.[5]

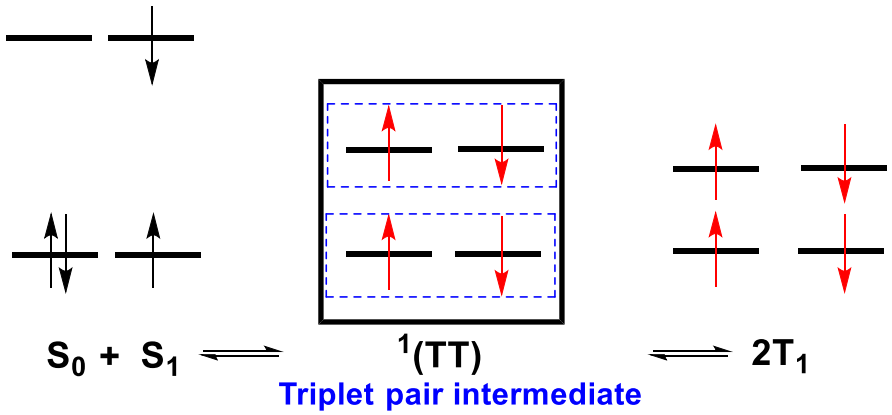

Figure 1.1. Schematic of singlet fission – a process where one singlet exciton is converted into two triplet excitons through a triplet pair intermediate.

SF was first proposed in 1965 to rationalize delayed fluorescence in anthracene crystals,[6] and intense research efforts in the SF field have been rekindled in the last decade due to the suggestion by Nozik et al. in 2006 that using materials capable of SF in conjunction with lower bandgap conventional absorbers, could potentially boost PCE and circumvent the SQ limit of singlet junction solar cells.[3] Extensive studies have focused primarily on acenes and diphenylisobenzofuran to unravel the underlying mechanism of SF.[7] It has been well established that SF in these materials can take place efficiently and rapidly between neighboring molecules. Because SF in these systems is an inherently intermolecular process, the rate and yield vary with intermolecular packing and coupling. Transient absorption spectroscopy (TAS) studies on a handful of oligomers[8] and polymers[9] have recently established that SF can also happen within isolated molecules,[10] provided the size of individual chromophores are large enough to localize two triplet excitons generated by SF. The intramolecular SF process is inherently less sensitive to intermolecular interactions. While the mechanism of singlet fission is the subject of intense study, it is generally agreed that photoexcitation generates a triplet pair ^{1}(TT) state either coherently or incoherently from the singlet exciton, and this state may subsequently separate into two triplets

($2xT_1$) in an overall spin-allowed process (Figure 1.1).[10-19] The energy requirement for singlet fission is often stated that the energy of the triplet pair ^{1}(TT) needs to be less than or equal to S_1, i.e., $E(S_1) \geq E^1(TT)$. However, it should be noted that in some systems such as carotenoids, fission occurs from higher S_n states since the S_1 is not optically accessible.[20,21] Also, SF can be observed in conjugated polymers with sufficiently energetic excitation, and with relatively high yields, provided that SF from higher excited singlet states outcompetes vibrational relaxation to S_1. [22,23]

Recent progress in understanding singlet fission has paved the way for the design of new SF materials and engineering of SF-based photovoltaic devices. If the two triplet excitons generated by SF can be effectively ionized at the donor/acceptor interface, it could potentially double the photocurrent at certain wavelengths and ultimately boost the efficiency of single junction photovoltaic devices. However, the electronic structure at the donor/acceptor interface must have a sufficiently low-lying lowest unoccupied molecular orbital (LUMO) to dissociate these typically low-energy triplet electron-hole pairs. By elaborate device design, singlet fission has been successfully implemented in solar cells with external quantum efficiencies (EQEs) of up to 126% and internal quantum efficiencies (IQEs) approaching 200%.[24,25]

1.3 Singlet fission based solar cells

For most organic donor-acceptor solar cells, the energy of the charge-transfer state (as estimated from the difference between highest occupied molecular orbital (HOMO) energy of the electron donor and the LUMO energy of electron acceptor)[26] is higher than the energy of SF-generated triplet electron-hole pairs. This mismatch prevents dissociation of the triplet excitons within heterojunction solar cells. To date, successful development of SF based photovoltaic

devices has been overwhelmingly limited to linear acenes (e.g. tetracene and pentacene), although there are notable exceptions. Pentacene (Pc) is a model system for singlet fission studies, as transient absorption studies on pentacene have revealed that SF in Pc occurs extremely fast (~80 fs) with a yield of 200%.[27] The ultrafast SF in pentacene that can outcompete alternative decay mechanisms of singlet excitons, coupled with its reasonable hole mobility,[28,29] make it a good candidate for SF-based solar cells. SF in tetracene can also produce two triplet excitons rapidly (within 200 ps)[30] with an efficiency approaching 200% in neat films.[31] Theoretical result has predicted that the ideal bandgap (T_1–S_0) with maximum efficiency for a SF-based solar cell is at ~ 1.0 eV, namely, the optimal T_1 energy of singlet fission materials is at ~ 1.0 eV. Different device structures have been designed to harvest triplet excitons generated by SF, and can be tentatively sorted into two classes. First, there are the donor-acceptor heterojunctions (either bulk or planar). To potentially overcome the SQ limit, a p-type singlet fission material must be combined with a red-absorbing acceptor to offset the loss of open-circuit voltage through capturing low-energy photons. The most promising acceptor material should have an optimal band at 0.9 ~ 1.0 eV and its LUMO level is deep enough to dissociate triplets. Second, there are singlet fission sensitized solar cells, where the SF material is integrated into a conventional (typically silicon) solar cell.

1.4 Donor-acceptor heterojunction

In 2010, Rao et al. employed TAS to demonstrate that the triplet excitons produced through SF can be separated at the pentacene/C_{60} heterojunction interface to form charges.[32] Since then, different device technologies have been developed to facilitate triplet exciton dissociation. The magnetic field response of the photocurrent has been widely used as a diagnostic tool to study singlet fission based photovoltaic devices.[24,33-35] Due to contributions from the Zeeman effect and

zero-field splitting of the triplet states, the SF rate slightly increases at low magnetic fields (H < 0.1 T), and then slows down with increasing magnetic fields (H > 0.2 T). If the triplets can be dissociated, the contribution of triplet excitons obtained from SF to the photocurrent of solar cells can be evaluated in-situ by applying a magnetic field.

One approach to engineer singlet fission solar cells is through a combination of SF donors and appropriate acceptors possessing low-lying LUMO energy levels. Using pentacene and 6,13-diphenyl-pentacene (DPP) as SF donors, Jadhav et al. studied triplet exciton dissociation in SF-based photovoltaic devices by varying the LUMO energy levels of acceptors outlined in Figure 1.2.[34] Based on the magnetic field dependence of the photocurrent, they found that the charge generation via triplet extraction is sensitive to slight variation of HOMO energy of donor and LUMO level of acceptor. For example, triplet excitons dissociate much better at the pentacene/C_{60} interface than the DPP/C_{60} interface, because the HOMO energy of DPP (5.2 ± 0.1 eV) is slightly deeper than pentacene (4.9 ± 0.1 eV), which leads to a larger charge-transfer state energy and increases the barrier for triplet dissociation. Triplet excitons produced by SF in DPP start to ionize when the acceptor is changed from C_{60} to N,N0-dioctyl-6,12-dicyano-3,4,9,10-tetracarboxyperylene diimide (PDI-CN_2) or N,N0-1H,1H-perfluorobutyl dicyanoperylenecarboxydiimide (PDIF-CN_2), which both exhibit a deeper LUMO level. Jadhav et al. also suggested that low band-gap nanocrystals (PbS and PbSe) could be promising acceptors, since they can effectively separate the triplet excitons of pentacene as well as harvest low-energy photons.

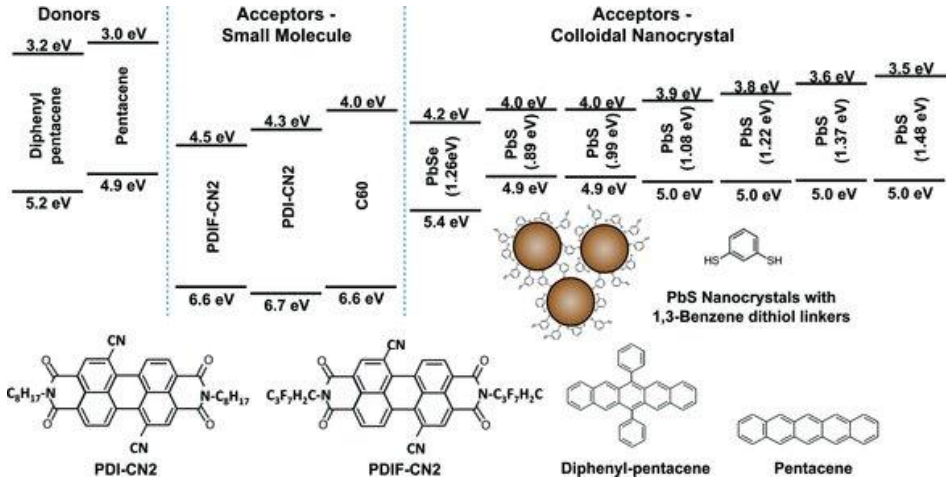

Figure 1.2. A comparison of energy levels and molecular structures studied in SF solar cells by Jadhav et al. Reproduced with permission.[34] Copyright 2012, John Wiley and Sons.

Ehrler et al.[36,37] explored the application of semiconductor nanocrystals as electron acceptors to dissociate the pentacene triplet exciton. The low band-gap nanocrystals can also serve as a long wavelength absorber to maximize light absorption. Their first report used lead sulfide (PbS) nanocrystals as acceptor and infrared absorber, achieving internal quantum efficiencies (IQE) exceeding 50% with a device structure of indium tin oxide (ITO)/pentacene (50 nm)/PbS nanocryctals (130 nm)/Al (Figure 1.3).[36] They demonstrated that the device performance can be improved by inserting a hole-blocking layer of 100 nm zinc oxide (ZnO) nanocrystals between the PbS nanocrystals and the metallic top contact.

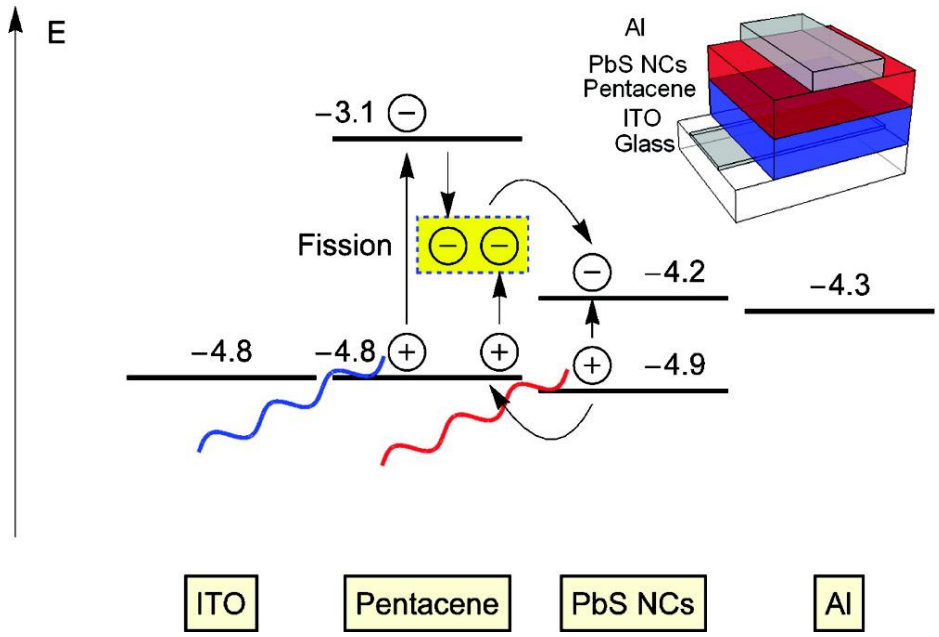

Figure 1.3. Schematic device structure, energy diagram and proposed working mechanism of pentacene/PbS nanocrystals solar cells studied by Ehrler et al. Reproduced with permission.[36] Copyright 2012, American Chemical Society.

In a subsequent publication, Ehrler et al.[37] changed the semiconductor nanocrystal acceptor to lead selenide (PbSe), and screened the low energy absorbers ranging from 0.67 – 1.20 eV (as measured in solution, Figure 1.4a). By integrating pentacene with these low band-gap inorganic acceptors, they showed that the triplet energy of pentacene is within the range of 0.85 eV to 1.00 eV in operating devices. With a device structure of (ITO)/pentacene (50 nm)/PbSe nanocryctals (0.98 eV, 150 nm)/Al, a PCE of 4.7% was achieved with an EQE up to 80% (Figure 1.4b).

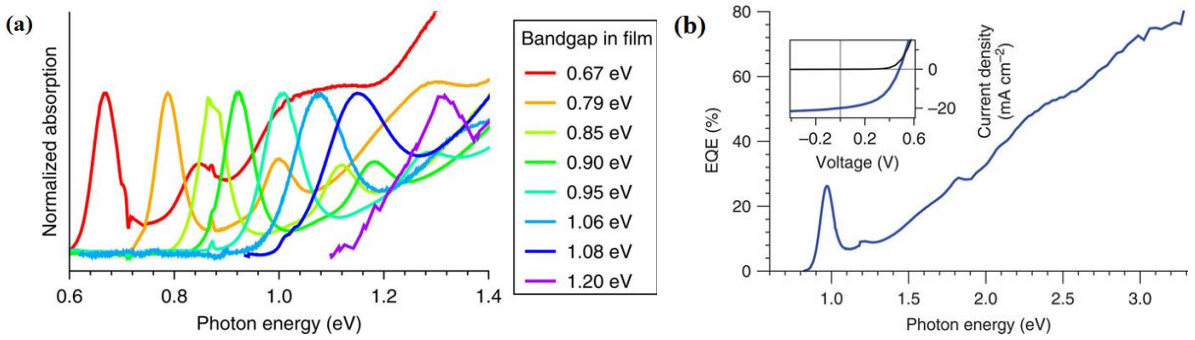

Figure 1.4. (a) Absorption spectra of the lead selenide (PbSe) nanocrystals studied by Ehrler et al. (b) EQE and current–voltage characteristics of the best pentacene/PbSe (0.98 eV) device. The top left inset shows the current-voltage data, with a power conversion efficiency of 4.7% under AM1.5G illumination. Reprinted with permission.[37] Copyright 2012, Nature Publishing Group.

Very recently, Yang et al.[38] reported solution-processed singlet fission solar cells made by combing PbS/PbSe nanocrystals with 6,13-bis-(triisopropylsilylethynyl)pentacene (TIPS-pentacene), which exhibits a dramatically improved solubility and stability in solution relative to pentacene. Contrary to previous pentacene/nanocrystal bilayer architectures studied by Ehrler et al., Yang et al. used an inverted device structure with a configuration of ITO/TiO_2/PbSe(PbS, 90~130 nm)/TIPS-Pc (13~20 nm)/MoO_x/Au (Figure 1.5a). They showed that the triplet ionization is dependent on the energy of the charge-transfer (CT) states, which varies with the conduction band energy of nanocrystals (Figure 1.5b). An IQE in TIPS-pentacene solution-processed devices up to 160 ± 40% was observed with the low acceptor level PbSe (1.0 eV) nanocrystals. It is worth noting that by using 1.25 eV PbS as an acceptor, a PCE over 4.8% was achieved with all active layers processed from solution. The promising PCE and IQE metrics suggest the great potential of singlet fission materials to improve the performance of solution-processable solar cells.

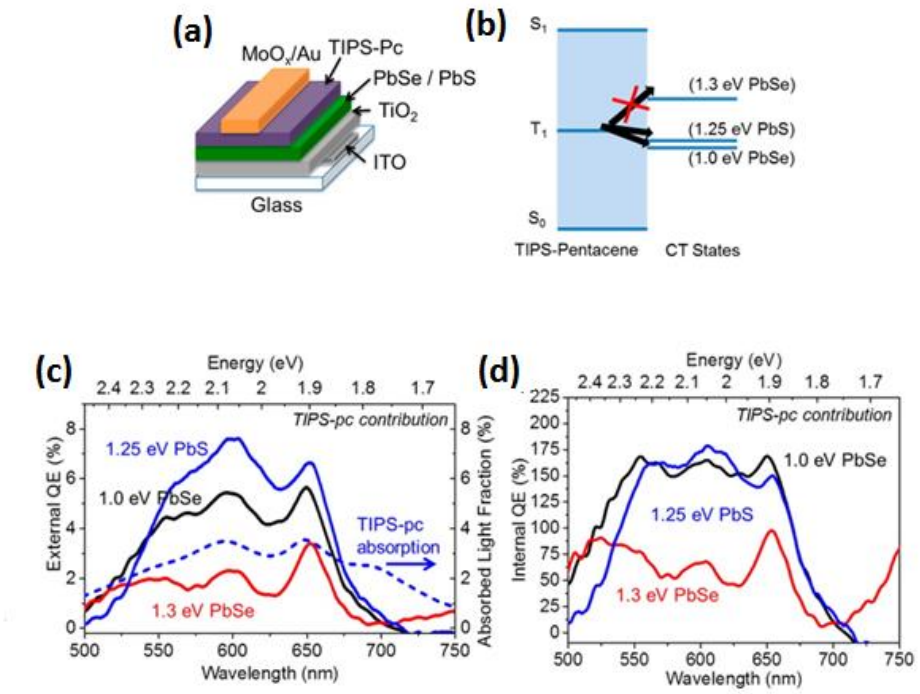

Figure 1.5. (a) Inverted device structure of the TIPS-pentacene/nanocrystal solar cells studied by Yang et al. (b) Energy alignment between the TIPS-pentacene triplet state and the charge transfer (CT) states with different nanocrystals bandgaps, the CT energy is estimated from the energy difference between the nanocrystal conduction band and the HOMO of TIPS-pentacene. (c) EQE contribution and modeled absorbed spectrum of TIPS-pentacene. (d) IQE of TIPS-pentacene in bilayer devices with nanocrystals of different bandgaps. Reproduced with permission from.[38] Copyright 2015, American Chemical Society.

While most studies of SF-based solar cells focused on using acenes as donors, Kawata et al.[39] explored the use of SF-capable non-polycyclic thienoquinoid (ThQ) compounds instead (Figure 1.6). The quinoid-biradical resonance of ThQ compounds lowers the triplet energy level, leading to efficient singlet fission in these compounds. They implemented these thienoquinoid compounds into a bilayer device with C_{60} or PDIF-CN_2 as an acceptor. Through a magnetic-field-dependent photocurrent study, they showed that SF generated triplets in ThQs can be dissociated in the co-evaporated blend using PDIF-CN_2 as an acceptor, with a device structure of ITO/PEDOT:PSS/ThQs:PDIF-CN_2 = 2:1 (45 nm)/BCP (10 nm)/Al. This result proved that triplets

generated by non-acene SF materials could also be ionized within a device, even though they had limited success in power conversion efficiency (PCE<1.1%).

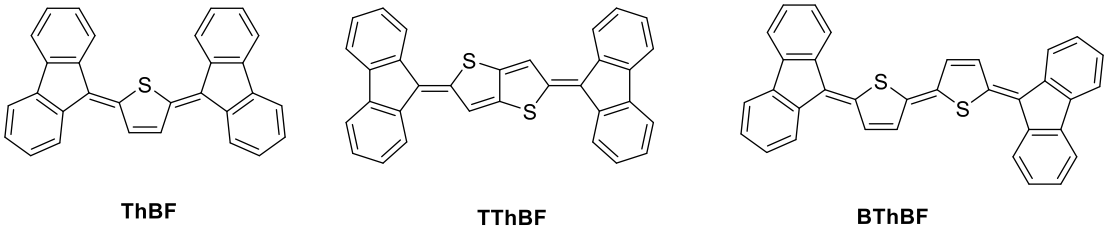

ThBF TThBF BThBF

Figure 1.6. Non-polycyclic thienoquinoidal compounds studied by Kawata et al.

In order to effectively implement singlet fission into organic solar cells with fullerene acceptors, a trilayer junction was explored by using an additional electron donor to increase the absorption of low energy photons by the active layer. Jadhav et al.[40] realized the first SF-based solar cell by adding copper phthalocyanine (CuPC) as an additional donor to the tetracene/C_{60} heterojunction (Figure 1.7). Tetracene absorbs light below 500 nm and undergoes singlet fission to produce two triplets with energy of ~1.2 eV. CuPc extends the light absorption to 700 nm, and its triplet energy (~1.1 eV) aligns well with tetracene. By modulating the photocurrent of the device under applied magnetic field, they showed that the singlet exciton fission yield of tetracene is preserved with the insertion of the CuPc layer, while the PCE is improved from 0.58% to 1.27%.

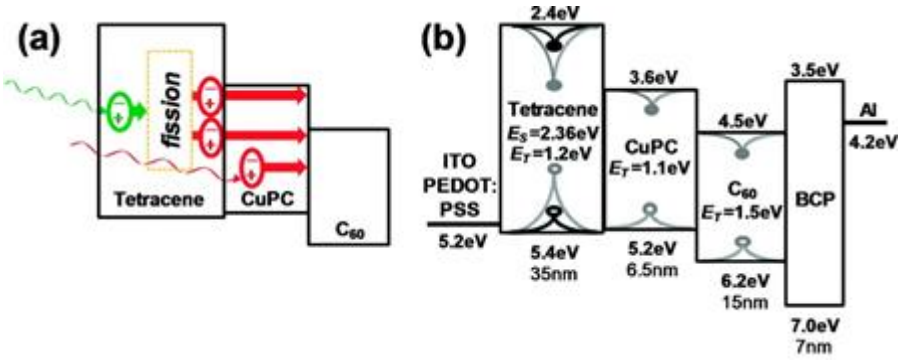

Figure 1.7. (a) Schematic of a three-layer SF-based organic solar cell in which the additional layer is a donor layer. (b) Energy alignment of complete device. Reproduced with permission.[40] Copyright 2011, American Chemical Society.

Congreve et al.[24] reported the first device that achieved an EQE of over 100% by combining poly(3-hexylthiophene) (P3HT) and pentacene donors with a C_{60} acceptor. The device architecture was ITO/PEDOT:PSS/P3HT (8 nm)/Pentacene (15 nm)/C_{60} (35 nm)/BCP/Ag (Figure 1.8). They showed that the P3HT acts as a triplet exciton blocking/hole extraction layer, and the photoexcited singlet excitons in P3HT can also be transferred to pentacene through Förster resonance energy transfer (FRET),[41] with the pentacene subsequently undergoing singlet fission. The result from modulating the photocurrent with magnetic field suggested that by confining the triplet excitons with the P3HT layer, the singlet fission yield approaches 200% within an operating device for pentacene films thicker than 5 nm. It should be noted that an MgF_2 antireflection layer was coated on the front surface of the glass substrate to maximize the light absorption. Soon after the work published by Congreve et al., Thompson et al.[25] demonstrated a state-of-the-art external quantum efficiency of 126% with the same device structure, by increasing the light absorption of the pentacene layer. The EQE of 126% is highest ever reported for any type of solar cells, demonstrating the potential of SF to increase the efficiency of organic solar cells.

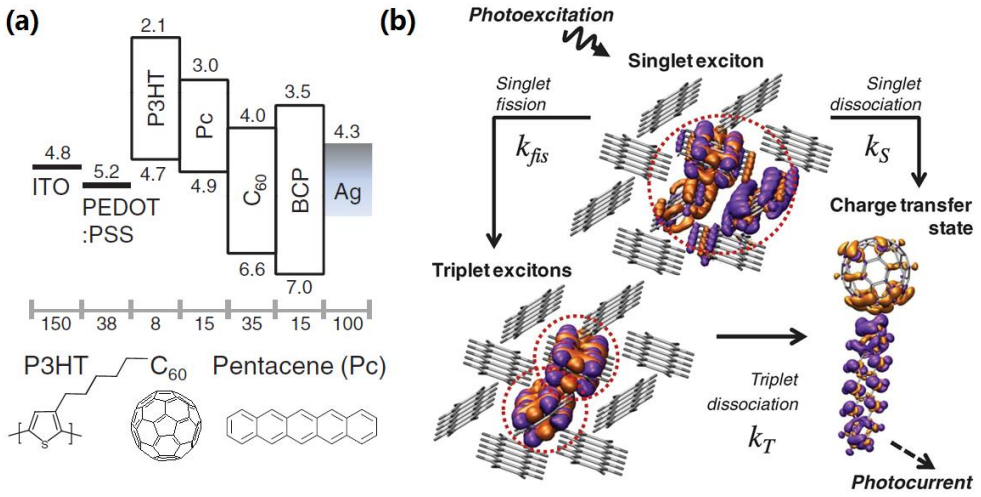

Figure 1.8. (a) Energy levels of full device and chemical structures studied by Congreve et al. (b) Singlet fission process in pentacene within the device. Reproduced with permission.[24] Copyright 2013, AAA of Science.

1.5 Singlet fission sensitized solar cell

An alternative approach to utilize singlet fission is through incorporation of this MEG processinto conventional solar cell technologies. Ehrler et al.[42] described a singlet fission sensitized silicon solar cell by coupling pentacene to amorphous silicon (a-Si), with a device configuration of ITO/pentacene (50 nm)/PbSe (1.1 eV, 25~50 nm)/a-Si (100 nm)/Al (Figure 1.9). A layer of PbSe nanocrystals with a bandgap of ~1.1 eV was inserted between pentacene and a-Si, in order to facilitate the dissociation of triplet excitons produced in pentacene and to help extract holes from the silicon layer. A device without the PbSe layer did not generate any photocurrent, presumably due to the destruction of pentacene when the Si was sputtered on. All three active layers were found to contribute to the photocurrent. Note that while the PCE of this SF sensitized solar cell is lower than traditional amorphous silicon solar cells, the rational design of inserting a

layer of semiconductor nanocrystals between the SF material and a-Si demonstrates a promising architecture for future study and optimization.

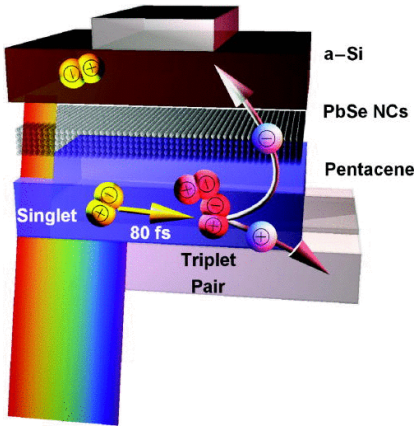

Figure 1.9. Schematic device structure of singlet fission sensitized silicon solar cell fabricated by Ehrler et al. Reproduced with permission.[42] Copyright 2012, AIP Publishing LLC.

An inherent character of singlet fission is that it doubles the photocurrent while simultaneously halving the voltage of a single-junction solar cell. This provides the possibility of using the SF solar cell as high band-gap sub-cell for parallel tandem solar cells, since the down-conversion process of singlet fission facilitates voltage matching of two sub-cells. Also, a solar cell with an SF component should be able to generate additional photocurrent from higher energy photons compared to a tandem cell without an SF component. Theoretical results by Pazos et al.[43] have therefore predicted that the maximum PCE of a singlet fission sensitized parallel tandem solar cell is about 45%. Pazos et al. also experimentally investigated such a SF-sensitized parallel tandem cell which consisted of a pentacne/C_{60} sub-cell paired with a monocrystalline silicon solar cell. The structure of pentacene sub-cell was same as the above-mentioned device fabricated by Congreve et al.,[24] and it was found that SF-generated triplet excitons contribute to the overall photocurrent of the tandem cell. The EQE of the tandem SF solar cell exceeded 100%; this cannot

be achieved with a single-junction silicon solar cell. The challenge here – as with all tandem devices – however, is that the architecture is very complex.

The efficient triplet exciton diffusion and dissociation are critical for engineering a high-performance SF-based solar cell. Research efforts have also been devoted to studying the triplet exciton dynamics to provide new insight into triplet exciton transport in the solid state. Poletayev et al. explored the triplet exciton diffusion in pentacene crystals and films using a bilayer device structure of ITO/Pc/PbS nanocrystals/Al. The triplet diffusion lengths in evaporated films and single crystals are 40-80 nm and 350-800 nm, respectively, as estimated from the TAS studies. This indicates that the morphology of active layer is critical for maximizing triplet exciton diffusion. They also demonstrated that the incorporation of a thin exciton blocking layer at the ITO/Pc interface is necessary for ensuring maximal triplet exciton dissociation of single-crystalline pentacene. Recently, Wan et al. (Nat. Chem. 2015, 7, 785) has shown the cooperative singlet and triplet exciton transport in tetracene crystals using femtosecond transient absorption microscopy. The endothermic singlet fission and the energetically allowable triplet fusion in tetracene results in an equilibrium between the singlet and triplet populations upon photoexcitation. They demonstrated that this equilibrium leads to more than one order of magnitude enhancement in the effective triplet exciton diffusion constant on picosecond to nanosecond timescales, which results from cooperative singlet–triplet transport. The cooperative singlet-triplet transport mechanism provides new insight into triplet transport in SF-based devices which has important implications for using SF materials for solar cells.

Independent studies by Tabachnyk et al.[44] and Thompson et al.[45] have demonstrated that the triplet excitons generated by singlet fission in acenes (pentacene and tetracene), can be directly and efficiently transferred to semiconductor nanocrystals (PbSe and PbS) through Dexter energy

transfer when the band-gap of the nanocrystals is close to the triplet energies of the acene. Ideally, the transferred triplet excitons can become emissive if their lifetime in the nanocrystal is sufficiently long, and a coating containing the acene and nanocrystal could be applied to a commercial solar cell. In this case, a singlet photon of light with excess energy is effectively down-converted into two photons. Such a process would work with no need for any electrical connection between the coating and the commercial solar cell. However, work remains to be done in this area: difficulties arise because small ligands are required to enable efficient triplet transfer, but larger ligands are preferred to effectively passivate the quantum dot.

For the successful implementation of acenes in SF devices, another challenge is their susceptibility to Diels-Alder reactions with fullerenes.[46-49] However, recent improvements in the field of non-fullerene acceptors may provide a viable solution moving forward.[50-55]

1.6 Recent progress in intramolecular singlet fission

The development of SF-based solar cells summarized above is constrained by the use of intermolecular singlet fission materials. The efficiency of SF in intermolecular materials is however highly sensitive to the crystal packing of the chromophore and the morphology of active layer. This sensitivity can be mitigated by using simple bilayer architectures to ensure a well-controlled morphology for the SF material. As discussed above, while this layered device structure has been commonly employed, this approach is in contrast to the most popular and highest performing approach of bulk-heterojunction architectures for organic photovoltaics (OPVs). An alternative approach to ensure SF efficiency is not lost with unfavorable morphology is to employ an intramolecular singlet fission (iSF) material, in which case SF does not depend sensitively on

intermolecular packing, but instead is an innate property of the molecule. While the utility of such an approach was recognized and candidate structures were theorized and synthesized,[56-61] it was not until 2015 that efficient systems were reported.[8,62-68] These early efforts towards intramolecular singlet fission materials, both theoretical and experimental, have been reviewed elsewhere.[7,30,69] Due to the novelty of iSF compounds, to the best of our knowledge, a solar cell that takes advantage of iSF chromophores to boost EQE has yet to be reported. Here we describe the advances in this field, focusing on the prospects of these materials as active layers in future devices.

1.7 Intramolecular singlet fission in acene derivatives

Because monomeric acenes have been widely used as a model system to study intermolecular SF, an intuitive approach to achieve intramolecular SF is through covalent coupling of two acene units. It has recently been demonstrated that dimers of acenes can undergo iSF with yields approaching 200%. The first reports focused on pentacene dimers, where singlet fission is typically exothermic by ~0.4 eV.[8,65,68] However, a more recent report has shown that this strategy is modular, and pentacene can be coupled with tetracene or even hexacene and still undergo efficient singlet fission.[62]

In this study, [62] pentacene was dimerized with anthracene, tetracene, pentacene or hexacene, and the photophysics of the resulting compounds were compared in dilute solution. In the case of solution SF, the ^{1}(TT) state is trapped, as the constrained nature of a dimer prevents triplet diffusion and separation of the ^{1}(TT) state to form free triplets ($2xT_1$). By varying the acene linked to pentacene, the energy of the singlet exciton (best described by the lower singlet energy component of the dimer) and the triplet pair (the sum of the triplet energy of each monomer) can be tuned.

Indeed, in the case of pentacene-anthracene (PA), iSF is significantly endothermic and iSF does not occur. Instead, the singlet exciton fluoresces for ~11 ns, similar to the singlet lifetime in monomeric TIPS pentacene. However, when the energetics are roughly isoergic (PT) or significantly exothermic (BP or PH), SF occurs with a surprisingly similar ~1ps time constant (Figure 1.10). The insensitivity of these rates to energetic driving force likely has implications for the mechanism of iSF in these compounds.

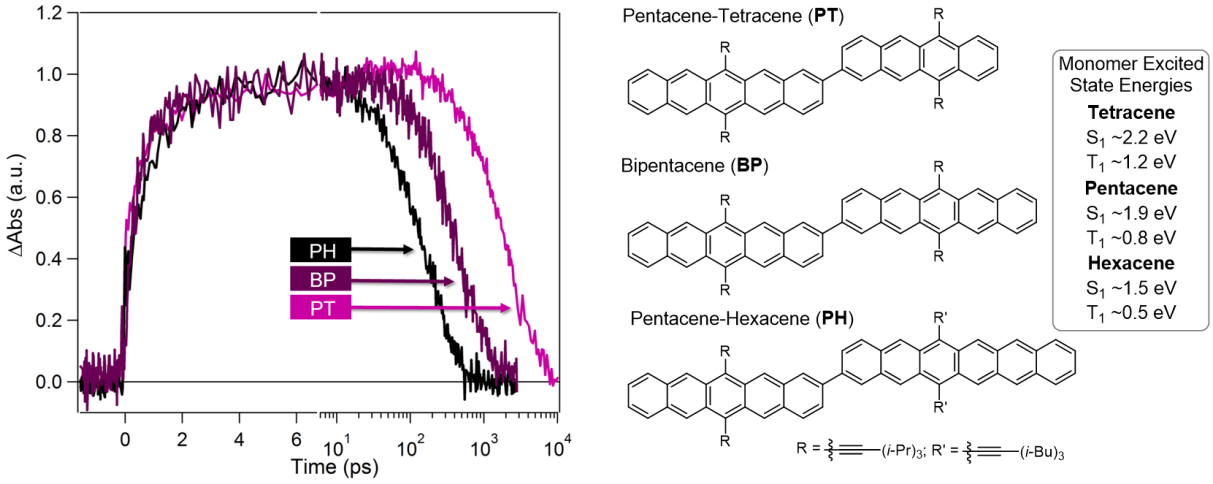

Figure 1.10. Kinetic traces at wavelengths where the triplet photoinduced absorption is preferentially probed, showing the temporal evolution of triplet pair signal in oligoacene heterodimers obtained by transient absorption spectroscopy in dilute solution. These kinetic traces reveal a minimal dependence of iSF rate on driving force, but a strong energy-gap-law dependence for the triplet pair recombination process. Note the change in scale from linear to log. Reproduced with permission.[62] Copyright 2016, John Wiley and Sons.

Furthermore, this series of compounds reveals that non-radiative recombination of triplet pairs is dictated by an energy gap law, similar to the well-known energy gap law for triplet excitons.[70] Therefore, the more energetic triplet pairs recombine to the ground state slower. Fundamentally, these compounds have enabled us to identify new physics of the trapped ^{1}(TT) state, a key intermediate in singlet fission, which is difficult to study in other systems due to its

short-lived nature in the solid state at room temperature.[12,71] From a practical perspective, this finding is important because it suggests an opportunity to address two challenges at once; the use of shorter oligoacenes yields higher energy triplets, thus increasing V_{OC}, and also lengthens the lifetime of the excited state. Longer excited state lifetimes provide more opportunity for separation and/or harvesting in eventual solid-state applications of these materials. With this information in mind, we turn our attention to the shortest singlet fission dimers reported, tetracene dimers from Korovina et al. [67]

Such tetracene dimers may prove to be the most promising materials for device applications of iSF materials. Recent results in tetracene dimer systems have shown that fission occurs in these materials in high (~154%) yields (Figure 1.11).[67] The dimers reported in this study form amorphous films in which SF does not exhibit a diffusive component, indicating the efficiency of the intramolecular process. In contrast, excitons generated in amorphous films of monomeric SF materials have to diffuse to sites where the chromophores have the correct orientation for the intermolecular process to occur .[72] While these results highlight the relative insensitivity of iSF chromophores to morphology and packing constraints, more crystalline systems are likely preferable for actual implementation, due to the need for efficient hole transport in the tetracene dimer for triplet and eventually hole transport.

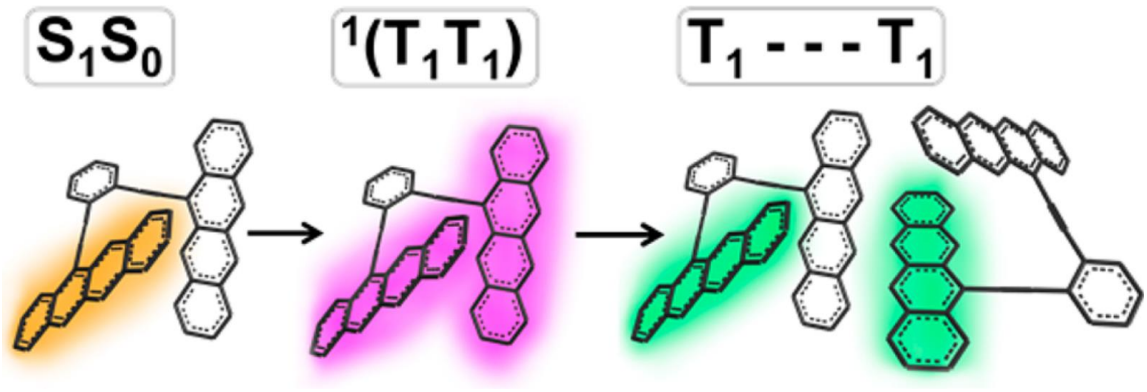

Figure 1.11. Tetracene dimers reported by Korovina et al. with desirable features such as high-yielding singlet fission, absence of a diffusive component in amorphous films, and high energy triplet excitons. Reproduced with permission.[67] Copyright 2016, American Chemical Society.

One issue with singlet fission dimers is that the triplet pair state, confined to a singlet molecule, typically recombines much faster than a triplet alone. While Korovina et al. have demonstrated that triplets in pairs in the solid state can separate by diffusion, in their work only some portion of the triplet pair population was able to be separated before recombining. To solve this problem, we must either enhance the rate of diffusion of the pair, or to reduce the rate of triplet pair recombination.

One possible solution to reduce the rate of triplet pair annihilation in iSF compounds is the use of a "bridge" between the relevant chromophores to spatially reduce coupling between the resultant triplets. Sanders et al.[8] demonstrated this effect by incorporating bridges with increasing numbers of phenyl rings between two pentacenes (Figure 1.12). While this strategy has proven effective for enhancement of triplet pair lifetime in solution, separation of the triplets in the solid state has not yet been reported for this class of compounds. The trade-off involved with inclusion of a bridge is that the bridge tends to slow singlet fission as well as triplet pair recombination.

However, the "bridge" strategy provides another option for rational design and optimization of iSF chromophores since the triplet lifetimes can be tuned appropriately to allow for their extraction.

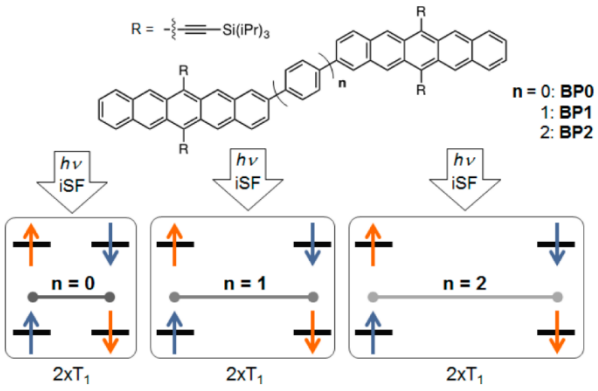

Figure 1.12. Introduction of phenyl spacers into pentacene dimers. Longer spacers enhance triplet lifetime but slow the rate of iSF. Reproduced with permission.[8] Copyright 2015, American Chemical Society.

Although experimental and theoretical results have already demonstrated that the triplet pair state is a crucial SF intermediate, understanding the exciton correlations of the ^{1}(TT) state is a remaining challenge. Dimers serve as an excellent platform for studying this state, as the two triplets are trapped adjacent to each other and cannot diffuse apart. Very recently, Sanders et al. studied the triplet pair dynamics in a series of asymmetric pentacene−tetracene (PTn, n = 0, 1, 2) heterodimers derived from the "bridge" motif.[73] The presence of long-lived delayed fluorescence in these compounds reveals a lifetime for correlated triplet pair states with singlet character on the order of 50 ns. Interestingly, long-lived multiexciton states eventually evolve to become dark, suggesting population of triplet states with higher spin multiplicity. Further studies with non-optical techniques will still be required to properly elucidate the spin physics at play.

While the intramolecular SF process is insensitive to the morphology and packing, an ordered morphology of the active layer is still highly desired for the triplet exciton transport and

extraction in iSF-based solar cells. The, fast recombination of triplet excitons generated by iSF localized on the same molecule presents a challenge for exciton dissociation in solar cell application. One promising way to tackle this issue is through forming highly ordered packing structure between the iSF donor material and low-band gap acceptor. The donor-acceptor charge transfer interaction would facilitate the triplet extraction, and attention needs to be paid to tune the morphology of active layers during device engineering.

1.8 Intramolecular singlet fission in donor-acceptor polymers

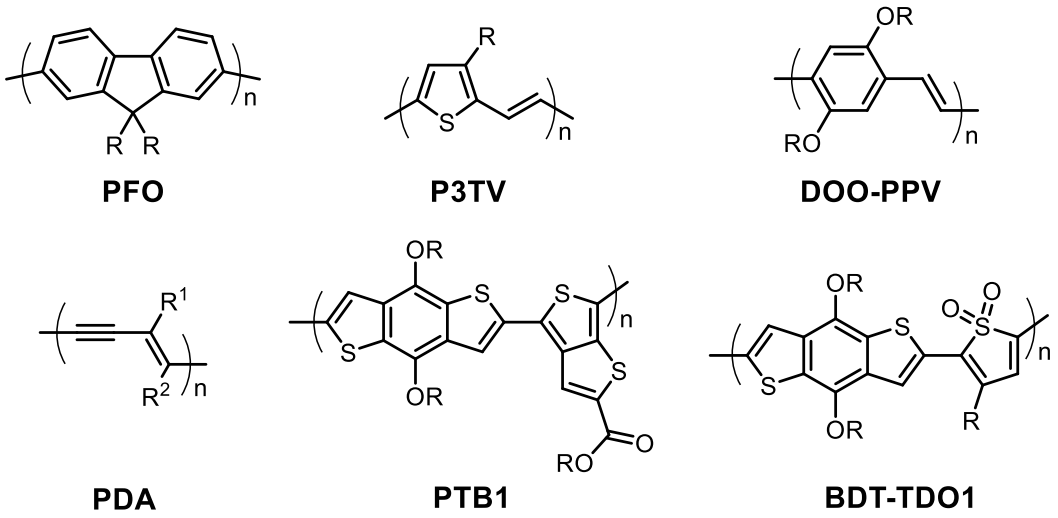

Figure 1.13. Structures of conjugated polymers that undergo singlet fission. The R groups represent solubilizing alkyl chains.

Most of the highest performing organic electronic devices employ conjugated polymers as the active material due to the ease of processing into thin films and efficiency of transport both along and between polymer chains. It is therefore promising that singlet fission has been observed in several conjugated polymers (Figure 1.13). Many of these systems require larger photon energy than the band gap, although there are some notable exceptions.

When the energy of the triplet pair ^{1}(TT) state is higher than the first optically excited state, SF can still occur. One mechanism shown in several reports involves the initial fusion of two singlets into a higher (S_n) state before fission into two triplets.[74-77] Although this scenario is not useful for multiexciton generation, the generation and fate of the triplets in such systems are still of interest. In particular, it was observed that singlet-singlet annihilation to form higher singlet excited states could subsequently populate ^{1}(TT) states by SF in polyfluorene (PFO) films.

Furthermore, the authors found that fewer ^{1}(TT) states formed in a more crystalline film of PFO, but that the more crystalline films had more effective dissociation of the ^{1}(TT) states relative to more amorphous films.[74] This result highlights the balance between many subtle factors at play and points out some challenges that will have to be overcome when engineering devices.

The generation of two triplets from a single excitation, when $E^1(TT) > E(S_1)$, and without singlet-singlet annihilation was reported by Musser et al.[78] In this case, excitation with sufficient energy in excess of the bandgap produces a vibrationally "hot" excited state, and SF occurs from this hot state in competition with vibrational relaxation. In this report, iSF was observed in poly(3-dodecylthienylenevinylene) (P3TV) and triplet yields increased with photon energy, indicating that SF was an activated process. Promisingly, a charged species in films of P3TV/PCBM blends had a similar photon energy dependence, implying that these triplets were being dissociated by the heterojunction. However, the authors noted that the PCE of P3TV solar cells rarely breach 1%. Zhai et al. [79] also studied SF in similar polymers poly(dioctyloxy)phenylenevinylene (DOO-PPV) and polydiacetylene (PDA) (Figure 1.13). The former was found to undergo activated intermolecular SF in films while the latter, like P3TV, undergoes iSF in solution. It was suggested that SF in conjugated polymers might be a "general process" that indeed warrants more research.

Donor-acceptor polymers typically outperform homopolymers in PCE, with PTB7 as a benchmark material in the OPV field.[80] A recent study by Kasai et al.[81] on the related polymer, PTB1, showed that it undergoes SF, albeit via an activated, interchain mechanism and with low yields. While it is difficult to ascertain the contribution of SF to PCE in devices based on PTB1, further understanding of SF in these high-performance materials can guide molecular design to better exploit it and employ it in novel device architectures.

In a similar development, Busby et al.[9] reported that the donor-acceptor polymer BDT-TDO1 (Figure 1.13) undergoes non-activated iSF with triplet yields of up to 170%. This is one of the highest yielding intramolecular systems reported besides the acene dimers discussed above. The donor-acceptor character imparts significant quinoidal character and results in a low triplet energy enabling singlet fission. While these materials demonstrated the possibility of efficient intramolecular singlet fission, they also featured low triplet energies and short triplet pair lifetimes which may present issues for the practical implementation of this specific system in SF devices. The mechanism of intrachain SF is also still not entirely clear, although it has been suggested that too much or too little intrachain charge transfer character in the initial excitation can be detrimental to fission yields.[19] A better understanding of the mechanism and design principles for these materials is still needed. If donor-acceptor iSF polymers with higher triplet energies are developed, they will be interesting to investigate as active layers in iSF devices.

1.9 Conclusions and Outlook

The implementation of singlet fission into devices exhibits great potential for boosting power conversion efficiency of third generation photovoltaic solar cells. An external quantum efficiency up to 126% has been achieved by directly harvesting triple excitons generated by SF within a layered donor-acceptor heterojunction device. Using singlet fission to enhance the photocurrent of conventional solar cells, an EQE over 100% was demonstrated for monocrystalline silicon solar cell by using a parallel tandem device.

To date, the greatest challenge faced by singlet fission based solar cells is how to achieve efficient triplet exciton diffusion and dissociation. To deal with the challenge, novel red-absorbing

acceptor materials with deep LUMOs need to be designed and developed, and research efforts should also be devoted to the device engineering. Michl et al. has pointed out that, a tandem solar cell composed of a blue-absorbing singlet fission donor and a red-absorbing acceptor is an ideal device architecture to maximize the efficiency of SF-based solar. While the best device structure for implementing singlet fission into single junction solar is dependent of the nature of SF. A bilayer heterojunction structure is most promising for intermolecular singlet fission, while a blended bulk heterojunction solar cell is ideal for intramolecular singlet fission.

Current achievement in engineering SF based solar cells is restricted to the use of intermolecular singlet fission materials, in particular acenes, in which the SF process is highly dependent on the packing and coupling of adjacent molecules. Due to the morphology-sensitive nature of intermolecular SF, most SF based solar cells are limited in using planar heterojunction device structure, and less success has been obtained for blended bulk heterojunction. Another drawback of acenes is that they can only absorb high energy photons with relatively small absorption coefficients, and a stronger absorber often has to be combined.

Recent progress in understanding the mechanism of singlet fission has established that this multiple exciton generation process can efficiently occur within an isolated chromophore, namely, intramolecular singlet fission. Unlike intermolecular SF, the field of iSF is still in its infancy and this process has yet to be investigated in functional devices. However, early results are promising and suggest the possibility of more and simpler device architectures in the future. Key challenges include the design and optimization of more chromophores. Besides donor-acceptor polymers and acene dimers discussed in detail above, quinoidal thiophenes might be another class of materials where iSF is prevalent.[66] Generally, desirable characteristics for iSF molecules to be exploited in

devices include fast fission rates, high triplet energies, long triplet pair lifetimes, and efficient diffusional separation of triplet pairs in the solid state.

The development of intramolecular SF conjugated polymers should open an avenue in engineering SF-based organic bulk-heterojunction solar cells, due to the morphology independent character of iSF as well as the ease of processing polymeric active layers into films. Also, the broadband absorption of conjugated polymers can make better use of sunlight. Recent improvements in the field of non-fullerene organic acceptors with tunable band-gaps[50-55] may further facilitate the implementation of SF-based organic solar cells, with all-solution-processable bulk heterojunction architectures.

1.10 References

(1) Green, M. A. *Prog. Photovoltaics* **2001**, *9*, 123.

(2) W. Shockley; H. J. Queisser *J. Appl. Phys.* **1961**, *32*, 510.

(3) Hanna, M. C.; Nozik, A. J. *J. Appl. Phys.* **2006**, *100*, 074510.

(4) Beard, M. C.; Luther, J. M.; Semonin, O. E.; Nozik, A. J. *Acc. Chem. Res.* **2013**, *46*, 1252.

(5) Smith, M. B.; Michl, J. *Chem. Rev.* **2010**, *110*, 6891.

(6) Singh, S.; Jones, W. J.; Siebrand, W.; Stoicheff, B. P.; Schneider, W. G. *J. Chem. Phys.* **1965**, *42*, 330.

(7) Smith, M. B.; Michl, J. *Annu. Rev. Phys. Chem.* **2013**, *64*, 361.

(8) Sanders, S. N.; Kumarasamy, E.; Pun, A. B.; Trinh, M. T.; Choi, B.; Xia, J.; Taffet, E. J.; Low, J. Z.; Miller, J. R.; Roy, X.; Zhu, X.-Y.; Steigerwald, M. L.; Sfei, M. Y.; Campos, L. M. *J. Am. Chem. Soc.* **2015**, *137*, 8965.

(9) Busby, E.; Xia, J.; QinWu; Low, J. Z.; Song, R.; Miller, J. R.; Zhu, X.-Y.; Campos, L. M.; Sfeir, M. Y. *Nat. Mater.* **2015**, *14*, 426.

(10) Monahan, N.; Zhu, X.-Y. *Annu. Rev. Phys. Chem.* **2015**, *66*, 601.

(11) Chan, W.-L.; Berkelbach, T. C.; Provorse, M. R.; Monahan, N. R.; Tritsch, J. R.; Hybertsen, M. S.; Reichman, D. R.; Gao, J.; Zhu, X. Y. *Acc. Chem. Res.* **2013**, *46*, 1321.

(12) Chan, W.-L.; Ligges, M.; Jailaubekov, A.; Kaake, L.; Miaja-Avila, L.; Zhu, X.-Y. *Science* **2011**, *334*, 1541.

(13) Chan, W.-L.; Ligges, M.; Zhu, X. Y. *Nat. Chem.* **2012**, *4*, 840.

(14) Bakulin, A. A.; Morgan, S. E.; Kehoe, T. B.; Wilson, M. W. B.; Chin, A. W.; Zigmantas, D.; Egorova, D.; Rao, A. *Nat. Chem.* **2015**, *8*, 16.

(15) Musser, A. J.; Liebel, M.; Schnedermann, C.; Wende, T.; Kehoe, T. B.; Rao, A.; Kukura, P. *Nat. Phys.* **2015**, *11*, 352.

(16) Zeng, T.; Hoffmann, R.; Ananth, N. *J. Am. Chem. Soc.* **2014**, *136*, 5755.

(17) Schrauben, J. N.; Ryerson, J. L.; Michl, J.; Johnson, J. C. *J. Am. Chem. Soc.* **2014**, *136*, 7363.

(18) Aryanpour, K.; Shukla, A.; Mazumdar, S. *J. Phys. Chem. C* **2015**, *119*, 6966.

(19) Aryanpour, K.; Dutta, T.; Huynh, U. N. V.; Vardeny, Z. V.; Mazumdar, S. *Phys. Rev. Lett.* **2015**, *115*, 267401.

(20) C. C. Gradinaru; J. T. M. Kennis; E. Papagiannakis; I. H. M. V. Stokkum; Cogdell, R. J.; G. R. Fleming; R. A. Niederman; Grondelle, R. V. *Proc. Natl. Acad. Sci.* **2001**, *98*, 2364.

(21) A. J. Musser; M. Maiuri; D. Brida; Cerullo, G.; R. H. Friend; Clark, J. *J. Am. Chem. Soc.* **2015**, *137*, 5130.

(22) Yost, S. R.; Lee, J.; Wilson, M. W. B.; Wu, T.; McMahon, D. P.; Parkhurst, R. R.; Thompson, N. J.; Congreve, D. N.; Rao, A.; Johnson, K.; Sfeir, M. Y.; Bawendi, M. G.; Swager, T. M.; Friend, R. H.; Baldo, M. A.; Van Voorhis, T. *Nat. Chem.* **2014**, *6*, 492.

(23) Renaud, N.; Grozema, F. C. *J. Phys. Chem. Lett.* **2015**, *6*, 360.

(24) D. N. Congreve; J. Lee; N. J. Thompson; E. Hontz; S. R. Yost; P. D. Reusswig; M. E. Bahlke; S. Reineke; T. V. Voorhis; Baldo, M. A. *Science* **2013**, *340*, 334.

(25) Thompson, N. J.; Congreve, D. N.; Goldberg, D.; Menon, V. M.; Baldo, M. A. *Appl. Phys. Lett.* **2013**, *103*, 263302.

(26) D. Veldman; S. C. J. Meskers; Janssen, R. A. J. *Adv. Funct. Mater.* **2009**, *19*, 1939.

(27) M. W. B. Wilson; A. Rao; J. Clark; R. S. S. Kumar; D. Brida; G. Cerullo; Friend, R. H. *J. Am. Chem. Soc.* **2011**, *133*, 11830.

(28) O. D. Jurchescu; M. Popinciuc; B. J. van Wees; Palstra, T. T. M. *Adv. Mater.* **2007**, *19*, 688.

(29) J. Mei; Y. Diao; A. L. Appleton; L. Fang; Bao, Z. *J. Am. Chem. Soc.* **2013**, *135*, 6724.

(30) Burdett, J. J.; Bardeen, C. J. *Acc. Chem. Res.* **2013**, *46*, 1312.

(31) T. C. Wu; N. J. Thompson; D. N. Congreve; E. Hontz; S. R. Yost; T. Van Voorhis; Baldo, M. A. *Appl. Phys. Lett.* **2014**, *104*, 193901.

(32) A. Rao; M. W. B. Wilson; J. M. Hodgkiss; S. Albert-Seifried; Bässler, H.; Friend, R. H. *J. Am. Chem. Soc.* **2010**, *132*, 12698.

(33) J. Lee; P. Jadhav; Baldo, M. A. *Appl. Phys. Lett.* **2009**, *95*, 033301.

(34) P. J. Jadhav; P. R. Brown; N. Thompson; B. Wunsch; A. Mohanty ; S. R. Yost ; E. Hontz ; T. Van Voorhis ; M. G. Bawendi ; V. Bulović; Baldo, M. A. *Adv. Mater.* **2012**, *24*, 6169.

(35) N. J. Thompson; E. Hontz; D. N. Congreve; M. E. Bahlke; S. Reineke; T. Van Voorhis; Baldo, M. A. *Adv. Mater.* **2014**, *26*, 1366.

(36) B. Ehrler; M. W. B. Wilson; A. Rao; R. H. Friend; Greenham, N. C. *Nano Lett.* **2012**, *12*, 1053.

(37) Ehrler, B.; Walker, B. J.; Böhm, M. L.; Wilson, M. W. B.; Vaynzof, Y.; Friend, R. H.; Greenham, N. C. *Nat. Commun.* **2012**, *3*, no. 1019.

(38) L. Yang; M. Tabachnyk; S. L. Bayliss; Böhm, M. L.; K. Broch; N. C. Greenham; R. H. Friend; Ehrler, B. *Nano Lett.* **2015**, *15*, 354.

(39) S. Kawata; Y.-J. Pu; A. Saito; Y. Kurashige; T. Beppu; H. Katagiri; M. Hada; Kido, J. *Adv. Mater.* **2016**, *28*, 1585.

(40) P. J. Jadhav; A. Mohanty; J. Sussman; J. Lee; Baldo, M. A. *Nano Lett.* **2011**, *11*, 1495.

(41) Reusswig, P. D.; Congreve, D. N.; Thompson, N. J.; Baldo, M. A. *Appl. Phys. Lett.* **2012**, *101*, 113304.

(42) B. Ehrler; K. P. Musselman; M. L. Böhm; R. H. Friend; Greenham, N. C. *Appl. Phys. Lett.* **2012**, *101*, 153507.

(43) L. M. Pazos; J. M. Lee; A. Kirch; M. Tabachnyk; R. H. Friend; Ehrler, B. *arXiv preprint* **2015**

(44) M. Tabachnyk; B. Ehrler; S. Gélinas; M. L. Böhm; B. J.Walker; K. P. Musselman; N. C. Greenham; Friend, R. H.; Rao, A. *Nat. Mater.* **2014**, *13*, 1033.

(45) Thompson, N. J.; B.Wilson, M. W.; Congreve, D. N.; Brown, P. R.; Scherer, J. M.; Bischof, T. S.; Wu, M.; Geva, N.; Welborn, M.; Voorhis, T. V.; Bulovic, V.; Bawendi, M. G.; Baldo, M. A. *Nat. Mater.* **2014**, *13*, 1039.

(46) Cao, Y.; Liang, Y.; Zhang, L.; Osuna, S.; Hoyt, A.-L. M.; Briseno, A. L.; Houk, K. N. *J. Am. Chem. Soc.* **2014**, *136*, 10743.

(47) Briggs, J. B.; Miller, G. P. *C. R. Chimie* **2006**, *9*, 916.

(48) Hudhomme, P. *C. R. Chimie* **2006**, *9*, 881.

(49) J. Mack; P.Miller, G. *Fullerene Sci. Technol.* **1997**, *5*, 607.

(50) Meng, D.; Sun, D.; Zhong, C.; Liu, T.; Fan, B.; Huo, L.; Li, Y.; Jiang, W.; Choi, H.; Kim, T.; Kim, J. Y.; Sun, Y.; Wang, Z.; Heeger, A. J. *J. Am. Chem. Soc.* **2016**, *138*, 375.

(51) Zhong, Y.; Trinh, M. T.; Chen, R.; Purdum, G. E.; Khlyabich, P. P.; Sezen, M.; Oh, S.; Zhu, H.; Fowler, B.; Zhang, B.; Wang, W.; Nam, C.-Y.; Sfeir, M. Y.; Black, C. T.;

Steigerwald, M. L.; Loo, Y.-L.; Ng, F.; Zhu, X. Y.; Nuckolls, C. *Nat. Commun.* **2015**, *6*, 8242.

(52) Zhong, Y.; Trinh, M. T.; Chen, R.; Wang, W.; Khlyabich, P. P.; Kumar, B.; Xu, Q.; Nam, C.-Y.; Sfeir, M. Y.; Black, C.; Steigerwald, M. L.; Loo, Y.-L.; Xiao, S.; Ng, F.; Zhu, X. Y.; Nuckolls, C. *J. Am. Chem. Soc.* **2014**, *136*, 15215.

(53) Lin, Y.; Wang, J.; Zhang, Z.-G.; Bai, H.; Li, Y.; Zhu, D.; Zhan, X. *Adv. Mater.* **2015**, *27*, 1170.

(54) Liu, Y.; Mu, C.; Jiang, K.; Zhao, J.; Li, Y.; Zhang, L.; Li, Z.; Lai, J. Y. L.; Hu, H.; Ma, T.; Hu, R.; Yu, D.; Huang, X.; Tang, B. Z.; Yan, H. *Adv. Mater.* **2015**, *27*, 1015.

(55) Sun, D.; Meng, D.; Cai, Y.; Fan, B.; Li, Y.; Jiang, W.; Huo, L.; Sun, Y.; Wang, Z. *J. Am. Chem. Soc.* **2015**, *137*, 11156.

(56) Müller, A. M.; Avlasevich, Y. S.; Schoeller, W. W.; Müllen, K.; Bardeen, C. J. *J. Am. Chem. Soc.* **2007**, *129*, 14240.

(57) Müller, A. M.; Avlasevich, Y. S.; Müllen, K.; Bardeen, C. J. *Chem. Phys. Lett.* **2006**, *421*, 518.

(58) Johnson, J. C.; Akdag, A.; Zamadar, M.; Chen, X.; Schwerin, A. F.; Paci, I.; Smith, M. B.; Havlas, Z.; Miller, J. R.; Ratner, M. A.; Nozik, A. J.; Michl, J. *J. Phys. Chem. B* **2013**, *117*, 4680.

(59) Schwerin, A. F.; Johnson, J. C.; Smith, M. B.; Sreearunothai, P.; Popović, D. K.; Černý, J. I.; Havlas, Z. K.; Paci, I.; Akdag, A.; MacLeod, M. K.; Chen, X.; David, D. E.; Ratner, M. A.; Miller, J. R.; Nozik, A. J.; Michl, J. *J. Phys. Chem. A* **2009**, *114*, 1457.

(60) Greyson, E. C.; Stepp, B. R.; Chen, X.; Schwerin, A. F.; Paci, I.; Smith, M. B.; Akdag, A.; Johnson, J. C.; Nozik, A. J.; Michl, J.; Ratner, M. A. *J. Phys. Chem. B* **2009**, *114*, 14223.

(61) Greyson, E. C.; Vura-Weis, J.; Michl, J.; Ratner, M. A. *J. Phys. Chem. B* **2010**, *114*, 14168.

(62) Sanders, S. N.; Kumarasamy, E.; Pun, A. B.; Steigerwald, M. L.; Sfeir, M. Y.; Campos, L. M. *Angew. Chem. Int. Ed.* **2016**, *55*, 3373.

(63) E. Busby; T. C. Berkelbach; B. Kumar; A. Chernikov; Y. Zhong; H. Hlaing; X.-Y. Zhu; T. F. Heinz; M. S. Hybertsen; M. Y. Sfeir; D. R. Reichman; C. Nuckolls; Yaffe, O. *J. Am. Chem. Soc.* **2014**, *136*, 10654.

(64) Low, J. Z.; Sanders, S. N.; Campos, L. M. *Chem. Mater.* **2015**, *27*, 5453.

(65) Lukman, S.; Musser, A. J.; Chen, K.; Athanasopoulos, S.; Yong, C. K.; Zeng, Z.; Ye, Q.; Chi, C.; Hodgkiss, J. M.; Wu, J.; Friend, R. H.; Greenham, N. C. *Adv. Funct. Mater.* **2015**, *25*, 5452.

(66) Varnavski, O.; Abeyasinghe, N.; Aragó, J.; Serrano-Pérez, J. J.; Ortí, E.; Navarrete, J. T. L.; Takimiya, K.; Casanova, D.; Casado, J.; GoodsonIII, T. *J. Phys. Chem. Lett.* **2015**, *6*, 1375.

(67) Korovina, N. V.; Das, S.; Nett, Z.; Feng, X.; Joy, J.; Haiges, R.; Krylov, A. I.; Bradforth, S. E.; Thompson, M. E. *J. Am. Chem. Soc.* **2016**, *138*, 617.

(68) Zirzlmeier, J.; Lehnherr, D.; Coto, P. B.; Chernick, E. T.; Casillas, R.; Basel, B. S.; Thoss, M.; Tykwinski, R. R.; Guldi, D. M. *Proc. Natl. Acad. Sci.* **2015**, *112*, 5325.

(69) Johnson, J. C.; Nozik, A. J.; Michl, J. *Acc. Chem. Res.* **2013**, *46*, 1290.

(70) J. S. Wilson ; Chawdhury, N.; M. R. A. Al-Mandhary; M. Younus; Khan., M. S.; P. R. Raithby; A. Köhler; Friend, R. H. *J. Am. Chem. Soc.* **2001**, *123*, 9412.

(71) Wilson, M. W. B.; Rao, A.; Johnson, K.; Gélinas, S.; di Pietro, R.; Clark, J.; Friend, R. H. *J. Am. Chem. Soc.* **2013**, *135*, 16680.

(72) S. T. Roberts; R. E. McAnally; J. N. Mastron; D. H. Webber; M. T. Whited; R. L. Brutchey; M. E. Thompson; Bradforth, S. E. *J. Am. Chem. Soc.* **2012**, *134*, 6388.

(73) Sanders, S. N.; Kumarasamy, E.; Pun, A. B.; Appavoo, K.; Steigerwald, M. L.; Campos, L. M.; Sfeir, M. Y. *J. Am. Chem. Soc.* **2016**, *138*, 7289.

(74) Tamai, Y.; Ohkita, H.; Benten, H.; Ito, S. *J. Phys. Chem. C* **2013**, *117*, 10277.

(75) Guo, J.; Ohkita, H.; Benten, H.; Ito, S. *J. Am. Chem. Soc.* **2009**, *131*, 16869.

(76) Kraabel, B.; Hulin, D.; Aslangul, C.; Lapersonne-Meyer, C.; Schott, M. *Chem. Phys.* **1998**, *227*, 83.

(77) Antognazza, M. R.; Lüer, L.; Polli, D.; Christensen, R. L.; Schrock, R. R.; Lanzani, G.; Cerullo, G. *Chem. Phys.* **2010**, *373*, 115.

(78) Musser, A. J.; Al-Hashimi, M.; Maiuri, M.; Brida, D.; Heeney, M.; Cerullo, G.; Friend, R. H.; Clark, J. *J. Am. Chem. Soc.* **2013**, *135*, 12747.

(79) Zhai, Y.; Sheng, C.; Vardeny, Z. V. *Phil. Trans. R. Soc. A* **2015**, *373*, 0140327.

(80) Liang, Y.; Xu, Z.; Xia, J.; Tsai, S.-T.; Wu, Y.; Li, G.; Ray, C.; Yu, L. *Adv. Mater.* **2010**, *22*, E135.

(81) Kasai, Y.; Tamai, Y.; Ohkita, H.; Benten, H.; Ito, S. *J. Am. Chem. Soc.* **2015**, *137*, 15980.

2 Quantitative Intramolecular Singlet Fission in Bipentacenes

2.1 Preface

This chapter is based on a manuscript entitled "Quantitative Intramolecular Singlet Fission in Bipentacenes" by Samuel N. Sanders, Elango Kumarasamy, Andrew B. Pun, M. Tuan Trinh, Bonnie Choi, Jianlong Xia, Elliot J. Taffet, Jonathan Z. Low, John R. Miller, Xavier Roy, X.-Y. Zhu, Michael L. Steigerwald, Matthew Y. Sfeir, Luis M. Campos published in the *Journal of the American Chemical Society*.[1]

I synthesized the molecules with essential help from Elango Kumarasamy, Andrew B. Pun, Jianlong Xia, and Elliot Taffet from Professor Luis Campos's group. I collected and processed the transient absorption data with assistance from M. Tuan Trinh from Professor Xiaoyang Zhu's group and Matthew Y. Sfeir.

2.2 Introduction

The third-generation of solar cells is based on materials that operate by non-conventional photophysical mechanisms to overcome the Shockley-Queisser limit.[2-4] In molecules and polymers, singlet fission (SF) is the process whereby two triplets are generated from a single photon.[5] Devices fabricated from singlet fission molecules have exceeded 100% external quantum efficiency,[6,7] but many fundamental challenges remain: a) there are a limited number of materials that undergo SF; b) appropriate heterojunctions must be engineered to extract the multiple excitons; and c) device architectures that exploit SF must be engineered. While the resurgent interest in SF has been catalyzed by solar cells, multiexcitonic materials can be also widely applicable in other optoelectronic thin-film technologies, such as photodetectors.[8]

One major hurdle to development of multiexcitonic devices is the need for chromophores that undergo SF independent of intermolecular interactions. For example, acenes can undergo SF only when neighboring chromophores are electronically coupled in the solid-state or by diffusional collisions in highly concentrated solutions. We refer to this process as intermolecular singlet fission (xSF),[6,8-13] where pentacene has surfaced as the prototypical material since its SF triplet quantum yield is quantitative (200%).[11] In fact, even in crystalline media, the crystal packing and morphology have a significant effect on fission rates, rendering practical applications more challenging.[14-17] A more suitable approach is to employ intramolecular singlet fission (iSF) active layers, but iSF has rarely been observed in organic materials, with yields before 2015 languishing below 30% and/or as an activated process.[18-20]

We have recently pioneered the design of organic materials based on strong-donor/strong-acceptor copolymers and small molecules that facilitate iSF through a photoexcited state with strong charge-transfer (CT)-character, exhibiting up to 170% triplet yield in a polymer.[21,22] Such design principles were founded on the CT-mediated mechanism of xSF. Interestingly, there is another strategy in molecular materials, which involves the covalent coupling of two xSF chromophores. As of 2014, several groups attempted to model and synthesize such dimers based on tetracene and diphenylisobenzofuran, only to find low experimental triplet yields (<10%).[23-29] However, it can be possible to improve the yields using covalently coupled pentacene dimers and by understanding how the conjugation within these chromophores affect iSF. During the course of revisions to this manuscript, Zirzlmeier *et al.* reported a pentacene dimer that exhibits 156% yield of triplets, along with two other dimers of the same family.[30] Such dimers are coupled at through the 6-position by a diethynylbenzene. While the ethynyl groups impart stability to the pentacenes, we envisioned that coupling through the 2-position would yield a modular platform to fine-tune

structural components that evade through-space interactions between the pentacenes, thus focusing on through-bond coupling as a function of distance (Figure 2.1). In this vein, we synthesized a series of singlet fission dimers by coupling pentacenes at the 2-position with, and without (oligo)phenylene spacers. Using these spacers, we can vary the proximity and extent of conjugation of the pentacenes, which allows for control of the rate of singlet fission and the rate of recombination of the two triplets. The ability to extend the lifetime of the triplet pair ($2xT_1$) is a major challenge in multiexcitonic devices based on iSF chromophores, where efficient charge extraction is essential for the overall performance of devices.

Here, we report soluble, stable derivatives of 2,2'-bipentacene that exhibit the maximum iSF yield, ~200%, via an intramolecular process on isolated molecules. We find that the singlet fission rate and triplet lifetimes can be tuned by varying the length of the spacer group. While the connectivity of the pentacenes in the reported dimers is similar to tetracene dimers previously proposed,[31] the chromophores in Figure 2.1 have key distinctions: a) since xSF in pentacene is known to be exothermic, covalently coupling two pentacenes can lead to a similarly energetically favored iSF process that stems from a delocalized singlet (in apparent contrast to localized singlets observed by Zirzlmeier et al.); and b) triisopropysilylacetylene (TIPS) groups render the product soluble and stable, resulting in facile and scalable synthesis.[32]

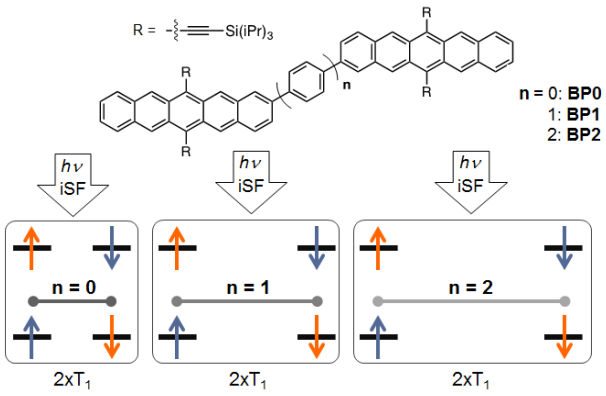

Figure 2.1. The pentacene chromophores of interest, where both are directly coupled (n = 0, BP0), and separated by one phenylene group (n = 1, BP1) or two (n = 2, BP2), which affect the triplet spectra, as well as the rates of fission and recombination.

2.3 Molecular Design

As a first approximation, we calculated the excited state energies. In order for SF to take place, the energy of the singlet state must be twice the energy of the triplet. In singlet fission, the singlet state evolves into a multiexcitonic state, which dephases into a spin-correlated pair of triplets. Thus, the product of singlet fission is referred to as the triplet pair, or $2xT_1$. Using a similar method to Greyson and co-workers,[31] we calculated the energy of iSF to be roughly isothermic for all three bipentacenes discussed. The satisfaction of the energetic requirement $2xT_1 \leq S_1$, within the margin of error for DFT energy calculations, suggests that these compounds are feasible candidates for iSF. Furthermore, DFT simulations, using the optimized S_0 ground state, reveal that the highest-occupied and lowest-unoccupied molecular orbitals (HOMO and LUMO, respectively) of the S_0 state are delocalized over the entire molecule. The lowest-energy excited singlet state, S_1, is optically allowed and in all three cases results primarily from the expected electronic excitation, *viz.*, moving an electron from the S_0 HOMO to the S_0 LUMO. Independent DFT calculations on the lowest-energy triplet, T_1, performed from the same optimized S_0 geometry, show that the two

singly occupied orbitals that characterize T_1 are localized on just one of the pentacene subunits in all three molecules. This localization is not surprising as it maximizes the stabilizing exchange interaction. The localization of T_1 suggests that the electronic structure of these molecules is appropriate to accommodate a second "isolated" triplet produced via iSF.

2.4 Steady State Spectroscopy

The steady state absorption spectra of **BP0**, **BP1**, and **BP2** in chloroform are compared to that of a single pentacene chromophore, TIPS-Pentacene (**TPc**) in Figure 2.2. The low enegy region of the spectra is qualitatively similar and red-shifted by approximately 50 meV in all bipentacenes. Additionally, a new set of high-energy peaks appears in **BP0**, broadening the absorption to include a greater portion of the visible spectrum. This feature is unique to the connectivity of these molecules, and is not observed in other oligopentacene derivatives.[33] We found that the bipentacene series all have molar extinction coefficients roughly twice that of **TPc**. Finally, concentration-dependence studies on all bipentacenes indicate no aggregation, which is typically manifested as red-shift in the absorption spectrum.[34] Similarly, the dependence of signal intensity on concentration adheres to Beers Law. The lack of aggregates is important to ensure that the photophysical measurements are probing molecules that are fully dissolved, and intermolecular coupling effects are not playing a role in the dynamics of the excited state.

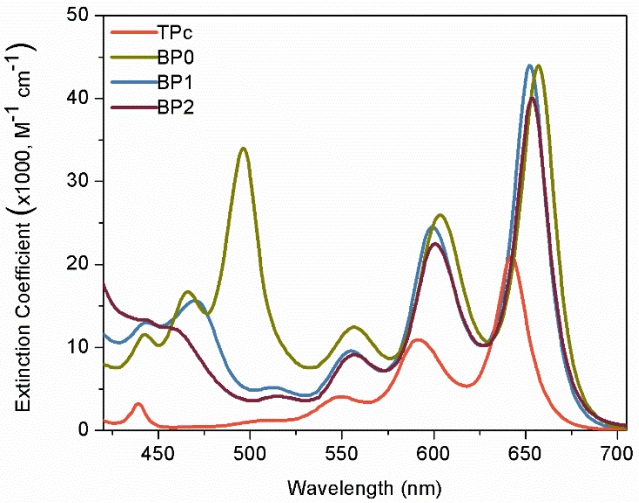

Figure 2.2. Comparison of TPc with UV-Vis spectra of pentacene dimers with 0, 1, and 2 para-phenylene spacers (BP0, BP1 and BP2 respectively).

2.5 Transient Absorption Spectroscopy

In order to evaluate and compare the photophysical dynamics of the materials, we first describe our observations of **BP0**, and we then proceed to compare the results to **BP1** and **BP2**. The key focus is to understand the effects of pentacene proximity on iSF. This relationship is probed by modulating the length of conjugated phenylene spacers. As shown in Figure 2.1, we postulate that the decreasing proximity of triplet sites from **BP0**, to **BP1** and to **BP2** will drastically affect the rates of iSF, quantum yields, and triplet-triplet recombination.

Employing ultrafast transient absorption spectroscopy (TAS), we observed a rapid conversion of photoexcited singlets into triplets, occurring on a sub-ps timescale in **BP0**. These two distinct populations can be clearly seen in 2D pseudo-color (ΔA) plots of transient absorption spectra as a function of probe wavelength and delay time (Figure 2.3A). Notably, the photoinduced absorption (PIA) features at 470 nm and 560 nm rapidly evolve into a new feature at 517 nm. The

amplitude of the feature at 517 nm rises for a few ps and then decays with a several hundred ps time constant back to the ground state (Figure 2.3C), during which the shape of the transient spectra remains constant. The negative feature at 660 nm persists for the duration of the conversion from singlet to triplet, and results from ground state bleaching of the lowest energy optical transition that can be seen in the linear absorption spectrum (Figure 2.2).

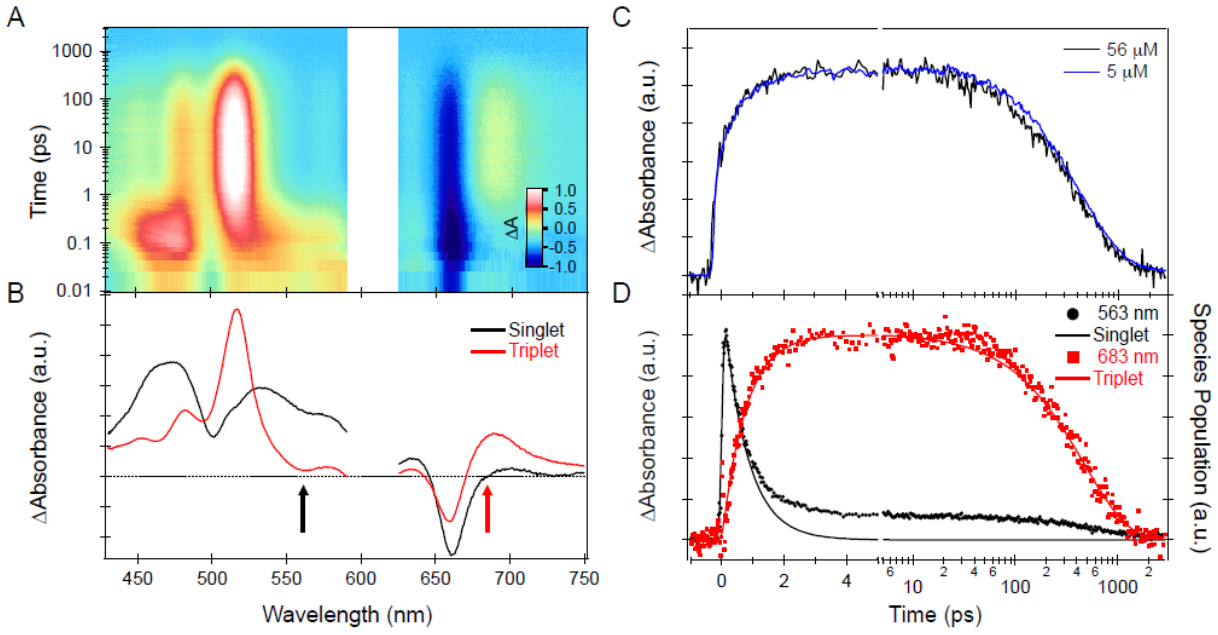

Figure 2.3. A) Normalized transient absorption data of **BP0** in chloroform (56 μM, 600 nm pump). Due to pump wavelength scatter, small portions of the data have been excluded for clarity. **B)** Deconvoluted transient spectra of singlet and triplet species as solved by global analysis. It should be noted that differences in the magnitude of bleach in panel B are attributable to overlap with the triplet spectrum, not to a reduction in bleach. **C)** A normalized spectral slice at 517 nm showing that the carrier dynamics are independent of concentration over an order of magnitude. **D)** Population evolution from global analysis is compared to raw data at wavelengths where primarily singlet (563 nm, black arrow in B) and triplet (683 nm, red arrow in B) dynamics are observed. The discrepancy at 563 nm is due to the ~ 20% overlap with a triplet photoinduced absorption feature.

Based on sensitization experiments along with the known TAS of **TPc** and related compounds, we assign the features that decay on the sub-ps timescale to the singlet state and the

slow decaying features to the triplet state.[9] The triplet spectrum can be clearly isolated at times > 5 ps, when features associated with the singlet manifold have decayed. However, to isolate the rapidly decaying singlet features and get an accurate time scale for fission, we use global analysis methods with a sequential kinetic decay model ($S_1 \rightarrow 2xT_1 \rightarrow S_0$).[35] The deconvoluted spectra that result from global analysis are shown in Figure 2.3B and the resulting species concentration profiles as a function of time are shown in Figure 2.3D (solid lines). We note that a triplet PIA feature overlaps spectrally with the position of the ground state bleach. As a result, the ground state recovery does not strictly correlate with the net magnitude of the bleach feature as a function of time. In other words, the net change in the bleach during the singlet decay is primarily due to the rise of the overlapping triplet PIA, and not due to the loss of excited state population. However, after accounting for the non-zero baseline, we find that the overall ground state bleach signal is conserved during the singlet fission process, a signature of a quantitative conversion of singlets to triplets.

Global analysis yields a time constant for singlet decay and concomitant triplet rise of 760 fs. From the spectral deconvolution, we identify regions in the unprocessed data where the singlet (563 nm) and the triplet (683 nm) can be preferentially observed. We note that these regions do not correspond to the peaks of the singlet and triplet PIA features. The extracted raw kinetic traces at these wavelengths are compared against the computed population profiles (Figure 2.3D) and good agreement is found with our model that correlates the rise of the triplet with the decay of the singlet. Similarly, the data at both wavelengths fits well with a common set of time constants that agree with those determined from global fitting.

2.6 Ultrafast Photoluminescence Spectroscopy

The fast decay of the singlet excitons was further confirmed by time-resolved ultrafast photoluminescence spectroscopy (UFPL). Photoluminescence is spin-allowed for singlet excitons, but spin-forbidden for triplets. Therefore, the conversion of a singlet into two triplets observed in TAS corresponds to conversion from an emissive (singlet) to non-emissive (two triplet) state in the time-resolved UFPL experiment. A time constant of ~0.7 ps for the decay of the photoluminescence is extracted by fitting the time-resolved emission signal measured at 675 nm, near the peak of the photoluminescence spectrum (Figure 2.4A). The sub-ps time constant for the decay of the singlet is in excellent agreement with transient absorption measurements, and taken together, these data support the assignment of quantitative, ultrafast, intramolecular singlet fission of a singlet exciton into two triplet excitons. We note that the emission lifetime in **TPc** is > 10 ns, more than four orders of magnitude longer than what is observed in **BP0**.[34] A small fraction (~ 3% of the overall amplitude) of longer-lived emission is observed that could originate from trace monomer in our sample.

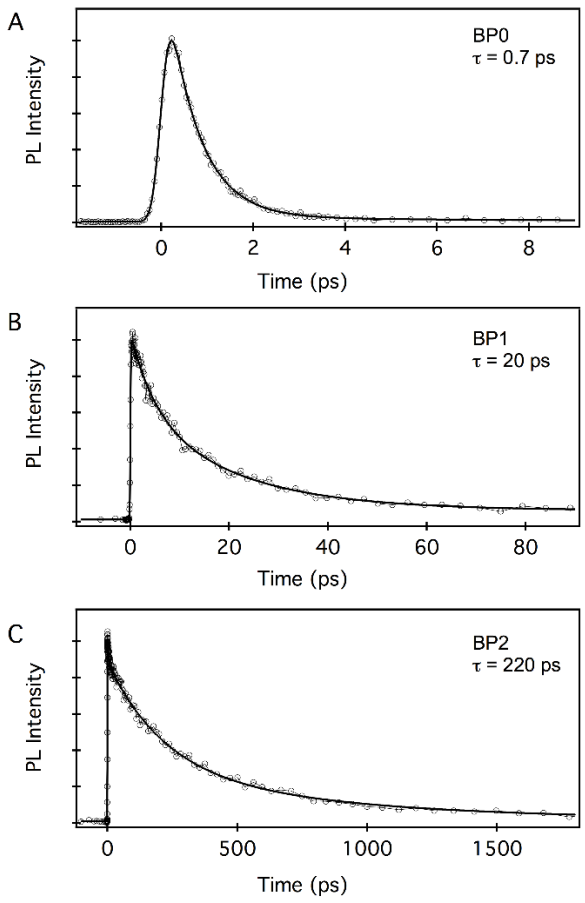

Figure 2.4. Ultrafast photoluminescence (UFPL) decay lifetimes (τ) of the emissive singlet state in A) **BP0**, B) **BP1**, and C) **BP2**.

Since triplet pairs created via intramolecular singlet fission in solution are confined to a single molecule and are unable to diffuse apart intermolecularly (as in the case of xSF), the triplet recombination dynamics are faster than in those resulting from typical intermolecular fission processes in the solid state. From transient absorption measurements (Figure 2.3), we determine that the triplet pair lifetime is ~450 ps in **BP0**, compared to > 100 ns in pentacene crystals.[36] Furthermore, we can confirm that the observed sub-ns lifetime is not the intrinsic lifetime of an individual triplet; since iSF occurs in dilute solution, we can utilize triplet sensitization techniques to directly compare the T_1 versus $2xT_1$ relaxation dynamics in **BP0** molecules.

2.7 Triplet Sensitization Measurements

Having obtained rates of singlet decay followed by population of the $2xT_1$ state, the absorption features of the triplet pairs must be compared to the single-triplet spectrum obtained through sensitization. The process involves photoexcitation of anthracene, which undergoes intersystem crossing and subsequently transfers an electron via diffusive collisions to the **BP** chromophores.[21,37,38] The absorption spectra of the triplet transient is recorded, and compared to the $2xT_1$ generated by singlet fission (Figure 2.5A). Interestingly, a subtle difference in the spectra is observed between individual triplets produced via sensitization and triplet pairs produced via singlet fission in **BP0**. This is evident in the feature at ~680 nm. The low energy PIA feature (typically assigned to $T_1 \rightarrow T_2$) is red-shifted by ~200 meV in the sensitization experiment, though much better agreement is seen in the higher energy ($T_1 \rightarrow T_3$) triplet PIA feature. This difference will be further discussed later, in comparison to the other two chromophores. The most striking difference between the individual triplet and the triplet pair state is observed in the decay timescale of triplet pairs (~450 ps), which is more than four orders of magnitude faster than that of individual triplets (> 18 μs, Figure 2.5D). This ultrafast timescale is in agreement with recent reports of fast triplet-triplet recombination, resulting from the iSF process.[21,30] We note that the formation and decay kinetics of the $2xT_1$ state have weak dependence on solvent, distinct from other fast singlet deactivation processes that have been observed in conjugated small molecule systems, such as intramolecular charge transfer.[39-42]

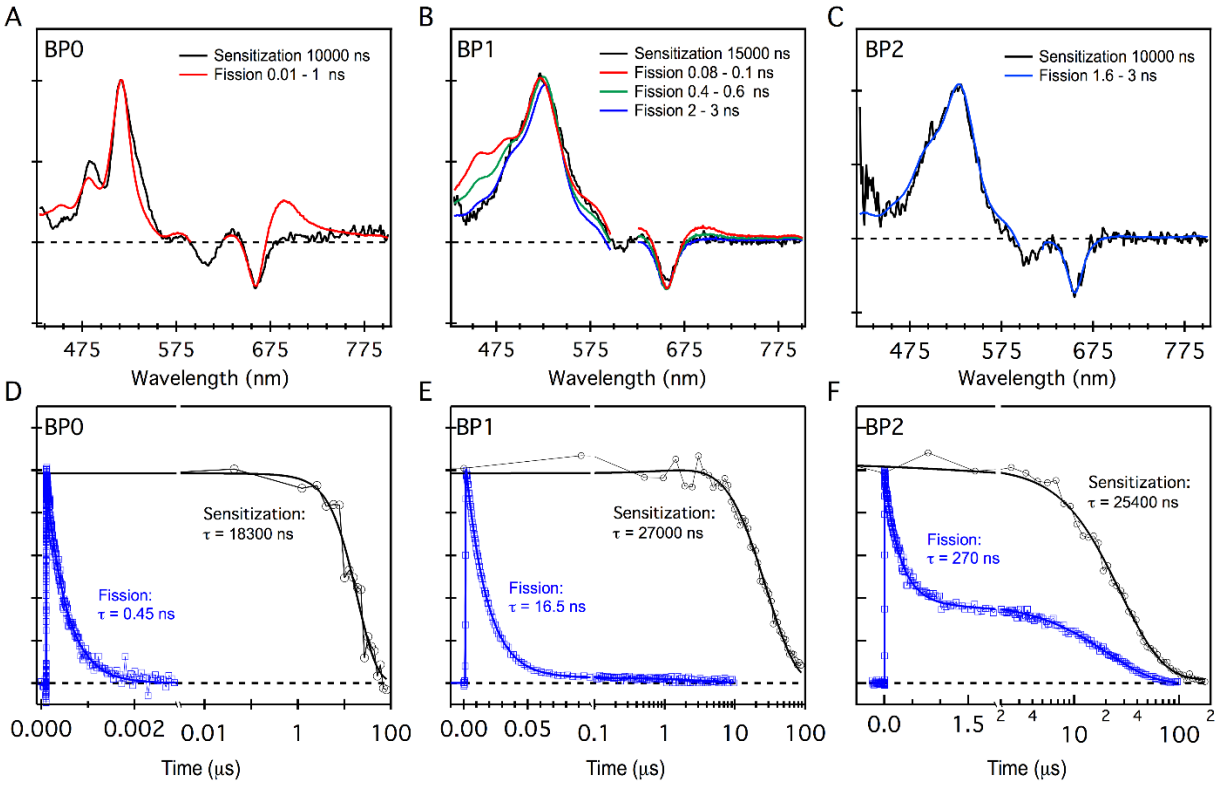

Figure 2.5. Comparison of spectra (A-C) and lifetimes (D-F) of triplets obtained from singlet fission, which produces two triplets, and triplet photosensitization, which populates just one triplet.

In **BP0**, fast triplet-triplet recombination and spectral differences between the T_1 and $2xT_1$ state suggests that significant electronic coupling occurs in the transition dipole moments of aligned pentacene triplets.[43] This coupling results from the close proximity of the two pentacenes and the highly planar geometry resulting from conjugation. While direct conjugation of the two pentacenes promotes efficient sub-ps fission, the resulting fast triplet lifetimes are detrimental to potential applications based on exciton harvesting. Furthermore, while there is no evidence to suggest any parasitic process that compete with iSF, spectral differences between one and two triplets preclude a direct yield determination to support the observation of a conserved ground state bleach signal during the conversion of singlets to triplets. To address these issues, we turn to **BP1** and **BP2**.

2.8 Comparison of BP0 with BP1 and BP2

In **BP1** and **BP2**, the proximity of the pentacenes is decreased by adding phenylene spacers. The inclusion of the spacers also results in additional rotational axes. Notably, this structural change negligibly affects the singlet state; the optical extinction coefficients and low-energy spectral positions are nearly identical in the three bipentacene compounds (Figure 2.2). Differences in the high-energy optical absorption features upon addition of the phenylene spacers likely result from differences in the symmetry of the molecules. Further investigation into the origin of these high-energy peaks in **BP0** is still underway.

Despite the similarities in the singlet states, systematically decreasing fission rates relative to **BP0** are observed with increasing spacer length. The ultrafast transient absorption data of **BP1** and **BP2** are qualitatively very similar to **BP0**, differing primarily by the rates of the singlet to triplet conversion. Because of more complex dynamics in the triplet manifold (discussed below), the fission rate is best determined using time-resolved photoluminescence. We find that the fission rate constant (τ_{SF}) evolves from 0.7 ps in **BP0** to 20 ps in **BP1**, and to 220 ps in **BP2** (Figure 2.4). While an order of magnitude decrease in the rate per phenylene spacer might seem dramatic, the long singlet exciton lifetime of **TPc** (13 ns) allows for effectively quantitative fission processes even in the long spacer limit.[34] Based on the emission dynamics, if we assume fission competes with the same intrinsic singlet decay rate as **TPc**, the fission yields are calculated to be 199.9%, 199.7%, and 196.7% for **BP0**, **BP1**, and **BP2**. These values are consistent with the measured PL quantum yields (1.6%, 4.4%, 5.0% respectively) when we account for emission from fluorescent impurities (1-4%) that are readily seen in time-resolved photoluminescence measurements.

Considering the design of the three chromophores, the varying separation between **BP0**, **BP1**, and **BP2** reduces the proximity of the two triplets localized on each pentacene moiety, in

addition to slowing down the rate of triplet-triplet recombination. Furthermore, the isolated triplet transitions can be observed when the pentacenes are sufficiently apart, resulting in the convergence of the T_1 and $2xT_1$ transient spectra. In **BP1**, the triplet PIA spectrum resembles **BP0** immediately after excitation, and differs from the sensitization spectrum on the low-energy side of the bleach (680 nm, Figure 2.5B). This state evolves over the next ~1 ns to match the single-triplet state, indicating that fully independent, uncoupled triplets are produced. Notably, the $2xT_1$ lifetime (16.5 ns) is much shorter than the single-triplet lifetime (27 □s) obtained from photosensitization (Figure 2.5E). In **BP2** however, the $2xT_1$ state immediately produced by iSF is spectrally indistinguishable from the single-triplet spectrum, indicating that fission directly produces decoupled triplets (Figure 2.5C). In the triplet recombination dynamics, a bimodal distribution is observed, with a relatively fast component exhibiting a lifetime of ~270 ns, and a long-lived component approaching that of the individual triplet lifetime (25 μs). The nature of this spectral evolution is likely related to conformational changes that occur within the molecule on long timescales, as it is independent of **BP2** concentration, but weakly solvent dependent (SI.7).

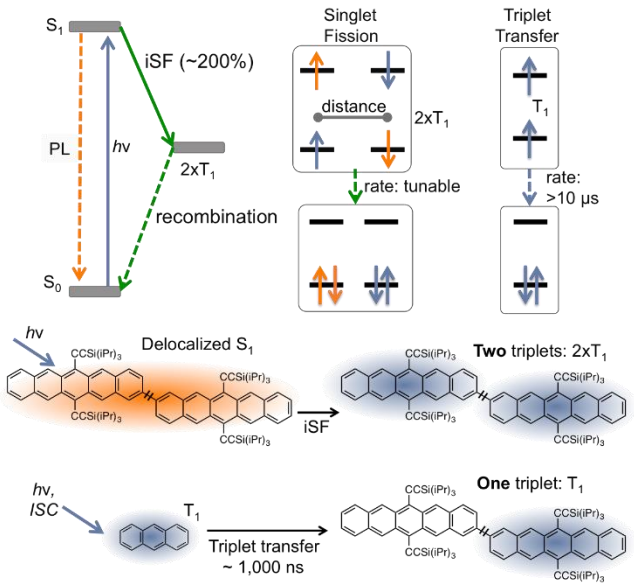

Figure 2.6. Comparison of bipentacenes under optical excitation, which results in ultrafast intramolecular singlet fission (iSF) producing a triplet pair that recombines in timescales varying from 0.45 ns up to 270 ns; and bipentacenes excited by photosensitization triplet transfer using anthracene to produce a single, long-lived triplet.

The differences in the transient optical spectra produced by singlet fission, which results from direct optical excitation, and triplet photosensitization, in which a single-triplet is transferred to the molecule are crucial to our assignment of intramolecular singlet fission. In the singlet fission process summarized in Figure 2.6, direct optical excitation of the bipentacene derivatives results in a delocalized singlet state, which undergoes a small amount of photoluminescence (< 5%) before decaying to produce two triplets ($2xT_1$). The two triplets recombine with a time constant ranging from 0.5 ns (**BP0**) to > 1 µs (**BP2**). During sensitization experiments, triplet energy transfer generates an individual triplet that decays to the ground state *via* a spin-forbidden relaxation process at a much slower timescale (>10 µs).

2.9 Singlet Fission Yield Determination

In all three bipentacene derivatives, the rapid conversion of singlets into the triplet pair in dilute solution is assigned to the dynamical process of iSF with a triplet yield approaching 200% that matches the best xSF solid-state systems. We base this on the fact that the singlet decay rate is orders of magnitude faster than the corresponding singlet lifetime of TIPS-Pen, and no other species besides the singlet and triplet features are identified in the transient absorption spectra. Furthermore, radiative losses, measured using steady-state photoluminescence, are minimal in these molecules. Similarly, we can rule out the presence of additional non-radiative decay channels, which have been shown to disrupt the correlation between the singlet decay and triplet rise.[21]

An additional way to determine the yield is through quantification of the ground-state bleach (GSB). While quantitative xSF has been shown to produce twice the GSB after fission due to production of two triplet excitons, in the case of the bipentacenes reported here, the conjugation of the chromophores results in a different situation. The DFT calculations reveal extensive delocalization of the singlet exciton, even in the case of **BP2**. Therefore, we expect the singlet exciton to bleach both pentacenes in the dimers. Indeed, transient absorption experiments controlling for photon flux and solution optical density reveal that, even for **BP2**, both pentacenes in the dimer are bleached by the singlet exciton.[34]

Because the singlet exciton fully bleaches the ground state transitions, in the case of quantitative iSF, we expect to observe a constant bleach during fission. Using a modified version of the bleach addition method pioneered by Eaton et al., we find no change in the bleach before and after iSF in any of the three bipentacenes.[44] Our analysis suggests that while the bleach signal may appear to reduce (**BP0**), remain constant (**BP1**) or intensify (**BP2**) during fission, in the case of dimers studied here, this perceived change is merely a result of overlap between GSB and PIA

from the singlet and/or triplet excitons, and not due to a change in population of excited chromophores.[30]

In **BP2**, the similarity of the T_1 and $2xT_1$ spectra allows for yet another iSF yield determination, in this case utilizing sensitization experiments to determine the triplet excited state absorption extinction coefficient. The iSF yield can then be directly computed from TAS using the Beer-Lambert Law. In **BP2**, the iSF yield is determined to be 201 ± 15%, consistent with our estimates of the maximum yield from the singlet decay rate of **TPc** monomer (196.7%). Our procedure uses **TPc** as an internal standard for a determination of both the singlet and triplet concentration, i.e., the calculation does not rely on literature values for the triplet extinction coefficient of the sensitizer. Crucially, this method is only valid in cases where the spectrum of the two triplets, produced by fission, matches that of a single triplet produced from sensitization. This result supports the assertion that no additional loss channels exist in these compounds. Furthermore, this result confirms that the constant bleach during fission is indeed indicative of near-quantitative fission yields. This yield information, as well as SF and triplet decay time constants are summarized below in Table 2.1.

We note that the distinct $2xT_1$ spectra observed after iSF in **BP0** and at early times in **BP1** are a unique feature iSF molecules with little separation between chromophores. We postulate that spectral shifting between T_1 and $2xT_1$ occurs because the triplet transition dipole moments are aligned and in close proximity.[43] This alignment occurs as long as the pentacene units are relatively planar; in **BP1**, the triplets live long enough for the molecular backbone to distort to a non-planar geometry. The electronic coupling observed here should not be confused with strongly coupled multiexciton states (such as the ME state that couples the singlet and triplet manifold). In both **BP0**

and **BP1**, we are observing singlet fission to produce independent triplet excitons, in which one or both excitons may be harvested for applications.

Table 2.1. Summary of relevant SF time constants, triplet lifetime, and triplet yields for compounds discussed in this work. *It should be noted that BP2 has a biexponential triplet decay, as discussed above, and the lifetime quoted is the shorter time constant.

Compound	τ_{SF}	$\tau_{Triplet\ Decay}$	Triplet Yield
BP0	760 fs	0.45 ns	~200%
BP1	20 ps	16.5 ns	~200%
BP2	220 ps	270* ns	~200%

2.10 Conclusions

We have designed and synthesized **BP0**, **BP1** and **BP2** as materials that can be used to understand how the excited state dynamics are dependent on molecular connectivity of the SF chromophores. Calculations demonstrate that iSF is energetically feasible in these molecules due to a localization of triplets on each pentacene unit, resulting from favorable exchange energy interactions. Unlike pentacene monomers, which depend on intermolecular interactions for singlet fission, these bipentacenes yield two triplets independent of intermolecular coupling. This intramolecular process is important because it is independent of packing order and can be observed in solution. Thus, the materials have potential to be studied and exploited in non-crystalline media, using high throughput processing techniques. We experimentally demonstrated that these molecules undergo quantitative, ultrafast intramolecular singlet fission using transient absorption

and time-resolved photoluminescence spectroscopy, similar to observations reported during the review of this manuscript.[30] Triplet sensitization was used to determine the nature of the observed transients and to elucidate the distinct triplet pair recombination dynamics. Similar to the other recently reported pentacene dimer system, we observe fast, high-yielding iSF.[30] However, in contrast, we employ progressively longer spacers to extend triplet pair lifetimes. In the limit of a two-phenylene spacer bridge, we achieve triplet pair lifetimes as long as 270 ns which may enable harvesting of two electron-hole pairs for devices with enhanced photocurrents. Currently, we are exploring the application of bipentacenes in devices, as well as SF of these molecules in the solid-state.

2.11 Detail on Transient Absorption Spectroscopy

BP0

Global and Target Analysis

Global (singular value decomposition-based) and target (differential equation-based) analysis is accomplished using the Glotaran software package (http://glotaran.org). The advantage of these methods is that they treat the full (~ 800 kinetic traces) data set in aggregate, yielding much more accurate fits of the rate constants and deconvoluted "spectra" which track the distribution of the rate constants as a function of wavelength. A simple sequential decay model (S1 → T1 → S0) is found to accurately reproduce the data set when pumping close to the band edge. Similar results can be accomplished using global (constrained) fits of real data slices rather than singular vectors. The results of global fitting at two raw kinetic traces is show in Figure 2.7

(with residuals) in which only two decay rates are used for the entire data set. This treatment accurately reproduces the correlated singlet decay and triplet rise, with time constants matching well with those extracted from the full data set analysis.

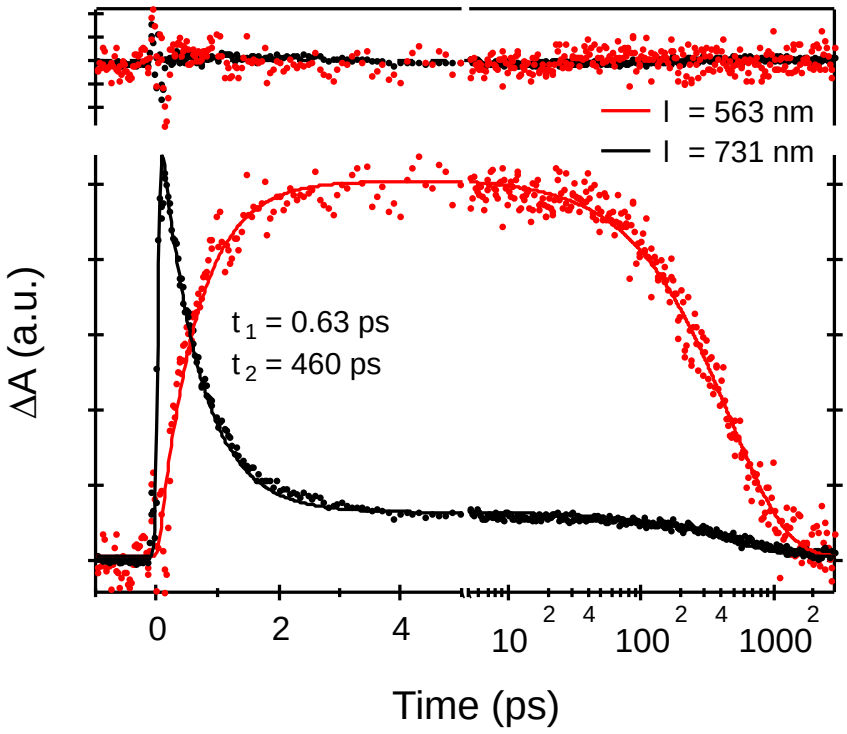

Figure 2.7. Two-exponential fit of two kinetic traces from raw data using two "globally" constrained rate constants.

Fluence Independent Dynamics of BP0

All dynamical behavior is independent of excitation fluence within the measured range (up to 100 μJ/cm^2). Single-wavelength kinetics at 567 nm (dominated by singlet response) and 688 nm (dominated by triplet response) are shown in Figure 2.8 (c = 50 μM in chloroform) as a function of the 600 nm pump fluence.

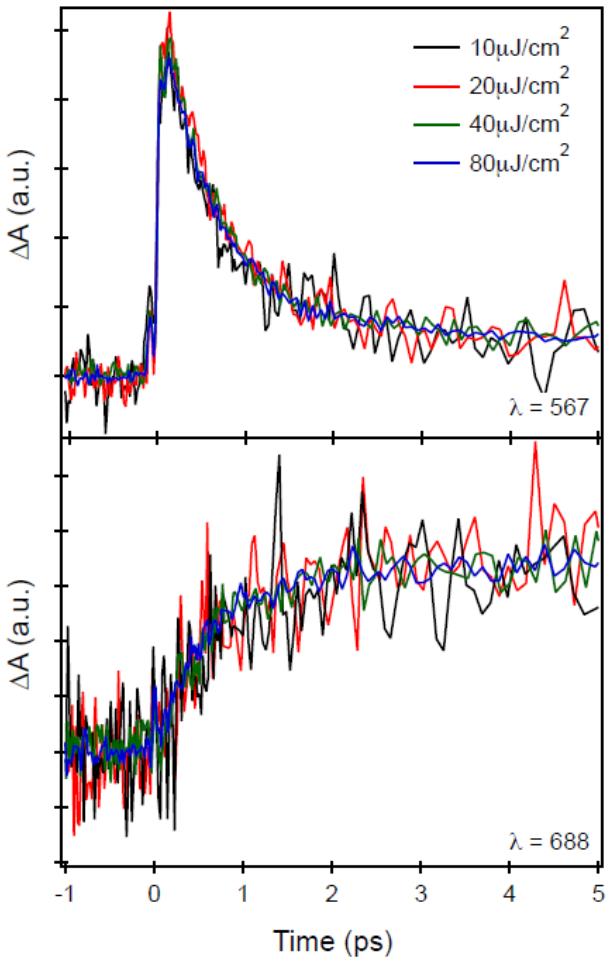

Figure 2.8. Comparison of normalized kinetic slices at 567 and 688 nm, excited with 600 nm pump with varying pump fluence.

Solvent Independent Dynamics of BP0

The fission rate and triplet decay dynamics are independent of solvent, although slight differences are seen in the relative amplitude of triplet photoinduced absorption features (Figures 2.3 and 2.4). In Figure 2.9, we show kinetic traces extracted from the raw data set of the rise at 567 nm (dominated by singlet response) and 688 nm (dominated by triplet response).

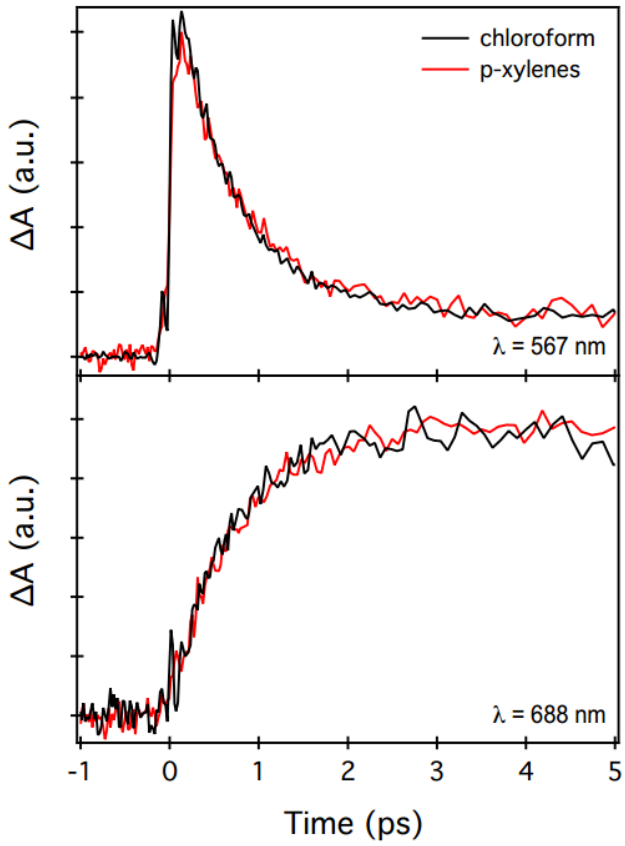

Figure 2.9. Comparison of kinetic slices at 567 and 688 nm, excited with 600 nm pump in chloroform and p-xylenes.

Excitation Wavelength Dependence of BP0

The singlet fission rate showed no dependence on photon energy, remaining constant at ~ 760 fs. However, the relaxation of the triplet pair, confined to a singlet molecule, was found to show more complex dynamics at higher excitation energy. Single wavelength kinetics at 688 nm (600 nm pump) are shown in Figure 2.10, where the constant rise of the triplet can be clearly seen along with a weakly energy dependent recombination process.

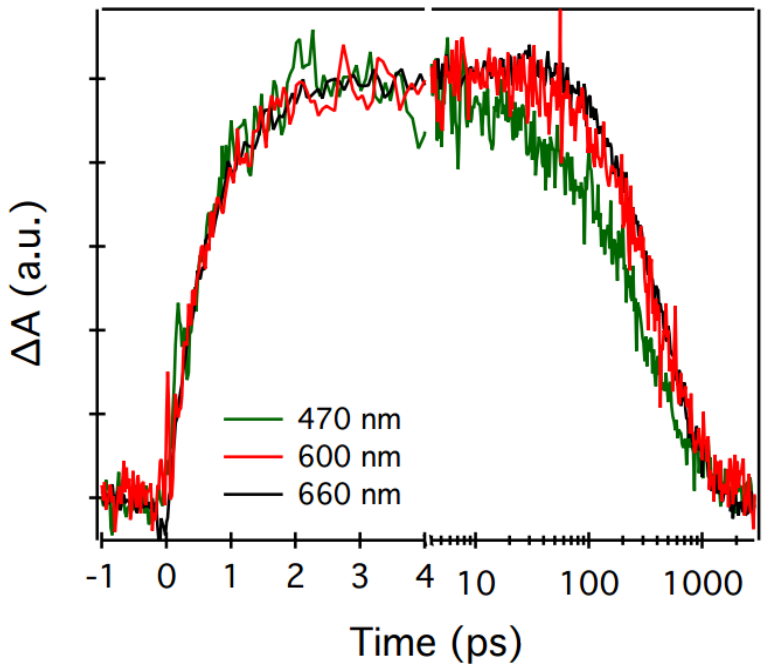

Figure 2.10. Kinetic data at 688 nm for difference pump photon wavelengths. An identical fission rate is seen in all three traces.

BP1

The raw femtosecond (top panel) and nanosecond (bottom panel) data is shown in Figure 2.11.

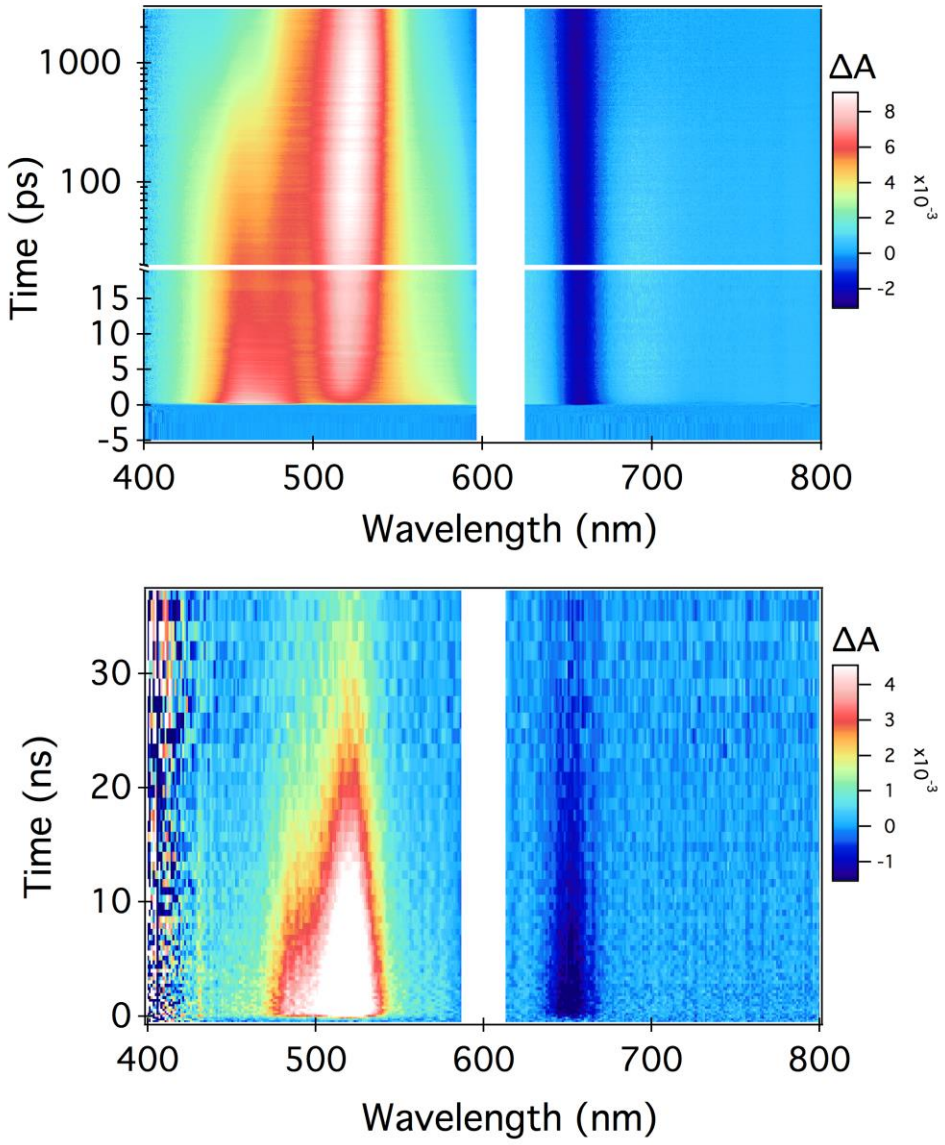

Figure 2.11. Femtosecond (top) and nanosecond (bottom) transient absorption data for BP1 excited at 600 nm in chloroform.

BP2

Transient Absorption of BP2

The raw femtosecond (top panel) and nanosecond (bottom panel) data is shown in Figure 2.12.

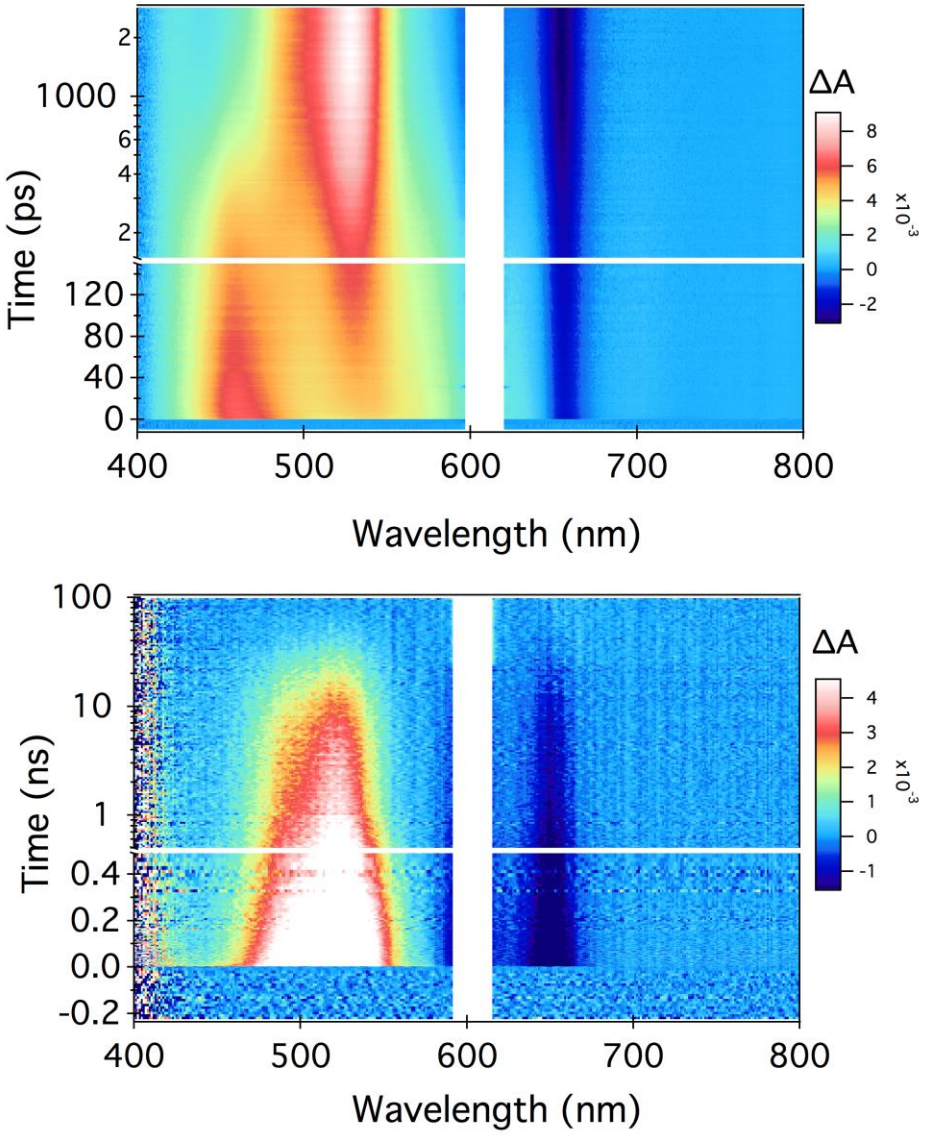

Figure 2.12. Femtosecond (top panel) and nanosecond (bottom panel) transient absorption data of BP2 excited at 600 nm in chloroform.

Solvent Dependent Dynamics of BP2

The triplet-triplet recombination of BP2 shows a weak solvent dependence, as shown in Figure 2.13.

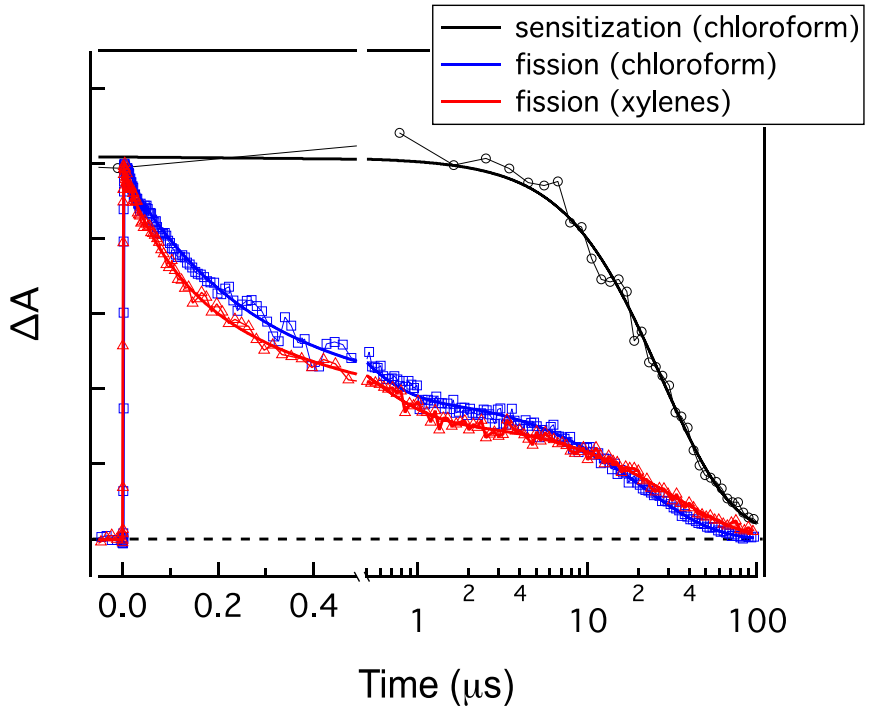

Figure 2.13. Triplet excited state absorption signal monitored at 525 nm. For fission studies, a 600 nm pump is used. For sensitization, 20 mM of anthracene is excited using a 360 nm pump pulse.

2.12 Details on Triplet Sensitization of BP0, BP1, and BP2

In Figure 2.5D-F, the triplet sensitization kinetics are offset to exclude the rise time, during which triplets are transferred to the BP compounds from the anthracene. The transfer time depends on concentration, and varies slightly between experiments. Typical rise times are on the order of 10 μs. Linear scale spectra are shown below in Figure 2.14 to illustrate the offsets used in Figure 2.5.

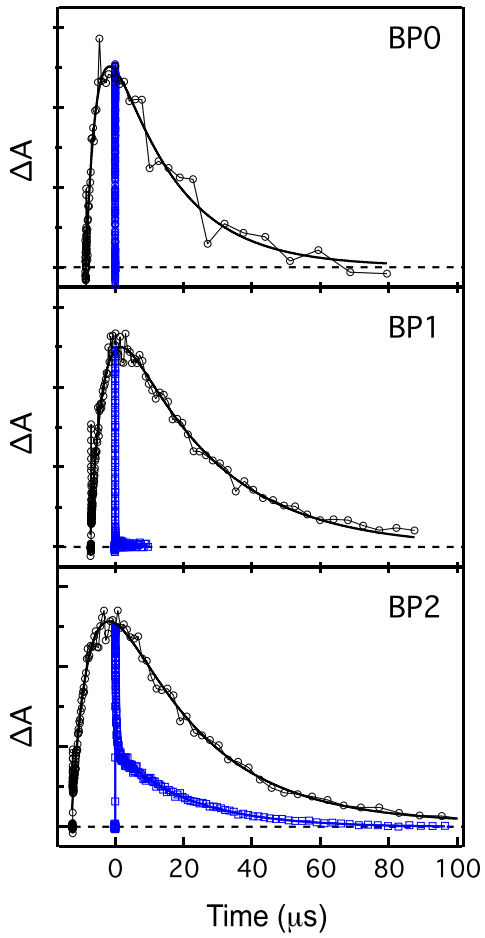

Figure 2.14. Decay of triplets produced via sensitization by anthracene in chloroform (black) and from direct optical excitation of the bipentacene which results in iSF (blue). Sensitization data was offset along the x axis so that the maximum signal occurs at time zero.

2.13 Details on Singlet Fission Yield Determination

Yield Determination via Ground State Bleach Dynamics

Correlating Extinction Coefficients to Ground State Bleach Signals

Solution	**O.D. @ 600 nm**	**(1-T) @ 600 nm**	**(M^{-1} cm^{-1})**
TIPS Pentacene	0.103	1-10^-0.103 = 0.211	21000
BP2	0.191	1-10^-0.191 = 0.356	40000

Excitation Conditions

Wavelength: 600 nm

Spot area (A) = 0.9 x 0.6 mm = 4.24e-3 cm^2

Spot volume (V) = A*l = 4.24e-3 * 0.2 = 8.48e-4 cm^3 = 8.48e-4 mL = 8.48e-7 L

TIPS-Pentacene

Bleach minimum (644 nm) = -1.39mOD (direct fitting)

Concentration of singlets: $c = \Delta A/(\varepsilon * l)$ = 1.39e-3/(21000*0.2) = 3.31e-07 M^{-1}

Number of photons incident = $c*V*N_A/(1-T)$ = 3.30952e-07 *8.48e-7*6.0221413e+23/0.211 = 8.04808e+11

BP2

Bleach minimum (651 nm) = -3.78 mOD (direct fitting)→ increase by 4% to account for baseline → 3.93 mOD

Triplet maximum (521 nm) = 10.7mOD (direct fitting)

Concentration of singlets: $c = \Delta A/(\varepsilon*l)$ = 3.78e-3/(40000*0.2) = 4.725e-07M^{-1} → 4.91e-07M^{-1}

Number of photons incident = 4.725e-07*8.48e-7*6.0221413e+23/0.356 = 6.77795e+11 → 7.04e+11

Error Determination

Since TIPS-Pentacene and BP2 are excited under identical conditions, the error in determining singlet (and triplet) concentrations from the magnitude of the transient signals can be estimated from the above analysis.

Ratio of $\Delta A\_2phBP/\Delta A\_TIPS = \varepsilon\_2phBP/\varepsilon\_TIPS * (1-T)\_2phBP/(1-T)\_TIPS$ → 3.93/1.39 = 40000/21000 * 0.356/0.211

2.82 = 3.2 → 1 = 1.13 → < 15% error bar

For the same number of singlets, the ground state bleach signal in **BP2** is approximately twice as large. This implies that the singlet exciton bleaches the entire **BP2** molecule. The raw data used for this determination is shown below in Figure 2.15.

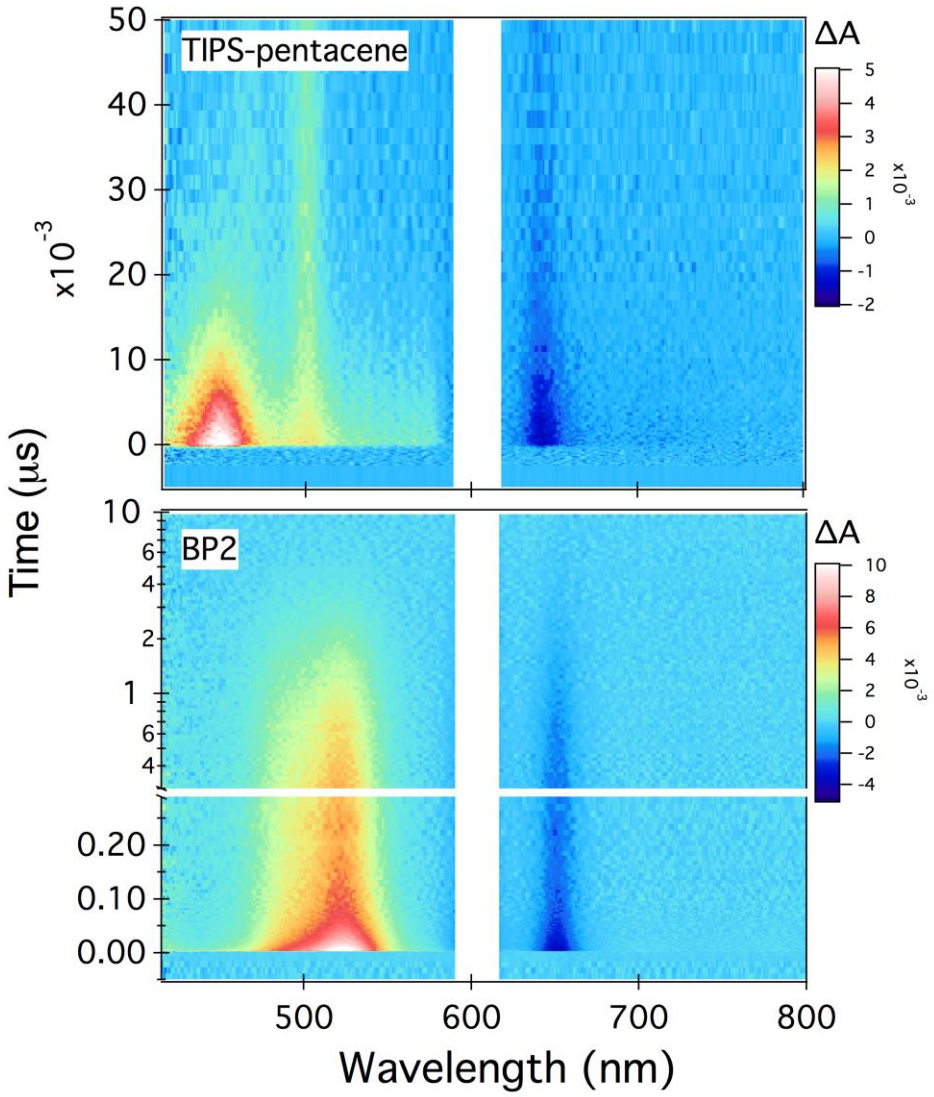

Figure 2.15. Raw transient absorption data for TIPS-pentacene and BP2 solutions with 600 nm excitation in chloroform.

The net change in the magnitude of the ground state bleach during fission is caused by the overlap of a singlet and triplet excited state absorption (ESA) features with the ground state bleach, and not due to a change in the population of excited molecules. In fact, in BP0, a net decay is observed; in BP1 the bleach is relatively constant; and in **BP2** a net rise is observed, primarily due to differences in the ESA spectra of the triplets. This can be clearly seen by inspection, where the difference in the on-resonance bleach minima is nearly identical to the difference in the off-resonance baseline. The overall fission yield can be estimated by fitting the bleach with a singlet Gaussian and a linear baseline; this is a modified version of the procedure suggested by Eaton, *et al*.[44]

The transient spectra during and immediately after iSF (solid lines) are shown for BP0 in the graph below (Figure 2.16). A simple one Gaussian fit with a cubic baseline is also shown (dotted lines) and the total areas of the resulting fits agree within 2%. This result confirms that the singlet fission process is quantitative.

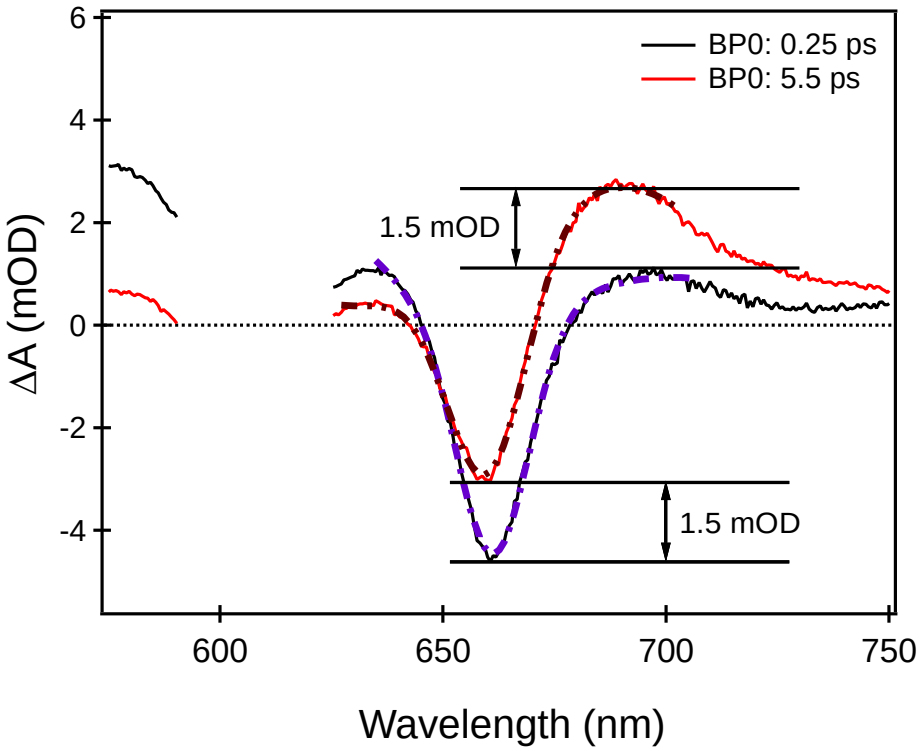

Figure 2.16. Transient spectra of **BP0** at 0.25 ps (black) curve and a singlet Gaussian fit to the bleach (purple dash). Transient spectra of **BP0** at 5.5 ps (red) curve and a singlet Gaussian fit to the bleach (maroon dash).

The transient spectra during and immediately after fission (solid lines) are shown for **BP1** in the graph below (Figure 2.17). A simple one Gaussian fit with a linear baseline is also shown (dotted lines) and the total areas of the resulting fits agree within 4%. This result confirms that the singlet fission process is quantitative.

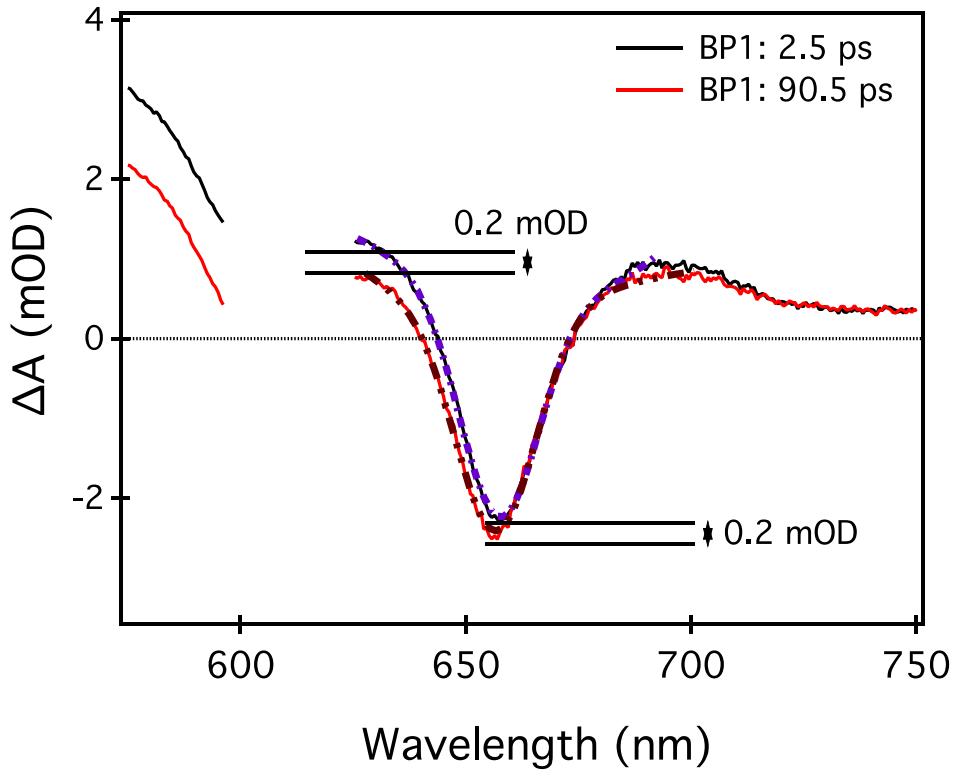

Figure 2.17. Transient spectra of **BP1** at 2.5 ps (black) curve and a singlet Gaussian fit to the bleach (purple dash). Transient spectra of **BP1** at 90.5 ps (red) curve and a singlet Gaussian fit to the bleach (maroon dash).

The transient spectra during and immediately after fission (solid lines) are shown for **BP2** in the graph below (Figure 2.18). A simple one Gaussian fit with a linear baseline is also shown (dotted lines) and the total areas of the resulting fits agree within 5%. This result confirms that the singlet fission process is quantitative.

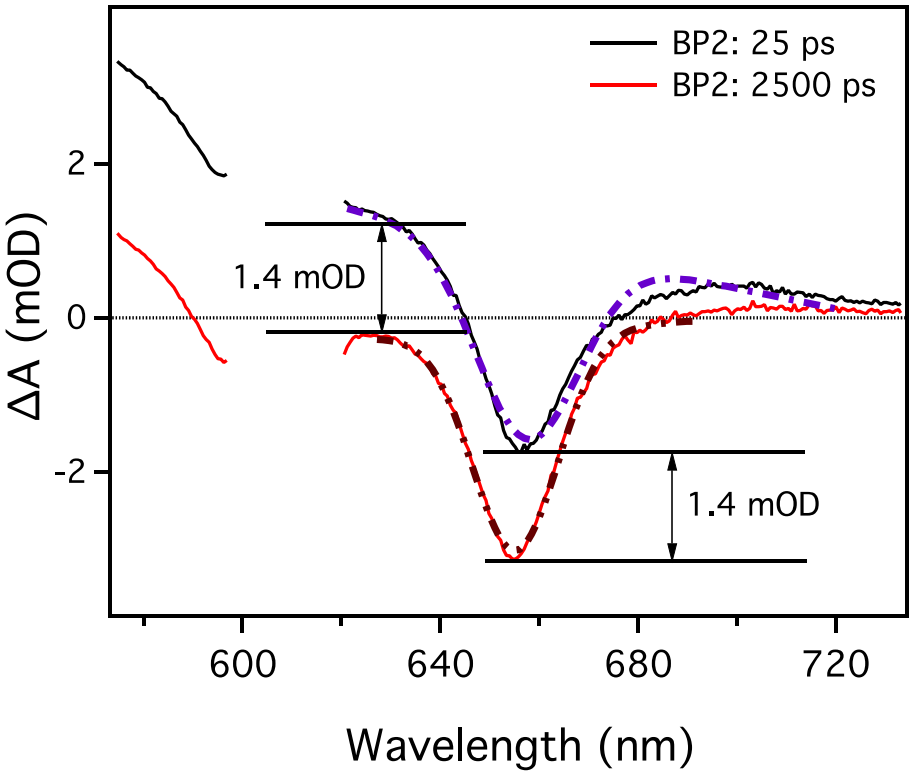

Figure 2.18. Transient spectra of **BP2** at 25 ps (black) curve and a singlet Gaussian fit to the bleach (purple dash). Transient spectra of **BP2** at 2500 ps (red) curve and a singlet Gaussian fit to the bleach (maroon dash).

Sensitization Yield Determination

An additional determination of the yield of triplet involves triplet sensitization experiments using a solution consisting of 20 mM anthracene and ~ 50 µM TIPS-pentacene/BP2 excited at 360 nm. Triplets are generated in the anthracene by intersystem crossing and are then transferred to BP2 via collisional energy transfer.

To serve as an internal standard, a solution of regular TIPS-pentacene was measured under identical conditions. This method ensures that accurate triplet excited state extinction coefficients are obtained for anthracene in chloroform. Unlike in BP2, a triplet exciton on TIPS-pentacene will bleach the entire molecule. As a result, we can use the magnitude of the ground state bleach signal after triplet sensitization to determine the number of triplets transferred to TIPS-pentacene. From this, we can back out the anthracene triplet extinction coefficient after accounting for the transfer efficiency. We have found that in chloroform, the triplet lifetime of anthracene is weakly concentration dependent; it was determined independently for each anthracene solution used.

20 mM Anthracene Solution 1: freshly prepared, degassed under Argon. Used for TIPS sensitization experiments.

$1/\langle\tau\rangle = \frac{\sum_i a_i^2 \tau_i}{\sum_i a_i \tau_i}$ = 1/((1/0.15395)^2*0.0020722

+(1/0.018131)^2*0.0022811)/((1/0.15395)*0.0020722 +(1/0.018131)*0.0022811)

= 1/50.45 µs = 0.0198 μs^{-1}

20 mM Anthracene Solution 2: freshly prepared, degassed under Argon. Used for BP2 sensitization experiments.

$1/\langle\tau\rangle = \frac{\sum_i a_i^2 \tau_i}{\sum_i a_i \tau_i}$ = 1((1/0.088763)^2*0.0024706

+(1/0.010821)^2*0.0024267)/((1/0.088763)*0.0024706 +(1/0.0024706)*0.0024267) = 1/20.83 μs = 0.0480 μs^{-1}

The raw data used for this sensitization yield determination are shown below in Figure 2.19 and Figure 2.20.

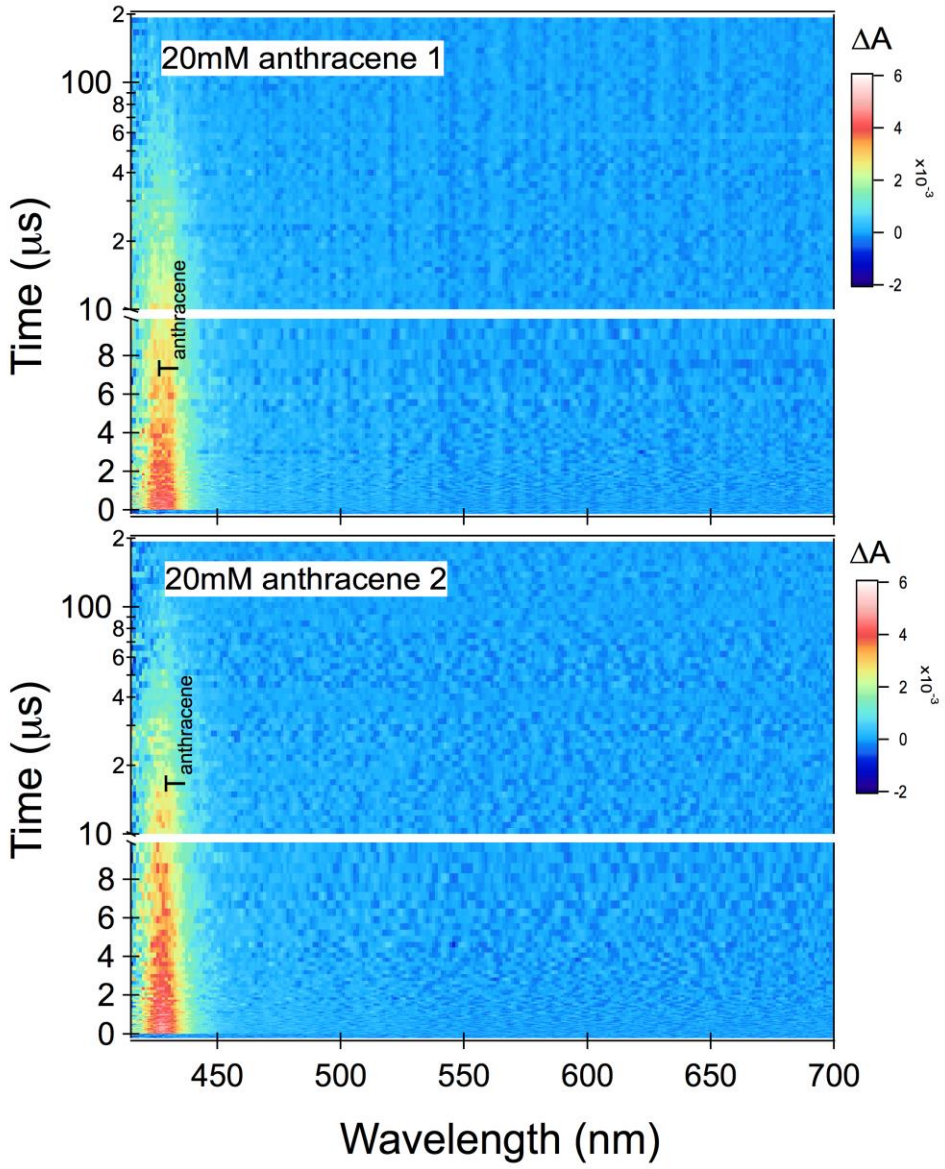

Figure 2.19. Raw sensitization data for 20 mM anthracene solutions with 360 nm excitation in chloroform.

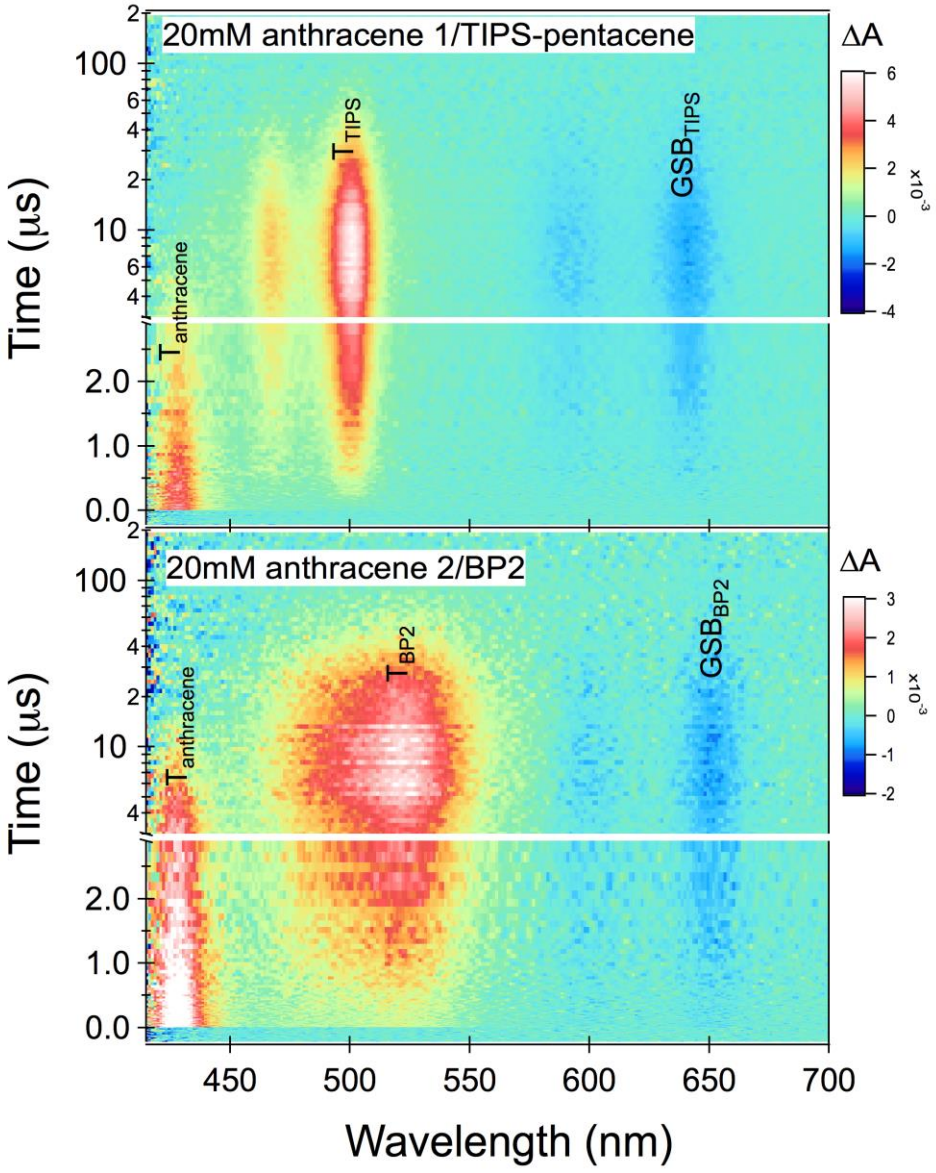

Figure 2.20. Raw sensitization data for 20mM anthracene (fresh solution #1)/TIPS-pentacene and 20 mM anthracene (Fresh solution #2)/BP2 with 360 nm excitation, both in chloroform.

In regular sensitization experiments, the raw transient signals are corrected for the transfer efficiency (ratio of the triplet rise rate constant over the sum of the triplet rise and anthracene triplet lifetime) and the triplet decay kinetics (ratio of the triplet rise over the triplet rise plus triplet decay rate constants).

20 mM Anthracene 1/TIPS Pentacene:

$1/\tau\_ET = 0.31306\ \mu s^{-1}$ (single exponential fit at 427 nm)

Triplet energy transfer efficient: 0.31306/(0.31306+0.0198) = 0.94

T_anth ΔA maximum (427) = 4.15 mOD

T_TIPS ΔA maximum (501) = 5.82 mOD

T_TIPS ΔA maximum (501) scaled by energy efficiency = 5.82/.94 = 6.19 mOD

T_TIPS ΔA maximum (501) scaled by T decay kinetics = 6.19 mOD

/0.31306/(0.31306+0.03951) = 6.19 mOD/0.89 = 6.96mOD

GSB ΔA minimum (640) = 1.34 mOD

GSB ΔA minimum (640) scaled by T decay kinetics and ET efficiency= 1.32/0.89/0.94 = 1.58 mOD

20 mM Anthracene 2/BP2:

$1/\tau\_ET = 0.1814\ \mu s^{-1}$ (single exponential fit at 427 nm)

Triplet energy transfer efficient: 0.1814 /(0.1814 +0.0480) = 0.79

T_anth ΔA maximum (427) = 4.13 mOD

T_2phBP ΔA maximum (522) = 2.71 mOD

T_2phBP ΔA maximum (522) scaled by ET efficiency = 2.71/.79 = 3.43 mOD

T_2phBP ΔA maximum (522) scaled by T decay kinetics = 3.43/ (.1814/(.1814 + .03327)) = 3.43/0.85 = 4.06 mOD

GSB ΔA minimum (650) = 0.714 mOD) → increase by 4% to account for baseline → 0.743 mOD

GSB ΔA minimum (650) scaled by T decay kinetics and ET efficiency = 0.734/.85/.79 = 1.09 mOD

Calculations:

Anthracene T-T ESA extinction coefficients, using the corrected GSB bleach signal of TIPS pentacene:

$$\frac{\mathrm{GSB_{TIPS}}\ \Delta A}{ESA_{ant}\ \Delta A} = \frac{\mathrm{GSB_{TIPS}}\ \varepsilon_S}{ESA_{ant}\ \varepsilon_T} = \frac{1.58}{4.15} = \frac{21000}{x}$$

$$ESA_{ant}\ \varepsilon = 55200\ M^{-1}\ cm^{-1}$$

2phBP T-T ESA extinction coefficients:

$$\frac{\mathrm{ESA_{2phBP}}\ \Delta A}{ESA_{ant}\ \Delta A} = \frac{\mathrm{ESA_{2phBP}}\ \varepsilon_T}{ESA_{ant}\ \varepsilon_T} = \frac{4.06}{4.13} = \frac{x}{55200}$$

$$ESA_{2phBP}\ \varepsilon_T = 54260\ M^{-1}\ cm^{-1}$$

2phBP fission yield:

$$\frac{\mathrm{c_{triplets}}}{c_{singlets}} = \frac{\Delta A/\epsilon_T l}{4.91\mathrm{e}-07} = \frac{0.0107/(54260 * 0.2)}{4.91\mathrm{e}-07} = \frac{9.86e-07}{4.91\mathrm{e}-07} = 2.01$$

Using the error estimation from part A, the overall fission yield is 201% +/- 15%.

2.14 Details on UV-Vis, Photoluminescence and PL Quantum Yield

UV-Vis Concentration Dependence Study

Shown in Figure 2.21 are UV-Visible steady state spectra taken at varying concentrations of BP0.

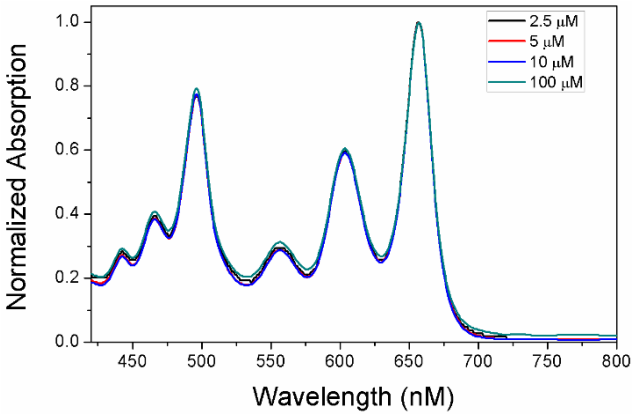

Figure 2.21. Normalized steady state absorption reveals no evidence of aggregation or change in spectral shape for **BP0**.

A representative determination of molar extinction coefficient for BP0 is shown below (Figure 2.22). Molar extinction coefficients for BP1 and BP2 were taken in the same manner.

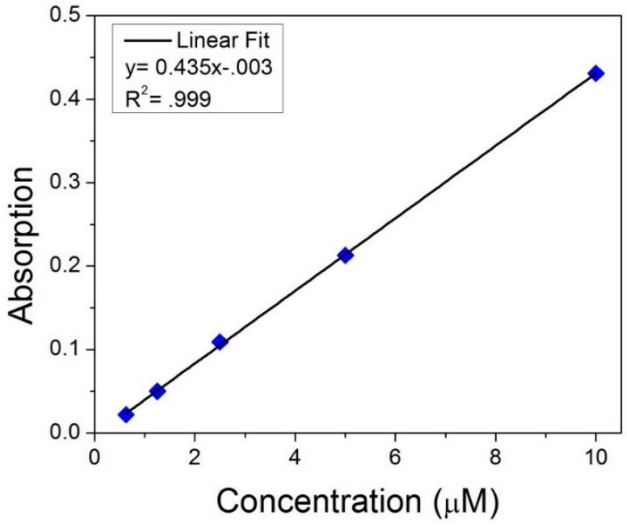

Figure 2.22. Beer's law of BP0 in chloroform yields a molar extinction coefficient of 44,000 $M^{-1}cm^{-1}$.

Concentration dependent UV-Visible steady state absorption measurements reveal no aggregation effects in BP1 or BP2 (Figures 2.23, 2.24).

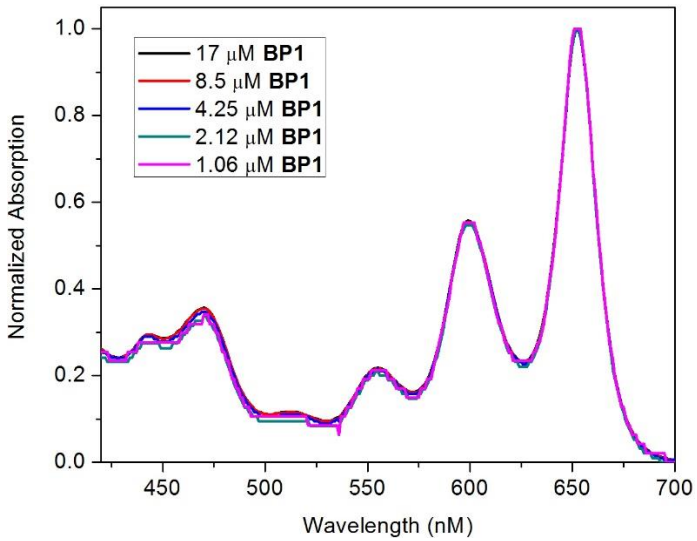

Figure 2.23. Normalized concentration dependent steady state absorption reveals no evidence for aggregation in BP1.

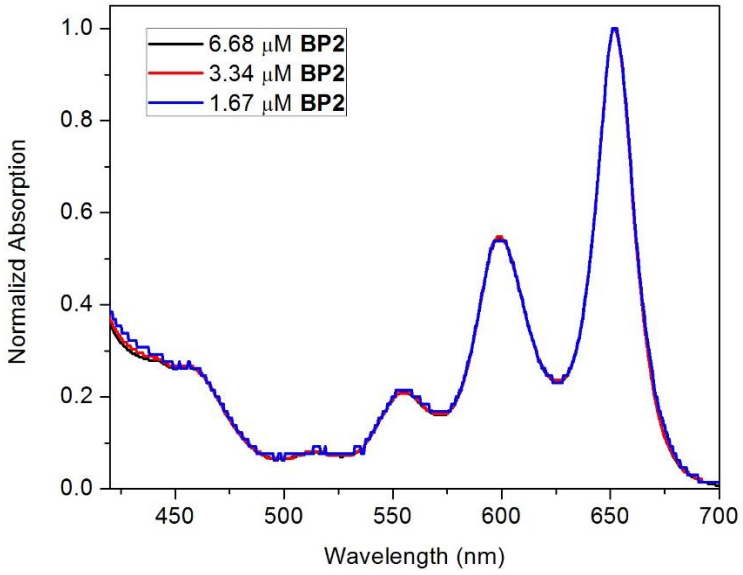

Figure 2.24. Normalized steady state absorption of BP2 reveals no concentration dependence.

Steady-state PL and Quantum Yield Determination

The photoluminescence spectrum (Figure 2.25) and quantum yield of BP0 (1.6%), BP1 (4.4%), and BP2 (5.0%) are measured relative to a dilute solution of TIPS-pentacene in chloroform, which has a published quantum yield of 75% in chloroform.[34] A high repetition rate (5 MHz) picosecond pulsed laser is used for photoexcitation at 543 nm. Emission is collected in reflection geometry and detected using a JY Horiba iHR320 spectrometer and liquid nitrogen cooled back-illuminated deep depleted CCD camera, with enhanced NIR sensitivity. The PL quantum yield is calculated by comparing the integrated PL spectrum after correcting for the optical densities of the different solutions.[45,46]

The photoluminescence quantum yield of BP2 is consistent with the value estimated from the measured singlet fission rate (1/220 ps) and the known PL lifetime (13 ns). It should be noted that the QY's quoted here are reflective of the upper bound of the QY of the compounds. Due to the photosensitive nature of pentacenes, despite careful handling, some small (on order of 1 to 4%) percentage of sample may have one of the two pentacenes in a dimer degrade during handling or measurement. This degradation results in some small portion of the sample that behaves effectively as monomeric pentacene, which has a much higher QY than the bipentacenes reported. The QY of BP0 reflects the small (few percent) fluorescent impurities that can be clearly seen in time-resolved PL measurements. Likely, the slightly higher QY of BP1 than expected based on the fission rate also results from some small amount of fluorescent impurity.

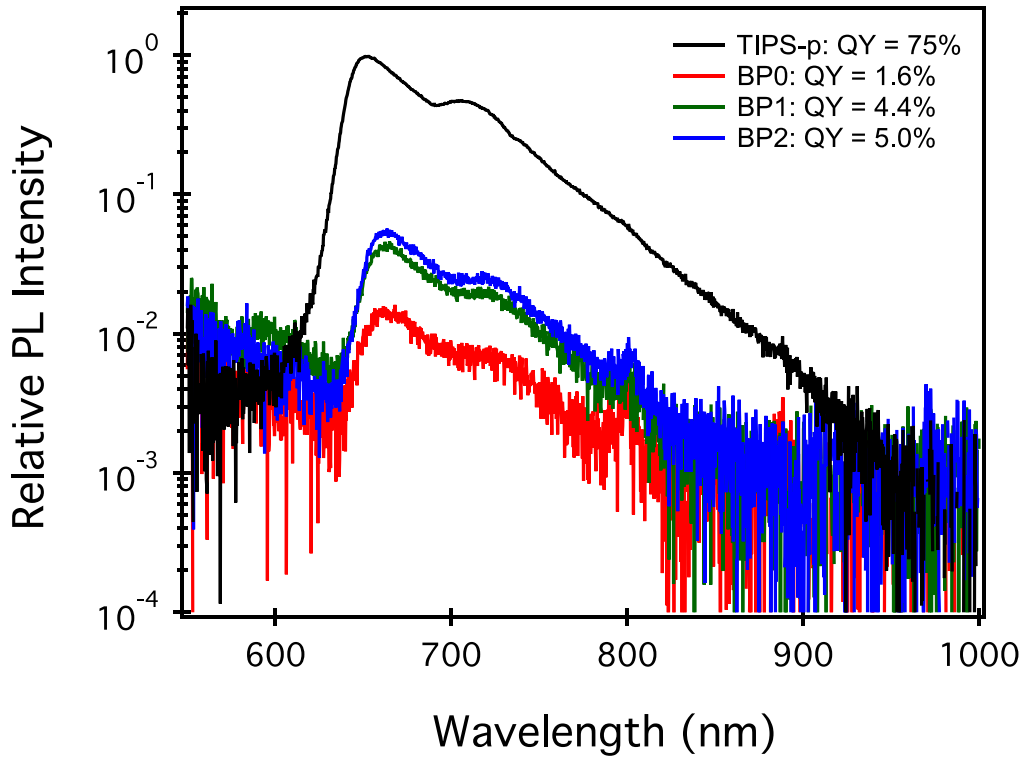

Figure 2.25. PL spectra for TIPS-pentacene (black), **BP0** (red), **BP1** (green), and **BP2** (blue) in chloroform using 543 nm laser excitation.

Ultrafast PL

The PL upconversion data presented in Figure 2.4 is used to determine the fission rate for BP1 and BP2. The data are fit with three exponentials convoluted with the Gaussian laser pulse. The longest time constant represents the small amplitude (few percent) impurities, whose PL resembles regular TIPS-pentacene. A fast time constant (~ 5 ps) is present in both BP1 and BP2 samples. Its origin is unknown, but as it is uncorrelated to the excited state population recovery monitored via TAS, it is assumed to be related to a vibrational or rotational relaxation process. In both BP1 and BP2, the fission rate is assumed to be the intermediate time constant, which dominates the PL decay, 20 ps in BP1 and 220 ps in BP2.

2.15 Details on Computational Methods

Calculations were done using Density Functional Theory (DFT) and Time Dependent DFT (TDDFT) with the B3LYP functional and the 6-31G** basis set. The ground state geometry was optimized using *Jaguar* (version 8.4, Schrodinger Inc., New York, NY, 2013). The same optimized ground state geometry was used to calculate all vertical excitations shown. All states were found using DFT except for the S_1 states, for which TDDFT was employed. To simplify the computation, trimethylsilyl groups were used in place of TIPS groups, which do not contribute electron density to the system.

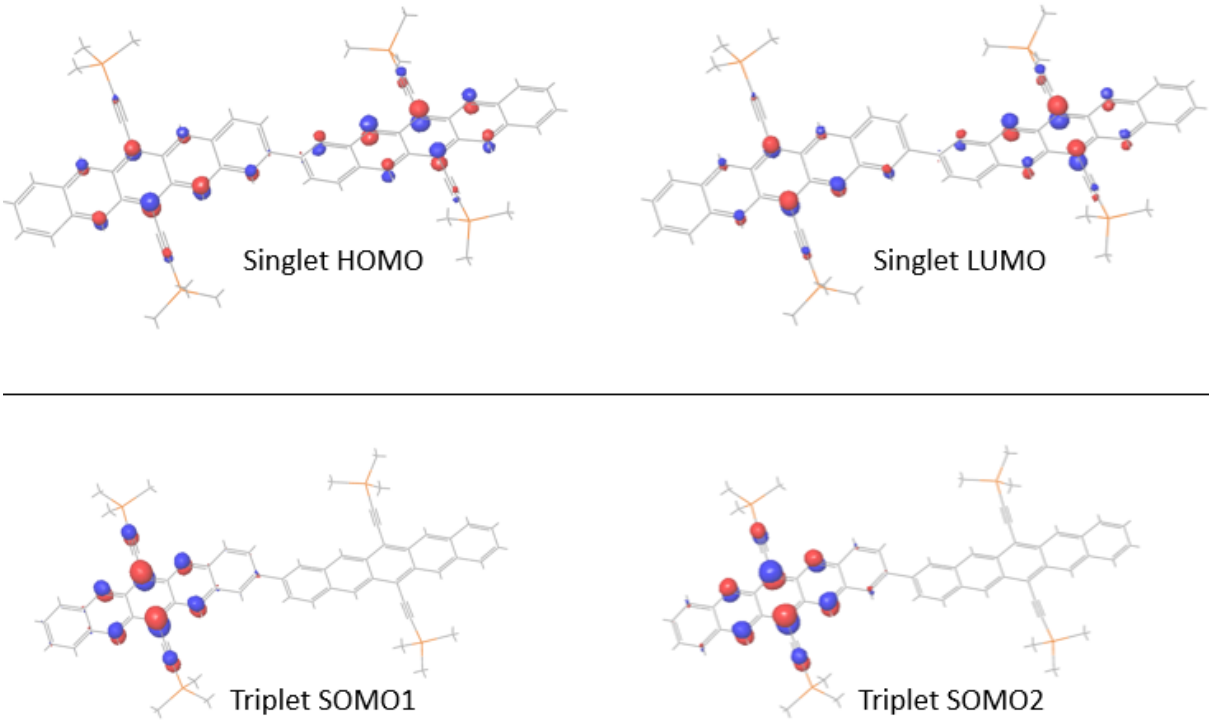

Figure 2.26. Electronic orbitals for singlet (HOMO and LUMO) and triplet (SOMO1 and SOMO2) states of **BP0**.

In Figure 2.26, the electron orbitals of the S_0 singlet state HOMO (highest occupied molecular orbital) and LUMO (lowest unoccupied molecular orbital) are given, as well as the T_1 triplet state SOMO1 (singly occupied molecular orbital) and SOMO2. The S_1 state is best described as a state whose electronic orbitals are essentially the same as those of the S_0 state, but a single electron has moved from the S_0 HOMO to the S_0 LUMO. As discussed in the main text, the HOMO and LUMO of S_0 (and therefore the two singly-occupied orbitals in S_1) feature significant delocalization across the entire molecule. However, presumably due to favorable exchange interaction, even in BP0, the most directly coupled dimer, the singly-occupied orbitals in T_1 reside on a single pentacene. This localization is important, in that it allows room for a second triplet to occupy the other pentacene, making the final two-triplet state formation in the singlet fission process favorable.

The exothermicity of the singlet fission process is defined as $E(S_1)$-$2E(T_1)$ under conditions of weak interchromophore coupling. The final state is more conveniently approximated, however, by the energy of the quintet state of the dimer, or $E(Q_1)$, in that the quintet state more closely describes the energetics of a two-triplet state.[31] For this computational study, the exothermicity of pentacene dimer fission was calculated from $E(S_1)$-$E(Q_1)$, though the triplet state energy also was calculated. Importantly, in all three bipentacenes studied, $E(Q_1)$ was nearly isoethermic with $2E(T_1)$, which suggests that fission in these compounds populates relatively isolated, non-interacting triplets.

Static DFT was used to calculate the total S_0 state energy of -3631.8772 Hartrees (Table 2.2). Appendix A lists the geometry optimization details of the final S_0 optimized geometry used to determine the S_1, T_1 and Q_1 optimized geometries. Relative to S_0, static DFT yielded a vertical Q_1 state energy of 1.43 eV and a vertical T_1 state energy of 0.724 eV. TDDFT calculations were

used to compute the vertical excited state energy of S_1, which was 1.52 eV above S_0. $E(S_1)$-$E(Q_1)$ was found to be 0.09 eV exothermic, which is in close agreement with the 0.3 eV fission exothermicity previously suggested for a similar dimer with no solubilizing chains.[31] Furthermore, the proximity of the $E(S_1)$-$2E(T_1)$ value to that calculated above implies that the ($2xT_1$) state of the pentacene dimer effectively consists of two isolated triplets, as suggested by the SOMO's. If each of the two triplets were to reside on either monomer of the pentacene dimer, this "double triplet state" would be equivalent to the combination of two independent triplets, as calculated here.

Table 2.2. Molecular states studied and associated final total energies.

State	BP0 State Energy (Hartree)	BP1 State energy (Hartree)	BP2 State Energy (Hartree)
S_0	-3631.8772	-3862.9415	-4094.0053
S_1	-3631.8212	-3862.8818	-4093.9445
T_1	-3631.8506	-3862.91017	-4093.9741
Q_1	-3631.8245	-3862.8789	-4093.9429

Table 2.3. List of calculated vertical excitation energies and relevant fission exothermicities.

Compound	$E(S_1)_{vert}$ (eV)	$E(T_1)_{vert}$ (eV)	$E(Q_1)_{vert}$ (eV)	$E(S_1)$-$2E(T_1)$ (eV)	$E(S_1)$-$E(Q_1)$ (eV)

BP0	1.52	0.724	1.43	0.072	0.09
BP1	1.63	0.85	1.70	-0.07	-0.07
BP2	1.66	0.85	1.70	-0.04	-0.04

Shown below (Figure 2.27) are the SOMO1 and SOMO2 for the triplet state of BP1. Again, the triplet is localized entirely on one pentacene unit, which is consistent with the general tendency of triplets to be more localized due to favorable exchange energy interactions.

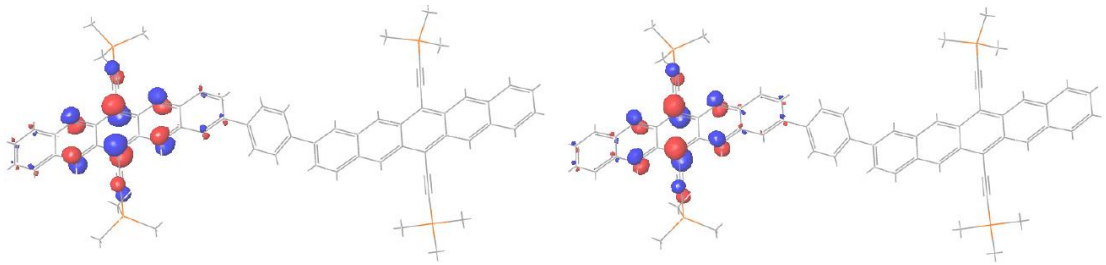

Triplet SOMO1 Triplet SOMO2

Figure 2.27. Electronic orbitals for the **BP1** T1 state, SOMO1 and SOMO2

TDDFT shows the BP1 S1 excited state results from the promotion of one electron from HOMO to LUMO (CI coefficient 0.99) plus the promotion of one electron from HOMO-1 to LUMO+1 (CI coefficient 0.14). This transition is entirely described by extensively delocalized molecular orbitals, as shown below in Figure 2.28.

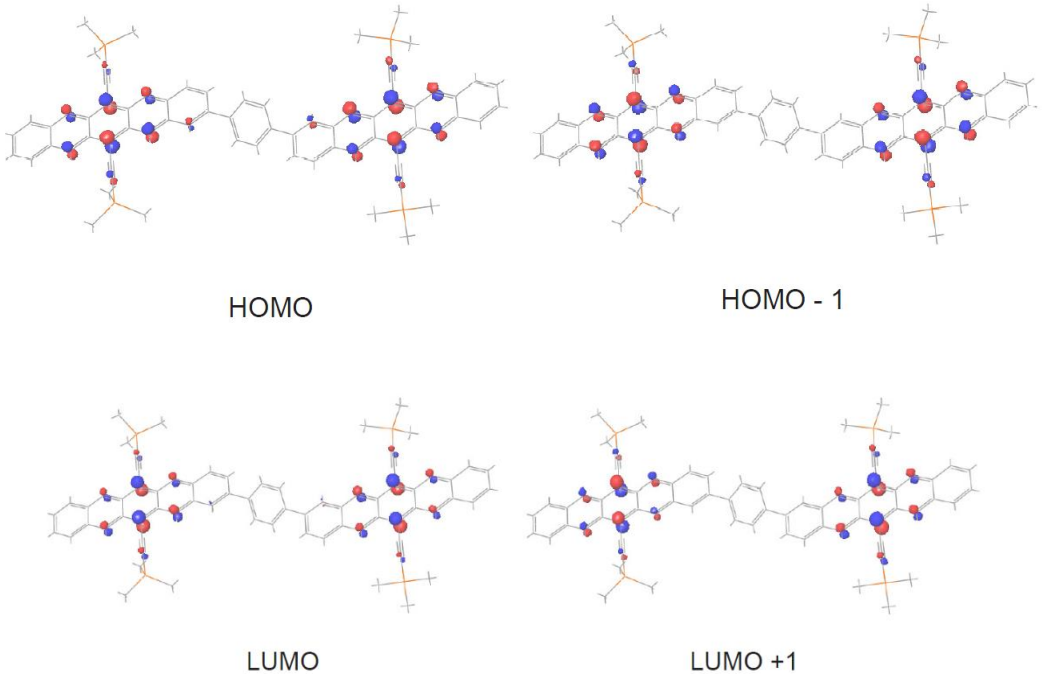

Figure 2.28. HOMO, HOMO-1, LUMO and LUMO-1 comprise the S1 excited state of **BP1**

DFT was then used to calculate the triplet state SOMO1 and SOMO2. Again, we find localized triplets, allowing for accommodation of two independent triplets on a single bipentacene molecule (Figure 2.29).

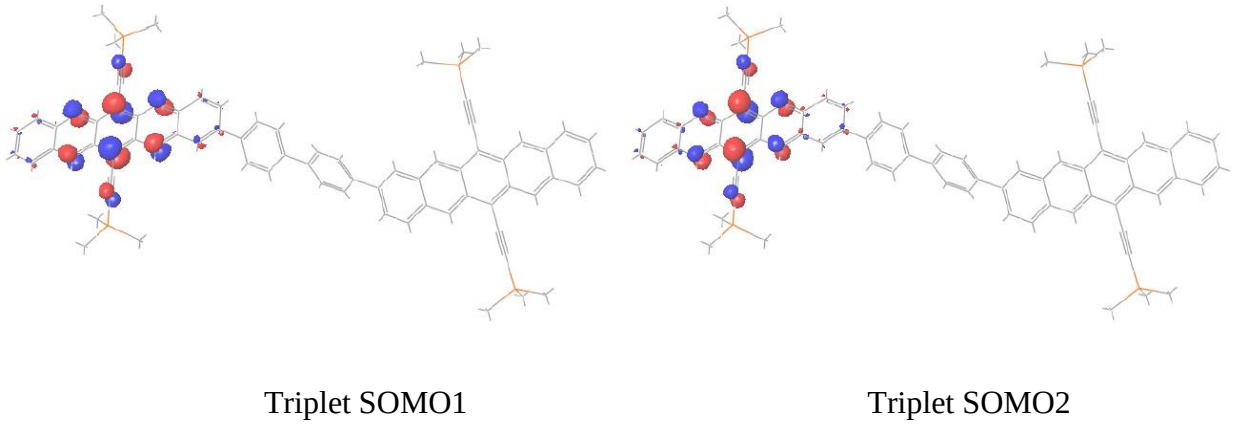

Figure 2.29. Triplet SOMO1 and SOMO2 for **BP2**, calculated by DFT

Finally, TDDFT shows this S1 excited state results from the promotion of one electron from HOMO to LUMO (CI coefficient 0.91) plus the promotion of one electron from HOMO-1 to LUMO+1 (CI coefficient 0.43). Crucially, even in this extreme of BP2, with the largest spacer between pentacene units, all of the molecular orbitals responsible for the S1 excited state are delocalized throughout the entire molecule. This extensive delocalization supports our spectroscopic finding that the singlet state bleaches all of the ground state transitions of the bipentacenes, and not just one pentacene subunit, as one might expect for a localized singlet (Figure 2.30).

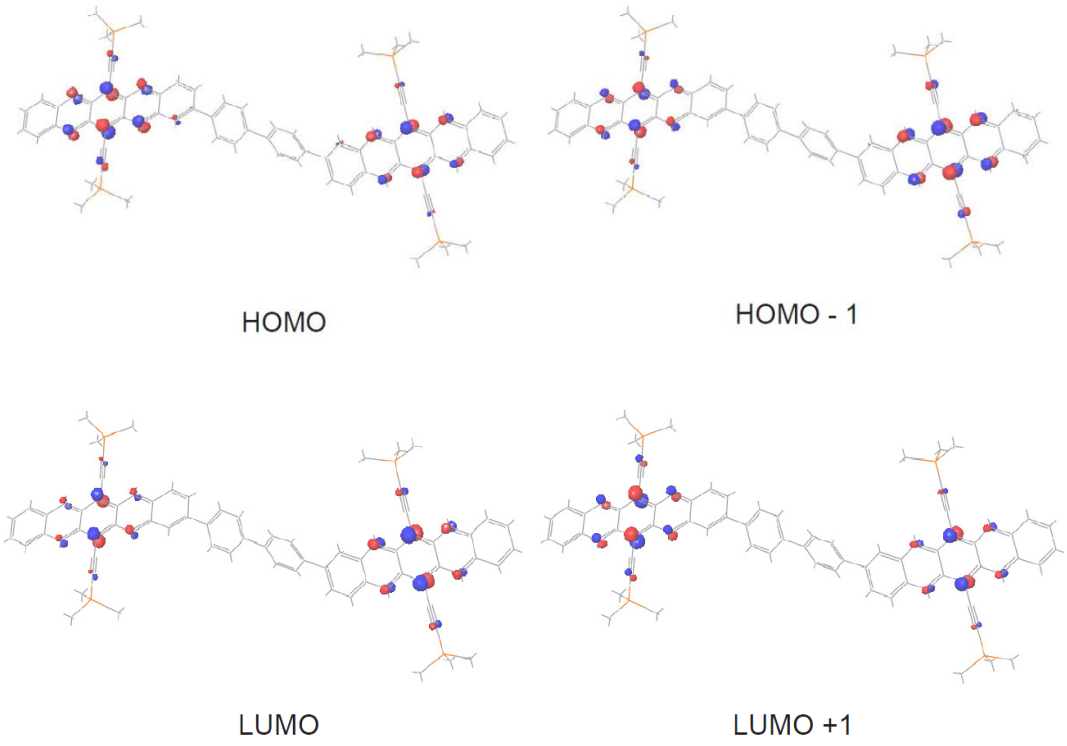

Figure 2.30. HOMO, HOMO-1, LUMO and LUMO-1 comprise the S1 excited state of BP1

2.16 Synthetic Details

General Methods

All commercially obtained reagents/solvents were used as received; chemicals were purchased from Alfa Aesar®, Sigma-Aldrich®, Acros organics®, TCI America®, Mallinckrodt®, and Oakwood® Products, and were used as received without further purification. Unless stated otherwise, reactions were conducted in oven-dried glassware under argon atmosphere. ^{1}H-NMR and ^{13}C-NMR spectra were recorded on Bruker 400 MHz (100 MHz for ^{13}C) and on 500 MHz (125 MHz for ^{13}C) spectrometers. Data from the ^{1}H-NMR and ^{13}C spectroscopy are reported as chemical shift (δ ppm) with the corresponding integration values. Coupling constants (*J*) are reported in hertz (Hz). Standard abbreviations indicating multiplicity were used as follows: s (singlet), b (broad), d (doublet), t (triplet), q (quartet), m (multiplet) and virt (virtual). The mass spectral data for the compounds were obtained from XEVO G2-XS Waters® equipped with a QTOF detector with multiple inlet and ionization capabilities including electrospray ionization (ESI), atmospheric pressure chemical ionization (APCI), and atmospheric solids analysis probe (ASAP). The base peaks were usually obtained as $[M]^+$ or $[M+H]^+$ ions. Anhydrous solvents were obtained from a Schlenk manifold with purification columns packed with activated alumina and supported copper catalyst (Glass Contour, Irvine, CA). All reactions were carried out under argon unless otherwise noted.

General Synthetic protocol for the synthesis of Bipentacenes

Synthesis of Bpin derivatives of TIPS pentacenes:

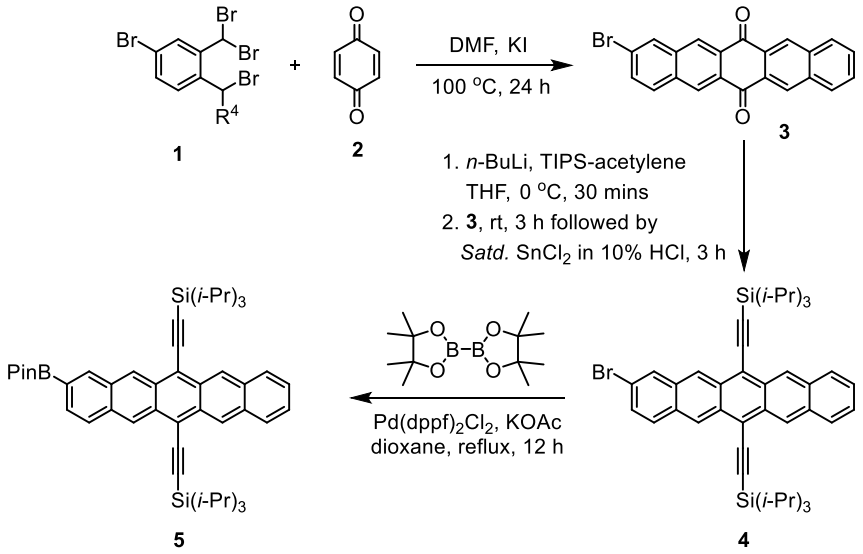

Synthesis of Bipentacenes:

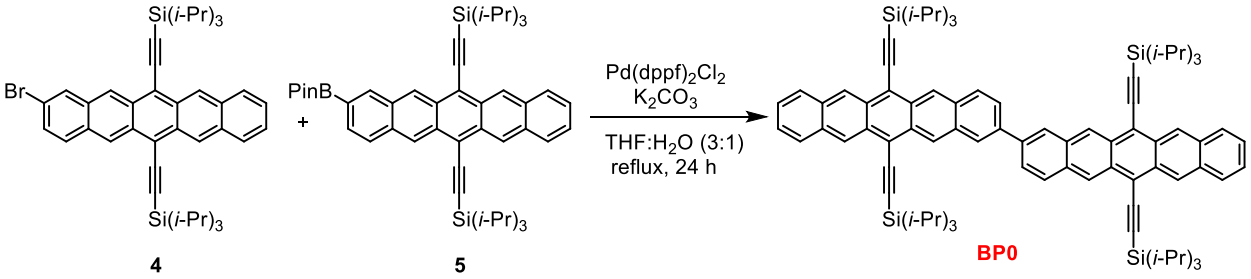

Synthesis of phenyl linked Bipentacenes:

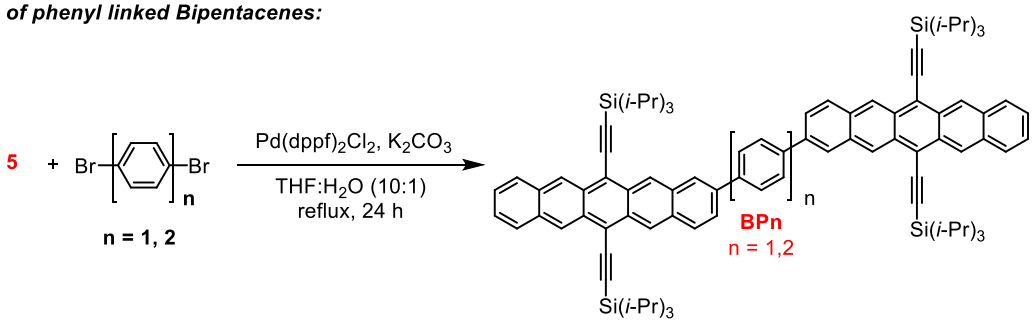

General procedure for the synthesis of BPin derivatives of pentacenes

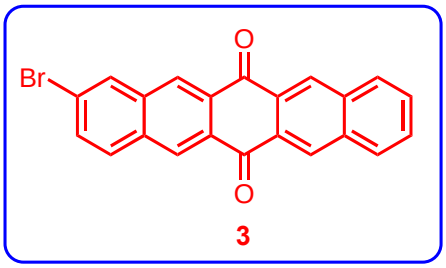

The 6,13-pentacenequinone derivatives were synthesized according to a procedure reported in the literature.[47] In a typical procedure a mixture of 2-(bromomethyl)-2-(dibromomethyl)benzene **1** (1.0 *equiv*), *p*-benzoquinone **2** and KI in dry DMF was heated to 100° C and maintained for 24 h. After the reaction, the mixture was cooled to rt and diluted with methanol. The slurry was filtered and the solid was washed with water and methanol. The resulting solid was collected and dried. The crude product was directly used for next step without further purification.

Due to limited solubility of the 6,13-pentacenequinones no characterization was performed.

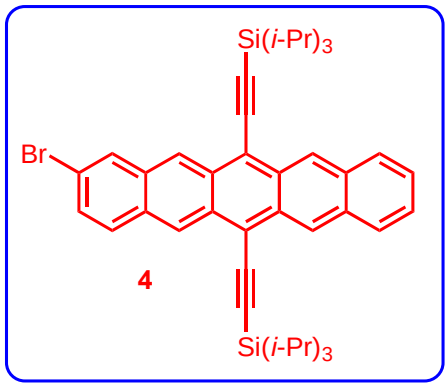

To a solution of (triisopropylsilyl)acetylene (3.5 *equiv.*) in dry and degassed THF (25 mL) in 200 mL Schlenk flask at -78 °C added *n*-butyl lithium (3.4 *equiv.*, 2.5 M in hexanes). This solution was allowed to stir at -78 °C for 1 h followed by the addition of **3** (4.0 g, 1.0 *equiv.*) under positive argon flow. The solution was allowed to warm to rt and stirred overnight (16 h) or until solid pentacenoquinone was no longer observed. To this clear, deep yellow solution was added of a saturated solution of tin (II) chloride dihydrate in 10% aqueous HCl solution (50 mL) during which the solution turned deep blue. The resulting mixture was stirred at rt for 1 h under dark and filtered over a pad of silica. The solid was washed with DCM and the

combined organic layer was washed with water (2 × 200 mL), dried over *anhyd.* Na_2SO_4, filtered and the solvent was removed under reduced pressure to get the crude product. The crude was purified by silica chromatography using hexanes as an eluent to obtain bromo pentacene derivative **4** as a deep blue solid in 65% yield.

^{1}H-NMR (500 MHz, $CDCl_3$, δ ppm): 9.34 (s, 1H), 9.32 (s, 1H), 9.29 (s, 1H), 9.22 (s, 1H), 8.16 (s, 1H), 8.01-7.99 (m, 2H), 7.87-7.86 (m, 1H), 7.48-7.44 (m, 3H) and 1.44-1.38 (m, 42H).

^{13}C-NMR (125 MHz, $CDCl_3$, δ ppm): 132.6, 132.5, 132.4, 130.9, 130.8, 130.7, 130.6, 130.4, 130.2, 130.18, 129.5, 128.7, 126.9, 126.4, 126.36, 126.2, 126.19, 125.5, 120.3, 118.7, 118.5, 107.7, 107.6, 104.4, 104.38, 19.02, 19.0 and 11.7.

MS (ESI): Calculated: 716.2869; Observed: 716.2863.

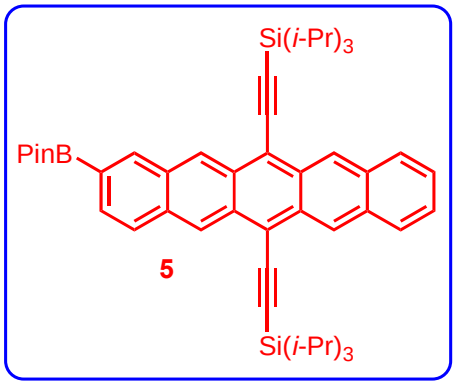

To a dry round bottomed flask was added **4** (4.0 g, 5.57 mmol), $Pd(dppf)_2Cl_2$·DCM (203 mg, 0.25 mmol), KOAc (1.91 g, 19.5 mmol), and bis(pinacolato)diboron (2.82g, 11.1 mmol). Sequential vacuum and argon were used to degas the mixture followed by the addition of degassed 1, 4 dioxane (70 mL). The mixture was heated to 80 °C and maintained for 12 h in the dark. After the reaction, the mixture was cooled to rt and the solvent was removed under reduced pressure. The crude was partitioned between DCM (250 mL) and water (200 mL). The organic layer was separated, washed with water (2 × 200 mL), dried over *anhyd.* Na_2SO_4, filtered and the solvent was removed under reduced pressure to get the crude product. The crude was purified by silica chromatography using mixtures of hexanes/DCM as an eluent to obtain BPin pentacenes derivative **5** as a deep blue solid in 49% yield.

^{1}H-NMR (400 MHz, $CDCl_3$, δ ppm): 9.34-9.32 (m, 2H), 9.30 (s, 1H), 9.27 (s, 1H), 8.51-8.507 (m, 1H), 7.98-7.95 (m, 2H), 7.93-7.90 (m, 1H), 7.72-7.70 (m, 1H), 7.42-7.40 (m, 2H), 1.44 (s, 12H) and 1.41-1.36 (m, 42H).

^{13}C-NMR (125 MHz, $CDCl_3$, δ ppm): 138.1, 133.2, 132.5, 132.4, 131.9, 131.3, 130.9, 132.90, 130.7, 129.8, 128.82, 128.80, 127.8, 127.7, 126.6, 126.4, 126.2, 126.18, 126.15, 118.97, 118.5, 107.6, 107.3, 104.8, 104.7, 84.2, 25.1, 19.20, 19.15 and 11.8.

MS (ESI): Calculated: 764.4616; Observed: 764.4617.

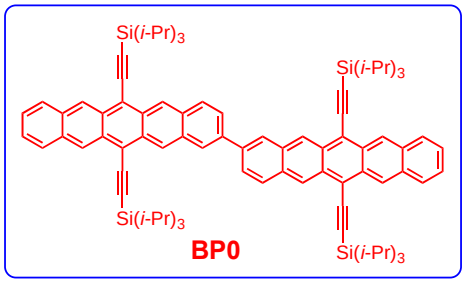

Synthesis of BP0: To a 20 mL sealed tube was added **4** (72 mg, 0.1 mmol), **5** (76 mg, 0.1 mmol), $Pd(dppf)_2Cl_2 \cdot DCM$ (4 mg, 0.005 mmol), and K_2CO_3 (240 mg, 1.7 mmol). Sequential vacuum and argon were used to degas the mixture followed by the addition of degassed H_2O (1 mL) and THF (3 mL). The resulting solution was heated to 70 °C and maintained for 24 h in dark. After the reaction, the solution was poured into a separatory funnel containing DCM (30 mL) and water (30 mL). The organic layer was separated, dried over *anhyd.* Na_2SO_4, filtered and the solvent was removed under reduced pressure to get the crude product. The crude was purified by silica chromatography using mixtures of hexanes/DCM as an eluent to obtain bipentacenes as deep purple solid in 77% yield.

^{1}H-NMR (500 MHz, $CDCl_3$, δ ppm): 9.45 (s, 2H), 9.39-9.36 (m, 6H), 8.38 (s, 2H), 8.19-8.17 (m, 2H), 8.03-8.01 (m, 4H), 7.97-7.95 (m, 2H), 7.47-7.45 (m, 4H) and 1.51-1.41 (m, 82H).

^{13}C-NMR (125 MHz, $CDCl_3$, δ ppm): 137.7, 132.5, 132.4, 132.3, 131.6, 131.0, 130.9, 130.8, 130.7, 129.6, 128.7, 126.8, 126.4, 126.2, 126.16, 126.1, 125.98, 118.5, 118.4, 107.4, 107.2, 104.7, 104.66, 19.0 and 11.7.

MS (ESI): Calculated: 1274.7348; Observed: 1274.7341.

Synthesis of phenyl linked bipentacenes

To a dry round bottomed flask was added 4,4'-dibromobiphenyl (*1.0 equiv*), BPin pentacene derivative **5** (294 mg, 0.39 mmol, *2.3 equiv*) K_2CO_3 (17 *equiv*) and $Pd(dppf)_2Cl_2 \cdot DCM$ (0.1 *equiv*). Sequential vacuum and argon were used to degas the mixture followed by the addition of degassed THF and H_2O (10:1 ratio, 110 mL). The mixture was heated to reflux and maintained for 24 h in

the dark. After the reaction, the mixture was cooled to rt and the solvent was removed under reduced pressure. The crude was purified by silica chromatography using mixtures of hexanes/chloroform as an eluent to obtain the product as a green solid.

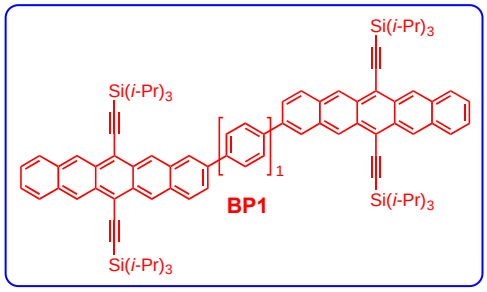

Yield = 57%

^{1}H-NMR (500 MHz, $CDCl_3$, 50° C, δ ppm): 9.42-9.35 (m, 8H), 8.27 (s, 2H), 8.14-8.12 (m, 2H), 8.02-7.99 (m, 8H), 7.84-7.82 (m, 2H), 7.45-7.43 (m, 4H) and 1.45-1.43 (m, 84H).

^{13}C-NMR (125 MHz, $CDCl_3$, δ ppm): Not obtained due to limited solubility.

MS (ESI): Calculated: 1350.7685; Observed: 1350.7676.

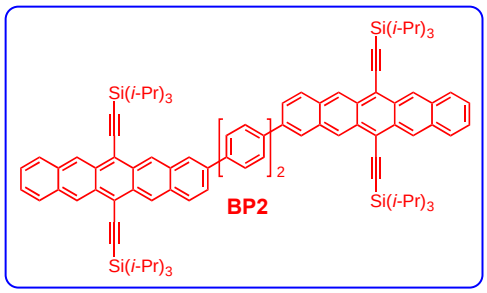

Yield = 79%

^{1}H-NMR (500 MHz, $CDCl_3$, 50° C, δ ppm): 9.41-9.35 (m, 8H), 8.25 (s, 2H), 8.13-8.11 (m, 2H), 8.02-7.998 (m, 4H), 7.97-7.95 (m, 4H), 7.91-7.89 (m, 4H), 7.83-7.80 (m, 2H), 7.45-7.43 (m, 4H) and 1.45-1.43 (m, 42H)

^{13}C-NMR (125 MHz, $CDCl_3$, δ ppm): Not obtained due to limited solubility.

MS (ESI): Calculated: 1426.7998; Observed: 1426.8003.

2.17 NMR Spectra

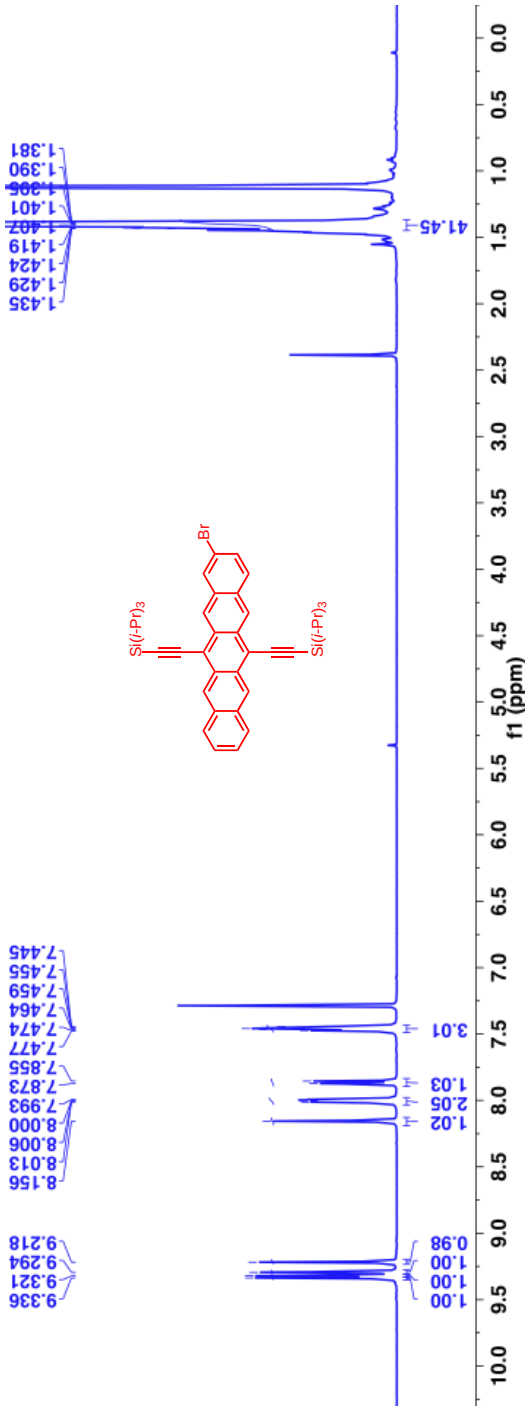

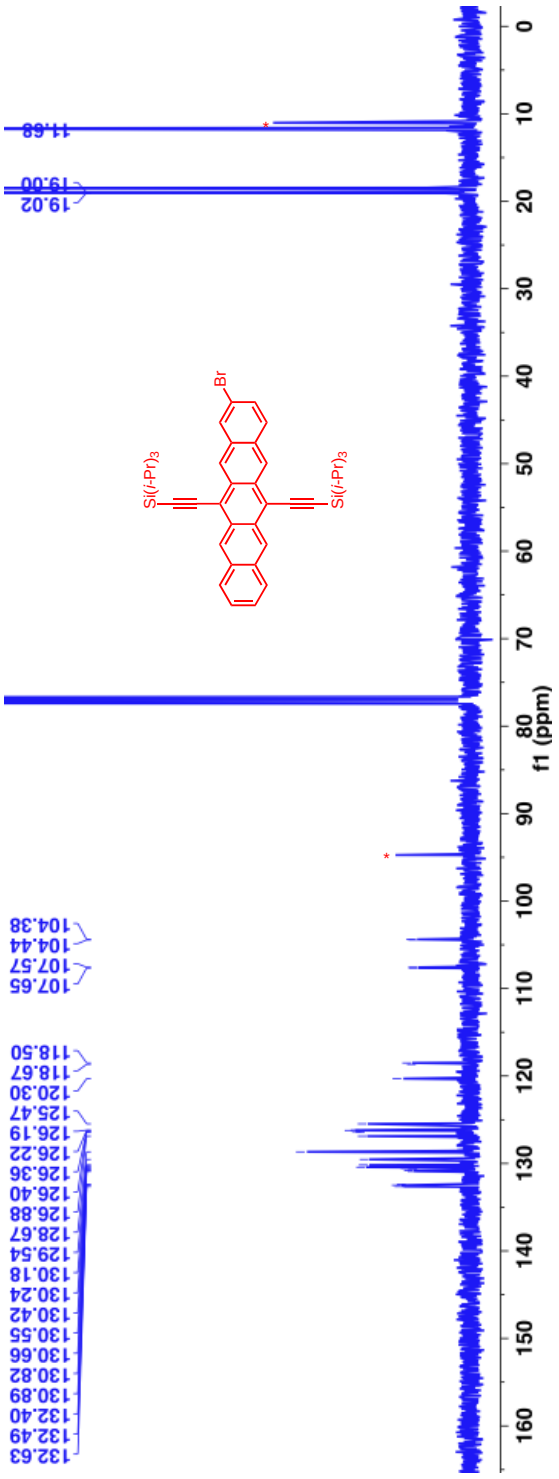

* = Residual TIPS acetylene

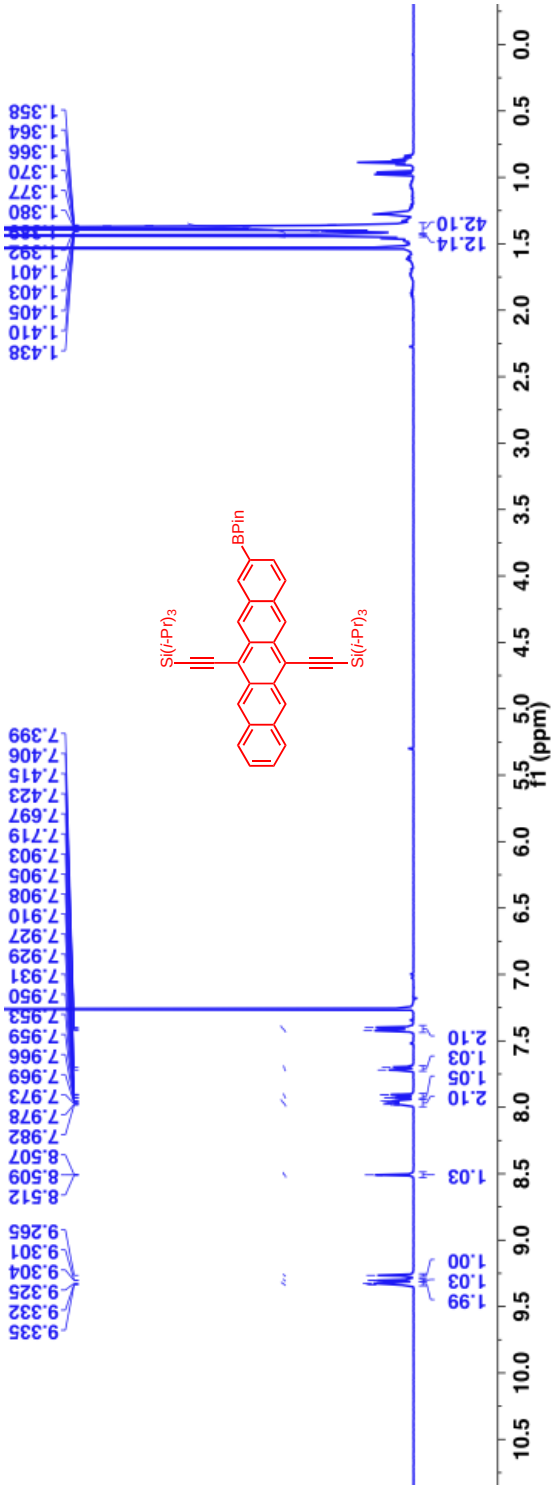
BPin
Si(i-Pr)3
Si(i-Pr)3
f1 (ppm)

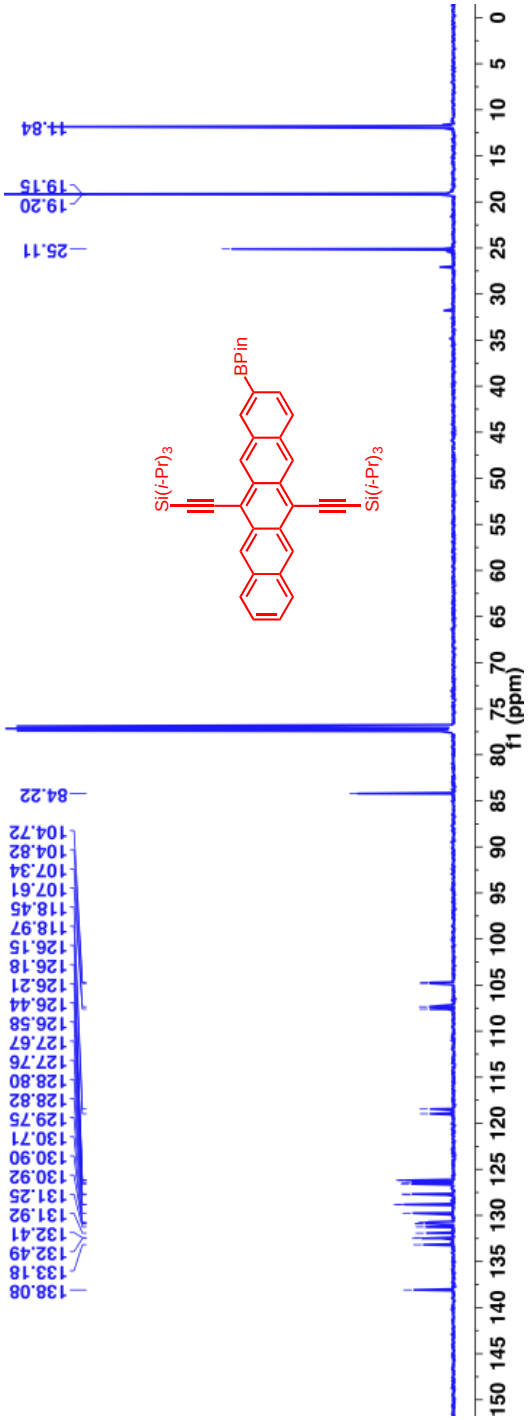
11.84
19.20
19.15
25.11
84.22
104.72
104.82
107.34
107.61
118.45
118.97
126.15
126.18
126.21
126.44
126.58
127.67
127.76
128.80
128.82
129.75
130.71
130.90
130.92
131.25
131.92
132.41
132.49
133.18
138.08
BPin
Si(i-Pr)3
Si(i-Pr)3
f1 (ppm)

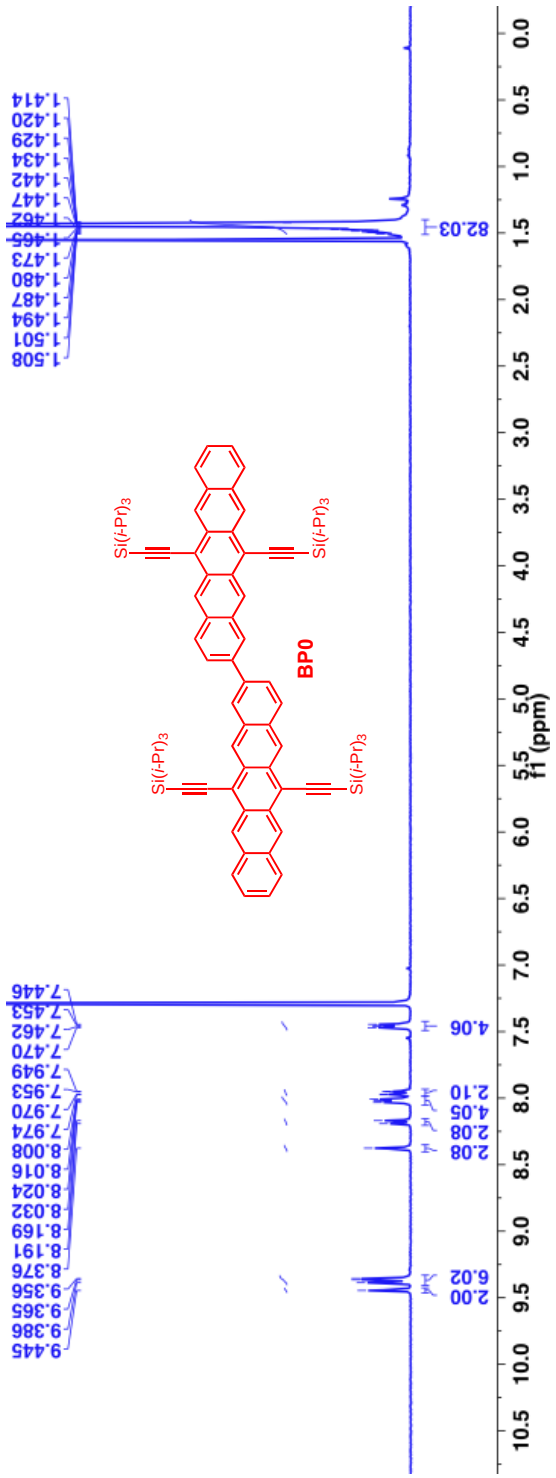
BP0
Si(i-Pr)3
Si(i-Pr)3
Si(i-Pr)3
Si(i-Pr)3
f1 (ppm)

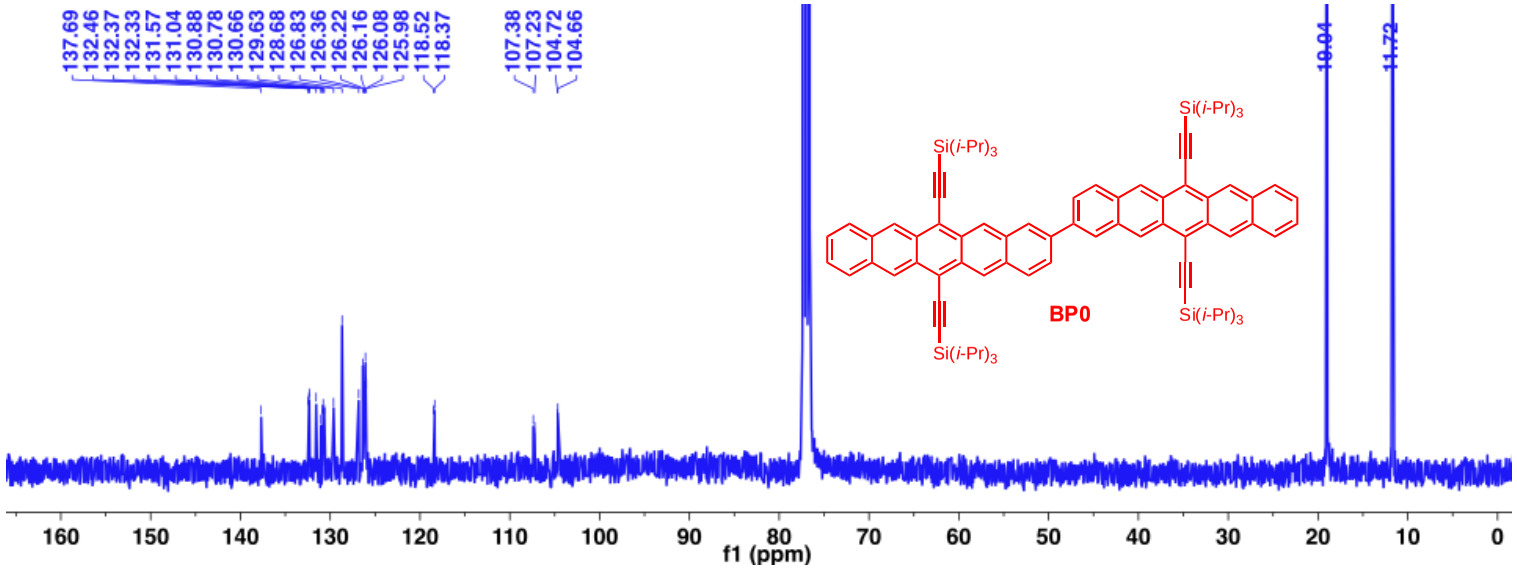
137.69
132.46
132.37
132.33
131.57
131.04
130.88
130.78
130.66
129.63
128.68
126.83
126.36
126.22
126.16
126.08
125.98
118.52
118.37
107.38
107.23
104.72
104.66
19.04
11.72
Si(i-Pr)3
Si(i-Pr)3
Si(i-Pr)3
Si(i-Pr)3
BP0
160
150
140
130
120
110
100
90
80
70
60
50
40
30
20
10
0
f1 (ppm)

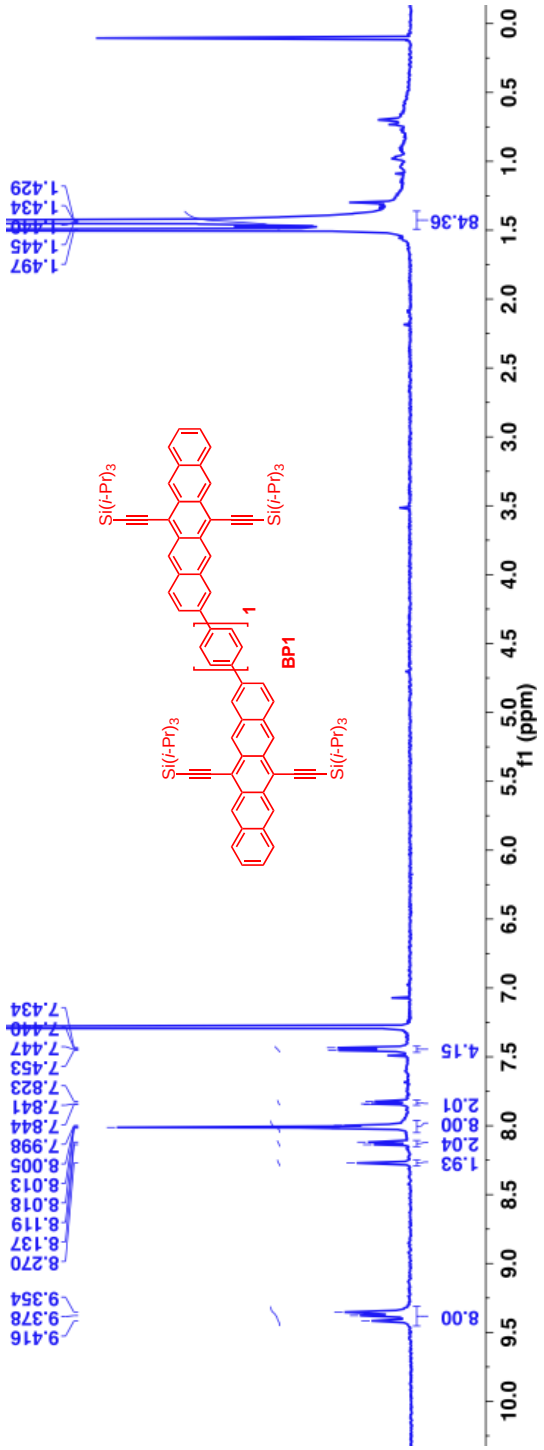
BP1
Si(i-Pr)3
f1 (ppm)

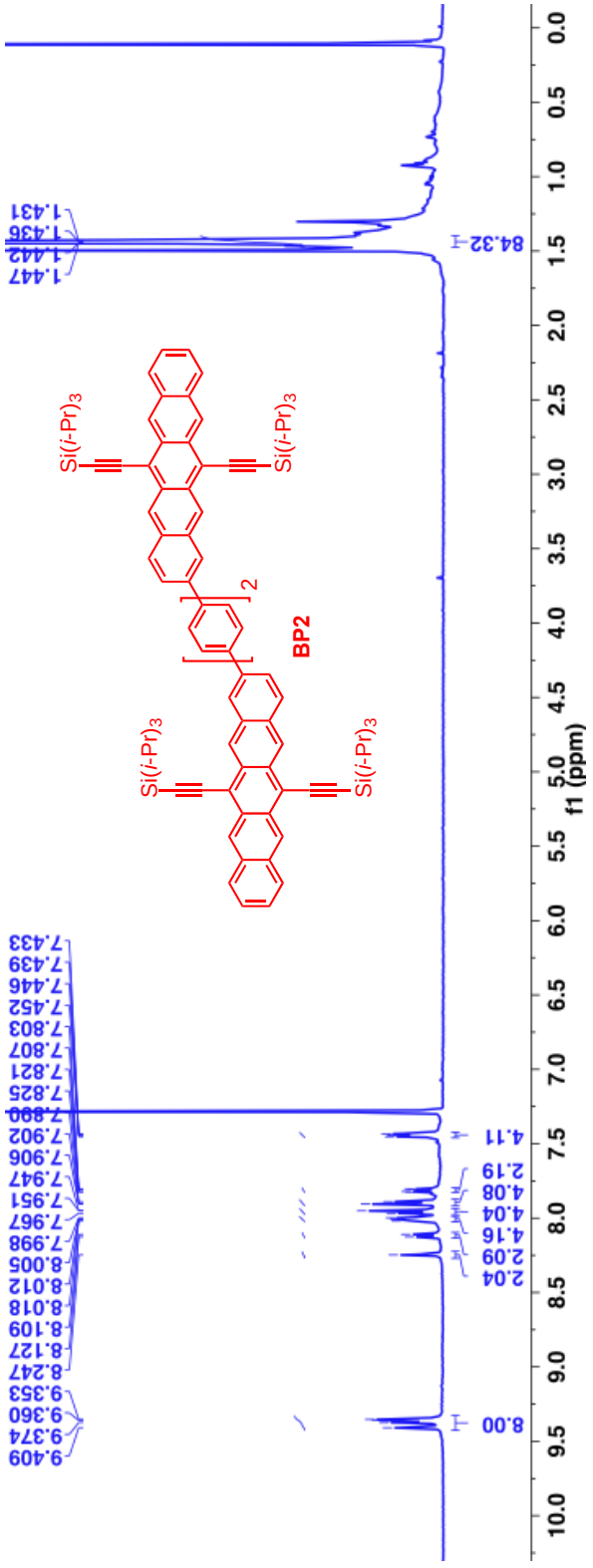
Si(i-Pr)3
Si(i-Pr)3
Si(i-Pr)3
Si(i-Pr)3
2
BP2
f1 (ppm)

2.18 Single Crystal X-Ray Diffraction

Single crystal X-ray diffraction data of **BP0** and **BP2** were collected on an Agilent SuperNova diffractometer using mirror-monochromated Cu Kα radiation. The crystals were mounted using a MiTeGen MicroMount cooled to 100 K with an Oxford-Diffraction Cryojet system. Data reduction was performed in CrysAlis.[48] Empirical correction and scaling was performed using ABSPACK, and face-indexed absorption correction was performed by analytical numeric methods.[49] Structure was solved using Superflip or ShelXS[50] and refined by full-matrix least-squares against F^2 using ShelXL[50] with the aid of Olex2.[51]

Single crystals of **BP0** were grown by slow evaporation of dichloromethane solution at room temperature for 1 week. A suitable crystal was selected and mounted with the aid of STP oil treatment and cooled to 100 K on the diffractometer. Complete data (99.2 %) was collected. 21545 reflections were collected (7221 unique, 5193 observed) with R(int) = 5.6 % and R(sigma) = 6.5 % after absorption correction (T_{max} = 0.969 and T_{min} = 0.790).

The structure was solved in P-1, and all non-H atoms were freely refined. Hydrogen atoms were placed in calculated positions and refined with riding coordinates and ADPs. The final refinement (7221 data, 427 parameters, 0 restraints) converged with R_1 ($F_o > 4\sigma(F_o)$) = 6.3 %, wR_2 = 17.8 %, S = 1.035. The largest Fourier features were 0.74 and -0.30 $e^-Å^3$.

Single crystals of **BP2** were grown by diffusion of methanol into a chloroform solution at room temperature for 5 days. A suitable crystal was selected and mounted with the aid of STP oil treatment and cooled to 100 K on the diffractometer. Complete data (98.5 %) was collected. 15442 reflections were collected (7930 unique, 5454 observed) with R(int) = 4.7 % and R(sigma) = 7.7 % after absorption correction (T_{max} = 1.000 and T_{min} = 0.894).

The structure was solved in P-1, and all non-H atoms were freely refined. Hydrogen atoms were placed in calculated positions and refined with riding coordinates and ADPs. The final refinement (7930 data, 481 parameters, 0 restraints) converged with R_1 ($F_o > 4\sigma(F_o)$) = 6.5 %, wR_2 = 18.7 %, S = 0.998. The largest Fourier features were 0.79 and -0.30 $e^-Å^3$.

Table 2.4. Selected crystallographic data for **BP0** and **BP2**

Parameter	**BP0**	**BP2**
Formula	$C_{88}H_{106}Si_4$	$C_{100}H_{114}Si_4$
MW	1276.08	1428.36
Lattice type	Triclinic	Triclinic
Space group	P-1	P-1
a (Å)	8.6287(3)	8.6151(5)
b (Å)	14.5001(6)	16.0135(11)
c (Å)	16.3117(8)	17.3223(9)
α (°)	70.296(4)	117.140(6)
β (°)	79.485(3)	90.356(5)
γ (°)	77.514(3)	101.870(5)
V ($Å^3$)	1862.55(14)	2067.4(2)
Z value	1	1

D_{calc} (g cm^{-3})	1.138	1.147
T (K)	100	100
GOF on F^2	1.035	0.998
R_1 [$F^2 > 4\sigma(F^2)$]	0.0626	0.0651
wR_2 (all data)	0.1785	0.1869

2.19 References

(1) Sanders, S. N.; Kumarasamy, E.; Pun, A. B.; Trinh, M. T.; Choi, B.; Xia, J.; Taffet, E. J.; Low, J. Z.; Miller, J. R.; Roy, X.; Zhu, X. Y.; Steigerwald, M. L.; Sfeir, M. Y.; Campos, L. M. *J. Am. Chem. Soc.* **2015**, *137*, 8965.

(2) Green, M. A. *Prog. Photovolt: Res. Appl.* **2001**, *9*, 123.

(3) Nozik, A. J. *Phys. E* **2002**, *14*, 115.

(4) Shockley, W.; Queisser, H. J. *J. Appl. Phys.* **1961**, *32*, 510.

(5) Singh, S.; Jones, W. J.; Siebrand, W.; Stoicheff, B. P.; Schneider, W. G. *J. Chem. Phys* **1965**, *42*, 330.

(6) Congreve, D. N.; Lee, J.; Thompson, N. J.; Hontz, E.; Yost, S. R.; Reusswig, P. D.; Bahlke, M. E.; Reineke, S.; Van Voorhis, T.; Baldo, M. A. *Science* **2013**, *340*, 334.

(7) Hanna, M. C.; Nozik, A. J. *J. Appl. Phys.* **2006**, *100*, 074510.

(8) Lee, J.; Jadhav, P.; Baldo, M. A. *Appl. Phys. Lett.* **2009**, *95*, 033301.

(9) Lee, J.; Jadhav, P.; Reusswig, P. D.; Yost, S. R.; Thompson, N. J.; Congreve, D. N.; Hontz, E.; Van Voorhis, T.; Baldo, M. A. *Acc. Chem. Res.* **2013**, *46*, 1300.

(10) Yost, S. R.; Lee, J.; WilsonMark, W. B.; Wu, T.; McMahon, D. P.; Parkhurst, R. R.; Thompson, N. J.; Congreve, D. N.; Rao, A.; Johnson, K.; Sfeir, M. Y.; Bawendi, M. G.; Swager, T. M.; Friend, R. H.; Baldo, M. A.; Van Voorhis, T. *Nat. Chem.* **2014**, *6*, 492.

(11) Chan, W.-L.; Ligges, M.; Jailaubekov, A.; Kaake, L.; Miaja-Avila, L.; Zhu, X.-Y. *Science* **2011**, *334*, 1541.

(12) Chan, W.-L.; Berkelbach, T. C.; Provorse, M. R.; Monahan, N. R.; Tritsch, J. R.; Hybertsen, M. S.; Reichman, D. R.; Gao, J.; Zhu, X. Y. *Acc. Chem. Res.* **2013**, *46*, 1321.

(13) Zeng, T.; Hoffmann, R.; Ananth, N. *J. Am. Chem. Soc.* **2014**, *136*, 5755.

(14) Pensack, R. D.; Tilley, A. J.; Parkin, S. R.; Lee, T. S.; Payne, M. M.; Gao, D.; Jahnke, A. A.; Oblinsky, D.; Li, P.-F.; Anthony, J. E.; Seferos, D. S.; Scholes, G. D. *J. Am. Chem. Soc.* **2015**, *137*, 6790.

(15) Piland, G. B.; Bardeen, C. J. *J. Phys. Chem. Lett.* **2015**, 1841.

(16) Roberts, S. T.; McAnally, R. E.; Mastron, J. N.; Webber, D. H.; Whited, M. T.; Brutchey, R. L.; Thompson, M. E.; Bradforth, S. E. *J. Am. Chem. Soc.* **2012**, *134*, 6388.

(17) Mastron, J. N.; Roberts, S. T.; McAnally, R. E.; Thompson, M. E.; Bradforth, S. E. *J. Phys. Chem. B* **2013**, *117*, 15519.

(18) Gradinaru, C. C.; Kennis, J. T. M.; Papagiannakis, E.; van Stokkum, I. H. M.; Cogdell, R. J.; Fleming, G. R.; Niederman, R. A.; van Grondelle, R. *Proc. Nat. Acad. Sci.* **2001**, *98*, 2364.

(19) Musser, A. J.; Al-Hashimi, M.; Maiuri, M.; Brida, D.; Heeney, M.; Cerullo, G.; Friend, R. H.; Clark, J. *J. Am. Chem. Soc.* **2013**, *135*, 12747.

(20) Trinh, M. T.; Zhong, Y.; Chen, Q.; Schiros, T.; Jockusch, S.; Sfeir, M. Y.; Steigerwald, M.; Nuckolls, C.; Zhu, X. *J. Phys. Chem. C* **2015**, *119*, 1312.

(21) Busby, E.; Xia, J.; Wu, Q.; Low, J. Z.; Rong, R.; Miller, J. R.; Zhu, X.-Y.; Campos, L. M.; Sfeir, M. Y. *Nat. Mater.* **2014**, *14*, 426.

(22) Varnavski, O.; Abeyasinghe, N.; Aragó, J.; Serrano-Pérez, J. J.; Ortí, E.; López Navarrete, J. T.; Takimiya, K.; Casanova, D.; Casado, J.; Goodson, T. *J. Phys. Chem. Lett.* **2015**, *6*, 1375.

(23) Burdett, J. J.; Bardeen, C. J. *Acc. Chem. Res.* **2013**, *46*, 1312.

(24) Vallett, P. J.; Snyder, J. L.; Damrauer, N. H. *J. Phys. Chem. A.* **2013**, *117*, 10824.

(25) Müller, A. M.; Avlasevich, Y. S.; Müllen, K.; Bardeen, C. J. *Chem. Phys. Lett.* **2006**, *421*, 518.

(26) Müller, A. M.; Avlasevich, Y. S.; Schoeller, W. W.; Müllen, K.; Bardeen, C. J. *J. Am. Chem. Soc.* **2007**, *129*, 14240.

(27) Smith, M. B. M., J. *Chem. Rev.* **2010**, *110*, 6891.

(28) Greyson, E. C.; Vura-Weis, J.; Michl, J.; Ratner, M. A. *J. Phys. Chem. B.* **2010**, *114*, 14168.

(29) Smith, M. B.; Michl, J. *Annu. Rev. Phys. Chem.* **2013**, *64*, 361.

(30) Zirzlmeier, J.; Lehnherr, D.; Coto, P. B.; Chernick, E. T.; Casillas, R.; Basel, B. S.; Thoss, M.; Tykwinski, R. R.; Guldi, D. M. *Proc. Natl Acad. Sci.* **2015**, *112*, 5325.

(31) Greyson, E. C.; Stepp, B. R.; Chen, X.; Schwerin, A. F.; Paci, I.; Smith, M. B.; Akdag, A.; Johnson, J. C.; Nozik, A. J.; Michl, J.; Ratner, M. A. *J. Phys. Chem. B* **2009**, *114*, 14223.

(32) Fudickar, W.; Linker, T. *J. Am. Chem. Soc.* **2012**, *134*, 15071.

(33) Lehnherr, D.; Tykwinski, R. R. *Materials* **2010**, *3*, 2772.

(34) Walker, B. J.; Musser, A. J.; Beljonne, D.; Friend, R. H. *Nat. Chem.* **2013**, *5*, 1019.

(35) Snellenburg, J. J. L., S. P.; Seger, R.; Mullen, K. M.; van Stokum, I. H. M. *J. Stat. Softw.* **2012**, *49*, 1.

(36) Poletayev, A. D.; Clark, J.; Wilson, M. W. B.; Rao, A.; Makino, Y.; Hotta, S.; Friend, R. H. *Adv. Mater.* **2014**, *26*, 919.

(37) Bensasson, R.; Land, E. J. *Trans. Faraday Soc.* **1971**, *67*, 1904.

(38) Turro, N. J. *Modern Molecular Photochemistry*; University Science Books, 1991.

(39) Rettig, W. *Angewandte Chemie International Edition in English* **1986**, *25*, 971.

(40) Rettig, W. *J. Mol. Struct.* **1982**, *84*, 303.

(41) Grabowski, Z. R.; Rotkiewicz, K.; Siemiarczuk, A. *J. Lumin.* **1979**, *18–19, Part 1*, 420.

(42) Fery-Forgues, S.; Fayet, J.-P.; Lopez, A. *Journal of Photochemistry and Photobiology A: Chemistry* **1993**, *70*, 229.

(43) Marciniak, H.; Pugliesi, I.; Nickel, B.; Lochbrunner, S. *Phys. Rev. B* **2009**, *79*, 235318.

(44) Eaton, S. W.; Shoer, L. E.; Karlen, S. D.; Dyar, S. M.; Margulies, E. A.; Veldkamp, B. S.; Ramanan, C.; Hartzler, D. A.; Savikhin, S.; Marks, T. J.; Wasielewski, M. R. *J. Am. Chem. Soc.* **2013**, *135*, 14701.

(45) Resch-Genger, U. R., Knut *Pure Appl. Chem.* **2013**, *85*, 2005.

(46) Brouwer, A. M. *Pure Appl. Chem.* **2011**, *83*, 2213.

(47) Plunkett, K. N.; Godula, K.; Nuckolls, C.; Tremblay, N.; Whalley, A. C.; Xiao, S. *Org. Lett.* **2009**, *11*, 2225.

(48) Busing, W. R.; Levy, H. A. *Acta Crystallographica* **1957**, *10*, 180.

(49) Clark, R. C.; Reid, J. S. *Acta Crystallogr A* **1995**, *51*, 887.

(50) Sheldrick, G. M. *Act. Cryst. A* **2008**, *64*, 112.

(51) Dolomanov, O. V.; Bourhis, L. J.; Gildea, R. J.; Howard, J. A. K.; Puschmann, H. *J Appl Crystallogr* **2009**, *42*, 339.

3 Properties of Poly- and Oligo-Pentacenes Synthesized from Modular Building Blocks

3.1 Preface

This chapter is based on a manuscript entitled "Properties of Poly- and Oligo-Pentacenes Synthesized from Modular Building Blocks" published in *Macromolecules*, authored by Elango Kumarasamy, Samuel N. Sanders, Andrew B. Pun, Saeed Ahmadi Vaselabadi, Jonathan Z. Low, Matthew Y. Sfeir, Michael L. Steigerwald, Gila Stein, and Luis M. Campos. Elango and I synthesized all the molecules with assistance from Andrew Pun. Saeed from the Stein group performed the X-Ray diffraction measurements and analysis. I collected all absoption spectra, while Matthew and Michael provided invaluable analysis of these spectra. Michael performed all calculations, while Jonathan was responsible for cyclic voltammetry measurements.

3.2 Introduction

Acenes are of great interest in the field of organic electronics due to their tunable optoelectronic properties, high charge carrier mobilities, and the observation of singlet exciton fission (SF) in crystals of tetracene and higher acenes.[1-10] Pentacene is of particular interest, as it is a benchmark material for organic field effect transistors (OFETs) and organic photovoltaics (OPVs), as well as fundamental studies of various optoelectronic properties.[11-15] However, pentacene has only limited stability and solubility in common organic solvents and is unstable in the presence of oxygen,[16] making it difficult to process by high throughput techniques.[3,17,18] To overcome these limitations, several functionalized pentacenes have been reported, which exhibit

enhanced solubility, stability, and tunable electronic properties.[12,19,20] Despite these improvements, over the course of nearly 80 years of significant research in pentacene chemistry and physics, there has been only one report of short conjugated oligomers, a scarce number of conjugated pentacene-containing polymers, and a pentacene homopolymer remains unknown.[21-26] In order to understand the effects of increasing the oligomerization length on the fundamental properties of oligomers and polymers of pentacenes, we developed building blocks to access oligomers (2-7) as well as polypentacene.

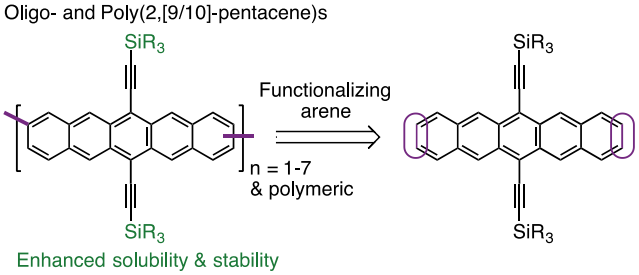

Scheme 3.1. Strategy for end functionalization of pentacene oligomers

Obtaining well-defined oligomeric materials is particularly attractive because they reveal detailed structure-property relationships, as in the case of thiophenes.[27-32] To date, pentacene has only been incorporated in alternating copolymers or as a pendant group on a polymer chain, not as a homopolymer.[21-26] Tykwinski and co-workers developed an attractive strategy where the pentacenes were not directly coupled, but included a diacetylene spacer in an alternating fashion linked at the 6 and 13 positions.[24] Unfortunately, higher oligomers (n > 4) could not be synthesized employing this strategy due to limited solubility, which results from the decreasing ratio of the solubilizing trialkylsilane unit to pentacene, upon oligomerization. This decreasing ratio can also be detrimental to stability, as the bulky alkylsilyl groups protect against the primary degradation pathways of dimerization and photo-oxidation.[19] An alternative strategy is needed to access higher

oligomers of conjugated pentacene and polypentacene in order to study the optoelectronic properties. Our strategy, shown in Scheme 3.1, employs coupling at the 2,[9/10] positions, which allows us to retain the solubilizing/stabilizing functionalities at the 6 and 13 positions on every monomer unit in the oligomer. This strategy overcomes previous limitations, finally allowing for synthesis and characterization of well-defined conjugated oligomers of pentacenes (n= 1-7), in addition to a soluble homopolymer of pentacene by step-growth polymerization.

3.3 Synthesis

The building blocks shown in Scheme 3.2 were designed to access well-defined pentacene oligomers and polypentacene, which are synthesized in multi-gram scales, and are soluble and stable. All materials stem from the primary pentacenes **1A** and **1A2**,[22] which are borylated to **1B** and **1B2** under mild conditions. Using these four primary building blocks, the secondary and tertiary building blocks are synthesized in good yields. Subsequent palladium-catalyzed cross-couplings in the combinations shown in Scheme 3.2 yield the oligopentacenes of interest.

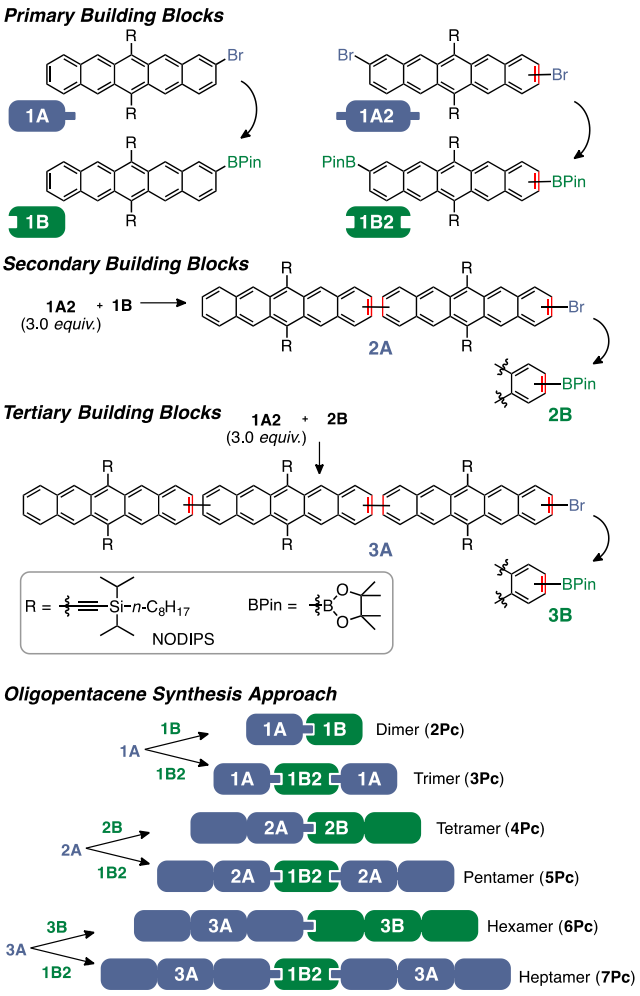

Scheme 3.2. Primary, secondary and tertiary building blocks used in our oligomer synthesis

Our initial attempts to synthesize oligopentacenes contained triisopropylsilylethynyl groups (TIPS) as the solubilizing unit. Unfortunately, TIPS was not sufficiently solubilizing for pentacene oligomers with more than three repeat units. To overcome this problem, we turned to *n*-octyl-diisopropylsilylethynyl (NODIPS), which Anthony and co-workers had previously demonstrated as a better solubilizing group for pentacenes.[33] The synthesis of the pentacene core has been well-established in the literature.[34-45] The oligopentacenes exhibit excellent solubility in solvents such as THF and chlorinated solvents (DCM and chloroform).

While this synthetic strategy is modular in nature and allows synthesis of higher oligomers, the products are regioisomeric mixtures because **1A2** is a mixture of 2,9-dibromopentacene (*anti*) and 2,10-dibromopentacene (*syn*) derivatives. We were interested in exploring the effect of this regioisomerism on the properties of the resultant oligomers. The two regioisomers of the trimer, ***syn*-3Pc** and ***anti*-3Pc** (Scheme 3.3), were synthesized using Bao and coworker's selective crystallization strategy for regiopure *syn* and *anti*-dibromopentacenequinone.[46] We compare the properties of these regiopure trimers below. Beyond trimer, exhaustive exploration of possible regioisomers was precluded by the exponentially increasing number of regioisomers, as well as the many steps and difficulties in acquiring large quantities of regiopure dibromoquinone starting material.

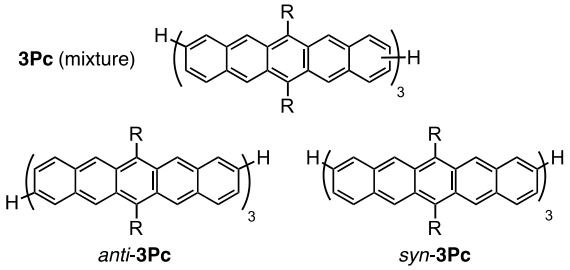

Scheme 3.3. Illustration of the possible regioisomers of the pentacene trimer

The oligomers up to **3Pc** were readily characterized by NMR spectroscopy and high-resolution mass spectrometry. However, NMR spectroscopic characterization of oligomers >**4Pc** was hampered by peak broadening which was prevalent even at elevated temperature (^{1}H-NMR at 50 °C). This peak broadening is the result of several factors such as the presence of regioisomers, similar location of aromatic protons on adjacent pentacenes and decreasing symmetry in higher oligomers. In order to definitively assign the identity of the oligomers **4-7Pc**, ^{1}H-NMR was corroborated by MALDI mass spectrometry.

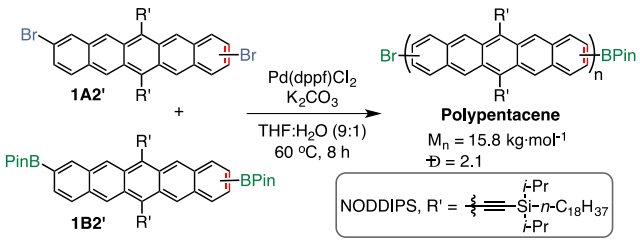

Scheme 3.4. Synthetic conditions used to prepare polypentacene

An effort to obtain polypentacene was carried out by step-growth polymerization of **1A2** and **1B2**. The initial attempt on polymerization at 65 °C for 3 days resulted in an insoluble black solid. Reduction of the temperature or reaction time only resulted in oligomers of pentacenes as determined by mass spectrometry. This result indicated that the NODIPS chain is insufficient to produce soluble polypentacenes.

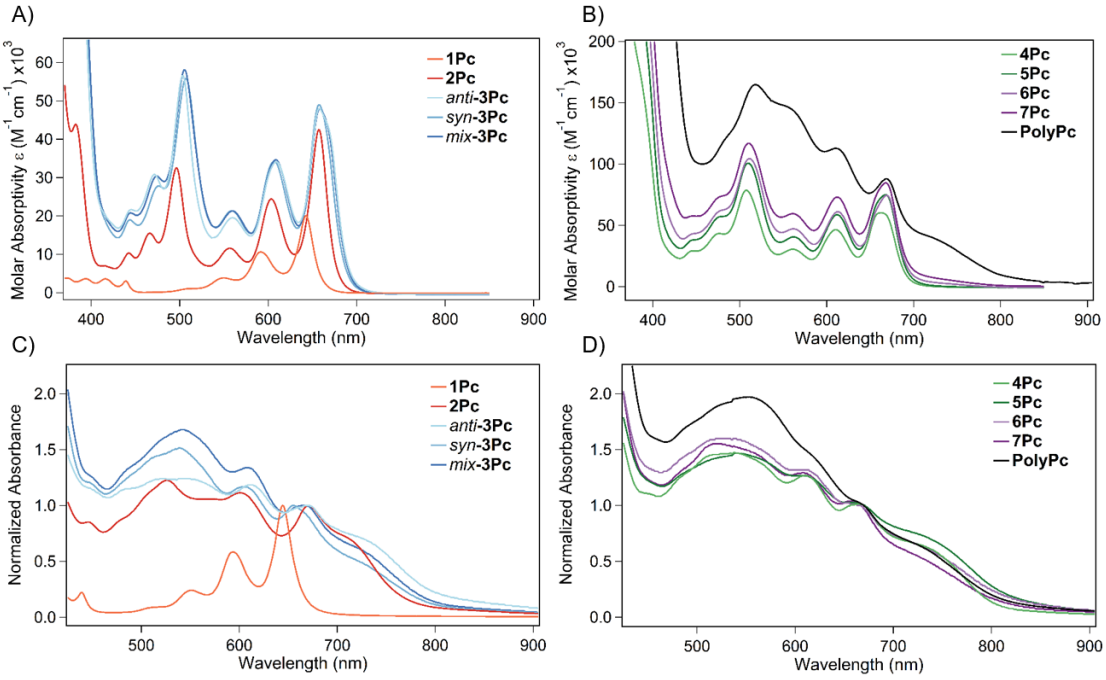

Figure 3.1. A) UV-vis spectra of oligomers 1Pc-3Pc measured in chloroform (12.5 μM). **B)** UV-vis of oligomers 4Pc-7Pc (12.5 μM) and PolyPc (arbitrary units for comparison) measured in chloroform. **C)** and **D)** UV-Vis of oligomers and PolyPc, drop cast from chloroform on a glass slide and plotted with the onset of absorption peak near 670 nm normalized to a value of 1.

We therefore substituted the C-8 chain in NODIPS with a C-18 chain to create the stronger solubilizing group, *n*-octadecyl-diisopropylsilylethynyl (NODDIPS). The polymerization was carried out between **1A2′** and **1B2′** at 60 °C to obtain a pentacene homopolymer (Scheme 3.4). The reaction time was limited to 8 h to access soluble polymers. The reaction mixture was precipitated into methanol and the solid was purified by Soxhlet extraction, consecutively with hexanes, chloroform and chlorobenzene. The molecular weight of the polypentacene from the chlorobenzene fraction was determined by gel permeation chromatography (GPC) using hot 1,2,4-trichlorochlorobenzene (150 °C) as the eluent against polyethylene standards. The polypentacene was found to have a number average molecular weight (M_n) of ~15.8 kg·mol^{-1} with Đ = 2.1.

3.4 Steady State Absorption

The optical properties of oligomers **1**-**7Pc**, regiopure **3Pc** and polypentacene were probed by steady state UV-visible absorption spectroscopy in solution and in thin-films (Figure 3.1). In solution, the oligomer spectra of **2Pc** through **7Pc** are qualitatively similar, with minimal redshift as the number of pentacenes increases. Notably, in solution, there are only minute differences in the UV-vis spectra of *syn*-**3Pc**, *anti*-**3Pc** and *mix*-**3Pc**. In the longer wavelength region (>550 nm) the oligomers all resemble the absorption spectrum of the monomer. However, in the dimer and each of the higher oligomers a new set of absorption peaks appear between 425 nm and 550 nm (which we interpret as a vibrational progression associated with a fundamental absorption described below). These peaks have not been previously observed in other pentacene-containing materials. The height of this new absorption maximum, relative to the height of the peak at the

onset of absorption, increases with oligomer length. The strong similarity of the long-wavelength region in the oligomers to that of the monomer lead us to conclude that these long-wavelength features in all of these molecules are due to intra-pentacene vibrational progressions. We verified this conclusion with electronic structure calculations on **1Pc**, **2Pc**, **3Pc**, and **4Pc**.

3.5 DFT Calculations

Excited state (TD-DFT) calculations suggest that the absorption peak at 650 nm in the monomer is due to the fundamental HOMO-to-LUMO transition. However, corresponding calculations on the dimer reveal a more complex situation. The HOMO in the dimer comprises two parts: one that resembles what would be the HOMO localized on one isolated pentacene ($homo_L$ in Figure 3.2), and another that resembles what would the HOMO on the other isolated pentacene ($homo_R$ in Figure 3.2). In the full HOMO and HOMO-1 of the molecule, these orbitals are combined with different phases: the HOMO is ($homo_L$ - $homo_R$), and the HOMO-1 is ($homo_L$ + $homo_R$). The situation for the lowest-energy unoccupied orbitals is similar: the molecular LUMO is approximated by (($lumo_L$ + $lumo_R$), and the molecular LUMO+1 by ($lumo_L$ - $lumo_R$). We propose that the lower-energy transition in the dimer effectively promotes an electron from the HOMO to the LUMO, and the higher-energy transition effectively promotes an electron from the HOMO-1 to the LUMO+1.

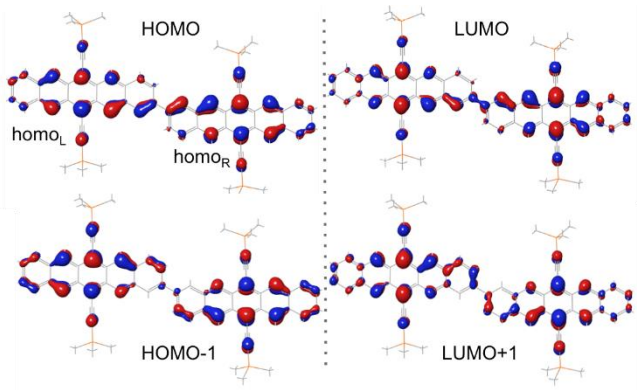

Figure 3.2. Highest occupied and lowest unoccupied molecular orbitals (HOMO and LUMO, respectively), along with the +1 and -1 orbitals.

The source of the energy separation between the two transitions lies in the nexus of the two pentacenes. In the HOMO there is a π-antibonding interaction between the two C atoms that form the pentacene-pentacene link; in the LUMO there is a π-bonding interaction in that space. By comparison in the HOMO-1 there is a π-bond between these two C atoms, and in the LUMO+1 there is a π-antibond. Thus the two "HOMO-to-LUMO" excitations are split by the formation versus destruction of the inter-pentacene π-interaction. In the lower-energy transition an unfavorable interaction is relieved in the ground state and a favorable interaction realized in the excited state; in the higher-energy transition the reverse is the case. We believe that similar effects occur in the higher oligomers. A complete discussion of these cases is complicated, particularly by the many geometrical degrees of freedom available to the higher oligomers. We will report more detailed results of these studies separately.

In the solution UV-vis, a modest red-shift of the onset of absorption is observed in the highest (n>4) oligomers, indicating weak aggregation in chloroform. This aggregation is weakly concentration dependent, as expected, and strongly solvent dependent. For example, less

aggregation was observed in solvents such as toluene, tetrachloroethylene and chloroform, while significant aggregation was observed in hexanes.

3.6 Solid-State Absorbance Spectra

Solid-state absorbance spectra were also obtained by drop casting oligomers on to a glass slide from chloroform. In the monomer **1Pc**, the solution and solid-state spectra are nearly identical, indicating that the bulky NODIPS chains effectively prevent any significant crystallinity in the solid state and result in a highly amorphous solid. On the other hand, starting from the dimer containing NODIPS, a large degree of interaction is evidenced in the solid-state UV-vis, presumably due to a "bricklayer" type packing that we have previously observed in the crystal structure of the dimer and possible for all oligomers beyond the monomer, **1Pc**. This interaction results in a loss of the clear vibronic peaks present in solution, as well as a significant red-shift of the absorption onset. Such significant solid-state interaction in these higher oligomers bodes well for their potential in electronic applications, where strong interactions resulting from planarity and π-π stacking are typically desirable for organic materials.[47,48] These strong interactions also help to explain the dramatic loss of solubility between monomeric TIPS-pentacene and the TIPS-pentacene dimer, which necessitated the use of the more solubilizing NODIPS chain for higher oligomers. Notably, there are fairly significant differences in the solid-state spectra of *syn*-**3Pc**, *anti*-**3Pc** and mixture of trimers, despite their similarity in solution. These differences are therefore attributable to different capacities for effective solid-state packing, as confirmed by grazing-incidence wide-angle x-ray scattering (GIWAXS), vide infra. However, beyond the trimer, there are only subtle differences among oligomers 4-7**Pc**, suggesting that these longer oligomers are starting to converge in their characteristics towards that of a polymer.

3.7 Photostability

Acenes are notorious for their degradation in presence of light and oxygen. Longer oligoacenes are also particularly susceptible to intermolecular Diels-Alders reactions upon thermal activation. To investigate the stability of oligopentacenes towards such undesirable processes, we carried out a qualitative photodegradation study involving irradiation of solutions of **1**-**3Pc** in the presence of oxygen at similar molarities with respect to pentacene monomer. The results indicate a significantly enhanced stability of oligomers relative to that of the monomer. The stark difference in stability enhancement may have its origin from the shortened excited state lifetime of the oligopentacenes and/or ultrafast deactivation of any photodegradation pathways specific to the singlet exciton. More comprehensive studies to understand the underpinnings of the stability of oligo- and poly-pentacenes are currently underway in our group.

3.8 Cyclic Voltametry

In order to investigate how the energy levels vary as a function of oligomer length, we carried out cyclic voltammetry to determine the oxidation and reduction potentials. The good solubility of the oligopentacenes enabled their measurement in dichloromethane against a Ag/Ag^+ reference. The highest occupied molecular orbital (HOMO) and lowest unoccupied molecular orbital (LUMO) levels were obtained by calibrating the onset of oxidation (or reduction, for LUMO) to the Fc/Fc^+ couple (Figure 3.3).[49] The convergence of the band gap in this oligopentacene series is evident both from the frontier energy levels and from the UV-vis data. Similar to the oligopentacenes linked by the central ring reported by Lehnherr et al., polymer-like behavior is approached starting

at **4Pc**.[24] The band gap decrease is a result of the HOMO being raised as successive pentacene units are added, while the LUMO remains fairly constant. The raising of the HOMO level with increasing oligomer length has also been reported for phenylene[50] and thiophene systems.[27] Repeated scans revealed that the compounds all display good redox stability within the potential window measured, with the exception of the heptamer which had an irreversible reduction wave.

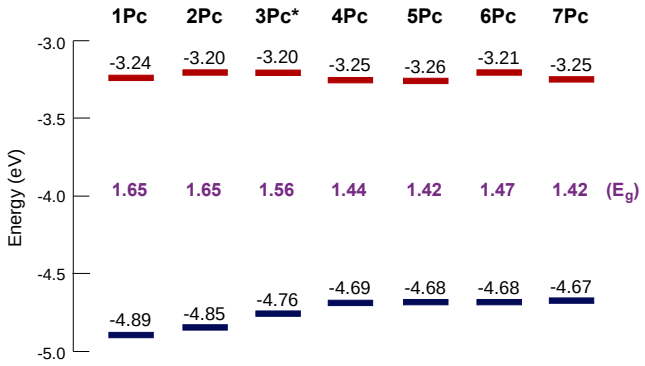

Figure 3.3. Electrochemical properties of oligopentacenes obtained from cyclic voltammetric studies. 3Pc* indicates the sample used was mix-3Pc.

3.9 Thermal Properties

Thermal gravimetric analysis (TGA) revealed excellent thermal stability of these pentacene oligomers, with all compounds exhibiting a decomposition temperature (T_d) of at least 370 °C under nitrogen flow. A summary of these values can be seen in Table 1. As the oligomer length increases there is no appreciable change in the T_d of the compounds, which is likely attributable to the almost identical empirical chemical formula of the oligomers. For example, the smallest oligomer (**2Pc**) has a T_d of 371 °C, while the largest oligomer, (**7Pc**) has a T_d of 382 °C.

The thermal transitions of these materials were studied by differential scanning calorimetry (DSC). Only **2Pc** exhibited phase transitions, with a glass transition temperature of 134 °C and a

melting point of 166 °C. However these transitions are only observed in the first heating cycle, due to the decomposition that is observed after the compound reaches its melting point under oxygen at high temperature. These non-reversible phase transitions agree with DSC performed on similar materials.[33] For the larger oligomers, no phase transitions were observed within the range of temperatures explored.

Table 3.1. Thermal properties of oligopentacene obtained by Thermogravimetric analysis (TGA)

Entry	Compound	Decomposition temperature, T_d [°C]
1	**2Pc**	371
2	Mixture-**3Pc**	373
3	*anti*-**3Pc**	374
4	*syn*-**3Pc**	372
5	**4Pc**	374
6	**5Pc**	380
7	**6Pc**	380
8	**7Pc**	382

The measurement was carried out under constant flow of nitrogen with heating rate of 10°C /min.

In order to gain insights into the packing interactions of these materials, grazing incidence wide angle X-ray scattering (GIWAXS) data was collected for all oligopentacene films at incidence angles in the range of 0.2-0.22°, which is above the critical angle of the oligopentacenes (ca. 0.17°) and below the critical angle of the substrate (ca. 0.24°). The crystal structure of these NODIPS-functionalized oligopentacenes has not been previously reported, and the crystalline content of these samples is too low for a detailed analysis (i.e., too few diffraction peaks). However, we have previously reported the crystal structure of **2Pc** where the TIPS solubilizing groups are used.[51] This compound, and several other classes of functionalized acenes[16,52-54] exhibit a triclinic unit cell (space group $P\bar{1}$) in bulk and thin films. We used these studies to guide interpretation of our data.

First, we investigate the morphology of the regiopure trimers and compare it to the mixed product to understand how any differences may arise from these two classes of materials. Figure 3.4A displays GIWAXS data for the annealed *anti*-**3Pc** thin film, and Figure 3.4B shows the out-of-plane line cuts ($q_y = 0$) of the same oligomer before and after annealing at 200 °C for 30 min. The 2D scattering pattern is largely diffuse, meaning the film has a high amorphous content, but there are signatures of oriented crystallites along the out-of-plane *z*-axis (spots/arcs along q_z rather than isotropic rings). Diffraction peaks in the as-cast film are weak and broad along the q_z axis, but annealing increases their intensity and narrows the line shape, which demonstrates that crystallinity is enhanced with heat treatment. Moreover, the first-order peak is detected at $q_z^* = 0.52$ Å^{-1}, corresponding with a periodicity of $d = 2\pi/q_z^* = 12.1$ Å, and higher-order peaks are detected at $2q_z^* = 1.05$ Å^{-1} and $3q_z^* = 1.58$ Å^{-1}. Using the lattice parameters for **1Pc**,[33] we attribute these peaks to scattering from {002} and {003} planes. A comparison between the predicted and observed values is included in Table 2. An additional peak is observed at $q_z = 1.33$ Å^{-1},

corresponding to an interlayer periodicity of 0.47 Å, which is consistent with scattering from {111} planes. Scattering from {001} planes is indicative of an edge-on crystallite orientation, where the direction of π-π stacking is in the plane of the film.

Table 3.2. Predicted positions of diffraction peaks for 6,13-bis(diisopropyloctylsilylethynyl)pentacene[33] and measured positions for *anti*-3Pc.

Plane	Predicted q_z (Å^{-1})	Measured q_z (Å^{-1})	Measure d d (Å)
(001)	0.51	0.52	12.1
(002)	1.03	1.05	0.60
(111)	1.24	1.33	0.47
(003)	1.54	1.58	0.40

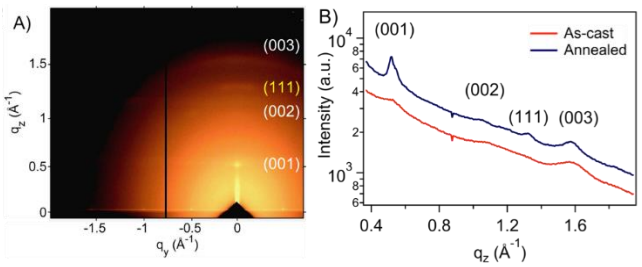

Figure 3.4. A) 2D GIWAXS patterns of the annealed *anti*-3Pc film (incident tangle α_i= 0.22°). **B)** Scattering profiles of as-cast and annealed *anti*-pentacene trimer (*anti*-3Pc) along the q_z-axis at q_y = 0 (out-of-plane profile).

Scattering from {111} planes is associated with a face-on orientation that is less favorable for transistors. *anti*-**3Pc** Adopts both of these orientations, which is consistent with other thin film studies of functionalized acenes.[33,52] Figure 3.5 summarizes the out-of-plane intensity profiles for all the oligopentacenes considered in this report. The highest crystallinity is observed in the annealed trimer series, where it is higher in the order *anti*-**3Pc** > mix-**3Pc** > *syn*-**3Pc**. All other higher oligomers (**4Pc**-**7Pc**) materials exhibit very low crystallinity, and annealing has little or no impact on ordering. This observation is reasonable as more regioisomers are created for higher oligomers, which can alter packing interactions. Understanding these fundamental details of poly- and oligo-pentacenes will be important in to design the appropriate architectures for device fabrication.

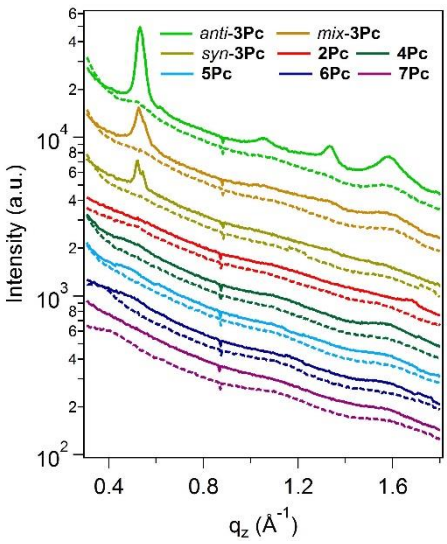

Figure 3.5. Out-of-plane line cuts I(q_z) for as-cast (dashed lines) and thermally annealed (at 200°C, solid lines) oligopentacene films. Incidence angle is $\alpha_i = 0.20°$.

3.10 Conclusions

We report a facile and scalable method for the synthesis of solution processable higher oligomers of pentacenes (**2Pc**-**7Pc**), in addition to the first pentacene homopolymer. Exploiting the arene functional handle allows for a constant ratio of solubilizing/stabilizing units to pentacene as oligomer length increases, which results in excellent solubility in common organic solvents. Importantly, regiopure pentacene trimers (*syn*-**3Pc** and *anti*-**3Pc**) were also synthesized and compared to the regiomixture trimer (*mix*-**3Pc**), revealing several interesting characteristics: while there were no significant changes in the solution UV-vis spectroscopy, the solid-state UV-vis signature was strongly affected by regioisomerism. We showed that changes are attributable to the different packing interactions of the different regioisomers, as characterized by GIWAXS. The crystallinity of *anti*-**3Pc** was significantly greater than *mix*-**Pc** and *syn*-**Pc**. GIWAXS also revealed minimal ordering in the higher oligomers, likely due to the presence of a large number of

regioisomers. In all cases, crystalline order was increased upon thermal annealing. The solution UV-vis spectroscopy revealed the occurrence of high-energy peak in the region between 425 nm and 550 nm that intensifies as the length of the oligomer increases. This absorption, which effectively increases the absorption profile in the visible region, is attributed to an inter-pentacene π to π^* transition. Cyclic voltammetry revealed an increase in the HOMO level for each homologous addition of pentacene, with polymer-like behavior approached at an oligomer length of four. The DSC and TGA experiments reveal that the oligopentacenes are thermally stable and have consistent decomposition temperature irrespective of oligomer length (371-382 °C). Except for **2Pc**, all the oligomers displayed no phase transition during the heating cycle while **2Pc** had non-reversible phase transition. The application of these oligo/polypentacenes in various semiconductor applications and determination of charge transport properties are currently under progress.

3.11 General Methods

General Methods: All commercially obtained reagents/solvents were used as received; chemicals were purchased from Alfa Aesar®, Sigma-Aldrich®, Acros organics®, TCI America®, Mallinckrodt®, and Oakwood® Products, and were used as received without further purification. Unless stated otherwise, reactions were conducted in oven-dried glassware under argon atmosphere. Anhydrous solvents were obtained from a Schlenk manifold with purification columns packed with activated alumina and supported copper catalyst (Glass Contour, Irvine, CA). All reactions were carried out under argon unless otherwise noted. ^{1}H-NMR and ^{13}C-NMR spectra were recorded on Bruker 400 MHz (100 MHz for ^{13}C) and on 500 MHz (125 MHz for ^{13}C)

spectrometers. Data from the ^{1}H-NMR and ^{13}C spectroscopy are reported as chemical shift (δ ppm) with the corresponding integration values. Coupling constants (*J*) are reported in hertz (Hz). Standard abbreviations indicating multiplicity were used as follows: s (singlet), b (broad), d (doublet), t (triplet), q (quartet), m (multiplet) and virt (virtual).

The mass spectral data for the compounds were obtained from XEVO G2-XS Waters® equipped with a QTOF detector with multiple inlet and ionization capabilities including electrospray ionization (ESI), atmospheric pressure chemical ionization (APCI), and atmospheric solids analysis probe (ASAP). The base peaks were usually obtained as $[M]^{+}$ or $[M+H]^{+}$ ions. MALDI measurements were carried out in Bruker UltrafleXtreme MALDI-TOF/TOF instrument. Samples were diluted in 0.5 mL of dichloromethane. 1 μL of sample was spotted onto MALDI target and 1ul of matrix was added (Dithranol, α-Cyano-4-hydroxycinnamic acid). Samples were analyzed on with various different methods such as different laser settings, detector settings, negative/positive ion mode.

Absorption spectra were obtained on a Shimadzu UV 1800 UV-Vis spectrophotometer. The TGA analysis was carried out in q500-2210 TA instrument. Differential Scanning Calorimetry (DSC) was performed on a TA Instruments DSC Q2000 fitted with a RCS90 refrigerated cooling system to determine the glass transition temperatures. DSC measurements were taken at a sampling rate of 10 °C/min in the temperature range of 0°C to 140°C. Photodegradation studies were performed using a UVP Black-Ray® bench lamp (115v, ~60Hz, 0.68 amps) fitted with two ~352 nm lamp (Sankyo Denki blacklight, 15W).

Gel permeation chromatography (GPC) analyses were carried out using an Agilent PL-GPC 50 integrated system (2 x PLgel Mini-MIX C columns, 5 micron, 4.6 mm ID) equipped with UV

and refractive index detectors. The GPC columns were eluted at a rate of 1.0 mL/min with 1,2,4-trichlorobenzene (150 ^{o}C) and were calibrated relative to monodisperse polyethylene standards.

3.12 General Protocol for the Synthesis of Oligopentacenes:

Synthesis of building blocks for oligopentacenes:

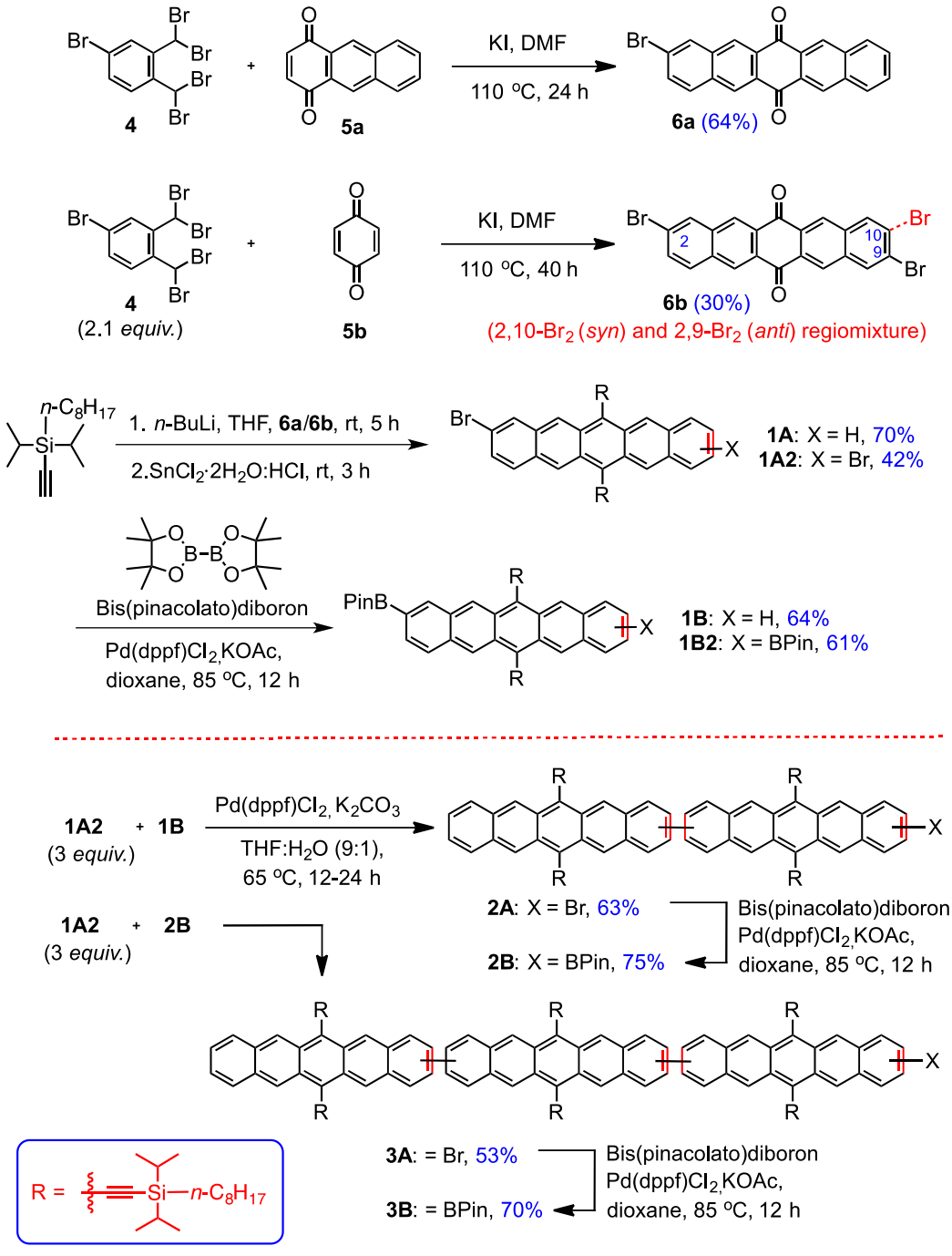

The compounds **6a-b** were synthesized according to a procedure reported in the literature.[22,34]

General Protocol for the synthesis of regiopure dibromo pentacenes 1A2

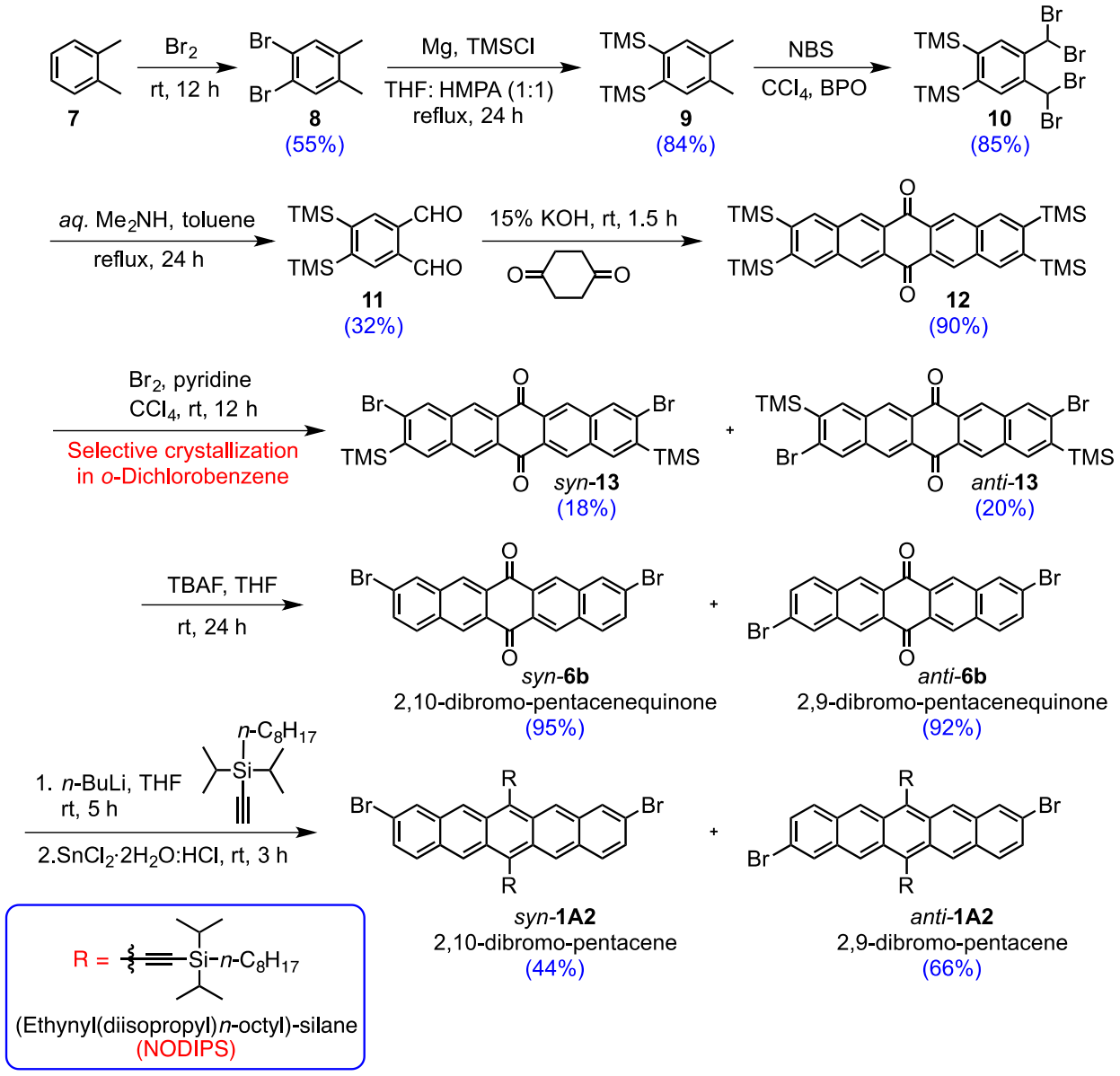

The regiopure dibromoquinones *syn*-**6b** and *anti*-**6b** were synthesized according to a procedure reported in the literature.[46,55]

Synthesis of bis(trimethylsilyl)-o-xylene:

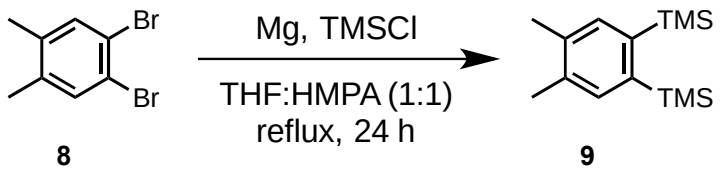

8 **9**

To a mixture of magnesium (5.52 g, 0.23 mol) and trimethylsilyl chloride (77 mL, 0.61 mol) in THF:HMPA (1:1, 200 mL) at 40 ^{o}C added 1 mL of dibromoethane (catalytic) followed by the addition of dibromoxylene **8** (20 g, 0.08 mol) in THF (15 mL) slowly over 15 mins. The resulting mixture was heated to reflux and maintained for 24 h. After the reaction, the mixture was cooled to rt, diluted with hexanes (300 mL) and filtered through celite carefully to remove magnesium chloride and excess magnesium. The solution was cooled to 0 ^{o}C and diluted with water (200 mL), stirred and the layers were separated. The aqueous layer was extracted with hexanes (2 × 100 mL) and the combined layer was dried over sodium sulfate, filtered and concentrated to get the crude. The crude was purified in column chromatography using hexanes as eluent.

^{1}H-NMR (400 MHz, $CDCl_3$, δ ppm): 7.52 (s, 2H), 2.35 (s, 6H) and (s, 18H).

^{13}C-NMR (100 MHz, $CDCl_3$, δ ppm): 143.0, 137.1, 136.1, 19.7 and 2.1.

Synthesis of *n*-octyl(diisopropyl)silylacetylene (NODIPS)

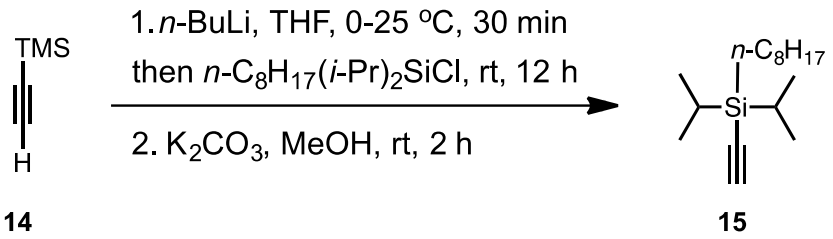

14 **15**

To a solution of TMS-acetylene **14** (7.43 g, 75.6 mmol) in dry THF (400 mL) at 0 °C under N_2 atmosphere *n*-BuLi (2.5 M in hexanes, 30.2 mL, 75.6 mmol) was added. The solution was warmed to rt and stirred for further 30 mins. A solution of *n*-octyl(diisopropyl)chlorosilane (21.8 g, 83.2 mmol) in THF (50 mL) was slowly added over 10 mins and the resulting solution was stirred at rt for 12 h. The reaction was diluted with water (200 mL), extracted with hexanes (3 × 75 mL) and the combined organic layer was dried, filtered and concentrated to get the crude. The crude was directly taken to next step.

To a mixture of crude product in methanol (500 mL) added K_2CO_3 (12.4 g, 89.8 mmol) and the mixture was stirred at rt for 2 h. After the reaction, the mixture was diluted with ice cold water (200 mL), extracted with hexanes (3 × 75 mL) and the combined organic layer was dried, filtered and concentrated to get the crude product. The crude was purified by silica gel column chromatography using hexanes as eluent.

Yield: 86% colorless oil

^{1}H-NMR (500 MHz, $CDCl_3$, δ ppm): 2.37 (s, 1H), 1.46-1.27 (m, 13H), 1.10-1.06 (m, 13H), 0.92-0.91 (m, 3H) and 0.67-0.64 (m, 2H).

^{13}C-NMR (125 MHz, $CDCl_3$, δ ppm): 94.5, 86.4, 33.8, 31.9, 29.3, 29.2, 24.3, 22.7, 18.1, 17.9, 14.1, 11.5 and 9.9.

Synthesis of *n*-octadecyl(diisopropyl)silylacetylene (NODDIPS):

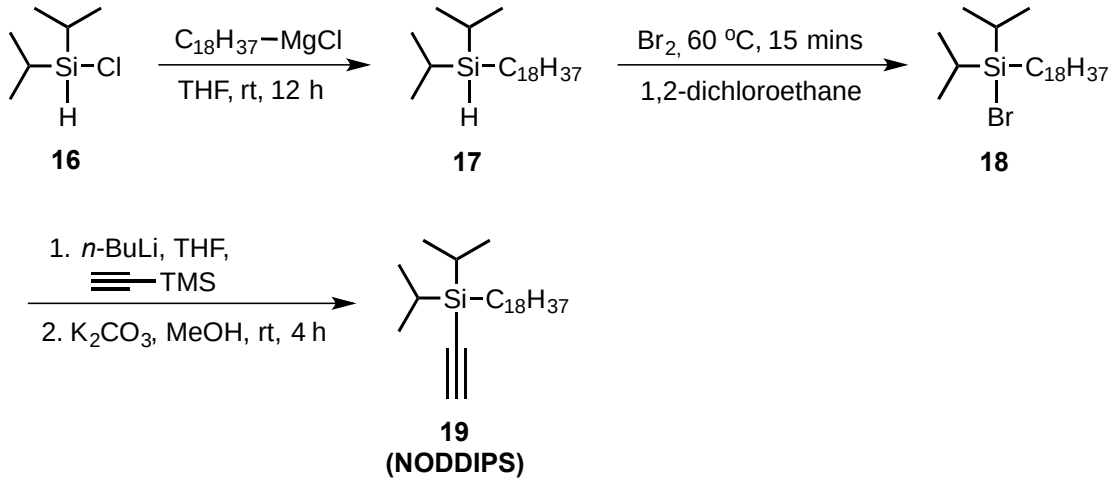

To a solution of diisopropylchlorosilane **16** (10.0 g, 66.3 mmol) in dry THF (80 mL) at 0 °C under N_2 atmosphere octadecylmagnesium chloride (0.5 M in THF, 121 mL, 60.3 mmol) was added slowly over 45 mins. The solution was warmed to rt and stirred for further 12 h. The reaction was diluted with water (200 mL), extracted with hexanes (3 × 75 mL) and the combined organic layer was dried, filtered and concentrated to get the crude. The crude was purified by column chromatography using hexanes.

^{1}H-NMR (400 MHz, $CDCl_3$, δ ppm): 3.46-3.43 (m, 1H), 1.33-1.29 (m, 34H), 1.07-1.04 (m, 14H) and 0.92 (t, 3H)

The silane derivative **17** from the above reaction in 1,2-dichloroethane at 0 °C was titrated with Br_2 until the color of the bromine persisted. The reaction mixture was heated to 60 °C and maintained for 15 mins. The reaction mixture was concentrated and the crude was taken to the next step with out further purification.

The conversion of **18** to **19** was achieved using the synthetic protocol described for the synthesis of NODIPS.

^{1}H-NMR (400 MHz, $CDCl_3$, δ ppm): 2.37 (s, 1H), 1.34-1.29 (m, 34H), 1.11-1.04 (m, 14H) and 0.91 (t, 3H)

Note: The product **17** contained quenched octadecane (~45%, characterized by ^{1}H-NMR using the methyl group as a handle). This impurity was carried all the way through NODDIPS **19**. This impurity was removed at the later stage where excess NODDIPS is removed at the pentacene-diol stage prior to $SnCl_2$ reduction to get the desired pentacene.

Synthesis of primary building blocks of pentacenes:

Synthesis of bromo derivatives of pentacenes:

To a solution of (*n*-octyl-diisopropylsilyl)acetylene/(*n*-octadecyl-diisopropylsilyl)acetylene (3.5 *equiv.*) in dry and degassed THF (40 mL) in 200 mL Schlenk flask at 0 °C added *n*-butyl lithium (3.4 *equiv.*, 2.5 M in hexanes). This solution was allowed to stir at 0 °C for 1 h followed by the addition of quinone **6a-b** (4.0 g, 1.0 *equiv.*) under positive argon flow. The solution was warmed to rt and stirred for further 5 h. The reaction was diluted with water (50 mL) and extracted with ethyl acetate (2 × 50 mL). The combined organic layer was washed with brine (30 mL), dried over sodium sulfate, filtered and concentrated to get the crude. The crude was purified in column chromatography using hexanes as eluent first to recover excess silylacetylene (NODIPS) and then with DCM to obtain intermediate diol product.

To a solution of diol in THF (40 mL) at 0 ^{o}C added a solution of tin (II) chloride dihydrate (10 *equiv.*) in 10% aqueous HCl solution (20 mL) during which the solution turned deep blue. The resulting mixture was stirred at rt for 3 h under dark and diluted with water (50 mL). The mixture was extracted with hexanes (2 × 50 mL). The combined organic layer was washed with brine (30 mL), dried over sodium sulfate, filtered and concentrated to get the crude. The crude was purified in column chromatography using hexanes as eluent to obtain the product.

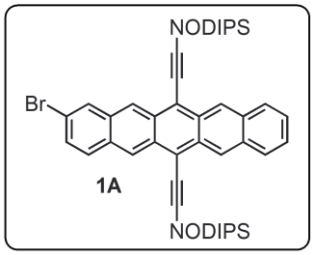

1A

Yield = 70%; Blue paste

^{1}H-NMR (400 MHz, $CDCl_3$, δ ppm): 9.39-9.38 (m, 2H), 9.35 (s, 1H), 9.28 (s, 1H), 8.25 (s, 1H), 8.10-8.08 (m, 2H), 7.95-7.93 (m, 1H), 7.54-

7.51 ((m, 3H), 1.90-1.81 (m, 4H), 1.64-1.57 (m, 4H), 1.49-1.33 (m, 44H), 1.07-1.02 (m, 4H) and 0.96-0.92 (m, 6H).

^{13}C-NMR (100 MHz, $CDCl_3$, δ ppm): 132.7, 132.6, 132.5, 130.9, 130.87, 130.7, 130.6, 130.4, 130.3, 130.27, 125.6, 128.7, 126.9, 126.5, 126.4, 126.2, 126.2, 125.5, 120.4, 118.7, 118.6, 107.98, 104.4, 34.1, 34.09, 32.1, 29.6, 29.58, 29.49, 29.46, 25.1, 25.0, 22.8, 18.8, 18.5, 14.2, 12.3 and 10.5.

MS (ESI): Calculated $[M]^+$: 856.4434; Observed: 856.4423.

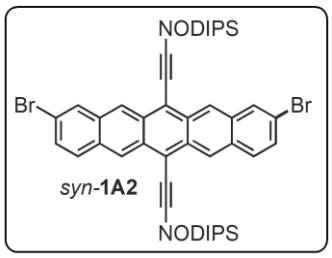

Yield = 44%; Blue paste solidifies over time

^{1}H-NMR (400 MHz, $CDCl_3$, δ ppm): 9.27 (s, 2H), 9.21 (s, 2H), 8.18 (s, 2H), 7.89-7.88 9.27 (m, 2H), 7.50-7.47 9.27 (m, 2H), 1.83-1.73 (m, 4H), 1.58-1.49 (m, 4H), 1.41-1.27 (m, 44H), 1.01-0.96 (m, 4H) and 0.88-0.85 (m, 6H).

^{13}C-NMR (125 MHz, $CDCl_3$, δ ppm): 132.8, 131.0, 130.5, 130.4, 130.35, 130.2, 129.8, 129.7, 126.95, 125.5, 120.6, 118.9, 118.6, 108.4, 108.2, 104.1, 103.98, 34.1, 34.09, 34.06, 32.0, 29.6, 28.59, 29.55, 29.49, 29.46, 29.43, 25.1, 25.04, 25.0, 22.8, 22.7, 18.8, 18.77, 18.5, 18.49, 14.2, 12.2, 10.5 and 10.45.

MS (ASAP): Calculated [M+H]: 935.3618; Observed: 935.3606.

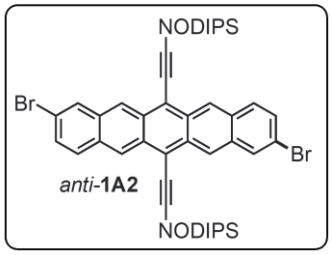

Yield = 55%; Blue paste solidifies over time

^{1}H-NMR (500 MHz, $CDCl_3$, δ ppm): 9.27 (s, 2H), 9.19 (s, 2H), 8.18 (s, 2H), 7.89-7.87 (m, 2H), 7.50-7.48 (m, 2H), 1.82-1.76 (m, 4H), 1.59-1.53 (m, 4H), 1.46-1.29 (m, 44H), 1.01-0.98 (m, 4H) and 0.89-0.88 (m, 6H).

^{13}C-NMR (125 MHz, $CDCl_3$, δ ppm): 132.7, 130.8, 130.76, 130.5, 130.4, 130.2, 129.7, 126.9, 125.6, 120.5, 118.8, 108.3, 104.0, 34.0, 32.0, 29.5, 29.4, 25.0, 22.7, 18.8, 18.5, 14.1, 12.2 and 10.4.

MS (ASAP): Calculated [M+H]: 935.3618; Observed: 935.3592.

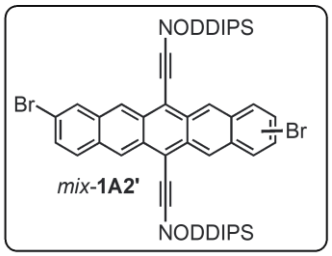

Yield = 30%; Blue paste solidifies over time

^{1}H-NMR (500 MHz, $CDCl_3$, δ ppm): 9.27-9.25 (m, 2H), 9.19-9.18 (m, 2H), 8.16 (m, 2H), 7.87-7.86 (m, 2H), 7.48-7.46 (m, 2H), 1.78-1.73 (m, 4H), 1.53-1.51 (m, 4H), 1.36-1.19 (m, 88H) and 0.89 (t, 6H).

^{13}C-NMR (125 MHz, $CDCl_3$, δ ppm): 132.8, 132.7, 131.0, 130.8, 130.7, 130.5, 130.4, 130.38, 130.34, 130.2, 129.74, 129.71, 126.96, 126.91, 125.6, 125.5, 120.6, 120.5, 118.9, 118.8, 118.6, 108.4, 108.3, 108.2, 34.1, 34.0, 33.9, 31.9, 29.8, 29.73, 29.70, 29.6, 29.56, 29.52, 29.40, 25.0, 24.98, 24.94, 22.7, 18.8, 18.73, 18.71, 18.5, 18.45, 18.43, 14.2, 12.1 and 10.4.

MS (ASAP): Calculated [M+H]: 1214.6669; Observed: 1214.6671.

Synthesis of bpin derivatives of pentacenes:

To a dry round bottomed flask was added **1A/1A2/1A2'** (4.0 g, 5.57 mmol), Pd(dppf)Cl_2·DCM (10 mol% for **1A** and 15 mol% for **1A2**/**1A2'**), KOAc (1.5 *equiv*. for **1A** and 3.0 *equiv*. for **1A2**/**1A2'**), and bis(pinacolato)diboron (1.5 *equiv*. for **1A** and 3.0 *equiv*. for **1A2**/**1A2'**). Sequential vacuum and argon were used to degas the mixture followed by the addition of dry and degassed 1, 4 dioxane (40 mL). The mixture was heated to 85 °C and maintained for 12 h in the dark. After the reaction, the mixture was cooled to rt and the solvent was removed under reduced pressure. The crude was purified by silica chromatography using mixtures of hexanes/chloroform as an eluent to obtain pure product.

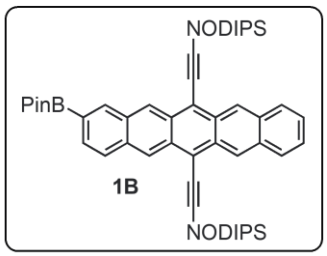

Yield = 64%; Blue paste

H-NMR (400 MHz, $CDCl_3$, δ ppm): 9.34-9.33 (m, 2H), 9.31 (s, 1H), 9.27 (s, 1H), 8.56 (s, 1H), 8.02-7.95 (m, 3H), 7.75-7.73 (m, 1H), 7.46-7.43 (m, 2H), 1.79-1.74 (m, 4H), 1.56-1.51 (m, 4H), 1.47 (s, 12H), 1.39-1.33 (m, 35H), 1.28-1.24 (m, 8H), 1.02-0.95 (m, 5H) and 0.87-0.82 (m, 6H).

^{13}C-NMR (125 MHz, $CDCl_3$, δ ppm): 138.2, 133.3, 132.5, 132.46, 131.98, 131.3, 130.9, 130.85, 130.7, 129.8, 128.8, 127.8, 127.6, 126.5, 126.4, 126.2, 118.96, 118.4, 107.9, 107.6, 104.7, 104.6, 84.1, 34.1, 32.1, 29.6, 29.5, 25.0, 22.8, 18.9, 18.8, 18.6, 18.56, 14.2, 12.3 and 10.6.

MS (ESI): Calculated $[M+Na]^+$: 927.6079; Observed: 927.6089.

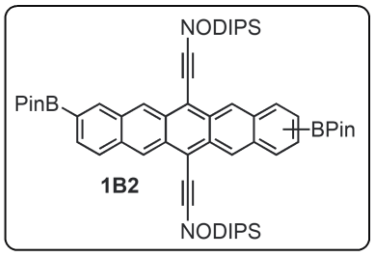

Yield = 61%; Sticky blue paste solidifies over time.

^{1}H-NMR (400 MHz, $CDCl_3$, δ ppm): 9.39 (s, 1H), 9.37 (s, 1H), 9.32 (s, 1H), 9.29 (s, 1H), 8.57 (s, 2H), 7.98-7.96 (m, 2H), 7.77-7.75 (m, 2H), 1.85-1.76 (m, 4H), 1.61-1.53 (m, 5H), 1.47 (s, 24H), 1.41-1.35 (m, 35H), 1.29-1.26 (m, 8H), 1.03-0.99 (m, 4H) and 0.88-0.83 (m, 6H).

^{13}C-NMR (125 MHz, $CDCl_3$, δ ppm): 138.1, 138.0, 134.8, 133.2, 133.1, 131.9, 131.86, 131.3, 131.2, 130.8, 130.7, 129.8, 129.7, 127.8, 127.7, 127.6, 127.55, 126.2, 126.1, 119.3, 118.8, 118.3, 108.1, 107.9, 107.6, 104.6, 104.5, 104.4, 84.1, 34.1, 34.0, 33.97, 32.0, 32.01, 29.5, 29.4, 29.40, 29.3, 24.99, 22.7, 18.9, 18.8, 18.78, 18.6, 18.55, 18.5, 14.2, 12.2, 10.5 and 10.49.

MS (APCI): Calculated $[M+Na]^+$: 1053.6931; Observed: 1053.6946.

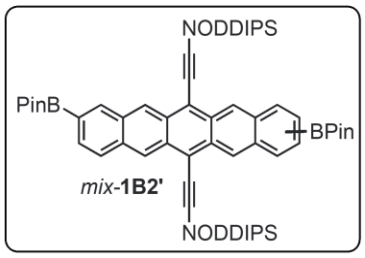

Yield = 80%; Sticky blue paste.

^{1}H-NMR (400 MHz, $CDCl_3$, δ ppm): 9.36-9.34 (m, 2H), 9.29-9.27 (m, 2H), 8.55 (s, 2H), 7.96-7.94 (m, 2H), 7.74-7.72 (m, 2H), 1.81-1.75 (m, 4H), 1.56-1.49 (m, 4H), 1.46 (s, 24H), 1.40-1.19 (m, 88H) and 0.89 (t, 6H).

^{13}C-NMR (125 MHz, $CDCl_3$, δ ppm): 138.0, 137.9, 133.1, 133.0, 131.8, 131.7, 131.2, 131.1, 130.7, 130.6, 129.7, 129.6, 127.8, 127.6, 127.52, 127.50, 126.1, 125.99, 119.3, 118.8, 118.2, 108.1, 107.8, 107.5, 104.5, 104.4, 104.3, 84.0, 33.99, 33.96, 33.90, 31.9, 29.8, 29.71, 29.70, 29.7, 29.5, 29.4, 29.37, 29.31, 24.9, 22.7, 18.8, 18.78, 18.72, 18.5, 18.5, 18.45, 14.1, 12.2 and 10.5.

MS (ESI): Calculated $[M+H]^+$: 1312.0242; Observed: 1312.0264.

Synthesis of pentacenes derivatives **2A** and **3A**

To a mixture of **1B** (to obtain **2A**) or **2B** (to obtain **3A**) (1.0 g, 1.0 *equiv.*), **1A2** (3.0 *equiv.*), Pd(dppf)Cl_2·DCM (5 mol%), and K_2CO_3 (5 *equiv.*) under argon atmosphere added dry and degassed THF:H_2O (9:1, 50 mL). The resulting mixture was heated to 65 °C and maintained for 24 h in the dark. After the reaction, the THF was evaporated and the residue was purified by silica chromatography using mixtures of hexanes/chloroform as an eluent to obtain the product.

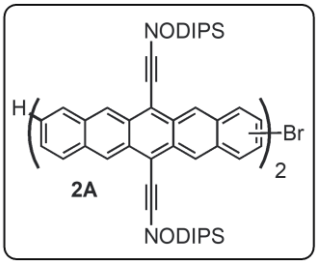

Yield = 63%; Dark purple solid.

^{1}H-NMR (400 MHz, $CDCl_3$, δ ppm): 9.43-9.41 (m, 2H), 9.36-9.30 (m, 5H), 9.23-9.22 (m, 1H), 8.38 (s, 2H), 8.19-8.17 (m, 3H), 8.04-7.95 (m, 4H), 7.89-7.88 (m, 1H), 7.49-7.45 (m, 3H), 1.84-1.78 (m, 8H), 1.45-1.28 (m, 85H), 1.22-1.18 (m, 10H), 1.03-0.99 (m, 9H), 0.88-0.85 (m, 6H) and 0.78-0.75 (m, 6H).

^{13}C-NMR (125 MHz, $CDCl_3$, δ ppm): 137.8, 137.5, 132.7, 132.69, 132.6, 132.4, 132.39, 132.36, 131.8, 131.7, 131.6, 131.3, 131.1, 131.0, 130.96, 130.91, 130.88, 130.85, 130.76, 130.67, 130.57, 130.4, 130.3, 130.29, 130.2, 129.6, 129.59, 128.7, 126.9, 126.4, 126.2, 126.1, 125.8, 125.5, 120.4, 118.8, 118.6, 118.5, 118.4, 118.3, 108.1, 108.0, 107.99, 107.9, 107.7, 107.5, 104.6, 104.5, 104.3, 34.13, 34.1, 34.09, 34.08, 34.07, 34.05, 32.0, 31.9, 29.6, 29.56, 29.54, 29.51, 29.45, 29.42, 29.40, 25.1, 25.06, 25.03, 25.0, 22.7, 22.69, 22.66, 22.64, 18.8, 18.79, 18.76, 18.5, 18.49, 14.1, 14.0, 12.23, 12.20, 10.52, 10.50 and 10.48.

MS (ESI): Calculated $[M+H]^+$: 1633.9685; Observed: 1633.9662.

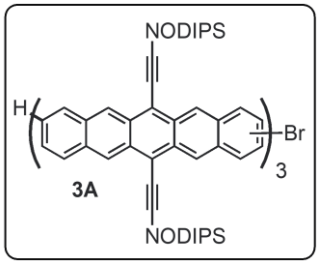

Yield = 53%; Dark purple solid.

^{1}H-NMR (500 MHz, 50 °C, $CDCl_3$, δ ppm): 9.46-9.24 (m, 12H), 8.39 (s, 4H), 8.20-8.17 (m, 5H), 8.03-7.96 (m, 6H), 7.89-7.87 (m, 1H), 7.49-7.44 (m, 3H), 1.89-1.83 (m, 13H), 1.59-1.58 (m, 14H), 1.47-1.21 (m, 127H), 1.07-1.02 (m, 14H), 0.89-0.86 (m, 8H) and 0.80-0.77 (m, 10H).

^{13}C-NMR (125 MHz, 50 °C, $CDCl_3$, δ ppm): 137.3, 137.2, 136.91, 136.90, 136.88, 136.8, 136.73, 136.72, 136.7, 136.6, 136.5, 132.78, 132.73, 132.68, 132.65, 132.58, 132.52, 132.46, 132.4, 132.37, 132.33, 131.9, 131.86, 131.75, 131.73, 131.69, 131.63, 131.3, 131.27, 131.21, 131.1, 130.99, 130.89, 130.83, 130.81, 130.74, 130.72, 130.63, 130.58, 130.34, 130.31, 130.23, 130.19, 130.15, 130.07, 129.5, 129.4, 129.37, 128.7, 128.6, 128.58, 126.96, 126.9, 126.85, 126.78, 126.31, 126.27, 126.15, 126.1, 125.9, 125.8, 125.6, 125.62, 125.56, 125.54, 125.50, 125.45, 125.37, 125.33, 120.37, 120.34, 120.29, 118.84, 118.81, 118.72, 118.69, 118.65, 118.63, 118.54, 118.50, 118.46, 118.4, 118.38, 108.1, 108.0, 107.99, 107.96, 107.90, 107.85, 107.78, 107.75, 107.63, 107.52, 107.49, 107.39, 104.90, 104.84, 104.82, 104.78, 104.75, 104.59, 104.57, 104.52, 34.06, 34.02, 34.0, 33.97, 31.95, 31.90, 31.88, 29.5, 29.47, 29.44, 29.36, 29.33, 25.1, 25.04, 25.00, 24.98, 24.95, 22.60, 22.57, 22.6, 18.9, 18.8, 18.76, 18.74, 18.57, 18.52, 18.50, 13.96, 13.90, 13.88, 13.81, 12.4, 12.38, 12.36, 12.34, 10.73, 10.7 and 10.65.

MALDI: Calculated: 2409.48; Observed: 2411.42.

Synthesis of pentacenes derivatives **2B** and **3B**

The compound **2B** and **3B** was obtained according to the procedure described for the synthesis of **1B**.

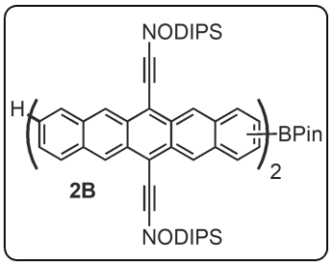

Yield = 75%; Dark purple solid.

^{1}H-NMR (400 MHz, $CDCl_3$, δ ppm): 9.46-9.31 (m, 8H), 8.58 (s, 1H), 8.39 (s, 2H), 8.19-8.17 (m, 2H), 7.99-7.96 (m, 5H), 7.77-7.75 (m, 1H), 7.47-7.45 (m, 2H), 1.84-1.79 (m, 8H), 1.47 (s, 12H), 1.43-1.37 (m, 69H), 1.30-1.19 (m, 26H), 1.03-0.99 (m, 9H), 0.88-0.86 (m, 6H) and 0.78-0.75 (m, 6H).

^{13}C-NMR (125 MHz, $CDCl_3$, δ ppm): 138.1, 137.7, 137.65, 133.2, 133.28, 132.6, 132.5, 132.4, 132.39, 131.9, 131.89, 131.7, 131.6, 131.3, 131.22, 131.20, 131.17, 131.06, 131.0, 130.9, 130.8,130.75, 130.69, 130.65, 129.7, 129.66, 128.7, 127.8, 127.6, 127.0, 126.9, 126.40, 126.2, 126.12, 126.10, 126.0, 125.96, 119.0, 118.9, 118.6, 118.5, 118.4, 118.3, 108.0, 107.9, 107.74, 107.71, 107.59, 107.55, 104.65, 104.58, 104.55, 104.5, 104.4, 84.1, 34.14, 34.1, 34.09, 34.05, 32.04, 32.01, 31.97, 31.9, 29.60, 29.54, 29.49, 29.46, 29.44, 25.10, 25.06, 25.03, 25.01, 22.73, 22.68, 18.88, 18.86, 18.82, 18.79, 18.59, 18.58, 18.54, 18.52, 14.2, 14.1, 12.3, 10.55 and 10.53.

MS (ESI): Calculated $[M]^+$: 1681.1354; Observed: 1681.1345.

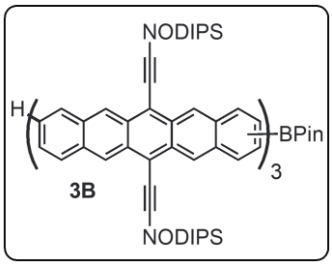

Yield = 70%; Dark purple solid.

^{1}H-NMR (500 MHz, 50 °C, $CDCl_3$, δ ppm): 9.46-9.31 (m, 12H), 8.58 (s, 1H), 8.39 (s, 4H), 8.20-8.17 (m, 4H), 8.03-7.98 (m, 7H), 7.78-7.75 (m, 1H), 7.46-7.43 (m, 2H), 1.86-1.84 (m, 12H), 1.59-1.58 (m, 14H), 1.48-1.39 (m, 110H), 1.31-1.21 (m, 31H), 1.06-1.03 (m, 13H) and 0.89-0.78 (m, 18H).

^{13}C-NMR (125 MHz, 50 °C, $CDCl_3$, δ ppm): 137.9, 137.85, 137.82, 137.81, 137.78, 137.74, 133.24, 133.22, 132.65, 132.62, 132.55, 132.46, 132.44, 131.97, 131.76, 131.73, 131.67, 131.3, 131.24, 131.14, 131.09, 130.98, 130.95, 130.8, 130.78, 130.72, 130.7, 129.7, 129.6, 128.6, 127.7, 127.4, 126.9, 126.8, 126.33, 126.22, 126.18, 125.98, 125.9, 118.6, 118.4, 107.76, 107.73, 107.57, 104, 73, 104.68, 104.65, 104.61, 104.55, 84.0, 34.0, 33.96, 33.91, 33.88, 31.9, 31.8, 29.4, 29.3, 22.6, 22.5, 22.46, 18.74, 18.72, 18.69, 18.67, 18.45, 18.43, 13.91, 13.85, 13.83, 13.76, 12.29 and 10.6.

MALDI: Calculated: 2457.65; Observed: 2458.59.

General procedure for the synthesis of oligopentacenes

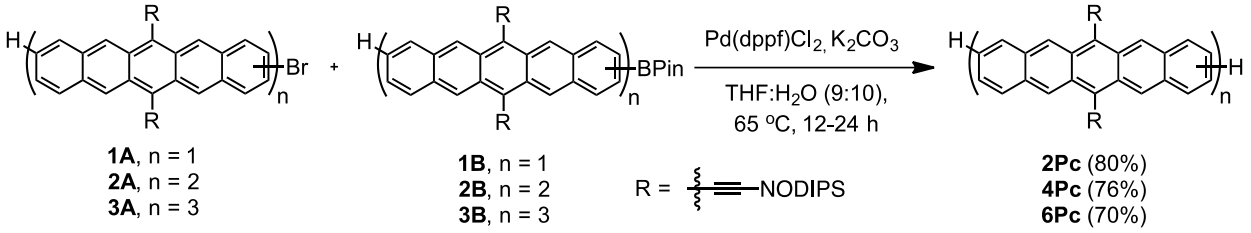

Even numbered oligopentacenes: A mixture of bromopentacene derivative **1A**/**2A**/**3A** (100 mg, 1.0 *equiv.*), BPin-pentacene derivative **1B**/**2B**/**3B** (1.2 *equiv.*), Pd(dppf)Cl_2·DCM (4 mg, 5 mol%), and K_2CO_3 (5 *equiv.*) in a dry round bottom flask was subjected to sequential vacuum and argon to degas the mixture followed by the addition of degassed H_2O (2 mL) and THF (18 mL). The resulting solution was heated to 65 °C and maintained for 24 h in dark. After the reaction, the solution was poured into a separatory funnel containing chloroform (30 mL) and water (30 mL). The organic layer was separated, dried over *anhyd.* Na_2SO_4, filtered and the solvent was removed under reduced pressure to get the crude product. The crude was purified by silica chromatography using mixtures of hexanes/DCM as an eluent to obtain even numbered oligomers of pentacenes as deep purple solid (dimer was obtained as a deep blue green solid).

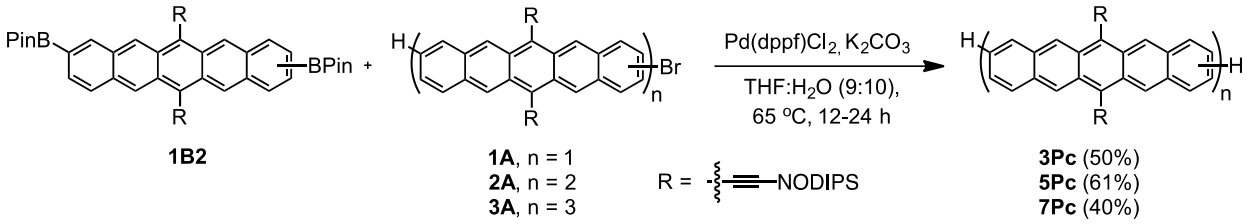

Odd numbered oligopentacenes*:* Similar procedure followed for the synthesis of odd numbered oligopentacenes except the 2.3 *equiv.* of bromo derivatives of pentacenes **1A**/**2A**/**3A** were used.

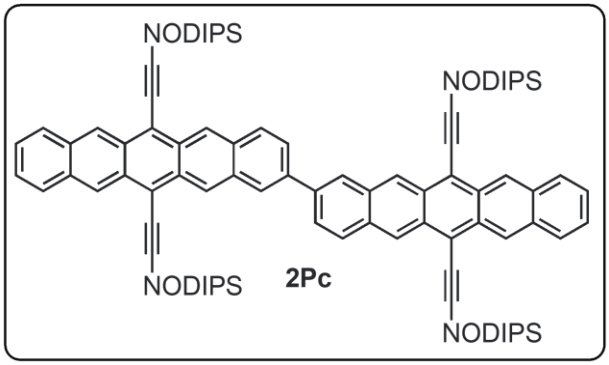

^{1}H-NMR (500 MHz, $CDCl_3$, δ ppm):): 9.43-9.35 (m, 8H), 8.39 (s, 2H), 8.20-8.18 (m, 2H), 8.05-8.03 (m, 4H), 7.97-7.97 (m, 2H), 4.47-7.45 (m, 4H), 1.87-1.79 (m, 8H), 1.87-1.79 (m, 8H), 1.60-1.54 (m, 8H), 1.44-1.38 (m, 66H), 1.32-1.21 (m, 22H), 1.04-1.00 (m, 8H), 0.89-0.87 (m, 6H) and 0.79-0.78 (m, 6H).

^{13}C-NMR (125 MHz, $CDCl_3$, δ ppm): 137.6, 132.5, 132.4, 132.35, 131.6, 131.0, 130.9, 130.8, 130.7, 129.6, 128.7, 126.9, 126.4, 126.2, 126.1, 125.9, 118.5, 118.4, 107.7, 107.5, 104.6, 104.5, 34.1, 34.05, 32.0, 31.9, 29.6, 29.5, 29.4, 29.39, 25.1, 24.99, 22.7, 22.6, 18.8, 18.75, 18.5, 18.48, 14.1, 14.0, 12.2, 10.5 and 10.5.

MS (ESI): Calculated $[M]^+$: 1555.0461; Observed: 1555.0502.

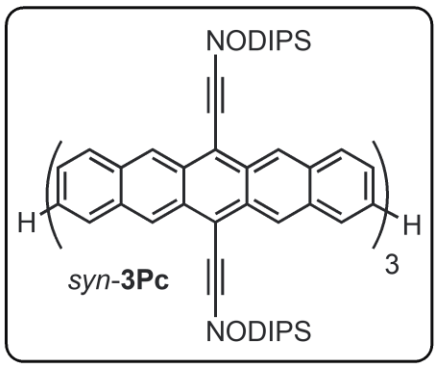

^{1}H-NMR (500 MHz, $CDCl_3$, δ ppm): 9.41-9.33 (m, 12H), 8.35-8.32 (m, 4H), 8.19-8.18 (m, 4H), 8.03-8.00 (m, 4H), 7.96-7.94 (m, 4H), 7.45-7.40 (m, 4H), 1.87-1.81 (m, 12H), 1.62-1.55 (m, 12H), 1.49-1.39 (m, 105H), 1.31-1.29 (m, 22H), 1.05-1.01 (m, 12H), 0.92-0.87 (m, 12H), 0.79-0.77 (m, 8H) and 0.70-0.68 (m, 3H).

^{13}C-NMR (125 MHz, $CDCl_3$, δ ppm): 137.5, 137.4, 132.5, 132.4, 132.36, 132.3, 131.6, 131.5, 131.1, 131.0, 130.9, 130.86, 130.7, 130.6, 129.6, 128.7, 126.9, 126.85, 126.3, 126.2, 126.1, 125.83, 125.80, 118.7, 118.5, 118.3, 107.8, 107.6, 107.5, 104.7, 104.6, 104.54, 104.51, 34.2, 34.1, 34.08,

34.06, 32.0, 31.9, 31.87, 31.6, 29.6, 29.56, 29.54, 29.51, 29.49, 29.44, 29.41, 29.39, 26.2, 25.1, 25.06, 25.0, 24.99, 24.8, 22.7, 22.67, 22.63, 22.59, 18.84, 18.83, 18.79, 18.76, 18.55, 18.52, 18.49, 14.14, 14.12, 14.05, 14.03, 13.95, 12.26, 12.25, 12.22, 10.56, 10.52 and 10.51.

MALDI: Calculated: 2331.57; Observed: 2332.54.

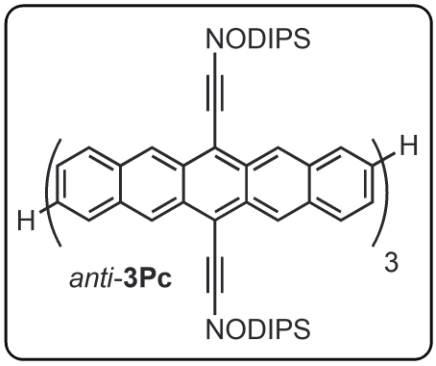

anti-**3Pc**

^{1}H-NMR (400 MHz, $CDCl_3$, δ ppm): 9.42-9.33 (m, 12H), 8.37 (m, 4H), 8.21-8.17 (m, 4H), 8.04-7.95 (m, 8H), 7.46-7.41 (m, 4H), 1.88-1.79 (m, 12H), 1.62-1.54 (m, 13H), 1.47-1.38 (m, 98H), 1.32-1.19 (m, 31H), 1.08-1.00 (m, 14H), 0.89-0.86 (m, 6H) and 0.81-0.76 (m, 12H).

^{13}C-NMR (125 MHz, $CDCl_3$, δ ppm): 136.5, 136.48, 136.45, 132.3, 132.23, 132.21, 132.19, 131.7, 131.6, 131.5, 130.9, 130.92, 130.88, 130.85, 130.7, 130.6, 129.4, 128.57, 128.54, 126.9, 126.86, 126.3, 126.2, 125.9, 125.8, 125.5, 125.4, 125.3, 118.4, 118.3, 107.4, 107.36, 107.29, 104.7, 104.6, 34.18, 34.14, 34.1, 32.0, 31.96, 31.95, 29.58, 29.56, 29.52, 29.45, 29.43, 29.42, 25.1, 25.07, 25.0, 22.7, 22.66, 22.64, 18.9, 18.85, 18.8, 18.6, 18.56, 18.53, 14.1, 14.06, 14.0, 12.32, 12.28, 12.25, 10.62, 10.57 and 10.55.

MALDI: Calculated: 2331.57; Observed: 2332.46.

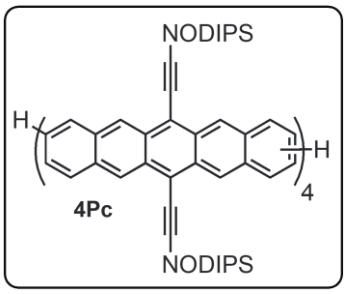

^{1}H-NMR (500 MHz, 50 °C, $CDCl_3$, δ ppm): 9.44-9.34 (m, 16H), 8.38 (s, 6H), 8.18 (s, 6H), 8.01-7.97 (m, 10H), 7.44 (s, 4H), 1.87-1.83 (m, 18H), 1.62-1.21 (m, 200H) and 0.89-0.79 (m, 30H).

MALDI: Calculated: 3108.08; Observed: 3109.14.

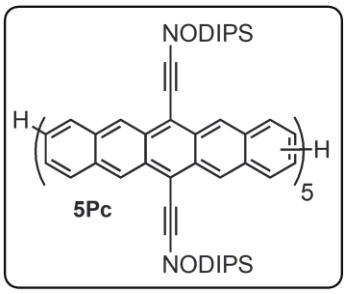

^{13}C-NMR ((500 MHz, 50 °C, $CDCl_3$, δ ppm): 9.38-9.34 (s, 20H), 8.39 (s, 8H), 8.18 (s, 8H), 7.97 (s, 12H), 7.44-7.42 (m, 4H), 1.87 (m, 21H), 1.61-1.03 (m, 258H) and 0.89-0.78 (m, 31H).

MALDI: Calculated: 3884.60; Observed: 3886.72.

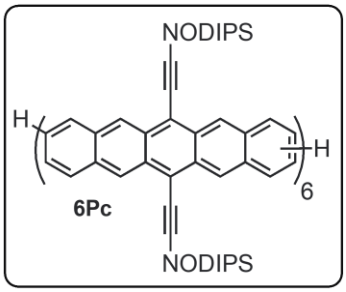

^{1}H-NMR (500 MHz, 50 °C, $CDCl_3$, δ ppm): 9.34 (bs, 24H), 8.39-7.97 (m, 38H) and 1.89-0.71 (m, 372H, water peak overlap)

MALDI: Calculated: 46661.10; Observed: 4663.05.

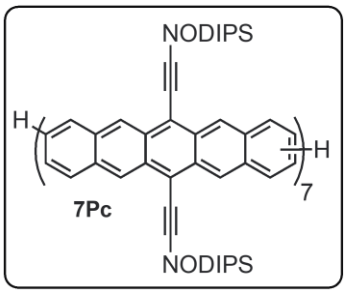

^{1}H-NMR (500 MHz, 50 °C, $CDCl_3$, δ ppm): 9.44-9.35 (m, 28H), 8.40 (s, 10H), 8.19-7.98 (m, 34H) and 1.88-0.78 (m, 434H, water peak overlap)

MALDI: Calculated: 5437.64; Observed: 5440.72.

General procedure for the homopolymer of pentacenes

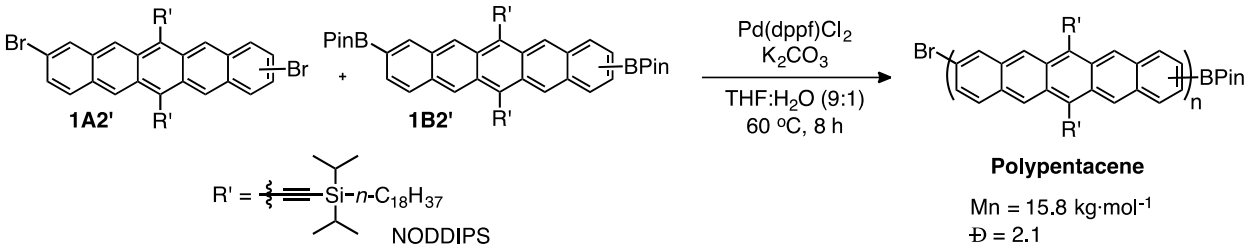

To a dry 20 mL vial added **1B2′** (50 mg, 1.0 *equiv.*), **1A2′ (**1.1 *equiv.***)**, Pd(dppf)Cl_2 (5 mol%) and K_2CO_3(5.0 *equiv.*). The vial was capped followed by sequential vacuum and argon was carried out 3 times to degas the mixture. Degassed H_2O (1.7 mL) and THF (15.3 mL) was added and the mixture was placed in an oil bath preheated to 60 ^oC. The reaction was carried out in dark for 8 h and then cooled to room temperature. The mixture was precipitated in methanol (75 mL), filtered and the solid was transferred to a Soxhlet thimble. The solid was extracted with hexanes, chloroform and finally chlorobenzene sequentially in dark and under argon atmosphere. The solutions were concentrated and the residue was precipitated in methanol, filtered, dried and stored.

The chloroform fraction yielded 33 mg of product and chlorobenzene fraction yielded 28 mg of the product.

3.13 Comparison of 1H-NMR Spectrum of syn and anti isomers of Pentacene Trimer

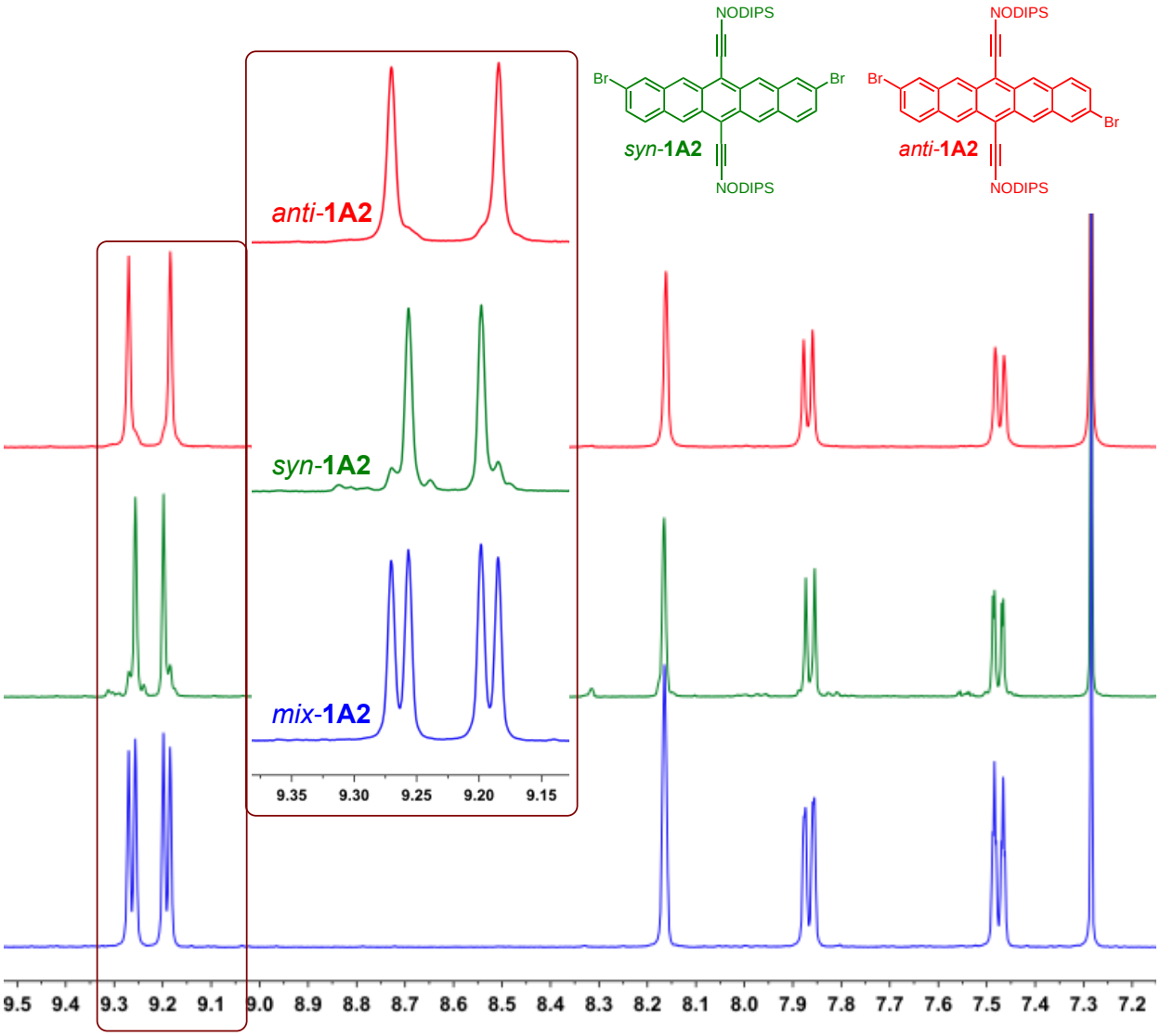

Figure 3.6. The NMR spectrum of mix-1A2 (bottom, blue), *syn*-1A2 (middle, green) and *anti*-1A2 (top, red) isomers. The aliphatic regions are omitted for clarity.

The NMR spectrum compares the aromatic regions of **3a** mixture with regiopure *syn* and *anti* isomers. The regiopurity of the *anti*-**1A2** is higher compared to *syn*-**1A2** that has small amount of (~12%) of *anti*-**1A2**.

3.14 Concentration Dependence in Steady-state Absorption of Oligopentacenes

Shown below are steady state UV-Visible absorption spectra for the oligopentacenes. The spectra were taken for known masses of oligomer in a measured volume of chloroform. Variation of the molarity was used to test for aggregation, which typically manifests as red-shifting of the absorbance onset and/or adherence to Beer's Law. The molarities are reported in the legend as molarity of pentacene for ease of comparison, not the molarity of the oligomer (each molarity represents a nearly identical mass of pentacene per volume of solution). The extinction coefficients are listed as $L^{-1}M^{-1}$, where the molarity is the moles of oligomer, in keeping with convention.

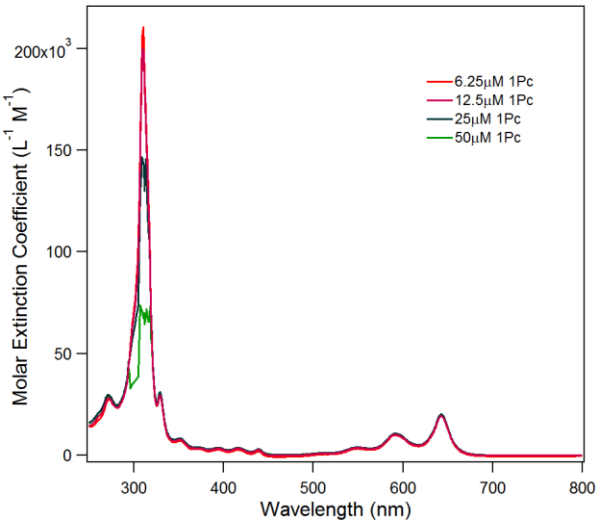
200x10^3
150
100
50
0
Molar Extinction Coefficient (L^-1 M^-1)
300
400
500
600
700
800
Wavelength (nm)
6.25μM 1Pc
12.5μM 1Pc
25μM 1Pc
50μM 1Pc

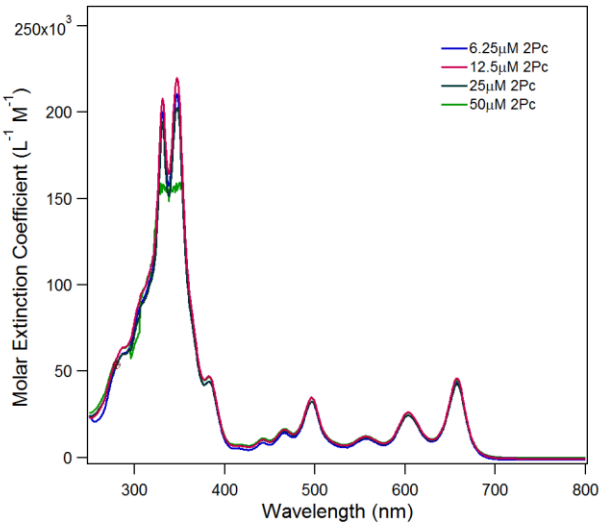
250x10^3
200
150
100
50
0
Molar Extinction Coefficient (L^-1 M^-1)
300
400
500
600
700
800
Wavelength (nm)
6.25μM 2Pc
12.5μM 2Pc
25μM 2Pc
50μM 2Pc

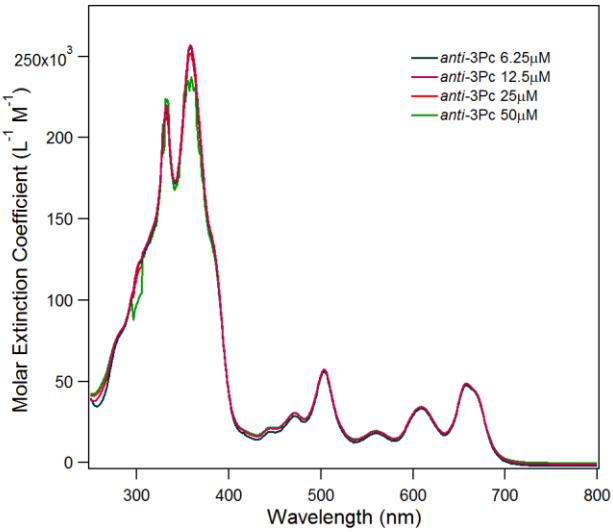
250x10^3
200
150
100
50
0
Molar Extinction Coefficient (L^-1 M^-1)
300
400
500
600
700
800
Wavelength (nm)
anti-3Pc 6.25μM
anti-3Pc 12.5μM
anti-3Pc 25μM
anti-3Pc 50μM

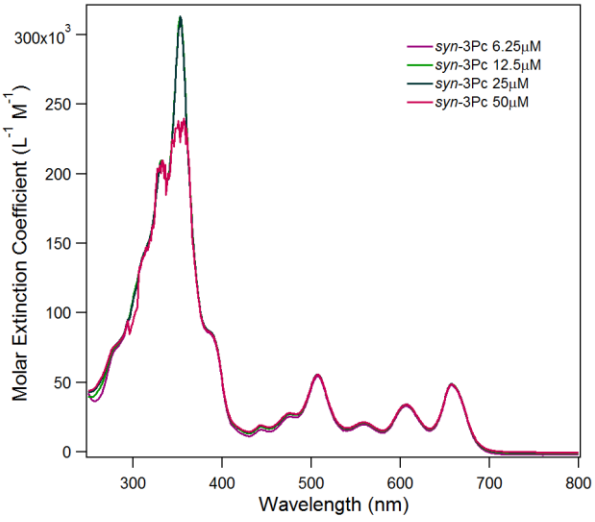
300x10^3
250
200
150
100
50
0
Molar Extinction Coefficient (L^-1 M^-1)
300
400
500
600
700
800
Wavelength (nm)
syn-3Pc 6.25μM
syn-3Pc 12.5μM
syn-3Pc 25μM
syn-3Pc 50μM

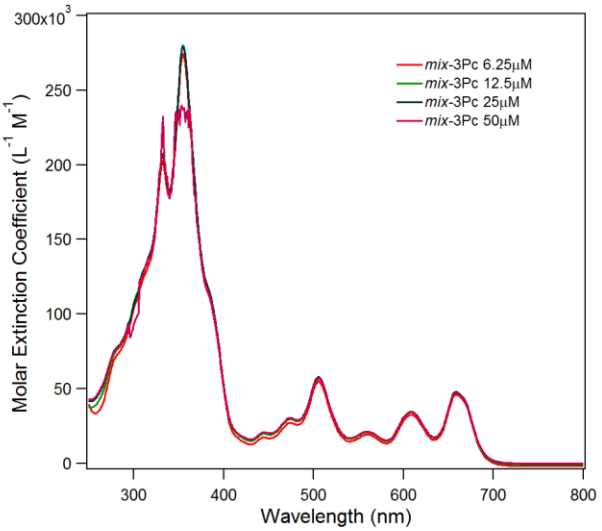
300x10^3
250
200
150
100
50
0
Molar Extinction Coefficient (L^-1 M^-1)
300
400
500
600
700
800
Wavelength (nm)
mix-3Pc 6.25μM
mix-3Pc 12.5μM
mix-3Pc 25μM
mix-3Pc 50μM

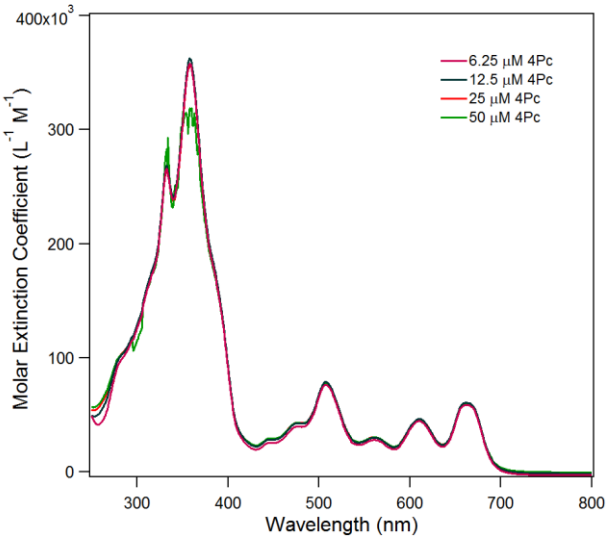
400x10^3
300
200
100
0
Molar Extinction Coefficient (L^-1 M^-1)
300
400
500
600
700
800
Wavelength (nm)
6.25 μM 4Pc
12.5 μM 4Pc
25 μM 4Pc
50 μM 4Pc

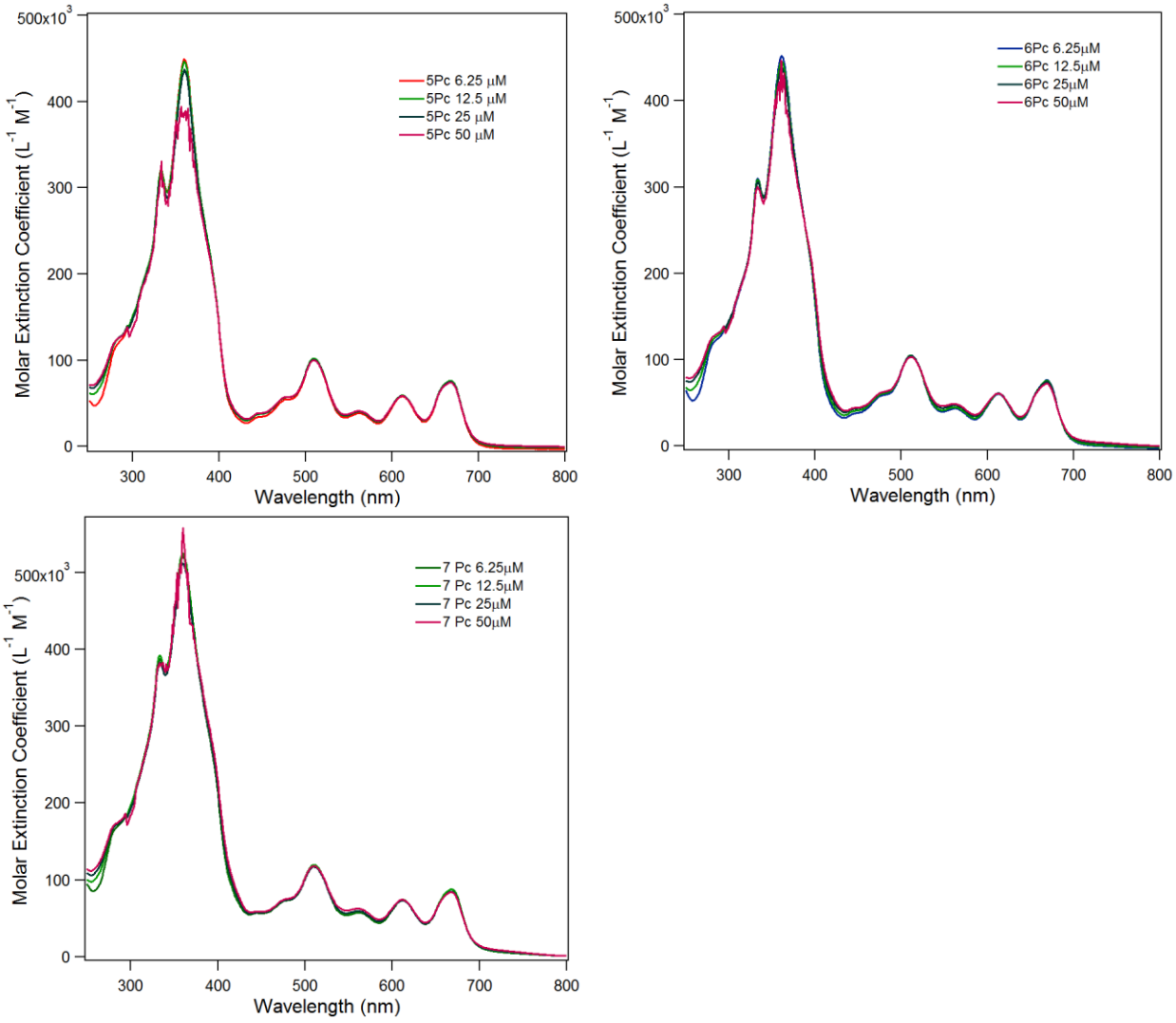

Figure 3.7. Steady-state absorption in chloroform for the oligomers reported. Note that the molarity listed in the legend is not the molarity of the oligomer, but rather the molarity of pentacene monomer for ease of comparison.

3.15 Solvent Dependence in Steady-state Absorption of Oligopentacenes

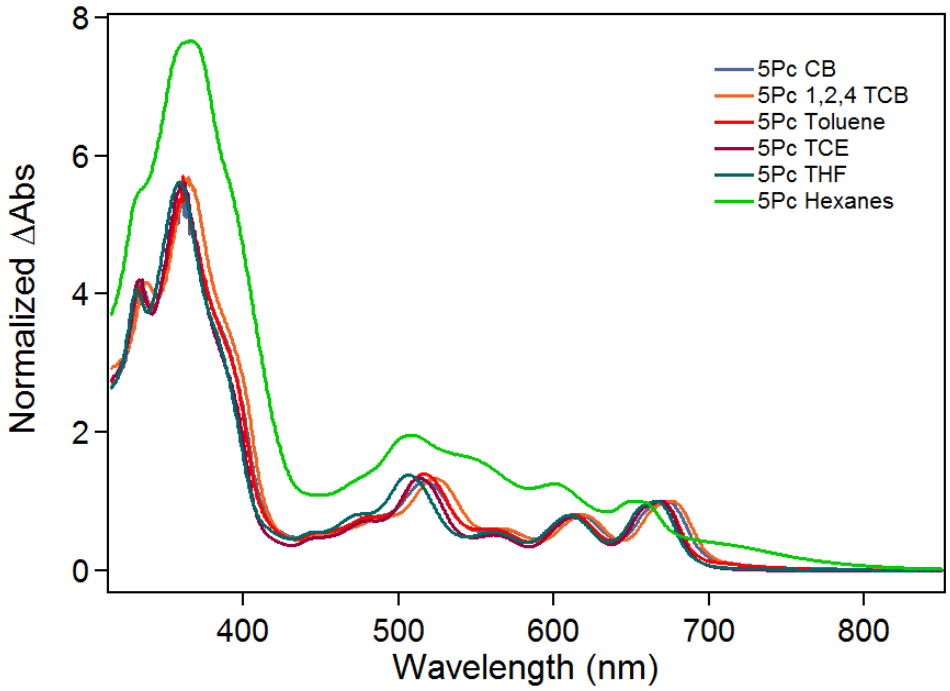

Figure 3.8. Solvent dependence study of pentamer 5Pc in different solvents

While the oligopentacenes were not found to have significant concentration-dependent aggregation, there was evidence for solvent-dependent aggregation. **5Pc** was chosen for an extensive solvent study. This compound has excellent solubility in a variety of solvents, such as chlorinated solvents (trichloroethene, TCE, 1,2,4 trichlorobenzene), aromatic solvents (toluene) and even polar, non-aromatic tetrahydrofuran, due to the strong solubilizing power of the NODIPS chains. However, while it is readily dispersed in hexanes, and will even pass a filter, steady-state absorption suggests significant aggregation in hexanes and other linear hydrocarbon solvents. This aggregation is revealed in a long tail to the absorbance near the onset of absorption and a spectrum which overall resembles the solid-state absorption spectrum.

3.16 Solvent Dependence of Polypentacene

The most significant aggregation was observed for polypentacene. Indeed, at room temperature, significant aggregation was observed in every solvent examined, as shown below.

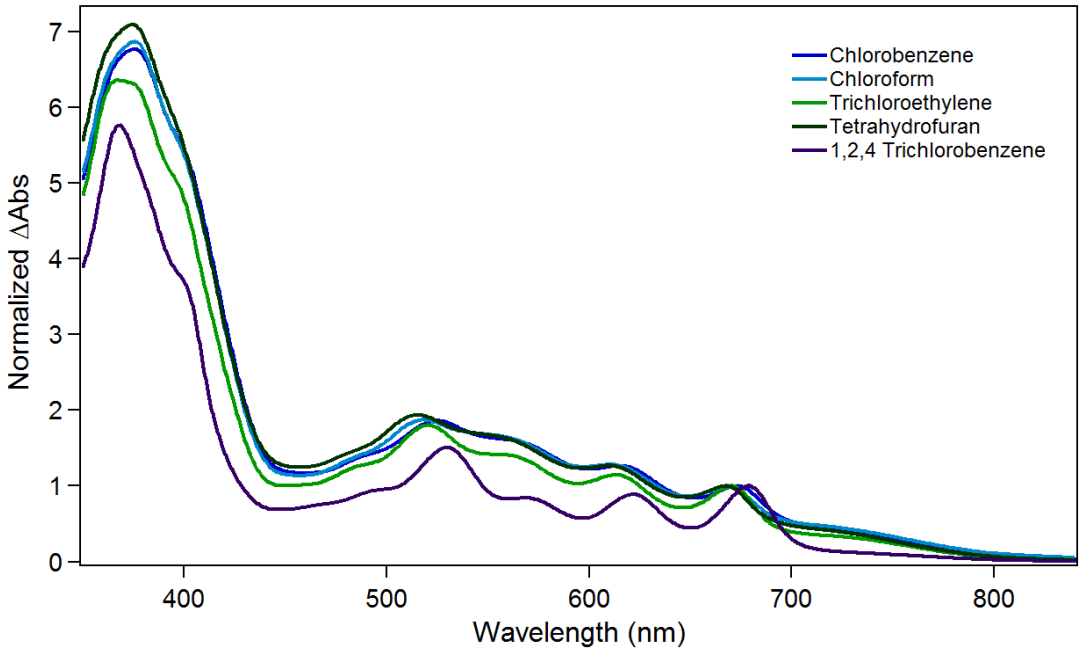

Figure 3.9. Comparison of UV-Visible steady state absorption of polypentacene in varying solvents, normalized to the height of the peak at the onset of absorption

Absorption spectra were taken in a variety of solvents, shown above. The optical density of the solutions were comparable, with the peak at the onset of absorption ranging from 0.13 to 0.24 in a 1 cm quartz cuvette. The spectra were normalized to the peak at the onset to allow for a comparison of spectral shape, which revealed significant aggregation in most solvents tested, manifesting in a red-shifting of the absorption spectra. The aggregation also results in less pronounced peaks associated with vibronic effects. The least evidence for aggregation was observed in 1,2,4 trichlorobenzene.

3.17 Qualitative Photodegradation Studies

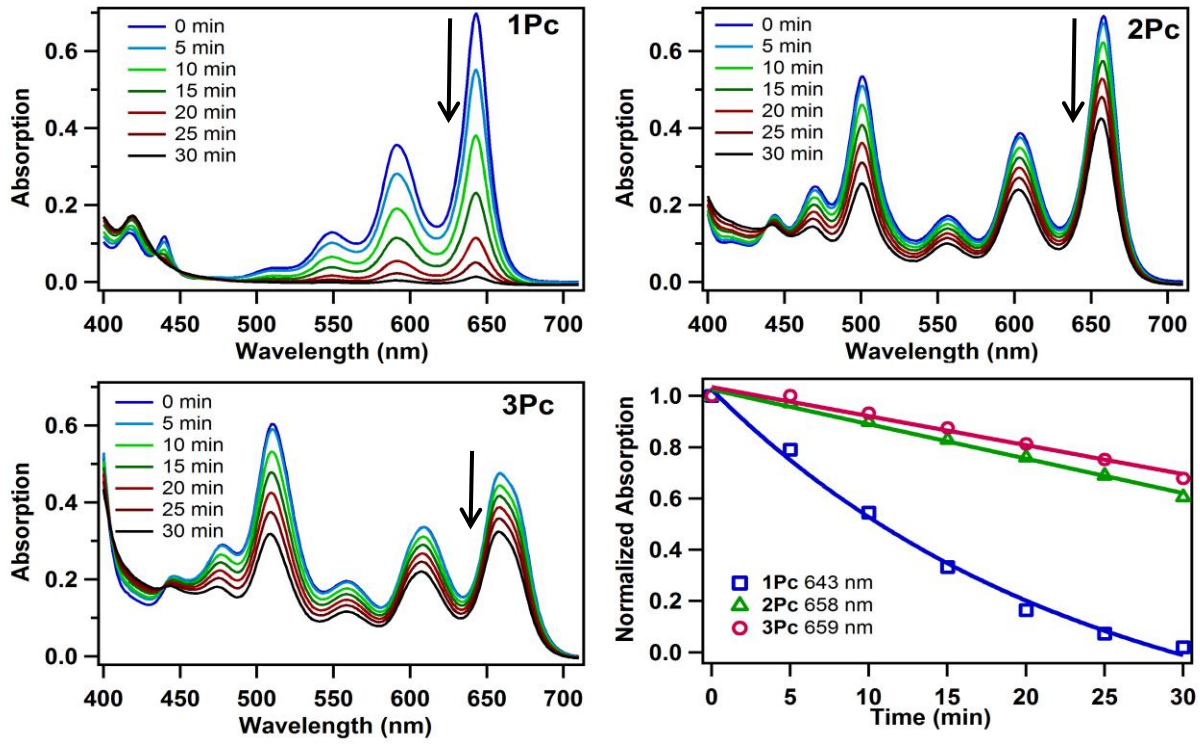

Figure 3.10. Degradation in solution, initially prepared to have ~ 30 µM pentacene repeat units relative to monomer solution in toluene, upon exposure to a ~350 nm lamp under ambient conditions. The absorbance at the maximum absorbance near the onset is plotted as a function of time (bottom right) and fitted with a single exponential.

To investigate the stability of oligomers of pentacene **2-3Pc** relative to pentacene monomer **1Pc**, we prepared toluene solutions of oligomers (~30 µM relative to pentacene monomer) in UV-vis cuvettes and exposed them to a ~350 nm lamp under ambient conditions open to air. Under exposure to the lamp light and oxygen, pentacenes are notorious for their degradation *via* cycloaddition reactions with other pentacene molecules or oxygen.

Because the light source available excites the molecules at 350 nm, and the oligomers **2Pc** and **3Pc** have molar absorptivities at this wavelength ~9 and ~7 times greater than the absorptivity

of monomer at that wavelength, resulting in a significantly larger number of photons absorbed by the oligomers during this experiment. Nevertheless, the oligomers show considerably greater stability than the monomer (Figure 3.10).

This stark difference in photostability may be the result of the starkly different photophysics of oligomers of pentacene relative to monomer. Our group has previously reported that the dimer undergoes singlet fission, where the singlet is converted to a triplet pair in under 1 ps and returns to the ground state with a time constant of ~0.45 ps. To our knowledge, the stability enhancement provided by oligomerization is the first possible implication of singlet fission as a mode of stability enhancement for acene materials, and the specific mechanism of this stabilization is of considerable interest and is underway in our group.

3.18 Cyclic Voltammetry

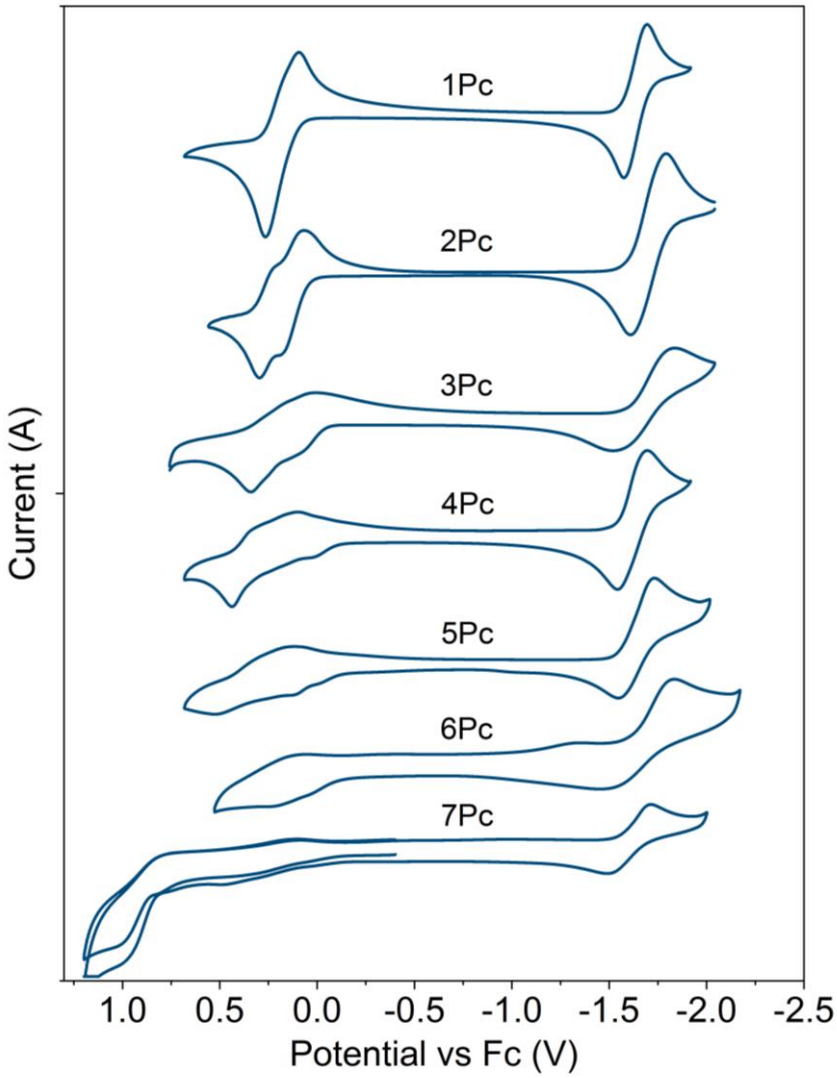

Figure 3.11. Cyclic voltammograms of pentacene oligomer series plotted against the ferrocene oxidation potential. A second sweep of 7Pc is shown to demonstrate the irreversibility.

CV measurements were done using a single cell set-up on a CH Instruments Electrochemical Analyzer potentiostat with a platinum working electrode, platinum wire counter electrode and Ag/AgCl reference electrode all purchased from BASi. Compounds were measured in dichloromethane solution at a concentration of 1-2mg/mL and 0.1 M of tetrabutylammoniumhexafluorophosphate ($TBAPF_6$) as supporting electrolyte. A scan rate of 0.2V/s was used throughout.

From the CVs shown in the figures 3.11 above, the HOMO (or LUMO) levels were extracted from the onset of oxidation (or reduction), which were calibrated against the ferrocene/ferrocenium (Fc/Fc^+) couple, assumed to be at -4.80 eV relative to vacuum. The oxidation peak of the Fc/Fc^+ measured had slight variations and was adjusted using: $E_{Fc} = -(4.80 - E_{Fc,\ measured})V$.[49]

To convert the redox onsets to the HOMO and LUMO levels, the following formulae were used:[49]

$$HOMO = -e(E_{onset,Ox} + (-E_{Fc}))\ (eV)$$

$$LUMO = -e(E_{onset,Red} + (-E_{Fc}))\ (eV)$$

The voltammograms for **1Pc**-**6Pc** showed reversible redox waves under the potential ranges measured. Moving out of these ranges generally resulted in irreversible behavior. The reduction wave of the heptamer was irreversible and diminished greatly after the first sweep. The oxidation wave also diminishes after successive sweeps. In figure 3.11, a full redox scan, starting with oxidation, is shown along with a 2^{nd} oxidation scan to show that the process is irreversible.

The HOMO and LUMO energies obtained from and CV and DFT measurements are provided in the following table. Qualitatively, these results are in good agreement between each other. However, quantitiave comparision is convoluted as so many parameters affect the DFT

obtained numbers. For instance, the basis set used for the calculation, energies of individual molecule in the absence of solvent and temperature at which these calculation were performed (0K vs 298K) can drastically affect the resulting energies of HOMO and LUMO.

Entry	Energies from CV		Energies from DFT	
	HOMO (eV)	LUMO (eV)	HOMO (eV)	LUMO (eV)
1Pc	-4.89	-3.24	-4.61	-2.71
2Pc	-4.85	-3.20	-4.56	-2.81
3Pc	-4.76	-3.20	-4.54	-2.86
4Pc	-4.69	-3.25	-4.54	-2.87
5Pc	-4.68	-3.26	-	-
6Pc	-4.68	-3.21	-	-
7Pc	-4.67	-3.25	-	-

3.19 Thermogravimetric and Differential Scanning Calorimetric Analysis

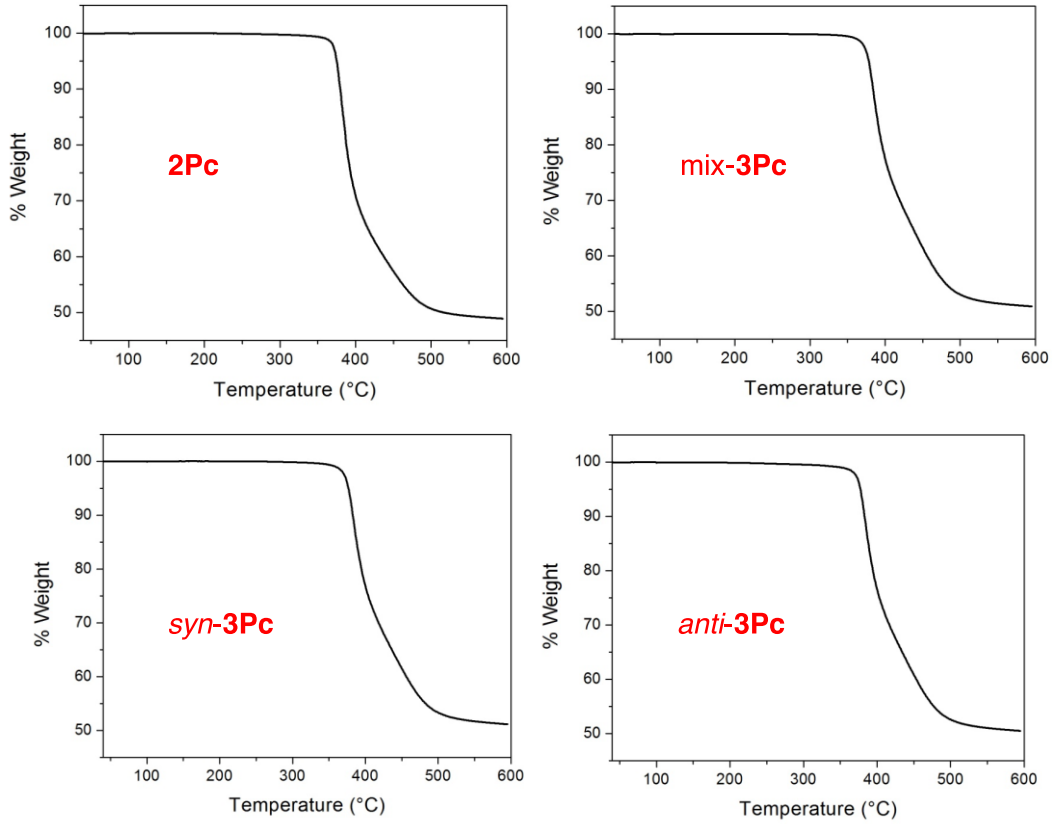

Figure 3.12. TGA graph of oligopentacenes **2Pc-3Pc**

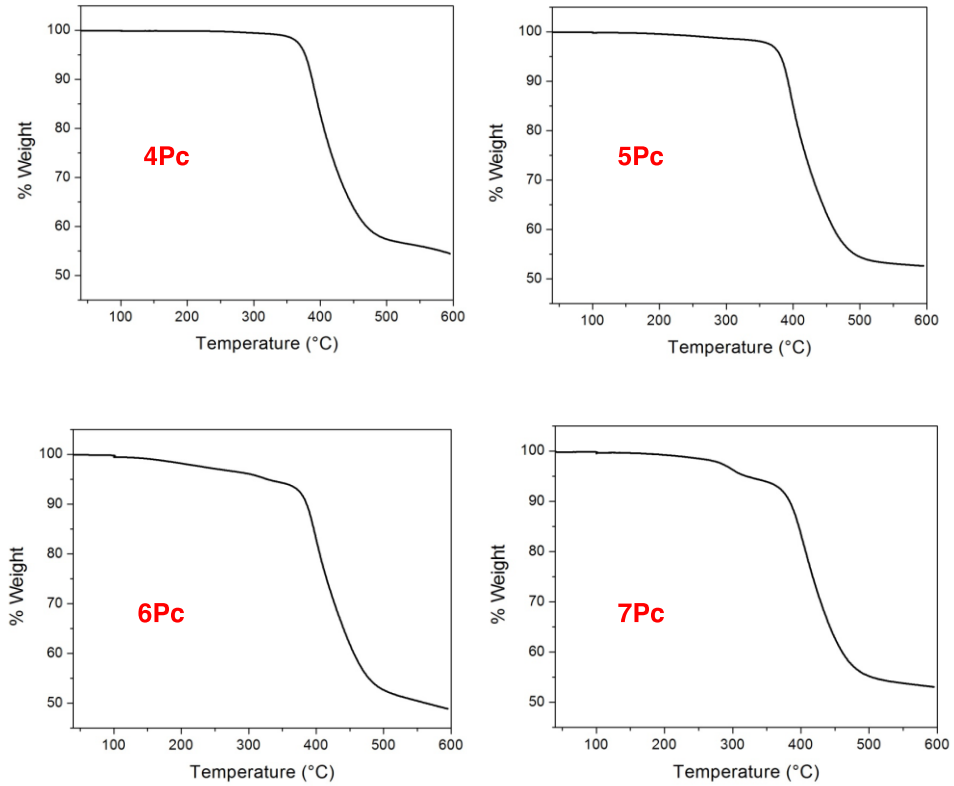

Figure 3.13. TGA graph of oligopentacenes **4Pc-7Pc**

Differential scanning calorimetry (DSC) was performed on a Q200 instrument (TA-instrument) under N_2 flow at a heating/cooling rate of 5 °C/min.

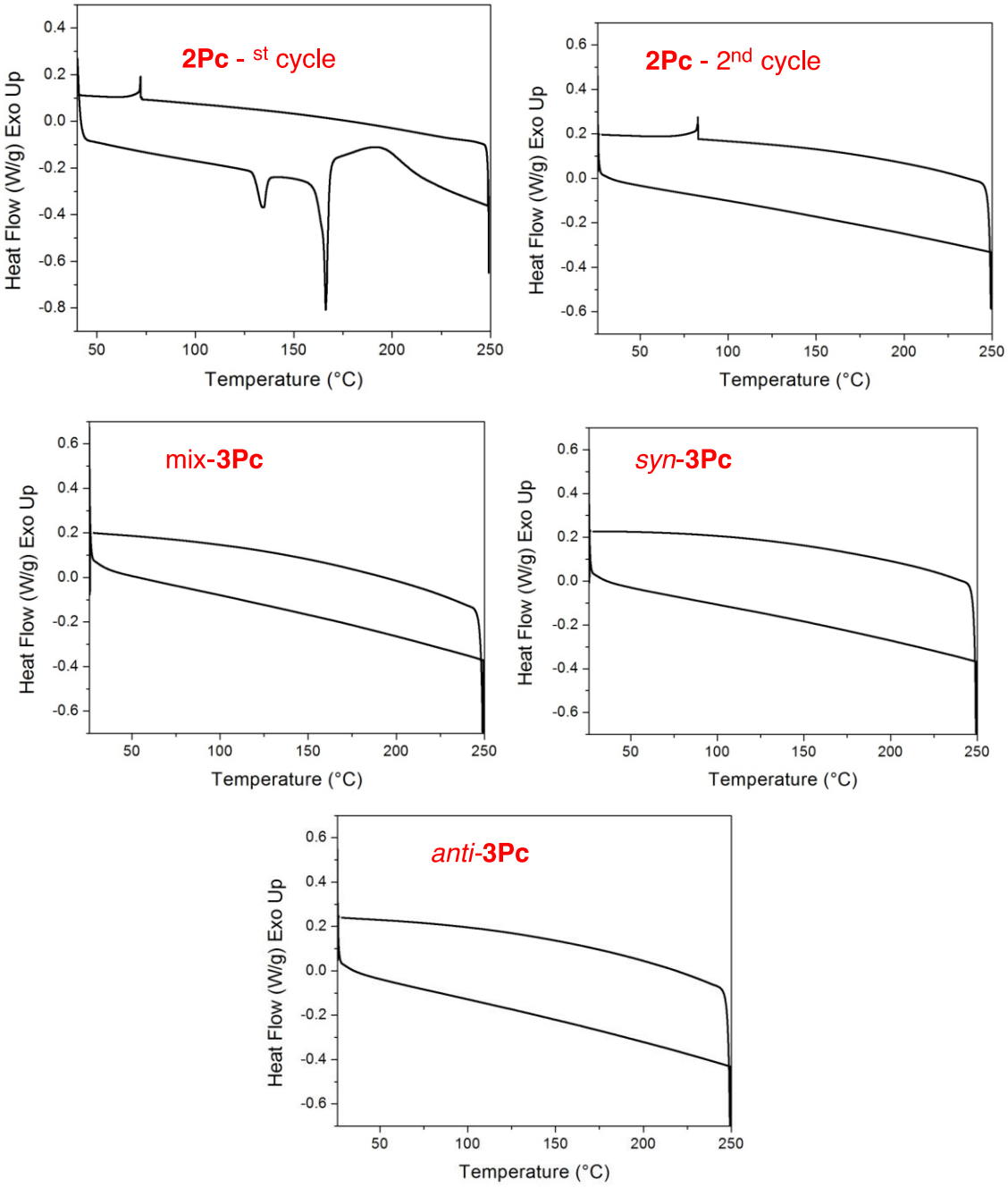

Figure 3.14. DSC traces of oligopentacenes **2Pc-3Pc**

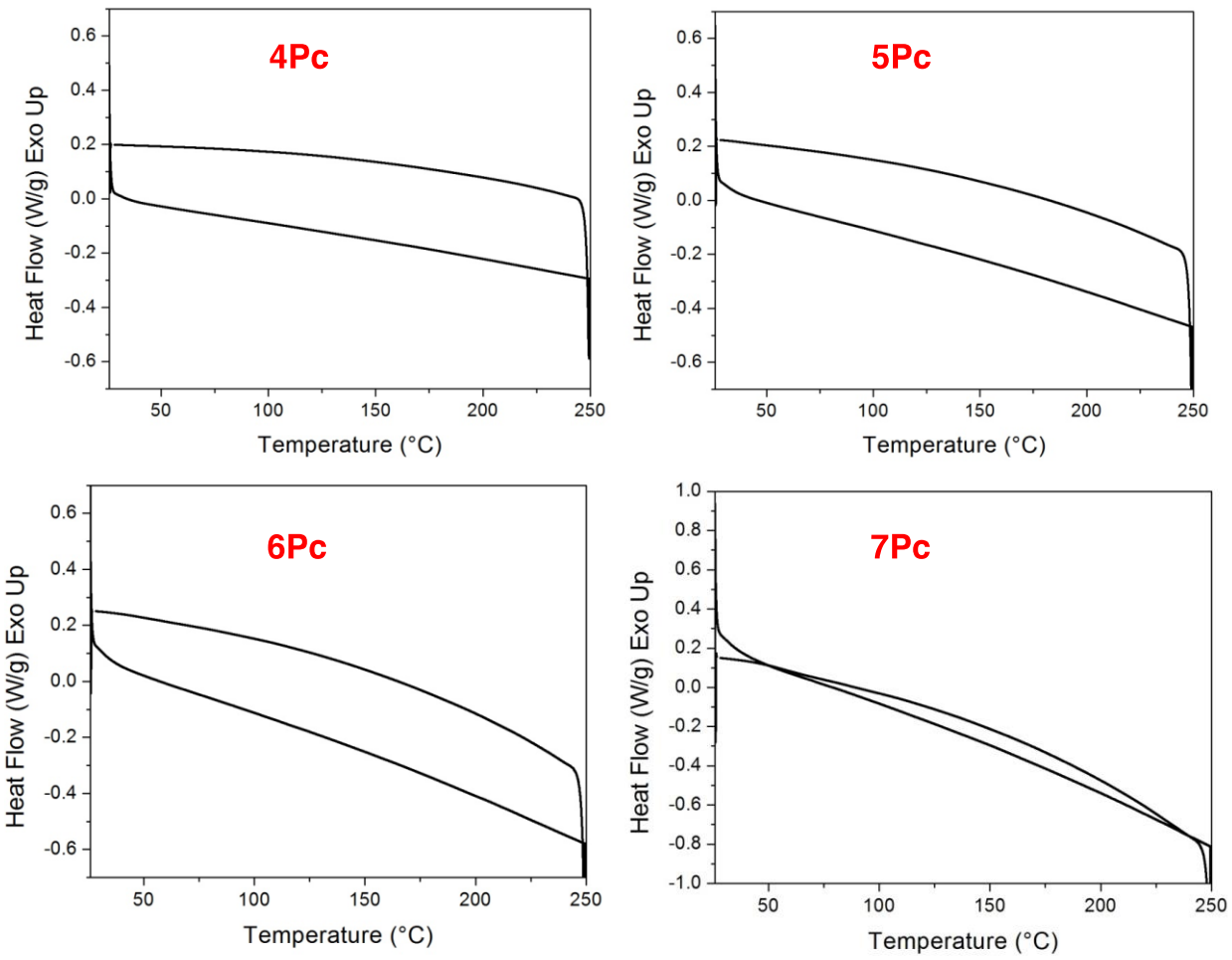

Figure 3.15. DSC traces of oligopentacenes **4Pc-7Pc**.

3.20 GIWAXS Analysis

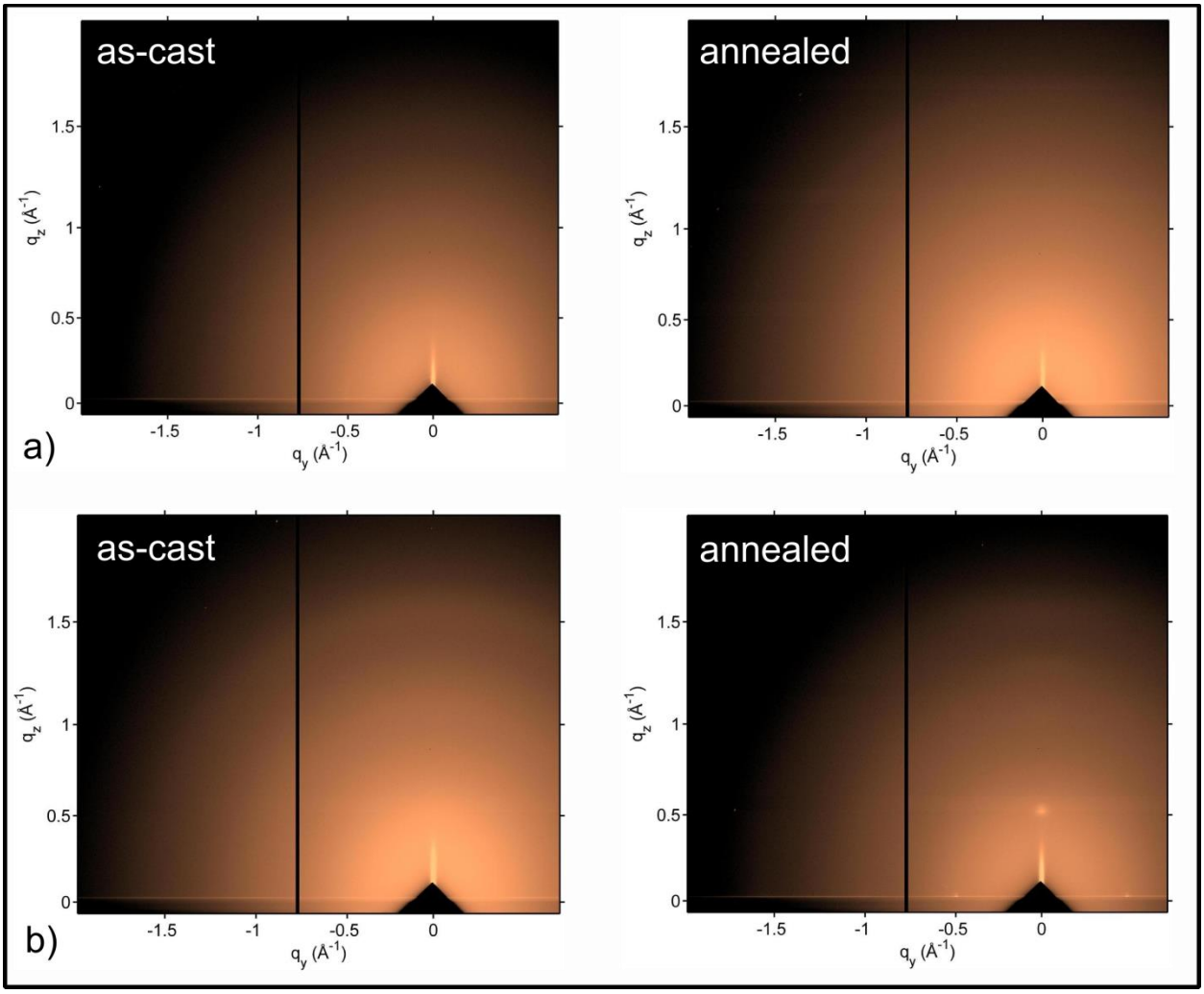

Figure 3.16. a) 2D GIWAXS patterns of pentacene dimer (**2Pc**); left side image is the as-cast, while the image on the right is the annealed thin film. **b)** Mixture of pentacene trimer (**mix-3Pc**) 2D GIWAXS patterns, for left) as-cast, and right) annealed thin films.

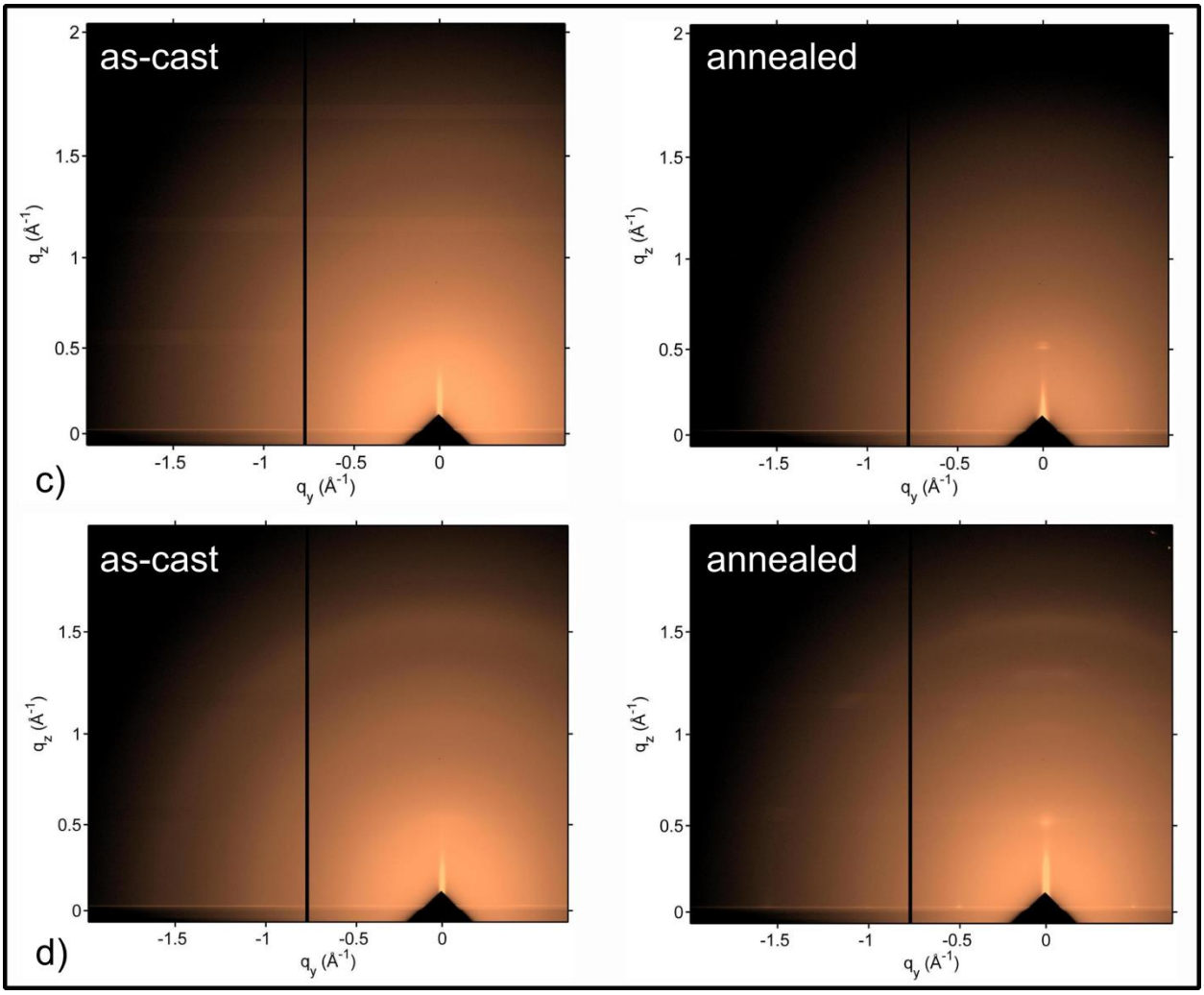

Figure 3.17. c) *syn*-Pentacene trimer (***syn*-3Pc**) 2D GIWAXS patterns; left side image is the as-cast, while the image on the right is the annealed thin film. **d)** 2D GIWAXS patterns of, left) as-cast, and right) annealed *anti*-pentacene trimer (***anti*-3Pc**) thin films.

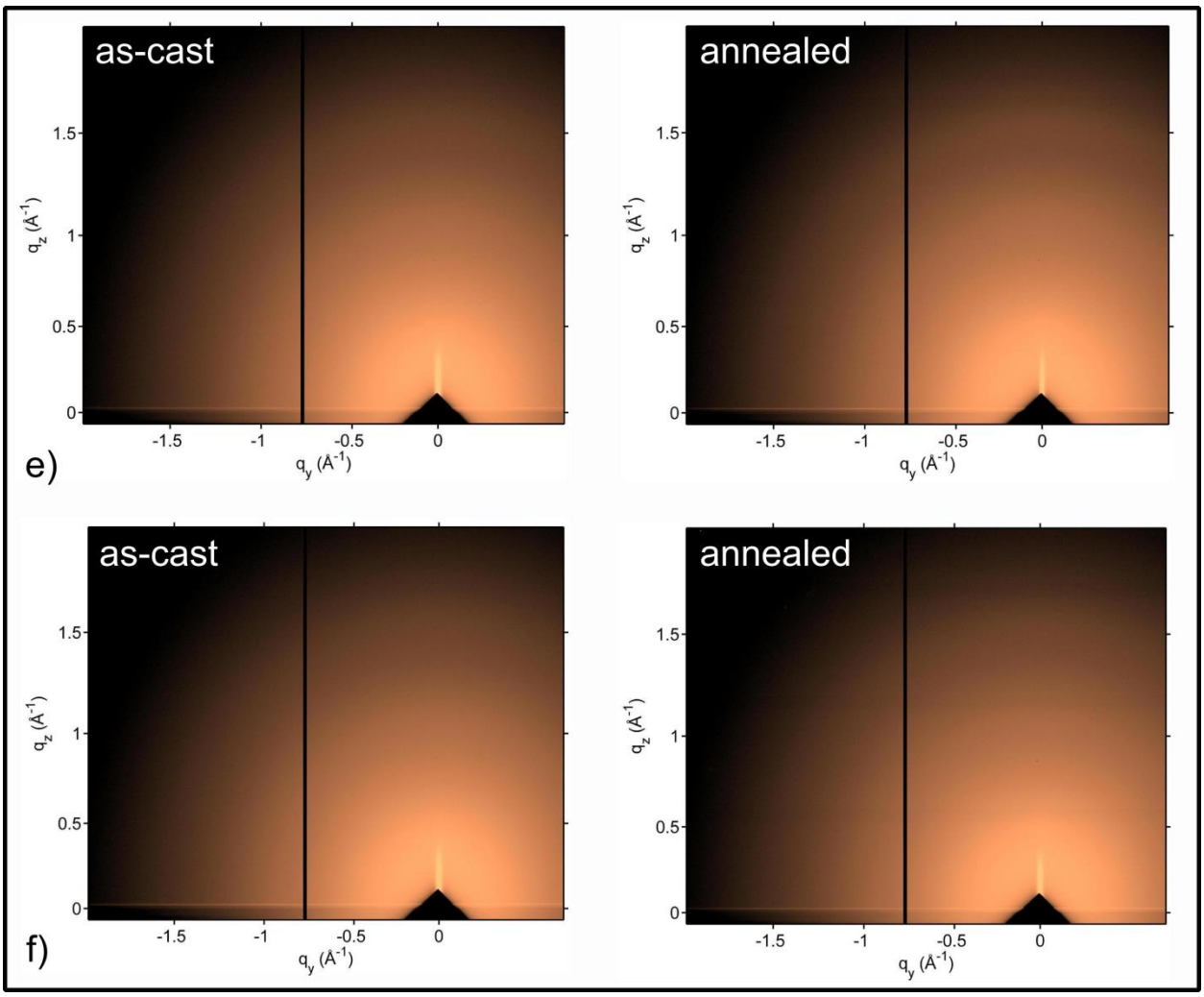

Figure 3.18. e) Pentacene tetramer (**4Pc**) 2D GIWAXS patterns; left side image is the as-cast, while the image on the right is the annealed thin film. **f)** 2D GIWAXS patterns of, left) as-cast, and right) annealed pentacene pentamer (**5Pc**) thin films.

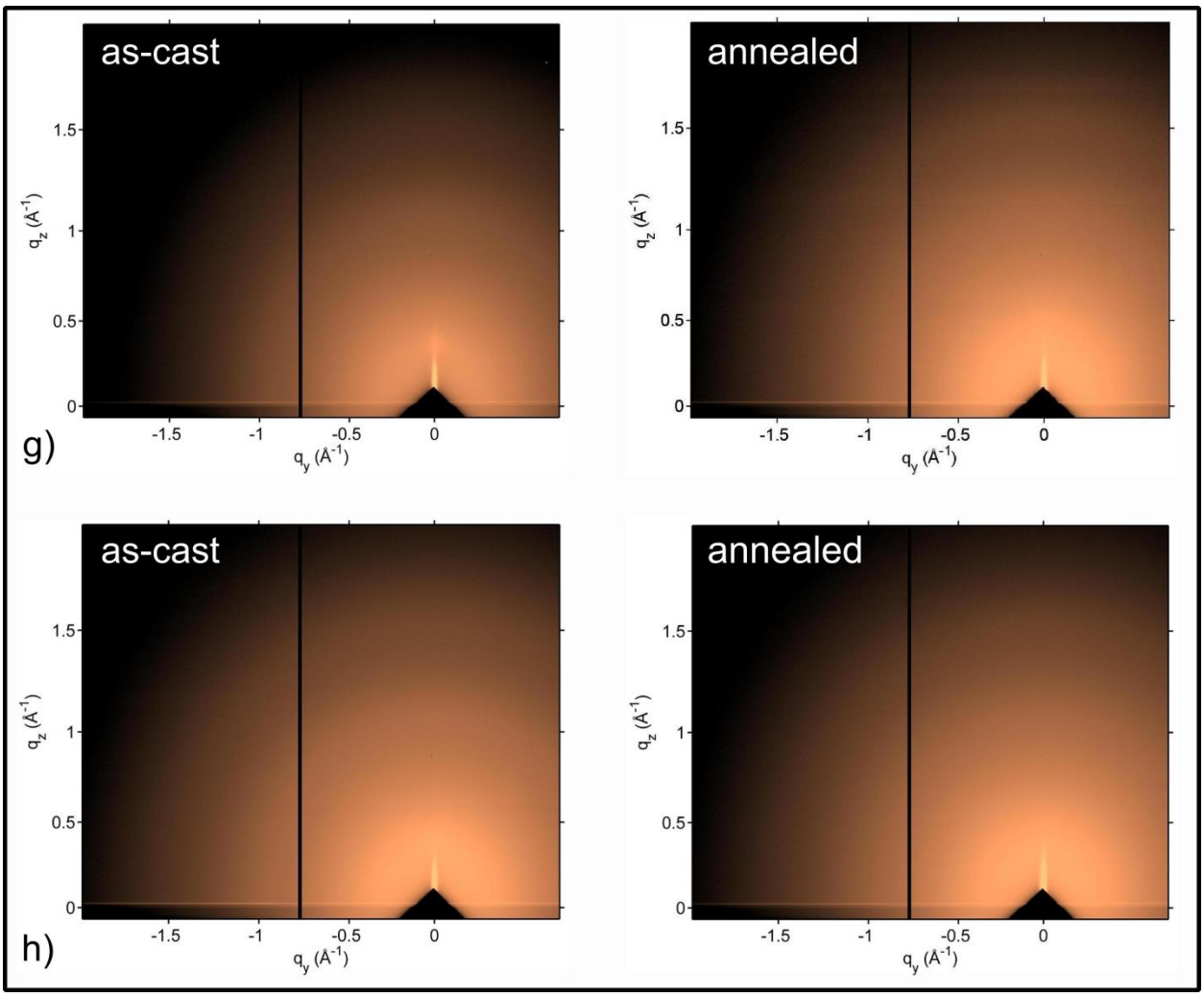

Figure 3.19: g) Pentacene hexamer (**6Pc**) 2D GIWAXS patterns; left side image is the as-cast, while the image on the right is the annealed thin film. **h)** 2D GIWAXS patterns of, left) as-cast, and right) annealed pentacene heptamer (**7Pc**) thin films.

3.21 Details of DFT and TD-DFT Calculations

All DFT and TD-DFT calculations were carried out using Jaguar, version 8.3, Schrodinger, Inc., New York, NY, 2014.

The geometries of **1Pc**, **2Pc**, **3Pc**, and **4Pc** were fully optimized at the B3LYP/6-31G** level. In the cases of the latter three molecules the variations in total energy with rotations about the pentacene-pentacene bonds are quite small over a wide range of angles, so there is latitude in the choice of geometrical optima with respect to these coordinates. In the cases of the trimer and tetramer we studied only the trans regioisomers. We have included the Cartesian coordinates for each molecule below. Additional geometrical data (distances, angles, torsional angles) is available on request.

Using TD-DFT we calculated the absorption spectrum for each molecule at its optimum geometry. Plots of these calculated spectra are available on request.

3.22 NMR Spectra of oligopentacenes and their intermediates

^{1}H-NMR (400 MHz, $CDCl_3$, δ ppm): 9.39-9.38 (m, 2H), 9.35 (s, 1H), 9.28 (s, 1H), 8.25 (s, 1H), 8.10-8.08 (m, 2H), 7.95-7.93 (m, 1H), 7.54-7.51 ((m, 3H), 1.90-1.81 (m, 4H), 1.64-1.57 (m, 4H), 1.49-1.33 (m, 44H), 1.07-1.02 (m, 4H) and 0.96-0.92 (m, 6H).

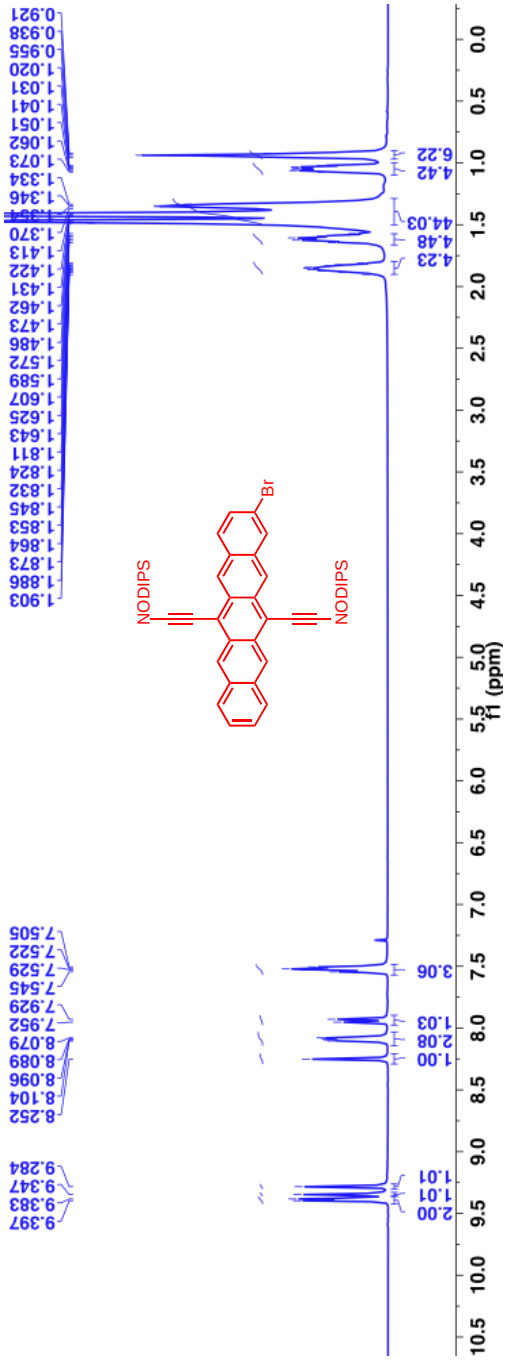

^{13}C-NMR (100 MHz, $CDCl_3$, δ ppm): 132.7, 132.6, 132.5, 130.9, 130.87, 130.7, 130.6, 130.4, 130.3, 130.27, 125.6, 128.7, 126.9, 126.5, 126.4, 126.2, 126.2, 125.5, 120.4, 118.7, 118.6, 107.98, 104.4, 34.1, 34.09, 32.1, 29.6, 29.58, 29.49, 29.46, 25.1, 25.0, 22.8, 18.8, 18.5, 14.2, 12.3 and 10.5.

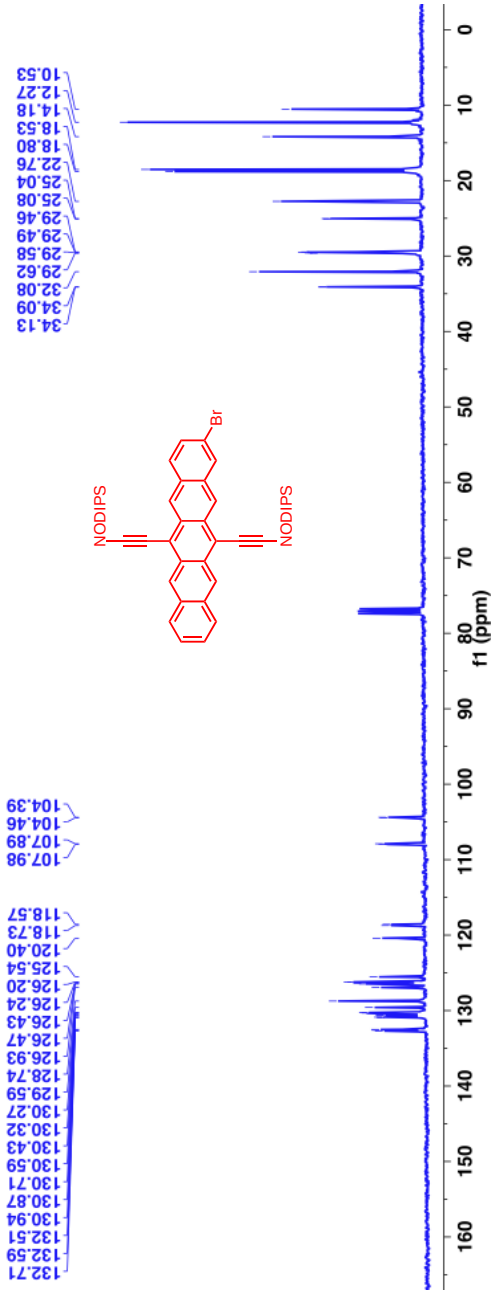

^{1}H-NMR (500 MHz, $CDCl_3$, δ ppm): 9.34-9.33 (m, 2H), 9.31 (s, 1H), 9.27 (s, 1H), 8.56 (s, 1H), 8.02-7.95 (m, 3H), 7.75-7.73 (m, 1H), 7.46-7.43 (m, 2H), 1.79-1.74 (m, 4H), 1.56-1.51 (m, 4H), 1.47 (s, 12H), 1.39-1.33 (m, 35H), 1.28-1.24 (m, 8H), 1.02-0.95 (m, 5H) and 0.87-0.82 (m, 6H).

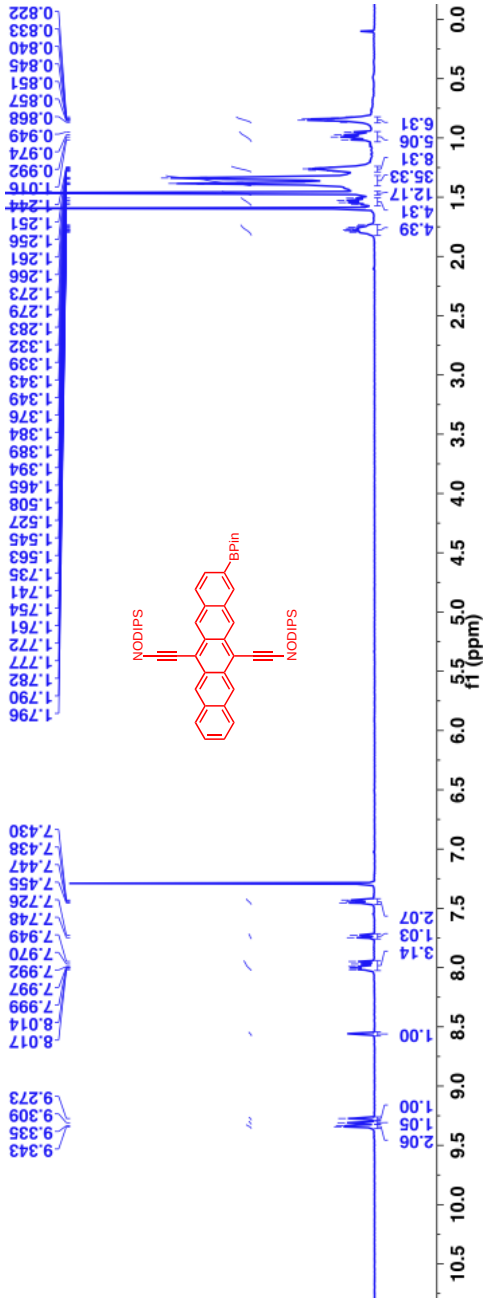

^{13}C-NMR (125 MHz, $CDCl_3$, δ ppm): 138.2, 133.3, 132.5, 132.46, 131.98, 131.3, 130.9, 130.85, 130.7, 129.8, 128.8, 127.8, 127.6, 126.5, 126.4, 126.2, 118.96, 118.4, 107.9, 107.6, 104.7, 104.6, 84.1, 34.1, 32.1, 29.6, 29.5, 25.0, 22.8, 18.9, 18.8, 18.6, 18.56, 14.2, 12.3 and 10.6.

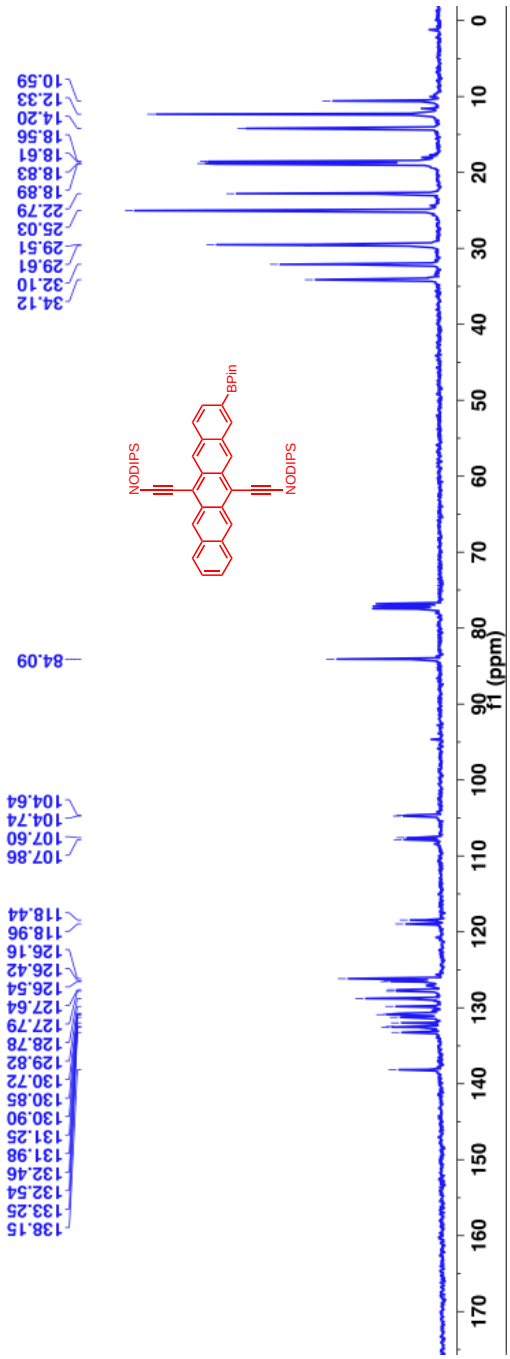

^{1}H-NMR (400 MHz, $CDCl_3$, δ ppm): 9.27 (s, 2H), 9.21 (s, 2H), 8.18 (s, 2H), 7.89-7.88 9.27 (m, 2H), 7.50-7.47 9.27 (m, 2H), 1.83-1.73 (m, 4H), 1.58-1.49 (m, 4H), 1.41-1.27 (m, 44H), 1.01-0.96 (m, 4H) and 0.88-0.85 (m, 6H).

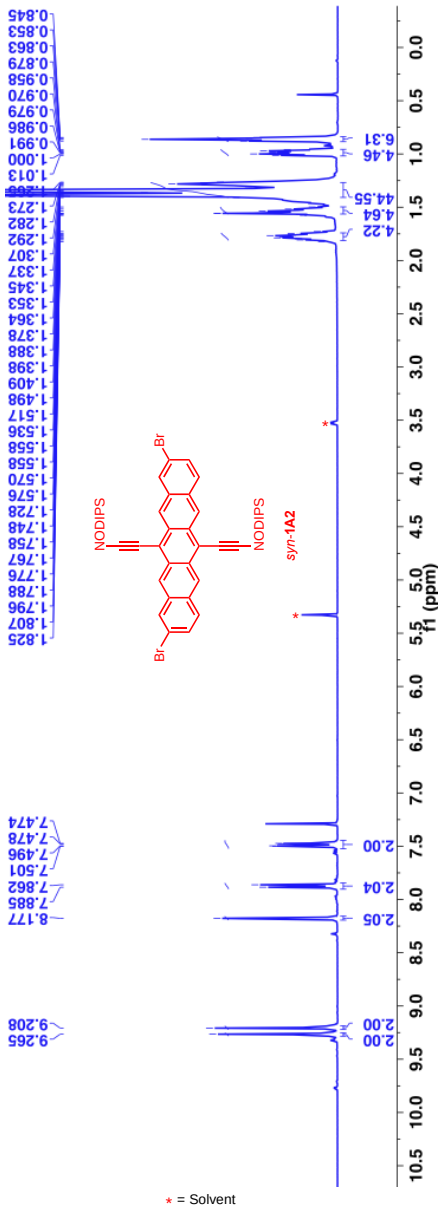

^{13}C-NMR (125 MHz, $CDCl_3$, δ ppm): 132.8, 131.0, 130.5, 130.4, 130.35, 130.2, 129.8, 129.7, 126.95, 125.5, 120.6, 118.9, 118.6, 108.4, 108.2, 104.1, 103.98, 34.1, 34.09, 34.06, 32.0, 29.6, 28.59, 29.55, 29.49, 29.46, 29.43, 25.1, 25.04, 25.0, 22.8, 22.7, 18.8, 18.77, 18.5, 18.49, 14.2, 12.2, 10.5 and 10.45.

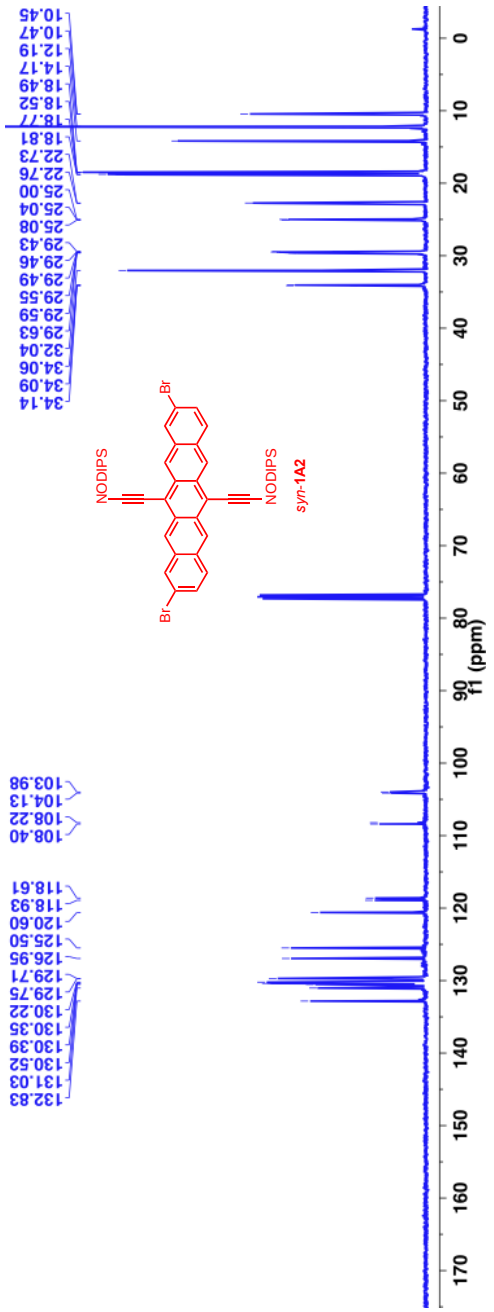

^{1}H-NMR (500 MHz, $CDCl_3$, δ ppm): 9.27 (s, 2H), 9.19 (s, 2H), 8.18 (s, 2H), 7.89-7.87 (m, 2H), 7.50-7.48 (m, 2H), 1.82-1.76 (m, 4H), 1.59-1.53 (m, 4H), 1.46-1.29 (m, 44H), 1.01-0.98 (m, 4H) and 0.89-0.88 (m, 6H).

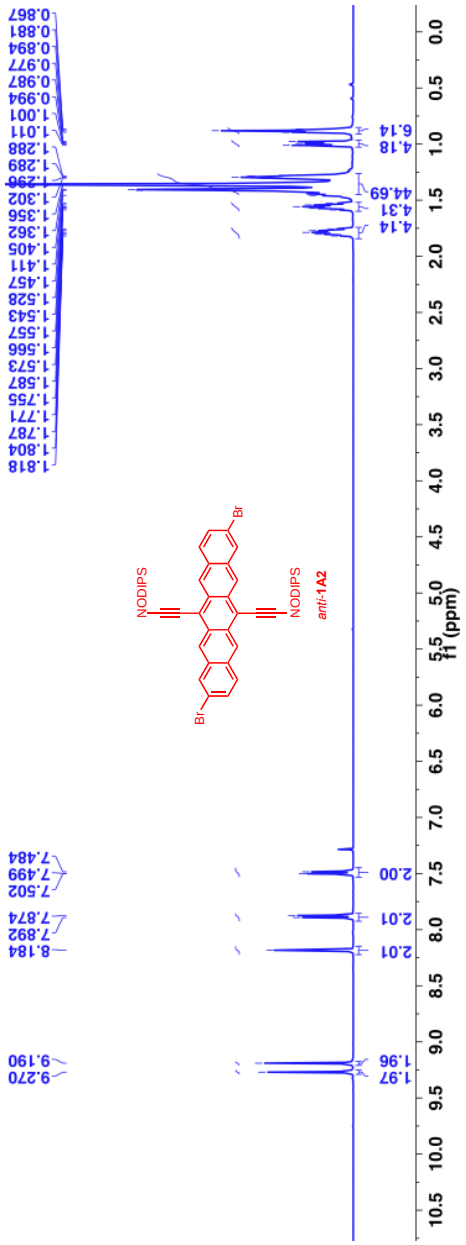

^{13}C-NMR (125 MHz, $CDCl_3$, δ ppm): 132.7, 130.8, 130.76, 130.5, 130.4, 130.2, 129.7, 126.9, 125.6, 120.5, 118.8, 108.3, 104.0, 34.0, 32.0, 29.5, 29.4, 25.0, 22.7, 18.8, 18.5, 14.1, 12.2 and 10.4.

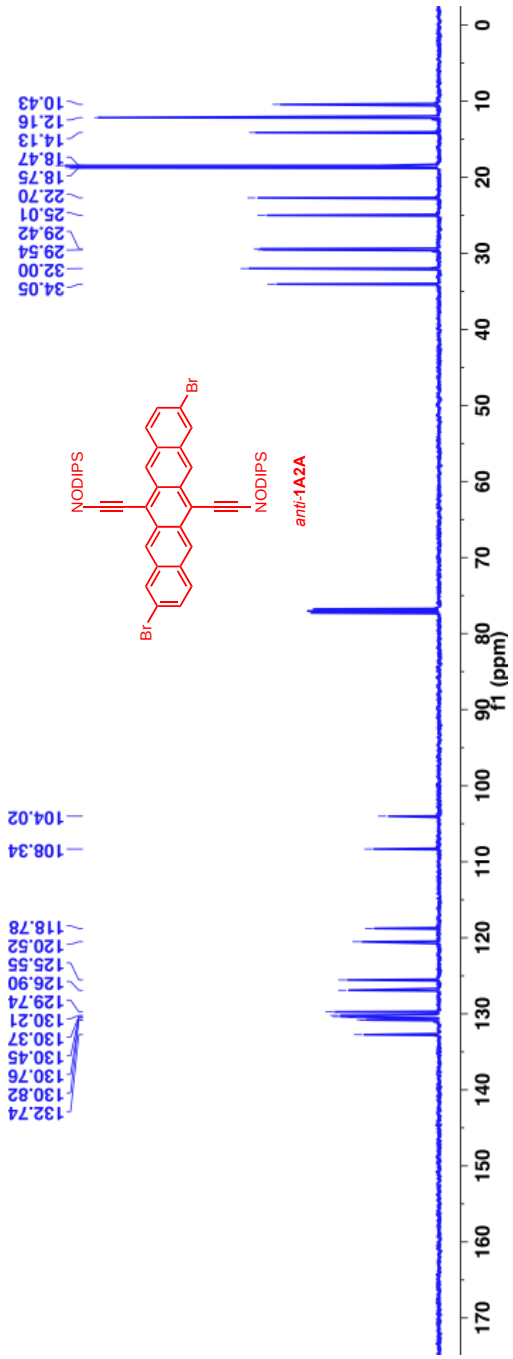

^{1}H-NMR (500 MHz, $CDCl_3$, δ ppm): 9.39 (s, 1H), 9.37 (s, 1H), 9.32 (s, 1H), 9.29 (s, 1H), 8.57 (s, 2H), 7.98-7.96 (m, 2H), 7.77-7.75 (m, 2H), 1.85-1.76 (m, 4H), 1.61-1.53 (m, 5H), 1.47 (s, 24H), 1.41-1.35 (m, 35H), 1.29-1.26 (m, 8H), 1.03-0.99 (m, 4H) and 0.88-0.83 (m, 6H).

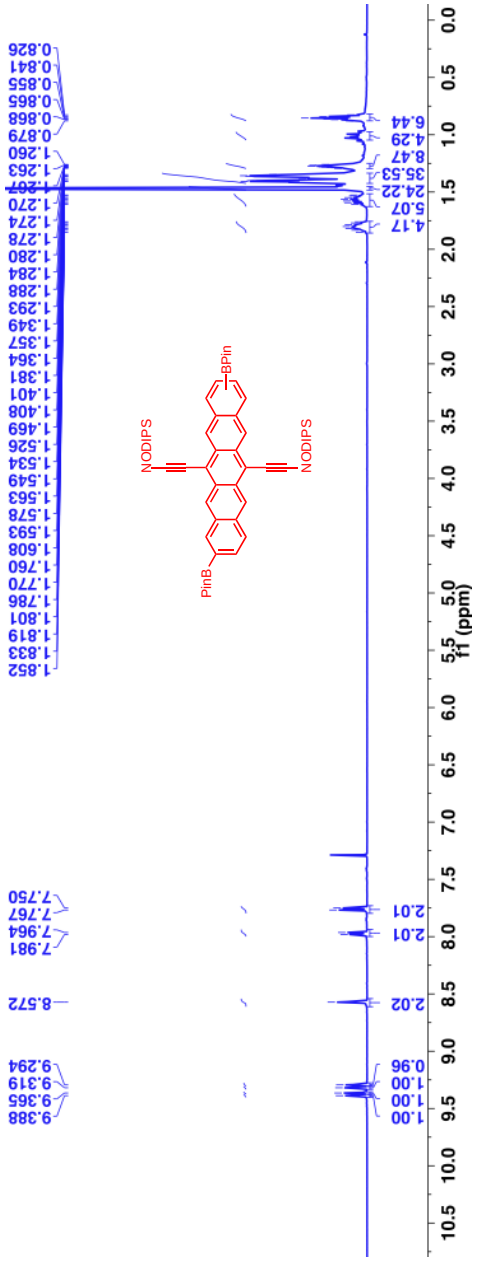

^{13}C-NMR (125 MHz, $CDCl_3$, δ ppm): 138.1, 138.0, 134.8, 133.2, 133.1, 131.9, 131.86, 131.3, 131.2, 130.8, 130.7, 129.8, 129.7, 127.8, 127.7, 127.6, 127.55, 126.2, 126.1, 119.3, 118.8, 118.3, 108.1, 107.9, 107.6, 104.6, 104.5, 104.4, 84.1, 34.1, 34.0, 33.97, 32.0, 32.01, 29.5, 29.4, 29.40, 29.3, 24.99, 22.7, 18.9, 18.8, 18.78, 18.6, 18.55, 18.5, 14.2, 12.2, 10.5 and 10.49.

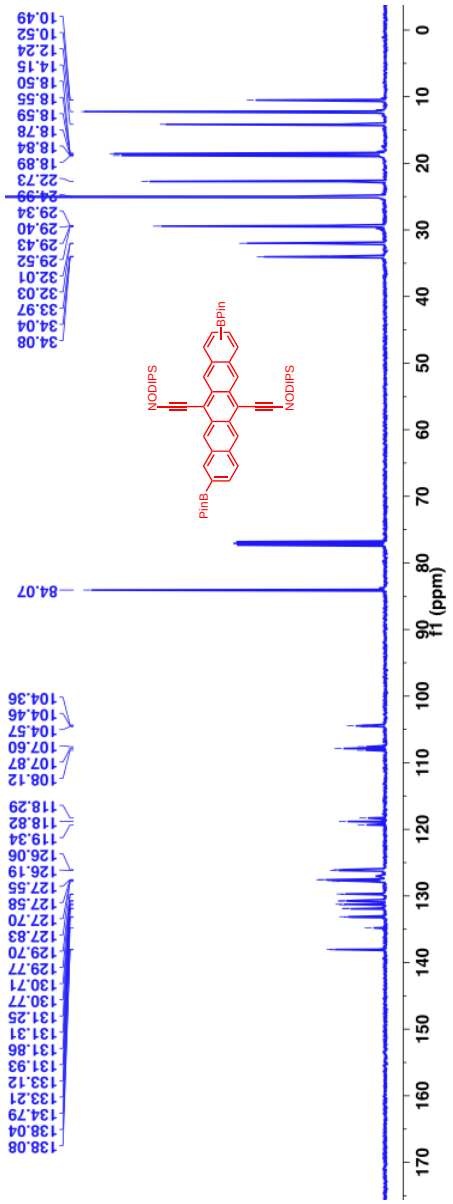

^{1}H-NMR (500 MHz, $CDCl_3$, δ ppm): 9.27-9.25 (m, 2H), 9.19-9.18 (m, 2H), 8.16 (m, 2H), 7.87-7.86 (m, 2H), 7.48-7.46 (m, 2H), 1.78-1.73 (m, 4H), 1.53-1.51 (m, 4H), 1.36-1.19 (m, 88H) and 0.89 (t, 6H).

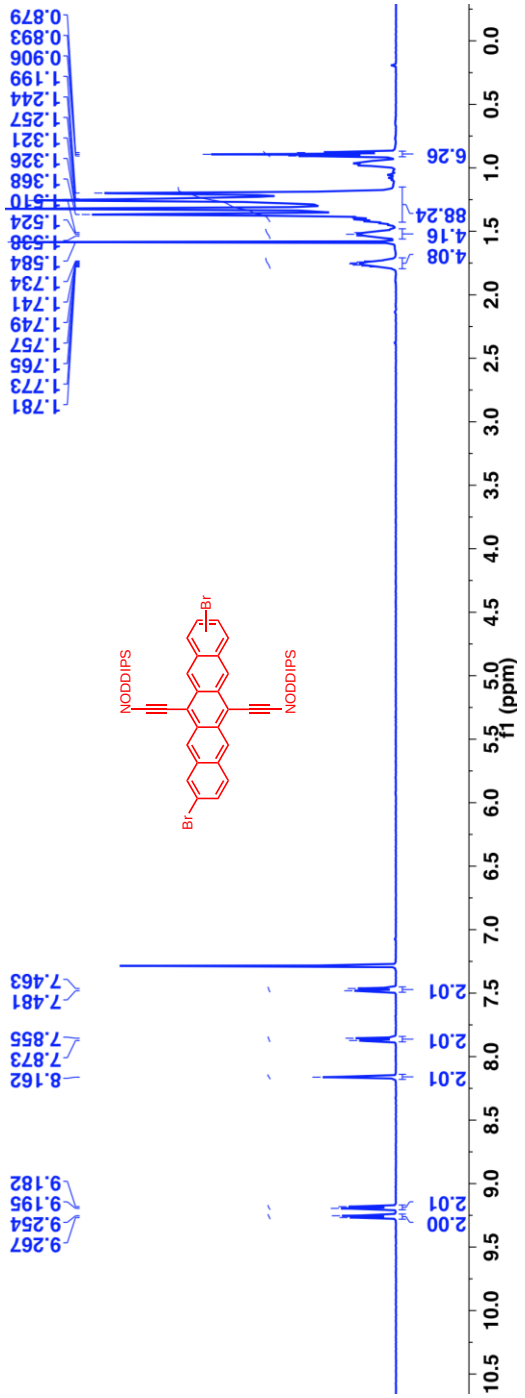

^{13}C-NMR (125 MHz, $CDCl_3$, δ ppm): 132.8, 132.7, 131.0, 130.8, 130.7, 130.5, 130.4, 130.38, 130.34, 130.2, 129.74, 129.71, 126.96, 126.91, 125.6, 125.5, 120.6, 120.5, 118.9, 118.8, 118.6, 108.4, 108.3, 108.2, 34.1, 34.0, 33.9, 31.9, 29.8, 29.73, 29.70, 29.6, 29.56, 29.52, 29.40, 25.0, 24.98, 24.94, 22.7, 18.8, 18.73, 18.71, 18.5, 18.45, 18.43, 14.2, 12.1 and 10.4.

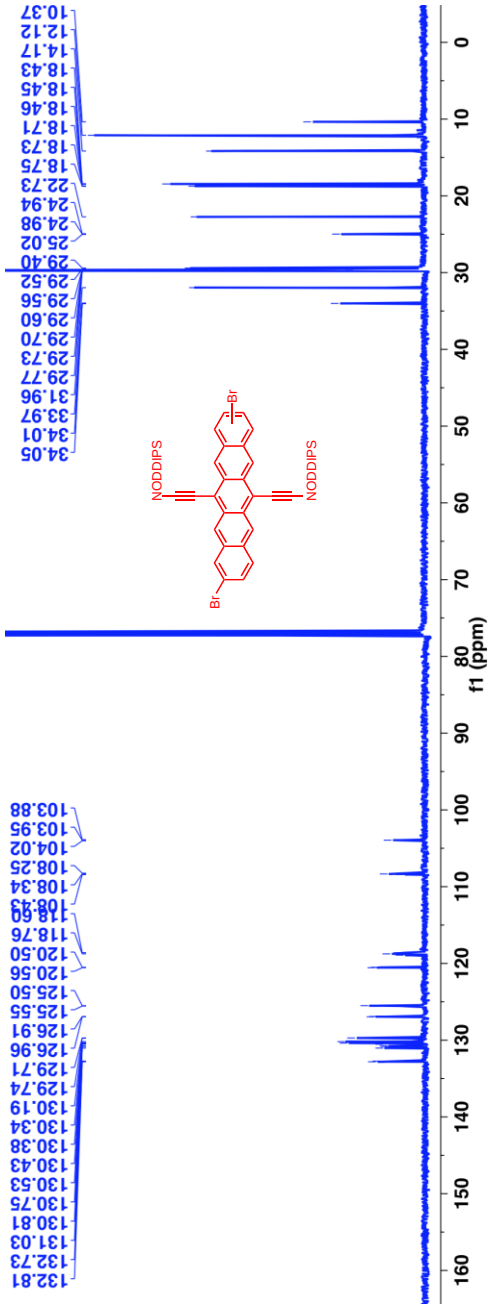

^{1}H-NMR (500 MHz, $CDCl_3$, δ ppm): 9.36-9.34 (m, 2H), 9.29-9.27 (m, 2H), 8.55 (s, 2H), 7.96-7.94 (m, 2H), 7.74-7.72 (m, 2H), 1.81-1.75 (m, 4H), 1.56-1.49 (m, 4H), 1.46 (s, 24H), 1.40-1.19 (m, 88H) and 0.89 (t, 6H).

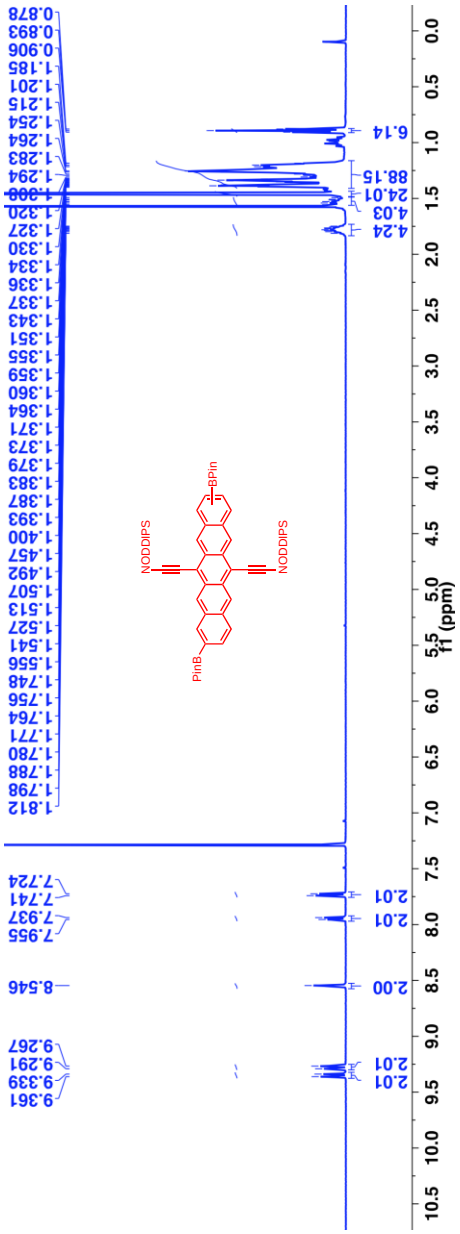

^{13}C-NMR (125 MHz, $CDCl_3$, δ ppm): 138.0, 137.9, 133.1, 133.0, 131.8, 131.7, 131.2, 131.1, 130.7, 130.6, 129.7, 129.6, 127.8, 127.6, 127.52, 127.50, 126.1, 125.99, 119.3, 118.8, 118.2, 108.1, 107.8, 107.5, 104.5, 104.4, 104.3, 84.0, 33.99, 33.96, 33.90, 31.9, 29.8, 29.71, 29.70, 29.7, 29.5, 29.4, 29.37, 29.31, 24.9, 22.7, 18.8, 18.78, 18.72, 18.5, 18.5, 18.45, 14.1, 12.2 and 10.5.

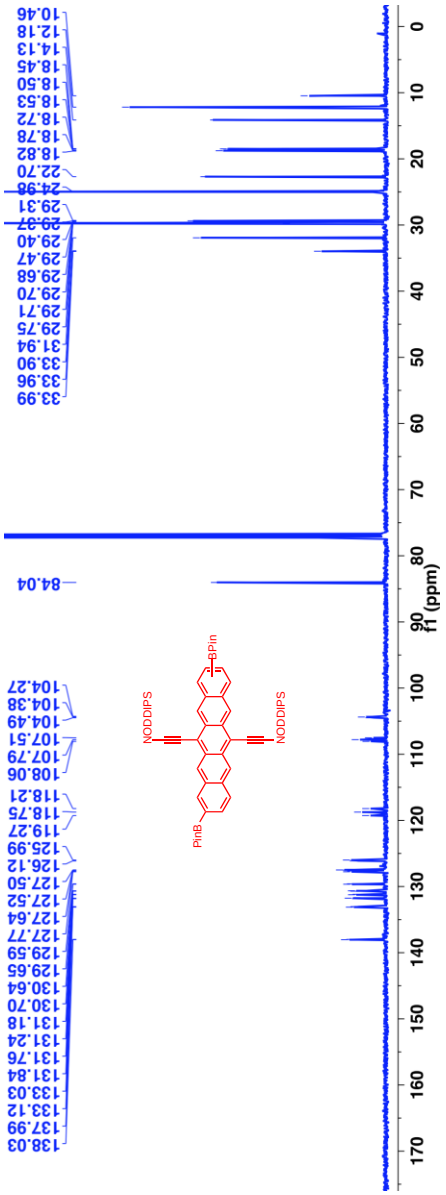

^{1}H-NMR (500 MHz, $CDCl_3$, δ ppm): 9.43-9.41 (m, 2H), 9.36-9.30 (m, 5H), 9.23-9.22 (m, 1H), 8.38 (s, 2H), 8.19-8.17 (m, 3H), 8.04-7.95 (m, 4H), 7.89-7.88 (m, 1H), 7.49-7.45 (m, 3H), 1.84-1.78 (m, 8H), 1.45-1.28 (m, 85H), 1.22-1.18 (m, 10H), 1.03-0.99 (m, 9H), 0.88-0.85 (m, 6H) and 0.78-0.75 (m, 6H).

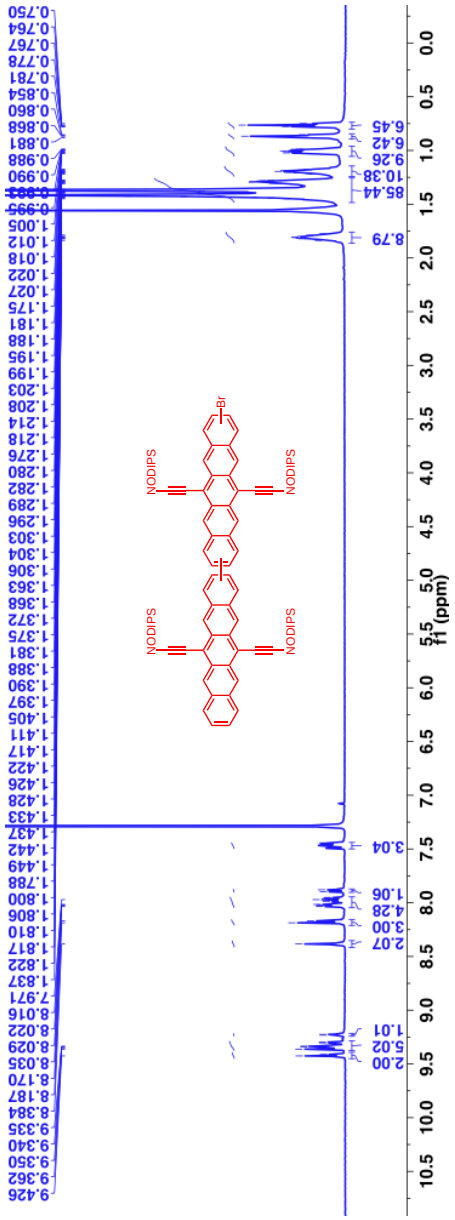

^{13}C-NMR (125 MHz, $CDCl_3$, δ ppm): 137.8, 137.5, 132.7, 132.69, 132.6, 132.4, 132.39, 132.36, 131.8, 131.7, 131.6, 131.3, 131.1, 131.0, 130.96, 130.91, 130.88, 130.85, 130.76, 130.67, 130.57, 130.4, 130.3, 130.29, 130.2, 129.6, 129.59, 128.7, 126.9, 126.4, 126.2, 126.1, 125.8, 125.5, 120.4, 118.8, 118.6, 118.5, 118.4, 118.3, 108.1, 108.0, 107.99, 107.9, 107.7, 107.5, 104.6, 104.5, 104.3, 34.13, 34.1, 34.09, 34.08, 34.07, 34.05, 32.0, 31.9, 29.6, 29.56, 29.54, 29.51, 29.45, 29.42, 29.40, 25.1, 25.06, 25.03, 25.0, 22.7, 22.69, 22.66, 22.64, 18.8, 18.79, 18.76, 18.5, 18.49, 14.1, 14.0, 12.23, 12.20, 10.52, 10.50 and 10.48.

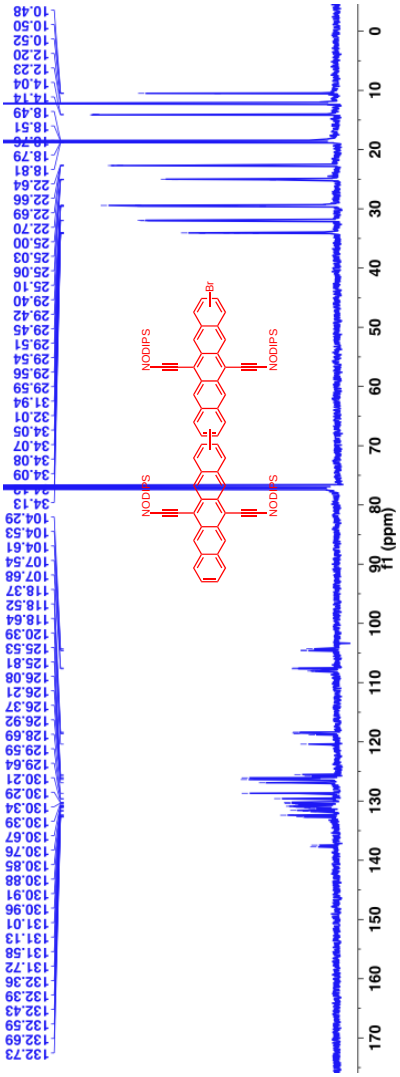

^{1}H-NMR (500 MHz, $CDCl_3$, δ ppm): 9.46-9.31 (m, 8H), 8.58 (s, 1H), 8.39 (s, 2H), 8.19-8.17 (m, 2H), 7.99-7.96 (m, 5H), 7.77-7.75 (m, 1H), 7.47-7.45 (m, 2H), 1.84-1.79 (m, 8H), 1.47 (s, 12H), 1.43-1.37 (m, 69H), 1.30-1.19 (m, 26H), 1.03-0.99 (m, 9H), 0.88-0.86 (m, 6H) and 0.78-0.75 (m, 6H).

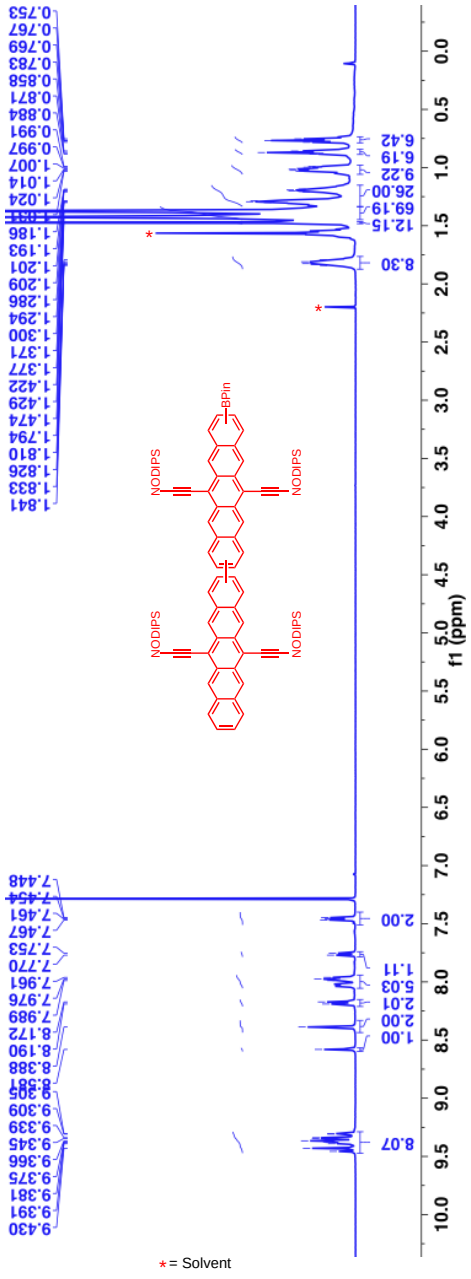

^{13}C-NMR (125 MHz, $CDCl_3$, δ ppm): 138.1, 137.7, 137.65, 133.2, 133.28, 132.6, 132.5, 132.4, 132.39, 131.9, 131.89, 131.7, 131.6, 131.3, 131.22, 131.20, 131.17, 131.06, 131.0, 130.9, 130.8,130.75, 130.69, 130.65, 129.7, 129.66, 128.7, 127.8, 127.6, 127.0, 126.9, 126.40, 126.2, 126.12, 126.10, 126.0, 125.96, 119.0, 118.9, 118.6, 118.5, 118.4, 118.3, 108.0, 107.9, 107.74, 107.71, 107.59, 107.55, 104.65, 104.58, 104.55, 104.5, 104.4, 84.1, 34.14, 34.1, 34.09, 34.05, 32.04, 32.01, 31.97, 31.9, 29.60, 29.54, 29.49, 29.46, 29.44, 25.10, 25.06, 25.03, 25.01, 22.73, 22.68, 18.88, 18.86, 18.82, 18.79, 18.59, 18.58, 18.54, 18.52, 14.2, 14.1, 12.3, 10.55 and 10.53.

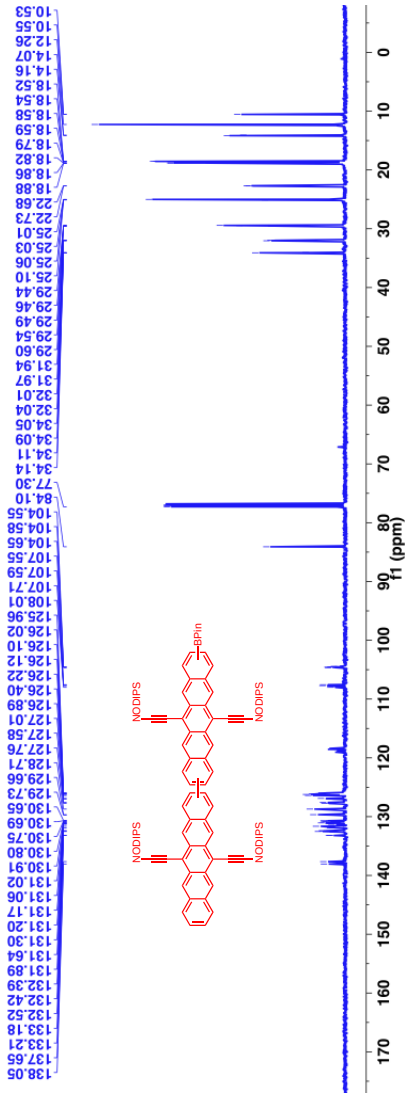

^{1}H-NMR (500 MHz, 50 °C, $CDCl_3$, δ ppm): 9.46-9.24 (m, 12H), 8.39 (s, 4H), 8.20-8.17 (m, 5H), 8.03-7.96 (m, 6H), 7.89-7.87 (m, 1H), 7.49-7.44 (m, 3H), 1.89-1.83 (m, 13H), 1.59-1.58 (m, 14H), 1.47-1.21 (m, 127H), 1.07-1.02 (m, 14H), 0.89-0.86 (m, 8H) and 0.80-0.77 (m, 10H).

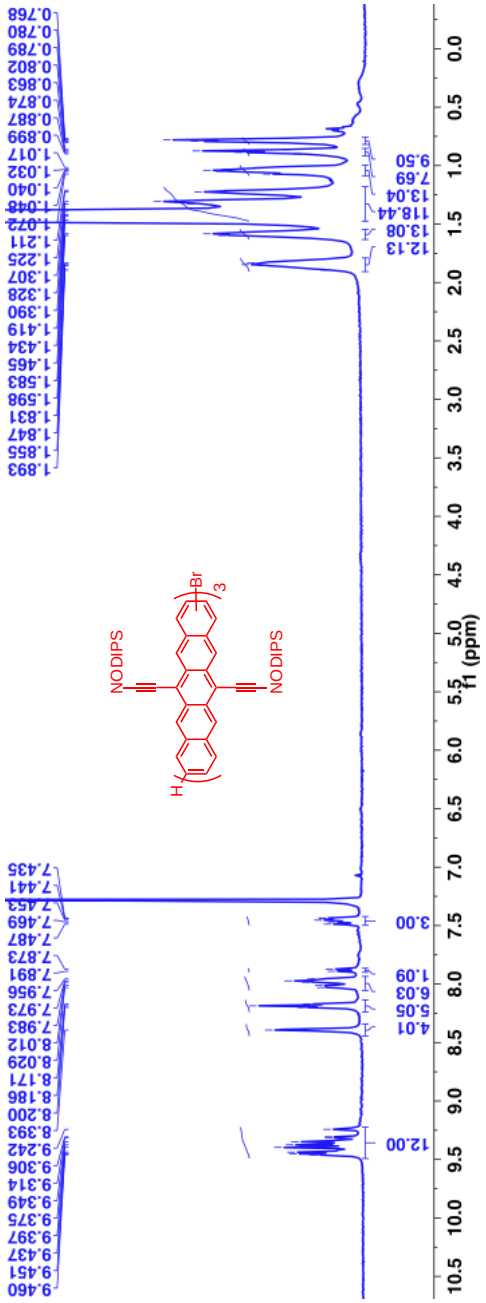

^{13}C-NMR (125 MHz, 50 °C, $CDCl_3$, δ ppm): 137.3, 137.2, 136.91, 136.90, 136.88, 136.8, 136.73, 136.72, 136.7, 136.6, 136.5, 132.78, 132.73, 132.68, 132.65, 132.58, 132.52, 132.46, 132.4, 132.37, 132.33, 131.9, 131.86, 131.75, 131.73, 131.69, 131.63, 131.3, 131.27, 131.21, 131.1, 130.99, 130.89, 130.83, 130.81, 130.74, 130.72, 130.63, 130.58, 130.34, 130.31, 130.23, 130.19, 130.15, 130.07, 129.5, 129.4, 129.37, 128.7, 128.6, 128.58, 126.96, 126.9, 126.85, 126.78, 126.31, 126.27, 126.15, 126.1, 125.9, 125.8, 125.6, 125.62, 125.56, 125.54, 125.50, 125.45, 125.37, 125.33, 120.37, 120.34, 120.29, 118.84, 118.81, 118.72, 118.69, 118.65, 118.63, 118.54, 118.50, 118.46, 118.4, 118.38, 108.1, 108.0, 107.99, 107.96, 107.90, 107.85, 107.78, 107.75, 107.63, 107.52, 107.49, 107.39, 104.90, 104.84, 104.82, 104.78, 104.75, 104.59, 104.57, 104.52, 34.06, 34.02, 34.0, 33.97, 31.95, 31.90, 31.88, 29.5, 29.47, 29.44, 29.36, 29.33, 25.1, 25.04, 25.00, 24.98, 24.95, 22.60, 22.57, 22.6, 18.9, 18.8, 18.76, 18.74, 18.57, 18.52, 18.50, 13.96, 13.90, 13.88, 13.81, 12.4, 12.38, 12.36, 12.34, 10.73, 10.7 and 10.65.

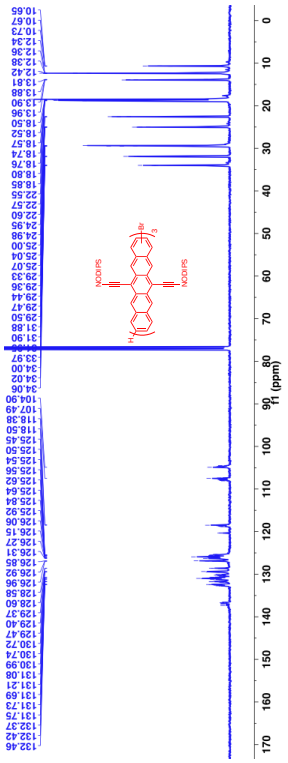

^{1}H-NMR (500 MHz, 50 °C, $CDCl_3$, δ ppm): 9.46-9.31 (m, 12H), 8.58 (s, 1H), 8.39 (s, 4H), 8.20-8.17 (m, 4H), 8.03-7.98 (m, 7H), 7.78-7.75 (m, 1H), 7.46-7.43 (m, 2H), 1.86-1.84 (m, 12H), 1.59-1.58 (m, 14H), 1.48-1.39 (m, 110H), 1.31-1.21 (m, 31H), 1.06-1.03 (m, 13H) and 0.89-0.78 (m, 18H).

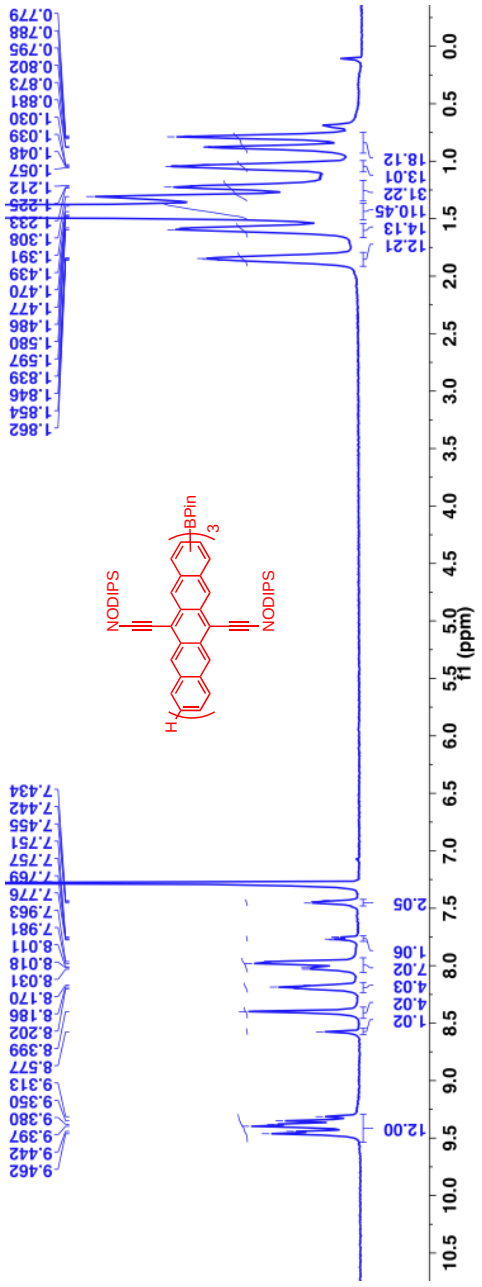

^{13}C-NMR (125 MHz, 50 °C, $CDCl_3$, δ ppm): 137.9, 137.85, 137.82, 137.81, 137.78, 137.74, 133.24, 133.22, 132.65, 132.62, 132.55, 132.46, 132.44, 131.97, 131.76, 131.73, 131.67, 131.3, 131.24, 131.14, 131.09, 130.98, 130.95, 130.8, 130.78, 130.72, 130.7, 129.7, 129.6, 128.6, 127.7, 127.4, 126.9, 126.8, 126.33, 126.22, 126.18, 125.98, 125.9, 118.6, 118.4, 107.76, 107.73, 107.57, 104, 73, 104.68, 104.65, 104.61, 104.55, 84.0, 34.0, 33.96, 33.91, 33.88, 31.9, 31.8, 29.4, 29.3, 22.6, 22.5, 22.46, 18.74, 18.72, 18.69, 18.67, 18.45, 18.43, 13.91, 13.85, 13.83, 13.76, 12.29 and 10.6.

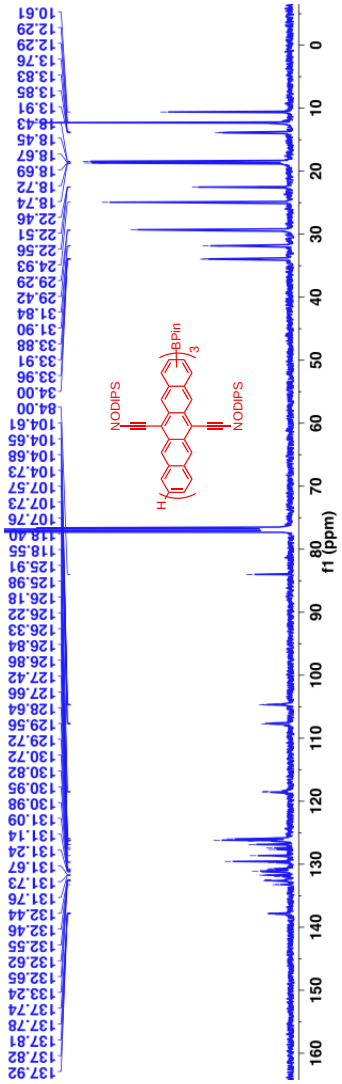

^{1}H-NMR (500 MHz, $CDCl_3$, δ ppm): 9.43-9.35 (m, 8H), 8.39 (s, 2H), 8.20-8.18 (m, 2H), 8.05-8.03 (m, 4H), 7.97-7.97 (m, 2H), 4.47-7.45 (m, 4H), 1.87-1.79 (m, 8H), 1.87-1.79 (m, 8H), 1.60-1.54 (m, 8H), 1.44-1.38 (m, 66H), 1.32-1.21 (m, 22H), 1.04-1.00 (m, 8H), 0.89-0.87 (m, 6H) and 0.79-0.78 (m, 6H).

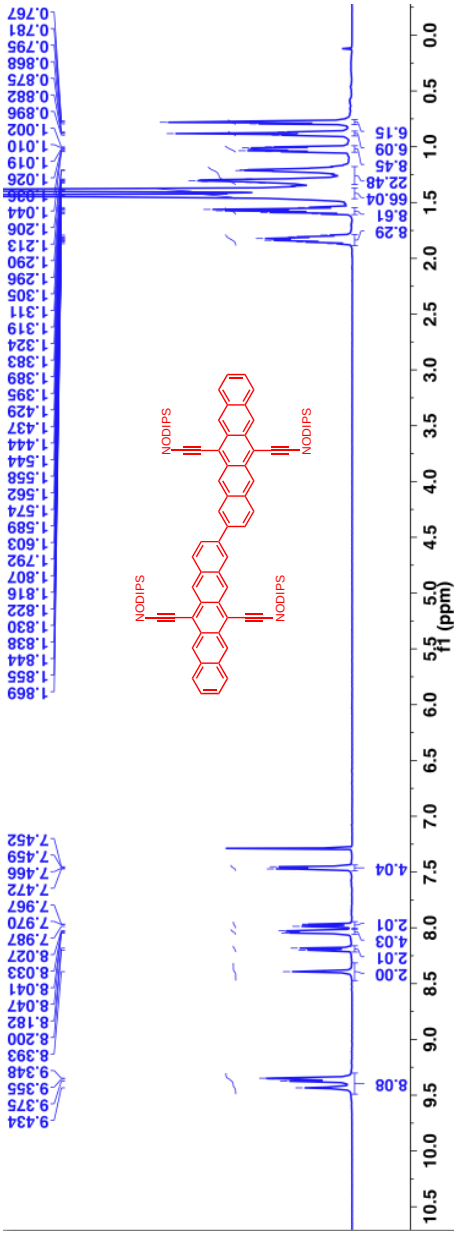

^{13}C-NMR (125 MHz, $CDCl_3$, δ ppm): 137.6, 132.5, 132.4, 132.35, 131.6, 131.0, 130.9, 130.8, 130.7, 129.6, 128.7, 126.9, 126.4, 126.2, 126.1, 125.9, 118.5, 118.4, 107.7, 107.5, 104.6, 104.5, 34.1, 34.05, 32.0, 31.9, 29.6, 29.5, 29.4, 29.39, 25.1, 24.99, 22.7, 22.6, 18.8, 18.75, 18.5, 18.48, 14.1, 14.0, 12.2, 10.5 and 10.5.

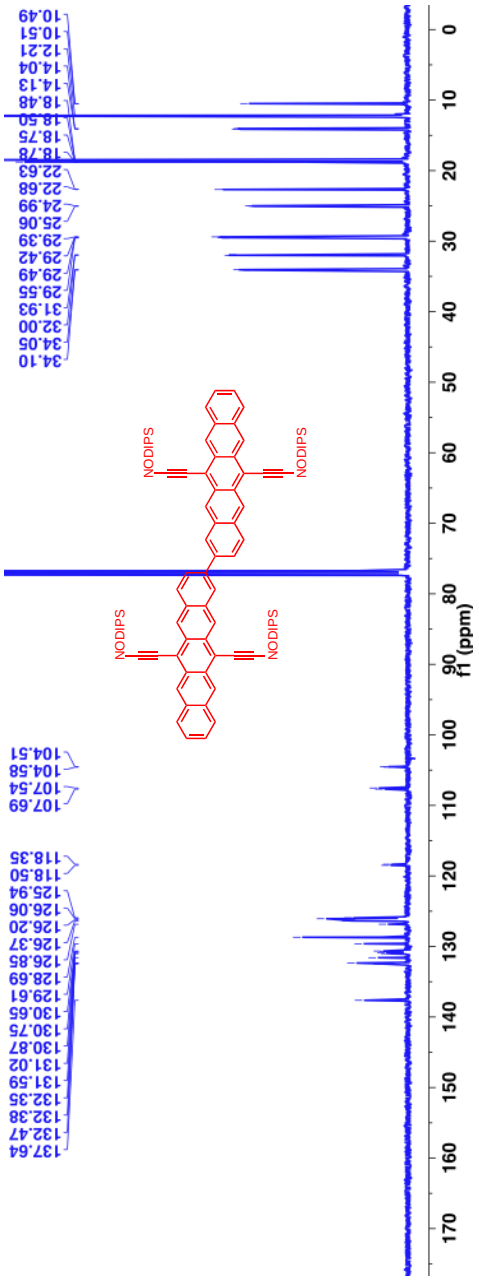

^{1}H-NMR (500 MHz, $CDCl_3$, δ ppm): 9.41-9.33 (m, 12H), 8.35-8.32 (m, 4H), 8.19-8.18 (m, 4H), 8.03-8.00 (m, 4H), 7.96-7.94 (m, 4H), 7.45-7.40 (m, 4H), 1.87-1.81 (m, 12H), 1.62-1.55 (m, 12H), 1.49-1.39 (m, 105H), 1.31-1.29 (m, 22H), 1.05-1.01 (m, 12H), 0.92-0.87 (m, 12H), 0.79-0.77 (m, 8H) and 0.70-0.68 (m, 3H).

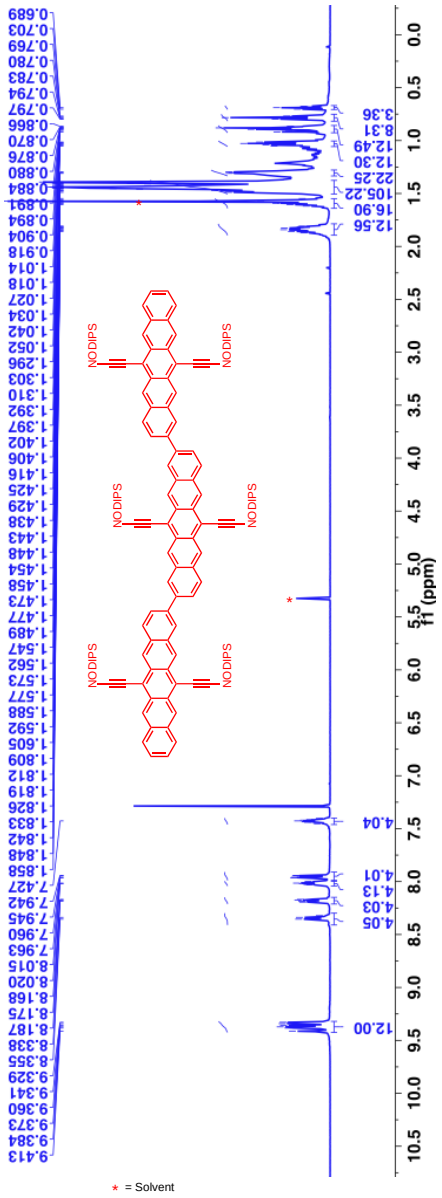

^{13}C-NMR (125 MHz, $CDCl_3$, δ ppm): 137.5, 137.4, 132.5, 132.4, 132.36, 132.3, 131.6, 131.5, 131.1, 131.0, 130.9, 130.86, 130.7, 130.6, 129.6, 128.7, 126.9, 126.85, 126.3, 126.2, 126.1, 125.83, 125.80, 118.7, 118.5, 118.3, 107.8, 107.6, 107.5, 104.7, 104.6, 104.54, 104.51, 34.2, 34.1, 34.08, 34.06, 32.0, 31.9, 31.87, 31.6, 29.6, 29.56, 29.54, 29.51, 29.49, 29.44, 29.41, 29.39, 26.2, 25.1, 25.06, 25.0, 24.99, 24.8, 22.7, 22.67, 22.63, 22.59, 18.84, 18.83, 18.79, 18.76, 18.55, 18.52, 18.49, 14.14, 14.12, 14.05, 14.03, 13.95, 12.26, 12.25, 12.22, 10.56, 10.52 and 10.51.

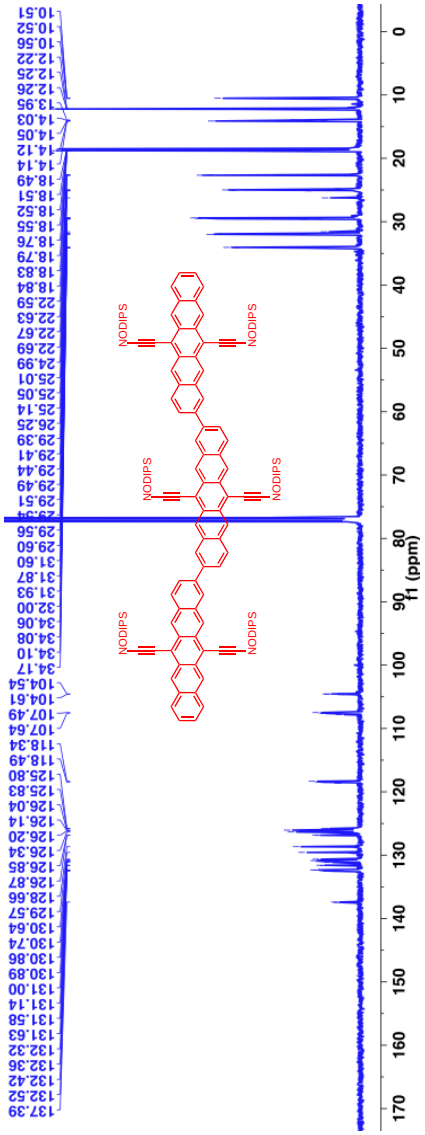

^{1}H-NMR (400 MHz, $CDCl_3$, δ ppm): 9.42-9.33 (m, 12H), 8.37 (m, 4H), 8.21-8.17 (m, 4H), 8.04-7.95 (m, 8H), 7.46-7.41 (m, 4H), 1.88-1.79 (m, 12H), 1.62-1.54 (m, 13H), 1.47-1.38 (m, 98H), 1.32-1.19 (m, 31H), 1.08-1.00 (m, 14H) 0.89-0.86 (m, 6H) and 0.81-0.76 (m, 12H)

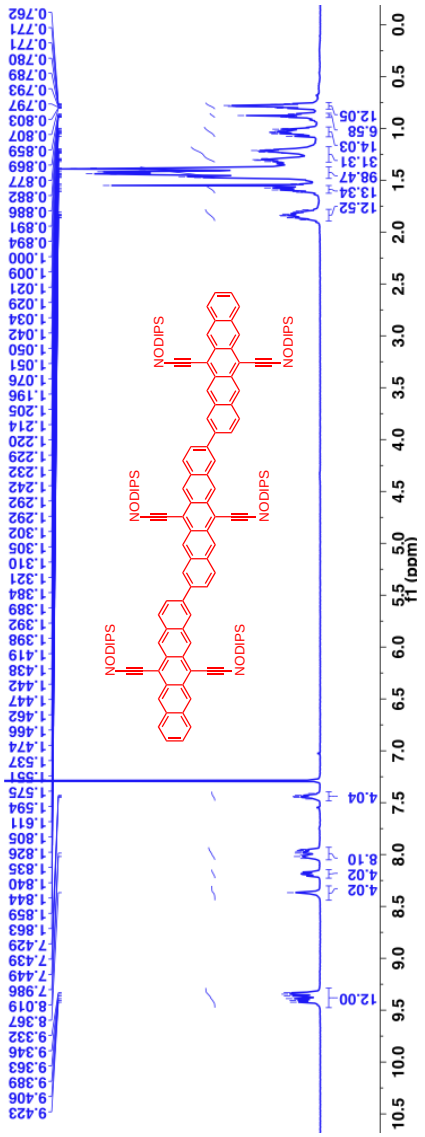

^{13}C-NMR (125 MHz, $CDCl_3$, δ ppm): 136.5, 136.48, 136.45, 132.3, 132.23, 132.21, 132.19, 131.7, 131.6, 131.5, 130.9, 130.92, 130.88, 130.85, 130.7, 130.6, 129.4, 128.57, 128.54, 126.9, 126.86, 126.3, 126.2, 125.9, 125.8, 125.5, 125.4, 125.3, 118.4, 118.3, 107.4, 107.36, 107.29, 104.7, 104.6, 34.18, 34.14, 34.1, 32.0, 31.96, 31.95, 29.58, 29.56, 29.52, 29.45, 29.43, 29.42, 25.1, 25.07, 25.0, 22.7, 22.66, 22.64, 18.9, 18.85, 18.8, 18.6, 18.56, 18.53, 14.1, 14.06, 14.0, 12.32, 12.28, 12.25, 10.62, 10.57 and 10.55.

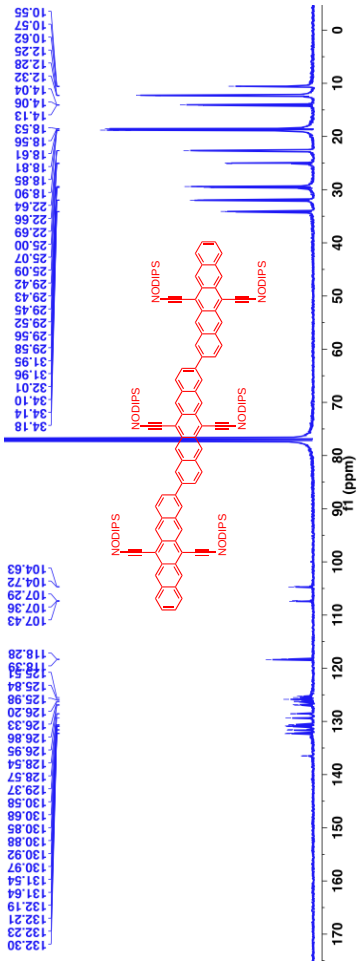

^{1}H-NMR (500 MHz, 50 °C, $CDCl_3$, δ ppm): 9.44-9.34 (m, 16H), 8.38 (s, 6H), 8.18 (s, 6H), 8.01-7.97 (m, 10H), 7.44 (s, 4H), 1.87-1.83 (m, 18H), 1.62-1.21 (m, 200H) and 0.89-0.79 (m, 30H).

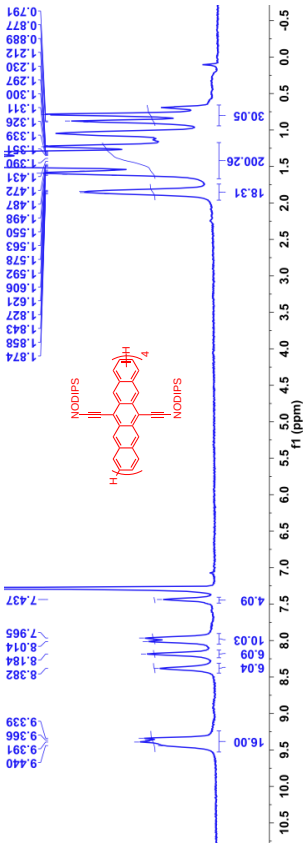

^{13}C-NMR ((500 MHz, 50 °C, $CDCl_3$, δ ppm): 9.38-9.34 (s, 20H), 8.39 (s, 8H), 8.18 (s, 8H), 7.97 (s, 12H), 7.44-7.42 (m, 4H), 1.87 (m, 21H), 1.61-1.03 (m, 258H) and 0.89-0.78 (m, 31H).

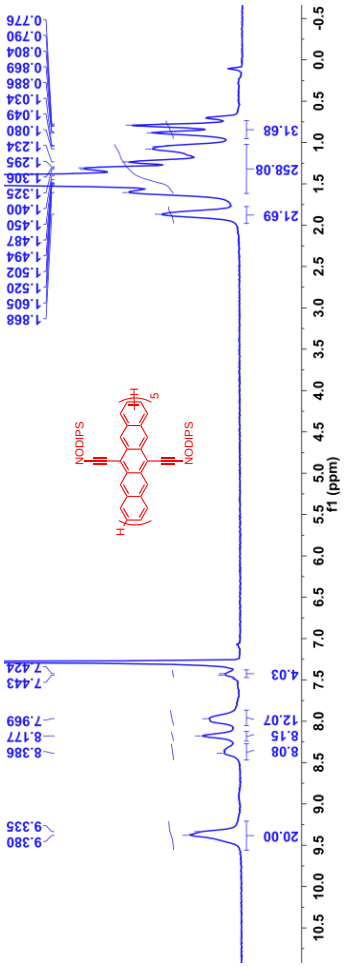

^{1}H-NMR (500 MHz, 50 °C, $CDCl_3$, δ ppm): 9.34 (bs, 24H), 8.39-7.97 (m, 38H) and 1.89-0.71 (m, 372H, water peak overlap)

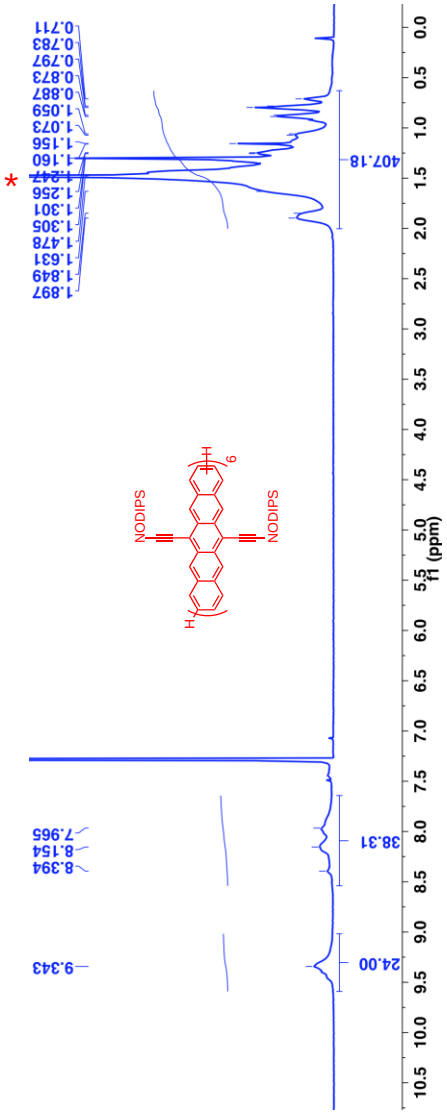

^{1}H-NMR (500 MHz, 50 °C, $CDCl_3$, δ ppm): 9.44-9.35 (m, 28H), 8.40 (s, 10H), 8.19-7.98 (m, 34H) and 1.88-0.78 (m, 434H, water peak overlap)

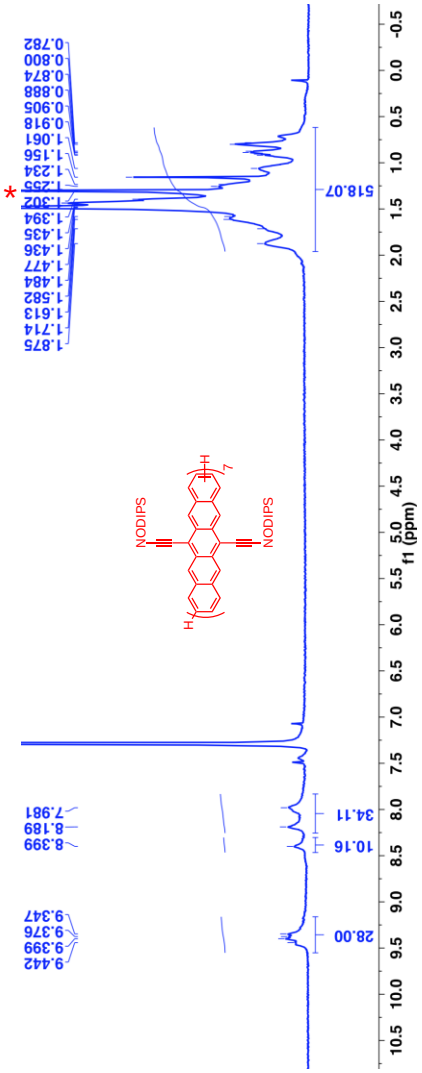

3.23 Matrix Assisted Laser Desorption Ionization Mass Spectra

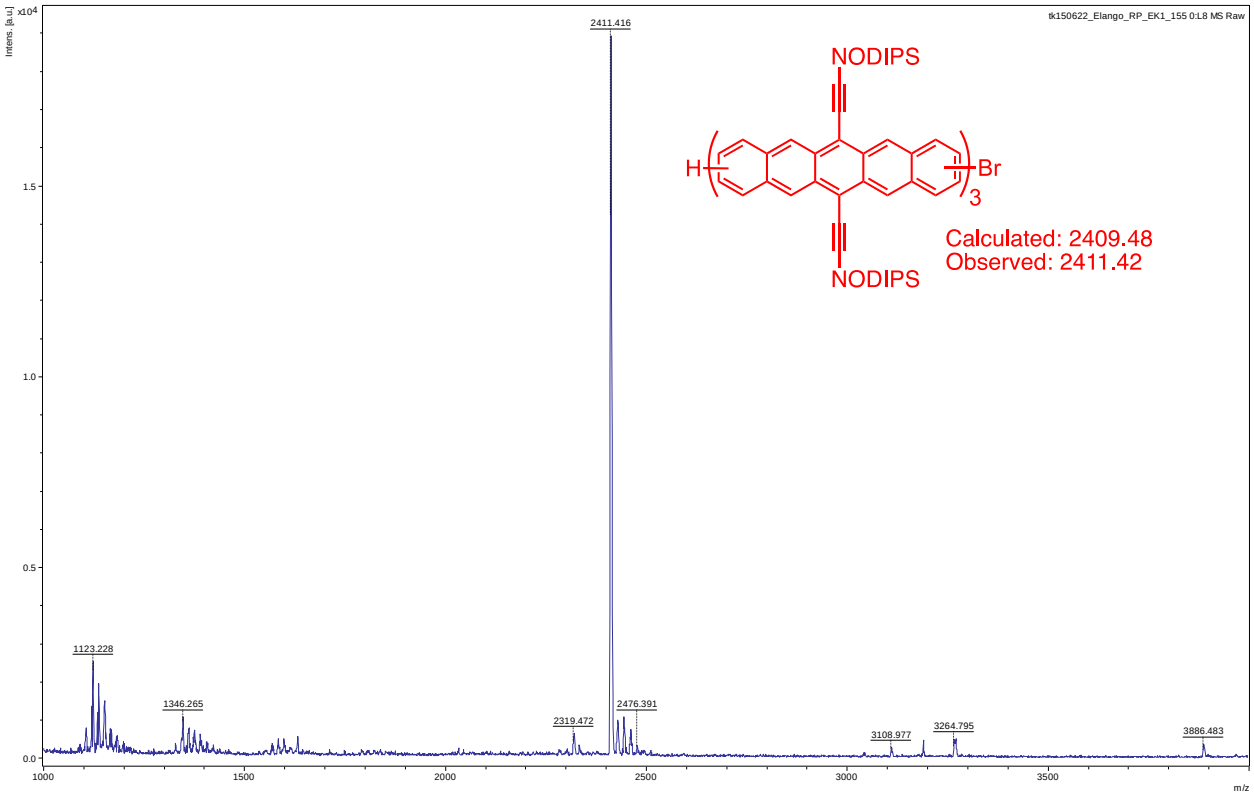

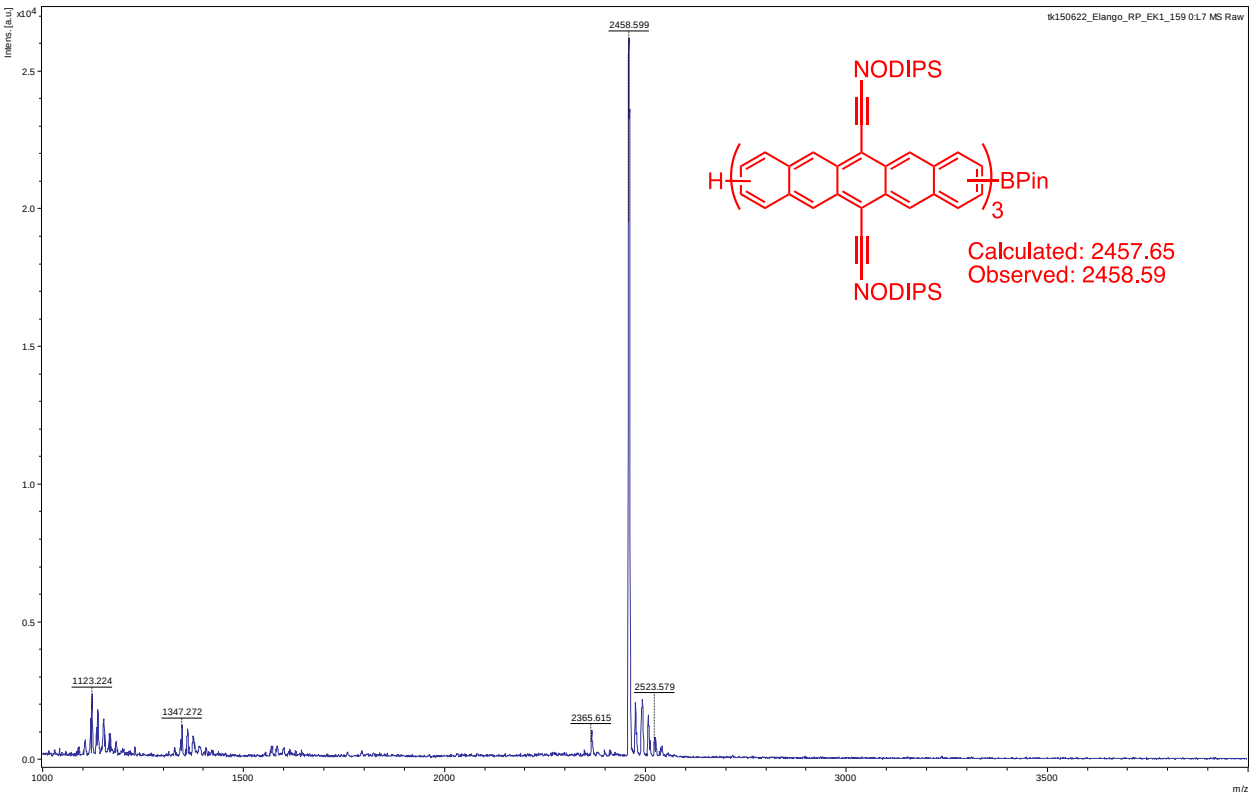
tk150622_Elango_RP_EK1_159 0:L7 MS Raw
Intens. [a.u.]
x10^4
2.5
2.0
1.5
1.0
0.5
0.0
2458.599
1123.224
1347.272
2365.615
2523.579
1000
1500
2000
2500
3000
3500
m/z
NODIPS
H
BPin
3
NODIPS
Calculated: 2457.65
Observed: 2458.59

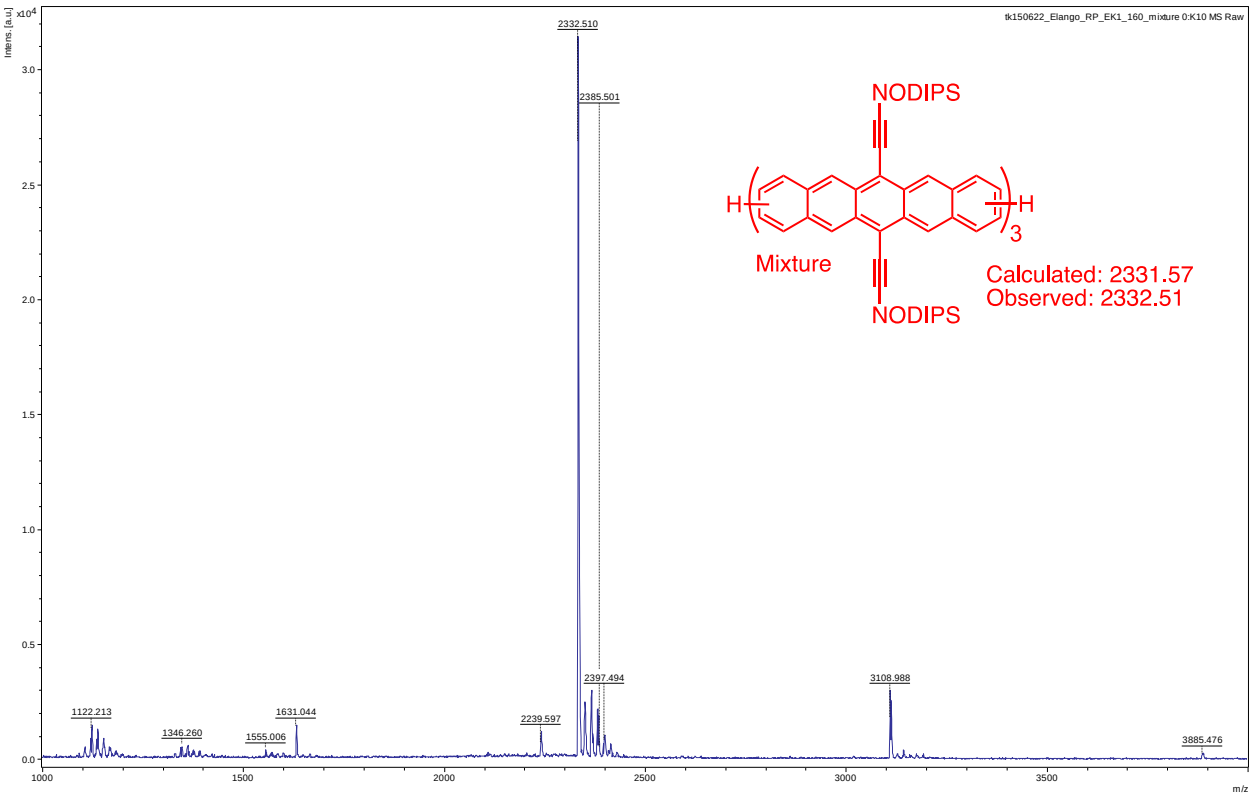
tk150622_Elango_RP_EK1_160_mixture 0:K10 MS Raw
Intens. [a.u.]
x10^4
3.0
2.5
2.0
1.5
1.0
0.5
0.0
1000
1500
2000
2500
3000
3500
m/z
2332.510
2385.501
2397.494
3108.988
1122.213
1346.260
1555.006
1631.044
2239.597
3885.476
NODIPS
H
H
3
Mixture
NODIPS
Calculated: 2331.57
Observed: 2332.51

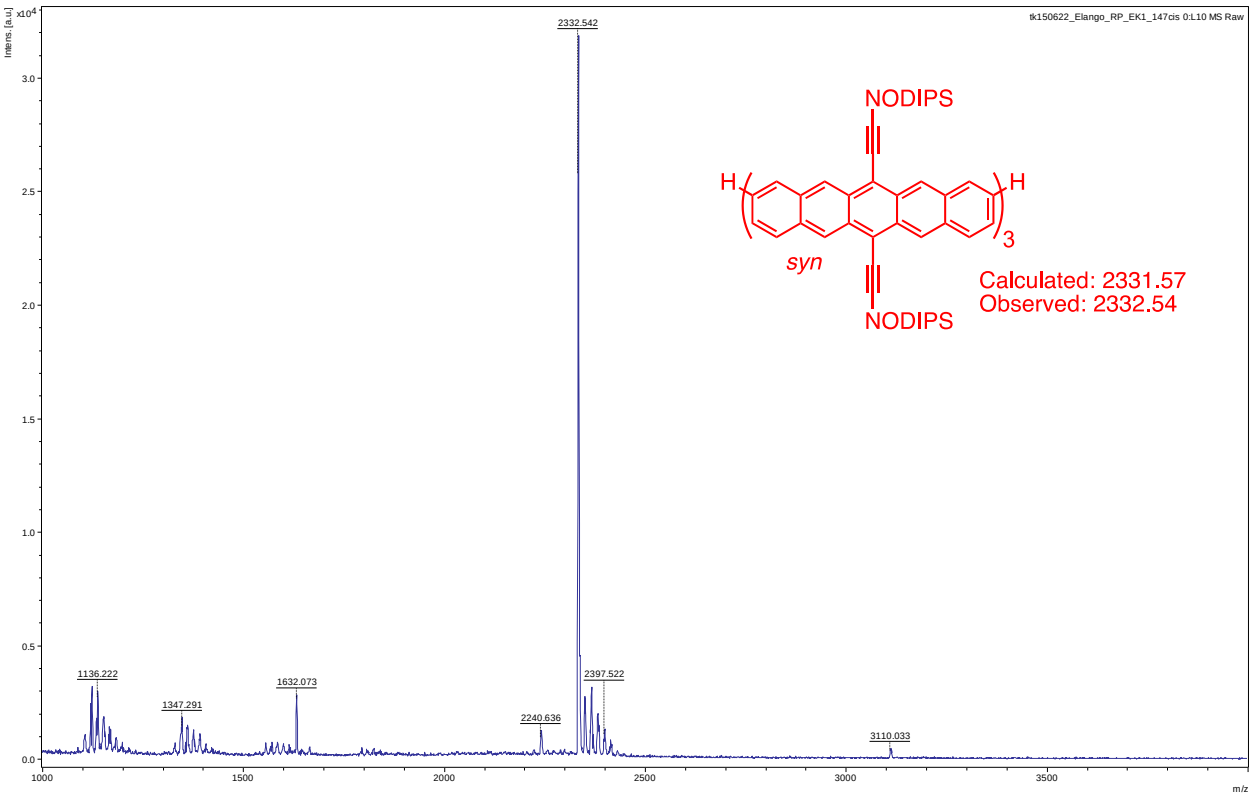
tk150622_Elango_RP_EK1_147cis 0:L10 MS Raw
Intens. [a.u.]
x10^4
3.0
2.5
2.0
1.5
1.0
0.5
0.0
1000
1500
2000
2500
3000
3500
m/z
2332.542
1136.222
1347.291
1632.073
2240.636
2397.522
3110.033
NODIPS
H
H
3
syn
NODIPS
Calculated: 2331.57
Observed: 2332.54

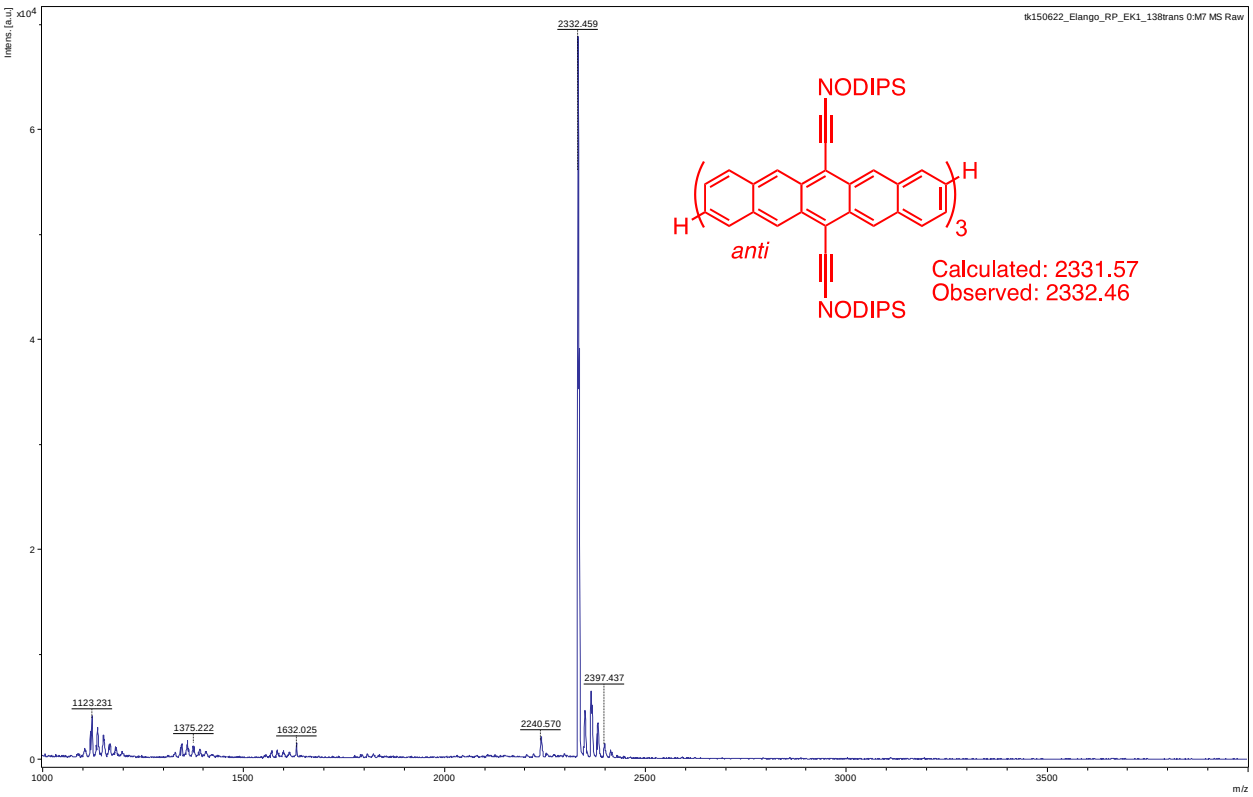
tk150622_Elango_RP_EK1_138trans 0:M7 MS Raw
Intens. [a.u.]
x10^4
6
4
2
0
2332.459
2397.437
1123.231
1375.222
1632.025
2240.570
1000
1500
2000
2500
3000
3500
m/z
NODIPS
H
H
3
anti
NODIPS
Calculated: 2331.57
Observed: 2332.46

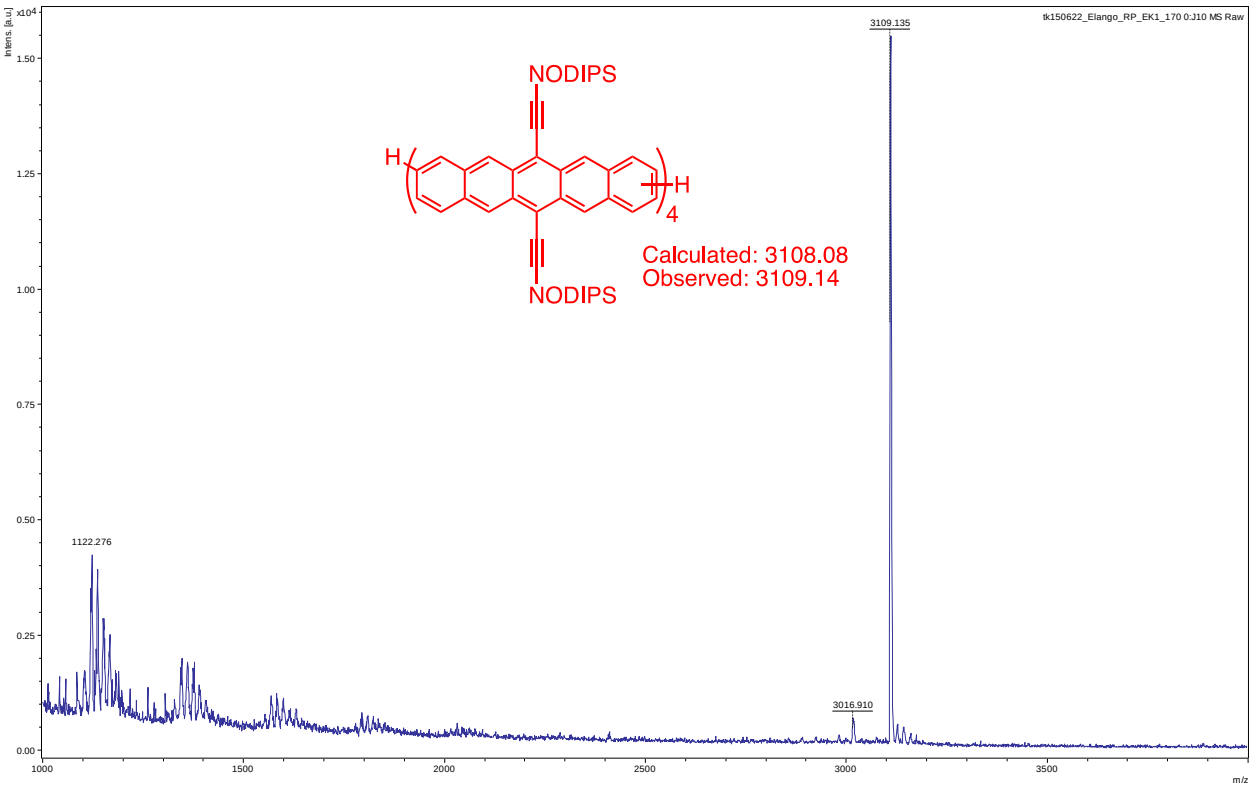
tk150622_Elango_RP_EK1_170 0:J10 MS Raw
Intens. [a.u.]
x10^4
1.50
1.25
1.00
0.75
0.50
0.25
0.00
1000
1500
2000
2500
3000
3500
m/z
3109.135
1122.276
3016.910
NODIPS
H
H
4
NODIPS
Calculated: 3108.08
Observed: 3109.14

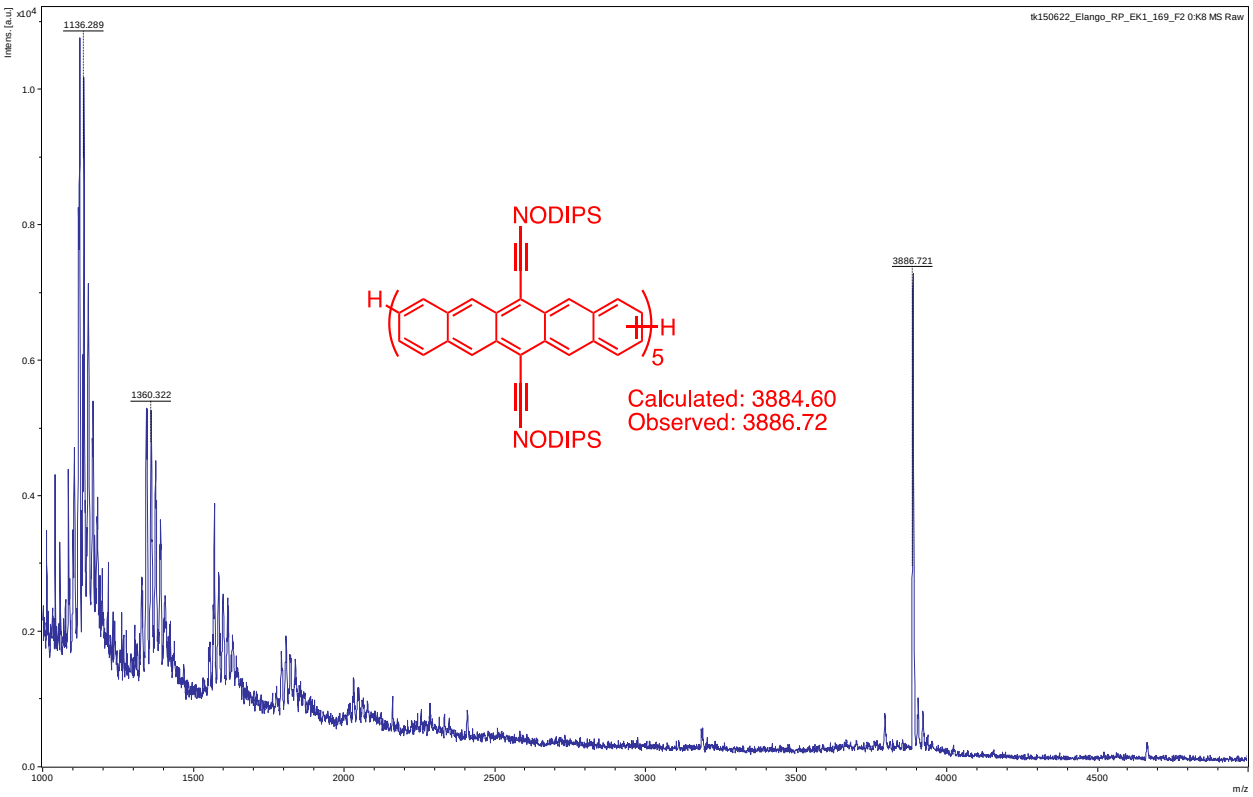
tk150622_Elango_RP_EK1_169_F2 0:K8 MS Raw
Intens. [a.u.]
x10^4
1.0
0.8
0.6
0.4
0.2
0.0
1136.289
1360.322
3886.721
1000
1500
2000
2500
3000
3500
4000
4500
m/z
NODIPS
H
H
5
NODIPS
Calculated: 3884.60
Observed: 3886.72

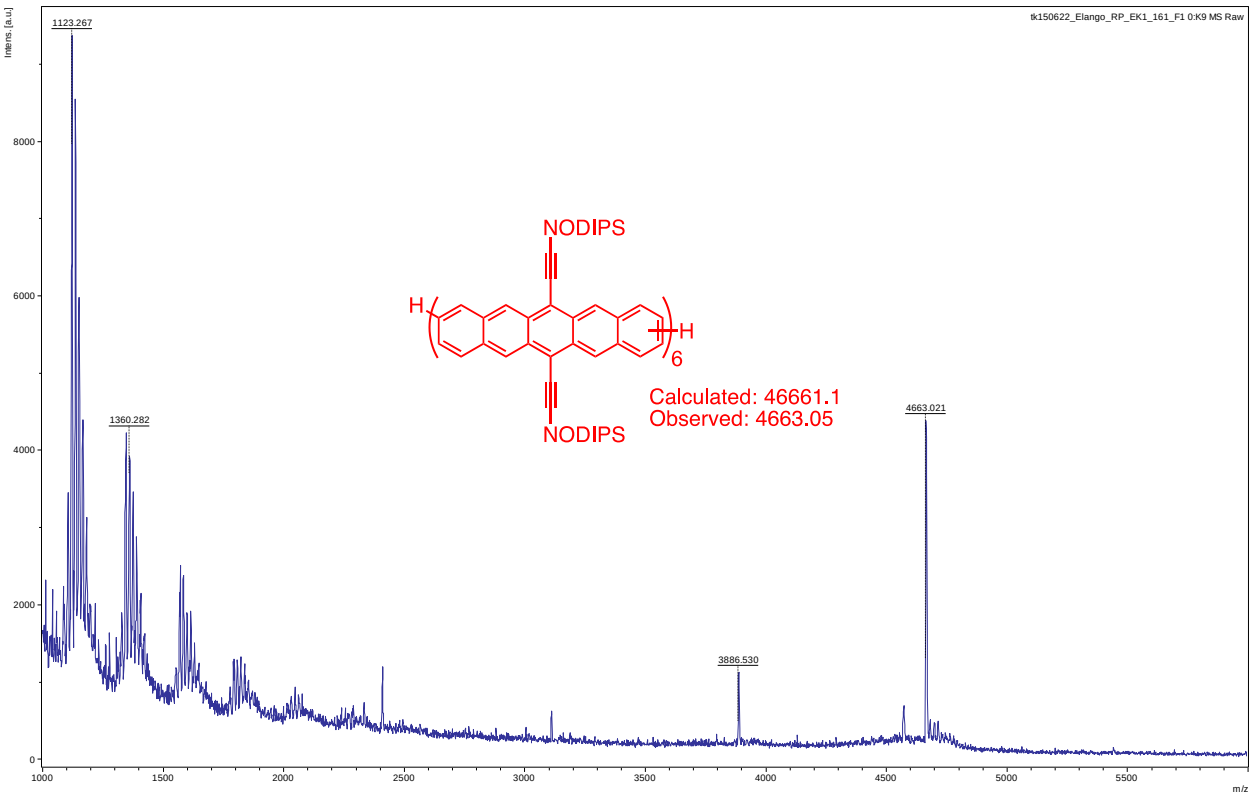
tk150622_Elango_RP_EK1_161_F1 0:K9 MS Raw
Intens. [a.u.]
1123.267
1360.282
3886.530
4663.021
NODIPS
H
H
6
NODIPS
Calculated: 46661.1
Observed: 4663.05
m/z

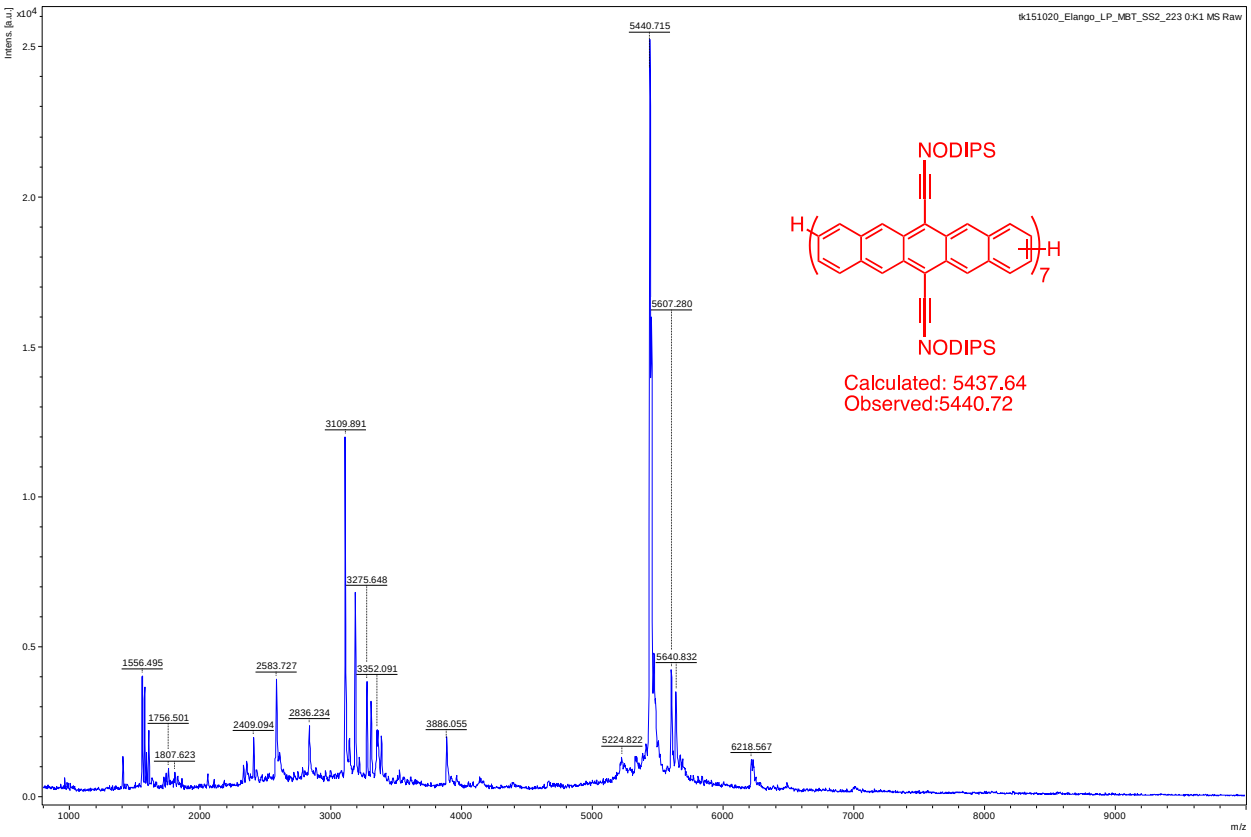

3.24 References

(1) Katz, H. E.; Bao, Z.; Gilat, S. L. *Acc. Chem. Res.* **2001**, *34*, 359.

(2) Ito, K.; Suzuki, T.; Sakamoto, Y.; Kubota, D.; Inoue, Y.; Sato, F.; Tokito, S. *Angew. Chem.* **2003**, *115*, 1191.

(3) Anthony, J. E. *Angew. Chem. Int. Ed.* **2008**, *47*, 452.

(4) Zade, S. S.; Bendikov, M. *Angew. Chem. Int. Ed.* **2010**, *49*, 4012.

(5) Ball, M.; Zhong, Y.; Wu, Y.; Schenck, C.; Ng, F.; Steigerwald, M.; Xiao, S.; Nuckolls, C. *Acc. Chem. Res.* **2015**, *48*, 267.

(6) Low, J. Z.; Sanders, S. N.; Campos, L. M. *Chem. Mater.* **2015**, *27*, 5453.

(7) Tsefrikas, V. M.; Scott, L. T. *Chem. Rev.* **2006**, *106*, 4868.

(8) Sundar, V. C.; Zaumseil, J.; Podzorov, V.; Menard, E.; Willett, R. L.; Someya, T.; Gershenson, M. E.; Rogers, J. A. *Science* **2004**, *303*, 1644.

(9) Bunz, U. H. F. *Acc. Chem. Res.* **2015**, *48*, 1676.

(10) Sanders, S. N.; Kumarasamy, E.; Pun, A. B.; Steigerwald, M. L.; Sfeir, M. Y.; Campos, L. M. *Angew. Chem. Int. Ed.* **2016**.

(11) Yen-Yi, L.; Gundlach, D. I.; Nelson, S. F.; Jackson, T. N. *Electron Devices, IEEE Transactions on* **1997**, *44*, 1325.

(12) Park, S. K.; Jackson, T. N.; Anthony, J. E.; Mourey, D. A. *Appl. Phys. Lett.* **2007**, *91*, 063514

(13) Afzali, A.; Dimitrakopoulos, C. D.; Breen, T. L. *J. Am. Chem. Soc.* **2002**, *124*, 8812.

(14) Jo, S. B.; Kim, H. H.; Lee, H.; Kang, B.; Lee, S.; Sim, M.; Kim, M.; Lee, W. H.; Cho, K. *ACS Nano* **2015**, *9*, 8206.

(15) Herwig, P. T.; Müllen, K. *Adv. Mater.* **1999**, *11*, 480.

(16) Anthony, J. E.; Brooks, J. S.; Eaton, D. L.; Parkin, S. R. *J. Am. Chem. Soc.* **2001**, *123*, 9482.

(17) Anthony, J. E. *Chem. Rev.* **2006**, *106*, 5028.

(18) Bendikov, M.; Wudl, F.; Perepichka, D. F. *Chem. Rev.* **2004**, *104*, 4891.

(19) Fudickar, W.; Linker, T. *J. Am. Chem. Soc.* **2012**, *134*, 15071.

(20) Maliakal, A.; Raghavachari, K.; Katz, H.; Chandross, E.; Siegrist, T. *Chem. Mater.* **2004**, *16*, 4980.

(21) Lehnherr, D.; Gao, J.; Hegmann, F. A.; Tykwinski, R. R. *J. Org. Chem.* **2009**, *74*, 5017.

(22) Okamoto, T.; Bao, Z. *J. Am. Chem. Soc.* **2007**, *129*, 10308.

(23) Lehnherr, D.; McDonald, R.; Ferguson, M. J.; Tykwinski, R. R. *Tetrahedron* **2008**, *64*, 11449.

(24) Lehnherr, D.; Murray, A. H.; McDonald, R.; Tykwinski, R. R. *Angew. Chem. Int. Ed.* **2010**, *49*, 6190.

(25) Tokito, S.; Weifurtner, K.-H.; Fujikawa, H.; Tsutsui, T.; Taga, Y. *Proc. SPIE-Int. Soc. Opt. Eng.* **2001**, *4105*, 69.

(26) Porz, M.; Paulus, F.; Höfle, S.; Lutz, T.; Lemmer, U.; Colsmann, A.; Bunz, U. H. F. *Macromol. Rapid Commun.* **2013**, *34*, 1611.

(27) Capozzi, B.; Dell, E. J.; Berkelbach, T. C.; Reichman, D. R.; Venkataraman, L.; Campos, L. M. *J. Am. Chem. Soc.* **2014**, *136*, 10486.

(28) Koch, F. P. V.; Smith, P.; Heeney, M. *J. Am. Chem. Soc.* **2013**, *135*, 13695.

(29) Koch, F. P. V.; Heeney, M.; Smith, P. *J. Am. Chem. Soc.* **2013**, *135*, 13699.

(30) Zhang, L.; Colella, N. S.; Liu, F.; Trahan, S.; Baral, J. K.; Winter, H. H.; Mannsfeld, S. C. B.; Briseno, A. L. *J. Am. Chem. Soc.* **2013**, *135*, 844.

(31) Liu, F.; Espejo, G. L.; Qiu, S.; Oliva, M. M.; Pina, J.; Seixas de Melo, J. S.; Casado, J.; Zhu, X. *J. Am. Chem. Soc.* **2015**, *137*, 10357.

(32) Müllen, K.; Wegner, G.; Electronic Materials: The Oligomer Approach; Wiley-VCH: New York: 1998.

(33) Chen, J.; Subramanian, S.; Parkin, S. R.; Siegler, M.; Gallup, K.; Haughn, C.; Martin, D. C.; Anthony, J. E. *J. Mater. Chem.* **2008**, *18*, 1961.

(34) Plunkett, K. N.; Godula, K.; Nuckolls, C.; Tremblay, N.; Whalley, A. C.; Xiao, S. *Org. Lett.* **2009**, *11*, 2225.

(35) Swartz, C. R.; Parkin, S. R.; Bullock, J. E.; Anthony, J. E.; Mayer, A. C.; Malliaras, G. G. *Org. Lett.* **2005**, *7*, 3163.

(36) Lehnherr, D.; Gao, J.; Hegmann, F. A.; Tykwinski, R. R. *Org. Lett.* **2008**, *10*, 4779.

(37) Anthony, J. E.; Eaton, D. L.; Parkin, S. R. *Org. Lett.* **2002**, *4*, 15.

(38) Lehnherr, D.; McDonald, R.; Tykwinski, R. R. *Org. Lett.* **2008**, *10*, 4163.

(39) Lehnherr, D.; Tykwinski, R. R. *Org. Lett.* **2007**, *9*, 4583.

(40) Miao, Q.; Chi, X.; Xiao, S.; Zeis, R.; Lefenfeld, M.; Siegrist, T.; Steigerwald, M. L.; Nuckolls, C. *J. Am. Chem. Soc.* **2006**, *128*, 1340.

(41) Payne, M. M.; Odom, S. A.; Parkin, S. R.; Anthony, J. E. *Org. Lett.* **2004**, *6*, 3325.

(42) Takahashi, T.; Kitamura, M.; Shen, B.; Nakajima, K. *J. Am. Chem. Soc.* **2000**, *122*, 12876.

(43) Lu, J.; Ho, D. M.; Vogelaar, N. J.; Kraml, C. M.; Bernhard, S.; Byrne, N.; Kim, L. R.; Pascal, R. A. *J. Am. Chem. Soc.* **2006**, *128*, 17043.

(44) Zhao, Y.; Mondal, R.; Neckers, D. C. *J. Org. Chem.* **2008**, *73*, 5506.

(45) Bénard, C. P.; Geng, Z.; Heuft, M. A.; VanCrey, K.; Fallis, A. G. *J. Org. Chem.* **2007**, *72*, 7229.

(46) Okamoto, T.; Reese, C.; Senatore, M. L.; Tang, M. L.; Jiang, Y.; Parkin, S. R.; Bao, Z. *Synth. Met.* **2010**, *160*, 2447.

(47) Wu, W.; Liu, Y.; Zhu, D. *Chem. Soc. Rev.* **2010**, *39*, 1489.

(48) Coropceanu, V.; Cornil, J.; da Silva Filho, D. A.; Olivier, Y.; Silbey, R.; Brédas, J.-L. *Chem. Rev.* **2007**, *107*, 926.

(49) You, J.; Dou, L.; Yoshimura, K.; Kato, T.; Ohya, K.; Moriarty, T.; Emery, K.; Chen, C.-C.; Gao, J.; Li, G.; Yang, Y. *Nat Commun* **2013**, *4*, 1446.

(50) Banerjee, M.; Shukla, R.; Rathore, R. *J. Am. Chem. Soc.* **2009**, *131*, 1780.

(51) Sanders, S. N.; Kumarasamy, E.; Pun, A. B.; Trinh, M. T.; Choi, B.; Xia, J.; Taffet, E. J.; Low, J. Z.; Miller, J. R.; Roy, X.; Zhu, X. Y.; Steigerwald, M. L.; Sfeir, M. Y.; Campos, L. M. *J. Am. Chem. Soc.* **2015**, *137*, 8965.

(52) Kline, R. J.; Hudson, S. D.; Zhang, X.; Gundlach, D. J.; Moad, A. J.; Jurchescu, O. D.; Jackson, T. N.; Subramanian, S.; Anthony, J. E.; Toney, M. F.; Richter, L. J. *Chem. Mater.* **2011**, *23*, 1194.

(53) Mannsfeld, S. C. B.; Tang, M. L.; Bao, Z. *Adv. Mater.* **2011**, *23*, 127.

(54) Kang, J.; Shin, N.; Jang, D. Y.; Prabhu, V. M.; Yoon, D. Y. *J. Am. Chem. Soc.* **2008**, *130*, 12273.

(55) Ashton, P. R.; Girreser, U.; Giuffrida, D.; Kohnke, F. H.; Mathias, J. P.; Raymo, F. M.; Slawin, A. M. Z.; Stoddart, J. F.; Williams, D. J. *J. Am. Chem. Soc.* **1993**, *115*, 5422.

4 Singlet Fission in Polypentacene

4.1 Preface

This chapter is based on a publication entitled "*Singlet Fission in Polypentacene*" published in the journal *Chem* by Samuel N. Sanders, Elango Kumarasamy, Andrew B. Pun, Michael L. Steigerwald, Matthew Y. Sfeir, and Luis M. Campos. Elango, Andrew and I synthesized all the molecules while I performed all the time resolved spectroscopy in the lab of Dr. Sfeir. Matt and Mike assisted in interpretation of the results.

4.2 Introduction

Singlet fission (SF) is the spin-conserved conversion of one singlet exciton into two triplet excitons.[1,2] Because this exciton multiplication process could be applied to exceed the Shockley-Queisser limit of solar power conversion efficiency, the development of new materials, understanding the mechanism of SF, and device optimization are crucial challenges in third-generation photovoltaics.[3] Initial studies were based on the highly efficient intermolecular SF (xSF) process,[1,2] while intramolecular SF (iSF) chromophores were scarce. However, various successful iSF systems have recently emerged, and interest has surged. These materials feature the practical advantages of a reduced dependence of singlet fission on morphology and packing interactions.[4,5] Furthermore, the study of iSF chromophores in solution can reveal valuable information to understand and optimize the singlet fission process through structure-property relationships.[4,6-13]

Recent breakthroughs in materials design and mechanistic understanding of SF have come from molecular dimers of pentacene,[6,7,9,11-13] in addition to heterodimers of oligoacenes.[8,14] One important finding is that triplet pairs generated in pentacene dimers exhibit spin correlations that

persist for >10 nanoseconds.[14] However, it is not clear what happens to these correlations when the number of pentacenes is increased through conjugation (oligomers and polymers), leading to more available triplet sites within each molecule, as in the case of crystalline pentacene (xSF).[15-27] With the limited number of iSF polymers, there is a lack of understanding of structure-property relationships connecting singlet fission in the building blocks to their polymer counterparts. Notably, in donor-acceptor materials, the strong electron correlations that promote singlet fission can also promote the formation of a low energy dark singlet state that is parasitic to singlet fission.[19] This dark state has complicated the systematic investigation of a wide variety of singlet fission polymers.[18] Further complicating the issue is the fact that in donor-acceptor materials, the singlet fission yield is very sensitive to the degree of charge transfer character.[15]

To overcome these issues, we postulate that polyacenes can provide valuable fundamental information about iSF and triplet pair dynamics because oligoacene dimers exhibit quantitative iSF yields, up to 200%.[9,10,14] Furthermore, in dimers, triplet pair generation occurs via a direct mechanism that stems from resonance between the photoexcited singlet and the triplet pair, with minimal contribution from charge transfer states.[6] Finally, these materials exhibit sharp and strongly absorbing triplet absorption resonances, which allow us to distinguish between correlated triplet pairs and free triplets.[9,14] Thus we have a valuable spectral probe for whether triplet pairs formed in these polymers (or oligomers) dissociate into free triplets.

With the above information in mind, we investigate the excited state dynamics of polypentacene (PPc) as a model system to understand iSF and the behavior of the triplet pairs within the extended chromophore backbone. It may be possible for the polymer to exhibit enhanced delocalization to promote faster iSF. Additionally, triplet pairs in polymers may, in principle, be able to dissociate and diffuse apart since the pentacenes are conjugated. On the other

hand, the possibility exists that spin-correlations are strong enough to keep the triplet pair bound until recombination occurs. As shown in Figure 4.1, we explore structure-property relationships in these materials by comparing the polymer photophysics with oligomers, from dimer to pentamer.[28-33]

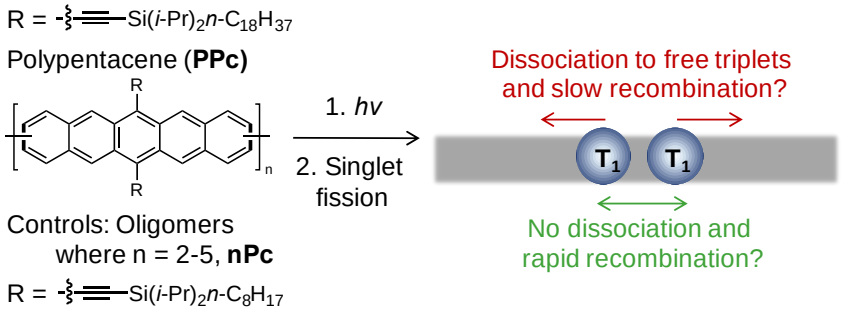

Figure 4.1. Singlet fission in polypentacene reveals that despite the extended polymeric system, triplet pairs do not dissociate into free triplets. Oligomers (n = 2-5) provide further insights into the excited state dynamics.

4.3 Materials Summary

We have recently reported the synthesis of a soluble polypentacene and its derivatives based on well-defined oligomers.[34] The polymer (PPc, M_n = 16 kg mol^{-1}, $Đ$ = 2.1) is synthesized by a Suzuki step-growth polymerization of bifunctional monomers, and is regiorandom as shown in Figure 4.1. As we have reported previously, oligopentacenes are significantly more photostable than monomeric pentacene. We also find them to be stable up to ~380 °C by thermogravimetric analysis, and therefore these materials make excellent candidates for study and implementation of iSF.[34]

4.4 Transient Absorption Spectroscopy

We focus on the singlet fission dynamics of these new materials in solution. Transient absorption data for PPc in 1,2,4-triclorobenzene (TCB) is shown in Figure 4.2. It is qualitatively similar to the published transient data for bipentacene, 2Pc, with a broad singlet photoinduced absorption feature extending from 400–600 nm that rapidly decays into a triplet absorption signal (peak ~530 nm).[9] From this data, we determine that PPc undergoes iSF with a time constant τ_{iSF}(PPc) = 0.54 ps, which is faster than for 2Pc in TCB (0.8 ps). Importantly, we do not find evidence for any competing processes, indicating iSF occurs quantitatively. Additionally, we observe that the time constant for triplet pair recombination in PPc (τ_{rec}[PPc] = 0.74 ns) is remarkably similar to 2Pc (τ_{rec}[2Pc] = 0.45 ns), and it is orders of magnitude shorter than that of a single triplet obtained by sensitization. The fact that the triplet pair lifetimes are similar in both polymer and dimer is indicative that triplet pairs do not dissociate along the backbone of the polymer. To better understand these excited state dynamics, we compare the photophysics of the oligomers, with n = 2 to 5 in Figure 4.1. Because the oligomers have different solubilizing chains from the polymer, they are used for a qualitative understanding of the polymer photophysics, but not for quantitative comparison to the polymer rate constants.

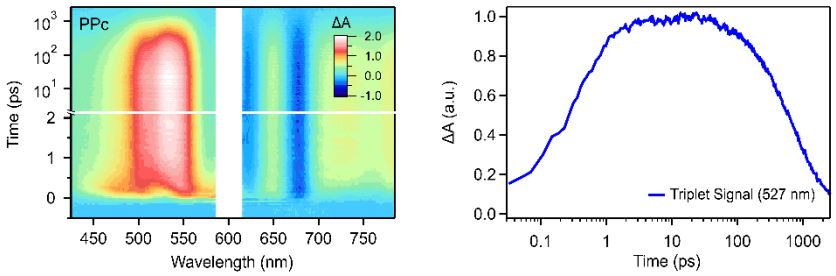

Figure 4.2. TAS of PPc in 1,2,4-tricholorobenzene (TCB) excited at 600 nm with ~25 μJ/cm^2 (left), and kinetics at 527 nm (right), a wavelength, which preferentially features the triplet pair rise and decay.

We observe a monotonic increase in the rate of triplet pair formation as a function of oligomer length for n = 2-5 (Figure 4.3). The evolution of the rate constants can be described using an empirical model that accounts for the ratio of "terminal" to "interior" pentacenes. We multiply the fraction of "terminal" pentacenes by the rate constant for the dimer, since they have one nearest neighbor. For interior pentacenes (with two nearest neighbors), we multiply by twice the rate constant of the dimer (eqn 1):

$$\Gamma_{iSF}^{n} = \frac{2}{n}\Gamma_{2Pc} + \frac{n-2}{n}2\Gamma_{2Pc} \qquad (1)$$

The dashed line in Figure 4.3 shows the result of this fit with Γ_{2Pc} as a fit parameter (1.4 ps^{-1}).

While it is clear that the singlet fission rate constant increases with increasing oligomer length, the mechanism is likely due to a combination of electronic and geometric factors. First, exciton delocalization has recently been implicated as an important driver of singlet fission,[14,35] with the singlet exciton being a linear combination of local excitations on individual pentacenes.[6] As such, it is likely that the singlet exciton samples the entire oligomer, even as its length is increased. Secondly, we have recently demonstrated that singlet fission rates are sensitive to the dihedral angle between the covalently coupled chromophores.[6] Therefore, the increased number of neighbors, on average, may lead to an increased occurrence of favorable geometries for iSF, increasing the rate. Furthermore, measurements of these oligomers in 1,1,2,2-tetrachloroethylene (TCE) are identical to TCB (Figure 4.3), showing that this process is only weakly sensitive to the properties of the solvent. The similar behavior in different solvents also helps rule out possibilities such as solvent-dependent aggregation contributing to the observed changes in SF rates, as the scaling for a solvent dependent aggregation process would likely change based on the solvent chosen.

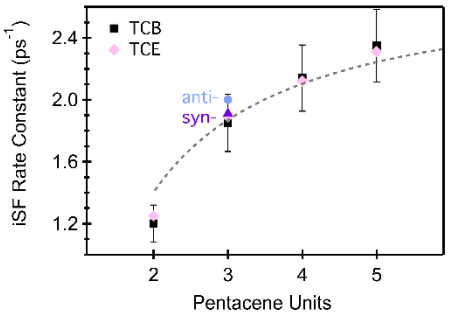

Figure 4.3. Rate constants for singlet fission in two solvents (1,2,4-trichlorobenzene, TCB, and 1,1,2,2-tetrachloroethylene, TCE) as a function of oligomer length.

In contrast to the singlet fission rate constant, we find that the triplet pair lifetime is nearly independent of oligomer length, with no dissociation into free triplets despite an increase in the number of available triplet sites. In dimers, we have previously reported that spin-correlated triplet pairs decay through a concerted recombination process that is dramatically faster than free triplet decay.[8,14] When energetics allow for equilibrium between singlet and triplet pair, delayed fluorescence *via* the singlet exciton is a viable decay channel, but in oligopentacenes linked at the 2' position, triplet recombination only occurs *via* internal conversion and is a dark process.[9,14] Moreover, the transient spectra of correlated triplet pairs in directly linked dimers differs from a free triplet, particularly in the NIR region of the spectrum.[9] The assignment of the NIR photoinduced absorption signal to the triplet pair has been established based on its identical decay kinetics to the $T_1 \rightarrow T_3$ photoinduced absorption feature in the visible. Therefore, we can readily distinguish triplet pairs from free triplets. Importantly, we can also distinguish between correlated triplet pairs on adjacent and non-adjacent pentacenes, as both the spectra and the recombination rate are sensitive to triplet pair separation.[9,14,36] Therefore, the triplet pair lifetime and the NIR spectral feature serve as a sensitive probe of the spatial distribution of triplets along the backbone of the oligomers.

Figure 4.4 shows the triplet pair recombination kinetics for the oligomers. In all cases, we find that the recombination remains relatively constant, with time constants of 0.62 ns in 3Pc, to 0.69 ns in 4Pc, and 0.7 ns in 5Pc. The free triplet lifetime is measured using triplet sensitization experiments to be >10 µs. In addition to the nearly identical lifetimes, the triplet pair spectra of the oligomers resemble the directly linked 2Pc compound, indicating that triplet pairs are preferentially located on nearest neighbor pentacenes. As such, triplet pairs remain bound in these systems and do not dissociate along the extended oligomer and polymer chains in any significant amount. These results show that, in order to slow down triplet pair recombination, it is more essential to separate the chromophores through covalent bridges, as in the case of pentacene dimers and heterodimers, rather than extending the backbone of the chromophore.

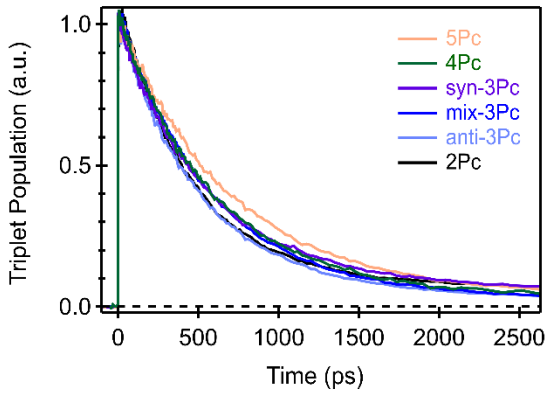

Figure 4.4. Triplet population, monitored at 527 nm in TCB after 600 nm excitation (~25 µJ/cm^2), shows a weak and complex relationship to oligomer length, but a slight trend toward longer triplet pair lifetimes for longer oligomers.

Interestingly, we find that there is no difference in the photophysics of different regioisomers. Since the oligomers and the polymer are mixtures of regioisomers, as we previously discussed, we also investigated the excited state dynamics of well-defined regioisomers of the trimer, syn-3Pc and anti-3Pc (see SI for details). We find that despite their different symmetry point groups, these

trimers exhibit nearly identical absorption spectra as well as iSF and recombination dynamics. Thus, we postulate that regioregularity does not significantly affect the individual chain photophysics of the pentacene polymer. However, as in other polymer systems, the degree of regioregularity might affect the interchain packing and the corresponding physical properties in the condensed phase, including the carrier dynamics and transport, which we are currently investigating.[37,38]

4.5 Conclusions

In conclusion, we have found that more extended pentacene systems feature enhanced rates of singlet fission. This phenomenon is not sensitive to the presence of regioisomers, as demonstrated by *syn* and *anti* trimers. Furthermore, while extended systems offer additional chromophores for diffusional separation of triplet excitons, we find that the triplet pairs remain bound, as evidenced by spectral differences and shorter lifetimes of these bound triplet pairs compared to free triplets.

4.6 Methods

Transient absorption spectroscopy was performed on oligomers dissolved in 1 or 2 mm quartz cuvettes in less than 100 μM concentration of pentacene repeat unit. These solutions were interrogated using a transient absorption spectroscopy system previously described by our group.[6] Briefly, a commercial Ti:sapphire laser system (SpectraPhysics) operating at a repetition rate of 1 kHz was used to seed a commercial optical parametric amplifier (LightConversion) which generated resonant pump pulses with ~100 fs time duration. A small portion of the 800 nm

fundamental was focused into a sapphire disk to generate supercontinuum probe light. Shot to shot detection of these pump and probe beams was accomplished by a fiber-coupled silicon (visible) or InGaAs (infrared) diode array. A mechanical delay stage was used to control pump probe delay, and excitation fluence in each measurement was approximately 25 $\mu J/cm^2$ and always less than 100 $\mu J/cm^2$.

Global Analysis was used to analyze the resulting transient absorption spectra. This analysis was accomplished using the Glotaran software package.[39] Global analysis yields accurate rate constants because is treats the entire dataset in aggregate. In each case, a decay model of $S_1 \rightarrow TT \rightarrow S_0$ was used to model the data. Typically, singlet fission rate was monoexponential and the triplet pair recombination rate was weakly biexponential.

4.7 Transient Absorption Spectra

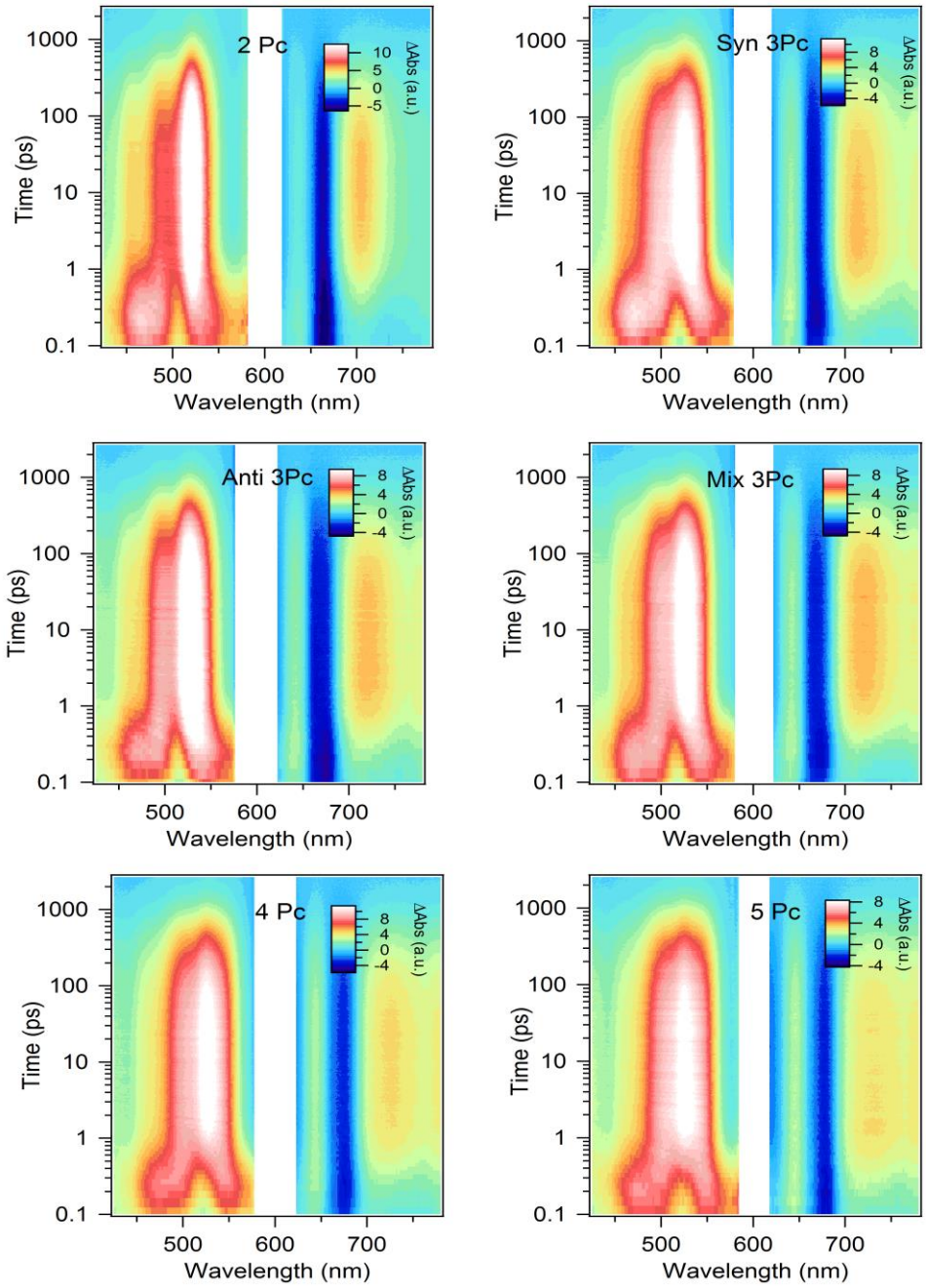

Figure 4.5. Transient absorption spectra of oligopentacenes dissolved below 100 µM (relative to pentacene monomers) in 1,2,4-trichlorobenzene (TCB) with excitation at 600 nm and approximately 25 µJ/cm^2

In every case, qualitatively similar behavior is observed for photoexcitation in TCB, where the photoexcited singlet exciton rapidly decays on a sub-picosecond timescale, concomitant with rise of the triplet pair photoinduced absorption.

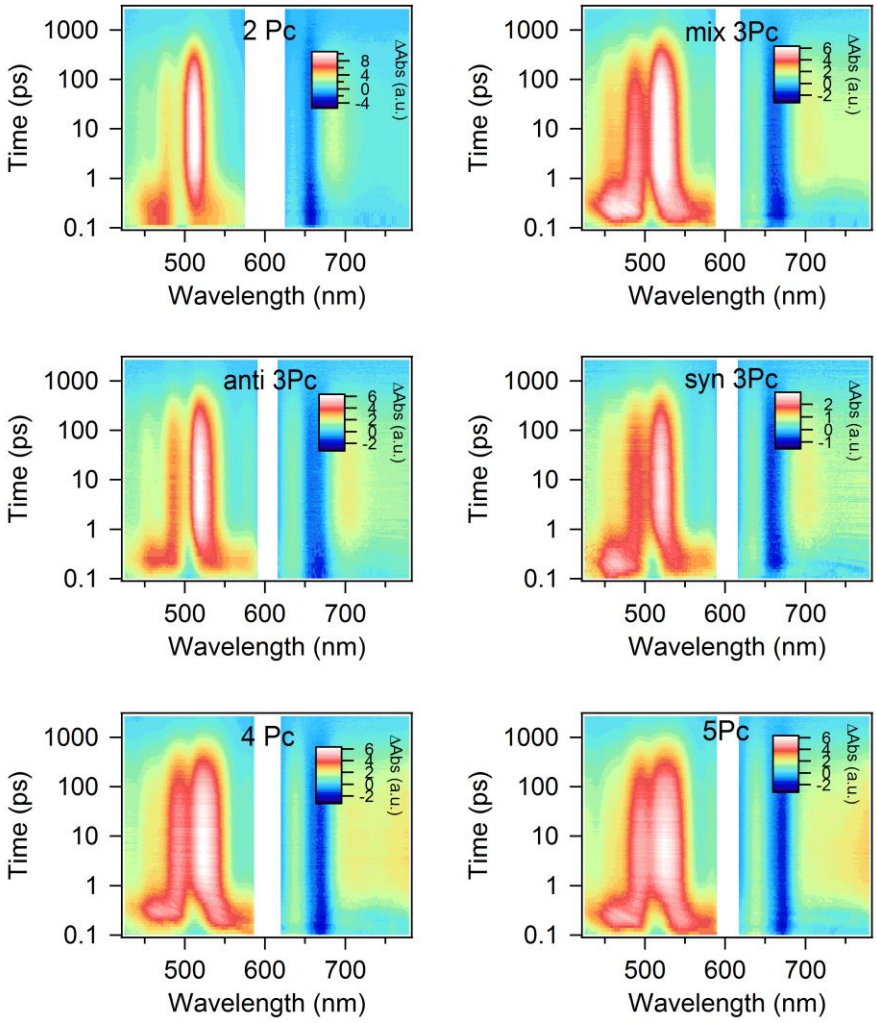

Figure 4.6. Transient absorption spectra of oligopentacenes dissolved below 100 μM (relative to pentacene monomers) in 1,1,2-trichloroethylene (TCE) with excitation at 600 nm and approximately 25 μJ/cm^2

Transient absorption spectroscopy in TCE for the oligomers reveals the weak dependence of the singlet fission process on the solvent. Indeed, global analysis of these datasets recovers singlet fission time constants nearly identical to those found by measurements in TCB.

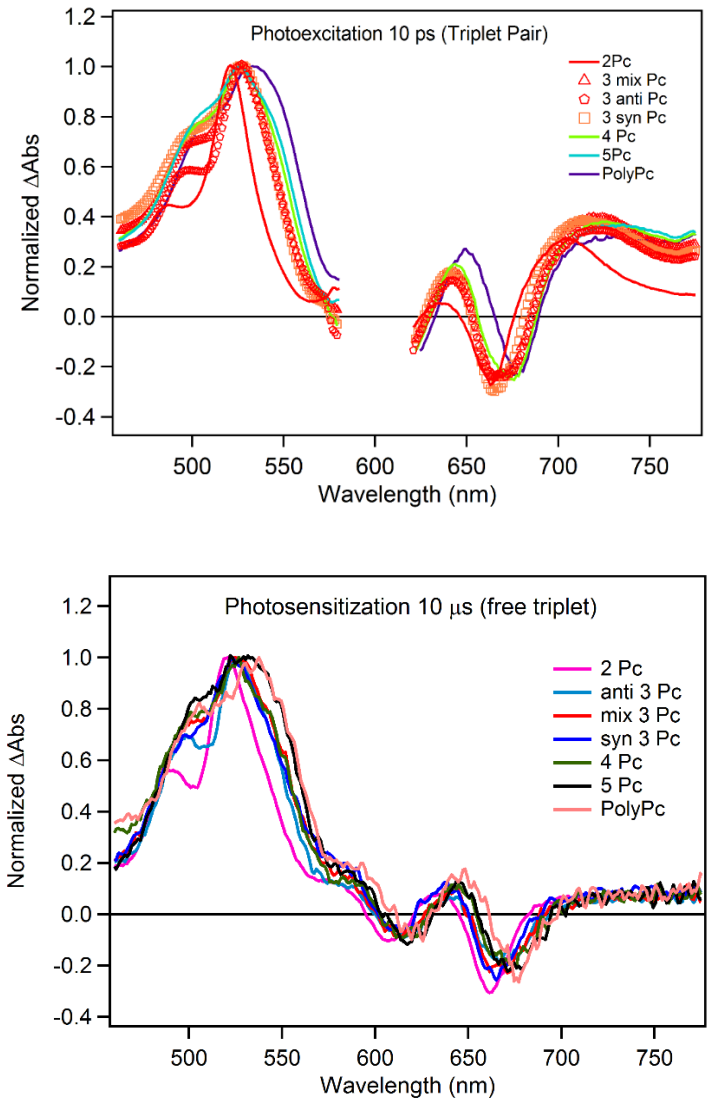

Figure 4.7. Photoinduced absorption spectra 10 ps after excitation for the oligomers in TCB reveal a triplet pair spectrum with a pronounced peak near 710 nm, indicative of a correlated triplet pair state.

The triplet pair spectra, produced by photoexcitation, are similar but not quite identical to the spectra of a single triplet, produced by triplet photosensitization experiments (more detail below). Interestingly, even in longer oligomers, a peak near 700 nm, previously assigned as indicative of a close-proximity triplet pair, is prominent for the triplet pair spectra but not the individual triplet spectra.[9] This difference in lineshape, combined with the shorter lifetimes of

triplet pairs (from photoexcitation) compared to the native triplet lifetimes (from photosensitization), all suggest that iSF in all the oligomers and polymer studied here produces triplet pairs which do not diffuse apart.

4.8 Linear Absorption Spectroscopy

We have previously reported the UV-Visible linear absorption spectra for the oligomers and polypentacene in chloroform. We have also shown the change in the linear absorption as a function of solvent for the pentamer and polymer. Here, we also report the linear absorption spectra in TCB for all oligomers and polypentacene. It should be noted that the molar absorptivity was found to be independent of concentration in the regime measured (below 100 μM) and is reported here normalized per-pentacene, compared to monomer with a molar absorptivity of ~19,000 $L^{-1}M^{-1}$ at the first maximum after the onset of absorption, near 660 nm. The only exception is polypentacene, where the normalization is arbitrary.

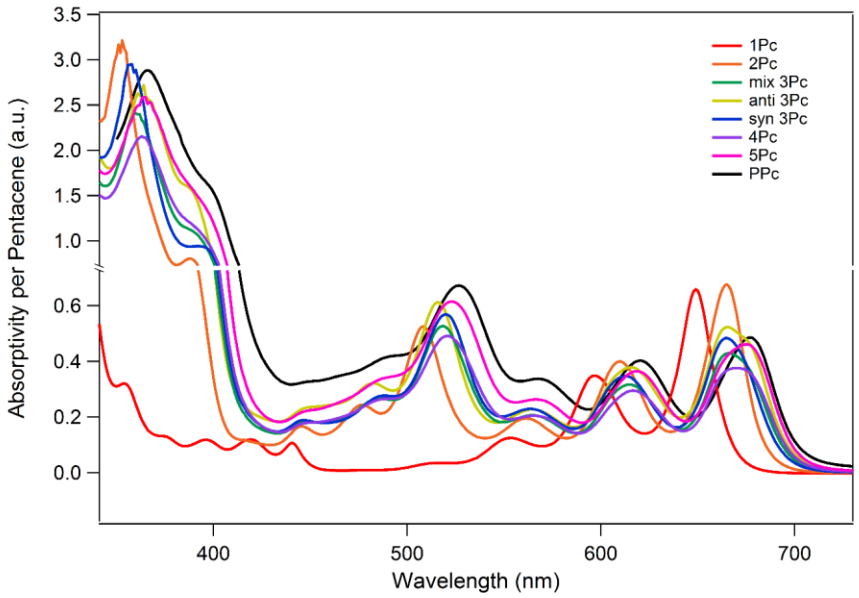

Figure 4.8. Linear absorption spectra for oligomers, scaled per-pentacene relative to monomer, as well as polypentacene (scaled arbitrarily), in TCB.

The linear absorption spectra reveal the absence of aggregation in these oligomers and polymer at the concentration regime considered (similar to that used for transient absorption spectroscopy). Aggregation of these molecules manifests as a red shifting of the onset of absorption and a broadening of the vibronic peaks which are well defined in well-dissolved solutions.

4.9 Triplet Photosensitization Measurements

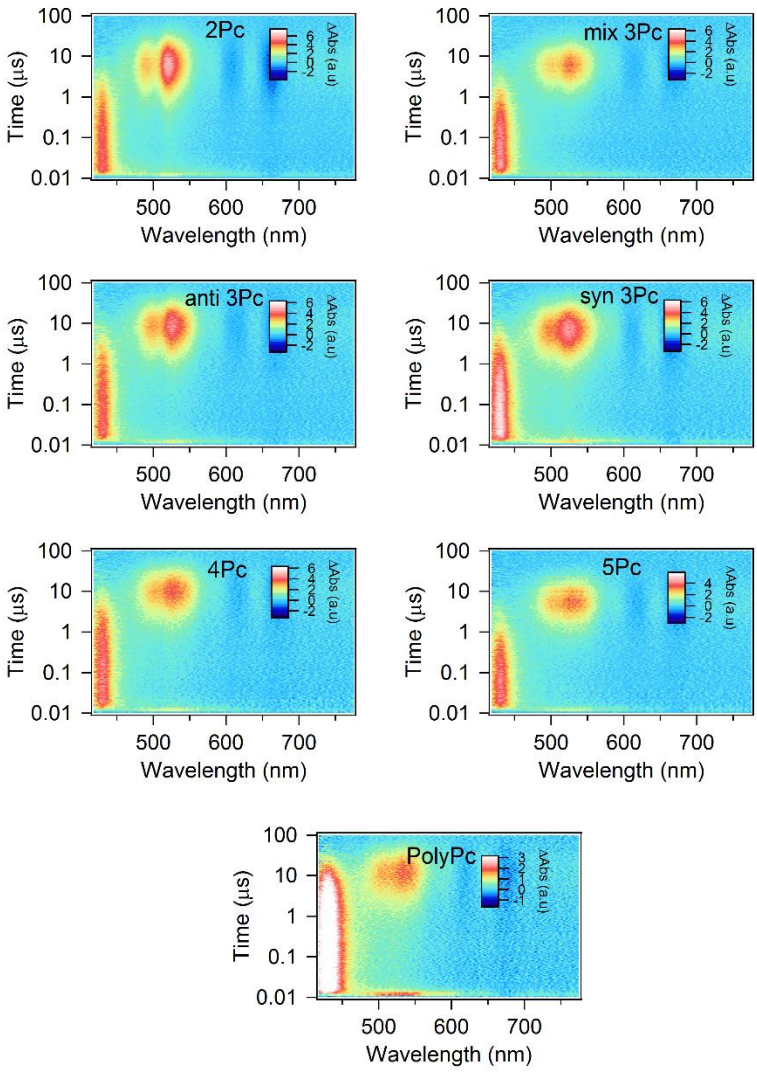

Figure 4.9. Nanosecond transient absorption spectroscopy of photosensitization experiments with 20 mM anthracene, excited at 360 nm with a ~25 µJ/cm^2 pulse in TCB

Triplet photosensitization experiments were performed to reveal the free triplet lifetime and spectrum. The compound of interest is dissolved along with a large excess of anthracene. Photoexcitation at 360 nm preferentially excites the anthracene, which undergoes intersystem crossing to form the anthracene triplet. Collisions in solution between anthracene triplet excitons and the pentacene derivative populate individual triplets on the pentacene chromophores which

are then interrogated optically to reveal the lifetime and spectrum of the free triplet exciton in these systems.

4.10 References

(1) Smith, M. B.; Michl, J. *Annu. Rev. Phys. Chem.* **2013**, *64*, 361.

(2) Smith, M. B.; Michl, J. *Chem. Rev.* **2010**, *110*, 6891.

(3) Hanna, M. C.; Nozik, A. J. *J. Appl. Phys.* **2006**, *100*, 074510.

(4) Korovina, N. V.; Das, S.; Nett, Z.; Feng, X.; Joy, J.; Haiges, R.; Krylov, A. I.; Bradforth, S. E.; Thompson, M. E. *J. Am. Chem. Soc.* **2016**, *138*, 617.

(5) Roberts, S. T.; McAnally, R. E.; Mastron, J. N.; Webber, D. H.; Whited, M. T.; Brutchey, R. L.; Thompson, M. E.; Bradforth, S. E. *J. Am. Chem. Soc.* **2012**, *134*, 6388.

(6) Fuemmeler, E. G.; Sanders, S. N.; Pun, A. B.; Kumarasamy, E.; Zeng, T.; Miyata, K.; Steigerwald, M. L.; Zhu, X. Y.; Sfeir, M. Y.; Campos, L. M.; Ananth, N. *ACS Cent. Sci.* **2016**, *2*, 316.

(7) Low, J. Z.; Sanders, S. N.; Campos, L. M. *Chem. Mater.* **2015**, *27*, 5453.

(8) Sanders, S. N.; Kumarasamy, E.; Pun, A. B.; Steigerwald, M. L.; Sfeir, M. Y.; Campos, L. M. *Angew. Chem. Int. Ed.* **2016**, *55*, 3373.

(9) Sanders, S. N.; Kumarasamy, E.; Pun, A. B.; Trinh, M. T.; Choi, B.; Xia, J.; Taffet, E. J.; Low, J. Z.; Miller, J. R.; Roy, X.; Zhu, X. Y.; Steigerwald, M. L.; Sfeir, M. Y.; Campos, L. M. *J. Am. Chem. Soc.* **2015**, *137*, 8965.

(10) Lukman, S.; Musser, A. J.; Chen, K.; Athanasopoulos, S.; Yong, C. K.; Zeng, Z.; Ye, Q.; Chi, C.; Hodgkiss, J. M.; Wu, J.; Friend, R. H.; Greenham, N. C. *Adv. Funct. Mater.* **2015**, *25*, 5452.

(11) Zirzlmeier, J.; Lehnherr, D.; Coto, P. B.; Chernick, E. T.; Casillas, R.; Basel, B. S.; Thoss, M.; Tykwinski, R. R.; Guldi, D. M. *Proc. Natl Acad. Sci.* **2015**, *112*, 5325.

(12) Sakuma, T.; Sakai, H.; Araki, Y.; Mori, T.; Wada, T.; Tkachenko, N. V.; Hasobe, T. *J. Phys. Chem. A* **2016**, *120*, 1867.

(13) Zirzlmeier, J.; Casillas, R.; Reddy, S. R.; Coto, P. B.; Lehnherr, D.; Chernick, E. T.; Papadopoulos, I.; Thoss, M.; Tykwinski, R. R.; Guldi, D. M. *Nanoscale* **2016**, *8*, 10113.

(14) Sanders, S. N.; Kumarasamy, E.; Pun, A. B.; Appavoo, K.; Steigerwald, M. L.; Campos, L. M.; Sfeir, M. Y. *J. Am. Chem. Soc.* **2016**, *138*, 7289.

(15) Aryanpour, K.; Dutta, T.; Huynh, U. N. V.; Vardeny, Z. V.; Mazumdar, S. *Phys. Rev. Lett.* **2015**, *115*, 267401.

(16) Musser, A. J.; Al-Hashimi, M.; Maiuri, M.; Brida, D.; Heeney, M.; Cerullo, G.; Friend, R. H.; Clark, J. *J. Am. Chem. Soc.* **2013**, *135*, 12747.

(17) Zhai, Y.; Sheng, C.; Vardeny, Z. V. *Philosophical Transactions of the Royal Society of London A: Mathematical, Physical and Engineering Sciences* **2015**, *373*.

(18) Busby, E.; Xia, J.; Low, J. Z.; Wu, Q.; Hoy, J.; Campos, L. M.; Sfeir, M. Y. *J. Phys. Chem. B* **2015**, *119*, 7644.

(19) Busby, E.; Xia, J.; Wu, Q.; Low, J. Z.; Rong, R.; Miller, J. R.; Zhu, X.-Y.; Campos, L. M.; Sfeir, M. Y. *Nat. Mater.* **2014**, *14*, 426.

(20) Austin, R. H.; Baker, G. L.; Etemad, S.; Thompson, R. *J. Chem. Phys.* **1989**, *90*, 6642.

(21) Jundt, C.; Klein, G.; Le Moigne, J. *Chem. Phys. Lett.* **1993**, *203*, 37.

(22) Wohlgenannt, M.; Graupner, W.; Leising, G.; Vardeny, Z. V. *Phys. Rev. B* **1999**, *60*, 5321.

(23) Kraabel, B.; Hulin, D.; Aslangul, C.; Lapersonne-Meyer, C.; Schott, M. *Chem. Phys.* **1998**, *227*, 83.

(24) Antognazza, M. R.; Lüer, L.; Polli, D.; Christensen, R. L.; Schrock, R. R.; Lanzani, G.; Cerullo, G. *Chem. Phys.* **2010**, *373*, 115.

(25) Lanzani, G.; Cerullo, G.; Zavelani-Rossi, M.; De Silvestri, S.; Comoretto, D.; Musso, G.; Dellepiane, G. *Phys. Rev. Lett.* **2001**, *87*, 187402.

(26) Guo, J.; Ohkita, H.; Benten, H.; Ito, S. *J. Am. Chem. Soc.* **2009**, *131*, 16869.

(27) Österbacka, R.; Wohlgenannt, M.; Shkunov, M.; Chinn, D.; Vardeny, Z. V. *J. Chem. Phys.* **2003**, *118*, 8905.

(28) Geerts, Y.; Klärner, G.; Müllen, K. In *Electronic Materials: The Oligomer Approach*; Wiley-VCH Verlag GmbH: 2007, p 1.

(29) Koch, F. P. V.; Smith, P.; Heeney, M. *J. Am. Chem. Soc.* **2013**, *135*, 13695.

(30) Meier, H.; Stalmach, U.; Kolshorn, H. *Acta Polym.* **1997**, *48*, 379.

(31) Liu, F.; Espejo, G. L.; Qiu, S.; Oliva, M. M.; Pina, J.; Seixas de Melo, J. S.; Casado, J.; Zhu, X. *J. Am. Chem. Soc.* **2015**, *137*, 10357.

(32) Varnavski, O.; Abeyasinghe, N.; Aragó, J.; Serrano-Pérez, J. J.; Ortí, E.; López Navarrete, J. T.; Takimiya, K.; Casanova, D.; Casado, J.; Goodson, T. *J. Phys. Chem. Lett.* **2015**, *6*, 1375.

(33) Dell, E. J.; Capozzi, B.; Xia, J.; Venkataraman, L.; Campos, L. M. *Nat. Chem.* **2015**, *7*, 209.

(34) Kumarasamy, E.; Sanders, S. N.; Pun, A. B.; Vaselabadi, S. A.; Low, J. Z.; Sfeir, M. Y.; Steigerwald, M. L.; Stein, G. E.; Campos, L. M. *Macromolecules* **2016**, *49*, 1279.

(35) Pensack, R. D.; Tilley, A. J.; Parkin, S. R.; Lee, T. S.; Payne, M. M.; Gao, D.; Jahnke, A. A.; Oblinsky, D. G.; Li, P.-F.; Anthony, J. E.; Seferos, D. S.; Scholes, G. D. *J. Am. Chem. Soc.* **2015**, *137*, 6790.

(36) Pensack, R. D.; Ostroumov, E. E.; Tilley, A. J.; Mazza, S.; Grieco, C.; Thorley, K. J.; Asbury, J. B.; Seferos, D. S.; Anthony, J. E.; Scholes, G. D. *J. Phys. Chem. Lett.* **2016**, 2370.

(37) Kline, R. J.; McGehee, M. D.; Kadnikova, E. N.; Liu, J.; Fréchet, J. M. J.; Toney, M. F. *Macromolecules* **2005**, *38*, 3312.

(38) Kim, Y.; Cook, S.; Tuladhar, S. M.; Choulis, S. A.; Nelson, J.; Durrant, J. R.; Bradley, D. D. C.; Giles, M.; McCulloch, I.; Ha, C.-S.; Ree, M. *Nat. Mater.* **2006**, *5*, 197.

(39) Snellenburg, J. J. L., S. P.; Seger, R.; Mullen, K. M.; van Stokum, I. H. M. *J. Stat. Soft.* **2012**, *49*, 1.

5 Tuning Singlet Fission in Pi-Bridge-Pi Chromophores

5.1 Preface

This chapter is based on a manuscript published in the *Journal of the American Chemical Society* entitled "Tuning Singlet Fission in Pi-Bridge-Pi Chromophores" by Elango Kumarasamy, Samuel N. Sanders, Murad J. Y. Tayebjee, Amir Asadpoordarvish, Timothy J. H. Hele, Eric G. Fuemmeler, Andrew B. Pun, Lauren M. Yablon, Jonathan Z. Low, Daniel W. Paley, Jacob C. Dean, Bonnie Choi, Gregory D. Scholes, Michael L. Steigerwald, Nandini Ananth, Dane R. McCamey, Matthew Y. Sfeir, and Luis M. Campos. Elango synthesized all the compounds while I performed all linear and transient absorption spectroscopy. Murad and Amir performed electron spin resonance spectroscopy in the laboratory of Prof. McCamey while Tim and Eric performed calculations in the lab of Prof. Nandini. Andrew assisted with linear absorption measurements, Lauren assisted with analyzing transient absorption data, and Jacob performed quantum yield measurements in the lab of professor Scholes. Mike assisted with interpretation of results while Bonnie and Dan solved the crystal structures.

5.2 Introduction

Understanding the fundamental dynamics of singlet fission (SF) chromophores with idealized properties for next-generation optoelectronic devices fuels the development of families of new materials.[1-6] This includes the important discovery of intramolecular singlet fission polymers and oligomers, where chromophore-chromophore interactions occur primarily through covalent bonds.[7-23] Several different bonding connectivity schemes have been demonstrated to activate singlet fission, where the triplet generation and decay kinetics have been shown to be

highly sensitive to the manner in which neighboring chromophores are linked. The interaction of chromophores in iSF compounds differs significantly from the through-space interactions primarily found in molecular crystals, where the through-space coupling between the chromophore coupling is greatly influenced by the morphology.[24-26,28-30] For instance, multiexponential singlet fission rates are observed in disordered systems when compared to monoexponentional kinetics in iSF systems.[31,32]

Given the sensitivity of SF to structure, it remains unclear how through-bond interactions promote fast and efficient singlet fission, especially focusing on the most basic pentacene dimer model. To date, several groups have reported that connecting two pentacenes using conjugated bridges can be used to promote efficient singlet fission, even when the proximity between the pentacenes is significantly decreased.[9,10,13,14] For example, when the bridge shown in Figure 5.1 is varied from one to three phenylene units, we have found that the rates of singlet fission and triplet pair recombination in pentacene dimers are drastically affected. The longer the conjugated bridge, the slower the rate of iSF and triplet pair recombination.[11] Similarly, Zirzlmeier et al. reported pentacene dimers that were connected through 6-position by *o*-, *m*-, *p*-diethynylbenzene spacers, which revealed that through-space and through-bond interactions play crucial role in singlet fission and triplet recombination dynamics. They also found that faster singlet fission was accompanied by faster triplet recombination.[9] Further, orthogonally connected dimers reported by Lukman et al. resulted in ultrafast singlet fission and were particularly sensitive to the polarity of the medium.[12,33] Recently, Liu et al. designed tetracene trimer through linear oligomerization which resulted in greatly enhanced iSF yield (96%) relative to a similar dimer. This SF enhancement was attributed to singlet exciton delocalization.[34] These studies all suggest that conjugation plays a significant role in driving singlet fission and triplet recombination. Such conclusion is further supported by

the fact that singlet fission is slower in twisted dimers that lack bridging units, where conjugation is decreased due to reduced overlap of the pi orbitals.[35]

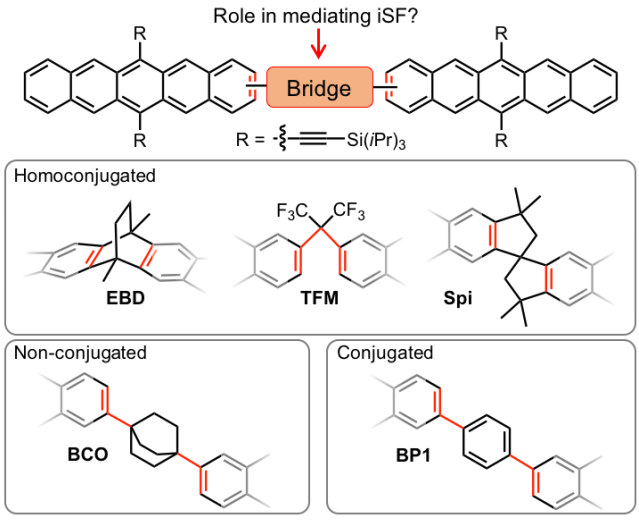

Figure 5.1. The pentacene-bridge-pentacene model showing the comparison between different bridging units. In the bottom representations, the pentacenes are omitted to highlight the nature of the bridging units.

Interestingly, many of aforementioned studies offer hints that conjugation may not be strictly necessary for singlet fission in pentacene-bridge-pentacene chromophores. A recent computational study suggests that singlet fission occurs by a direct mechanism in bipentacene, in contrast to the charge transfer mediated (step-wise) mechanism widely perceived to be dominant in intermolecular singlet fission of crystalline pentacene.[35] One of the key predictions from this study was that very weak chromophore-chromophore coupling could permit ultrafast singlet fission. The process is viable through an avoided crossing, when resonance between the singlet exciton and triplet pair states is reached through a vibrational mode. However, the ultimate limits of this hypothesis have not yet been tested, i.e., it is unknown what happens in the excited state when both through-space and through-bond interactions are extremely weak.

We investigate how homoconjugated and non-conjugated bridging units affect the excited state dynamics of pentacene dimers. We particularly focus on understating how singlet fission and triplet pair recombination behave in the limit of weakly coupled pentacene dimers (Figure 5.1). In homoconjugated dimers, the two pentacene chromophores are separated by a saturated sp^3 carbon, thus the pentacene-pentacene coupling and/or electron delocalization is expected to be weaker than in conjugated systems (such as BP1, Figure 5.1).[11] We postulate that this π-sigma-π bonding scheme will make the excited state dynamics much less sensitive to subtle variations in the geometry of the bridge as compared to analogous conjugated dimers.[36] Additionally, these systems are suited to introduce more than one sp^3 carbon in the bridge to yield non-conjugated dimers, thus allowing us to probe the limits of weak coupling interactions.

5.3 Materials Design

The chromophores shown in Figure 5.1 were designed as follows: In both the ethanobenzo[*b*]decacence derivative (EBD)[20-22] and the spirobi[cyclopenta[*b*]pentacene] derivative (Spi) the pentacenes are locked in a rigid fashion. The pentacenes in EBD are more planar than in Spi, where the two chromophores are nearly orthogonal to each other. In the bistrifluoromethyl derivative (TFM), the two pentacene units are connected by single saturated carbon, giving the pentacenes some freedom to rotate relative to one another. Finally, we use a bicyclooctane spacer (BCO) to mimic the distance imposed by the conjugated phenylene spacer in BP1, which has been previously reported.[11]

5.4 Steady-State Optical Properties

The UV-visible absorption spectra of the dimers are shown in Figure 5.2, and are plotted alongside the spectrum of TIPS-pentacene for comparison. In all cases the dimer spectra are qualitatively similar to the monomer spectra, allowing us to assign dimer transitions from the known spectrum of pentacene.[37] The absorption around 650 nm corresponds to an intra-monomer HOMO to LUMO excitation polarized along the short-axis of the monomer, and is slightly red-shifted in Spi (by ~12 nm), possibly due to a small interaction between pi systems of the monomers. The intense absorption in the UV around 310 nm corresponds to a long-axis polarized transition and the weak absorption around 440 nm to an almost-forbidden long-axis transition.

Both the 650 nm and 440 nm transitions are accompanied by vibrational stretching progressions commonly seen in acene spectra. Some dimers exhibit a splitting of the 310 nm absorption, whereby the dipole moments along the long-axis of each monomer can combine in-phase or out-of-phase, giving two distinct absorptions. This is clearest when the long-axes of the monomers are approximately 90° apart (as for Spi) and absent if the long-axes are in the same (as for BP1). The redshift in the high-energy features in BP1 is potentially due to greater interactions between the chromophores through a conjugated linker.

Although changes in the absorption spectrum (where present) can indicate the extent of chromophore interaction, the inter-chromophore coupling responsible for SF is not available from UV-vis spectra, since the relevant CT and TT states (or adiabatic states with that character) are generally dark and the UV-vis spectrum probes the adiabatic electronic states, not localized/diabatic states from whose coupling SF rates can be determined.[35,38]

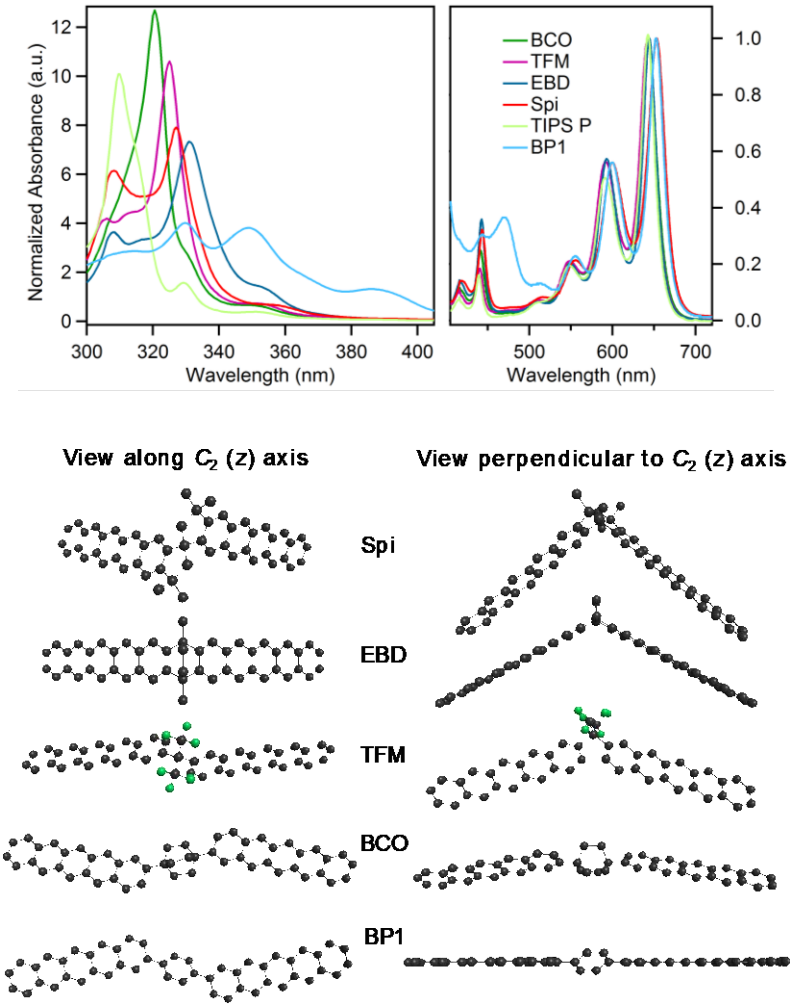

Figure 5.2. Top: UV-Visible absorption spectra with TIPS-pentacene and BP1 included for reference. Bottom: Calculated structures using density functional theory. Hydrogens and TIPS substituents at the 6,13-position of pentacene are omitted for clarity.

5.5 Transient Absorption Spectroscopy of Homoconjugated Dimers

We use broadband transient absorption spectroscopy (TAS) to study the excited state dynamics of these molecules in dilute solution. The measurements are carried out in a standard nearly collinear transmission geometry. A 100 fs pump pulse is tuned to excite a vibronic feature associated with the lowest energy optical transition (~ 600 nm) and a supercontinuum white light

was used as probe. Both femto- (mechanical delay) and nanosecond (electronic delay) broadband probes are employed in conjunction with this same pump pulse to extend the dynamic range of measurement from 100 fs – 100 μs. Figure 5.3 shows the resulting 2D color plots produced by photoexcitation of the pentacene dimers with a fluence of ~25 μJ/cm^2 in chloroform.

We find that efficient singlet fission occurs in all of the homoconjugated pentacene dimers (EBD, TFM, Spi). Moreover, despite the significantly different geometries, singlet fission rates are quite similar among the homoconjugated dimers as EBD, TFM and Spi undergo iSF with time constants of 10 ps, 50 ps and 55 ps, respectively. Singlet fission is assigned following the widely accepted criteria.[7,9-12,14,19,23,33-35,39-43] Briefly, the singlet decay is assigned by correlating the time constants associated with the decay of prompt fluorescence (using photoluminescence upconversion techniques) to features in the transient absorption spectra. From this, we determine that the photoexcited singlet exciton is associated with photoinduced absorption bands near ~460 nm and 520 nm, and find that the singlet decays on <100 ps timescales.

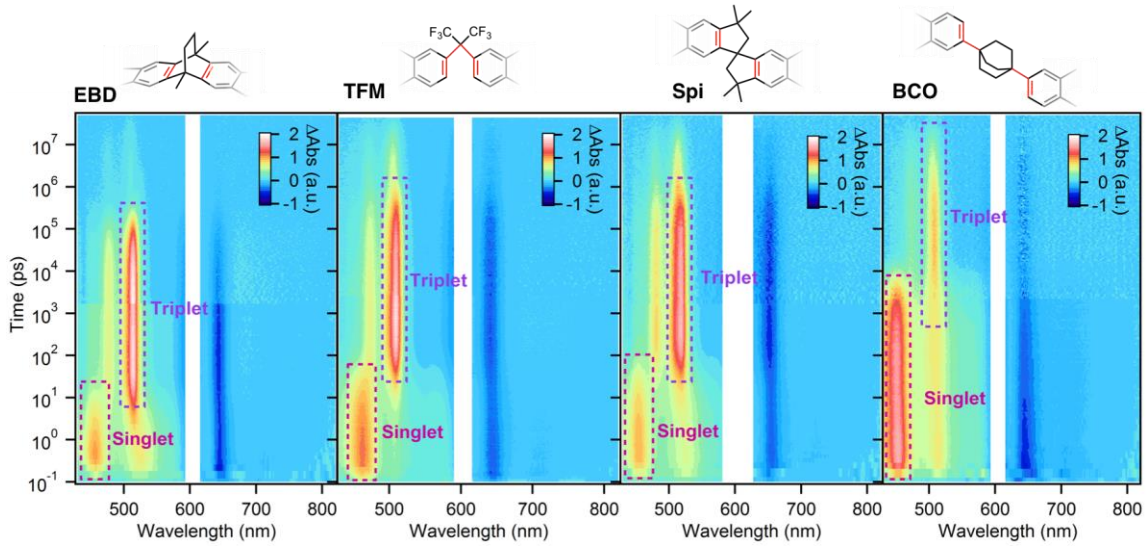

Figure 5.3. Transient absorption spectroscopy in dilute chloroform solution with 600 nm excitation (~25 μJ/cm^2) reveals evolution of the photoexcited singlet into triplets with singlet fission and triplet pair recombination rates that depend strongly dependent on the properties of the

bridge. In the structures of the bridges, red color indicates the connectivity of pentacene units, and the color scales have been normalized to facilitate comparison and are therefore reported in arbitrary units (a.u.). Data prior to ~2.7 ns is collected using a mechanical delay, while the same pump pulse and an electronically controlled probe were used to generate data after ~2.7 ns.

The triplet pair state also shows similar dynamics within the set of homoconjugated dimers and is assigned by comparing the products of singlet fission to triplet sensitization studies. From this comparison, we find that the primary triplet feature in the transient absorption spectra is a prominent photoinduced absorption near ~510 nm. This feature can be used to monitor the triplet decay dynamics. Similar to other dimer systems, we find that the rise of the triplet pair is concomitant to the decay of the singlet, indicating that no parasitic processes or other intermediates are present, as has been widely suggested in the literature.[10-12,14,16,44] This allows us to quantify the yields using kinetic arguments, since the only significant competing relaxation process is a 12.3 ns radiative decay. Using these arguments, we calculate that the singlet fission yields exceed 198%. As will be discussed later, using electron spin resonance measurements, we also show that the triplet pairs that are formed from singlet fission remain spin coupled across the homoconjugated bridge. Similar to other dimers with long lived triplet pairs, this leads to a biexponential recombination process, with a dominant short lifetime component (< 1 μs) in ESR and TA representing the spin coupled state and a weaker component with a time constant of ~20 μs lifetime that is assigned to a minority species of free pentacene triplets formed *via* dissociation of the triplet pair. For EBD, TFM and Spi the spin coupled triplet pair lifetimes are extremely long, 174 ns, 531 ns, and 705 ns, respectively.

Akin to conjugated pentacene dimers, we suggest that iSF proceeds through a direct mechanism in homoconjugated dimers, without significant mediation from charge transfer (CT) states. This is based on the following evidence: (i) the prohibitively high-lying energy of CT states

with large center-center distances which we calculate using electronic structure theory methods, compared to molecular crystals, where additional electronic bandwidth also help to bring singlet exciton and CT states into resonance (ii) the discovery of a viable direct mechanism based on vibrationally induced degeneracy between S_1 and TT, despite weak coupling,[35] and (iii) a weak and non-monotonic dependence of SF rates on solvent polarity or polarizability.[11,35,41,45]

Here, the effect of changing the conjugation motif is highlighted by comparison to a previously reported conjugated dimer (BP1, Figure 5.4, Table 5.1). BP1, which constitutes two pentacenes connected by a *p*-phenylene bridge (Figure 5.1), is the conjugated dimer with the closest singlet fission time constant (20 ps) to the homoconjugated dimers investigated here.[11] From inspection, we clearly see that the electronic coupling between the chromophores is significantly affected by through-bond interactions; singlet fission in BP1, where pentacenes are connected through four sp^2 hybridized carbons, has a time constant similar to homoconjugated dimers, where pentacene chromophores are separated by just one sp^3 hybridized carbon.

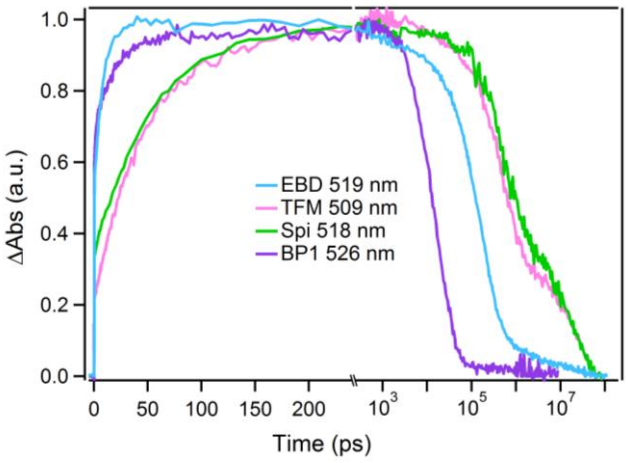

Figure 5.4. Normalized kinetics monitored at the maximum of the triplet photoinduced absorption of TFM, EBD, Spi, and BCO as dilute solutions in chloroform following 600 nm excitation (~25 μJ/cm^2).

Despite the faster time constants for triplet pair generation as compared to conjugated BP1, triplet pair recombination is > 10 times slower in EBD. Similarly, while singlet fission is slower by a factor of approximately 2.5, the triplet pair recombination is slower by a factor of > 30 in TFM and > 40 in Spi. These results indicate that singlet fission and triplet pair recombination are not governed by the exact same pentacene-pentacene coupling relationship. This is an important observation because breaking the relationship between the rate of triplet generation (fast singlet fission) and decay rates (slow recombination) can play a fundamental role in optoelectronic devices, where maximizing the overall triplet pair lifetime is beneficial for harvesting that energy. While it has been observed in twisted dimers that reducing the coupling between pentacene chromophores preferentially extends the triplet pair lifetime,[35] this is the first family of materials with fast rates of iSF, and drastically different rates of triplet pair recombination. While it is worth noting that solid-state dynamics are relevant to devices, solution studies isolate through-bond singlet fission. In the solid-state, through-bond singlet fission can be complemented by through-space singlet fission, adding an additional SF channel. Though it must be noted that characterization of the through-bond SF in solution is informative to the properties of the new materials and their potential utility.

Table 5.1. Time constants for: rate of iSF (τ_{iSF}), triplet pair lifetimes ($\tau_{[TT]}$), and individual triplet decay ($\tau_{[T]}$, obtained from slower triplet decay component).

Compound	τ_{iSF} (ps)	$\tau_{(TT)}$ (ns)	$\tau_{(T)}$ (ns)
BP1[11]	20	16.5	---
EBD	10	174	24,300

TFM	50	531	23,000
Spi	55	705	19,600
BCO	~20,000	1,800	18,000

5.6 Transient Absorption Spectroscopy of a Non-Conjugated Dimer.

Surprisingly, we find that BCO, a non-conjugated pentacene dimer separated by 4 sp^3 hybridized carbons, is capable of singlet fission (Figure 5.3). A similar methodology to other dimers was used to identify singlet fission and assign the relevant rate constants. It is remarkable that singlet fission can proceed even in the limit of extremely weak electronic coupling, as evidenced by the long singlet lifetime (7.6 ns). Despite the similar interchromophore separation as conjugated BP1, the rate constant for singlet fission in BCO slower by a factor of nearly 1000. Again, this allows us to deduce the important role of conjugation in facilitating fast and efficient singlet fission.

5.7 Identification of Triplet-Triplet Pairs with Electron Spin Resonance Spectroscopy

We establish that singlet fission is operative, producing triplet pairs as opposed to free triplet generation by intersystem crossing, by correlating transient absorption and electron spin resonance studies (Figure 5.5). Like other iSF dimers, transient absorption studies show that the triplet population decays biexponentially, indicating the presence of triplet pairs (TT) with an enhanced recombination rate (Figure 5.6) and a minority population of free triplets decay with the expected

rate for an individual triplet. These biexponential decay dynamics have also been observed in other systems[11,14,39,40] and do not change as a function of concentration or other experimental parameters.

The biexponential dynamics in the TA experiments were further probed by transient electronic spin resonance (tr-ESR) measurements. tr-ESR spectroscopy has previously been used to identify coupled triplet-triplet pairs, (TT), and uncoupled triplets, T, in bipentacenes.[39] Figure 5.5 shows the 80K pulsed laser, continuous microwave tr-ESR spectra of Spi and BCO in toluene, using microwave frequencies of 9.681092 and 9.615778 GHz, respectively. The spectra are plotted as a function of g-factor to highlight the identical location of resonances, which arise from the g-factor and zero-field splitting parameters of individual pentacene triplets (g~2.0023, D~1100MHz and E~20MHz, in accordance with previous ESR studies of the pentacene chromophore[39,46,47]). Transition resonance peaks for magnetic fields applied along the x/y molecular axes are marked on the plot.

In both Spi and BCO the $^5(TT)_0$ quintet state is generated faster than the time resolution of the experiment. The absorptive/emissive resonances for the $^5(TT)_0 \rightarrow {}^5(TT)_{\pm}$ transitions are separated by (D-3E)/3, as is expected for strongly coupled triplets (J>D,E). After several hundred nanoseconds uncoupled triplets are generated, probably via a geometric relaxation that reduces the inter-triplet exchange coupling, J. This gives rise to absorptive/emissive $T_0 \rightarrow T_{\pm}$ transitions separated by D-3E. The absorption/emission structure is indicative of the selective population of T_0, as is expected for triplets generated by fission.[48]

We confirm the assigned spin multiplicities using pulsed laser, pulsed microwave measurements of the $^5(TT)_0 \rightarrow {}^5(TT)_+$ and $T_0 \rightarrow T_+$ transitions, which yielded a Rabi nutation frequency ratio of 1.64±0.05, in agreement with the expected value of $\sqrt{3}$=1.73 for strongly coupled triplet pairs.[39,49] The strong coupling regime in ESR measurements of these materials

refers to exchange energies that are only ≳ 20 GHz. It is likely that the triplet-triplet pair coupling in BCO is actually weak on an electronic energy scale and this gives rise to the relatively large values of τ_{iSF} and $\tau_{(TT)}$.

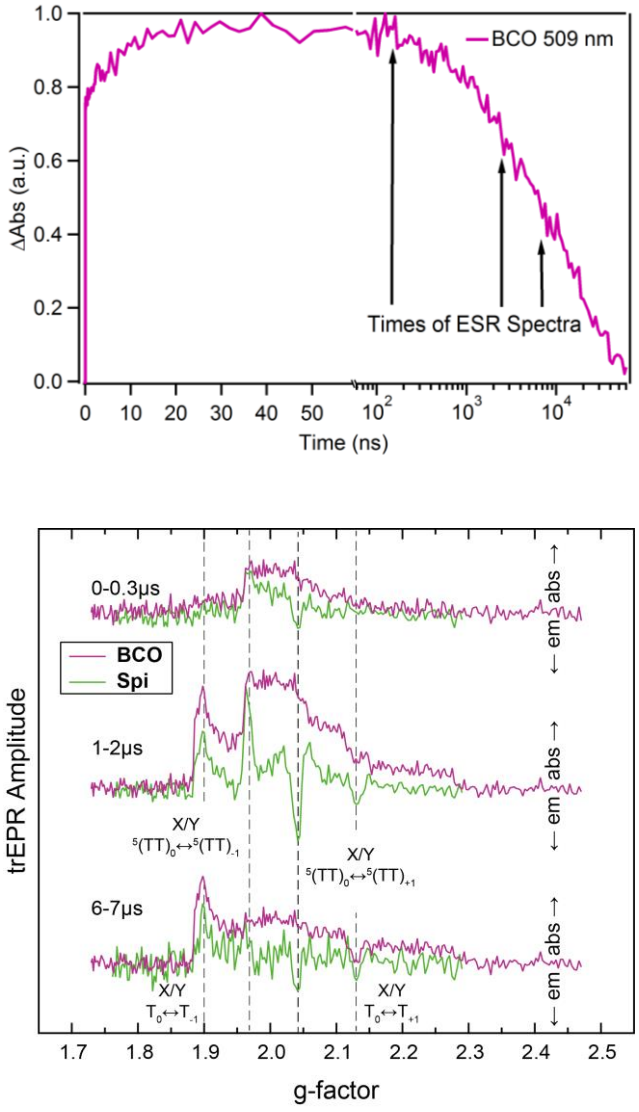

Figure 5.5. Top: Transient absorption kinetics near the triplet absorption maximum, with arrows indicating times selected for ESR spectra. Bottom: Transient ESR spectra of **Spi** and **BCO** in toluene at given time delays after laser excitation at 599 nm, ~70 μJ/pulse. Dashed lines mark locations of $(TT)_0$ and T_0 transition resonances.

These measurements allow us to confirm that no other parasitic decay channels besides radiative recombination are present in these dimers. Unlike in homoconjugated dimers, where the yield is nearly quantitative, radiative recombination in BCO is a significant loss channel. We estimate the singlet fission yield to be ~76% based on kinetic competition of SF with the typical ~12.3 ns radiative lifetime of TIPS-pentacene.[50] Importantly, the similarity between the triplet pair and free triplet transient spectra allows us to directly determined the SF yield using triplet sensitizations methods.[11] Indeed, a cross-sectional yield determination, where we compare the triplet signal at a given fluence to that produced by transfer of a known number of triplets from an external, well-characterized sensitizer, finds a yield of 63%. If any other parasitic decay processes were occurring, the sensitization methods would yield a significantly lower value for the singlet fission yield. This compound shows that fully incoherent singlet fission can occur even in the limit of extremely weak electronic coupling, as long as the excited state lifetimes permit reasonable kinetic competition with ground state repopulation.

5.8 Conclusions

Through the evaluation of a family of materials, we have found that the conjugation motif of the interpentacene bridge is instrumental in mediating singlet fission in pentacene dimers. The concept of intrachromophore coupling interactions in pi-bridge-pi molecules was tested using homoconjugated and non-conjugated bridging moieties. In these systems, homoconjugated bridges can yield singlet fission rates that are faster than a conjugated bridge, while maintaining slower triplet pair recombination. We also found that SF can occur in the case of a non-conjugated bridge, although the process is much slower than SF in a similar sized conjugated bridge. We further characterized the formation of triplet pairs through singlet fission using ESR measurements. This

study demonstrates the importance of the bridge design in such compounds and emphasizes that bridge effects must be play a key role in understanding SF and triplet pair recombination.

5.9 Details of Transient Absorption and Triplet Photosensitization Experiments

Details of the transient absorption experiments have been described previously.[1,6,16] Briefly, a 1 kHz amplified Ti:Sapphire system equipped with an optical parametric amplifier is used to generate resonant pump pulses with a pulse width of ~ 100 fs. This laser is also used to generate a femtosecond supercontinuum probe in a thin sapphire plate that is mechanically delayed with respect to the pump pulse. A nanosecond supercontinuum probe pulse generated in a fiber laser (Leukos) is alternately employed using an electronically delayed configuration to investigate longer delayed times. The pump pulse is the same for both probe configurations. The measurements are conducted at concentrations below 100 μM, and typically ~50 μM in bipentacene unless otherwise noted.

Triplet photosensitization measurements were performed to ascertain the spectrum and lifetime of individual triplets in these systems. In these measurements, ~20 mM of anthracene is dissolved in chloroform along with <100 μM bipentacene. Photoexcitation of the anthracene at 360 nm (~100 μJ/cm^2), followed by intersystem crossing and collisions with bipentacenes results in population of individual triplets in the pentacene molecules of interest. This process can be seen as the photoinduced absorption (PIA) from the anthracene triplet, most prominent near 420 nm, decays; while the pentacene triplet PIA, most prominent near 520 nm, rise in each case (Figure 5.6).

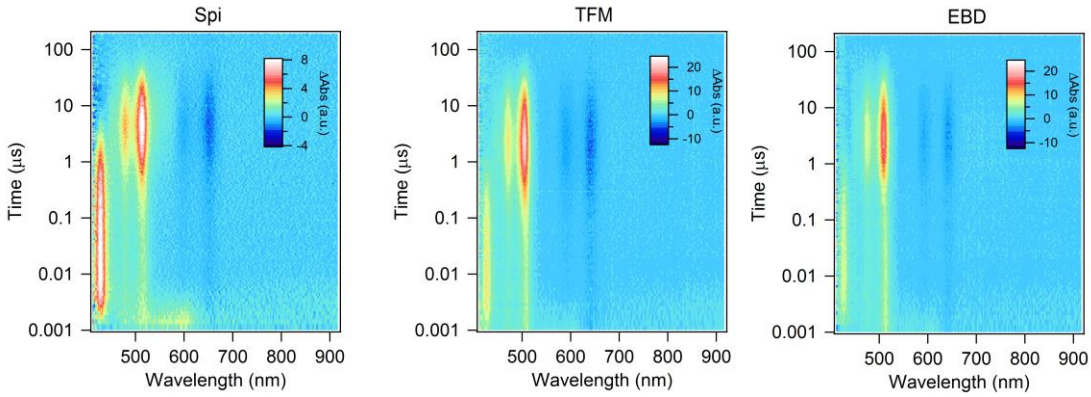

Figure 5.6. Triplet photosensitization measurements of bipentacene (~50 µM) and ~20 mM anthracene dissolved in chloroform, with excitation at 360 nm (~100 µJ/cM^2) preferentially exciting anthracene molecules. Color scale is reported in arbitrary units.

If we examine the spectrum of the PIA after sufficient time has passed, so that only pentacene triplets remain, we can ascertain the spectrum of an individual pentacene triplet in these systems. We can then compare this spectrum to spectrum produced by direct photoexcitation, which we expect to produce triplet pairs if singlet fission is operative. Shown below in Figure 5.7, these comparisons confirm that the state produced by direct photoexcitation of the bipentacenes (orange traces) can be assigned as triplet excitons. We note that some modest discrepancies are expected, as interactions between the two triplets in a pair can perturb the spectrum relative to that of individual triplets populated in sensitization experiments.[11,51]

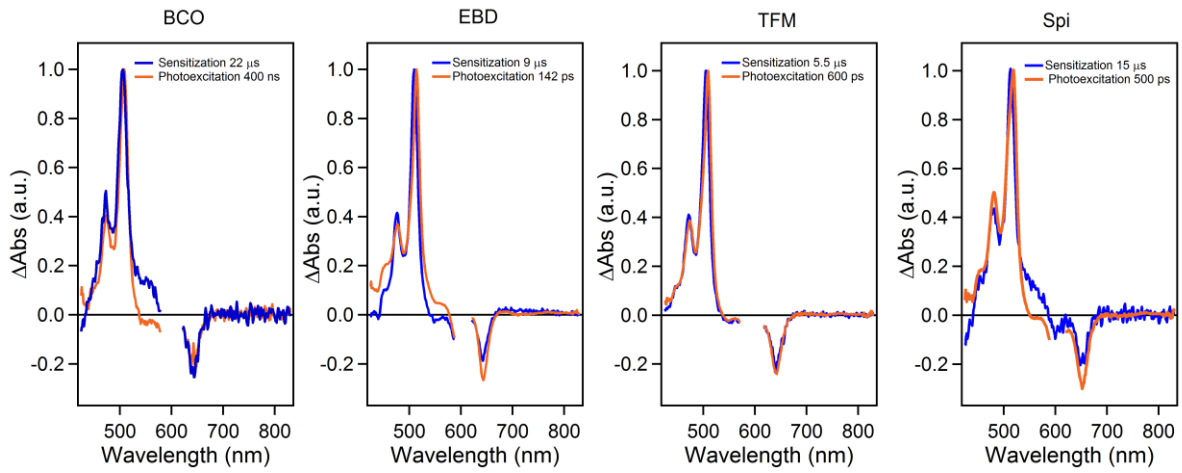

Figure 5.7. Comparison of spectral shape produced by photoexcitation (orange traces, triplet pair spectra) versus photosensitization (blue traces, individual triplet spectra), with each trace normalized to the maximum value.

5.10 Sensitization Yield Determination for BCO

The same sensitization experiments were performed for BCO. However, in this case, we have undertaken further, quantitative measurements of PIA produced by photoexcitation to also determine a cross-sectional triplet yield for this compound. This process is explained in detail below.

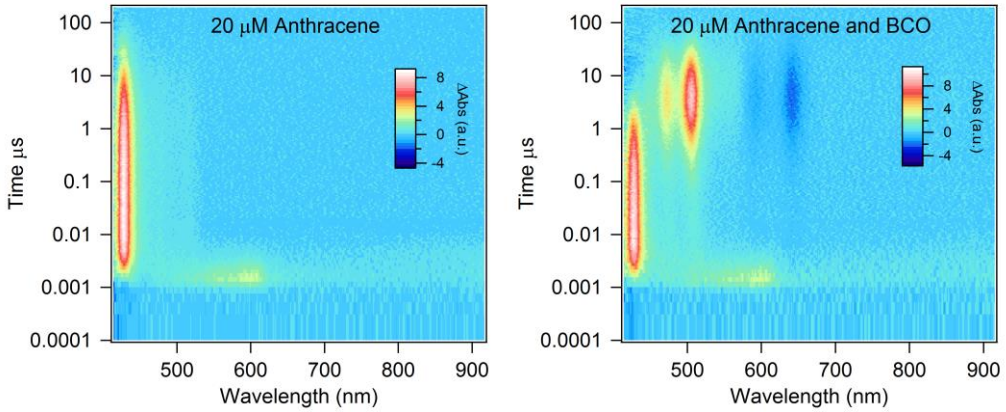

Figure 5.8. Photosensitization measurements for BCO, sensitized by ~20 mm anthracene in chloroform by the same procedure described above, where the color scale is in units of mOD.

Raw 2D color plots of sensitization experiments used to determine the triplet absorptivity for BCO. The intrinsic lifetime of the 20 μM anthracene solution is found to be ~45 μs. In the presence of the BCO, the lifetime was truncated to ~1.96 μs, giving a transfer efficiency of 92.3%. Comparing the ratio of triplet absorption at the λ_{max} for anthracene, known as 55,200, to the triplet absorption of the BCO ~507nm, and accounting for decay of BCO triplet signal during transfer (23 μs triplet lifetime), we find the molar absorptivity of the BCO triplet:

$$\varepsilon_{T-T}(BCOBP) = \frac{0.00951}{0.01081} * 55200 * \frac{1}{.959} * \frac{1}{.923} = 54{,}862 M^{-1} cm^{-1}$$

Solution	O.D. at 600 nm	(1-T) at 600 nm	$M^{-1}cm^{-1}$
TIPS Pentacene	0.2873	0.48	21000
BCO	0.3653	0.57	47000

The concentration of singlets in the TIPS pentacene sample is estimated from the maximum of the GSB signal of -0.0018187, as well as the molar absorptivity and cuvette length, as shown below.

$$Concentration\ (TIPS\ pent\ singlet) = \frac{-0.0018187}{21000 * 0.1} = 8.66 * 10^{-7} M$$

The singlet concentration for the BCO sample is then found under the same excitation conditions by simply comparing the number of photons absorbed:

$$Concentration\ (BCO\ singlet) = 8.66 * 10^{-7} * \frac{57}{48} = 1.03 * 10^{-6} M$$

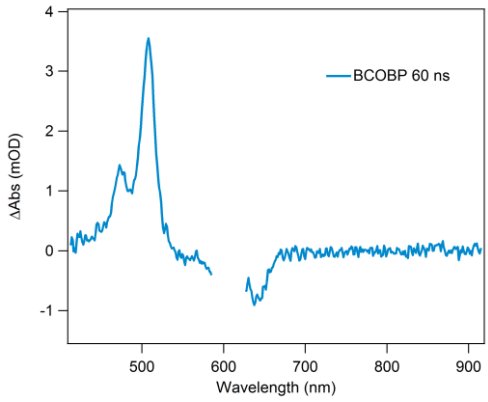

Figure 5.9. Photoinduced absorption in chloroform for BCO at 60 ns, used for yield calculation.

The triplet concentration can be found using the following relationship:

$$Triplet\ concentration = \frac{\Delta A}{\varepsilon_{T-T} * l} = \frac{.00355}{54862 * .1} = 6.47 * 10^{-7} M$$

Comparing the triplet concentration at 60 ns (Figure 5.9), after singlet decay is complete, but triplet decay has not substantially occurred, we find the triplet yield:

$$Yield\ (triplets) = \frac{6.47 * 10^{-7}}{1.03 * 10^{-6}} = 0.63$$

The triplet yield of 63 % is consistent with a simple kinetic argument. The intrinsic lifetime of TIPS pentacene in chloroform is 12.3 ns. The singlet in BCO decays with a monoexponential 7.6 ns lifetime. Assuming dimer has similar intrinsic dynamics to monomer, we can estimate a singlet fission rate and yield from the reduction in singlet lifetime:

$$\frac{1}{7.6\ ns} = \frac{1}{12.3} + \frac{1}{SF\ time\ constant}$$

SF time constant is therefore approximated as 20 ns. Competition between a 20 ns process (singlet fission) and a 12.3 ns process (radiative and non-radiative monomer decay) predicts:

$$\frac{12.3}{12.3 + 20} = 0.38$$

Based on these kinetics, we should expect 38% of the singlet excitons to undergo SF. Therefore, we expect a ~74% triplet yield if SF is the only triplet formation mechanism. The yield determined by sensitization of 63% agrees well with a SF dominated mechanism for triplet formation and is much too high to be explained by intersystem crossing (in which case only 38% triplet yield would be expected). The slightly lower actual triplet yield could be explained by a small contribution to triplet formation from ISC, but the expected 76% yield is certainly within the margin of error for the triplet yield calculations. The significant contributions from SF are also unambiguously characterized by the population of triplet pair states observed in tr-ESR experiments, described in the main text.

5.11 Details of Linear Absorption Spectroscopy

In Figure 5.10 is the UV-vis reproduced from the main text, but with units of molar absorptivity.

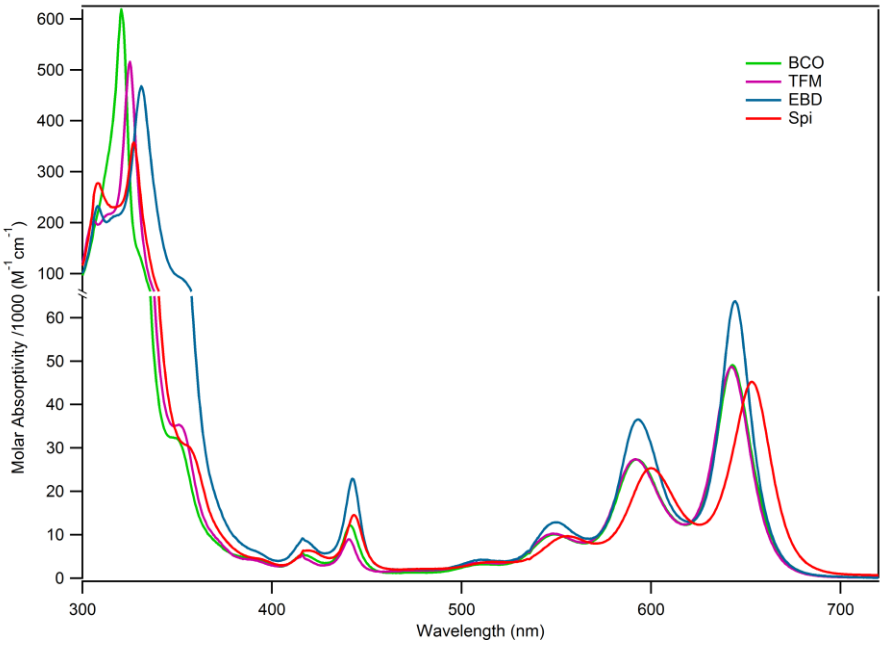

Figure 5.10. UV-visible absorption spectra for the pentacene dimers investigated in this manuscript in units of molar absorptivity.

In general, the absorptivity for the dimers is approximately twice that of the TIPS pentacene monomer (~20,000 $M^{-1}cm^{-1}$) near the absorption maximum ~650 nm.

5.12 Details of Photoluminescence Upconversion Spectroscopy

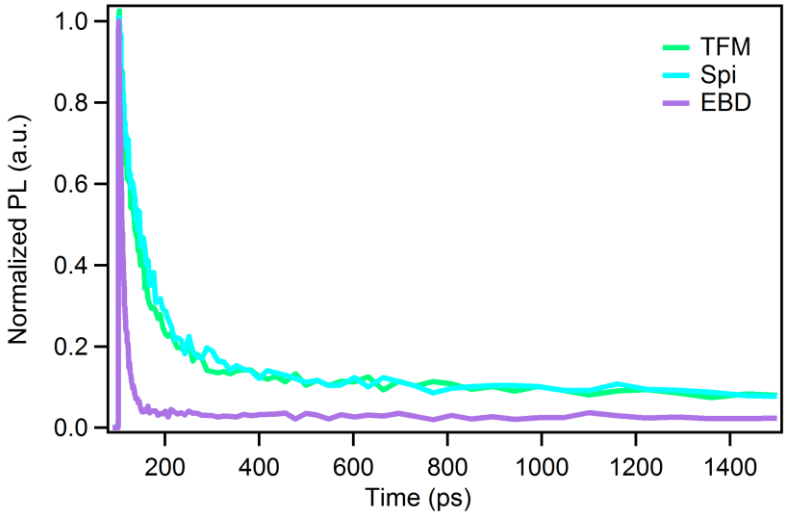

Figure 5.11. Decay of photoluminescence for ~50 μM solutions in chloroform, monitored at 680 nm after photoexcitation at 600 nm (~50μJ/cm^2).

Upconverted photoluminescence as a function of time is shown in Figure 5.11 for excitation in chloroform at 600 nm and monitoring at 680 nm. The singlet decay is correlated well with the singlet decay time constants found in transient absorption spectroscopy. Some residual PL, most notable in TFM and Spi, has a lifetime of ~12 ns and is attributed to monomeric pentacene impurity emission.

5.13 Solvent Dependence on Singlet Fission Rate for Spi

Below in Figure 5.12, we plot the rates of singlet fission for the pentacene dimers studied in this manuscript as a function of solvent. These rate assignments are achieved by modeling transient absorption data using global analysis in the program Glotaran.[52] The two dimensional color plots,

showing induced absorption as a function of time and wavelength, which are inputted to determine singlet fission rate constants, are shown below for the different dimers and solvents.

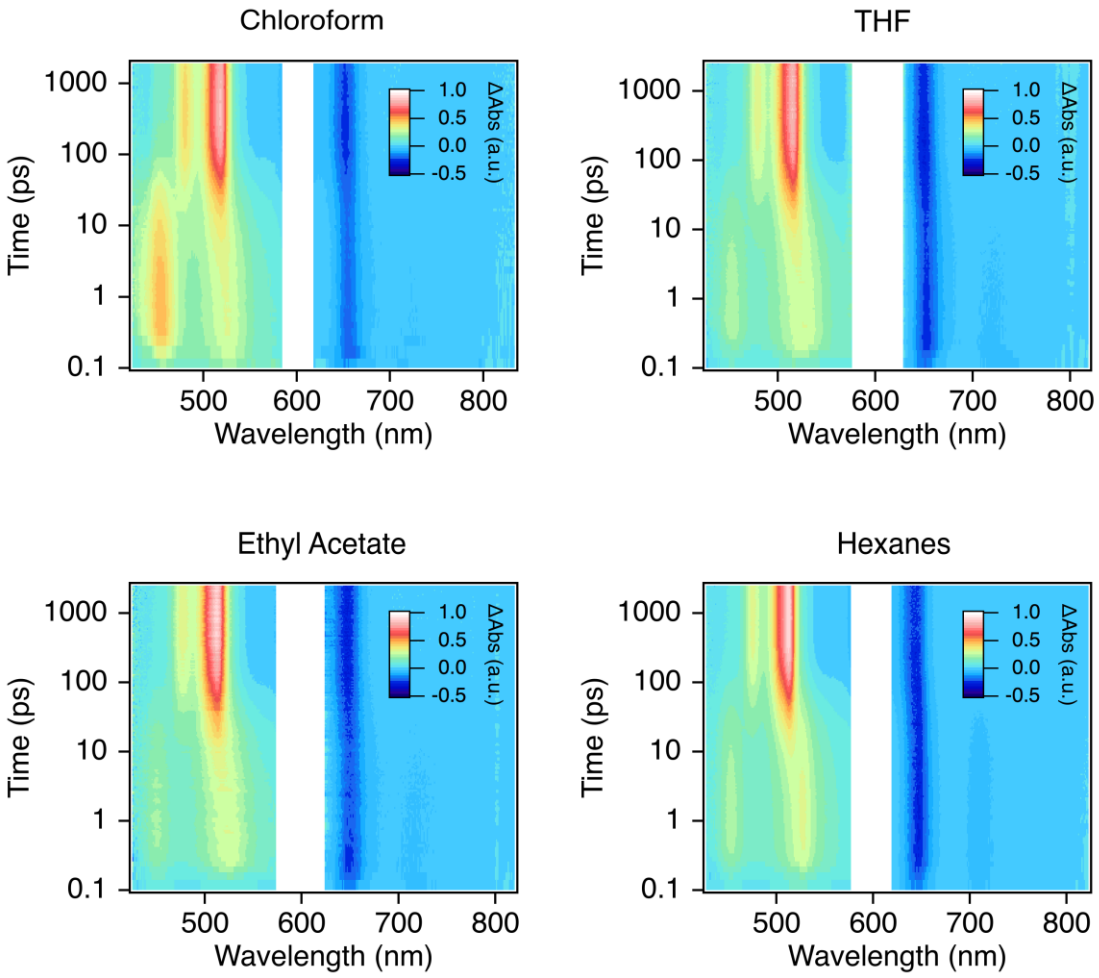

Figure 5.12. Transient absorption data of Spi in different solvents, with excitation at 600 nm (~50μJ/cm^2).

5.14 Solvent Dependence on Singlet Fission Rate for BCO

Shown below in Figure 5.13 are the transient absorption color plots for BCO in different solvents. These data were recorded using an electronically controlled delay between pulse and probe. While the ~0.5 ns time resolution of this technique results in relatively poor time resolution near time 0, it is sufficient to assign the >7 ns time constants for singlet fission in this system.

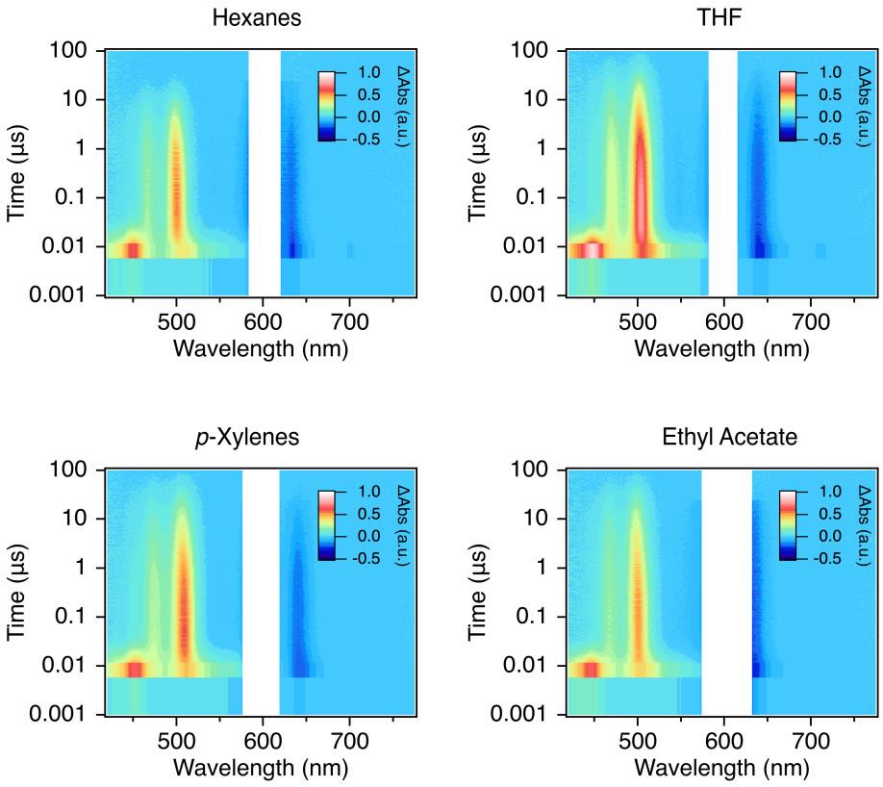

Figure 5.13. Transient absorption data of **BCO** in different solvents, with excitation at 600 nm (~50µJ/cm^2). the instrument response is approximately 0.5 ns while singlet decay ranges from about 7–11 ns, making the dynamics sufficiently resolved for assignment of accurate rate constants

5.15 Solvent Dependence on Singlet Fission Rate for EBD

Shown below in Figure 5.14 are transient absorption spectra for EBD in different solvents.

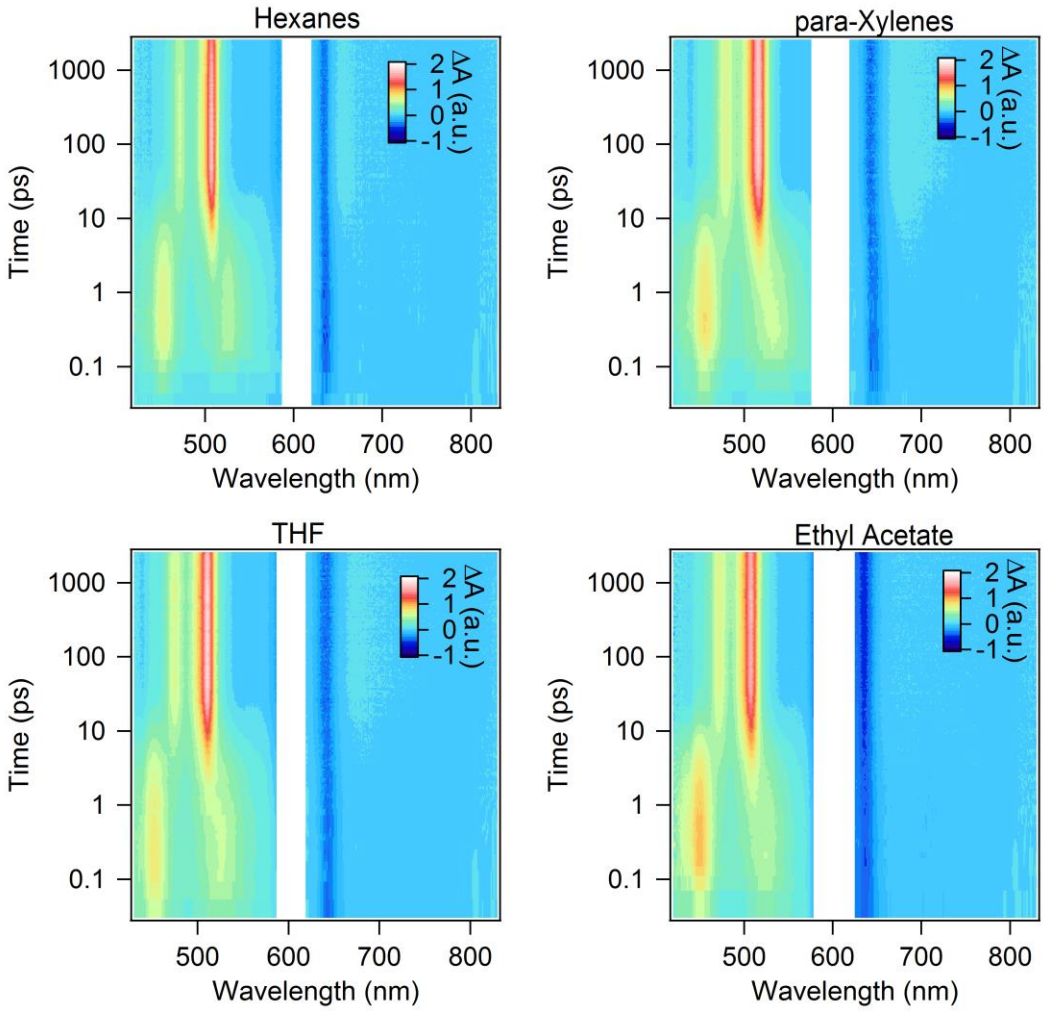

Figure 5.14. Transient absorption spectra of EBD in different solvents, with excitation at 600 nm (~50μJ/cm^2).

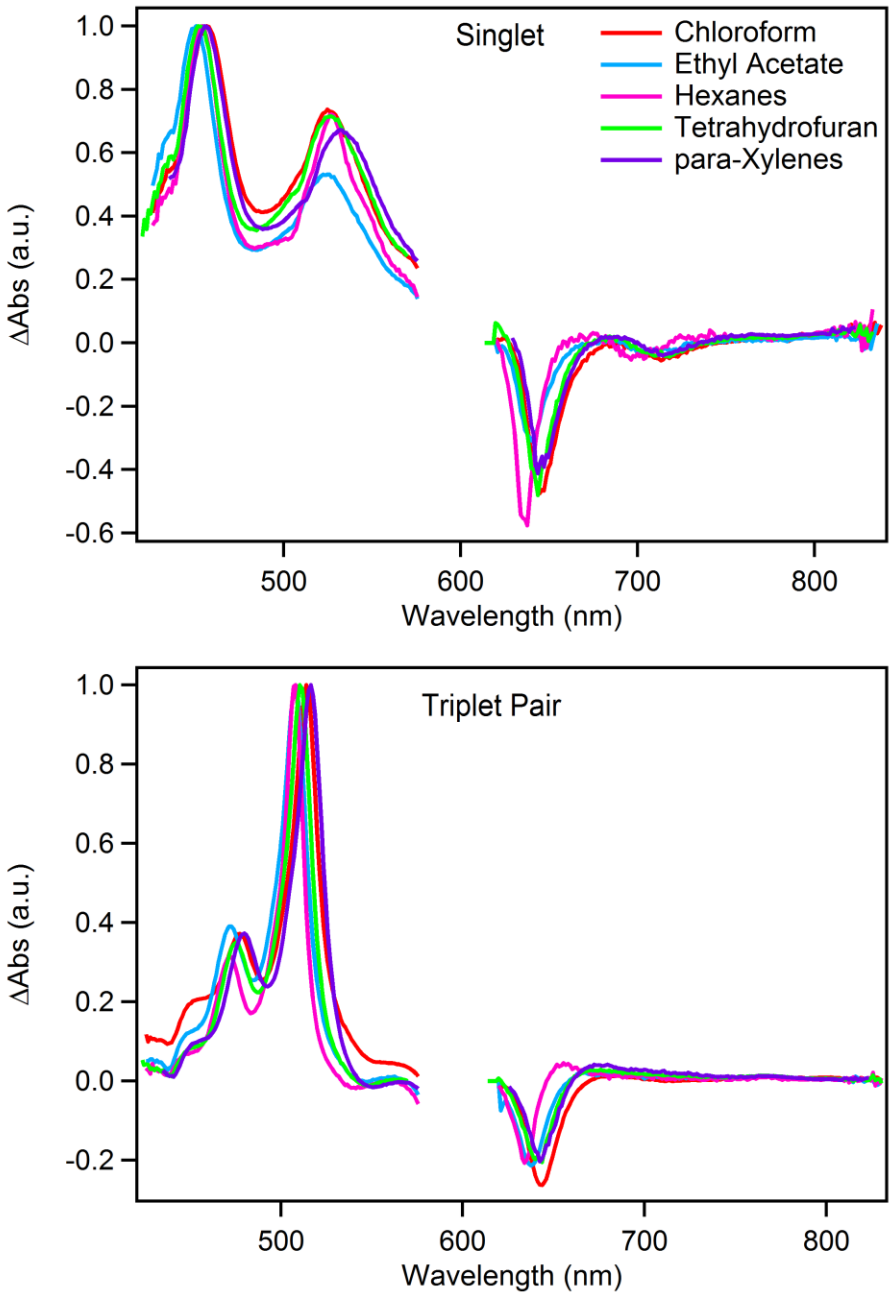

Figure 5.15. Transient spectra of the singlet and triplet pair of EBD in different solvents, derived from a global analysis sequential decay model.

5.16 Solvent Dependence on Singlet Fission Rate for TFM

Shown in Figure 5.16 are the transient absorption spectra for TFM in different solvents. These data sets were used to determine singlet fission rates, given in the main text.

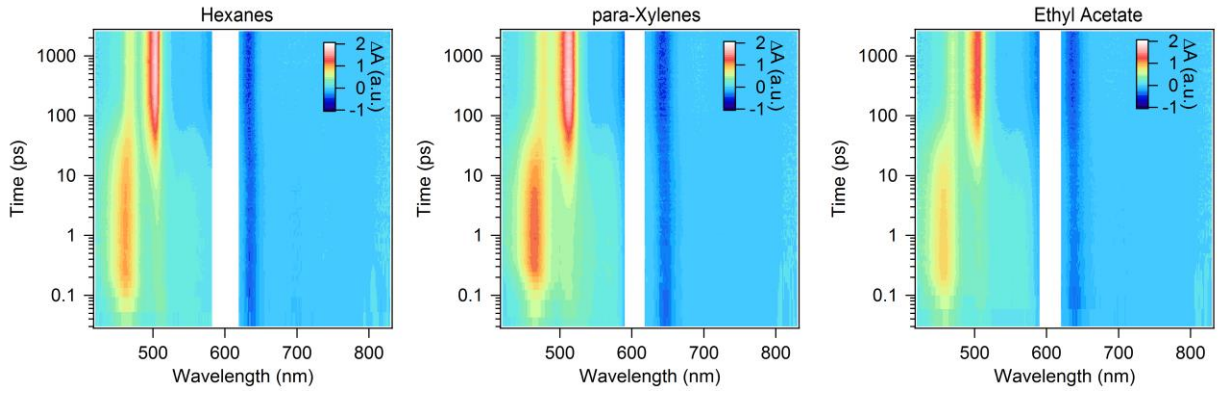

Figure 5.16. Transient absorption data for TFM in different solvents with excitation at 600 nm (~50μJ/cm^2).

5.17 Global Analysis: Spectra and Time Constants

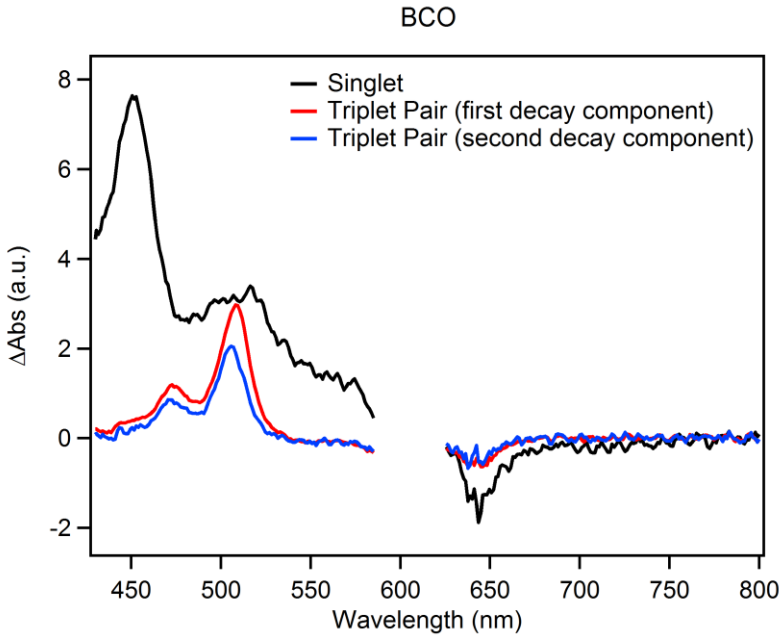

Figure 5.17. Spectra isolated from global analysis of longer-timescale, electronically controlled delay data for BCO in chloroform from 600 nm, ~50μJ/CM^2 excitation.

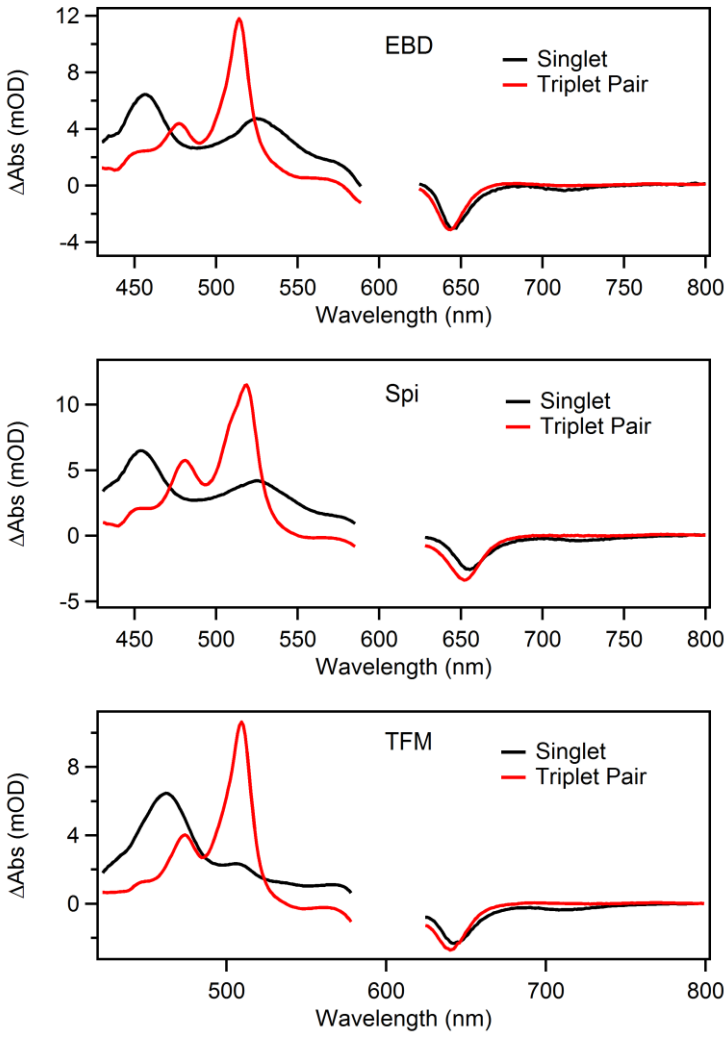

Figure 5.18. Spectra isolated from global analysis of ultrafast transient absorption data (first ~2.7 ns, mechanically controlled delay) for the singlet and triplet pair in chloroform.

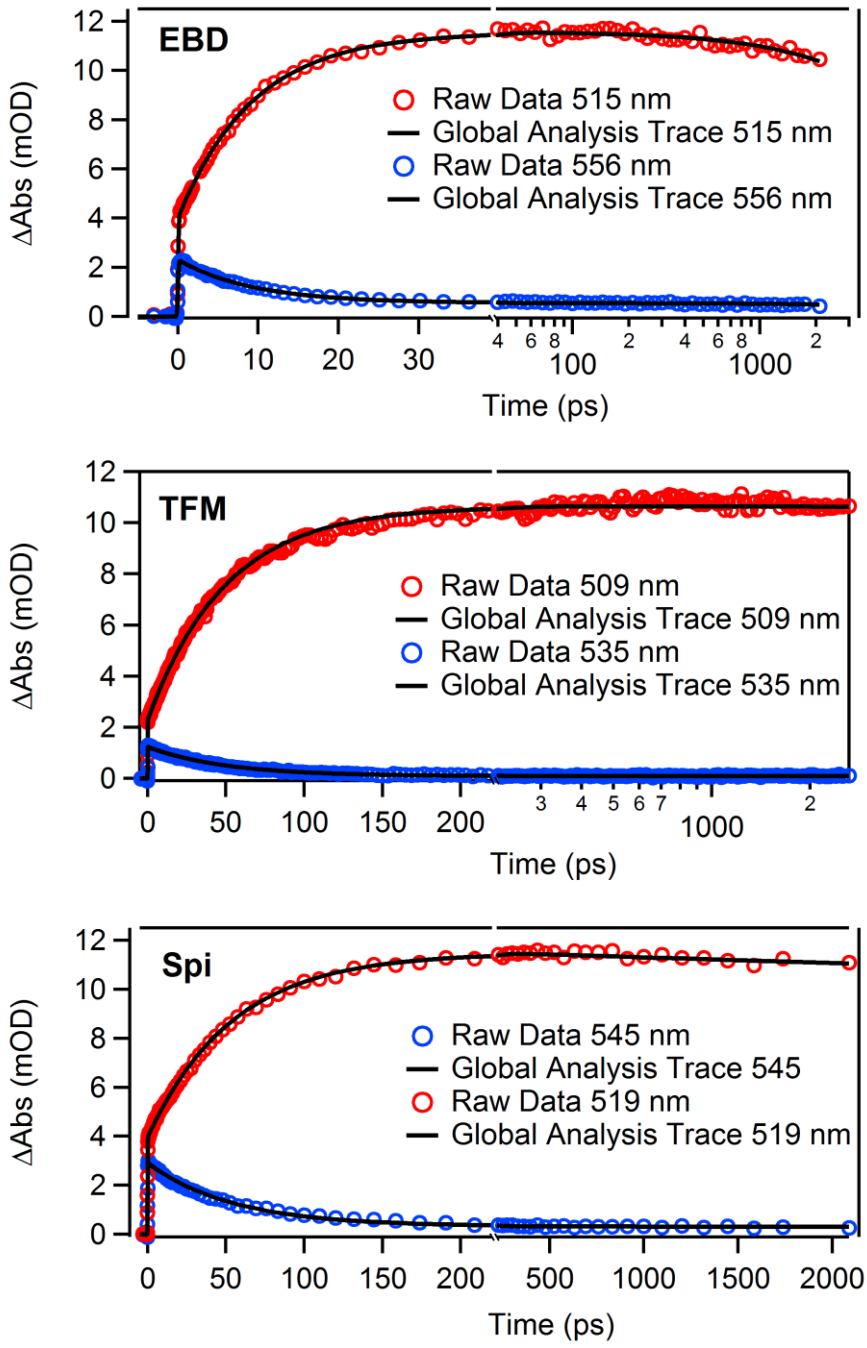

Figure 5.19. Comparison of kinetic cuts through the raw transient absorption data (chloroform as solvent) to the fits derived from a sequential decay model of the singlet into a triplet pair. The corresponding 2D color plots from which these cuts are derived are found in the main text.

5.18 Solvent Dependence of Singlet Fission and Triplet Pair Recombination for BCO

Shown in Figure 5.20 are the time constants for singlet fission in BCO as a function of solvent. Like the homoconjugated pentacene dimers in the main text, there is no clear trend with solvent polarizability. However, there is a modest trend towards faster singlet fission rates in more polar solvents. However, as shown on the right, triplet pair recombination time constants, given by the first exponent for triplet recombination in BCO, also accelerate in more polar solvents. The similarity of these trends points towards a more mundane explanation for these modest trends in these systems with large pentacene center-to-center distances, where CT states are high above the singlet state. The modest trend here is unlikely to necessitate mediation by virtual charge transfer states, as these states are not, to our knowledge, implicated in enhancing triplet pair recombination rates. Whether the modest rate enhancements over massive polarity ranges reported here are due to geometric differences in solvents of different polarities, differences in solvent reorganization energies, or other factors is still an open question. Regardless, it seems that the direct mechanism is dominant for this series of molecules.

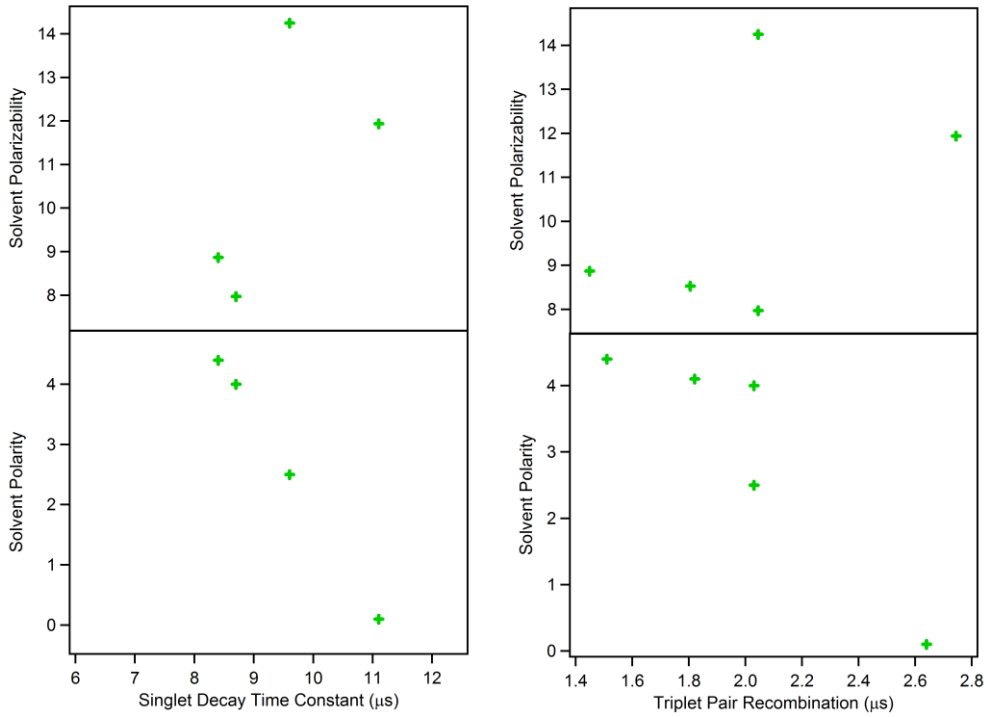

Figure 5.20. Time constants of singlet decay and triplet pair recombination for **BCO** as a function of solvent polarity (p') and polarizability (α). the polarity[53] and polarizability[54] values respectively, for hexanes (0.1, 11.94), p-xylenes (2.5, 14.25), chloroform (4.1, 8.53), tetrahydrofuran (4.0, 7.97), ethyl acetate (4.4, 8.87).

5.19 Solvent Dependence of Singlet Fission of TFM, Spi and EBD

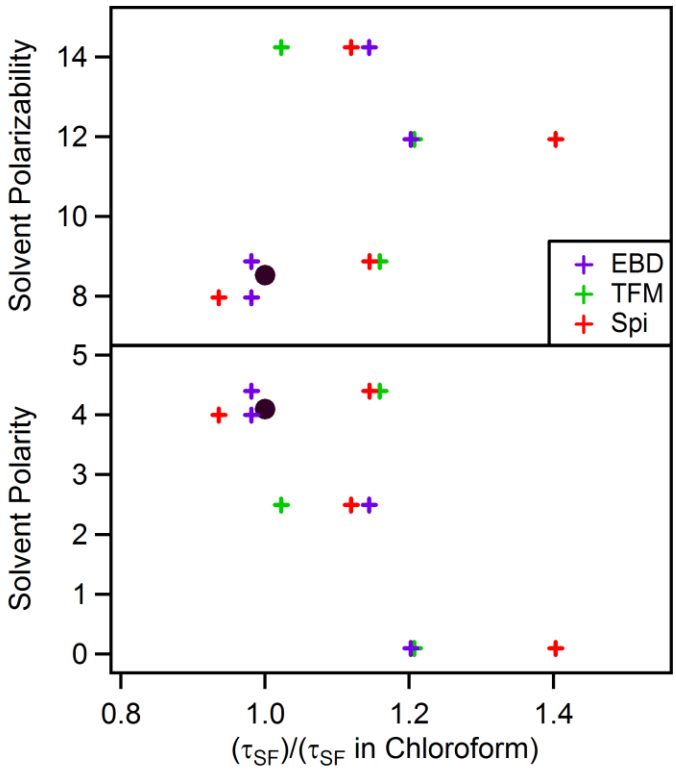

Figure 5.21. Singlet fission time constants, normalized to the time constant in chloroform, as a function of solvent polarity (p') or polarizability (α)

Table 5.2. Summary of time constants in picoseconds for singlet fission (or singlet decay in the case of **BCO**) of dimers in different solvents.

	Hexanes	*p*-Xylenes	THF	Chloroform	Ethyl acetate
EBD	12.5 ps	11.9 ps	10.2 ps	10.4 ps	10.2 ps
TFM	60 ps	50.8 ps	n/a	49.7 ps	57.6 ps
Spi	76.5 ps	61 ps	51 ps	54.5 ps	62.4 ps
BCO	11000 ps	9600 ps	8700 ps	7600 ps	8400 ps

Table 5.3. Summary of time constants in microseconds for triplet pair recombination of dimers in different solvents.

	Hexanes	*p*-Xylenes	THF	Chloroform	Ethyl acetate
BCO	2.64 µs	2.03 µs	2.03 µs	1.82 µs	1.51 µs

5.20 Fluence Independent Dynamics in BCO

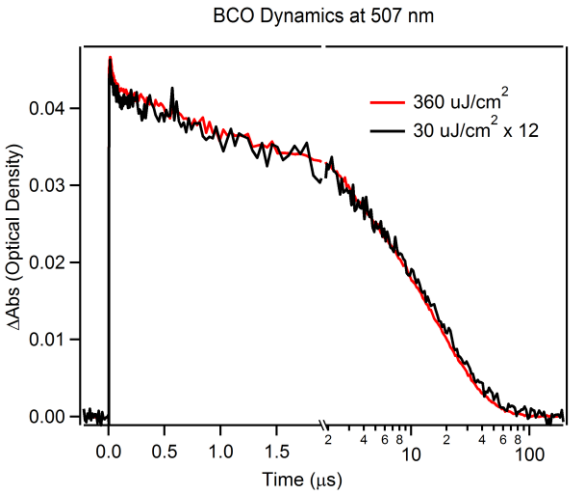

Figure 5.22. Kinetic traces at 507 nm for low (30 μJ/cm^2) and high (360 μJ/cm^2) pump fluence reveal fluence independent dynamics.

5.21 Electronic structure theory: general methods

In accordance with previous work the Si(*i*Pr$_3$) groups were replaced with Hydrogens as they do not substantially affect the electronic structure.[35] All calculations used the GAMESS-US package[55], some of which were run on XSEDE resources.[56]

Structural optimization was undertaken using density functional theory (DFT) with the B3LYP functional and a 6-31G* basis. To accelerate convergence of the optimization a Hessian was initially obtained at the restricted Hartree-Fock (RHF) level using a SBKJC pseudopotential basis, and used to initialize the DFT calculation.

The TFM, Spi, and BCO structures were optimized in the C_2 point group, BP1 in the C_i point group and EBD in the C_{2v} point group.

Due to the large size and high computational cost, multiconfigurational calculations used an SBKJC basis with *d* functions on carbon and fluorine (if present) added from the 6-31G* basis set. This has previously been demonstrated as being sufficient for an accurate description of the excited states of pentacene and its dimers[35,57].

CASSCF calculations used a RHF reference and were state-averaged over singlet states with equal weights. For TFM, Spi and BCO the state averaging was over the lowest four states of A symmetry and the lowest four states of B symmetry. For BP1 this was over the lowest four states of A_g symmetry and the lowest four states of A_u symmetry. For EBD, state averaging was over the lowest two singlet states of A_1, A_2, B_1 and B_2 point groups. The number of configuration interaction states to be found by the CASSCF calculation was adjusted on a case-by-case basis in order to include as many singlet states as were requested (since triplet and quintet states were also included in the configuration interaction states).

The CASSCF calculations all used a four orbital, four electron (4o4e) active space comprising the HOMO-1, HOMO, LUMO and LUMO+1 of the dimer. Previous research has shown that for quantitative accuracy an 8o8e active space (or larger) may be necessary for accurate excitation energies, though diabatizing the resulting states or assigning their character can be challenging.[35,57] Preliminary calculations with 8o8e active spaces on these molecules, which due to the linkers are larger than the pentacene dimers previously studied by these methods, were found to be unfeasible on the grounds of computational cost and numerical instability. We therefore consider 4o4e calculations, whose excitation energies are only qualitatively accurate, but whose character can be clearly described as excitonic, charge-resonance and multiexciton (see below).[58]

For accurate excitation energies, second order perturbation theory (MRMP) was applied using multiconfigurational quasidegenerate perturbation theory (MCQDPT) with the standard intruder state avoidance parameter of 0.02 E_h.[2,57]

In accordance with previous research, we assign the character of: ground state (GS); local (intra-monomer) exciton (EX); charge-resonance states (CR), sometimes referred to as charge-transfer; and multiexciton (triplet-triplet with zero overall spin) (ME).[58] States with character of a double excitation within a monomer (sometimes referred to as "dg" or "gd") can be used for inferring the relative signs of orbitals, but are otherwise not considered further.

GS and ME always transform as the totally symmetric representation, whereas EX and CR states commonly arise as symmetric and antisymmetric pairs. Here we consider only the antisymmetric EX and CR states, since in general only the antisymmetric pair is bright (has a substantial dipole moment from the ground state, as can be inferred from symmetry arguments), and it is expected that this will couple to the antisymmetric CR state (since the nuclear kinetic energy operator is totally symmetric). In practice, the weak coupling in these systems means that the symmetric and antisymmetric pairs are expected to be of very similar energy.

To summarize, the point groups and irreps used are:

Point group	C_2	C_i	C_{2v}
Associated molecules	TFM, Spi, BCO	BP1	EBD
GS and ME symmetry	A	A_g	A_1
EX and CR symmetry	B	A_u	B_2

To assign the character of the excitations we use the dimer molecular orbitals linear combination of fragment orbitals (DMO-LCFMO) procedure,[59] which has previously been used to describe singlet fission.[58] In brief, this involves writing out the linear combination of determinants of the states we wish to describe in the monomer basis (suitably symmetry-adapted to spin and point group) and transforming to dimer orbitals, leading to a configuration interaction (CI) expansion in the basis of dimer orbitals. By the symmetry of the molecules (see above) the dimer orbitals must be either in-phase or out-of-phase combinations of monomer orbitals (such as A or B in the C_2 point group), and we make the small additional assumption that the dimer HOMO and HOMO-1 are well-described as in-phase and out-of-phase combinations of the monomer HOMOs only (not mixing in other monomer orbitals), and similarly for the dimer LUMO and LUMO+1. This is expected to be a good approximation in weakly coupled dimers such as those investigated in this article.

We then match the resulting CI expansions against the adiabatic states produced by the electronic structure theory calculations (in this case the CASSCF states which are then perturbed with MCQDPT) to assign the character of the state. In cases where different characters have the same linear combination of determinants except for a relative sign, such as EX and CR, we infer the relative signs of the orbitals from the CI expansion of the ME state and/or doubly excited states. For the B_2 irrep in EBD where there is no accessible symmetry-allowed state for comparison, the state closest in energy to the experimental bright excitation is assigned as EX.

We stress that this is not a localization or (quasi)diabatization calculation; the adiabatic states are not transformed, merely assigned to given ‘characters’. Excitations are assigned as follows:

Excitation energy (eV)	EBD	TFM	Spi	BCO	BP1
Local excitation (EX)	1.95	1.69	1.62	1.70	1.66
Multiexciton (ME)	2.42	1.68	1.59	1.69	1.64
Charge-resonance (CR)	3.11	2.89	2.73	3.27	3.10

For all pentacene dimers the CR state is over 1eV higher in energy than EX. All the states for EBD are anomalously high in energy (particularly ME) and we expect this is due to the higher symmetry (see above) such that fewer determinants can be used to variationally optimize a given CI expansion.

The high energy of the CR states is probably attributable to the spatial separation of the monomers (see Fig 5.2) and the consequential Coulombic penalty to separating charges. Except for the anomalous EBD results, the simple Coulombic explanation is supported by the energy of the CR state increasing as the monomers are pushed further apart by the linker (see Fig 5.2), and in the case of BCO and BP1 which have a similar spatial orientation, as the through-bond coupling between the monomers decreases:

$E_{CT}(Spi) < E_{CT}(TFM) < E_{CT}(BP1) < E_{CT}(BCO)$.

Although these results are only qualitative and do not rule out a SF mechanism mediated by charge resonance (or other) states, they open the possibility of a direct pathway, consistent with earlier findings that singlet fission in bipentacenes occurs via a direct mechanism mediated by vibronic coupling.[35]

5.22 Single Crystal X-Ray Diffraction

Data for pentacene dimers TFM and BCO were collected on an Agilent SuperNova diffractometer using mirror-monochromated Cu Kα radiation. Data collection, integration, scaling (ABSPACK) and absorption correction (face-indexed Gaussian integration[60] or numeric analytical methods[61]) were performed in CrysAlisPro. Structure solution was performed using ShelXT. Subsequent refinement was performed by full-matrix least-squares on F^2 in ShelXL.[62] Olex2[63] was used for viewing and to prepare CIF files. ORTEP graphics were prepared in CrystalMaker. Thermal ellipsoids are rendered at the 50% probability level.

Crystal structure of BCO:

The structure solved readily in P-1 with one molecule in the asymmetric unit. The ethylene bridges of the BCO moiety were disordered by a 180 deg. rotation about the bridgehead-bridgehead axis. The two disordered components were located in difference maps and refined with standard similarity and rigid-bond restraints.

The four independent Si(*i*-Pr)$_3$ groups were all disordered over two or three positions. A packing diagram showed that the minor positions of each group would collide with the major position of a different group, so therefore the disorder was modeled with a single free variable for the occupancies of all four independent silyl groups. One isopropyl group was disordered over three positions, which were modeled with the use of a SUMP restraint for the total site occupancy. Every independent position of a silyl group was made equivalent with a SAME instruction (a total of 9 equivalent silyl groups, since 3 were disordered over 2 positions and 1 was disordered over 3 positions.) All atoms were refined anisotropically with the disordered atoms stabilized by a RIGU

restraint and a short-range SIMU restraint for overlapping ADPs. Hydrogen atoms were placed in calculated positions and refined with riding isotropic ADPs and coordinates.

Crystal structure of TFM:

The structure initially appeared to be ordered in C2/c, crystallizing on a twofold axis with ½ molecule in the asymmetric unit. The refinement of this model proceeded to R1 ~10% but suffered from large, unusual anisotropic ADPs for many atoms in the pentacene core. When these sites were split, the ratio of disordered components refined to 1:1, which suggested a possible special-position disorder generated by the twofold axis. Half of the split sites were transformed by the twofold axis, giving a model with 1 molecule in the asymmetric unit, and the whole molecule was placed in PART -1. When the two pentacene halves were restrained with a SAME instruction, the refinement proceeded normally from that point with all ADPs well-behaved and with the agreement factors improved by several %. All silyl groups had one or alkyl groups further disordered over two positions; these were located with some difficulty because the difference maps were always contaminated by density from another silyl group related by the twofold axis. Each independent $Si(^{i}Pr)_3$ group and each individual $Si\text{-}C_3H_7$ moiety was made similar with SAME instructions.

Due to the special-position disorder, a RIGU restraint was required for all atoms. Disordered silyl groups were further restrained with SIMU instructions. Hydrogen atoms were placed in calculated positions and refined with riding isotropic ADPs and coordinates.

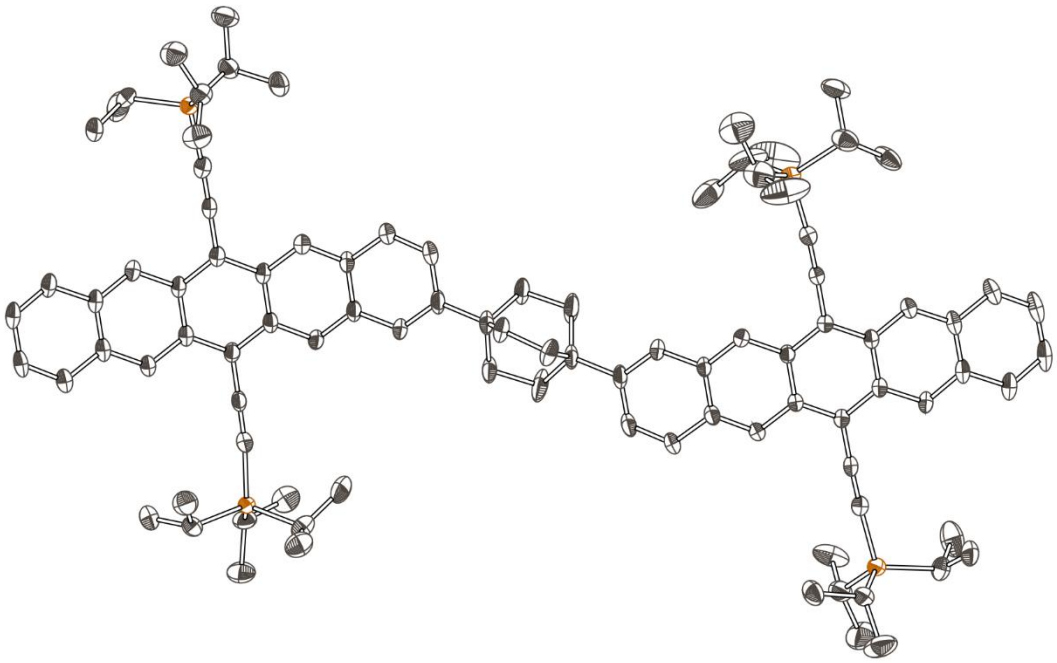

Figure 5.23. Molecular structure of BCO. Hydrogen atoms and the minor positions of disordered atoms are omitted for clarity.

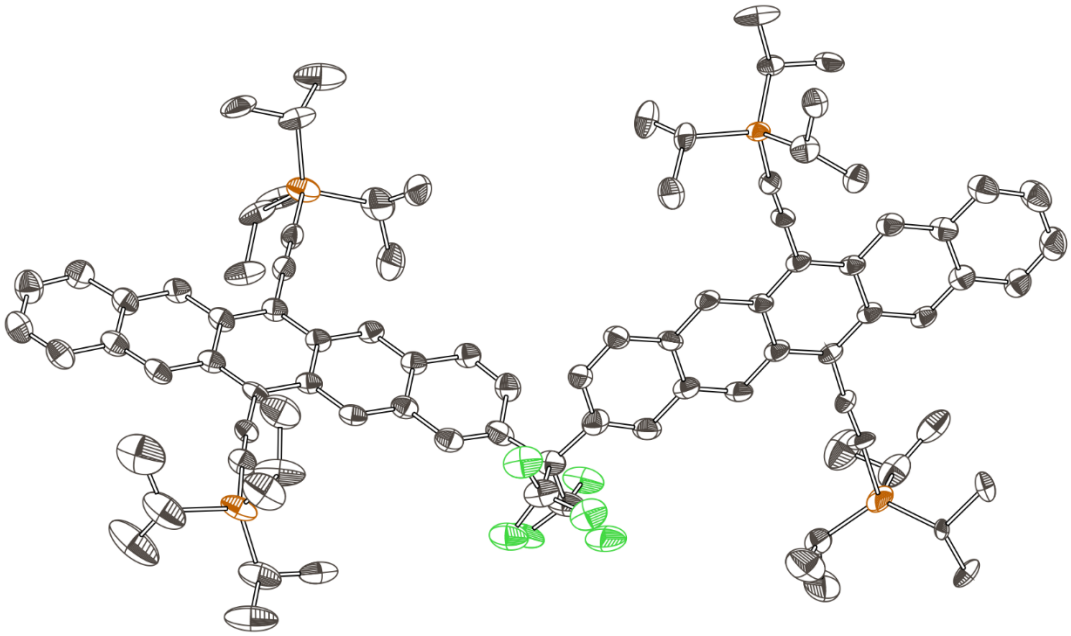

Figure 5.24. Molecular structure of TFM. Hydrogen atoms and the minor positions of disordered atoms are omitted for clarity.

Compound	BCO	TFM
Formula	$C_{96}H_{118}Si_4$	$C_{91}H_{106}F_6Si_4$
MW	1384.26	1426.11
Space group	P-1	C2/c
a (Å)	8.93370(19)	26.5637(5)
b (Å)	20.7978(5)	7.89746(9)
c (Å)	23.4696(6)	41.3109(9)
α (°)	98.332(2)	90
β (°)	90.9598(18)	106.605(2)
γ (°)	95.4335(19)	90
V (Å^3)	4293.21(17)	8305.0(3)
Z	2	4
ρ_{calc} (g cm^{-3})	1.071	1.141
T (K)	100	100
λ (Å)	1.54184	1.54184
$2\theta_{min}$, $2\theta_{max}$	9, 143	9, 143
Nref	77120	136992
R(int), R(σ)	.0741, .0564	.0544, .0167
μ(mm^{-1})	0.959	1.113
Size (mm)	.26 x .11 x .04	.25 x .18 x .03
T_{max}, T_{min}	.967, .871	.971, .801
Data	16580	8069
Restraints	1761	3210
Parameters	1346	1148
R_1(obs)	0.0931	0.0726
wR_2(all)	0.2655	0.2035
S	1.074	1.107
Peak, hole (e$^-$ Å^{-3})	0.76, -0.39	0.41, -0.30

5.23 General Synthetic Methods

All commercially obtained reagents/solvents were used as received; chemicals were purchased from Alfa Aesar®, Sigma-Aldrich®, Acros organics®, TCI America®, Mallinckrodt®, and Oakwood® Products, and were used as received without further purification. Unless stated otherwise, reactions were conducted in oven-dried glassware under argon atmosphere. The yields reported in the synthesis are not optimized. ^{1}H-NMR and ^{13}C-NMR spectra were recorded on Bruker 400 MHz (100 MHz for ^{13}C) and on 500 MHz (125 MHz for ^{13}C) spectrometers. Data from the ^{1}H-NMR and ^{13}C spectroscopy are reported as chemical shift (δ ppm) with the corresponding integration values. Coupling constants (*J*) are reported in hertz (Hz). Standard abbreviations indicating multiplicity were used as follows: s (singlet), b (broad), d (doublet), t (triplet), q (quartet), m (multiplet) and virt (virtual). The mass spectral data for the compounds were obtained from XEVO G2-XS Waters® equipped with a QTOF detector with multiple inlet and ionization capabilities including electrospray ionization (ESI), atmospheric pressure chemical ionization (APCI), and atmospheric solids analysis probe (ASAP). The base peaks were usually obtained as $[M]^{+}$ or $[M+H]^{+}$ ions.

Anhydrous solvents were obtained from a Schlenk manifold with purification columns packed with activated alumina and supported copper catalyst (Glass Contour, Irvine, CA). All reactions were carried out under argon unless otherwise noted.

5.24 Details of Electron Spin Resonance Studies

Pulsed laser, continuous microwave and pulsed laser, pulsed microwave measurements were carried out using the method described in our previous report.[39] BCO and Spiro were dissolved in

toluene and transferred to a sealed quartz ESR tube under a nitrogen environment. UV-visible absorption spectroscopy was used to ensure that no aggregation had occurred. Experiments were undertaken using a Bruker Elexsys E580. he samples were transferred to a cryogenically cooled (Oxford Instruments, CF935) resonator (Bruker, MD5) attached to an X-band microwave source (Bruker, Super X FT-ESR Bridge). A ~7 ns 599 nm laser pulse was used to excite the sample (Opotek, OPOLETTE). In BCO nutation frequency measurements, the nutation pulse was applied 1.7 μs and 700 ns after the laser pulse at 362.6 mT (9.626926 GHz) and 349.4 mT (9.626885 GHz), respectively. The data was Fourier transformed to establish the nutation frequency of a given transition.

5.25 General Protocol for the Synthesis of Spacer Derivatives

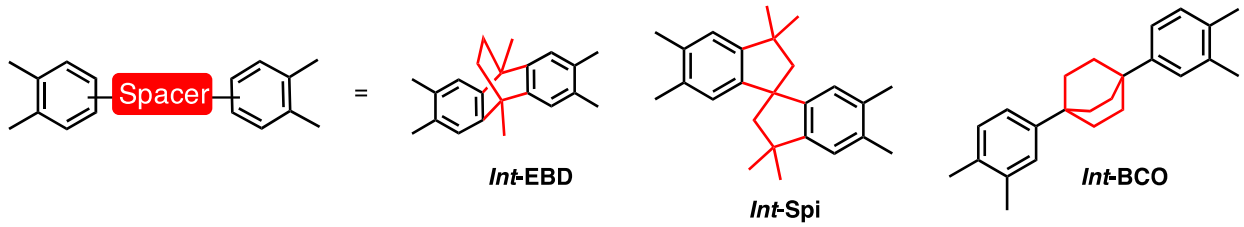

General protocol for the synthesis of spacer derivatives

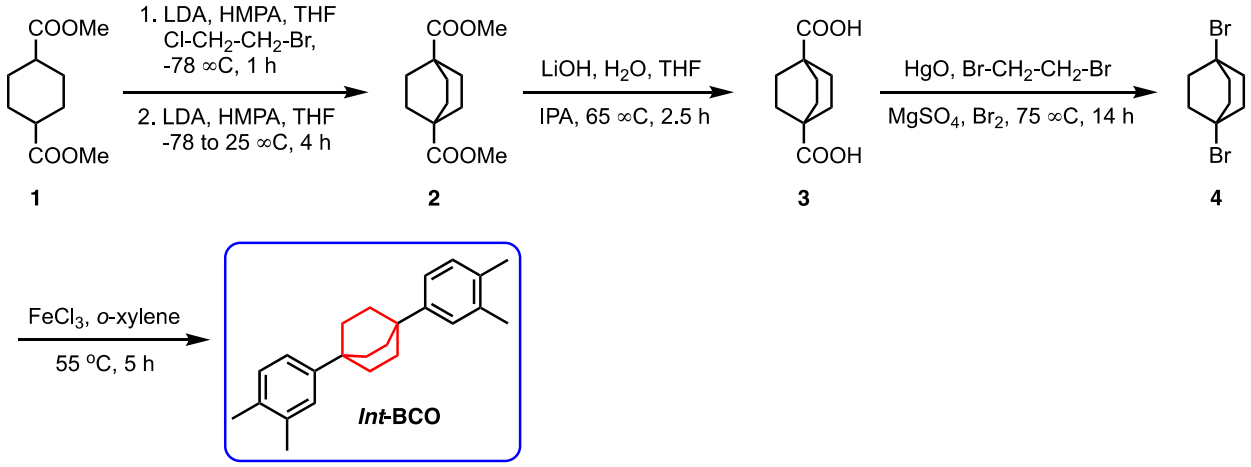

The compounds *Int*-EBD[64], *Int*-Spi[65] and 4[66-68] were synthesized using procedures reported in the literature.

Synthesis of Pentacene Dimers with Homo/Nonconjugated bridge:

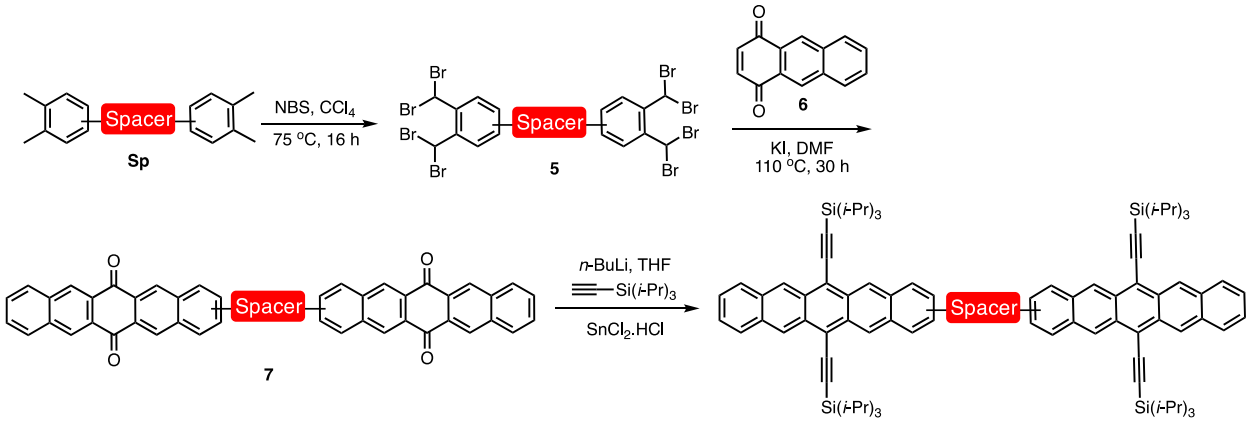

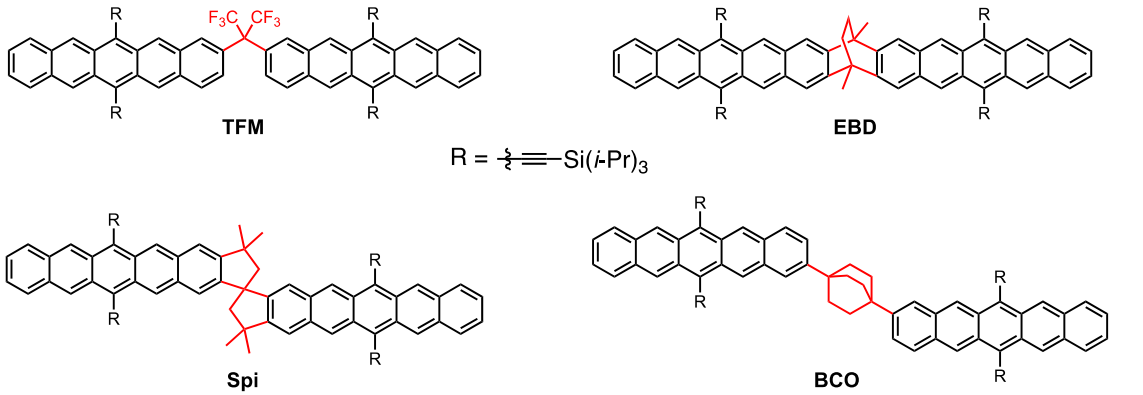

Synthesis of 1,4-bis(3,4-dimethylphenyl)bicyclo[2.2.2]octane:

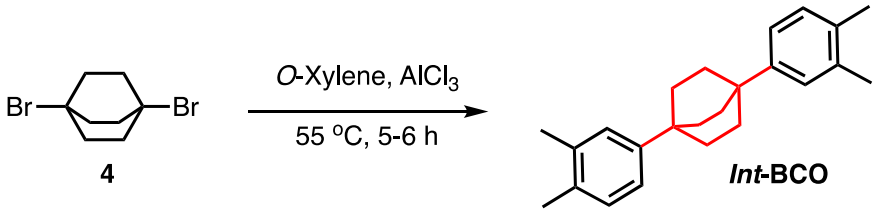

The compound SP-3 was synthesized according to a procedure reported in the literature. To a solution of 1,4-dibromobicyclo[2.2.2]octane 4[66-68] in dry *o*-xylene under argon atmosphere added *anhyd.* $AlCl_3$ and the mixture was stirred at room temperature for 10 minutes. The mixture heated to 55 °C and maintained for 5-6 h. The reaction was monitored by NMR spectroscopy and after the reaction was complete the solution was cooled to room temperature. The solution was quenched with cold water and the aqueous layer was extracted with ethyl acetate. The combined organic layer was washed with water and brine solution. The organic layer was dried over *anhyd.* Na_2SO_4, filter and concentrated to get the crude. The crude was purified by column chromatography using hexanes:ethyl acetate mixture to get the pure product.

Yield: 70% pale white solid

^{1}H-NMR (400 MHz, $CDCl_3$, δ ppm): 7.21 (s, 2H), 7.18-7.13 (m, 4H), 2.33 (s, 6H), 2.29 (s, 3H) and 2.00 (s, 12H).

^{13}C-NMR (100 MHz, $CDCl_3$, δ ppm): 147.6, 136.1, 133.7, 129.4, 126.97, 122.9, 34.6, 32.95, 20.1 and 19.3.

MS (ASAP): Calculated $[M]^+$: 318.2348; Observed: 318.2347.

Synthesis of Octabromo Derivatives:

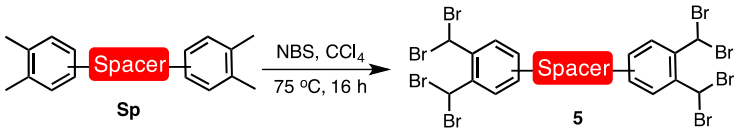

To a mixture of tetramethyl derivative 0.5 g in CCl_4 (15 mL) at room temperature under N_2 atmosphere added benzoyl peroxide and N-bromosuccinimide (4.2 *equiv.).* The mixture was heated to 80 °C and maintained for 4 h. The second portion of benzoyl peroxide and N-bromosuccinimide (4.2 *equiv.)* was added and the reaction was continued for further 12 h. The reaction was cooled and filtered off succinimide. The solid was washed with minimal amount of DCM. The combined organic layer was washed with 1N NaOH (15 mL), DM water (15 mL) and brine solution (15 mL). The organic layer was dried, filtered and concentrated to get the crude. The crude was directly taken to next step.

Note: Complete octabromination was not observed. Nevertheless, the material obtained was taken to next step.

Synthesis of Bipentacenequinone Derivative:

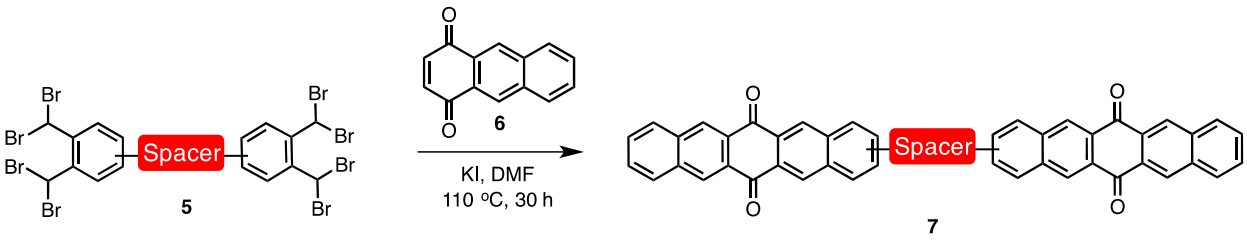

A mixture of octabromo derivative 1.6 g, KI (12 *equiv.*) and the quinone (2.2 *equiv.*) in dry DMF (30 mL) under argon atmosphere was heated to 110 °C and maintained for 30 h. After the reaction, the mixture was cooled to room temperature and diluted DM water (30 mL) stirred for 10 minutes

and filtered. The solid was washed with methanol and acetone. The solid was directly taken to next step without further purification.

Synthesis of Homo/Nonconjugated Bipentacene:

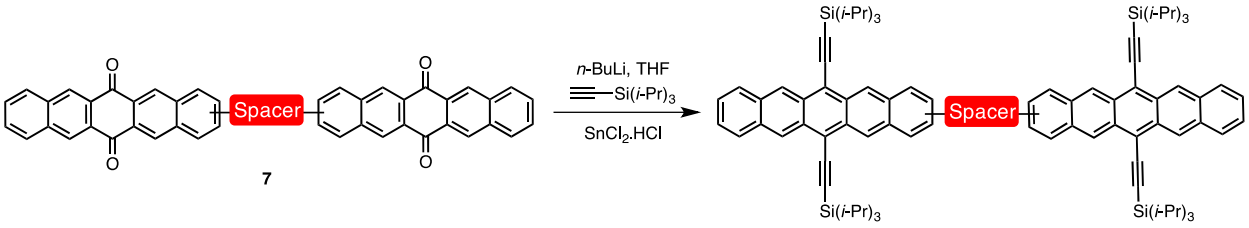

To a solution of (triisopropylsilyl)acetylene (12 equiv.) in dry and degassed THF (25 mL) in 250 mL two neck flask at 0 °C added *n*-butyl lithium (11.5 equiv., 2.5 M in hexanes). This solution was allowed to stir at 30 minutes followed by the addition of pentacenequinone (0.6 g, 1.0 equiv.) under positive argon flow. The solution was allowed to warm to room temperature and stirred overnight during which the solid pentacenequinone was completely dissolved. To this clear, deep yellow solution was added of a saturated solution of tin (II) chloride dihydrate (10 equiv.) in 10% aqueous HCl solution (8 mL) during which the solution turned deep blue. The resulting mixture was stirred at rt for 1 h under dark and filtered over a pad of silica. The solid was washed with DCM and the combined organic layer was washed with water (2 × 20 mL), dried over *anhyd.* Na_2SO_4, filtered and the solvent was removed under reduced pressure to get the crude product. The crude was purified by silica chromatography using mixture of DCM:hexanes as an eluent to obtain pentacene dimer derivatives.

5.26 NMR Spectra

Yield = 17% (for three steps); MS (ES+): Calculated $[M]^+$: 1354.7998; Observed: 1354.8072.

^{1}H-NMR (500 MHz, $CDCl_3$, δ ppm): 9.31 (s, 4H), 9.28 (s, 4H), 7.99-7.97 (m, 4H), 7.85 (s, 4H), 7.43-7.41 (m, 4H), 2.28 (s, 6H), 2.01 (s, 4H) and 1.48-1.40 (m, 84H).

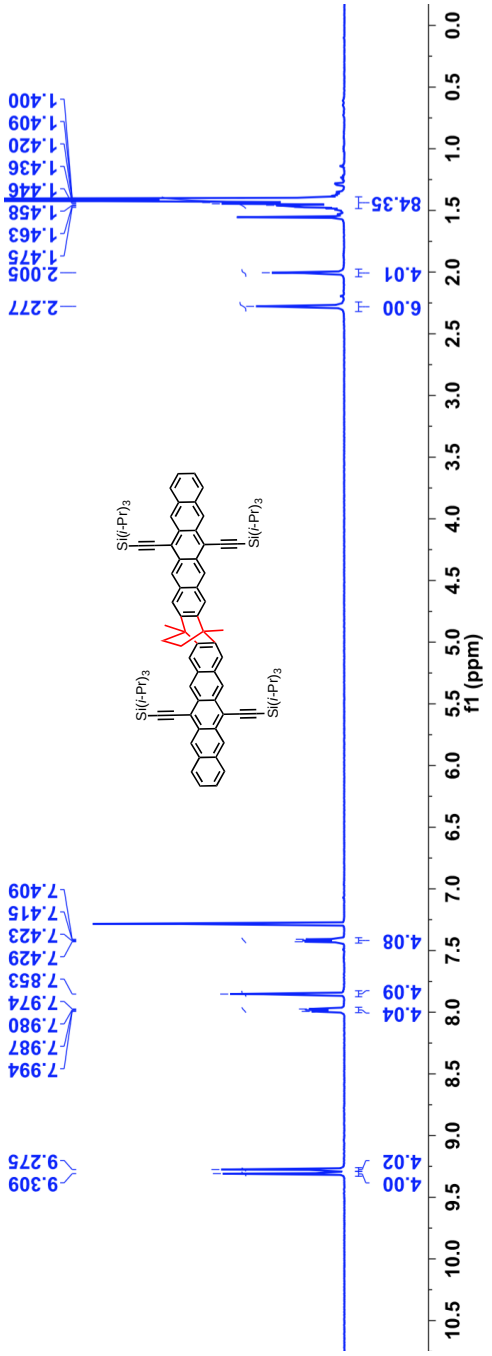

^{13}C-NMR (125 MHz, $CDCl_3$, δ ppm): 144.3, 132.1, 131.8, 130.7, 130.5, 128.7, 126.2, 125.9, 125.7, 119.1, 118.0, 106.8, 104.9, 41.2, 35.2, 19.1, 18.95 and 11.7.

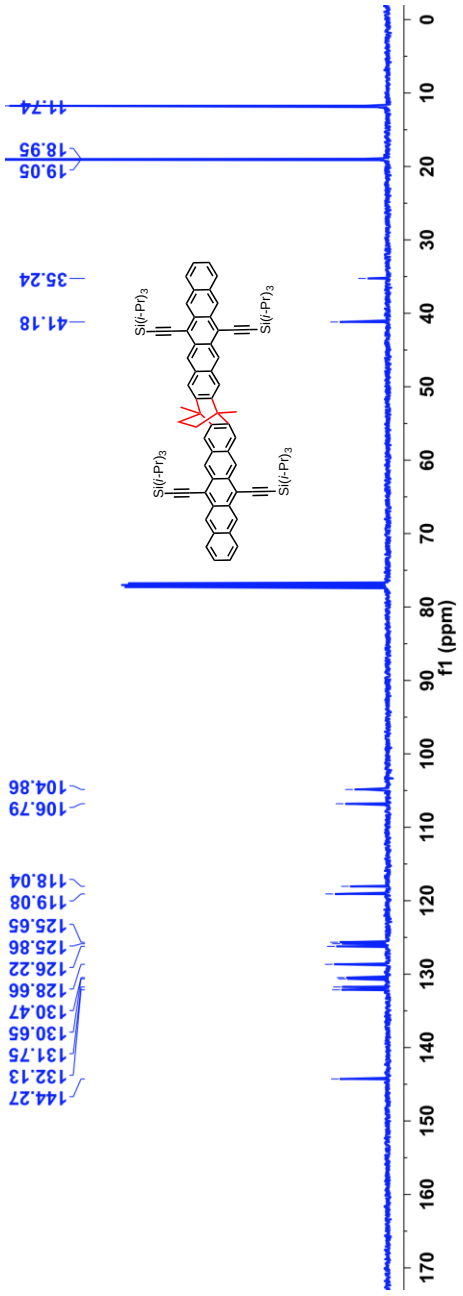

Yield = 15% (for three steps); MS (ES+): Calculated $[M]^+$: 1396.8467; Observed: 1396.8496.

^{1}H-NMR (400 MHz, $CDCl_3$, δ ppm): 9.35 (s, 2H), 9.33 (s, 2H), 9.28 (s, 2H), 9.14 (s, 2H), 7.99-7.94 (m, 4H), 7.83 (s, 2H), 7.51 (s, 2H), 7.42-7.39 (m, 4H), 2.71-2.62 (m, 4H), 1.73 (s, 6H), 1.63 (s, 6H), 1.48-1.43 (m, 42H) and 1.24-1.21 (m, 42H).

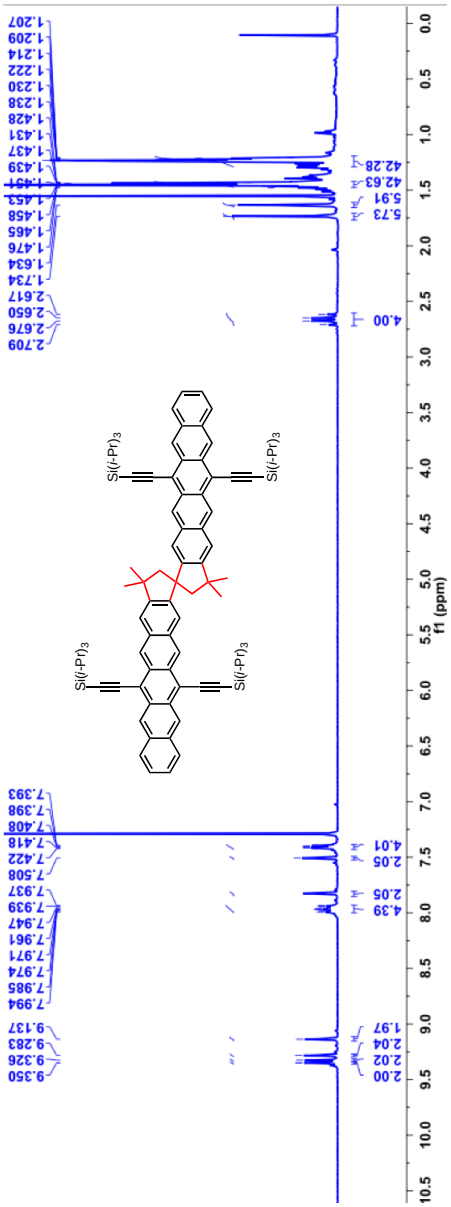

^{13}C-NMR (125 MHz, $CDCl_3$, δ ppm): 153.2, 152.96, 132.9, 132.8, 132.2, 130.7, 130.5, 130.3, 128.7, 126.3, 126.2, 125.9, 125.4, 123.1, 120.1, 118.2, 117.9, 107.2, 106.8, 104.99, 104.7, 60.3, 56.9, 43.2, 32.0, 30.7, 19.1, 18.9, 11.8 and 11.6.

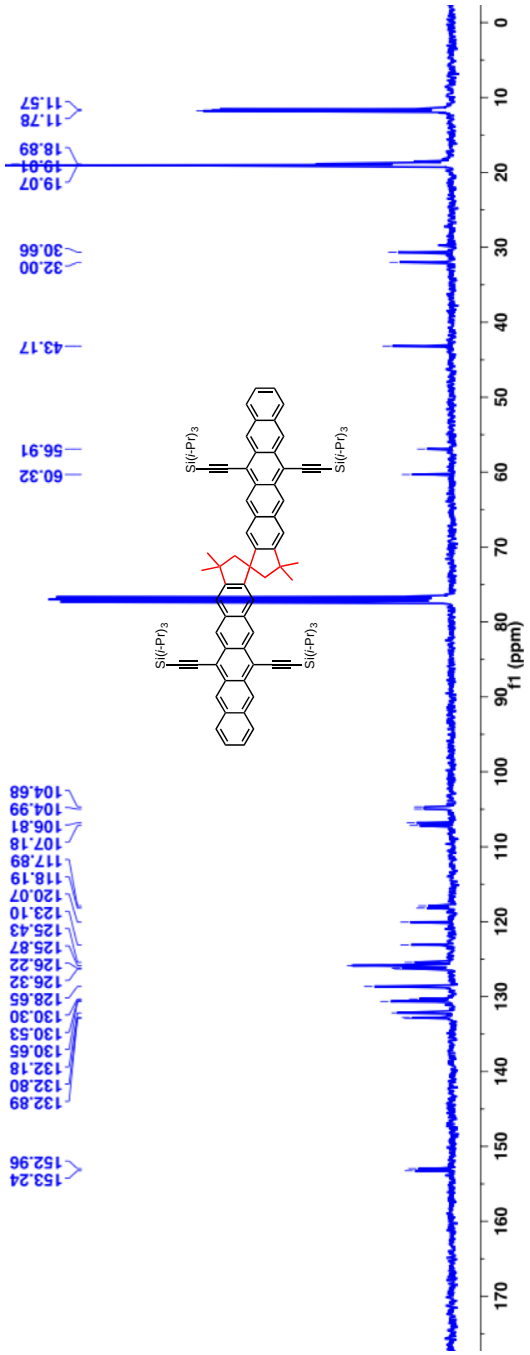

^{1}H-NMR (400 MHz, $CDCl_3$, δ ppm): 7.21 (s, 2H), 7.18-7.13 (m, 4H), 2.33 (s, 6H), 2.29 (s, 3H) and 2.00 (s, 12H).

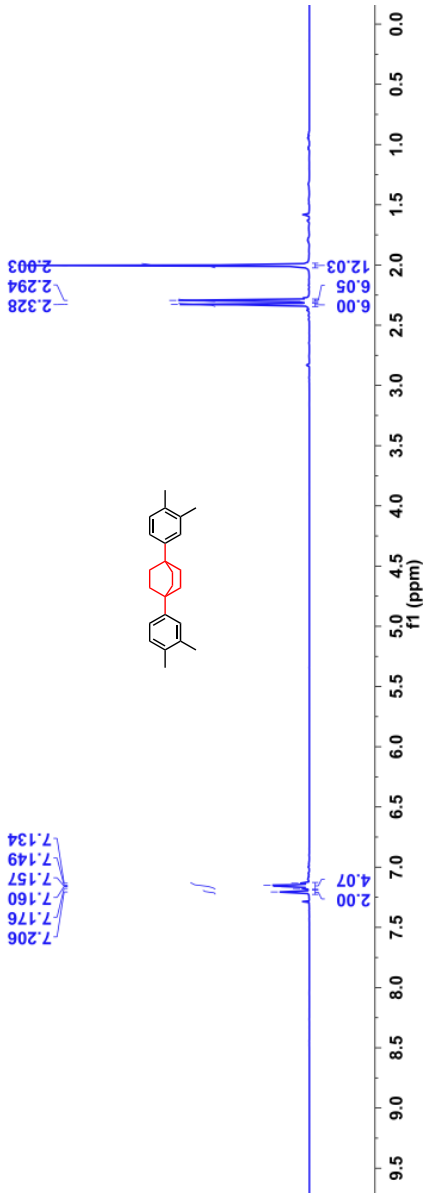

^{13}C-NMR (125 MHz, $CDCl_3$, δ ppm): 147.6, 136.1, 133.7, 129.4, 126.97, 122.9, 34.6, 32.95, 20.1 and 19.3.

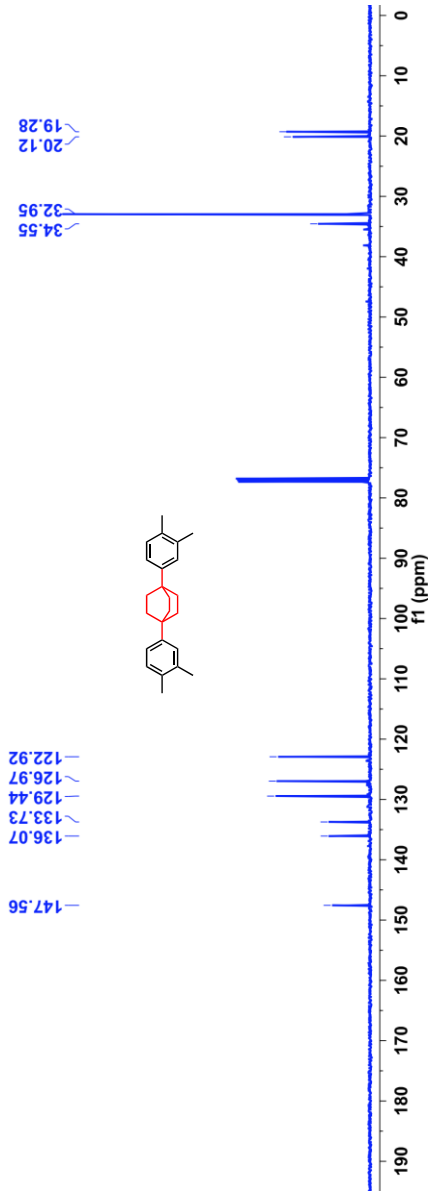

Yield = 19% (for three steps); MS (ES+): Calculated $[M]^+$: 1382.8311; Observed: 1382.8315.

^{1}H-NMR (500 MHz, $CDCl_3$, δ ppm): 9.34-9.29 (m, 8H), 8.01-7.98 (s, 6H), 7.85 (s, 2H), 7.62-7.59 (m, 2H), 7.45-7.43 (m, 4H), 2.24 (s, 12H) and 1.43-1.39 (m, 84H).

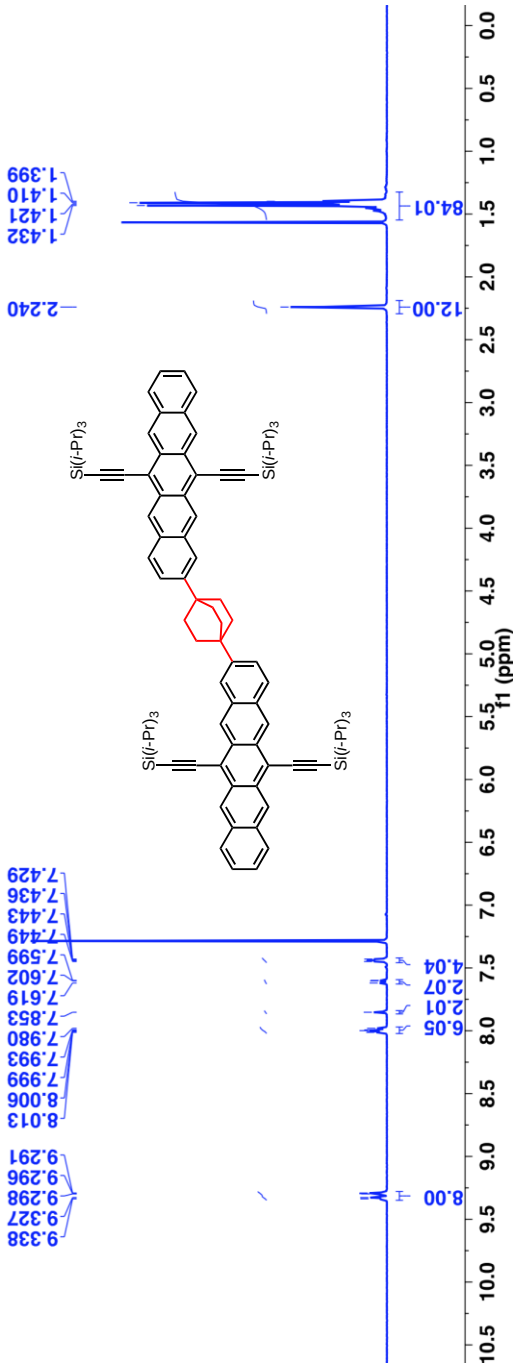

^{13}C-NMR (125 MHz, $CDCl_3$, δ ppm): 147.1, 132.5, 132.3, 132.2, 131.3, 130.9, 130.6, 130.5, 128.7, 128.4, 126.3, 125.97, 125.9, 125.7, 123.0, 118.3, 118.1, 106.97,104.8, 35.6, 31.97, 19.1, 19.0, 11.74 and 11.72.

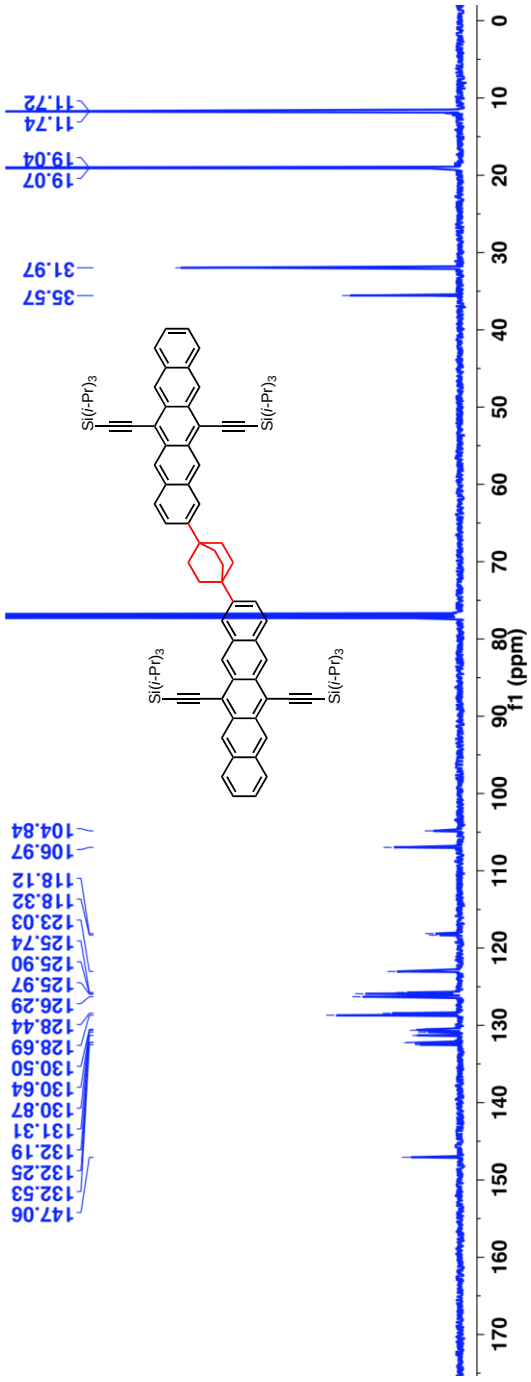

5.27 References

(1) Smith, M. B.; Michl, J. *Annu. Rev. Phys. Chem.* 2013, *64*, 361.

(2) Smith, M. B.; Michl, J. *Chem. Rev.* 2010, *110*, 6891.

(3) Hanna, M. C.; Nozik, A. J. *J. Appl. Phys.* 2006, *100*, 074510.

(4) Tayebjee, M. J. Y.; Gray-Weale, A. A.; Schmidt, T. W. *J. Phys. Chem. Lett.* 2012, *3*, 2749.

(5) Tayebjee, M. J. Y.; Hirst, L. C.; Ekins-Daukes, N. J.; Schmidt, T. W. *J. Appl. Phys.* 2010, *108*, 124506.

(6) Tayebjee, M. J. Y.; McCamey, D. R.; Schmidt, T. W. *J. Phys. Chem. Lett.* 2015, *6*, 2367.

(7) Low, J. Z.; Sanders, S. N.; Campos, L. M. *Chem. Mater.* 2015, *27*, 5453.

(8) Stern, H. L.; Musser, A. J.; Friend, R. H. In *Photochemistry; Singlet exciton fission in solution*; The Royal Society of Chemistry: Cambridge, UK, 2016; Vol. 43, p 270.

(9) Zirzlmeier, J.; Lehnherr, D.; Coto, P. B.; Chernick, E. T.; Casillas, R.; Basel, B. S.; Thoss, M.; Tykwinski, R. R.; Guldi, D. M. *Proc. Natl Acad. Sci.* 2015, *112*, 5325.

(10) Sanders, S. N.; Kumarasamy, E.; Pun, A. B.; Steigerwald, M. L.; Sfeir, M. Y.; Campos, L. M. *Angew. Chem. Int. Ed.* 2016, *55*, 3373.

(11) Sanders, S. N.; Kumarasamy, E.; Pun, A. B.; Trinh, M. T.; Choi, B.; Xia, J.; Taffet, E. J.; Low, J. Z.; Miller, J. R.; Roy, X.; Zhu, X. Y.; Steigerwald, M. L.; Sfeir, M. Y.; Campos, L. M. *J. Am. Chem. Soc.* 2015, *137*, 8965.

(12) Lukman, S.; Musser, A. J.; Chen, K.; Athanasopoulos, S.; Yong, C. K.; Zeng, Z.; Ye, Q.; Chi, C.; Hodgkiss, J. M.; Wu, J.; Friend, R. H.; Greenham, N. C. *Adv. Funct. Mater.* 2015, *25*, 5452.

(13) Korovina, N. V.; Das, S.; Nett, Z.; Feng, X.; Joy, J.; Haiges, R.; Krylov, A. I.; Bradforth, S. E.; Thompson, M. E. *J. Am. Chem. Soc.* 2016, *138*, 617.

(14) Sakuma, T.; Sakai, H.; Araki, Y.; Mori, T.; Wada, T.; Tkachenko, N. V.; Hasobe, T. *J. Phys. Chem. A* 2016, *120*, 1867.

(15) Busby, E.; Xia, J.; Low, J. Z.; Wu, Q.; Hoy, J.; Campos, L. M.; Sfeir, M. Y. *J. Phys. Chem. B* 2015, *119*, 7644.

(16) Busby, E.; Xia, J.; Wu, Q.; Low, J. Z.; Rong, R.; Miller, J. R.; Zhu, X.-Y.; Campos, L. M.; Sfeir, M. Y. *Nat. Mater.* 2014, *14*, 426.

(17) Varnavski, O.; Abeyasinghe, N.; Aragó, J.; Serrano-Pérez, J. J.; Ortí, E.; López Navarrete, J. T.; Takimiya, K.; Casanova, D.; Casado, J.; Goodson, T. *J. Phys. Chem. Lett.* 2015, *6*, 1375.

(18) Kasai, Y.; Tamai, Y.; Ohkita, H.; Benten, H.; Ito, S. *J. Am. Chem. Soc.* 2015, *137*, 15980.

(19) Xia, J.; Sanders, S. N.; Cheng, W.; Low, J. Z.; Liu, J.; Campos, L. M.; Sun, T. *Adv. Mater.* 2016, 1601652.

(20) Alguire, E. C.; Subotnik, J. E.; Damrauer, N. H. *J. Phys. Chem. A* 2015, *119*, 299.

(21) Cook, J. D.; Carey, T. J.; Damrauer, N. H. *J. Phys. Chem. A* 2016, *120*, 4473.

(22) Vallett, P. J.; Snyder, J. L.; Damrauer, N. H. *J. Phys. Chem. A.* 2013, *117*, 10824.

(23) Basel, B. S.; Zirzlmeier, J.; Hetzer, C.; Phelan, B. T.; Krzyaniak, M. D.; Reddy, S. R.; Coto, P. B.; Horwitz, N. E.; Young, R. M.; White, F. J.; Hampel, F.; Clark, T.; Thoss, M.; Tykwinski, R. R.; Wasielewski, M. R.; Guldi, D. M. *Nat. Commun.* 2017, *8*, 15171.

(24) Yost, S. R.; Lee, J.; Wilson, M. W. B.; Wu, T.; McMahon, D. P.; Parkhurst, R. R.; Thompson, N. J.; Congreve, D. N.; Rao, A.; Johnson, K.; Sfeir, M. Y.; Bawendi, M. G.; Swager, T. M.; Friend, R. H.; Baldo, M. A.; Van Voorhis, T. *Nat. Chem.* 2014, *6*, 492.

(25) Mauck, C. M.; Hartnett, P. E.; Margulies, E. A.; Ma, L.; Miller, C. E.; Schatz, G. C.; Marks, T. J.; Wasielewski, M. R. *J. Am. Chem. Soc.* 2016, *138*, 11749.

(26) Eaton, S. W.; Miller, S. A.; Margulies, E. A.; Shoer, L. E.; Schaller, R. D.; Wasielewski, M. R. *J. Phys. Chem. A* 2015, *119*, 4151.

(27) Ryerson, J. L.; Schrauben, J. N.; Ferguson, A. J.; Sahoo, S. C.; Naumov, P.; Havlas, Z.; Michl, J.; Nozik, A. J.; Johnson, J. C. *J. Phys. Chem. C* 2014, *118*, 12121.

(28) Dillon, R. J.; Piland, G. B.; Bardeen, C. J. *J. Am. Chem. Soc.* 2013, *135*, 17278.

(29) Kolata, K.; Breuer, T.; Witte, G.; Chatterjee, S. *ACS Nano* 2014, *8*, 7377.

(30) Wang, L.; Olivier, Y.; Prezhdo, O. V.; Beljonne, D. *J. Phys. Chem. Lett.* 2014, *5*, 3345.

(31) Mastron, J. N.; Roberts, S. T.; McAnally, R. E.; Thompson, M. E.; Bradforth, S. E. *J. Phys. Chem. B* 2013, *117*, 15519.

(32) Roberts, S. T.; McAnally, R. E.; Mastron, J. N.; Webber, D. H.; Whited, M. T.; Brutchey, R. L.; Thompson, M. E.; Bradforth, S. E. *J. Am. Chem. Soc.* 2012, *134*, 6388.

(33) Lukman, S.; Chen, K.; Hodgkiss, J. M.; Turban, D. H. P.; Hine, N. D. M.; Dong, S.; Wu, J.; Greenham, N. C.; Musser, A. J. *Nat. Commun.* 2016, *7*, 13622.

(34) Liu, H.; Wang, R.; Shen, L.; Xu, Y.; Xiao, M.; Zhang, C.; Li, X. *Org. Lett.* 2017, *19*, 580.

(35) Fuemmeler, E. G.; Sanders, S. N.; Pun, A. B.; Kumarasamy, E.; Zeng, T.; Miyata, K.; Steigerwald, M. L.; Zhu, X. Y.; Sfeir, M. Y.; Campos, L. M.; Ananth, N. *ACS Cent. Sci.* 2016, *2*, 316.

(36) Su, T. A.; Li, H.; Klausen, R. S.; Widawsky, J. R.; Batra, A.; Steigerwald, M. L.; Venkataraman, L.; Nuckolls, C. *J. Am. Chem. Soc.* 2016, *138*, 7791.

(37) Halasinski, T. M.; Hudgins, D. M.; Salama, F.; Allamandola, L. J.; Bally, T. *J. Phys. Chem. A* 2000, *104*, 7484.

(38) Berkelbach, T. C.; Hybertsen, M. S.; Reichman, D. R. *J. Chem. Phys.* 2013, *138*, 114103.

(39) Tayebjee, M. J. Y.; Sanders, S. N.; Kumarasamy, E.; Campos, L. M.; Sfeir, M. Y.; McCamey, D. R. *Nat. Phys.* 2017, *13*, 182.

(40) Sanders, S. N.; Kumarasamy, E.; Pun, A. B.; Appavoo, K.; Steigerwald, M. L.; Campos, L. M.; Sfeir, M. Y. *J. Am. Chem. Soc.* 2016, *138*, 7289.

(41) Sanders, S. N.; Kumarasamy, E.; Pun, A. B.; Steigerwald, M. L.; Sfeir, M. Y.; Campos, L. M. *Chem* 2016, *1*, 505.

(42) Margulies, E. A.; Logsdon, J. L.; Miller, C. E.; Ma, L.; Simonoff, E.; Young, R. M.; Schatz, G. C.; Wasielewski, M. R. *J. Am. Chem. Soc.* 2017, *139*, 663.

(43) Zirzlmeier, J.; Casillas, R.; Reddy, S. R.; Coto, P. B.; Lehnherr, D.; Chernick, E. T.; Papadopoulos, I.; Thoss, M.; Tykwinski, R. R.; Guldi, D. M. *Nanoscale* 2016, *8*, 10113.

(44) Trinh, M. T.; Pinkard, A.; Pun, A. B.; Sanders, S. N.; Kumarasamy, E.; Sfeir, M. Y.; Campos, L. M.; Roy, X.; Zhu, X.-Y. *Science Advances* 2017, *3*.

(45) Kumarasamy, E.; Sanders, S. N.; Pun, A. B.; Vaselabadi, S. A.; Low, J. Z.; Sfeir, M. Y.; Steigerwald, M. L.; Stein, G. E.; Campos, L. M. *Macromolecules* 2016, *49*, 1279.

(46) Bayliss, S. L.; Thorley, K. J.; Anthony, J. E.; Bouchiat, H.; Greenham, N. C.; Chepelianskii, A. D. *Phys. Rev. B* 2015, *92*, 115432.

(47) Van Strien, A. J.; Schmidt, J. *Chem. Phys. Lett.* 1980, *70*, 513.

(48) Swenberg, C. E.; van Metter, R.; Ratner, M. *Chem. Phys. Lett.* 1972, *16*, 482.

(49) Weiss, L. R.; Bayliss, S. L.; Kraffert, F.; Thorley, K. J.; Anthony, J. E.; Bittl, R.; Friend, R. H.; Rao, A.; Greenham, N. C.; Behrends, J. *Nat. Phys.* 2017, *13*, 176.

(50) Walker, B. J.; Musser, A. J.; Beljonne, D.; Friend, R. H. *Nat. Chem.* 2013, *5*, 1019.

(51) Scholes, G. D. *J. Phys. Chem. A* 2015, *119*, 12669.

(52) Snellenburg, J. J. L., S. P.; Seger, R.; Mullen, K. M.; van Stokum, I. H. M. *J. Stat. Soft.* 2012, *49*, 1.

(53) Snyder, L. R.; Kirkland, J. J.; Glajch, J. L. In *Practical HPLC Method Development*; John Wiley & Sons, Inc.: 1997, p 721.

(54) Bosque, R.; Sales, J. *J. Chem. Inform. Comput. Sci.* 2002, *42*, 1154.

(55) Schmidt, M. W.; Baldridge, K. K.; Boatz, J. A.; Elbert, S. T.; Gordon, M. S.; Jensen, J. H.; Koseki, S.; Matsunaga, N.; Nguyen, K. A.; Su, S.; Windus, T. L.; Dupuis, M.; Montgomery, J. A. *J. Comput. Chem.* 1993, *14*, 1347.

(56) Towns, J.; Cockerill, T.; Dahan, M.; Foster, I.; Gaither, K.; Grimshaw, A.; Hazlewood, V.; Lathrop, S.; Lifka, D.; Peterson, G. D. *Comput. Sci. Eng.* 2014, *16*, 62.

(57) Zeng, T.; Hoffmann, R.; Ananth, N. *J. Am. Chem. Soc.* 2014, *136*, 5755.

(58) Feng, X.; Luzanov, A. V.; Krylov, A. I. *J. Phys. Chem. Lett.* 2013, *4*, 3845.

(59) Pieniazek, P. A. K., A. I.; Bradforth, S. E. *J. Chem. Phys.* 2007, *127*, 044317.

(60) Blanc, E.; Schwarzenbach, D.; Flack, H. D. *J. Appl. Crystallogr.* 1991, *24*, 1035.

(61) Clark, R. C.; Reid, J. S. *Act. Cryst. A* 1995, *51*, 887.

(62) Sheldrick, G. M. *Act. Cryst. A* 2008, *64*, 112.

(63) Dolomanov, O. V.; Bourhis, L. J.; Gildea, R. J.; Howard, J. A. K.; Puschmann, H. *J. Appl. Crystallogr.* 2009, *42*, 339.

(64) Rogan, Y.; Malpass-Evans, R.; Carta, M.; Lee, M.; Jansen, J. C.; Bernardo, P.; Clarizia, G.; Tocci, E.; Friess, K.; Lanc, M.; McKeown, N. B. *J. Mater. Chem. A* 2014, *2*, 4874.

(65) Rogan, Y.; Starannikova, L.; Ryzhikh, V.; Yampolskii, Y.; Bernardo, P.; Bazzarelli, F.; Jansen, J. C.; McKeown, N. B. *Polym. Chem.* 2013, *4*, 3813.

(66) Royalty, S. M.; Burns, J. F.; Scicinski, J. J.; Jagdmann, J. G. E.; Foglesong, R. J.; Griffin, K. R.; Dyakonov, T.; Middlemiss, D. WO 2006012395 A2; 2006.

(67) Bennett, B. L.; Elsner, J.; Erdman, P.; Hilgraf, R.; LeBrun, L. A.; McCarrick, M.; Moghaddam, M. F.; Nagy, M. A.; Norris, S.; Paisner, D. A. US2013/0029987A1, 2013.

(68) Wiberg, K. B.; Pratt, W. E.; Bailey, W. F. *J. Am. Chem. Soc.* 1977, *99*, 2297.

6 Quintet Multiexciton Dynamics in Singlet Fission

6.1 Preface

This chapter is based on a manuscript entitled “Quintet Multiexciton Dynamics in Singlet Fission” published in *Nature Physics* by Murad J. Y. Tayebjee, Samuel N. Sanders, Elango Kumarasamy, Luis M. Campos, Matthew Y. Sfeir and Dane R. McCamey. Murad performed all electron spin resonance spectroscopy in the laboratory of Prof. McCamey. Elango and I synthesized all molecules in the laboratory of Prof. Campos, while I performed all transient absorption spectroscopy in the laboratory of Dr. Sfeir.

6.2 Introduction

Singlet fission (SF), the multiplication of a singlet exciton into two triplet excitons, is of practical interest for its potential to enhance efficiencies of photodetectors and photovoltaics.[1-4] Despite the large body of literature devoted to understanding SF, fundamental questions persist concerning the energetic and mechanistic requirements. For example, while a basic tenet of any physical process is conservation of energy, SF proceeds efficiently in tetracene molecular crystals even though the enthalpy of the final states (two triplet excitons) exceeds that of the initial state (singlet exciton).[5] This apparent violation of energy conservation has been explored since the discovery of SF itself in the late 1960s, without a definitive resolution.[6-9] Similarly, angular momentum conservation must hold for the SF process to proceed rapidly and efficiently. This requires that the initial product of SF is a spin correlated (multiexciton state) with net singlet character. While indirect evidence for these multiexciton states has been observed,[6,10,11] their spin character, dynamics, and energetic have not been quantified. These parameters are critical for

understanding the energy cascade that leads to uncoupled triplets. For example, it is important to determine the role of electron correlations in promoting SF in so-called "endothermic" SF materials.

The primary difficulty in studying multiexciton states is their transient nature. SF has been observed primarily in crystalline solids, where correlated (TT) pairs rapidly dissociate at room temperature and diffuse apart. However, covalently linked SF dimers (Figure 1a) offer significant advantages for detailed mechanistic studies of SF due to their chemical tunability and solution processability.[12-17] Recently, several reports have shown efficient intramolecular SF in isolated acene dimers and demonstrated that modifying their structure can systematically tune the rate of triplet generation and decay.[18-22] For example, we have previously employed acene heterodimers, systematically varying the energy of the (TT) pairs produced by SF, and uncovered an energy gap law which governs non-radiative (TT) pair recombination.[23] The advantages of these systems extend to the condensed phase, as tetracene dimers have recently been reported to undergo SF regardless of film morphology.[18] Importantly, dimers permit the study of a constrained (TT) pair, i.e., diffusion apart is forbidden since only two triplet sites exist in an isolated molecule. While these systems are ideal models for investigating the fundamental photophysics of SF, we stress that their utility is not limited to basic science as their modularity, tunability, and processability will be advantageous for designing triplet harvesting interfaces.

The details of SF are elusive in part because of their complexity (Figure 1b). In efficient SF systems, a photogenerated singlet exciton decays rapidly by forming multiple triplets, with timescales ranging as fast as ~80 fs in pentacene molecular crystals[24,25] and ~700 fs in directly linked bipentacene dimers.[21] The primary product of SF is a spin correlated triplet-triplet pair of multiplicity M, labelled ^{M}(TT). If one considers only coupling of the angular momentum of two

triplets, nine total (TT) pair states can be constructed (using Clebsch-Gordan coefficients for example) with one out of the nine possible (TT) pair states being a singlet. However, fine structure interactions couple the different states, such that the solutions to the full spin Hamiltonian do not have pure spin multiplicity. Even in the absence of spin-orbit coupling, the end result is that the singlet ^{1}(TT) and quintet ^{5}(TT) triplet-triplet pair states are mixed.[26] Excitation into S_1 therefore results in (TT) pair states with both singlet and quintet character,[27] and that the relative ratio of the two (as well as the total number of states containing partial singlet character) will be a function of the applied magnetic field.[26] While these phenomena have been indirectly observed as variations in the optical and transport properties of SF materials in the presence of an applied external field,[27-33] quintet states have never been directly and unambiguously identified. However, independent, uncoupled triplets have been observed in SF materials, suggesting that (TT) pair states may dissociate if a geometric reorganization gives rise to a lower energy uncoupled triplet (T_1) state. The full energy cascade is shown schematically in Figure 1b,c. The role of the quintet state in SF has often been unnecessarily[1] dismissed since it was assumed to be too high in energy to be accessed, although recent computational studies suggest the energetic splitting between ^{5}(TT) and ^{1}(TT) is only ~10 meV in tetracene dimers.[18] Previous electron spin resonance (ESR) measurements of $T_0 \rightarrow T_{\pm 1}$ polarized transitions have been used to infer that triplet states are populated via SF, [34-36] however no direct observation of the spin properties of the TT pair state have been reported.

We exploit intramolecular SF dimers as a stable, soluble and modular system to study the fundamental spin physics and dynamics of correlated (TT) pair states resulting from SF using transient absorption and time resolved electron spin resonance (tr-ESR) spectroscopy. We use pentacene dimers bridged by either two (BP2) or three (BP3) phenylene bridges (Figure 1a) as we

have previously shown that these bridges result in long (TT) pair lifetimes, reaching timescales suitable for investigation via tr-ESR. Previous results using transient absorption have shown quantitative SF in this class of molecules and the absence of any parasitic singlet exciton decay pathways introduced by dimerization,[21] making them ideal for this study. We present time-resolved ESR data which unambiguously demonstrates the generation of (TT) pair states with overall spin $S = 2$ (quintet) by intramolecular SF in bipentacene compounds, as shown in Figure 1. By comparing quintet states in two separate molecules, we show that molecular structure and chromophore-chromophore interactions significantly affect the dynamics of this previously unobserved state. These systems represent a facile way to populate and study the quintet state in closed shell organic molecules.

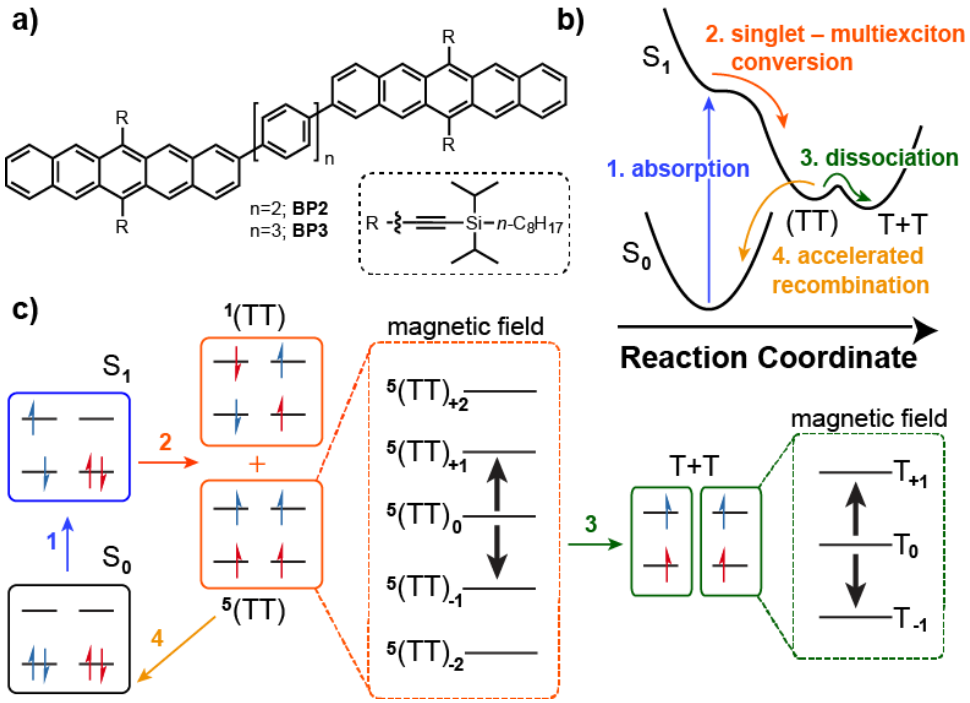

Figure 6.1. Molecular structure and Jablonksi diagram of the singlet fission system. a, Bipentacenes, BPn, with n phenylene linkers b, After photoexcitation, SF generates a (TT) pair state, which eventually dissociates via a conformational transition to yield isolated triplets. c, Schematic representation of the low field spin states that are observed in transient absorption and high field spin states observed in ESR measurements.

6.3 Singlet Fission Dynamics in Bipentacene

The SF dynamics of BP3 are similar to those we have previously reported for BP2 (Figure 2a).[21] Briefly, a photoexcited singlet evolves into a (TT) pair with a time constant that increases with increasing bridge length. SF has been previously identified in this class of materials by comparing the transient spectra of the (TT) pairs generated by direct photoexcitation to that of individual triplets that are populated on the molecules via collision energy transfer (sensitization). The most prominent feature associated with triplet states is a photo-induced absorption (PIA) signal associated with the $T_1 \rightarrow T_3$ transition that occurs at ~ 520 nm (Fig. 2b), which forms in BP3 with a time constant of ~ 6.4 ns (see Supplementary Information). The relatively long SF time constant in BP3 (compared to ~ 200 ps in BP2) means that SF is not quantitative, and a significant fraction of excited state population is lost due to radiative recombination. However, recombination of (TT) pairs slows down as well, making this molecule an ideal candidate for electron spin resonance studies.

The triplet photoinduced absorption feature of BP3 nm exhibits multiexponential decay kinetics, similar to those we have previously reported for BP2, with a primary recombination process occurring with a lifetime of ~ 200 ns and a weaker secondary component with a lifetime of ~ 20 μs (Fig. 2c).[21] The longer decay component is similar to that of an individual triplet in sensitization studies (see Supplementary Information). In analogous pentacene-tetracene heterodimers, we have shown that delayed fluorescence is possible during the initial fast decay component while the (TT) pair remains spin correlated, but not the longer component, due to the near degeneracy of the singlet and (TT) pair state.[37]SU While SF in these bipentacenes is too exothermic to permit delayed fluorescence, the similarity of the decay kinetic suggests that (TT)

pairs remain spin correlated into an overall singlet for 100 – 1000 ns. However, since the individual triplet and (TT) pair spectra are nearly identical in these compounds (Figure 2b), the PIA intensity is strictly proportional to the total number of triplets and cannot be used to resolve spin states. In order to resolve spin correlations in the (TT) pair states, we now turn to tr-ESR spectroscopy.

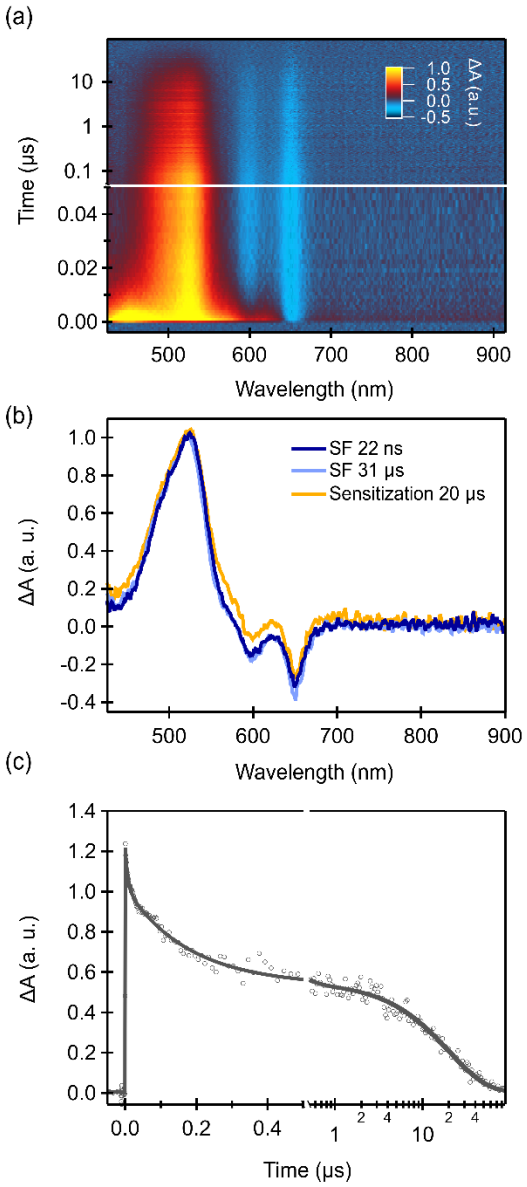

Figure 6.2. Identifying Singlet Fission Dynamics *via* Transient Absorption. a, Transient absorption data as a function of time and probe wavelength for a 50 μM solution of BP3 in

chloroform under a pump fluence of ~ 25 μJ/cm^2 with 360 nm excitation. b, The transient spectra of the (TT) pairs generated by SF are identical at early (22 ns, dark blue) and late (31 μs, light blue) times in the decay and nearly identical to individual triplets generated via sensitization (yellow). c, The decay kinetics at the maximum of the triplet photoinduced absorption (520 nm) are multiexponential, with time constants of ~ 500 ns and 20 μs.

To understand the signal that is expected in a tr-ESR experiment, it is necessary to consider the total spin Hamiltonian of a pair of triplets,

$$\widehat{\mathcal{H}} = \widehat{H}_z + \widehat{H}_{zfs} + \widehat{H}_{ee}, \qquad 1$$

which contains Zeeman, zero-field interaction, and spin-spin terms (explicit forms are given in the Supplementary Information). The first two terms respectively split the energy of states with different m_s and of individual triplets at zero-field. The spin-spin interaction is comprised of an isotropic term which splits states with different multiplicities and a symmetric term which accounts for directional spin-spin coupling.[38,39] ESR measurements are taken at high magnetic fields (B ~ 350 mT), and solutions to $\widehat{H}_z$ have pure spin states given by

$$\left| {}^1(\mathrm{TT})\right\rangle = \frac{1}{\sqrt{3}}(|00\rangle - |+-\rangle - |-+\rangle)$$

$$\left| {}^5(\mathrm{TT})_{\pm 1}\right\rangle = \frac{1}{\sqrt{2}}(|\pm 0\rangle + |0\pm\rangle)$$

$$\left| {}^5(\mathrm{TT})_{0}\right\rangle = \frac{1}{\sqrt{6}}(2|00\rangle + |+-\rangle + |-+\rangle)$$

$$\left| {}^5(\mathrm{TT})_{\pm 2}\right\rangle = |\pm\pm\rangle$$

$$\left| {}^3(\mathrm{TT})_{\pm 1}\right\rangle = \frac{1}{\sqrt{2}}(|\pm 0\rangle - |0\pm\rangle)$$

$$\left| {}^3(\mathrm{TT})_{0}\right\rangle = \frac{1}{\sqrt{2}}(|+-\rangle - |-+\rangle)$$

The splitting of the (TT) pair states under high magnetic field is depicted schematically in Figure 1c. The $|00\rangle$ and $2^{-\frac{1}{2}}(|+-\rangle + |-+\rangle)$ states have singlet character,[26,29] and upon dephasing of the SF generated $^1(TT)_0$, the $^5(TT)_0$ eigenstate of the Zeeman operator is also occupied. Moreover, the symmetric $^1(TT)$ and $^5(TT)$ states can be mixed by the fine structure operators ($\widehat{H}_{zfs}$ and $\widehat{H}_{ee}$), while the asymmetric $^3(TT)_0$ states remain as pure triplets.[39,40] As such, the SF generated (TT) pair tr-ESR spectra will be dominated by absorption/emission from $^5(TT)_0$ to $^5(TT)_{\pm1}$ transitions along with smaller contributions resulting from singlet character admixture.

6.4 Evolution of Correlated Quintet States into Isolated Triplets in BP3.

Figure 6.3(a) and (b) respectively show the simulated energy levels and ESR spectrum of BP3 immediately following optical excitation, measured at 40K. As expected the spectrum in (b) is dominated by $^5(TT)_0$ to $^5(TT)_{\pm1}$ transitions which are observed as peaks at 336.4 and 348.8 mT (red and green dashed lines). However the integrated absorption exceeds the emission and a shoulder is observed at ~360 mT. In order to account for these smaller features we incorporate a spin-spin coupling matrix into our model which gives rise to mixing between states of different multiplicities. With an isotropic coupling of $J_{iso} = 1.99 \times 10^4$ MHz and a directional spin-spin coupling of $X = 38$ MHz the $^1(TT)_0$ and $^5(TT)_{-2}$ states mix within the field range of our experiment; this allows for an additional absorptive transition to be simulated (blue dashed line) and an excellent fit of the data. The dominance of isotropic (TT) exchange coupling over anisotropic spin-spin coupling is indicative of a through space interaction rather than a dipole-dipole interaction.[38] Given the separation between the two pentacenes is ~16Å, we expect the spin-spin dipole-dipole interaction component, *X*, to be on the order of 10 MHz.[39] The positive isotropic coupling gives

rise to a ~80μeV splitting between the singlet and quintet manifolds[40] and the peaks of the $^5(TT)_0$ to $^5(TT)_{\pm1}$ transitions will be observed at $g \pm (D - 3E)/6$, where D is the zero-field splitting parameter of the pentacene triplet.[41] The dependence of resonance fields of the $^5(TT)_0 \leftrightarrow {}^5(TT)_{\pm1}$ transitions on J_{iso} is given below.

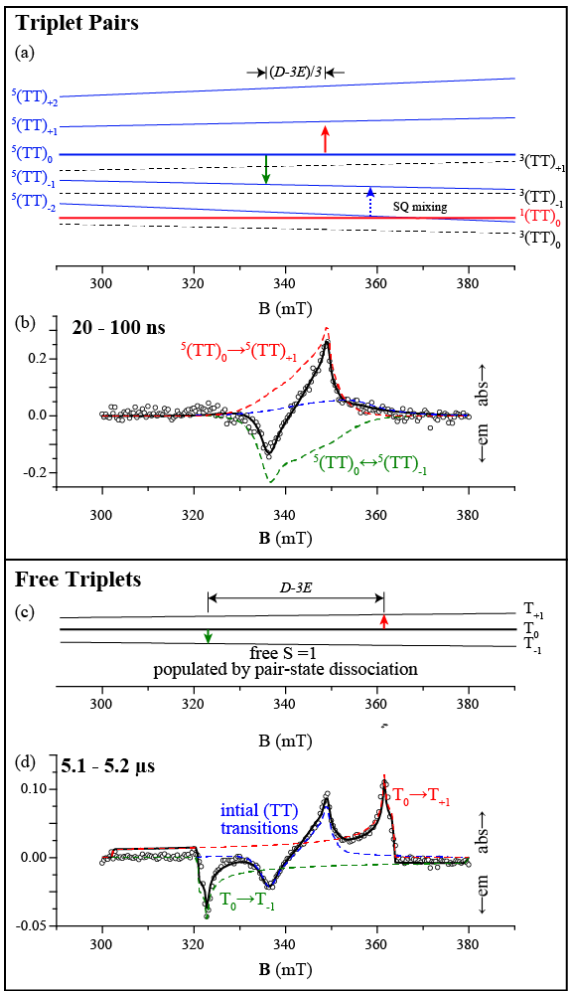

Figure 6.3. Identifying Quintet and Triplet spin states via time resolved Electron Spin Resonance. a, solutions to the Hamiltonian of (TT) pairs, where singlet-quintet mixing is denoted SQ. ESR resonances are also marked at $\boldsymbol{g \pm (D - 3E)/6}$ for $\boldsymbol{^5(TT)_{\pm1} \leftrightarrow {}^5(TT)_0}$. When a dipolar coupling term is included in $\boldsymbol{H_{ee}}$ the resonances depart from these values. c, free triplet resonances as a function of magnetic field strength with ESR resonances marked at $\boldsymbol{g \pm (D - 3E)/2}$ for the $\boldsymbol{T_{\pm1} \leftrightarrow T_0}$ transitions. b, Transitions observed within the experiment time resolution, 20-100ns

after optical excitation in BP3 at 40K, dominated by a quintet signal. d, After several microseconds the spectrum is the sum of the initial (TT) and dissociated triplet transitions. Data are represented by open circles, individual transitions are dashed lines, and the cumulative spectrum is given as a solid black line. The simulations above were carried out using the *g*-factors and zfs parameters listed in the Supplementary Information.

The outer pair at $g \pm (D - 3E)/2$ grows in over several hundred nanoseconds (

Figure 6.4.). We consider three possible transitions for the outer pair based on the positions of their resonance fields: (i) triplet-triplet pair ${}^5(\mathrm{TT})_{\pm 2} \leftrightarrow {}^5(\mathrm{TT})_{\pm 1}$ which are populated via thermalization within the quintet manifold (ii) triplet-triplet pair ${}^3(\mathrm{TT})_{\mp 1} \leftrightarrow {}^3(\mathrm{TT})_0$ which could be populated via spin-orbit coupling between the ^{5}(TT) and ^{3}(TT) manifolds, or (iii) $\mathrm{T}_{\pm 1} \leftrightarrow \mathrm{T}_0$ of the dissociated triplet. We can ignore the former explanation since we would expect the ${}^5(\mathrm{TT})_{\pm 1} \leftrightarrow {}^5(\mathrm{TT})_0$ transitions to also be present, however these are absent at times >5μs (Figure 4). We also discount the possibility of the triplet-triplet pair ${}^3(\mathrm{TT})_{\mp 1} \leftrightarrow {}^3(\mathrm{TT})_0$ transitions since the initial spin polarization favours the ${}^5(\mathrm{TT})_0$ state and the ${}^3(\mathrm{TT})_{\mp 1} \leftrightarrow {}^3(\mathrm{TT})_0$ is anti-polarized with respect to the experimental data. In addition this would require significant spin-orbit coupling for the ${}^5(\mathrm{TT}) \rightarrow {}^3(\mathrm{TT})$ transition to occur. Finally, the weak signal at long times are indicative of a thermalizing triplet which has a similar lifetime to the transient absorption signal of triplets generated by sensitization. As such, we attribute the long-lived signal to dissociated triplets which are initially polarized in the T_0 state to give the spectra in Figure 6.3(c,d). Note that, similar to the initial spectrum, the integrated absorption exceeds the integrated emission, providing further evidence that state-mixing gives rise to the populating of the ${}^5(\mathrm{TT})_{-2}$ state which dissociates into two T_{-1} triplets. Combining these observations, we are able to generate the physical description in Figure 6.1**Error! Reference source not found.**. Measurements at both higher (80K) and lower (20K) temperatures show qualitatively consistent results.

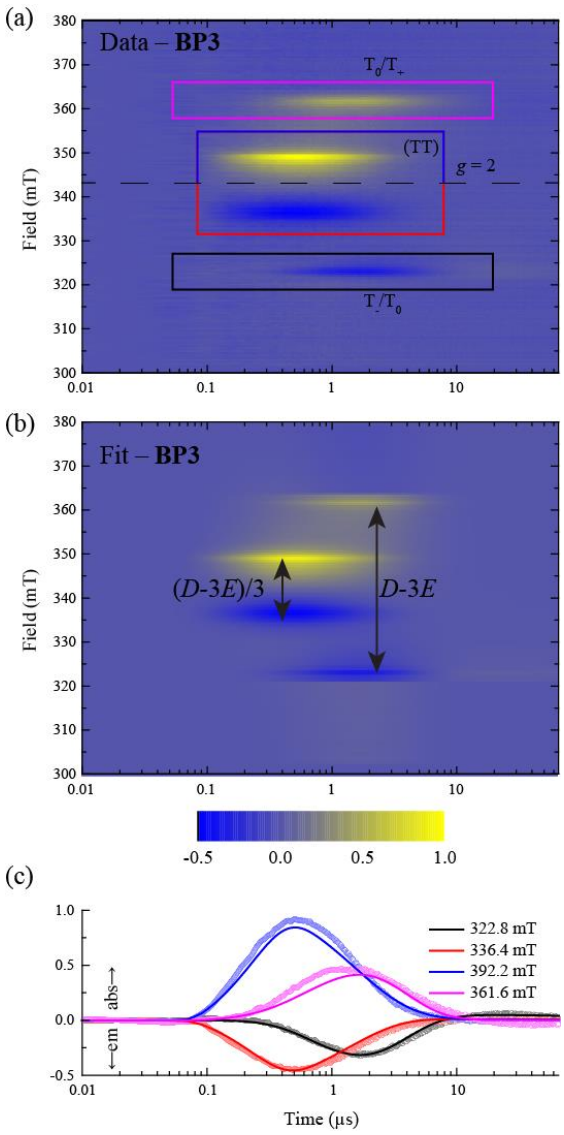

Figure 6.4. Spin dynamics of singlet fission. a, The 2D ESR spectra of BP3 at 40K and b, simulated data generated from fitting the experimental results. c, Transients taken at the peak of each of the four features in (a) and (b) where open circles are data and solid lines are fits. The initial quintet population evolves into two non-interacting triplets, either both in the T_0 state or one in T_{+1} and the other in T_{-1}, with a characteristic timescale $\tau_d/4 = 3.0\pm0.1$ μs (see Supplementary Information for details of the dynamical model).

Each spectrum was fit with the sum of a polarized coupled triplet-pair and free triplet transitions. We find D = 1.138 GHz in good agreement with previously reported values in TIPS-pentacene thin films ($D = 1.2$ GHz)[30] and crystalline pentacene ($D = 1.381$ GHz)[42] suggesting a

similar triplet exciton radius. A near isotropic g was also reported[42] and was used in our fitting for simplicity. The 2D traces were fit by globally fitting the simulated transitions governed by $\frac{d\mathbf{p}}{dt} = \mathbf{Mp}$ where p is a 1×6 column vector of the populations of the states involved in SF (^{5}(TT) and the two mixed singlet-quintet states shown in Figure 6.3(a) and the subsequent decay to three dissociated triplets. The matrix **M** includes rates of triplet-pair dissociation, recombination, reverse intersystem crossing of the dissociated triplet, and thermalization within the triplet manifold. **M** is explicitly given in the Supplementary Information. By comparing panels (a) and (b) in

Figure 6.4. we see that this model is able to describe the data extremely well. The resulting fitted transients at spectral peaks are given in Figure 4 (c).

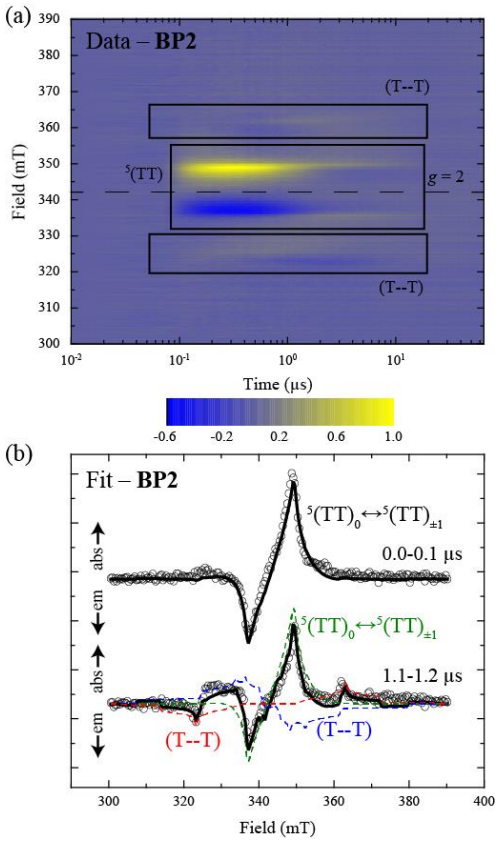

Figure 6.5. Singlet fission generates weakly coupled triplets in BP2. a, The 2D ESR spectra of BP2 at 80K. b, ESR traces integrated over two time intervals. The (TT) pairs generated upon

fission are strongly coupled. As the system relaxes the spectral signature of weakly coupled triplets emerges.

6.5 Time Resolved ESR on BP2

The measurements on BP2 give similar results to BP3, as shown in 6.5(a). As with BP3, the initial spectrum is simulated using coupled (TT) pairs where $\widehat{H}_{ee}$ is dominated by the exchange interactions (J_{iso} = 29.2 GHz) and is much larger than intra-triplet interactions (*D*: 1.093 GHz, *E*: 13 MHz). The coupling magnitude is greater in BP2 due to the shorter phenyl bridge giving rise to larger exchange contributions. In contrast to BP3, the spectrum which evolves from this initial state (see Figure 6.5b) is not well described by $T_0 \rightarrow T_{\pm 1}$ transitions of isolated triplets. In particular, the absorptive feature observed between 325 and 335 mT cannot be reproduced. Rather, the resulting triplets remain weakly coupled with $J_{iso} = -301$ MHz. The minor discrepancies with the fit may arise from small energy differences between distributions of nuclear configurations and hence values of J_{iso} (see Supplementary Information) due to rotatations about biaryl bonds[43]. This result confirms that the signal is comprised of the interaction of two triplets and could not have been generated by intersystem crossing of a single triplet from the pair-state to the ground state. Since the later signal is weak, although no signal from an uncoupled triplet was detected, we do not discount the possibility that the weakly coupled triplets decay independently of each other.

6.6 The Effect of Correlations on Triplet-triplet pair Dissociation

The plethora of long-lived electronic and spin correlations that exist in (TT) pairs suggests that complex dissociation kinetics will occur in these materials. Since the intensity of ESR transitions are proportional to the population difference between the two spin states involved it is difficult to ascertain whether signals decay as a result of recombination or thermalization within a

spin manifold. To obtain a more direct measure of the entire triplet population, we use transient absorption spectroscopy to measure the decay kinetics at a number of temperatures ranging from 7 to 300 K, of BP2 and BP3 molecules embedded in an inert dielectric matrix (see Methods). We have found that the matrix subtly affects the triplet generation and decay kinetics relative to solution experiments, but does not affect the qualitative processes under investigation, where singlet fission produces a (TT) pair which decays with biexponential kinetics (see Supplementary Information). We note that since transient absorption measurements are performed at zero external magnetic field, a quantitative comparison cannot be made to high field ESR measurements due to different mixing of singlet and quintet states and reverse intersystem crossing rates. However, this will not impact the qualitative photophysics. Therefore, the augmentation of the tr-ESR dataset with transient absorption spectroscopy is instructive for understanding the dissociation mechanism of (TT) pairs.

Using the assignments from ESR experiments, we can now unambiguously conclude that spin correlated triplet-triplet pairs in the ^{1}(TT) and ^{5}(TT) manifold exist during the first 100 – 500 ns and decay *via* concerted recombination to the ground state and *via* dissociation into two T_1 states. The nature of the dissociated triplet state is highly materials dependent since in BP2, where the chromophores are in closer proximity than BP3, weak electronic coupling persists. We extract the effective dissociation time constant by globally fitting the broadband transient absorption data using a sequential model such that $S_1 \rightarrow {}^{M}(TT) \rightarrow 2 \times T_1$. We find that as the temperature is decreased, the proportion of isolated (or weakly coupled) triplets also decreases (Figure 6). However, the scaling with temperature of the effective dissociation rate constant (k) associated with the $^{M}(TT) \rightarrow T_1$ conversion is not well described by simple empirical Arrhenius behaviour, and instead shows a saturation behaviour below ~ 50 K for both BP2 and BP3. This unusual

temperature dependence reflects the complex spin and electronic coupling interactions in (TT) pair states and suggests that a significant contribution from conformational distortion is needed to overcome activation barriers to dissociation. This is not surprising given the strong link between phonon modes and the triplet generation process.[44-46]

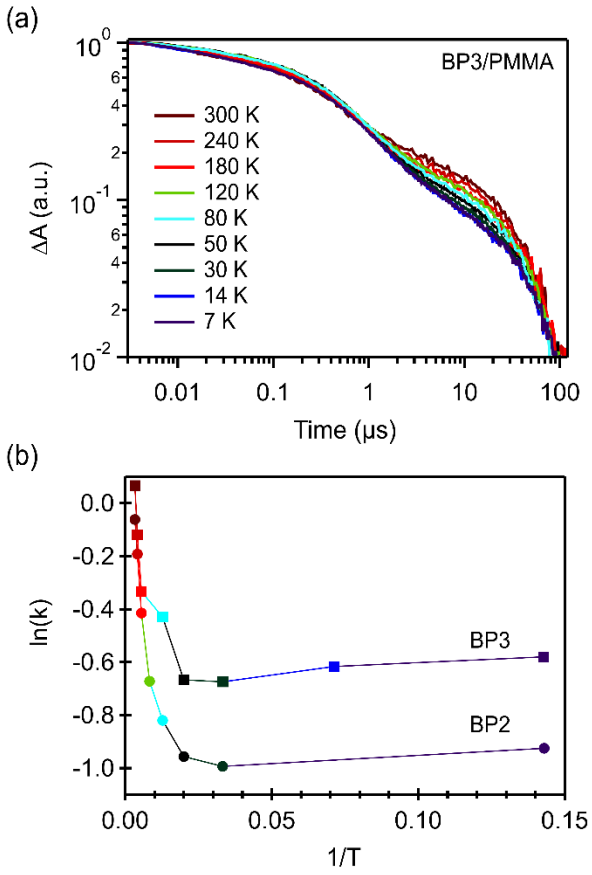

Figure 6.6. Temperature Dependent Dissociation Kinetics. a, The amplitude of the long decay component of the triplet signal of BP3 in a poly(methyl methacrylate) matrix is reduced as the temperature is reduced. b, The associated rate constant for dissociation of (TT) pairs into uncorrelated (or weakly coupled) triplets (k) for BP2 and BP3 shows a complex, non-Arrhenius behavior as a function of temperature.

6.7 Conclusions

We have used tr-ESR alongside TA PIA to identify the nature and dynamics of the spin-states involved in SF in pentacene dimers. We experimentally identify (TT) pair states with quintet character, which dissociate into two uncoupled (BP3) or weakly coupled (BP2) triplets on a time scale of ~5 μs. This dissociation is strongly thermally activated above T ~50 K, with only weak temperature dependence at lower temperatures. This observation of temperature dependent (TT) pair dissociation has precedent in previous models proposed by Tayebjee et al. when investigating the time-resolved photoluminescence of tetracene thin films,[6] and theoretical predictions by Krylov and coworkers,[47] however the combination of tr-ESR and TA in the present work represents the first unambiguous observation of this phenomenon. The results presented here provide design rules for optimising SF materials for device applications: the coupling between the chromophores will need to be strong enough to allow efficient generation of (TT) pairs but weak enough that the (TT) pair can still dissociate. The ease of preparation and modular molecular structure of the system used in this work will significantly aid future studies in this direction. Finally, we note that this work represents the first experimental observation of a quintet state in a closed shell organic molecule.

6.8 Methods

Pulsed laser, continuous wave tr-ESR

BP2 and BP3 were dissolved in toluene (0.2mM and 0.3mM) and transferred to a sealed quartz ESR tube under a nitrogen environment. UV-visible absorption spectroscopy was used to ensure that no aggregation had occurred. Experiments were undertaken using a Bruker Elexsys

E580. The samples were transferred to a cryogenically cooled (Oxford Instruments, CF935) resonator (Bruker, MD5) attached to an X-band microwave source (Bruker, Super X FT-EPR Bridge) operating at 9.61467GHz (Figures 3 and 4) or 9.61647GHz (Figure 5). Excitation to the first excited singlet state was achieved using a tunable ~7ns pulsed laser source (Opotek, Opolette). The resulting temporal resolution is approximately 100ns. Microwave absorption/emission was measured as a function of delay after the laser pulse for each field strength. The resulting spectral data was fit using Easyspin 5.01,[48] as outlined in the Supplementary Information.

Transient Absorption

BP2 or BP3 was dissolved in toluene along with commercial polymethyl methacrylate (PMMA). The solutions were drop cast on a sapphire window and the toluene allowed to evaporate. Concentration of BP2 and BP3 was adjusted to produce a dispersion of bipentacene in PMMA with suitable optical density for transient absorption spectroscopy, and UV-Visible spectroscopy was used to confirm successful dispersion of the bipentacene and absence of any aggregation effects. This sample was placed in a cryostat under vacuum and interrogated using a transient absorption spectroscopy setup, the details of which have been described recently.[23] Excitation with ~100 fs pulses tuned to 600 nm and broadband detection in the visible regime yielded the transient spectra.

6.9 Temperature Dependence of Transient Absorption Spectroscopy

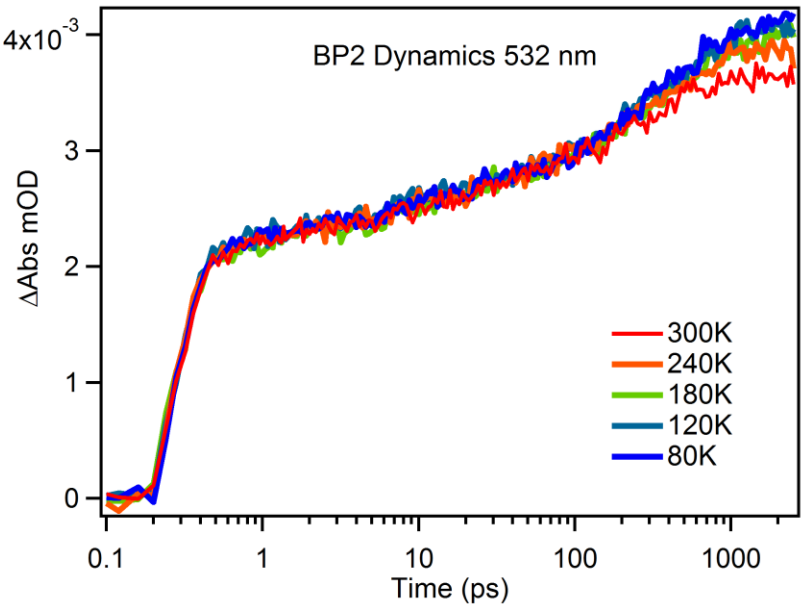

Figure 6.7. Triplet rise of BP2 in PMMA matrix, excited at 600 nm at 25 μJ/cm^2 and probed at the maximum triplet photoinduced absorption of 532 nm**.**

6.10 Global Analysis of Transient Absorption Results

Singlet fission for BP2 in the PMMA matrix, as probed here at the wavelength of maximum absorbance for the triplet exciton, is only weakly temperature dependent.

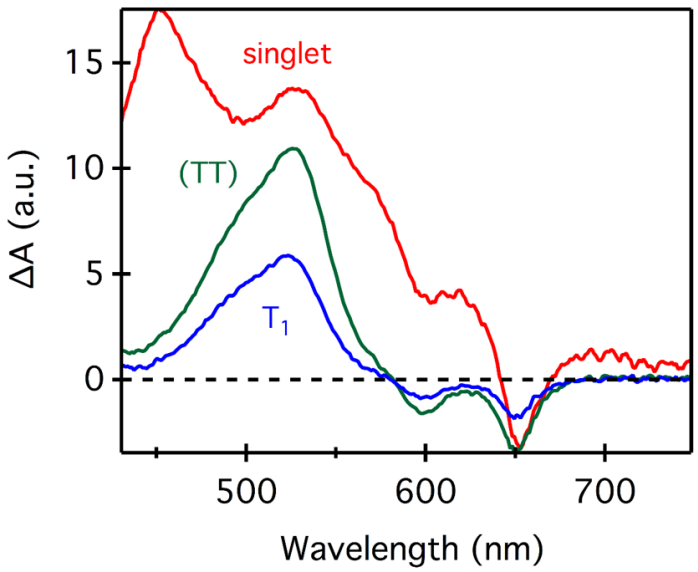

Figure 6.8. Singular value decomposition of transient species for BP3 in chloroform, excited at 360 nm, reveals a photoexcited triplet which decays into a (TT) state and then a (T) state, both of which feature similar spectra

Global analysis for transient absorption of BP3 in chloroform, excited at 360 nm (*~25 μJ/cm^2)* reveals three different species. The singlet exciton is populated initially and decays with a time constant of 6.4 ns to populate the triplet pair state which decays with time constants of 200 ns into the dissociated triplet state which (as shown in main text) that is spectrally indistinguishable from (TT), but decays with a slower time constant of 20 μs, similar to the triplet lifetime determined by sensitization experiments (see below).

6.11 Details of Triplet Sensitization Measurements

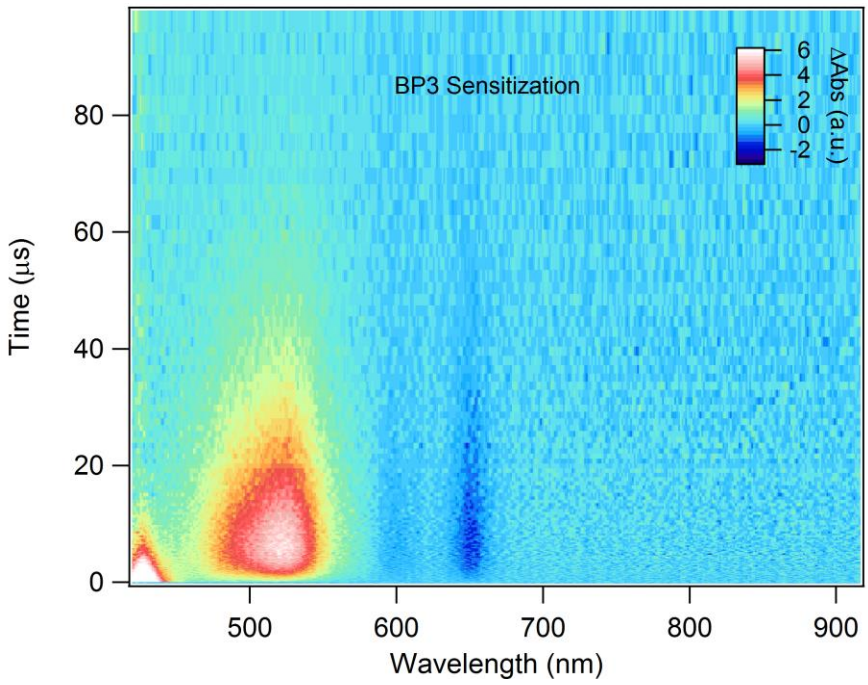

Figure 6.9. Triplet photosensitization of BP3 in chloroform, where triplet transfer from photoexcited anthracene populates individual triplet states on the bipentacene.

We have previously reported triplet photosensitization of BP2 by anthracene in chloroform. Here, we report the same technique applied to BP3. A solution of BP3 at less than 100 µM is dissolved along with ~20 mM anthracene in chlororform. The solution is degassed with bubbling argon, and 360 nm excitation, in this case *~50 µJ/cm*^{2}, populates anthracene triplets via intersystem crossing. Their photoinduced absorption can be seen prominently near 418 nm, and decays rapidly as transfer occurs and the signal near 520 nm corresponding to the BP3 triplet photoinduced absorption rises. Fitting the tail of the BP3 triplet after transfer has completed reveals a native 22 µs triplet lifetime for this compound.

6.12 Transient Absorption Color Plots for BP2 and BP3

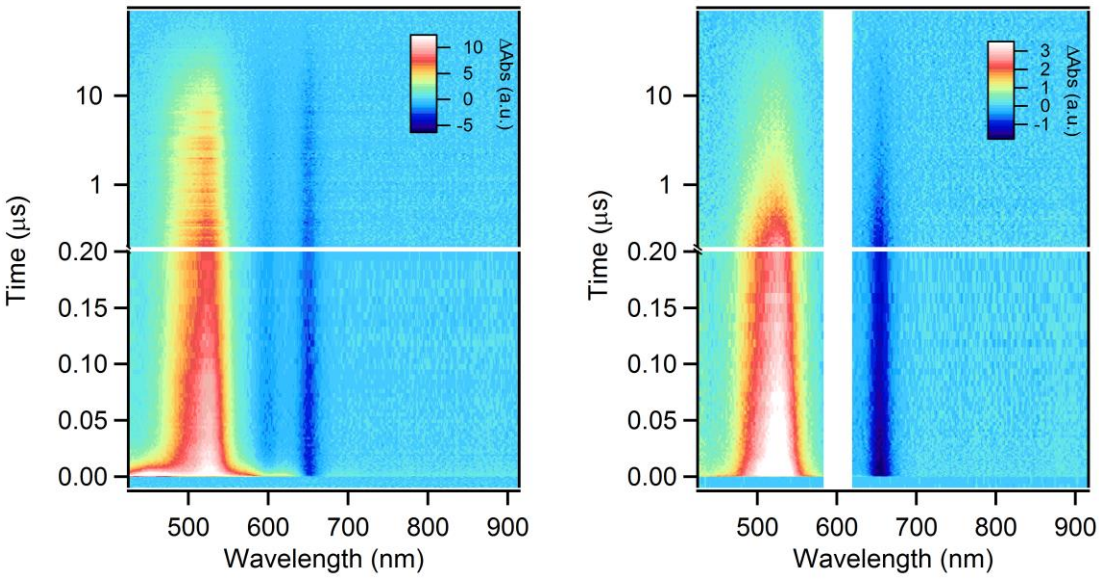

Figure 6.10. Transient absorption spectroscopy for BP3 excited in chloroform at 360 nm or in PMMA matrix at 600 nm, both at approximately 25 µJ/cm^2

The rates of singlet fission and triplet pair recombination change comparing BP3 in chloroform to the matrix, but the qualitative behavior is unchanged. In either case, singlet fission produce a triplet pair which recombines with two primary decay exponents.

General Synthetic Methods

All commercially obtained reagents/solvents were used as received; chemicals were purchased from Alfa Aesar®, Sigma-Aldrich®, Acros organics®, TCI America®, Mallinckrodt®, and Oakwood® Products, and were used as received without further purification. Unless stated

otherwise, reactions were conducted in oven-dried glassware under argon atmosphere. ^{1}H-NMR and ^{13}C-NMR spectra were recorded on Bruker 400 MHz (100 MHz for ^{13}C) and on 500 MHz (125 MHz for ^{13}C) spectrometers. Data from the ^{1}H-NMR and ^{13}C spectroscopy are reported as chemical shift (δ ppm) with the corresponding integration values. Coupling constants (*J*) are reported in hertz (Hz). Standard abbreviations indicating multiplicity were used as follows: s (singlet), b (broad), d (doublet), t (triplet), q (quartet), m (multiplet) and virt (virtual).

The mass spectral data for the compounds were obtained from XEVO G2-XS Waters® equipped with a QTOF detector with multiple inlet and ionization capabilities including electrospray ionization (ESI), atmospheric pressure chemical ionization (APCI), and atmospheric solids analysis probe (ASAP). The base peaks were usually obtained as $[M]^{+}$ or $[M+H]^{+}$ ions.

Absorption spectra were obtained on a Shimadzu UV 1800 UV-Vis spectrophotometer. Anhydrous solvents were obtained from a Schlenk manifold with purification columns packed with activated alumina and supported copper catalyst (Glass Contour, Irvine, CA). All reactions were carried out under argon unless otherwise noted.

Synthesis of bipentacene with Phenylene spacer BP2 and BP3:

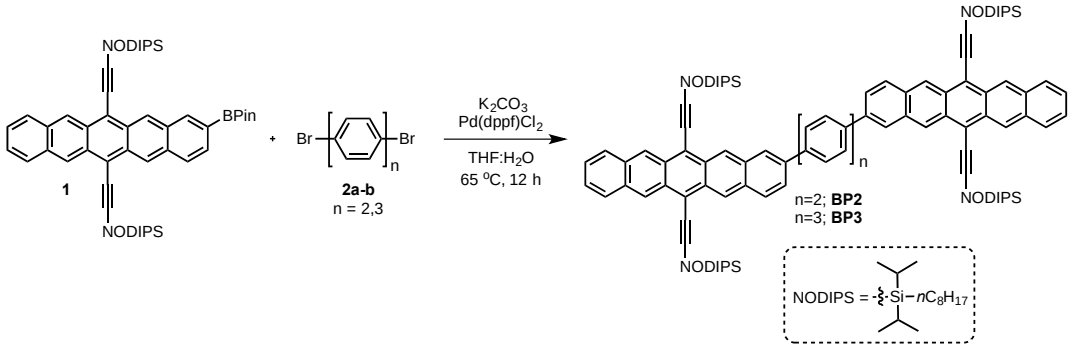

Procedure: To a dry flask, bpin-pentacene derivative 1[49] (250 mg, 2.3 *equiv.*), Dibromo-phenylene derivative 2a-b (1.0 *equiv.*), $Pd(dppf)Cl_2$ (0.1 *equiv.*) and K_2CO_3 (5.0 *equiv.*) were added. The

mixture was subjected to sequential vacuum and argon to remove oxygen followed by the addition of dry, degassed THF:H_2O (9:1, 60 mL). The reaction mixture was heated to 65 ^oC and maintained for 12 h in the dark. After the reaction, the solvent was evaporated and the crude mixture was purified in a silica column chromatography using hexanes:chloroform mixture as eluent.

Yield = 56% for BP2 and 43% for BP3.

MS (ESI): Calculated: 1707.1112; Observed: 1707.1128.

^{1}H-NMR (500 MHz, $CDCl_3$, δ ppm): 9.39-9.33 (m, 8H), 8.26 (s, 2H), 8.14-8.12 (m, 2H), 8.04-8.01 (m, 4H), 7.96-7.95 (m, 4H), 7.89-7.87 (m, 4H), 7.83-7.80 (m, 2H), 7.46-7.44 (m, 4H), 1.84-1.78 (m, 8H), 1.59-1.53 (m, 9H), 1.42-1.37 (m, 69H), 1.29-1.24 (m, 18H), 1.03-0.99 (m, 8H) and 0.88-0.82 (m, 12H).

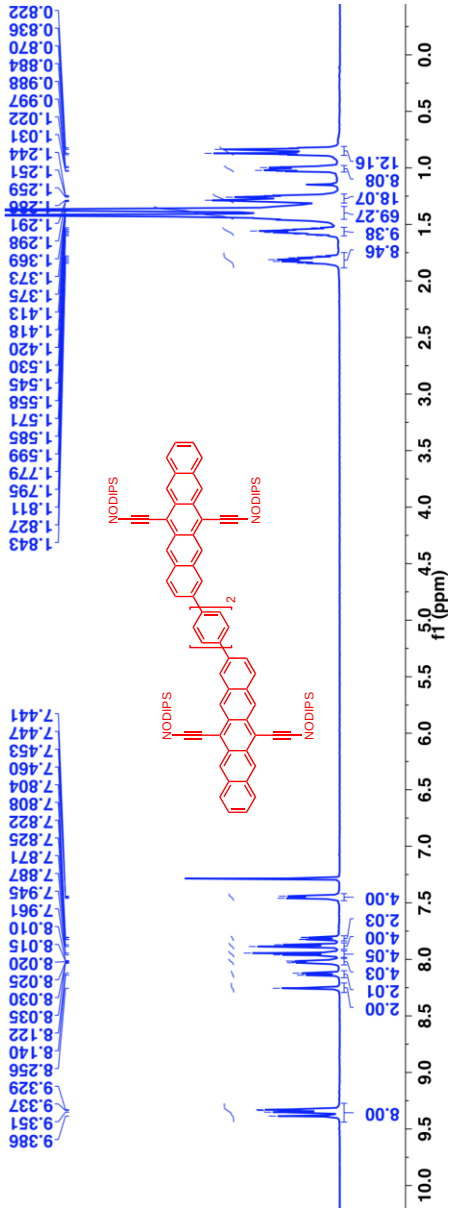

^{13}C-NMR (125 MHz, $CDCl_3$, δ ppm): 139.6, 139.55, 1332.5, 132.4, 132.3, 131.6, 130.97, 130.8, 130.76, 130.6, 129.4, 128.7, 127.5, 127.4, 126.7, 126.4, 126.3, 126.2, 126.1, 125.7, 118.5, 118.3, 107.6, 107.5, 104.7, 104.6, 34.14, 34.10, 32.04, 32.0, 29.6, 29.5, 29.48, 29.44, 25.1, 25.0, 22.7, 18.8, 18.79, 18.54, 18.52, 14.2, 14.1, 12.3, 10.6 and 10.5.

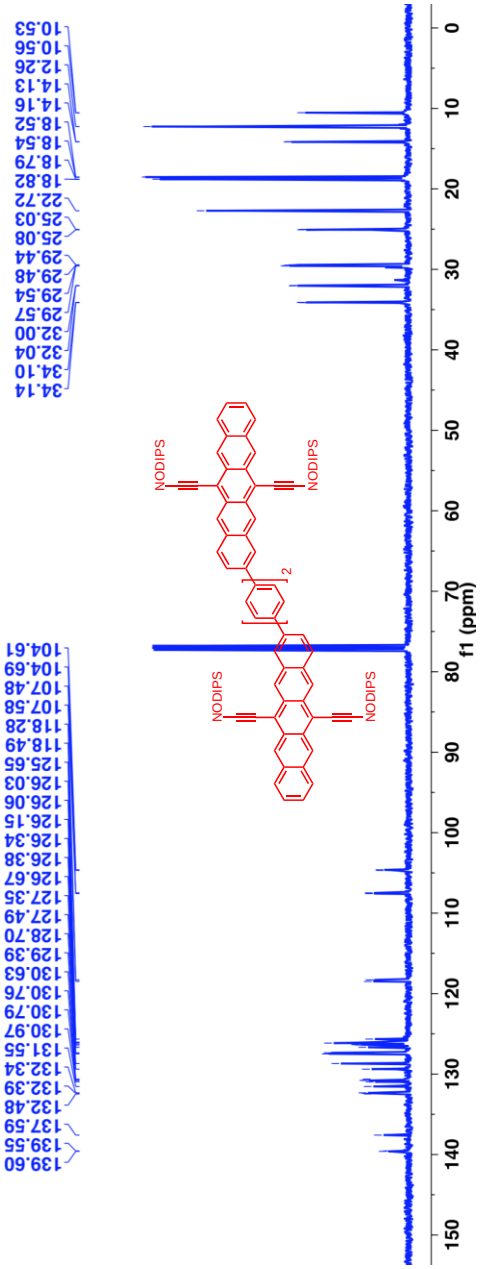

MS (ESI): Calculated: 1783.1427; Observed: 1783.1441.

^{1}H-NMR (500 MHz, $CDCl_3$, δ ppm): 9.38-9.33 (m, 8H), 8.26 (s, 2H), 8.14-8.12 (m, 2H), 8.03-8.01 (m, 4H), 7.97-7.95 (m, 4H), 7.89-7.81 (m, 10H), 7.46-7.44 (m, 4H), 1.83-1.79 (m, 8H), 1.41-1.28 (m, 95H), 1.02-0.98 (m, 9H) and 0.86-0.83 (m, 12H).

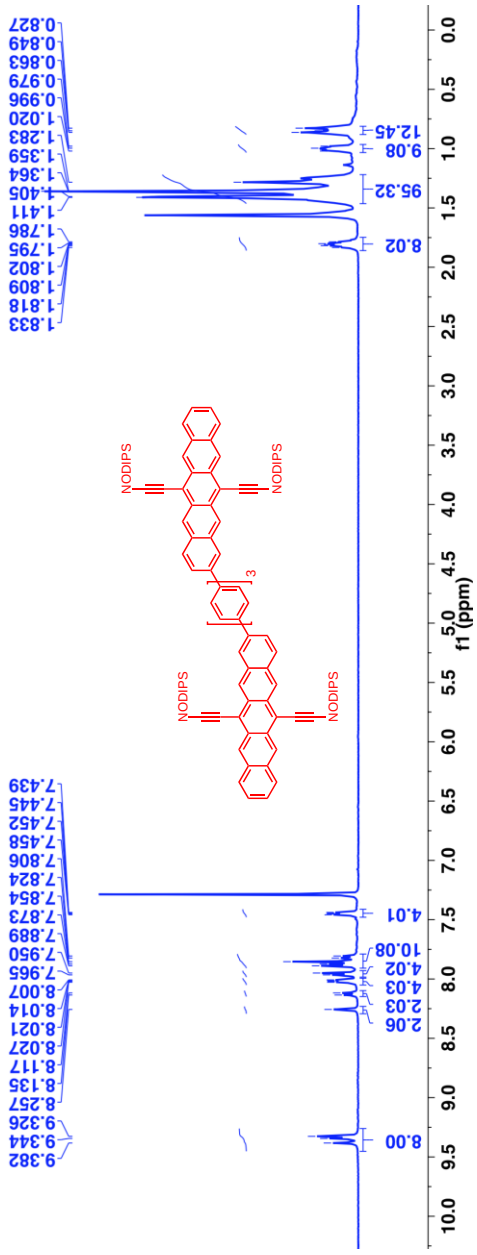

^{13}C-NMR (125 MHz, $CDCl_3$, δ ppm): 139.8, 139.7, 139.6, 137.7, 132.5, 132.4, 132.3, 131.5, 130.95, 130.8, 130.7, 130.6, 129.4, 128.7, 127.6, 127.5, 127.4, 126.6, 126.4, 126.3, 126.2, 126.15, 126.05, 125.7, 118.5, 118.3, 107.6, 107.5, 104.6, 104.55, 34.1, 34.06, 32.0, 31.97, 29.53, 29.50, 29.44, 29.40, 25.0, 24.99, 22.68, 18.8, 18.75, 18.5, 18.48, 14.13, 14.10, 12.2, 10.51 and 10.50.

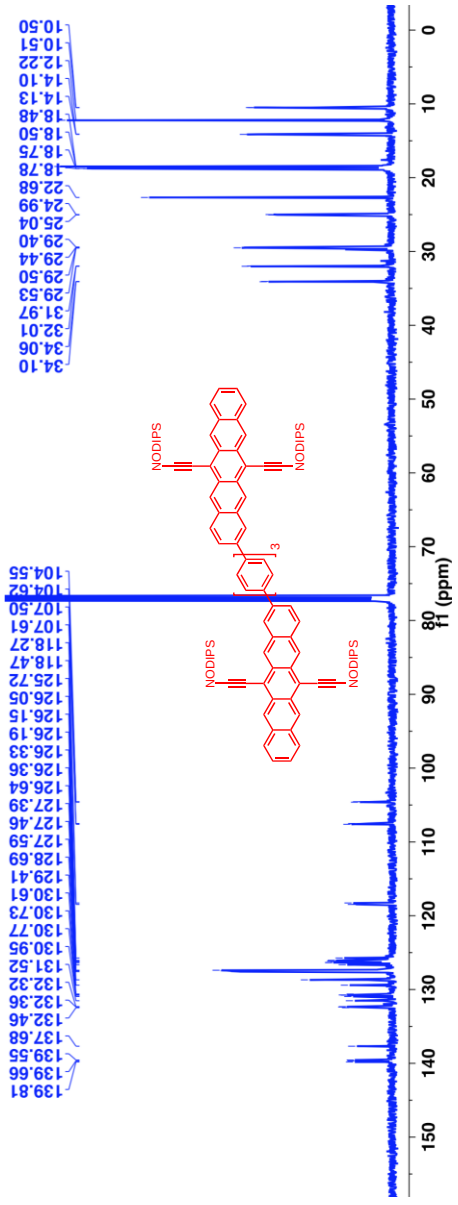

13. References

(1) Smith, M. B.; Michl, J. *Chemical Reviews* **2010**, *110*, 6891.

(2) Tayebjee, M. J. Y.; McCamey, D. R.; Schmidt, T. W. *J. Phys. Chem. Lett.* **2015**, *6*, 2367.

(3) Smith, M. B.; Michl, J. *Annual Review of Physical Chemistry* **2013**, *64*, 361.

(4) Hanna, M. C.; Nozik, A. J. *Journal of Applied Physics* **2006**, *100*, 74510.

(5) Tomkiewicz, Y.; Groff, R. P.; Avakian, P. *Journal of Chemical Physics* **1971**, *54*, 4504.

(6) Tayebjee, M. J. Y.; Clady, R. G. C. R.; Schmidt, T. W. *Physical Chemistry Chemical Physics* **2013**, *15*, 14797.

(7) Burdett, J. J.; Gosztola, D.; Bardeen, C. J. *Journal of Chemical Physics* **2011**, *135*, 214508.

(8) Burdett, J. J.; Muller, A. M.; Gosztola, D.; Bardeen, C. J. *Journal of Chemical Physics* **2010**, *133*, 144506.

(9) Wilson, M. W. B.; Rao, A.; Johnson, K.; Gélinas, S.; di Pietro, R.; Clark, J.; Friend, R. H. *J. Am. Chem. Soc.* **2013**, *135*, 16680.

(10) Walker, B. J.; Musser, A. J.; Beljonne, D.; Friend, R. H. *Nature Chemistry* **2013**, *5*, 1019.

(11) Stern, H. L.; Musser, A. J.; Gelinas, S.; Parkinson, P.; Herz, L. M.; Bruzek, M. J.; Anthony, J.; Friend, R. H.; Walker, B. J. *Proc. Natl Acad. Sci.* **2015**, *112*, 7656.

(12) Akdag, A.; Wahab, A.; Beran, P.; Rulíšek, L.; Dron, P. I.; Ludvík, J.; Michl, J. *J. Org. Chem.* **2015**, *80*, 80.

(13) Greyson, E. C.; Stepp, B. R.; Chen, X.; Schwerin, A. F.; Paci, I.; Smith, M. B.; Akdag, A.; Johnson, J. C.; Nozik, A. J.; Michl, J.; Ratner, M. A. *The Journal of Physical Chemistry B* **2010**, *114*, 14223.

(14) Low, J. Z.; Sanders, S. N.; Campos, L. M. *Chem. Mater.* **2015**, *27*, 5453.

(15) Müller, A. M.; Avlasevich, Y. S.; Müllen, K.; Bardeen, C. J. *Chemical Physics Letters* **2006**, *421*, 518.

(16) Müller, A. M.; Avlasevich, Y. S.; Schoeller, W. W.; Müllen, K.; Bardeen, C. J. *Journal of the American Chemical Society* **2007**, *129*, 14240.

(17) Zeng, T.; Goel, P. *J. Phys. Chem. Lett.* **2016**, *7*, 1351.

(18) Korovina, N. V.; Das, S.; Nett, Z.; Feng, X.; Joy, J.; Haiges, R.; Krylov, A. I.; Bradforth, S. E.; Thompson, M. E. *J. Am. Chem. Soc.* **2016**, *138*, 617.

(19) Lukman, S.; Musser, A. J.; Chen, K.; Athanasopoulos, S.; Yong, C. K.; Zeng, Z.; Ye, Q.; Chi, C.; Hodgkiss, J. M.; Wu, J.; Friend, R. H.; Greenham, N. C. *Adv. Funct. Mater.* **2015**, *25*, 5452.

(20) Sakuma, T.; Sakai, H.; Araki, Y.; Mori, T.; Wada, T.; Tkachenko, N. V.; Hasobe, T. *The Journal of Physical Chemistry A* **2016**, *120*, 1867.

(21) Sanders, S. N.; Kumarasamy, E.; Pun, A. B.; Trinh, M. T.; Choi, B.; Xia, J.; Taffet, E. J.; Low, J. Z.; Miller, J. R.; Roy, X.; Zhu, X. Y.; Steigerwald, M. L.; Sfeir, M. Y.; Campos, L. M. *J. Am. Chem. Soc.* **2015**, *137*, 8965.

(22) Zirzlmeier, J.; Lehnherr, D.; Coto, P. B.; Chernick, E. T.; Casillas, R.; Basel, B. S.; Thoss, M.; Tykwinski, R. R.; Guldi, D. M. *Proc. Natl Acad. Sci.* **2015**, *112*, 5325.

(23) Sanders, S. N.; Kumarasamy, E.; Pun, A. B.; Steigerwald, M. L.; Sfeir, M. Y.; Campos, L. M. *Angewandte Chemie* **2016**, *128*, 3434.

(24) Rao, A.; Wilson, M. W. B.; Albert-Seifried, S.; Di Pietro, R.; Friend, R. H. *Physical Review B* **2011**, *84*, 195411.

(25) Wilson, M. W. B.; Rao, A.; Clark, J.; Kumar, R. S. S.; Brida, D.; Cerullo, G.; Friend, R. H. *Journal of the American Chemical Society* **2011**, *133*, 11830.

(26) Merrifield, R. E. *Pure and Applied Chemistry* **1971**, *27*, 481.

(27) Burdett, J. J.; Bardeen, C. J. *J. Am. Chem. Soc.* **2012**, *134*, 8597.

(28) Bayliss, S. L.; Chepelianskii, A. D.; Sepe, A.; Walker, B. J.; Ehrler, B.; Bruzek, M. J.; Anthony, J. E.; Greenham, N. C. *Phys. Rev. Lett.* **2014**, *112*, 238701.

(29) Piland, G. B.; Burdett, J. J.; Kurunthu, D.; Bardeen, C. J. *J. Phys. Chem. C* **2013**, *117*, 1224.

(30) Bayliss, S. L.; Thorley, K. J.; Anthony, J. E.; Bouchiat, H.; Greenham, N. C.; Chepelianskii, A. D. *Phys. Rev. B* **2015**, *92*, 115432.

(31) Congreve, D. N.; Lee, J.; Thompson, N. J.; Hontz, E.; Yost, S. R.; Reusswig, P. D.; Bahlke, M. E.; Reineke, S.; Van Voorhis, T.; Baldo, M. A. *Science* **2013**, *340*, 334.

(32) Jadhav, P. J.; Mohanty, A.; Sussman, J.; Lee, J.; Baldo, M. A. *Nano Letters* **2011**, *11*, 1495.

(33) Thompson, N. J.; Hontz, E.; Chang, W.; Van Voorhis, T.; Baldo, M. *Magnetic Field Dependence of Singlet Fission in Solutions of Diphenyl Tetracene*, 2015; Vol. 373.

(34) Agostini, G.; Corvaja, C.; Giacometti, G.; Pasimeni, L. *Chemical Physics* **1993**, *173*, 177.

(35) Yarmus, L.; Rosenthal, J.; Chopp, M. *Chemical Physics Letters* **1972**, *16*, 477.

(36) Swenberg, C. E.; van Metter, R.; Ratner, M. *Chem. Phys. Lett.* **1972**, *16*, 482.

(37) Sanders, S. N.; Kumarasamy, E.; Pun, A. B.; Appavoo, K.; Steigerwald, M. L.; Campos, L. M.; Sfeir, M. Y. *J. Am. Chem. Soc.* **2016**, *138*, 7289.

(38) Jeschke, G.; Spiess, H.-W. In *Novel NMR and EPR techniques*; Dolinšek, J., Vilfan, M., Žumer, S., Eds. 2006; Vol. 63, p 21.

(39) Bencini, A.; Gatteschi, D. *EPR of Exchange Coupled Systems*; Springer-Verlag: Berlin, 1990.

(40) Snaathorst, D.; Keijzers, C. P. *Molecular Physics* **1984**, *51*, 509.

(41) Benk, H.; Sixl, H. *Molecular Physics* **1981**, *42*, 779.

(42) Van Strien, A. J.; Schmidt, J. *Chem. Phys. Lett.* **1980**, *70*, 513.

(43) Kumarasamy, E.; Sanders, S. N.; Pun, A. B.; Vaselabadi, S. A.; Low, J. Z.; Sfeir, M. Y.; Steigerwald, M. L.; Stein, G. E.; Campos, L. M. *Macromolecules* **2016**, *49*, 1279.

(44) Zeng, T.; Hoffmann, R.; Ananth, N. *Journal of the American Chemical Society* **2014**, *136*, 5755.

(45) Bakulin, A. A.; Morgan, S. E.; Kehoe, T. B.; Wilson, M. W. B.; Chin, A. W.; Zigmantas, D.; Egorova, D.; Rao, A. *Nat Chem* **2016**, *8*, 16.

(46) Musser, A. J.; Liebel, M.; Schnedermann, C.; Wende, T.; Kehoe, T. B.; Rao, A.; Kukura, P. *Nature Physics* **2015**, *11*, 352.

(47) Feng, X.; Krylov, A. I. *Physical Chemistry Chemical Physics* **2016**, *18*, 7751.

(48) Stoll, S.; Schweiger, A. *Journal of Magnetic Resonance* **2006**, *178*, 42.

(49) Kumarasamy, E.; Sanders, S. N.; Pun, A. B.; Vaselabadi, S. A.; Low, J. Z.; Sfeir, M. Y.; Steigerwald, M. L.; Stein, G. E.; Campos, L. M. *Macromolecules* **2016**, *49*, 1279.

7 Intramolecular Singlet Fission in Oligoacene Heterodimers

7.1 Preface

This chapter is based on a publication entitled "Intramolecular Singlet Fission in Oligoacene Heterodimers" published in *Angewandtie Chemie* by Samuel N. Sanders, Elango Kumarasamy, Andrew B. Pun, Michael L. Steigerwald, Matthew Y. Sfeir, Luis M. Campos. Elango, Andrew and I synthesized all molecules in the laboratory of Professor Campos while I performed all spectroscopic work in the laboratory of Dr. Sfeir.

7.2 Introduction

Singlet exciton fission has attracted renewed interest in the last decade due to its potential to enhance power conversion efficiencies of single junction solar cells beyond the Shockley-Queisser Limit.[1-6] The recent discovery of an efficient intramolecular singlet fission (iSF) process in conjugated polymers and small molecules has dramatically increased the quantity and variety of materials that exhibit this process.[7-13] Moreover, the mechanism of triplet pair formation and decay may be quite different in dimers of oligoacenes relative to their monomer counterparts in the solid state, where singlet fission is an intermolecular process (xSF). For example, donor-acceptor polymers reported by our group are presumed to undergo SF *via* charge transfer (CT) states, similar to the leading hypothesis for the mechanism for solid state SF.[7,14-16] However, there is no intrinsic CT character in molecular dimers, yet they have been reported to undergo SF at faster rates than the donor-acceptor polymers. There are various important aspects that are still being actively investigated in terms of electronic structure, excited state energies and dynamics.[17-24] Thus it is

important to elucidate the mechanistic and energetic requirements for iSF in order to optimize the design of practical SF chromophores.

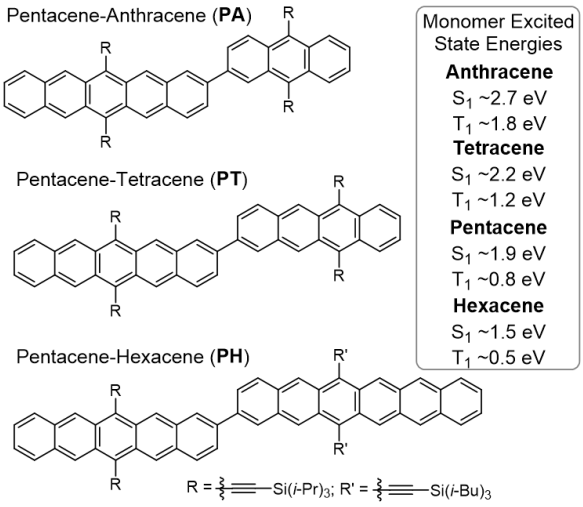

Scheme 7.1 Oligoacene heterodimers and the excited state energies of the respective monomers.

Molecular dimers made up of two covalently linked SF-capable monomers have long been considered as candidates for iSF.[25,26] Early work on tetracene dimers showed low iSF yields, presumably because of the endothermicity of the iSF process or the connectivity employed.[27,28] Pentacene dimers, on the other hand, have recently been reported to undergo iSF quantitatively.[10,12] The potential to develop families of oligoacene dimers through systematic studies has motivated us to revisit the concept of singlet fission in oligoacene "mixtures", which was briefly explored in the 1970s when several groups studied crystals of one type of acene doped with another type of acene.[29-31] In this vein, we explore iSF in asymmetric systems where two different oligoacene monomers are covalently linked (Scheme 1). This design feature allows us to systematically adjust the energetics of the iSF process, affecting both the driving force for singlet fission and the total energy of the resulting triplet pair. In these heterodimers, we demonstrate that the relevant singlet energy for iSF is given by the lower singlet state energy monomer, and the resulting triplet pair is

a sum of the individual monomer triplets. Therefore, the fundamental equation for energy conservation is $E(S_1[X]) \geq E(T_1[X]) + E(T_1[Y])$, in a dimer comprising monomer X coupled to Y. For example, the pentacene-tetracene heterodimer is nearly isoergic (S_1[**Pentacene**] ~1.9 eV, T_1[**Pentacene**] ~0.8 eV, T_1[**Tetracene**] ~1.2eV), while our previously reported bipentacene molecule is exoergic (S_1[**Pentacene**] > 2xT_1[**Pentacene**]).[10,32-35] Furthermore, since pentacene-anthracene is significantly endoergic ($E(S_1$[**Pentacene**]) < $E(T_1$[**Pentacene**]) + $E(T_1$[**Anthracene**])), it is not expected to undergo iSF. Here, we test this hypothesis and demonstrate that asymmetric dimers undergo fast and efficient iSF, provided that the singlet state is not significantly lower in energy than the resulting triplet pair. We also find that subsequent decay of the triplet pairs formed in iSF-capable heterodimers is primarily non-radiative, and it obeys the energy gap law for non-radiative recombination.[36-38]

In order to investigate singlet fission in oligoacene heterodimers, the molecules shown in Scheme 1 were synthesized *via* Suzuki coupling chemistry (See SI for details).[10] The compounds are labeled as **PA**, **PT**, **PH**, where **P**, **A**, **T** and **H** refers to pentacene, anthracene, tetracene, and hexacene respectively. We also compare these results to bipentacene (**BP**), which we recently reported, in which two pentacenes are similarly covalently attached at the 2-position. The inclusion of tri-isopropylsilyl acetylene (TIPS), or in the case of hexacene, tri-isobutylsilyl acetylene groups (TIBS), renders these heterodimers soluble and relatively stable in solution.[39-43]

7.3 Steady State Absorption

The steady state absorption spectra of the heterodimers show the characteristic features of both monomers (Figure 1A). In **PA**, **PT,** and **PH**, we observe the prominent low-energy singlet

transition peak associated with TIPS-pentacene (S_1[**P**]) at ~660 nm and, respectively, its complement, with the anthracene peak (S_1[**A**]) at ~ 470 nm, the tetracene peak (S_1[**T**]) at ~550 nm, and the hexacene peak (S_1[**H**]) at ~750 nm. A small redshift is observed in the dimers, relative to the monomer features. When coupling pentacenes at the 2-position, we also observe a high-energy feature in the ground state absorption. That feature, previously reported for 2,2' bipentacene (**BP**), is also observed in these compounds.[10] It can be seen clearly in Figure 1A for **PA**, but this peak in **PT** and **PH** has been omitted for clarity (see SI for full spectra). This high-energy feature is specific to directly coupled acenes at the position shown, and does not correspond to a peak in the parent monomers.

7.4 Transient Absorption Spectroscopy

We use broadband transient absorption spectroscopy (TAS) to understand the exciton dynamics in these molecules. Since we are probing the energetic requirements for iSF, the chromophores are pumped at the lower singlet energy selectively (**P** transitions for **PA** and **PT**, and **H** transitions for **PH**) to determine if iSF occurs without significant excess excitation energy. Figure 1B shows the resulting 2D plot of the spectral evolution of the transient absorption spectra as a function of time.

In the case of **PA**, where iSF is expected to be significantly endothermic, we observe no significant spectral changes of the singlet state features. In fact, the photophysics of this heterodimer are similar to TIPS-pentacene, with a photoexcited singlet that decays with a ~11.5 ns time constant primarily through a radiative pathway. The singlet lifetime is long enough to permit a small amount of triplet formation via intersystem crossing (ISC). By comparing the

magnitude of the ground state bleach in the singlet and triplet manifold, we calculate a triplet yield of ~10% giving an ISC time constant of 104 ns.[34] The triplet relaxation dynamics are similar to TIPS-pentacene as well, with a decay time of 17.4 μs. This result verifies that, in the case where energetics are not appropriate for iSF, no additional decay pathways are present in these compounds beyond the typical monomer excited state deactivation.

However, in **PT** and **PH**, singlet fission is roughly isoergic and exothermic, respectively. In these systems, TAS reveals dynamics similar to those observed in **BP**, where the photoexcited singlet rapidly decays into a triplet signal in dilute solution, consistent with iSF.[10] The triplet pair feature produced by iSF is dominated by the photoinduced absorption of the larger acene in each case, as the triplet absorption cross-section increases with increasing acene length.[32,34,44]

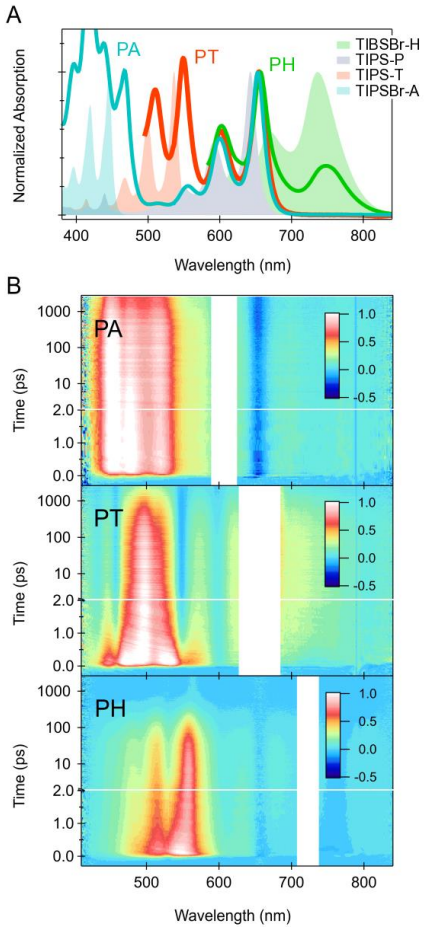

Figure 7.1. (A) Steady-state absorption spectra of **PA**, **PT** and **PH**, along with a TIPS-anthracene derivative, TIPS-tetracene, TIPS-pentacene and a TIBS-hexacene derivative. Absorption spectra are taken in chloroform and normalized at the pentacene absorption feature. (B) Transient absorption spectra of **PA** excited at 600 nm, **PT** excited at 660 nm and **PH** excited at 730 nm, at fluence of 25 $\mu J/cm^2$ in chloroform. In each case, warmer colors represent increased absorption after excitation, and cooler colors represent decreased absorption.

The triplet pair features ground-state bleach (GSB) characteristics of both monomers in magnitudes corresponding to the relative absorption heights in the linear spectra, as expected for a triplet pair where both monomers are bleached.

The time constants for singlet fission (τ_{iSF}) and triplet pair ($2xT_1$) decay (τ_{2xT1}) are shown in Table 1. Since there is no indication of a parasitic process that would compete with the singlet fission process, and the rates of SF are all orders of magnitude faster than fluorescence or internal

conversion in **PT** and **PH**, the data is consistent with a quantitative iSF process. In other words, the rates of singlet decay and triplet formation are directly correlated, and the yields are determined only by the kinetic competition between iSF and the intrinsic decay processes (~ 10 ns).[7,10,32,34] This is in stark contrast to the dynamics observed in **PA**.

Table 7.1. Time constants for singlet fission (τ_{iSF}) and triplet pair recombination (τ_{2xT1}) for the pentacene-tetracene (**PT**) and pentacene-hexacene (**PH**) heterodimers, compared to bipentacene (**BP**, homodimer).

Compound*	**τ_{ISC} (ps)**	**τ_{T1} (ns)**
PA	1.0 x 10^5	1.74 x 10^4
iSF Compound	**τ_{iSF} (ps)**	**τ_{2xT1} (ns)**
PT	0.83	2.4
BP	0.76	0.45
PH	1.2	0.21

*Compound **PA**: S_1 lifetime = 11.5 ns, ~ 10% T yield.

Beyond the kinetics, the heterodimers enable us to probe the spatial dynamics of iSF since, due to asymmetry, the relative spectral weight of GSB in **P** and **T** will change when converting between different exciton states. Even though we qualitatively describe the absorption spectra of the heterodimers as combinations of the absorption features due to the individual monomers, when we pump the longer-wavelength absorption in any of the heterodimers both ground-state absorptions are bleached, although the longer-wavelength absorption is bleached more thoroughly than the shorter-wavelength absorption. This asymmetry in bleaching is in contrast to

quantitative bleaching of both chromophores in bipentacenes, and it arises from the greater portion of the excited singlet wavefunction residing on the monomer unit that is associated with the lower-energy excited state.[10,12] Averaging over vibrational and rotational degrees of freedom in the ensemble of molecules can thus lead to some partial bleaching (not quantitative, but non-zero) of the higher singlet-energy chromophore in the singlet.

7.5 Triplet Photosensitization Experiments

In order to characterize the triplet pair, we compare singlet fission studies with sensitization experiments, in which the triplet states are populated in the heterodimers via collisional transfer from a triplet donor (anthracene) in excess concentration (Figure 2). In the case of the heterodimers, the anthracene can collide with and populate a triplet on either monomer. Interestingly, we do not observe any triplet transfer, despite the inequivalent triplet energies of the monomers. Presumably, the triplets cannot transfer in the heterodimers reported here because of the absence of the significant wavefunction overlap required for Dexter energy transfer, due to the highly-localized nature of acene triplets. [10,45] Given the pump energy employed in the sensitization experiments, individual molecules contain just one triplet exciton. Therefore, the spectra of individual triplets would appear significantly different from the triplet pair spectra produced by iSF. However, the ensemble contains a roughly even number of triplets on each monomer and can therefore be compared to iSF, which generates triplet pairs.

The photoinduced absorption (PIA) spectra of the T_1 resulting from sensitization and $2xT_1$ resulting from singlet fission are similar, but not identical. Modest spectral shifts of magnitude and/or wavelength of the PIA are found, consistent with reports of directly coupled pentacene

dimers.[10-12] These shifts result from the strong correlation of the triplet pair when in close proximity, as demonstrated previously.[10] While these spectra are similar, the dynamics are significantly different. In general, the triplet pairs produced from iSF tend to decay on much shorter timescales than individual triplets. In the case of **PT** and **PH**, the lifetime of the $2xT_1$ is less than 3 ns, as opposed to tens of microseconds for their individual T_1.[32,34,44] The correlated triplet pair decay is apparent since both the pentacene and tetracene GSB signals decay at the same rate.

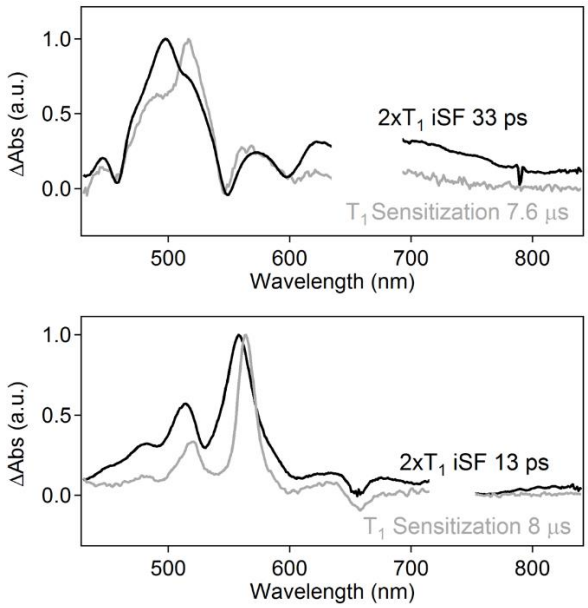

Figure 7.2. Comparison of triplet transient absorption spectra obtained by photosensitization (single T_1) and singlet fission ($2xT_1$) in **PT** and **PH**.

While energetics have a dramatic impact on whether or not iSF will occur, the rates of iSF for **PT**, **BP**, and **PH** are surprisingly insensitive to the driving force, each being ~1ps. In contrast, the recombination kinetics have a clear dependence on overall triplet pair energy. The lifetime of the triplet pair decreases following the trend, **PT** > **BP** > **PH**, in agreement with the trend of decreasing energy of the triplet state (Figure 3). The triplet pair lifetime varies from 0.21 ns to 2.4 ns as the expected triplet pair energy decreases from ~2.0 eV to ~1.3 eV. In all cases, the triplet

pair is significantly less emissive than the singlet, and these lifetimes are much shorter than the radiative lifetime of the monomers. Therefore, the decay in the directly linked acene series is primarily non-radiative and can be explained by invoking a simple energy gap argument for non-radiative decay processes, where the rate of such a multiphonon process is inversely proportionate to the number of photons needed, i.e. the energy above the ground state.[36-38]

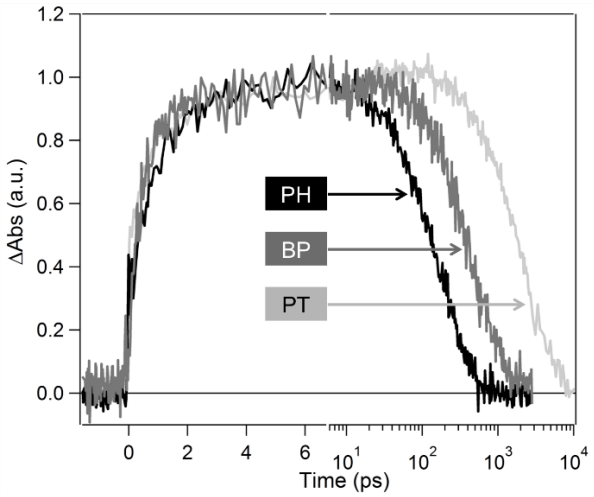

Figure 7.3. Rise and decay kinetic traces of the triplet pair in **PH**, **BP**, and **PT**, probed at the λ_{max} of the triplet excited state absorption spectra (683, 712, 707 nm respectively).

In summary, we have synthesized and characterized a series of pentacene-oligoacene heterodimers. In **PA**, iSF is significantly endothermic and does not occur. Instead, the compound undergoes the slow singlet state deactivation processes of internal conversion, fluorescence and a small amount of ISC. However, in **PT** and **PH**, where iSF is energetically feasible, iSF occurs with ~1 ps time constant, as demonstrated by ultrafast transient absorption spectroscopy and triplet photosensitization experiments. Triplet pair recombination adheres to the energy gap law, but formation of the triplet pair appears to be insensitive to the driving force in iSF heterodimers. This study opens up a new possibility to tune the excited state dynamics of singlet fission in oligoacenes. Additionally, these heterodimers offer a broadly applicable strategy for creating iSF materials

where energetics can be tuned and spectrally resolved monomer transitions can be exploited for detailed mechanistic studies of singlet fission.

7.6 Methods

Transient Absorption Spectroscopy. Transient absorption spectroscopy was performed using a commercial Ti:Sapphire laser system (SpectraPhysics |800 nm|100fs|3.5mJ|1kHz). A commercial optical parametric amplifier (LightConversion) was used to generate excitation light. Supercontinuum probe light was generated by focusing the 800 nm fundamental into a sapphire disc. The probe light was split into signal and reference beams, which were detected on a shot-by-shot basis by a fibre-coupled silicon (visible) or InGaAs (infrared) diode array. The pump–probe delay was controlled by a mechanical delay stage (Newport).

Global Analysis. Global (singular value decomposition-based) and target (differential equation-based) analysis were performed with the Glotaran software package (http://glotaran.org). These methods yield more accurate fits of rate constants because they treat the full data set in aggregate. A simple sequential decay model ($S_1 \rightarrow T_1 \rightarrow S_0$) was sufficient to accurately reproduce the exciton dynamics for **PH** and **PT**.

Triplet Photosensitization. A solution of ~20 mM anthracene in chloroform, along with a much smaller concentration of heterodimer (~50 μM) was excited by 360 nm pump light. This pump pulse primarily excites anthracene which, following intersystem crossing (ISC), results in

anthracene triplets. Diffusional collisions subsequently transfer these triplets to the heterodimer. An optical probe pulse then interrogates the resulting triplet state.

7.7 Details of Global Analysis

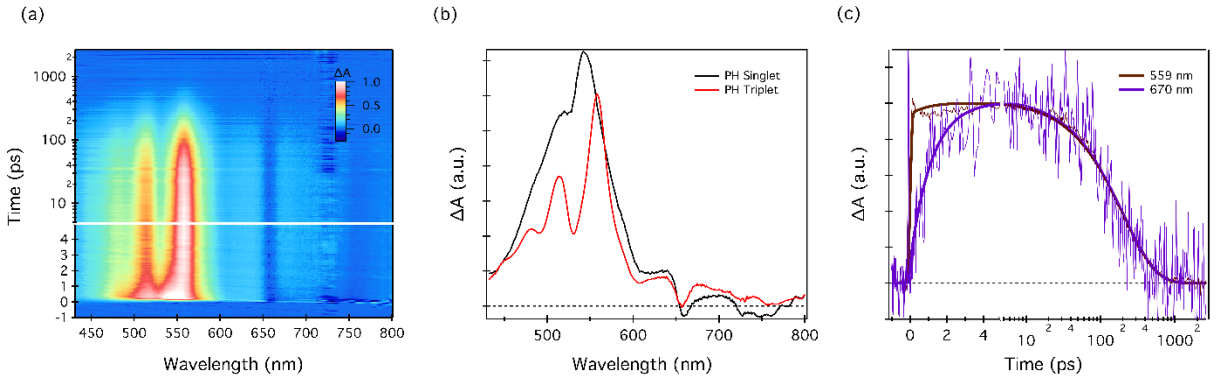

Figure 7.4. a) Transient absorption spectroscopy of **PH** as a dilute solution in chloroform. b) singlet and triplet spectra identified by global analysis C) Single wavelength cuts at the peak of the triplet PIA (559 nm), which is also nearly an isosbestic point, and at 670 nm, where the singlet PIA(photoinduced absorption) is 0, showing rise and decay of the triplet.

Measurements were taken as two scans on a dilute solution freshly prepared from pure solid **PH** and degassed with argon. The first and second scan were compared to ensure reproducibility. The similarity of the first and second scans indicate that the sample was stable enough under these conditions to produce reliable spectroscopic data. Indeed, the remarkable stability of this hexacene-containing compound under laser excitation may be in part due to the fast singlet excited state deactivation provided by singlet fission. Because the singlet exciton is involved in photodegradation reactions, this deactivation seems to result in fission compounds with enhanced stability relative to their monomeric counterparts.[39]

Notably, despite selectively pumping transitions associated with the hexacene monomer at 730 nm, where monomeric pentacene does not absorb, a clear signature of pentacene GSB is observed in the singlet as well as the triplet pair.

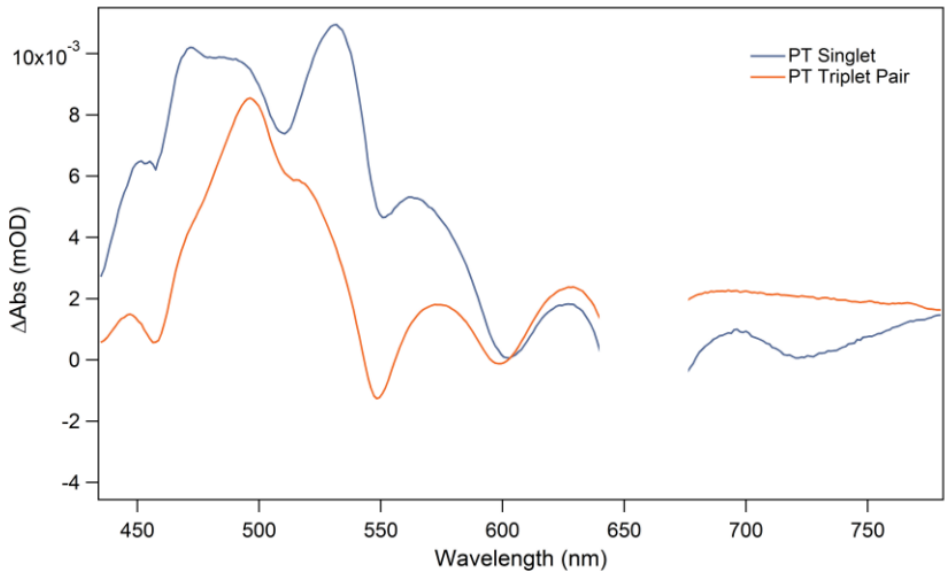

Figure 7.5. Singlet and triplet species for **PT** isolated from global analysis. Data is from transient absorption spectroscopy of **PT** dissolved as a dilute solution in chloroform and pumped at 660 nm**.**

Similarly, global analysis isolates only two species for TAS data of PT probed in dilute solution, the singlet and triplet pair. Again, we pump where the longer acene absorbs. In this case we pump at 660 nm where pentacene monomer absorbs and tetracene monomer does not. However, even in the singlet exciton we absorb clear GSB signal of both pentacene transitions (near 600nm) as well as tetracene transitions (near 550 nm). While quantitative analysis is obscured by the large degree of overlap with PIA in this region, it appears that there is somewhat more bleach of the pentacene than tetracene in the singlet exciton. This may reflect a preferential localization of the singlet to some degree on the monomer with a lower singlet energy. Overall, the presence of GSB for both monomers in the singlet is consistent with a picture of SF from a delocalized singlet exciton as reported previously by our group and others.[10,12]

7.8 Details of Photoluminescence Experiments

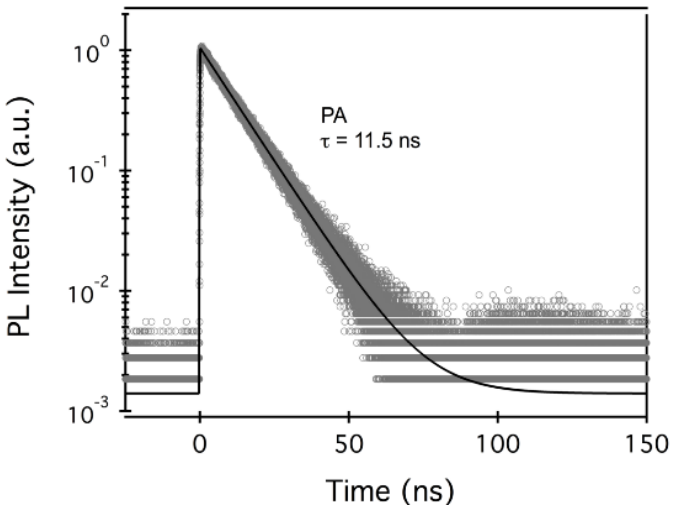

Figure 7.6. Time correlated singlet photon counting can be used to monitor the long-lived, emissive singlet exciton observed in PA.

Time correlated single photon counting was used to probe the decay of the singlet exciton in **PA**. Notably, the 11.5 ns decay observed is in excellent agreement with the 11.3 ns lifetime for the singlet observed in transient absorption spectroscopy. Single photon counting was not successfully employed to probe singlet decay in **PH** or **PT**, as neither is appreciably fluorescent and the singlet lifetimes are much shorter than the time resolution of this technique.

7.9 Transient Absorption Spectroscopy of PA

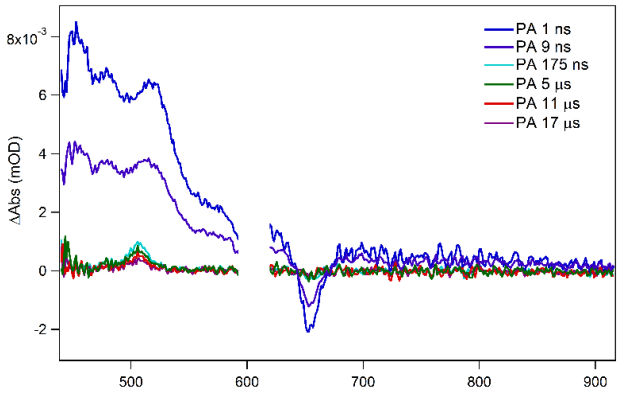

Figure 7.7. Spectral cuts taken at different times reveal the decay of the singlet exciton in **PA** to yield a small population of triplets.

Spectral line cuts reveal minimal spectral evolution of the photoexcited singlet in **PA** and its decay with an 11 ns time constant. Following the decay of the singlet, a very small triplet population remains, consistent with triplets formed *via* intersystem crossing on a slow timescale to create long-lived, individual triplets which subsequently decay with a ~20 µs lifetime, similar to the intrinsic lifetime of TIPS pentacene triplet excitons.

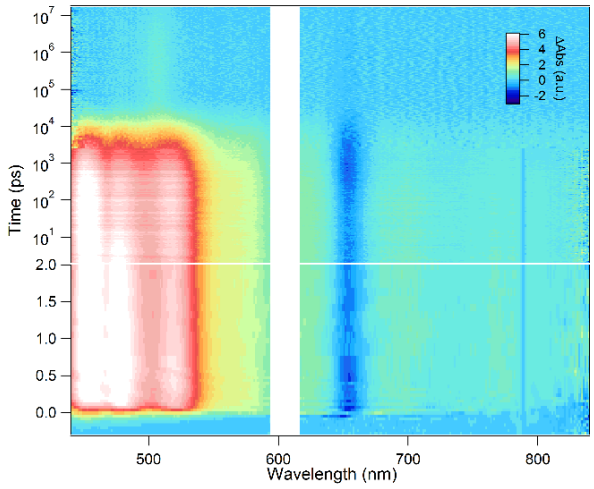

Figure 7.8. Full 2D color plot obtained from transient absorption spectroscopy of PA in chloroform excited at 600 nm.

While the **PA** color plot for the first 3 ns of measurement is shown in the main text, here we have given the full data set. Again, in this data we observe the decay of the singlet, primarily through fluorescence and internal conversion. The small population of triplets produced are spectrally similar to TIPS pentacene triplet excitons and feature a pentacene bleach with roughly 10% the area of the pentacene bleach observed in the photoexcited singlet. Therefore, a rough estimate of the magnitude of the ISC yield is ~10%.

7.10 Details of Triplet Photosensitization Experiments

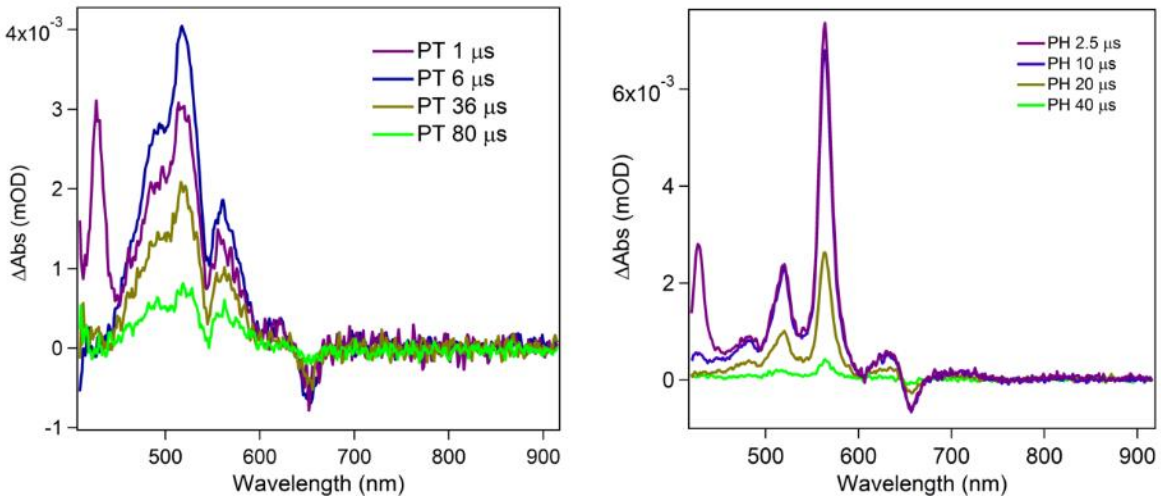

Figure 7.9. Spectral cuts from sensitization experiments of heterodimers dissolved along with a significant excess of anthracene in chloroform. The signal at early times near 418 nm is due to anthracene triplet photoinduced absorption, and therefore it decays as triplets are transferred to the heterodimer.

Data from sensitization of **PH** and **PT**, where the peak in the earliest time cut is from the anthracene sensitizer triplet photoinduced absorption. This peak vanishes as triplets are transferred to the heterodimer. The minimal evolution of the spectrum after sensitization reveals an absence of triplet transfer within the heterodimers. If triplets were to transfer from pentacene (higher energy triplet) to hexacene (lower energy triplet), the PIA would shift in magnitude considerably and the pentacene GSB would recover much faster than the hexacene GSB. Similarly, in **PT**, if the higher energy tetracene triplets were to transfer to pentacene, the tetracene bleach would recover faster than the pentacene bleach. None of this evidence for Dexter triplet transfer on a competitive timescale with intersystem crossing to the ground state is observed. Therefore, sensitization in **PH** and **PT** produces a static distribution of triplets and these populations decay independently. Since production of a tetracene, pentacene or hexacene triplet by diffusional collisions occurs with a

similar probability, the resultant spectra can be approximately compared to the triplet pair (exactly one triplet per monomer) produced by fission. However, triplets on each monomer have different lifetimes, and so the spectrum shifts slightly over time as the relative population changes. Therefore, to most accurately compare to the triplet pair, we use a relatively early time cut (main text) before the relative populations shift significantly.

7.11 Details of UV Visible Absorption Spectroscopy

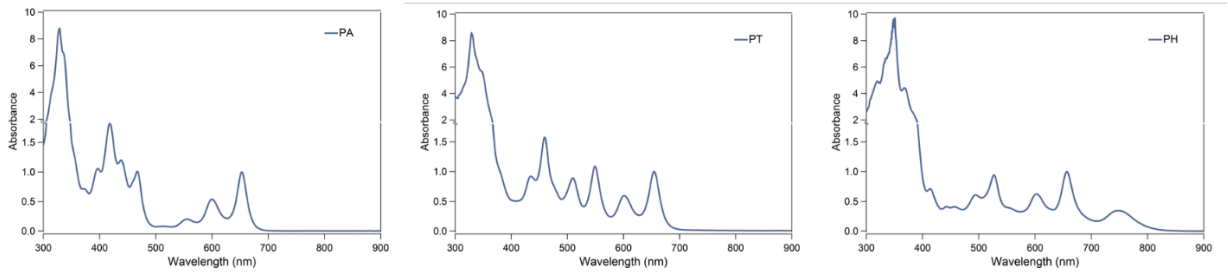

Figure 7.9. Steady state UV-visible absorption performed on dilute solutions of heterodimer in chloroform and normalized to the pentacene absorption near 660 nm.

UV-visible spectroscopy in chloroform in all heterodimers reported here revealed sets of peaks associated with each individual monomer. For example, peaks associated with TIBS-hexacene appear with an onset near 800 nm in **PH**, while peaks associated with TIPS-pentacene appear with an onset near 660 nm, and peaks associated with TIPS-anthracene appear near 460 nm. In addition to these features, we typically observe a new set of high energy peaks when dimerizing oligoacenes at the 2 position. These peaks have been reported before, and appear sensitive to the chromophores dimerized. For example, they appear near 540 nm in **PH**, near 480 nm in **PT**, and near 420 nm in **PA**. We are actively investigating the origin of these peaks, and will report the results of DFT calculations in due course. However, the interpretation of this UV-vis

absorption feature is beyond the scope of this manuscript, where we focus on singlet fission energetics in these heterodimers.

7.12 General Synthetic Methods

All commercially obtained reagents/solvents were used as received; chemicals were purchased from Alfa Aesar®, Sigma-Aldrich®, Acros organics®, TCI America®, Mallinckrodt®, and Oakwood® Products, and were used as received without further purification. Unless stated otherwise, reactions were conducted in oven-dried glassware under argon atmosphere. ^{1}H-NMR and ^{13}C-NMR spectra were recorded on Bruker 400 MHz (100 MHz for ^{13}C) and on 500 MHz (125 MHz for ^{13}C) spectrometers. Data from the ^{1}H-NMR and ^{13}C spectroscopy are reported as chemical shift (δ ppm) with the corresponding integration values. Coupling constants (*J*) are reported in hertz (Hz). Standard abbreviations indicating multiplicity were used as follows: s (singlet), b (broad), d (doublet), t (triplet), q (quartet), m (multiplet) and virt (virtual).

The mass spectral data for the compounds were obtained from XEVO G2-XS Waters® equipped with a QTOF detector with multiple inlet and ionization capabilities including electrospray ionization (ESI), atmospheric pressure chemical ionization (APCI), and atmospheric solids analysis probe (ASAP). The base peaks were usually obtained as $[M]^+$ or $[M+H]^+$ ions.

Absorption spectra were obtained on a Shimadzu UV 1800 UV-Vis spectrophotometer. Anhydrous solvents were obtained from a Schlenk manifold with purification columns packed with activated alumina and supported copper catalyst (Glass Contour, Irvine, CA). All reactions were carried out under argon unless otherwise noted.

General Protocol for the synthesis of Heterodimers:

Synthesis of tetracene-pentacene derivatives **PT** and **PA**:

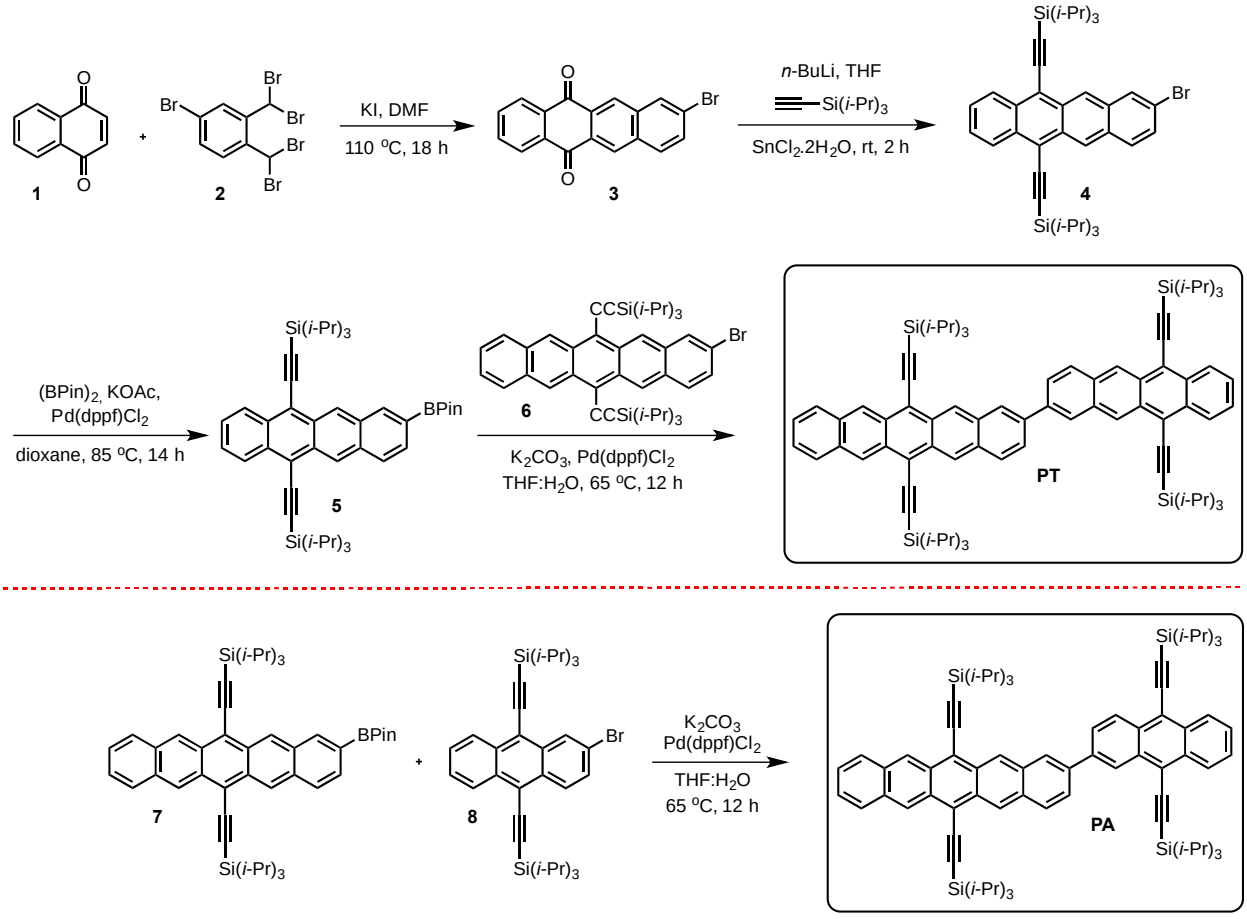

*Synthesis of Hexacene-pentacene derivatives **PH**:*

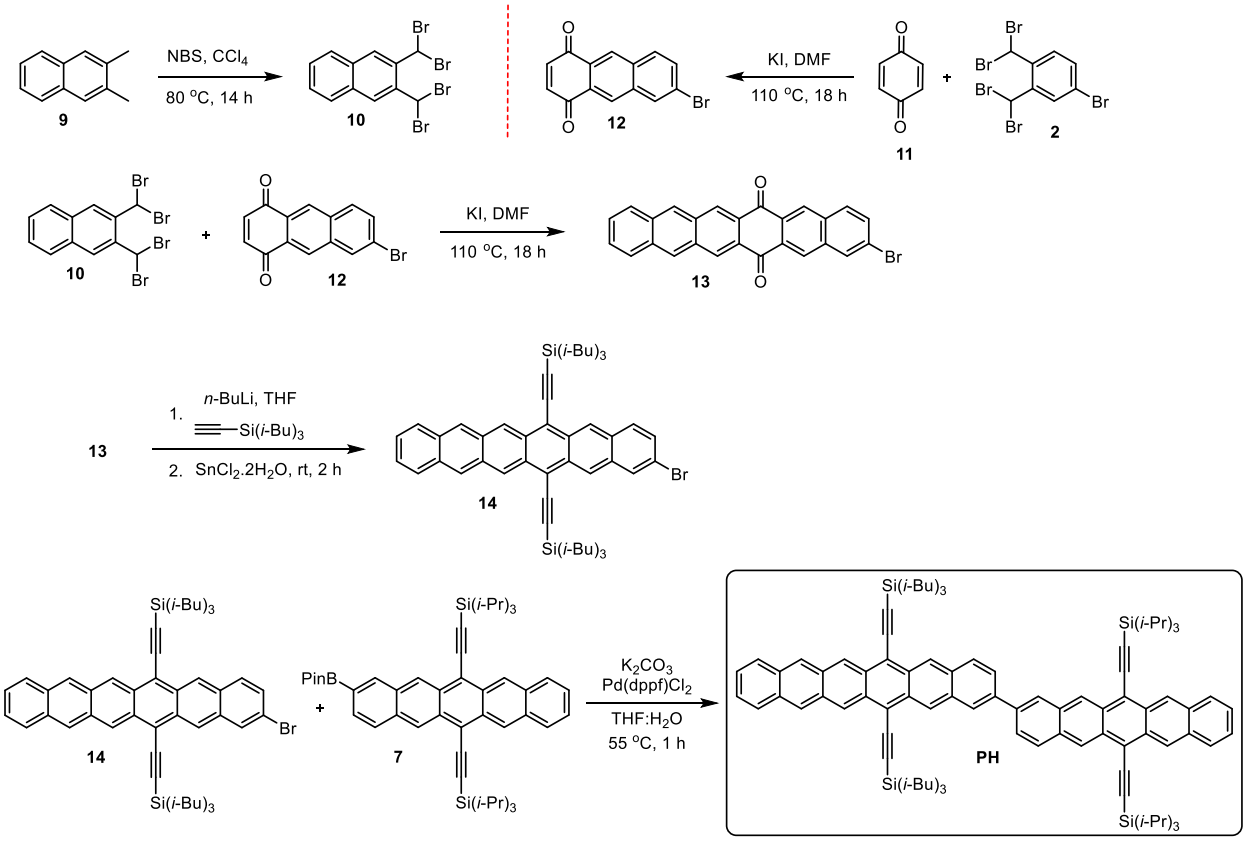

The bromo pentacene **6**, Bpin pentacene **7** and Bromo anthracene **8** were synthesized according to a procedures reported in the literature.[10,46]

Synthetic procedures for tetracene-pentacene dimers:

Synthesis of bromo-tetracenequinone **3**:

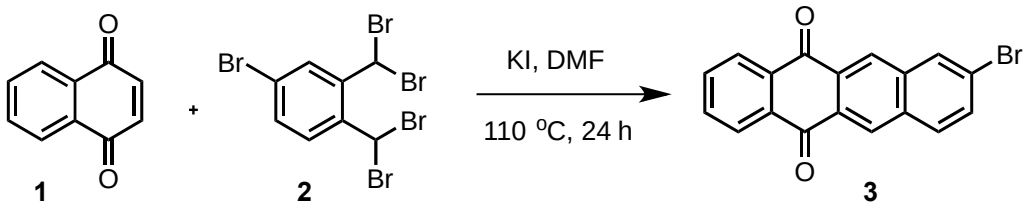

Procedure: To a 250 mL flask, **1** (1.6 g, 10.0 mmol, 1.0 *equiv.*), **2** (5.0 g 10.0 mmol, 1.0 *equiv.*) and potassium iodide (6.5 g, 40 mmol, 4.0 *equiv.*) were added. Sequential vacuum and argon were used to remove oxygen, at which point dry and degassed DMF (120 mL) was added and the mixture was heated at 110 °C for 18 h. After the reaction, the mixture was cooled to room temperature, poured into 200 mL of methanol and filtered. The solid was then washed with DI water (100 mL), methanol (50 mL) and chloroform (50 mL) to yield 1.8 g (53% yield) of shiny, golden solid.

Due to the minimal solubility of the product, no characterization was undertaken and the product was carried forward to the next step.

*Synthesis of bromo-TIPS-tetracene **4**:*

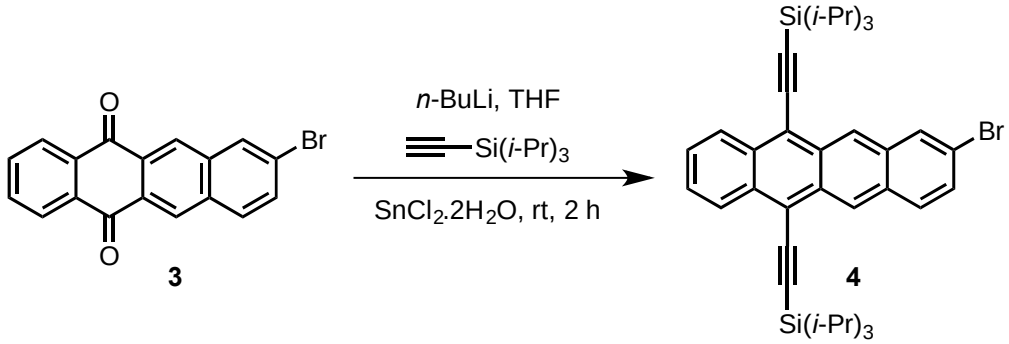

Procedure: To a 50 mL schlenk flask, triisopropylsilylacetylene (3.6 mL,16 mmol, 3.0 *equiv.*) and dry THF (20 mL) were added under argon. At -78 °C, 2.5 M *n*-butyl lithium in hexanes (6.0 mL, 15 mmol, 2.8 *equiv.*) was added. The mixture was warmed to 0 °C and stirred for 45 min, at which point tetracenequinone **3** (1.6 g, 5.4 mmol, 1.0 *equiv.*) was added and the mixture was stirred at room temperature for 16 h. To the clear brown mixture, an excess of 10% aq. HCl solution and saturated with $SnCl_2 \cdot 2H_2O$, was added, turning the solution deep red. After 30 minutes stirring at room temperature, this mixture was partitioned between water (150 mL) and DCM (100 mL). The aqueous layer was extracted with DCM (2 × 80 mL). The combined organic phase was dried over Na_2SO_4, filtered and concentrated under reduced pressure. The crude product was purified by column chromatography over silica (100% hexanes to isolate 1.6 g of product as deep red solid (50% yield).

^{1}H-NMR (500 MHz, $CDCl_3$, δ ppm): 9.29 (s, 1H), 9.22 (s, 1H), 8.66-8.63 (m, 2H), 8.19 (s, 1H), 7.91-7.89 (m, 1H), 7.60-7.57 (m, 2H), 7.53-7.51 (m, 1H) and 1.40-1.33 (m, 42H)

^{13}C-NMR (125 MHz, $CDCl_3$, δ ppm): 133.0, 132.8, 132.6, 130.7, 130.4, 130.3, 130.2, 130.1, 129.5, 127.4, 127.4, 127.1, 126.9, 126.8, 125.5, 120.3, 118.9, 118.7, 106.3, 106.2, 103.67, 103.65, 18.98, 18.96 and 11.6.

MS (ESI): Calculated: 667.2788; Observed: 667.2791

Synthesis of Bpin-TIPS-tetracene **5**:

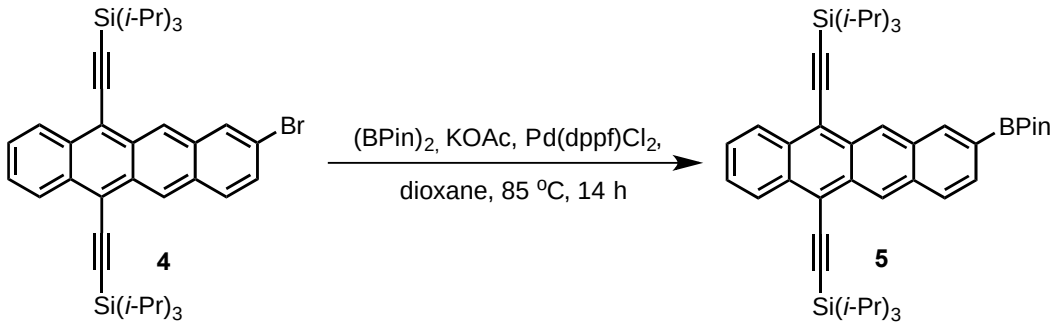

Procedure: To a 20 mL sealed tube was added Bromo tetracene derivative **4** (1.0 g, 1.5 mmol, 1.0 *equiv.*), bis(pinacolato)diboron (0.58 g, 2.3 mmol, 1.5 *equiv.*), $Pd(dppf)Cl_2$·DCM (61 mg, 0.07 mmol, 0.05 *equiv.*) and KOAc (0.52 g, 5.3 mmol, 3.5 *equiv.*). This tube was degassed by sequential vacuum and argon, followed by the addition of dry and degassed dioxane (7 mL). The mixture was heated to 85 °C and maintained for 14 h in the dark. The reaction mixture was partitioned between water (50 ML) and DCM (50 mL). The aqueous layer was extracted with DCM (50 mL). The combined organic phase was dried over Na_2SO_4, filtered and solvent removed under reduced pressure. The crude reaction mixture was purified by silica column chromatography using a mixture of hexanes and DCM as eluent to yield 320 mg (30% yield) of bright red product.

^{1}H-NMR (500 MHz, $CDCl_3$, δ ppm): 9.44 (s, 1H), 9.39 (s, 1H), 8.76-8.72 (m, 2H), 8.66 (s, 1H), 8.09-8.07 (m, 1H), 7.89-7.87 (m, 1H), 7.64-7.62 (m, 2H), 1.49 (s, 12H) and 1.43-1.37 (m, 42H).

^{13}C-NMR (125 MHz, $CDCl_3$, δ ppm): 137.8, 133.1, 132.9, 132.8, 131.7, 130.96, 130.4, 129.8, 127.6, 127.5, 127.4, 126.9, 126.7, 126.1, 119.1, 118.6, 106.2, 105.9, 103.9, 103.8, 84.1, 24.9, 19.1, 19.0 and 11.7

MS (ESI): Calculated: 714.4465; Observed: 714.4460.

Synthesis of pentacene-tetracene dimer **PT**:

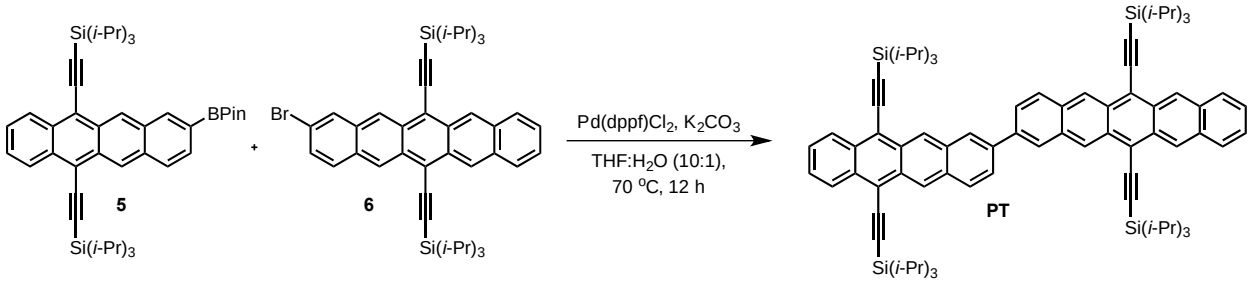

Procedure: To a sealed tube was added bromo pentacene derivative **6** (100 mg, 0.12 mmol, 1 *equiv.*), Bpin-tetracene derivative **5** (96 mg, 0.14 mmol, 1.2 *equiv.*), Pd(dppf)Cl_2DCM (9.8 mg, 0.01 mmol, 0.1 *equiv.*), and K_2CO_3 (282 mg, 2.04 mmol, 17 *equiv.*). Sequential vacuum and argon were used to degas the solids, followed by the addition of degassed THF (10 mL) and degassed water (1 mL). The mixture was heated to 70 °C and maintained for 12 h in the dark. The crude reaction mixture was concentrated and purified by chromatography on silica gel (DCM:Hexanes) to yield 55 mg of dark reddish brown solid (37% yield).

^{1}H-NMR (500 MHz, $CDCl_3$, δ ppm): 9.45-9.35 (m, 6H), 8.69-8.67 (m, 2H), 8.41-8.37 (m, 2H), 8.23-8.17 (m, 2H), 8.03-7.94 (m, 4H), 7.61-7.59 (m, 2H), 7.46-7.44 (m, 2H) and 1.44-1.37 (m, 84H).

^{13}C-NMR (125 MHz, $CDCl_3$, 50° C, δ ppm): 137.9, 137.8, 132.9, 132.8, 132.5, 132.4, 131.6, 130.9, 130.7, 129.6, 129.5, 128.6, 127.5, 126.8, 126.7, 126.69, 126.3, 126.2, 126.0, 125.9, 118.8, 118.7, 107.4, 107.2, 106.1, 105.96, 104.8, 104.1, 104.06, 29.7, 19.01, 19.00, 18.96, 18.94, 11.8 and 11.7.

MS (ESI): Calculated: 1224.7215; Observed: 1224.7212.

Synthesis of pentacene-Anthracene dimer **PA**:

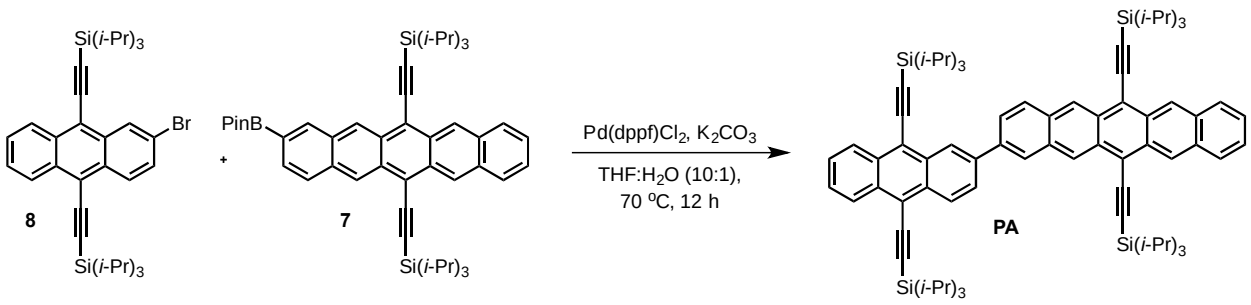

Procedure: To a sealed tube was added bromo anthracene derivative **8** (129 mg, 0.18 mmol, 1.2 *equiv.*), Bpin-pentacene derivative **7** (100 mg, 0.15 mmol, 1.0 *equiv.*), Pd(dppf)Cl_2DCM (12.2 mg, 0.015 mmol, 0.1 *equiv.*), and K_2CO_3 (352 mg, 2.55 mmol, 17 *equiv.*). Sequential vacuum and argon were used to degas the solids, followed by the addition of degassed THF (45 mL) and degassed water (5 mL). The mixture was heated to 70 °C and maintained for 12 h in the dark. The crude reaction mixture was concentrated and purified by chromatography on silica gel (DCM:Hexanes) to yield 120 mg of green solid (68% yield).

^{1}H-NMR (500 MHz, $CDCl_3$, δ ppm): 9.39-9.36 (m, 4H), 9.10 (s, 1H), 8.84-8.82 (m, 1H), 8.72-8.69 (m, 2H), 8.36 (s, 1H), 8.14-8.11 (m, 2H), 8.03-8.01 (m, 2H), 7.96-7.94 (m, 1H), 7.68-7.66 (m, 2H), 7.47-7.45 (m, 2H), 1.44-1.41 (m, 42H) and 1.35-1.33 (m, 42H).

^{13}C-NMR (125 MHz, $CDCl_3$, 50° C, δ ppm): 138.9, 138.1, 132.8, 132.7, 132.6, 132.5, 132.4, 132.3, 131.8, 131.6, 130.95, 130.9, 130.8, 130.7, 129.4, 128.7, 128.1, 127.4, 127.3, 127.0, 126.9, 126.7, 126.65, 126.54, 126.4, 126.37, 126.3, 126.1, 125.5, 119.0, 118.7, 118.5, 118.4, 107.4, 1-7.2, 105.4, 104.9, 104.7, 103.5, 103.3, 19.1, 19.0, 18.97, 18.94, 11.7, 11.6 and 11.5.

MS (ESI): Calculated: 1174.7059; Observed: 1174.7051.

Synthesis of bromo anthraquinone **12**:

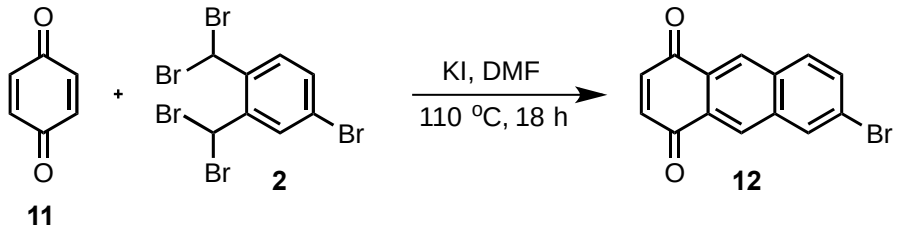

Procedure: To a 250 mL round bottom flask was added benzoquinone **11** (30.2 g, 280 mmol, 7 *equiv.*), bromo derivative **2** (20.0 g, 40 mmol, 1.0 *equiv.*) and KI (26.5 g, 160 mmol, 4.0 *equiv.*). Sequential vacuum and argon were used to degas the solids, at which point dry and degassed DMF (360 mL) was added and the reaction was stirred at 110 °C for 18 h. The mixture was cooled and poured into 1:1 water methanol mixture (400 mL). The resulting precipitate was filtered, then placed in a separatory funnel where it was separated between 1L of DCM and 1L of water. The solvent was removed *in vacuo* and loaded onto a silica gel column, where elution with DCM:hexanes yielded 4.8 g of yellowish orange powder product (42% yield).

^{1}H-NMR (500 MHz, $CDCl_3$, δ ppm): 8.62 (s, 1H), 8.55 (s, 1H), 8.26-8.25 (m, 1H), 7.97-7.95 (m, 1H), 7.80-7.78 (m, 1H) and 7.11 (s, 2H).

^{13}C-NMR (125 MHz, $CDCl_3$, δ ppm): 184.3, 140.1, 140.0, 135.8, 133.2, 133.1, 132.2, 131.6, 129.2, 128.8, 128.7, 127.7, 124.2

MS (ESI): Calculated: 286.9708; Observed: 286.9699.

Synthesis of bromo hexacenequinone **13**:

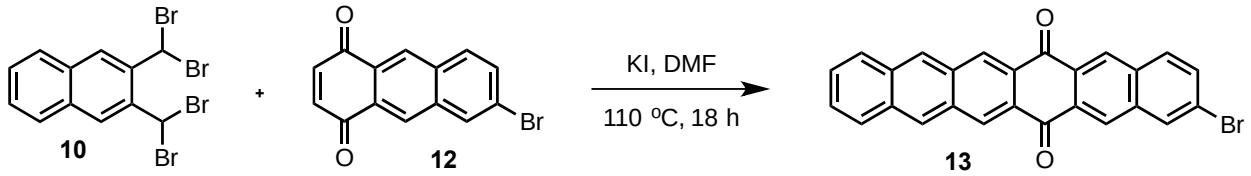

Procedure: To a 250 mL RBF were added naphthalene tetrabromide **10** (2.13 g, 4.5 mmol, 1.0 *equiv.*), 6-bromoanthracene-1,4-dione **12** (1.3 g, 4.5 mmol), and KI (3.0 g, 18 mmol, 4.0 *equiv.*). Sequential vacuum and argon were used to remove oxygen followed by the addition of dry and degassed DMF (100 mL). The mixture was heated at 110 °C for 18 h after which it was cooled to room temperature, poured into DI water (100 mL) and filtered. The solid was washed with methanol (50 mL), dichloromethane (150 mL), water (50 mL) until the filtrate was clear to yield 400 mg of brown solid product (20% yield).

No characterization was carried out due to limited solubility of the product.

Synthesis of bromo hexacene **14**:

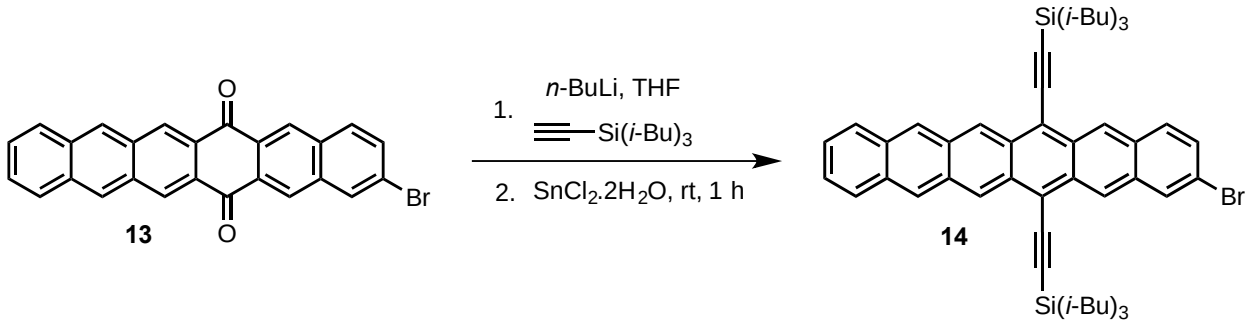

Procedure: To a 250 mL schlenk flask was added tri-isobutylsilylacetylene (1.7 g, 5 *equiv.*) and hexanes (25 mL). The mixture was cooled to 0 °C under argon and 2.5 M *n*-butyl lithium solution in hexanes (2.9 mL, 7.15 mmol, 4.8 *equiv.*) were added and the mixture was stirred one hour. To

this solution bromo hexacenequinone **13** (650 mg, mmol, 1.0 *equiv.*) was added as well as dry, degassed hexanes (70 mL) and THF (10 mL). This solution was stirred at room temperature overnight and the solvent was then removed *in vacuo.* The crude reaction mixture was purified in a silica plug first eluting with hexanes to remove excess acetylene followed by DCM to obtain bromo-hexacene diol product.

The bromo-hexacene diol was dissolved in dry and degassed THF (20 mL) to which a solution of excess $SnCl_2.2H_2O$ in 10 mL of 10% aq.HCl was added at room temperature and stirred in the dark until TLC indicated completion of the reduction (~ 1 h). Extraction between DCM and water (50 mL each) followed by drying of the organic phase over Na_2SO_4 and removal of solvent *in vacuo* gave a crude green solid which was purified by column chromatography to yield 236 mg of green powder (19% yield).

^{1}H-NMR (500 MHz, $CDCl_3$, δ ppm): 9.59-9.58 (m, 2H), 9.19 (s, 1H), 9.13 (s, 1H), 8.64-8.63 (m, 2H), 8.12 (s, 1H), 7.97-7.96 (m, 2H), 7.83-7.81 (m, 1H), 7.47-7.45 (m, 1H), 7.37-7.35 (m, 2H), 2.32-2.25 (m, 6H), 1.29-1.28 (36H) and 1.07-1.05 (m, 12H).

^{13}C-NMR (125 MHz, $CDCl_3$, δ ppm): 132.9, 132.4, 132.3, 131.2, 130.9, 130.8, 130.5, 130.4, 130.3, 130.2, 129.7, 128.5, 126.9, 126.8, 126.7, 126.6, 125.63, 125.62, 125.5, 120.4, 118.5, 118.4, 110.95, 110.8, 104.8, 104.7, 26.6, 25.5 and 25.4

MS (ASAP): Calculated: 851.4043; Observed: 851.4044.

Synthesis of pentacene-hexacene dimer **PH**:

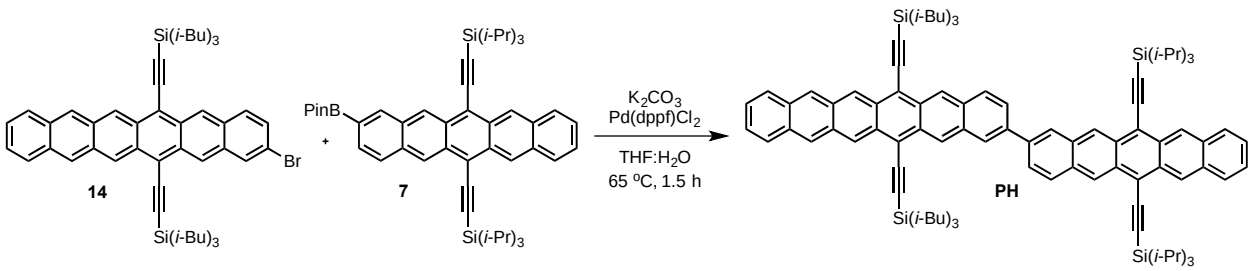

Procedure: To a dry round bottomed flask was added bromohexacene derivative **14** (30 mg, 0.035 mmol, 1.0 *equiv*), Bpin pentacene derivative **7** (32mg, 0.042 mmol, 1.2 *equiv*.) K_2CO_3 (83 mg, 0.6 mmol, 17 *equiv.*) and Pd(dppf)Cl_2·DCM (2.9 mg, 0.0035 mmol, 0.1 *equiv*.). Sequential vacuum and argon were used to degas the mixture followed by the addition of degassed THF and H_2O (9:1 ratio, 20 mL). The mixture was heated to 55 °C and maintained for 1.5 h in the dark. The reaction was cooled to room temperature, concentrated and the crude was purified using by silica chromatography using mixtures of hexanes/DCM as an eluent to obtain the product as a purple solid (30 mg, 60%).

Note: The column was run quickly and using N_2 pressure instead of air. The solvent was evaporated under dark and stored under argon and in dark. The spectroscopic measurements were undertaken shortly after purification, and repeated twice to ensure reproducibility. The product decomposed over 2 months, as evidenced from its green color even when stored under argon and away from light.

^{1}H-NMR (500 MHz, $CDCl_3$, δ ppm): 9.59 (s, 2H), 9.41 (s, 1H), 9.37-9.35 (m, 3H), 9.32 (s, 1H), 9.27 (s, 1H), 8.64 (s, 2H), 8.34-8.29 (m, 2H), 8.18-8.16 (m, 1H), 8.12-8.10 (m, 1H), 8.03-8.01 (m, 2H), 7.97-7.91 (m, 4H), 7.46-7.44 (m, 2H), 7.36-7.34 (m, 2H), 2.34-2.26 (m, 6H), 1.45-1.43 (m, 42H), 1.30-1.29 (m, 36H) and 1.08-1.06 (m, 12H).

^{13}C-NMR (125 MHz, $CDCl_3$, δ ppm): 137.8, 137.64, 137.60, 136.1, 135.9, 132.7, 132.5, 132.4, 132.33, 132.31, 131.8, 131.6, 131.4, 131.35, 131.2, 131.0, 130.9, 130.8, 130.78, 130.76, 130.7, 130.43, 130.3, 130.2, 129.6, 129.5, 128.9, 128.5, 126.9, 126.8, 126.7, 126.6, 126.4, 126.36, 126.33, 126.21, 126.19, 126.08, 126.0, 125.8, 125.5, 118.5, 118.4, 118.2, 110.6, 110.5, 107.4, 107.2, 105.0, 104.9, 104.72, 104.67, 29.7, 26.65, 25.53, 25.52, 25.49, 19.07, 19.05 and 11.73.

MS (APCI): Calculated: 1408.8441; Observed: 1408.8467.

^{1}H-NMR (500 MHz, $CDCl_3$, δ ppm): 9.29 (s, 1H), 9.22 (s, 1H), 8.66-8.63 (m, 2H), 8.19 (s, 1H), 7.91-7.89 (m, 1H), 7.60-7.57 (m, 2H), 7.53-7.51 (m, 1H) and 1.40-1.33 (m, 42H)

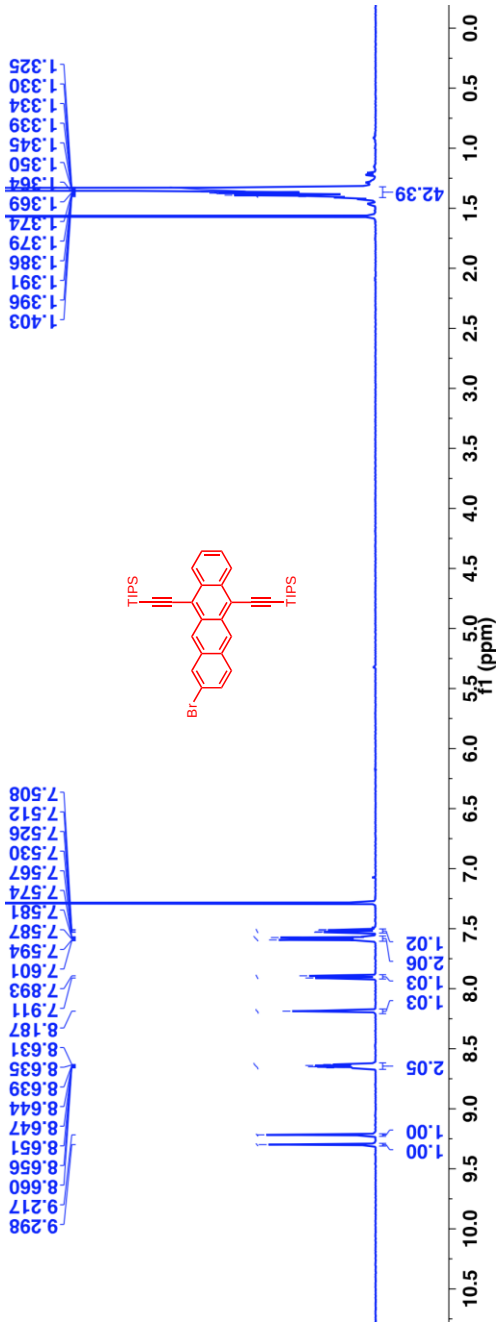

^{13}C-NMR (125 MHz, $CDCl_3$, δ ppm): 133.0, 132.8, 132.6, 130.7, 130.4, 130.3, 130.2, 130.1, 129.5, 127.4, 127.4, 127.1, 126.9, 126.8, 125.5, 120.3, 118.9, 118.7, 106.3, 106.2, 103.67, 103.65, 18.98, 18.96 and 11.6.

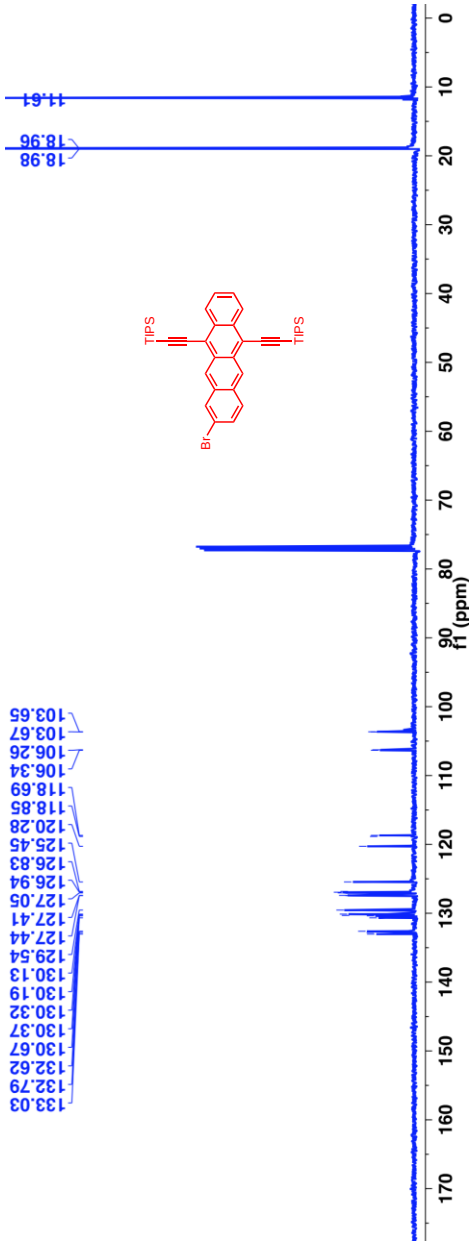

^{1}H-NMR (500 MHz, $CDCl_3$, δ ppm): 9.44 (s, 1H), 9.39 (s, 1H), 8.76-8.72 (m, 2H), 8.66 (s, 1H), 8.09-8.07 (m, 1H), 7.89-7.87 (m, 1H), 7.64-7.62 (m, 2H), 1.49 (s, 12H) and 1.43-1.37 (m, 42H).

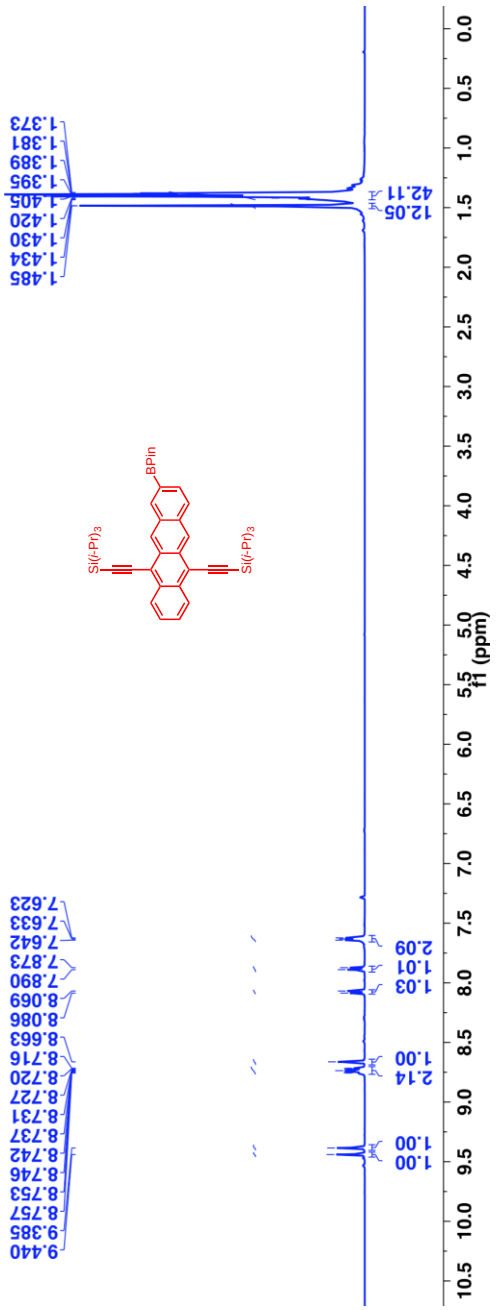

^{13}C-NMR (125 MHz, $CDCl_3$, δ ppm): 137.8, 133.1, 132.9, 132.8, 131.7, 130.96, 130.4, 129.8, 127.6, 127.5, 127.4, 126.9, 126.7, 126.1, 119.1, 118.6, 106.2, 105.9, 103.9, 103.8, 84.1, 24.9, 19.1, 19.0 and 11.7

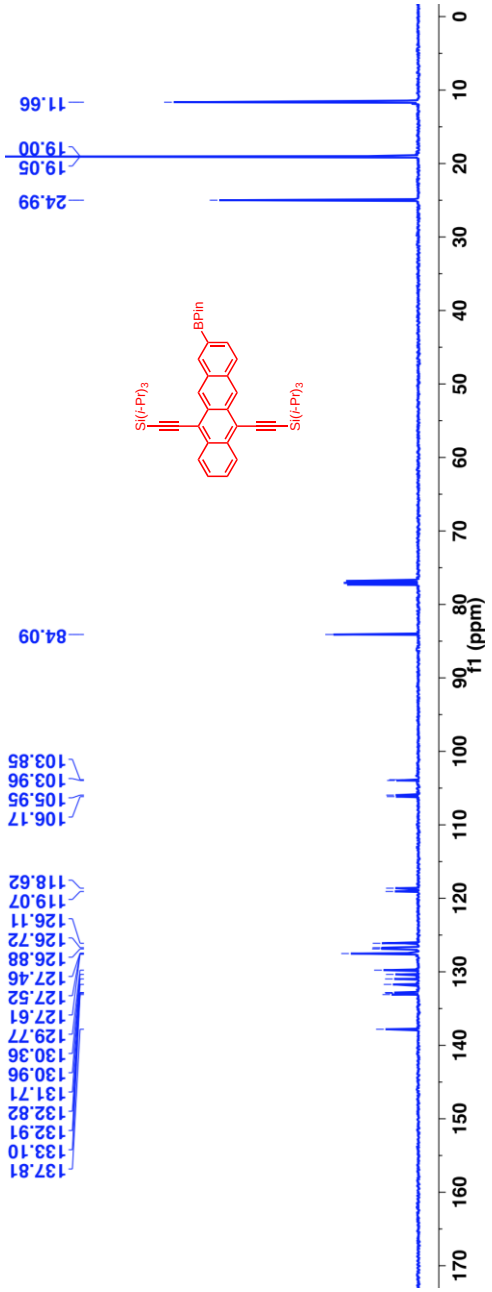

^{1}H-NMR (500 MHz, $CDCl_3$, δ ppm): 9.45-9.35 (m, 6H), 8.69-8.67 (m, 2H), 8.41-8.37 (m, 2H), 8.23-8.17 (m, 2H), 8.03-7.94 (m, 4H), 7.61-7.59 (m, 2H), 7.46-7.44 (m, 2H) and 1.44-1.37 (m, 84H).

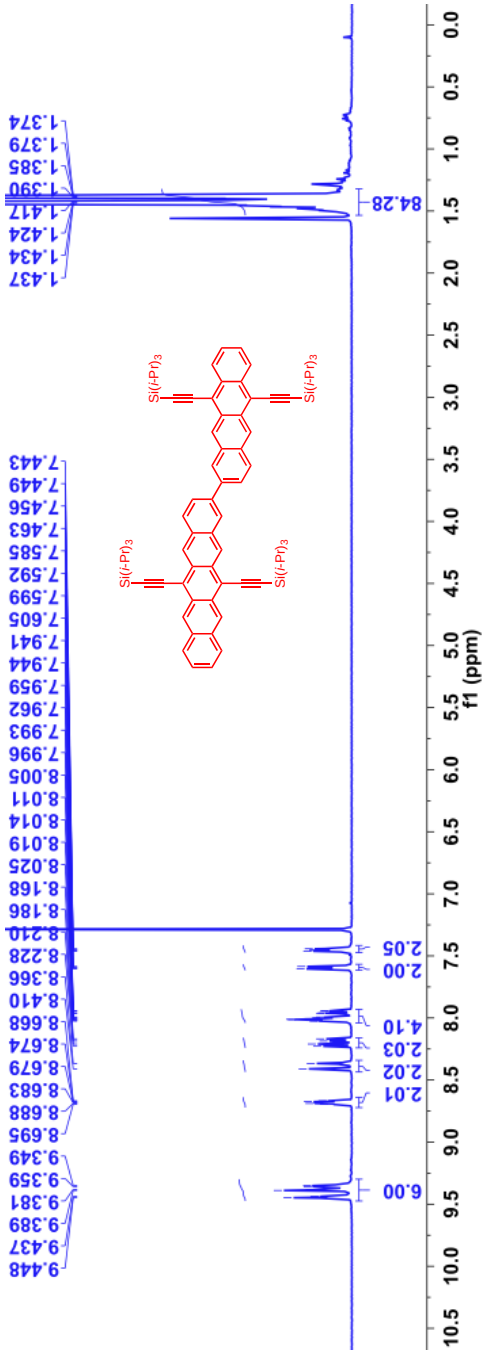

^{13}C-NMR (125 MHz, $CDCl_3$, 50° C, δ ppm): 137.9, 137.8, 132.9, 132.8, 132.5, 132.4, 131.6, 130.9, 130.7, 129.6, 129.5, 128.6, 127.5, 126.8, 126.7, 126.69, 126.3, 126.2, 126.0, 125.9, 118.8, 118.7, 107.4, 107.2, 106.1, 105.96, 104.8, 104.1, 104.06, 29.7, 19.01, 19.00, 18.96, 18.94, 11.8 and 11.7.

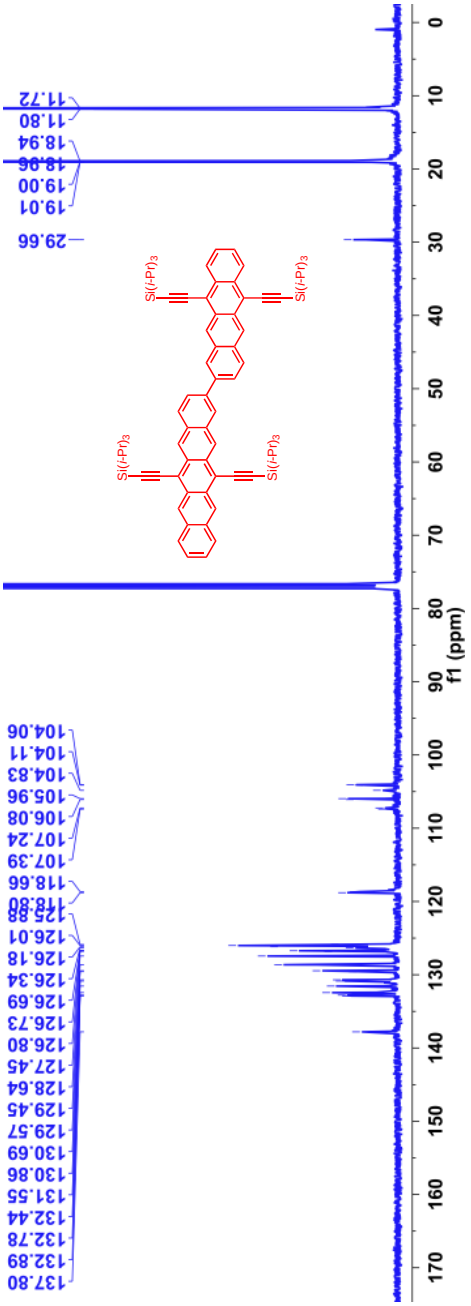

^{1}H-NMR (500 MHz, $CDCl_3$, δ ppm): 9.39-9.36 (m, 4H), 9.10 (s, 1H), 8.84-8.82 (m, 1H), 8.72-8.69 (m, 2H), 8.36 (s, 1H), 8.14-8.11 (m, 2H), 8.03-8.01 (m, 2H), 7.96-7.94 (m, 1H), 7.68-7.66 (m, 2H), 7.47-7.45 (m, 2H), 1.44-1.41 (m, 42H) and 1.35-1.33 (m, 42H).

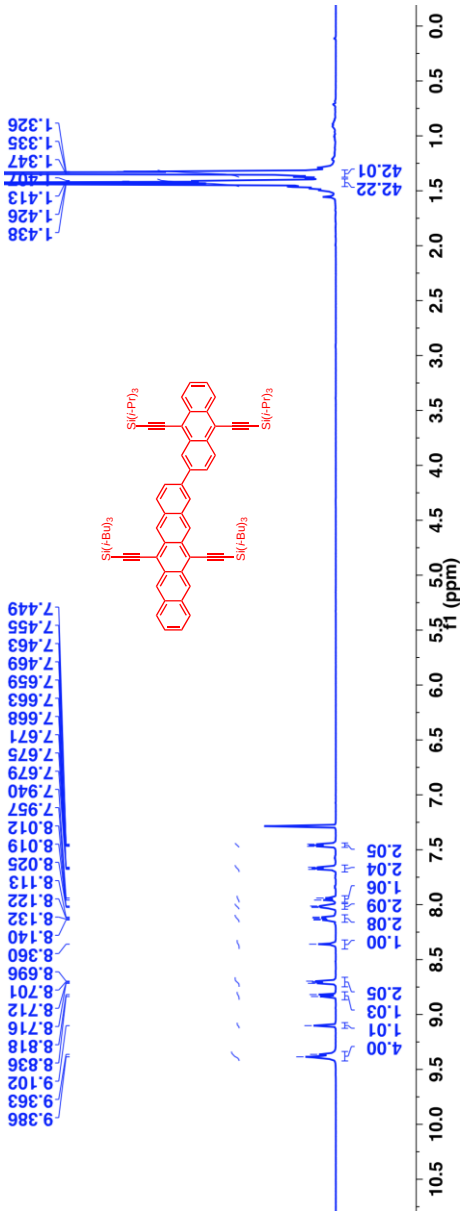

^{13}C-NMR (125 MHz, $CDCl_3$, 50° C, δ ppm): 138.9, 138.1, 132.8, 132.7, 132.6, 132.5, 132.4, 132.3, 131.8, 131.6, 130.95, 130.9, 130.8, 130.7, 129.4, 128.7, 128.1, 127.4, 127.3, 127.0, 126.9, 126.7, 126.65, 126.54, 126.4, 126.37, 126.3, 126.1, 125.5, 119.0, 118.7, 118.5, 118.4, 107.4, 1-7.2, 105.4, 104.9, 104.7, 103.5, 103.3, 19.1, 19.0, 18.97, 18.94, 11.7, 11.6 and 11.5.

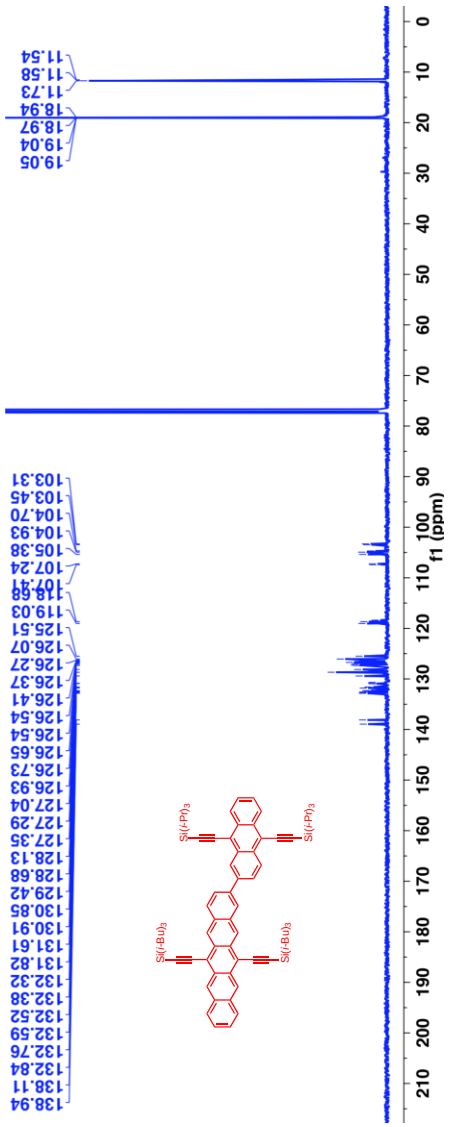

^{1}H-NMR (500 MHz, $CDCl_3$, δ ppm): 8.62 (s, 1H), 8.55 (s, 1H), 8.26-8.25 (m, 1H), 7.97-7.95 (m, 1H), 7.80-7.78 (m, 1H) and 7.11 (s, 2H).

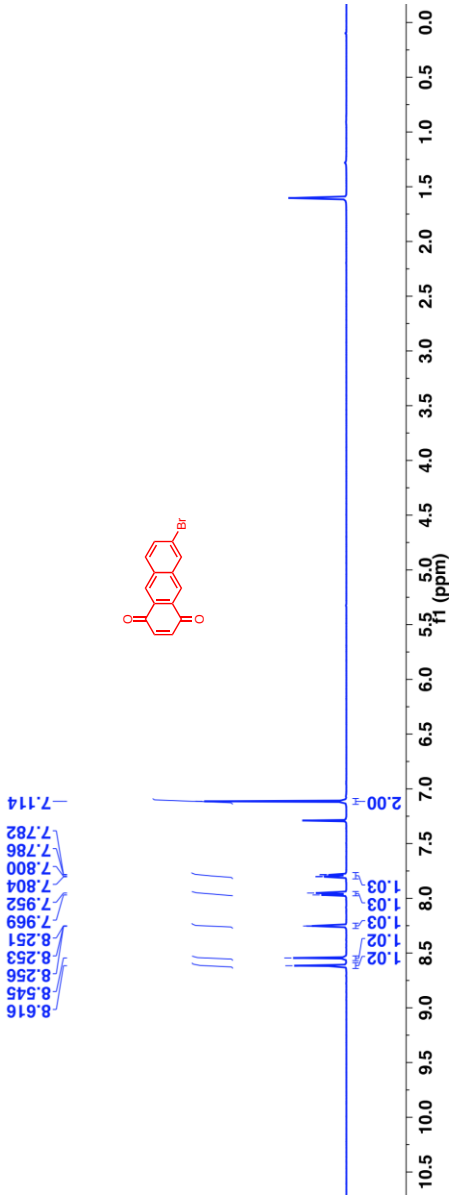

^{13}C-NMR (125 MHz, $CDCl_3$, δ ppm): 184.3, 140.1, 140.0, 135.8, 133.2, 133.1, 132.2, 131.6, 129.2, 128.8, 128.7, 127.7 and 124.2.

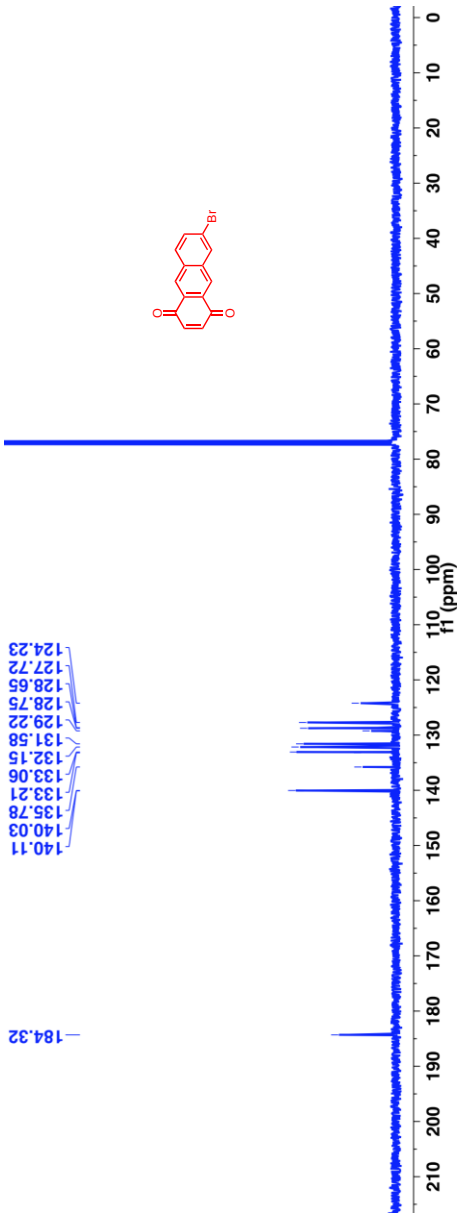

^{1}H-NMR (500 MHz, $CDCl_3$, δ ppm): 9.59-9.58 (m, 2H), 9.19 (s, 1H), 9.13 (s, 1H), 8.64-8.63 (m, 2H), 8.12 (s, 1H), 7.97-7.96 (m, 2H), 7.83-7.81 (m, 1H), 7.47-7.45 (m, 1H), 7.37-7.35 (m, 2H), 2.32-2.25 (m, 6H), 1.29-1.28 (36H) and 1.07-1.05 (m, 12H).

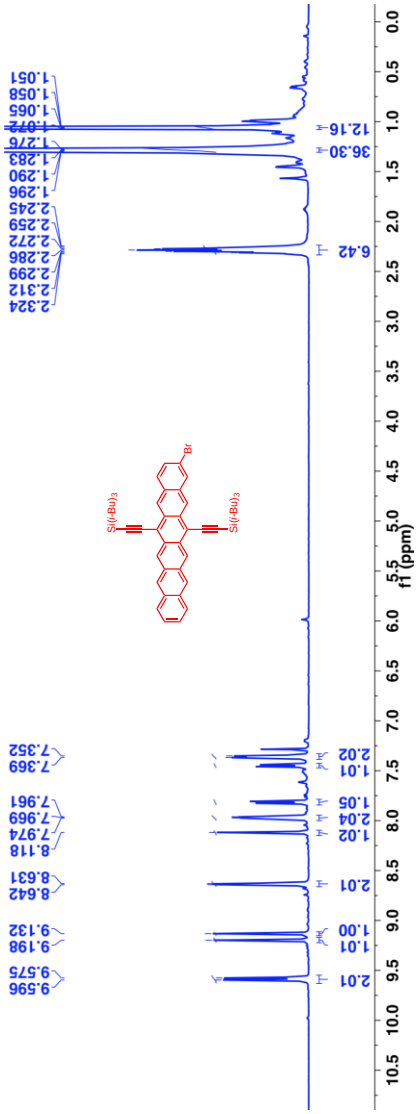

^{13}C-NMR (125 MHz, $CDCl_3$, δ ppm): 132.9, 132.4, 132.3, 131.2, 130.9, 130.8, 130.5, 130.4, 130.3, 130.2, 129.7, 128.5, 126.9, 126.8, 126.7, 126.6, 125.63, 125.62, 125.5, 120.4, 118.5, 118.4, 110.95, 110.8, 104.8, 104.7, 26.6, 25.5 and 25.4

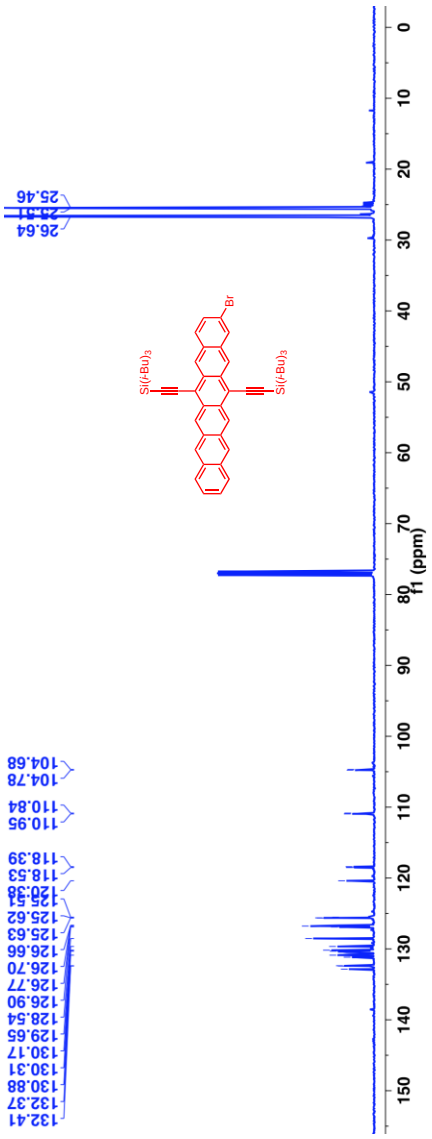

^{1}H-NMR (500 MHz, $CDCl_3$, δ ppm): 9.59 (s, 2H), 9.41 (s, 1H), 9.37-9.35 (m, 3H), 9.32 (s, 1H), 9.27 (s, 1H), 8.64 (s, 2H), 8.34-8.29 (m, 2H), 8.18-8.16 (m, 1H), 8.12-8.10 (m, 1H), 8.03-8.01 (m, 2H), 7.97-7.91 (m, 4H), 7.46-7.44 (m, 2H), 7.36-7.34 (m, 2H), 2.34-2.26 (m, 6H), 1.45-1.43 (m, 42H), 1.30-1.29 (m, 36H) and 1.08-1.06 (m, 12H).

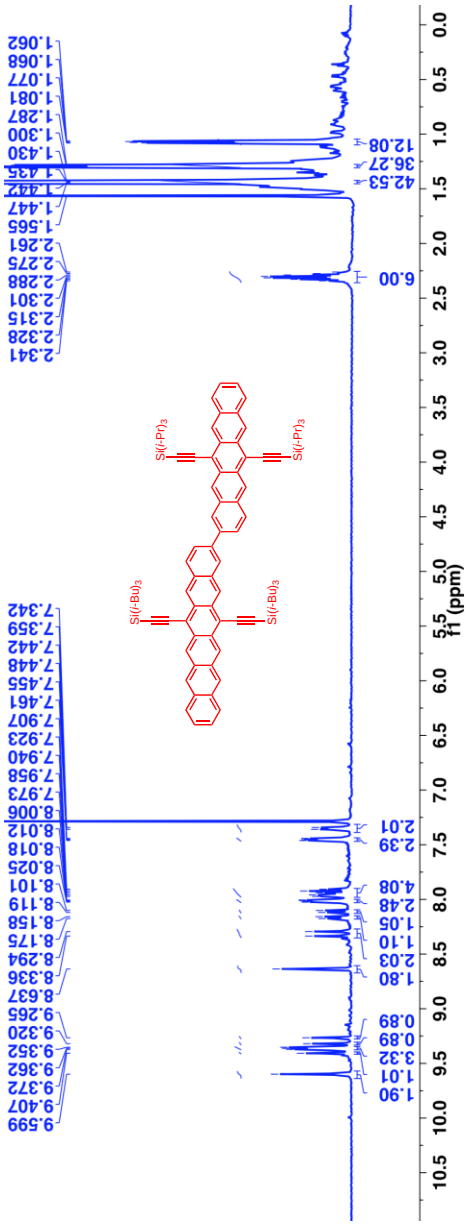

^{1}H-NMR (125 MHz, $CDCl_3$, δ ppm): ^{13}C-NMR (125 MHz, $CDCl_3$, δ ppm): 137.8, 137.64, 137.60, 136.1, 135.9, 132.7, 132.5, 132.4, 132.33, 132.31, 131.8, 131.6, 131.4, 131.35, 131.2, 131.0, 130.9, 130.8, 130.78, 130.76, 130.7, 130.43, 130.3, 130.2, 129.6, 129.5, 128.9, 128.5, 126.9, 126.8, 126.7, 126.6, 126.4, 126.36, 126.33, 126.21, 126.19, 126.08, 126.0, 125.8, 125.5, 118.5, 118.4, 118.2, 110.6, 110.5, 107.4, 107.2, 105.0, 104.9, 104.72, 104.67, 29.7, 26.65, 25.53, 25.52, 25.49, 19.07, 19.05 and 11.73.

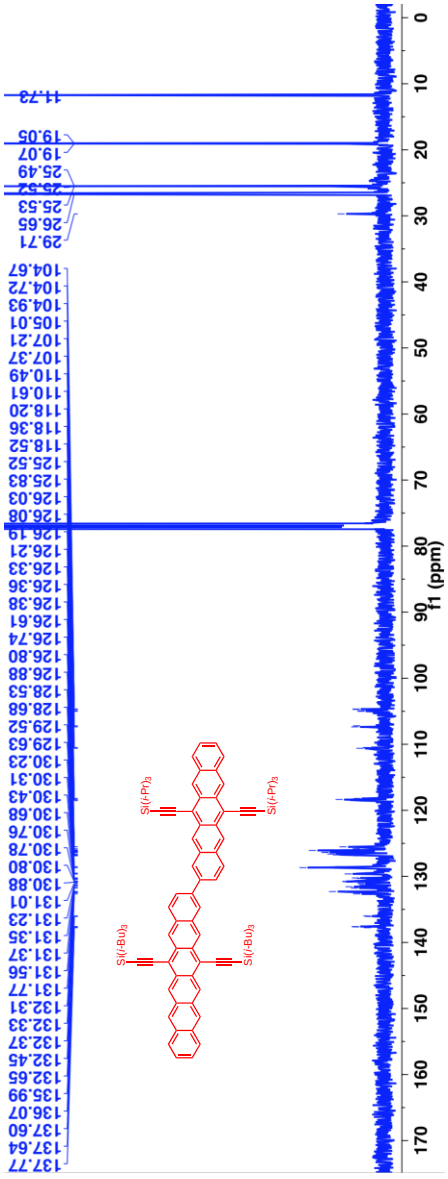

7.13 References

(1) Hanna, M. C.; Nozik, A. J. *J. Appl. Phys.* **2006**, *100*, 074510.

(2) Smith, M. B.; Michl, J. *Annu. Rev. Phys. Chem.* **2013**, *64*, 361.

(3) Smith, M. B.; Michl, J. *Chem. Rev.* **2010**, *110*, 6891.

(4) Paci, I.; Johnson, J. C.; Chen, X.; Rana, G.; Popović, D.; David, D. E.; Nozik, A. J.; Ratner, M. A.; Michl, J. *J. Am. Chem. Soc.* **2006**, *128*, 16546.

(5) Congreve, D. N.; Lee, J.; Thompson, N. J.; Hontz, E.; Yost, S. R.; Reusswig, P. D.; Bahlke, M. E.; Reineke, S.; Van Voorhis, T.; Baldo, M. A. *Science* **2013**, *340*, 334.

(6) Lee, J.; Jadhav, P.; Reusswig, P. D.; Yost, S. R.; Thompson, N. J.; Congreve, D. N.; Hontz, E.; Van Voorhis, T.; Baldo, M. A. *Acc. Chem. Res.* **2013**, *46*, 1300.

(7) Busby, E.; Xia, J.; Wu, Q.; Low, J. Z.; Rong, R.; Miller, J. R.; Zhu, X.-Y.; Campos, L. M.; Sfeir, M. Y. *Nat. Mater.* **2014**, *14*, 426.

(8) Busby, E.; Xia, J.; Low, J. Z.; Wu, Q.; Hoy, J.; Campos, L. M.; Sfeir, M. Y. *J. Phys. Chem. B* **2015**, *119*, 7644.

(9) Low, J. Z.; Sanders, S. N.; Campos, L. M. *Chem. Mater.* **2015**, *27*, 5453.

(10) Sanders, S. N.; Kumarasamy, E.; Pun, A. B.; Trinh, M. T.; Choi, B.; Xia, J.; Taffet, E. J.; Low, J. Z.; Miller, J. R.; Roy, X.; Zhu, X. Y.; Steigerwald, M. L.; Sfeir, M. Y.; Campos, L. M. *J. Am. Chem. Soc.* **2015**, *137*, 8965.

(11) Zirzlmeier, J.; Lehnherr, D.; Coto, P. B.; Chernick, E. T.; Casillas, R.; Basel, B. S.; Thoss, M.; Tykwinski, R. R.; Guldi, D. M. *Proc. Natl Acad. Sci.* **2015**, *112*, 5325.

(12) Lukman, S.; Musser, A. J.; Chen, K.; Athanasopoulos, S.; Yong, C. K.; Zeng, Z.; Ye, Q.; Chi, C.; Hodgkiss, J. M.; Wu, J.; Friend, R. H.; Greenham, N. C. *Adv. Funct. Mater.* **2015**, *25*, 5452.

(13) Varnavski, O. P.; Abeyasinghe, N.; Aragó, J.; Serrano-Perez, J. J.; Ortí, E.; López Navarrete, J. T.; Takimiya, K.; Casado, J.; Goodson III, T. G. *J. Phys. Chem. Lett.* **2015**, *6*, 1375.

(14) Monahan, N.; Zhu, X.-Y. *Annu. Rev. Phys. Chem.* **2015**, *66*, 601.

(15) Zeng, T.; Hoffmann, R.; Ananth, N. *J. Am. Chem. Soc.* **2014**, *136*, 5755.

(16) Aryanpour, K.; Dutta, T.; Huynh, U. N. V.; Vardeny, Z. V.; Mazumdar, S. *Phys. Rev. Lett.* **2015**, *115*, 267401.

(17) Mastron, J. N.; Roberts, S. T.; McAnally, R. E.; Thompson, M. E.; Bradforth, S. E. *J. Phys. Chem. B* **2013**, *117*, 15519.

(18) Roberts, S. T.; McAnally, R. E.; Mastron, J. N.; Webber, D. H.; Whited, M. T.; Brutchey, R. L.; Thompson, M. E.; Bradforth, S. E. *J. Am. Chem. Soc.* **2012**, *134*, 6388.

(19) Pensack, R. D.; Tilley, A. J.; Parkin, S. R.; Lee, T. S.; Payne, M. M.; Gao, D.; Jahnke, A. A.; Oblinsky, D.; Li, P.-F.; Anthony, J. E.; Seferos, D. S.; Scholes, G. D. *J. Am. Chem. Soc.* **2015**.

(20) Yost, S. R.; Lee, J.; Wilson, M. W. B.; Wu, T.; McMahon, D. P.; Parkhurst, R. R.; Thompson, N. J.; Congreve, D. N.; Rao, A.; Johnson, K.; Sfeir, M. Y.; Bawendi, M. G.; Swager, T. M.; Friend, R. H.; Baldo, M. A.; Van Voorhis, T. *Nat. Chem.* **2014**, *6*, 492.

(21) Chien, A. D.; Molina, A. R.; Abeyasinghe, N.; Varnavski, O. P.; Goodson, T.; Zimmerman, P. M. *J. Phys. Chem. C* **2015**, *119*, 28258.

(22) Zimmerman, P. M.; Bell, F.; Casanova, D.; Head-Gordon, M. *J. Am. Chem. Soc.* **2011**, *133*, 19944.

(23) Matsika, S.; Feng, X.; Luzanov, A. V.; Krylov, A. I. *J. Phys. Chem. A* **2014**, *118*, 11943.

(24) Feng, X.; Luzanov, A. V.; Krylov, A. I. *J. Phys. Chem. Lett.* **2013**, *4*, 3845.

(25) Alguire, E. C.; Subotnik, J. E.; Damrauer, N. H. *J. Phys. Chem. A* **2015**, *119*, 299.

(26) Vallett, P. J.; Snyder, J. L.; Damrauer, N. H. *J. Phys. Chem. A.* **2013**, *117*, 10824.

(27) Müller, A. M.; Avlasevich, Y. S.; Müllen, K.; Bardeen, C. J. *Chem. Phys. Lett.* **2006**, *421*, 518.

(28) Müller, A. M.; Avlasevich, Y. S.; Schoeller, W. W.; Müllen, K.; Bardeen, C. J. *J. Am. Chem. Soc.* **2007**, *129*, 14240.

(29) Trlifaj, M. *Czech J Phys* **1977**, *27*, 190.

(30) Charbr, M.; Williams, D. F. *Chem. Phys. Lett.* **1977**, *49*, 599.

(31) Geacintov, N. E.; Burgos, J.; Pope, M.; Strom, C. *Chem. Phys. Lett.* **1971**, *11*, 504.

(32) Stern, H. L.; Musser, A. J.; Gelinas, S.; Parkinson, P.; Herz, L. M.; Bruzek, M. J.; Anthony, J.; Friend, R. H.; Walker, B. J. *Proc. Natl Acad. Sci.* **2015**, *112*, 7656.

(33) Houk, K. N.; Lee, P. S.; Nendel, M. *J. Org. Chem.* **2001**, *66*, 5517.

(34) Walker, B. J.; Musser, A. J.; Beljonne, D.; Friend, R. H. *Nat. Chem.* **2013**, *5*, 1019.

(35) Yang, L.; Tabachnyk, M.; Bayliss, S. L.; Böhm, M. L.; Broch, K.; Greenham, N. C.; Friend, R. H.; Ehrler, B. *Nano Lett.* **2014**, *15*, 354.

(36) Wilson, J. S.; Chawdhury, N.; Al-Mandhary, M. R. A.; Younus, M.; Khan, M. S.; Raithby, P. R.; Köhler, A.; Friend, R. H. *J. Am. Chem. Soc.* **2001**, *123*, 9412.

(37) Caspar, J. V.; Meyer, T. J. *J. Phys. Chem.* **1983**, *87*, 952.

(38) Englman, R.; Jortner, J. *Mol. Phys.* **1970**, *18*, 145.

(39) Fudickar, W.; Linker, T. *J. Am. Chem. Soc.* **2012**, *134*, 15071.

(40) Anthony, J. E.; Eaton, D. L.; Parkin, S. R. *Org. Lett.* **2002**, *4*, 15.

(41) Anthony, J. E.; Brooks, J. S.; Eaton, D. L.; Parkin, S. R. *J. Am. Chem. Soc.* **2001**, *123*, 9482.

(42) Payne, M. M.; Parkin, S. R.; Anthony, J. E. *J. Am. Chem. Soc.* **2005**, *127*, 8028.

(43) Purushothaman, B.; Parkin, S. R.; Anthony, J. E. *Org. Lett.* **2010**, *12*, 2060.

(44) Angliker, H.; Rommel, E.; Wirz, J. *Chem. Phys. Lett.* **1982**, *87*, 208.

(45) Dexter, D. L. *J. Chem. Phys.* **1953**, *21*, 836.

(46) Goto, K.; Yamaguchi, R.; Hiroto, S.; Ueno, H.; Kawai, T.; Shinokubo, H. *Angew. Chem. Int. Ed.* **2012**, *51*, 10333.

8 Exciton Correlations in Intramolecular Singlet Fission

8.1 Preface

This chapter is based on a manuscript published in the Journal of the American Chemical Society entitled “Exciton Correlations in Intramolecular Singlet Fission” by Samuel N. Sanders, Elango Kumarasamy, Andrew B. Pun, Kannatassen Appavoo, Michael L. Steigerwald, Luis M. Campos, Matthew Y. Sfeir. Elango, Andrew and I synthesized all molecules in the Campos Lab while Kannatassen and I performed all spectroscopy in the Sfeir Lab. Dr Steigerwald performed all theoretical modeling.

8.2 Introduction

Multiple exciton generation from a single photon has tremendous potential for technological applications and has generated wide interest in organic singlet exciton fission (SF) compounds.[1-9] A few basic requirements for SF have been developed from advanced theoretical and spectroscopic studies of molecular crystals, which can be used to set the foundation for materials design and fuel the development of next generation devices.[10-22] For example, it has been well established that materials only undergo singlet fission when strong interchromophore electronic interactions are present, extending the spatial distribution of the singlet state over neighboring molecules.[23-26] Additionally, the materials must meet the energy conservation requirement – the singlet state must be greater than or equal to the triplet pair state.[5] Furthermore, it is understood that in molecular crystals, uncorrelated triplets rapidly form at room temperature from a multiexciton state and

diffuse apart, though non-geminate triplet-triplet annihilation can repopulate the singlet state when the energetics of the system permit it. [12,13,27-31]

While the initial and final states of SF have been widely studied, details of the dynamics that occur during singlet fission, e.g., between the singlet and correlated multiexciton (triplet pair) state, have been more difficult to discern. This uncertainty has stemmed from both the short lifetime of the correlated state in condensed phase systems and the similarity of the correlated and uncorrelated triplet pair spectral signatures.[14,32-34] These issues have led to the development of artificial systems designed to isolate exciton correlations, by either slowing down the dynamics of singlet fission, using high concentration solutions for example, or by introducing distinct spectral signatures for singlet fission, as in doped single-crystals.[35-37] Still, there is a lack of a comprehensive understanding of the correlated triplet pair exciton, including a detailed understanding of its formation and decay dynamics.

The recent discovery of efficient intramolecular singlet fission (iSF) materials based on molecular dimers and polymers has expanded the quantity and variety of materials that undergo singlet fission.[9,38-42] They also offer a unique platform to study the dynamical evolution of multiexciton states since the system can be constrained such that exactly two triplet sites exist on the molecule. This restriction prevents separation *via* diffusion, ensuring that all bimolecular recombination processes are geminate. Therefore, this system allows us to identify distinct dynamical processes attributable to a triplet pair. Furthermore, in oligoacene dimers, we can systematically tune the interchromophore interactions, e.g., their proximity, connectivity, or planarity to dramatically modify the triplet pair generation and recombination kinetics.[41,43]

Here, we take advantage of differences in the optical characteristics between tetracene and pentacene to study the exciton dynamics or iSF in a family of pentacene-tetracene heterodimers

(Figure 8.1). The asymmetry of these dimers results from inequivalent singlet and triplet energies in the parent monomers, yielding distinct spectral features associated with excitation of the individual chromophores in the dimer.[43] Critically, this allows us to monitor directly the spatial dynamics of the singlet exciton, as well as both the triplet pair states produced *via* singlet fission and the individual triplet states populated *via* sensitization. By varying the bridge length in the dimer, we can directly show how interchromophore separation affects the triplet formation and relaxation processes.

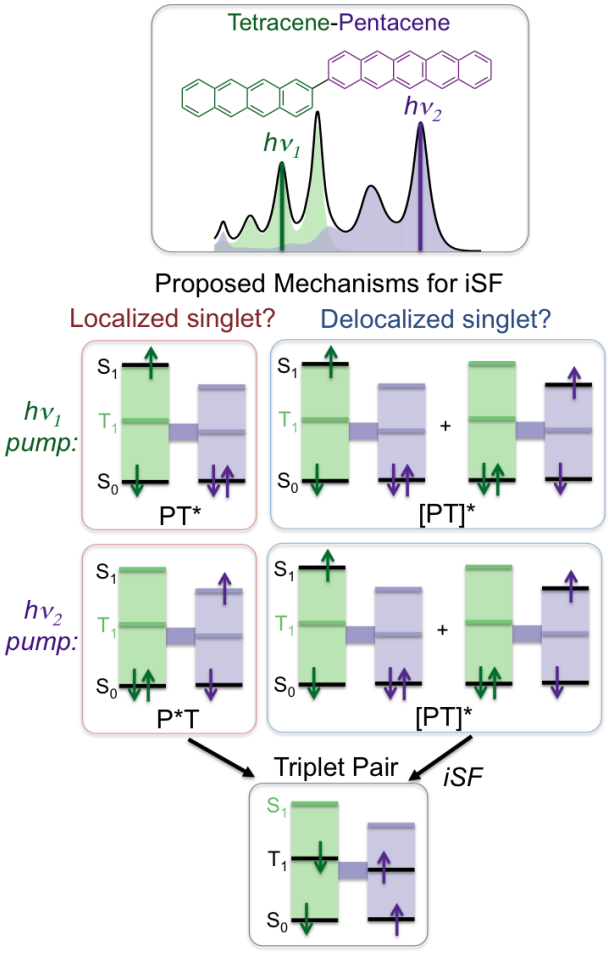

Figure 8.1. (Top) Representation of the absorption spectra of pentacene (purple) and tetracene (green) chromophores, along with their summed absorption (black line). (Middle) Depiction of the competing paths for intramolecular singlet fission based on localized (left) and delocalized (right) singlet states. Asymmetric dimers allow us to demonstrate the delocalization of the singlet exciton

in iSF compounds. (Bottom) The product of singlet fission is a triplet pair, with one triplet localized on each chromophore.

The spatial resolution provided by asymmetric dimers is critical for understanding singlet fission, including the role of exciton correlations. For example, while varying the connectivity in pentacene dimers has yielded valuable information about the kinetics of iSF, there is still considerable debate surrounding the role of singlet exciton delocalization in promoting singlet fission. The understanding of the nature of the photoexcited singlet is of particular interest because it has been suggested that delocalization may be important for promoting rapid singlet fission, and dimers are an ideal model system to further examine this possibility.[44] In a study on ethynylbenzene-separated dimers, the authors propose that the initial photoexcited singlet is localized on one of the two pentacenes in the dimer (P*P). From the time-resolved transient absorption spectra, an apparent rise of the bleach during singlet fission is reported, which is interpreted as fission from a highly localized singlet state, in contrast to what is observed in condensed phase systems.[42,45] On the other hand, two other studies, including our own, report pentacene dimers in which the singlet exciton is initially distributed over both monomers ([PP]*) and demonstrate that overlapping excited state absorption signals associated with the singlet can complicate the single-wavelength kinetics.[40,41] These two competing mechanisms are shown schematically in Figure 1 for the asymmetric pentacene-tetracene (PT) dimers studied here.

Here, we use the term delocalized singlet to describe the situation in which the optically bright state is a linear combination of two locally excited states: [PT]* = [aPT* + bP*T]. This picture of a linear combination of locally excited configurations is an example of the mixing of alternatives that is familiar to organic chemistry as the interaction of valence-bond resonance structures. As Pauling originally described[46], the closer in energy the two alternative structures are, the more important the mixing; in bipentacenes the two alternatives are degenerate while in the

present case the two, PT* and P*T, are energetically distinct, albeit nearly degenerate. This picture of locally excited monomer state mixing is supported by multireference electronic structure calculations on both non-covalent[15,47] and covalent pentacene dimers[48] and by the experimental absorption spectra of bipentacence[41] and pentacene-tetracene heterodimers (Figure 2), in which the monomer and dimer singlet energies differ by only ~ 30 meV. Since there is no systematic dependence on spacer length, the effects are likely related to a change in the effective dielectric screening due to the proximity of an additional chromophore and its associated solubilizing groups. We note that this "delocalization" is what Pauling referred to as resonance delocalization, and it should not be confused with simple orbital delocalization that results in a particle-in-a-box picture. The latter would dramatically shift the energy of the dimer relative to the monomer, the former yields comparatively minor energy consequences. Throughout this manuscript, we use the term delocalization to refer to this resonance delocalization: the linear combination of locally excited states on either the pentacene or tetracene monomer.

The distinct pentacene and tetracene absorption features provide a clear test of a delocalized singlet, in which case an instantaneous bleach of the tetracene spectral features would result when pumping lower energy pentacene absorption features. In contrast to bipentacene dimers, this method is direct and does not rely on resolving complex overlapping transient signals. Similarly, the distinguishability of the individual components in PT allows for direct study of their dynamical evolution, which is not possible in symmetric molecules. This includes the ability to differentiate between concerted and sequential triplet pair decay.

Here, we address these fundamental, unanswered questions by unambiguously characterizing the intrinsic excited state dynamics, from triplet pair formation and recombination, with exquisite spatial and spectral resolution. We use a series of PT heterodimers containing

phenylene spacers between the chromophores to show that the photogenerated singlets are delocalized over both monomers ([PT]*) and that triplet pair formation depends, to some extent, on the extent of singlet delocalization. Furthermore, our study indicates that iSF primarily yields correlated triplet pairs, which exhibit concerted decay processes. This includes a triplet-triplet annihilation process that results in delayed fluorescence, but also a non-radiative internal conversion mechanism, which is distinct from individual triplet decay processes. These decay processes occur rapidly despite the fact that individual triplets are not able to diffuse across the bridge, as determined *via* triplet sensitization experiments. In bridged compounds, a minority population of uncorrelated triplets are formed with a yield that increases with bridge length.

8.3 Synthesis

In order to investigate singlet fission in heterodimers, the pentacene-tetracene heterodimers shown in Figure 2 were synthesized *via* a modular Suzuki coupling strategy that we have adopted for the coupling of various acene building blocks.[41] The compounds are labeled as PTn, where P refers to pentacene, T refers to tetracene, and n refers to the number of phenylene spacers in the linker series, where n = 0, 1, 2. The inclusion of tri-isopropylsilyl acetylene (TIPS) groups renders these heterodimers soluble and stable in solution.[49-51]

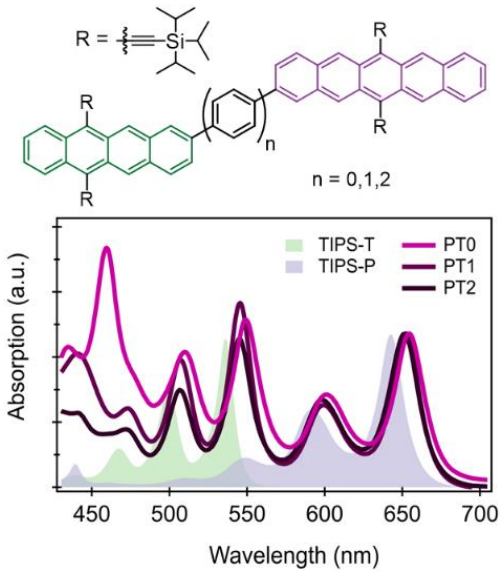

Figure 8.2. Chemical structure (top) and steady-state absorption spectra (bottom) of the PT0, PT1, and PT2 compounds (n=0, 1 or 2) along with TIPS-tetracene and TIPS-pentacene. Absorption spectra are taken in chloroform and normalized at the lowest energy absorption feature.

8.4 Absorption Features

The steady state absorption of the PTn heterodimers shows the characteristic absorption features of both monomers, with the prominent low-energy TIPS-pentacene peak at ~660 nm and the tetracene peak at ~550 nm (Figure 8.2). The relative intensity of the pentacene and tetracene features in the heterodimer spectrum varies among the different compounds, but not systematically with spacer length. Compared to our model absorption (direct sum of monomers) in Figure 8.1, we observe a small redshift relative to the monomer of both pentacene and tetracene features. The high energy feature observed in PT0 is similar to BP0, our previously reported bipentacene, shifted by ~ 40 nm. This feature is specific to directly linked dimers, and does not correspond to a peak in the parent monomers.[41]

8.5 Singlet Delocalization and Exciton Fission

We use broadband transient absorption spectroscopy to understand the exciton dynamics in these molecules. Qualitatively, the dynamics of PTn compounds are similar to those observed in their bipentacene analogs (here referred to as BPn, with n similarly representing the number of phenylene spacers), with a photoexcited singlet exciton rapidly decaying into a triplet pair in dilute solution, consistent with iSF (Figure 8.3). The assignment of the singlet and triplet states is accomplished similar to previous work from our group and others for pentacene dimers.[40-42,52] A brief but thorough discussion of the assignments is found below, with a more extensive discussion in the SI. We assign the singlet excited state absorption features using the correspondence of their temporal decay to the prompt fluorescence signal.

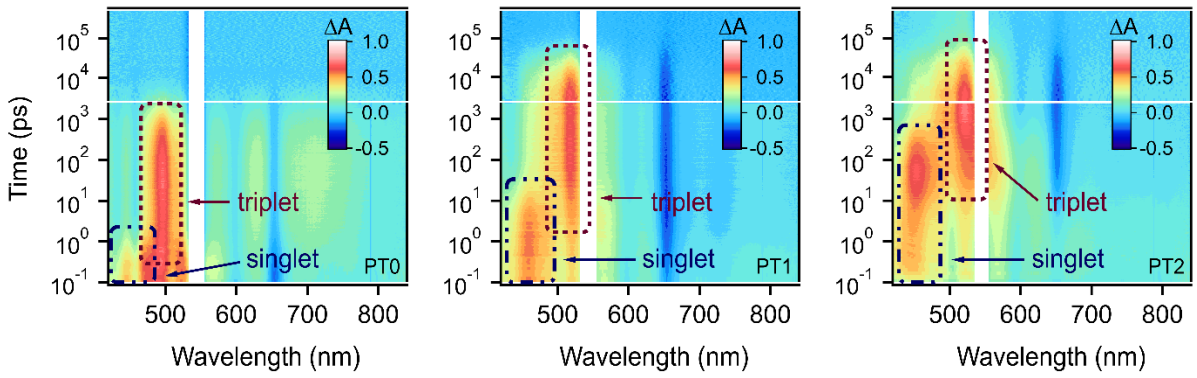

Figure 8.3. Transient absorption spectra of PT0, PT1 and PT2 (left to right), excited at 545 nm (~ 25 μJ/cm^2) in chloroform. The most prominent singlet (dot dash) and triplet (dash) excited state absorption features are outlined for clarity.

We assign the triplet excited state absorption features by comparing the transient spectra of the triplet pair (generated by direct photoexcitation followed by singlet fission) to an individual triplet generated by sensitization. Furthermore, we find that the triplet spectra in these compounds are nearly identical to those in symmetric bipentacene dimers, due to the much large extinction

coefficient of a pentacene triplet relative to a tetracene triplet.[35,53] Finally, we note that the dynamics are concentration independent, ruling out excimer-type singlet deactivation processes.

In contrast to homodimers, the compounds have two unique ground state bleach signals associated with tetracene (~ 550 nm) and pentacene (~ 660 nm) that can be used to track the relative occupation of excitons on each chromophore. Features associated with the triplet pair produced by iSF are dominated by the pentacene $T_1 \rightarrow T_3$ triplet excited state absorption (500 - 520 nm, dash line in Figure 3) due to the much larger triplet absorption cross-section of TIPS-pentacene relative to TIPS-tetracene.[35,53] As observed in homodimers, the singlet fission rate slows down with increasing chromophore separation (larger number of phenyl ring spacers), with time constants of 0.83 ps, 18.3 ps, and 640 ps for PT0, PT1, and PT2, respectively. There is no indication of a parasitic process that would affect the iSF yield. In other words, the rates of singlet decay and triplet formation are directly correlated, and the yields are determined only by the kinetic competition between iSF and the intrinsic monomer decay processes (~ 13 ns).[35,39,41,53]

We find that delocalized singlet excitons are essential for fast and efficient singlet fission. In PTn, the photoexcited singlet exciton contains a signature of both the tetracene and pentacene ground state bleach, even when selectively pumping the absorption features associated with the pentacene monomer. This can be clearly seen by inspection of Figure 8.4a (top panel), which shows the isolated transient spectra corresponding to the singlet, solved by global analysis methods.[54] Here, a pump pulse at 600 nm, resonant with a vibrationally excited S_1 state of pentacene, results in an impulsive bleach of tetracene absorption features at 550 nm. Indistinguishable SF dynamics are observed for direct resonant pumping of the pentacene absorption at 660 nm. The bleach of both chromophores implies a singlet exciton that is delocalized to some extent over the whole molecule.

Interestingly, in PT1 and PT2 (Figure 8.4a), the relative magnitude of the tetracene bleach is reduced when selectively pumping pentacene-associated absorption features as the spacer length is increased. The reduced contribution of the tetracene ground state bleach signals suggests that the singlet wavefunction contains a larger relative fraction of a localized pentacene excitation. This conclusion is supported by density functional theory calculations of the LUMO of these molecules as a function of linker length. While more sophisticated electronic structure methods are necessary to accurately describe the electron correlations these molecules, these calculations illustrate the general trend that the singlet wavefunction starts to resemble a localized pentacene excitation as the length of the bridge increases. Because the pentacene monomer has a smaller singlet energy than tetracene, it is reasonable to expect some preference of the singlet exciton for the pentacene subunit as the electronic coupling is reduced. Following iSF, the isolated triplet pair spectra show the prominent ground state bleach features of pentacene and tetracene in similar magnitude (bottom panel in Figure 8.4a), as is expected for a triplet pair state with one triplet on each chromophore.

Exciting PT1 or PT2 (Figure 8.4b) with a 545 nm pump pulse that is resonant with the tetracene component results in a hot singlet state, which shows an enhanced tetracene ground state bleach signal. The hot singlet state cools rapidly with time constants of ~ 1 ps in PT1 and ~ 12 ps in PT2 to a state nearly identical to the singlet populated under pentacene resonant pumping conditions. During cooling, the relative intensity of the pentacene ground state bleach increases relative to the tetracene ground state bleach features. As cooling in each molecule is much faster than the corresponding overall singlet lifetime, the population and subsequent cooling of this hot exciton has a negligible effect on the overall iSF time constant (~ 19 ps in PT1 and ~ 600 ps in PT2 with 545 nm pump).

The experimentally observed trend towards a more localized singlet (reduced tetracene ground state bleach signal) as the spacer length increases may have relevance to the observed SF rates. Similar SF rates are observed for PT0 and PT1 as compared to BP0 and BP1, respectively. However, in PT2, singlet fission is considerably slower (640 ps time constant) than BP2 (220 ps time constant). Using a similar electronic structure calculation for symmetric BPn as for PTn compounds, we find that the degeneracy of the monomers results in a more delocalized singlet for similar linker lengths.[41] This result suggests that singlet exciton delocalization may be an important or even essential design principle for iSF.

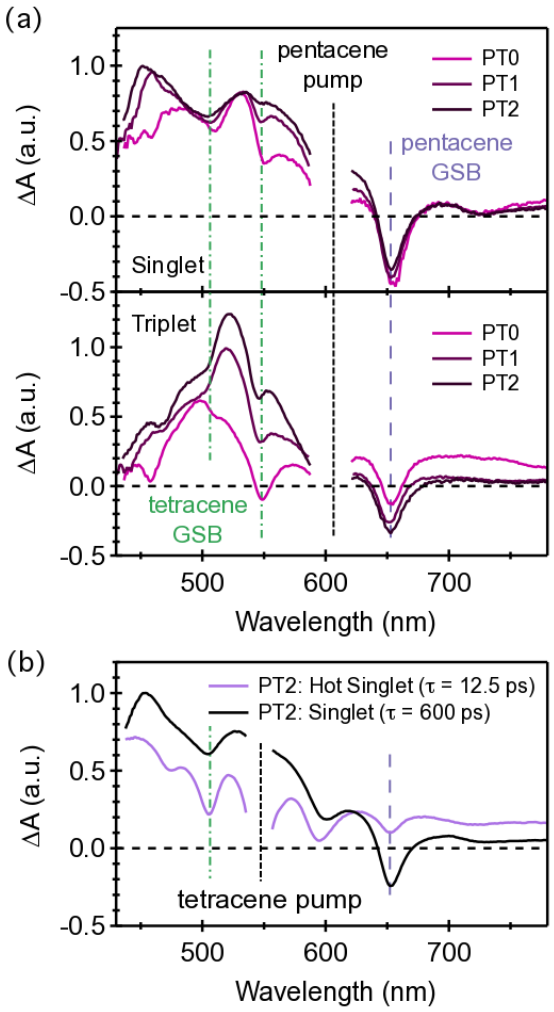

Figure 8.4. (a) Singlet and triplet pair excited absorption spectra from global analysis show that both the pentacene (purple dashed line) and tetracene (green dashed line) ground state bleach are present before (in unequal proportions) and after iSF (in similar proportions) when selectively pumping the low energy pentacene absorption features. (b) When a tetracene absorption peak is resonantly excited, an additional hot exciton state is observed that cools in 12.5 ps. This relaxed singlet state is nearly identical to the state observed when resonantly pumping pentacene, and subsequently undergoes iSF.

8.6 Sensitized Triplet Dynamics

The asymmetric oligoacene dimers also allow us to track the different recombination processes associated with the two inequivalent triplet sites. To this end, we utilize sensitization

experiments, in which pentacene and tetracene triplets are individually populated via collisional transfer from a triplet donor (anthracene) in excess concentration. Because anthracene can transfer an individual triplet to pentacene or tetracene with similar probability, we observe a roughly even mixture of pentacene and tetracene triplets after sensitization, as evidenced by the similar ground state bleach magnitudes for pentacene and tetracene (Figure 8.5).

We find that the triplets are not mobile, but instead remain localized on one half of the dimer. These localized, individual triplets decay with different time constants depending on whether the tetracene or pentacene sub-units are populated. Interestingly, we do not observe triplet transfer within a single heterodimer, e.g., from the higher energy tetracene triplet state to the lower energy pentacene triplet. This process would result in the exclusive population of pentacene triplets at later times. However, we observe the continued presence of both pentacene and tetracene ground state bleach signals at very long timescales. In fact, at long times, the tetracene ground state bleach actually increases relative to the pentacene ground state bleach (Figure 8.5) because tetracene triplets exhibit longer triplet lifetimes than pentacene triplets in agreement with the energy gap law.[55-57] These decay dynamics indicate that both inter- and intramolecular triplet transport from tetracene to pentacene is slow compared to recombination. Presumably, the lack of triplet energy transfer is due to the minimal wave function overlap between the pentacene and tetracene triplet, which are both highly localized due to favorable exchange energy interactions, precluding Dexter energy transfer.[58]

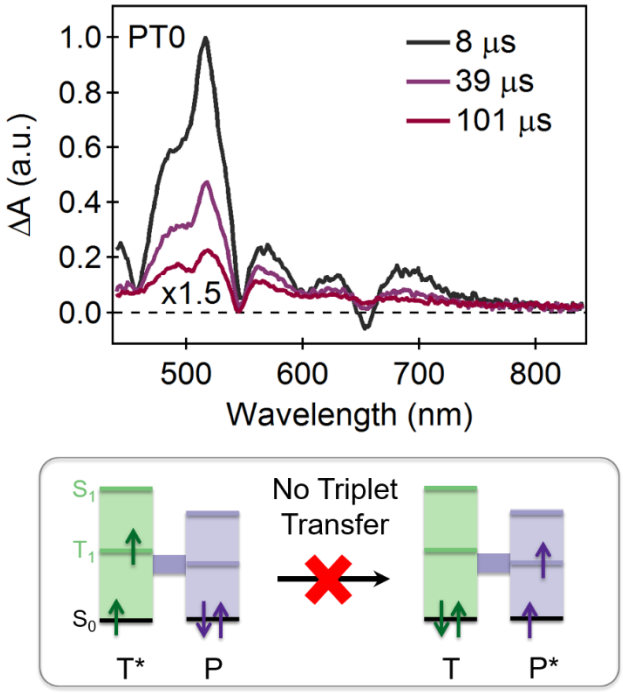

Figure 8.5. Representative sensitization data showing similar weights of GSB on pentacene and tetracene, and the lack of triplet transfer, even at long times.

8.7 Electronic Correlations in Triplet Pairs

Since the ensemble of molecules contains an even population distribution of T_1 in both pentacene and tetracene upon singlet fission (direct photoexcitation), we can directly compare the differential absorption of triplet pairs to single triplets generated by photosensitization and probe differences related to electronic interactions in triplet pairs. In contrast to sensitization experiments, where roughly half the triplet excitons reside on a pentacene monomer and half reside on a tetracene monomer, the product of iSF is one pentacene and one tetracene triplet on the same molecule. While differences would be apparent in individual molecules populated with an individual triplet or triplet pair, the ensembles averages are similar, showing both pentacene and tetracene optical features (Figure 8.6a,b). Similar to our previous work on BPn[41], we observe the

convergence of the individual triplet spectrum (mixture of individual pentacene and individual tetracene triplets) and that of the triplet pair as the phenylene bridges are introduced to spatially separate the triplets.

We stress that despite the convergence of the photoexcitation and photosensitization transient spectra in the bridged compounds, the recombination of the triplet pair and isolated triplet remain quite distinct (Figure 8.6c), indicating a correlated triplet pair (multiexciton) state. Here, we denote a correlated triplet pair as ${}^{M}(TT)$ where M is the appropriate multiplicity (e.g., M = 1 for a net singlet) in contrast to an individual triplet denoted as T_1. For example, the primary decay components of the triplet pair in PT0, PT1, and PT2 are 2.4, ns, 36 ns, and 45 ns, respectively, while individual triplets populated by sensitization in these systems decay in tens of microseconds (Figure 8.6d). The time scales associated with triplet pair decay are summarized in Table 1. In transient absorption, a weaker secondary component with a longer lifetime is observed in the triplet pair decay kinetics of PT1 and PT2. This feature is discussed in detail below. Unlike the sensitized individual triplet decay, the transient spectra as a function of time do not evolve and show the same relative spectral weight for tetracene and pentacene features as a function of time. Our ability to spectrally resolve concerted triplet pair decay in heterodimers allows us to explain a similar effect that was observed in symmetric dimers, where triplet pair lifetimes are orders of magnitude shorter than sensitized triplet lifetimes.

In these heterodimers, the presence of a delayed fluorescence signal allows us to further differentiate between signals originating from correlated triplet pairs and uncorrelated triplets. In our PTn compounds, correlated triplet pairs are nearly isoenergetic to the singlet, and as a result, population transfer between the singlet and triplet manifolds (Figure 8.7a) can occur if angular momentum conservation is satisfied. Since the triplet pairs produced by iSF are correlated into an

overall singlet, $^1(TT)$, facile coupling back to the singlet exciton via a quasi-first order process state results in a long-lived delayed fluorescence signal. The effect of this delayed fluorescence signal can be clearly seen in measurements of the photoluminescence quantum yield (Figure 7b). In contrast to analogous BPn compounds, where no delayed fluorescence is observed due to unfavorable energetics, the emission from these molecules is quite strong, with the PT2 quantum yield reaching 20% of monomeric TIPS-pentacene.

We have measured the delayed fluorescence of the correlated triplet pair using photon-counting techniques (Figure 8.7c). The emission lifetimes for delayed fluorescence are identical to the primary decay component of the triplet pair lifetime as measured using nanosecond transient absorption, confirming our assignment of the state to $^1(TT)$, a triplet pair that is correlated into an overall singlet. Electronic correlations in the spatially constrained triplet pair make the observed triplet-triplet annihilation process quasi-first order, in contrast to second order non-geminate diffusional annihilation in molecular crystals. The longer microsecond timescale component in transient absorption measurements of the PT1 and PT2 compounds with, ~5% and 20% of the total amplitude, respectively, is not present in the measurements of the fluorescence decays. As such, we assign these signals to a minority population of dark triplets, which can no longer couple back to the singlet manifold, that form in PT1 and PT2 due to an additional slow relaxation process. These species are either triplet pairs with non-singlet spin multiplicity, i.e., $^3(TT)$ or $^5(TT)$, or fully localized, independent triplets (2 x T_1). The small population of uncorrelated triplets makes it difficult to determine their exact nature and decay dynamics using optical techniques alone. A more rigorous determination of their spin properties is necessary and is underway in our group.

From the evidence described above, we conclude that correlations exist during the primary (faster) decay component of the triplet pair. To summarize, this is based on 1) the concerted decay

of features corresponding to pentacene and tetracene triplets are observed, 2) the recombination kinetics are faster in the triplet pair than in the corresponding individual triplets (Figure 8.6d), and 8.3) the primary decay component observed in transient absorption measurements corresponds to decay of a delayed fluorescence signal, indicating net singlet character. The presence of both correlated triplet pairs and uncorrelated triplets in these compounds explains the multiexponential triplet decay dynamics we have previously reported for BP1 and BP2 compounds.[41] However, in the previous study we were unable to directly differentiate between triplet states because of the symmetric nature of the BPn compounds and the lack of delayed fluorescence. It is striking that despite the highly localized nature of an individual triplet, strong long-range electronic correlations exist in triplet pairs bridged by multiple phenylene spacers. This observation is especially notable in light of our observation that intramolecular triplet transport is not present in these systems, as demonstrated in Figure 8.5.

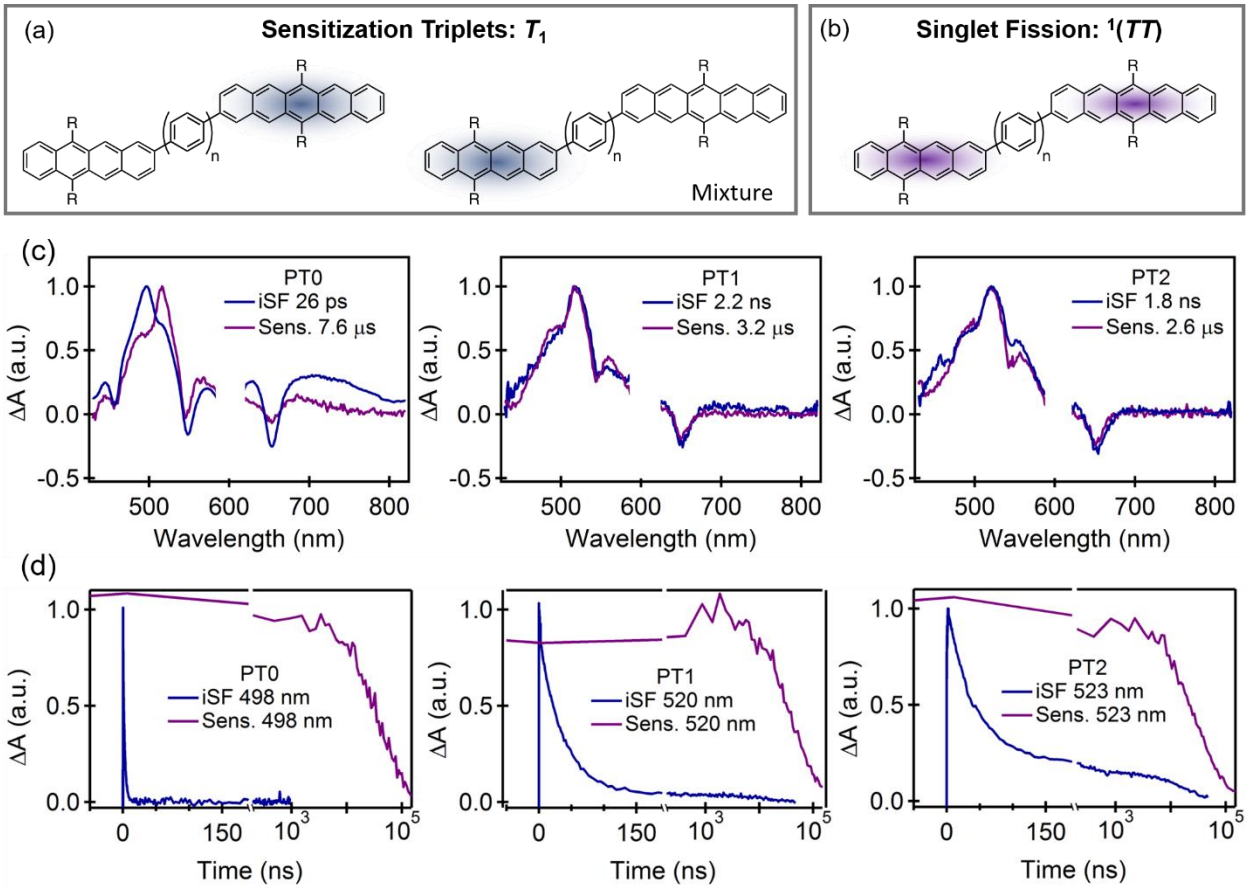

Figure 8.6. a) Photosensitization experiment, where triplets are populated roughly equally on pentacene and tetracene subunits, and b) singlet fission experiment where a triplet pair is populated. The spectral comparison in c) reveals that significant spectral mismatch is only observed when the subunits are directly linked (**PT0**), resulting in a strongly correlated triplet pair. The kinetic comparison in d) shows the lifetime of triplet pairs is shorter than sensitization-populated triplets, but can be extended by inclusion of a longer bridge.

We note that the longer tail observed in time-resolved photoluminescence measurements of **PT0** results from the small amount of fluorescent impurities (TIPS-pentacene monomer) which exist at a level of < 1%. This impurity is visible only in fluorescence measurements because of the high sensitivity of this technique and the long lifetime of the impurity relative to the triplet pair recombination. These signals are similar to what has also been reported in bipentacene compounds.[41] Impurity signals are not directly visible in PT1 and PT2 because of the longer-lived delayed fluorescence signal.

8.8 Analysis of Triplet Pair Recombination Processes

The time evolution of the photoexcited singlet and correlated triplet pair populations are summarized in the diagram in Figure 8.7a, and marked with their corresponding rate constants. Here we use a dark state (*D*) to represent correlated triplet pairs that have decayed either non-radiatively back to the ground state or relaxed into uncorrelated triplets. As such, in our model S_0' is a modified ground state that represents only species that have decayed radiatively from the singlet. This representation allows the overall process to be modeled using a set of coupled differential equations, which were solved numerically to determine the triplet-triplet annihilation rate constant (k_{TTA}). For example, the equation governing the evolution of the correlated triplet pair is:

$$\frac{d[\,{}^1(TT)]}{dt} = k_{iSF}[S_1] - k_{TTA}\left[\,{}^1(TT)\right] - k_D\left[\,{}^1(TT)\right]$$

The iSF rate constant (k_{iSF}) and overall triplet pair population dynamics $[\,{}^1(TT)]_t$ were directly determined *via* global analysis of transient absorption measurements. The radiative decay constant (k_R) from the S_1 state was assumed to be identical to monomeric TIPS-pentacene based on previous measurements of pentacene-anthracene heterodimers.[43] In our full model, we have included the effects of a small impurity contribution (at a level of 0.7%) that is observable in photoluminescence measurements.

The triplet-triplet annihilation rate constant (k_{TTA}) is uniquely determined when our solution reproduces the experimental fluorescence quantum yield, time-resolved decay measurements (proportional to the singlet population as a function of time), and the triplet pair population dynamics. In Figure 8.7b, the dotted lines are the modeled fluorescence quantum yield values (relative to TIPS-pentacene), determined from $[S_0']$ at $t = \infty$, for the k_{TTA} values are listed

in Table 8.1. Similarly, the modeled populations of the singlet state (including the impurity contribution) as a function of time are plotted as the solid lines in Figure 8.7c. With additional spacer length, triplet-triplet annihilation slows down with a similar scaling behavior as the singlet fission rate constants in these compounds.

The rate constants representing direct decay from the triplet pair (k_D) were similarly determined from fitting. In BPn compounds, where no TTA is possible, the triplet pair decay constant is identical to k_D. However, in PTn, triplet-triplet annihilation and subsequent radiative decay modifies the overall triplet pair decay rate, such that it deviates from k_D. In PT1 and PT2, the presence of TTA shortens the overall triplet pair lifetime since decay from the singlet manifold via delayed fluorescence is a viable relaxation channel. Interestingly, the opposite effect is seen in PT0. Since in this system, the singlet lifetime is longer than k_D, interconversion between the singlet and triplet manifolds extends the total lifetime of the triplet pair state. Because the excited singlet is longer lived than the triplet pair, this equilibration actually increases the overall triplet pair lifetime by ~ 6% relative to the rate of k_D. These data are summarized in Table 8.1.

Table 8.1. Time constants for iSF, triplet-triplet annihilation, triplet pair lifetime, and direct triplet pair relaxation for the bipentacene (BPn) series[41] as well as heterodimers (PTn) reported here.

Compound	$1/k_{iSF}$ (ps)	$1/k_{TTA}$ (ps)	$\tau_{1(TT)}$	$1/k_D$ (ns)
PT0	0.83	10	2.4	2.3
PT1	18.3	480	36	40
PT2	640	9300	45	51

BP0	0.76	-	0.45	0.45
BP1	20	-	16.5	16.5
BP2	220	-	270	270

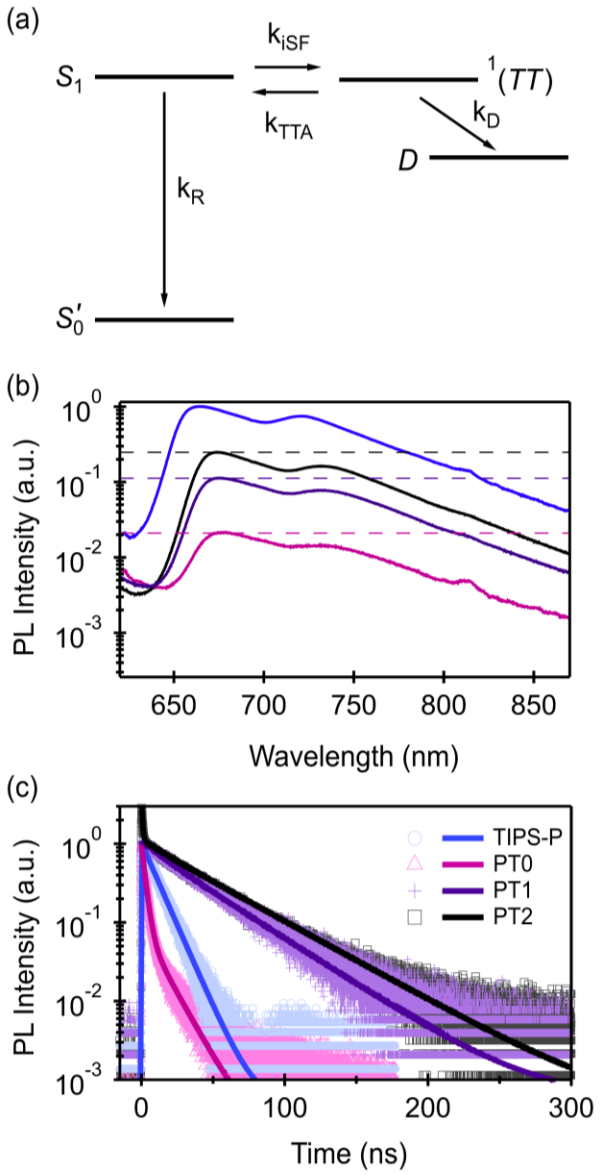

Figure 8.7. Representation of primary kinetic processes and associated rate constants governing the excited state relaxation dynamics after populating the heterodimer singlet (S_1) and triplet pair $^1(TT)$ state, including singlet fission (k_{iSF}), triplet-triplet annihilation (k_{TTA}), radiative recombination (k_R) and triplet pair relaxation (k_D). b) Measured photoluminescence spectra (solid lines) of **PT0**, **PT1**, and **PT2** relative to TIPS-pentacene monomer (561 nm excitation, chloroform as solvent). In **PT0**, the impurity emission decays slower than the heterodimer emission, allowing us to determine the relative concentration and decay lifetime. For heterodimers, the triplet-triplet annihilation rate constant (k_{TTA}) is determined by matching the calculated photoluminescence quantum yield (dotted lines) to the experimental ones, using the method described in the text. c) Measured (symbols) and calculated (solid lines) fluorescence decay curves. These lifetimes correspond to the triplet pair lifetimes measured using transient absorption, indicating that delayed fluorescence is occurring.

While PT1 and PT2 have similar triplet pair lifetimes (36 vs. 45 ns), PT2 forms a significantly larger number of uncorrelated triplets. Based on the amplitude of the long tail of the transient absorption triplet signal in Figure 8.6d, we determine that approximately 25% of triplet pairs in PT2 form uncorrelated triplets compared to only ~ 5% in PT1. A related phenomenon is the greater similarity of the triplet pair lifetime between PT1 and PT2 as compared to BP1 and BP2. Based on the energy gap law, the more energetic triplet pair states in PTn should have slower non-radiative decay relative to the BPn series.[43,55-57] While the energy gap law justifies a 3.88 times longer PT0 lifetime relative to BP0, PT1 has only a 2.44 times longer lifetime than BP1, and PT2 has a 5.4 times shorter lifetime than BP2. This effect is not well captured in our model since our analysis indicates that the overall triplet pair lifetime is only weakly sensitive to k_{TTA} until k_{iSF} becomes comparable to k_R. As such, the enhanced delayed fluorescence observed in PT2 does not appear to be primarily responsible for the shorter than expected triplet pair lifetime. This deviation from the energy gap law is notable and not fully accounted for by the accelerated relaxation into uncorrelated triplets.

8.9 Conclusions

We have synthesized a series of phenylene-spaced pentacene-tetracene heterodimers. These compounds undergo iSF, as demonstrated by ultrafast transient absorption spectroscopy, triplet photosensitization experiments and time-resolved PL spectroscopy. The spectral differentiation of the pentacene and tetracene ground state absorption allows us to track the spatial dynamics of the exciton population in time. In particular, the impulsive appearance of tetracene-associated features when selectively exciting low energy pentacene-associated absorption features shows that a delocalized singlet exciton is the primary product of photoexcitation. However, we find that the

extent of delocalization in these asymmetric dimers is dependent on the bridge length. As the delocalization becomes minimal in the longest bridged compound, the rate of singlet fission slows considerably, suggesting delocalization is important for promoting fast and efficient singlet fission. Furthermore, we find that the primary product of intramolecular singlet fission is a correlated triplet pair (multiexciton state). This state exhibits delayed fluorescence because it is correlated into an overall singlet. Because they primarily decay *via* a correlated process, the tetracene and pentacene triplets decay at the same rate. However, at long times, a triplet signal remains which does not correspond to a delayed fluorescence signal. This observation allows us identify a process in which correlated triplet pairs relax into a state which is not correlated into a singlet. Overall, the novel heterodimer platform enables detailed insights into exciton correlations during singlet fission, which are not accessible with other systems.

8.10 Methods

*Transient Absorption Spectroscopy***.** Transient absorption spectroscopy was performed using a commercial Ti:Sapphire laser system (1kHz repetition rate). A commercial optical parametric amplifier (LightConversion) was used to generate pump pulses with approximately 100 fs pulsewidths. For femtosecond measurements, supercontinuum probe light was generated by focusing the 800 nm fundamental into a sapphire disc. The probe light was split into signal and reference beams, which were detected on a shot-by-shot basis by a fibre-coupled silicon (visible) or InGaAs (infrared) diode array. The pump–probe delay was controlled by a mechanical delay stage. For longer delay times (ns – μs), a separate sub-ns supercontinuum laser is used to generate probe pulses that are electronically synchronized to the ultrafast laser (Ultrafast Systems EOS). All transient absorption spectroscopy was performed on compounds dissolved as a dilute (25-100

μM) solution in chloroform, except for sensitization experiments which are described below. Unless otherwise noted, pump fluences were ~ 25 μJ/cm^2.

*Global Analysis***.** Global analysis was performed with the Glotaran software package (http://glotaran.org).[1] These methods yield more accurate fits of rate constants because they treat the full data set in aggregate. A simple sequential decay model ($S_1 \rightarrow T_1 \rightarrow S_0$) was sufficient to accurately reproduce the exciton dynamics when pumping near the band edge for PT0, PT1 and PT2. When pumping resonant with the tetracene absorption, the sequential decay model was modified to include a hot and relaxed singlet state: $S_{1\text{hot}} \rightarrow S_{1\text{relaxed}} \rightarrow T_1 \rightarrow S_0$.

*Ultrafast Photoluminescence Spectroscopy***.** Ultrafast photoluminescence was measured by the upconversion technique. Briefly, a ~100 μM solution in chloroform was resonantly excited with 560 nm, 100 fs laser pulse. Sum frequency generation was achieved by mixing the spontaneous emission with a "gate" pulse in a nonlinear crystal. The magnitude of the unconverted optical signal was proportional to the instantaneous photoluminescence intensity and was measured at intervals of delay between excitation and gate pulse. The spectral resolution of this measurement was ~10 nm, and cross correlation of scattered light from the excitation pulse with the optical gate pulse found a time resolution of ~250 fs.

*Triplet Photosensitization***.** A solution of~20mM anthracene in chloroform, along with a much smaller concentration of heterodimer (~50 μM) was excited by 360 nm pump light. This pump pulse primarily excites anthracene which generates triplets by intersystem crossing (ISC). Diffusional collisions subsequently transfer these triplets to the heterodimer. Transient absorption measurements are used to track the population dynamics as a function of time.

*Steady-state and Time-resolved Photoluminescence***.** Briefly, the output from a picosecond supercontinuum laser (Fianium SC450-PP) was spectrally filtered using a narrow bandpass filter (561 nm with 2 nm bandwidth). We photoexcited ~50 μM solutions of PT0, PT1, and PT2 in chloroform at fluences of ~ 50 nJ/cm^2. Steady-state emission spectra were recorded using a spectrometer and liquid nitrogen cooled CCD camera (JY Horiba). Delayed photoluminescence data were measured using a spectrometer equipped with an avalanche photodiode and time-correlated single photon counting electronics (Picoquant). The instrument response of this system is ~ 100 ps.

8.11 Ultrafast Spectroscopy

Triplet Photosensitization Measurements of PT0, PT1, and PT2

Triplet photosensitization was employed to study the spectra and dynamics of the native triplets in the pentacene-tetracene heterodimers, and to compare these characteristics to the triplet pairs produced by singlet fission. In all three cases, we initially populate triplets with a roughly even pentacene and tetracene population, as evidenced by the similar heights of GSB for the two monomers. Because there is minimal wavefunction overlap between the pentacene and tetracene triplets, as discussed further in the theory section, we do not observe triplet transfer from the higher energy tetracene to pentacene triplet. The lack of transfer is evidenced by the uncorrelated decay of the pentacene and tetracene GSB's, as well as the longer lifetime of the triplet GSB. If there was transfer on a competitive timescale, it would result in exclusive population of the pentacene GSB at long times.

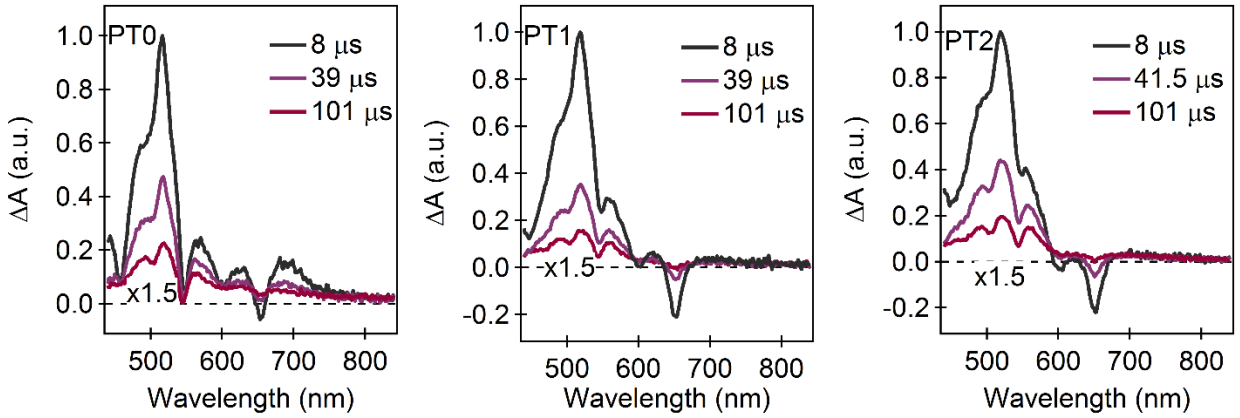

Figure 8.8. Triplet photosensitization on the PTn series reveals similar results for all three compounds, with uncorrelated decay of the pentacene and tetracene triplets, as well as a longer lifetime for the tetracene triplet and an absence of triplet transfer, as discussed in the main text. The 101 μs spectral slice is scaled by 1.5 to facilitate visualization.

The raw data used to create the spectral slices above is also shown in 2D color plots below.

8.12 Assignment of the Triplet Pair State

We assign the triplet pair state in a similar manner to symmetric bipentacene molecules.[2]

We assign the singlet excited state absorption features using the correspondence of their temporal

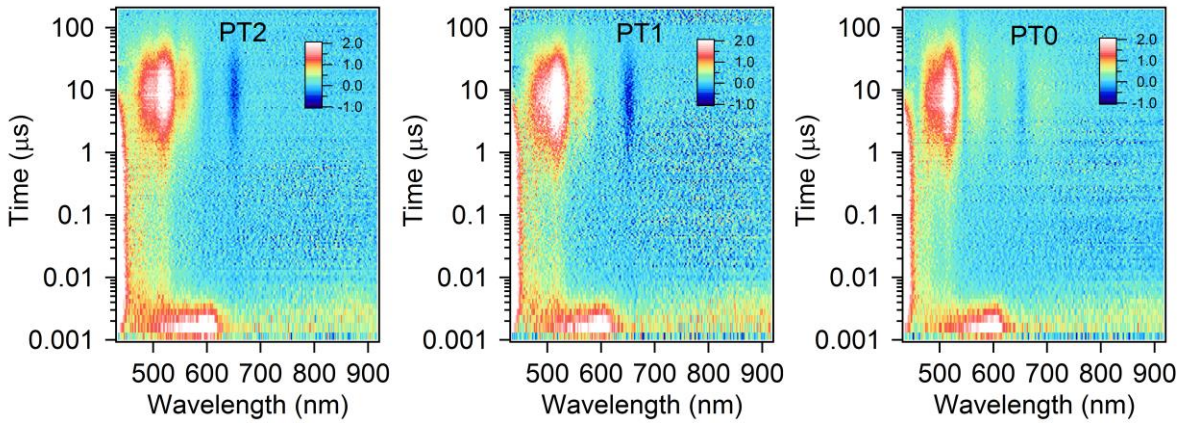

Figure 8.9. Raw data from triplet photosensitization, where the photoinduced absorption near 420 nm corresponds to anthracene triplet excited state transitions. The decay of that signal corresponds primarily with transfer to the rise of the heterodimer triplet signal. The color scale is represented in arbitrary units.

decay to the prompt fluorescence signal, measured using photoluminescence upconversion spectroscopy. The prompt fluorescence dominates the early time with a weaker delayed fluorescence signal visible as the longer lived tails whose decay are not resolved in this measurement (3 ns dynamic range). The decay of the delayed fluorecence is measured using time-correlated single photon counting methods, and is discussed in detail in the main mauscript.

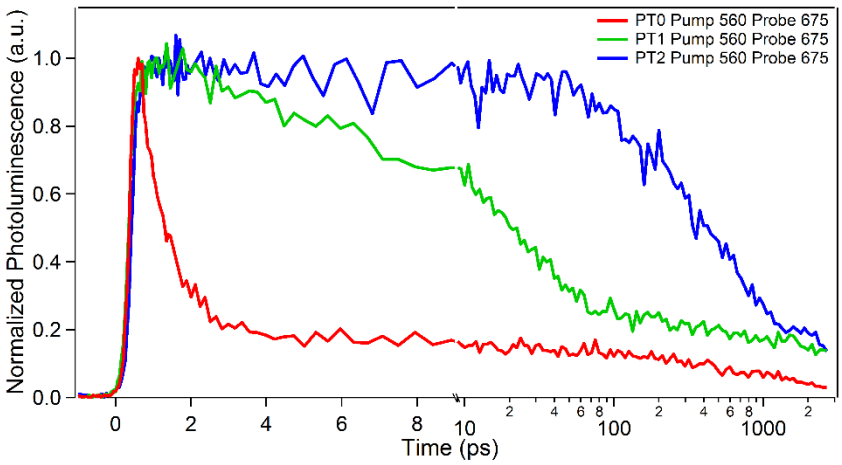

Figure 8.10. Photoluminescence upconversion spectroscopy shows the decay of the photoexcited singlet (first exponent of decay) in agreement with time constants for singlet decay determined by TA spectroscopy. The residual PL observed (second exponent) in the pentacene-tetracene dimers is delayed fluorescence, which we further probe with time correlated single photon counting, as discussed below

The assignment of triplet transient absorption features is based on the correspondence of the triplet pair transient spectra to that of an individual triplet populated via sensitization. The singlet fission and sensitization data for PTn are found in Figure 6c. Here, the triplet pair state can be readily distinguished from the photoexited singlet state primarily by the appearance of the strong pentacene $T_1 \rightarrow T_3$ excited state absorption feature at ~ 530 nm after singlet fission (Figure 8.4a). The triplet pair states in symmetric bipentacene (BPn) dimers have nearly identical transient spectra to those in asymmetric PTn heterodimers since the excited state absorption cross-section

of pentacene is much greater than that of tetracene.[3,4] The triplet pair states are optically dark (non-emissive) in bipentacene but emissive in PTn because of energetic considerations that bring the singlet and triplet pair state into near resonance.

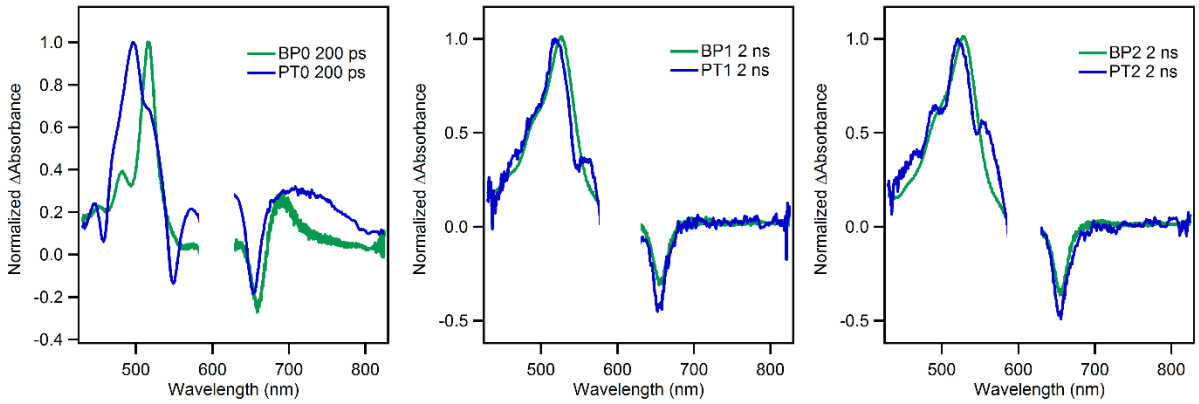

Figure 8.11. The triplet pair spectra of **PTn** compounds (blue) are nearly identical to those of their corresponding **BPn** analogs (green) due to the much larger cross section of the triplet excited state absorption signal of pentacene as compared to tetracene.

Furthermore, in all PT compounds, the transient spectra of the emissive correlated triplet pair state (~ 40ns lifetime in PT1 and ~ 50 ns lifetime in PT2) and the dark uncorrelated triplet state (> 1μs lifetime) state are nearly identical. The unchanging transient spectra are consistent with the evolution of a triplet pair correlated into an overall singlet to individual triplet molecules, but incompatible with an evolution from a relaxed emissive singlet state to another dark electronic configuration. The static spectrum of the correlated triplet pair as a function of time indicates a correlated decay process, in stark contrast to the decay of uncorrelated triplets, such as those produced in sensitization experiments.

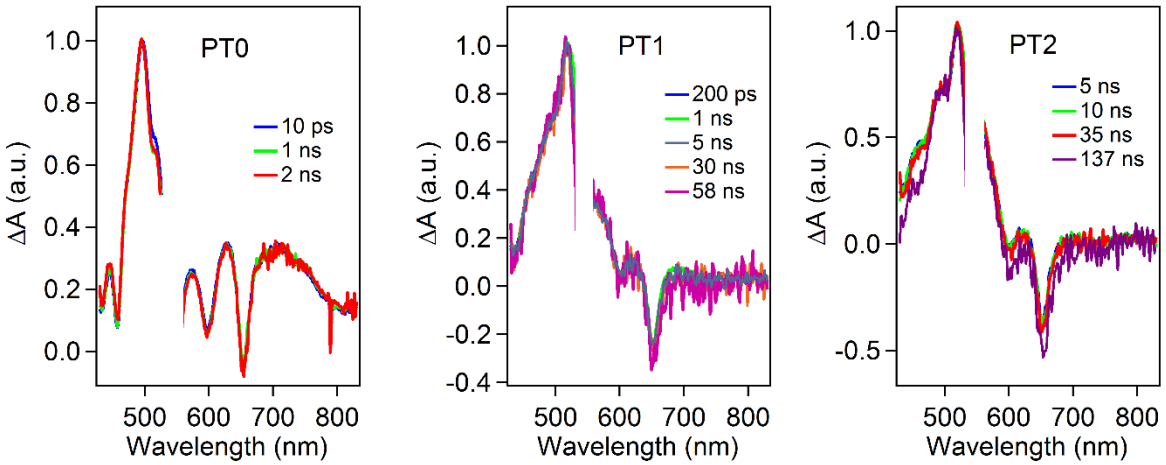

Figure 8.12. Transient absorption spectroscopy reveals a static triplet pair spectrum during the correlated triplet pair decay. Transient spectra corresponding to an uncorrelated triplet state for **PT1** (58 ns) and **PT2** (137 ns) are nearly identical to the correlated triplet pair.

Finally, the carrier dynamics are independent of the concentration. These characteristics rule out electronic states resulting from excimer-type singlets.

8.13 Concentration, Pump Wavelength and Fluence Independent Singlet Fission in PT0, PT1, and PT2

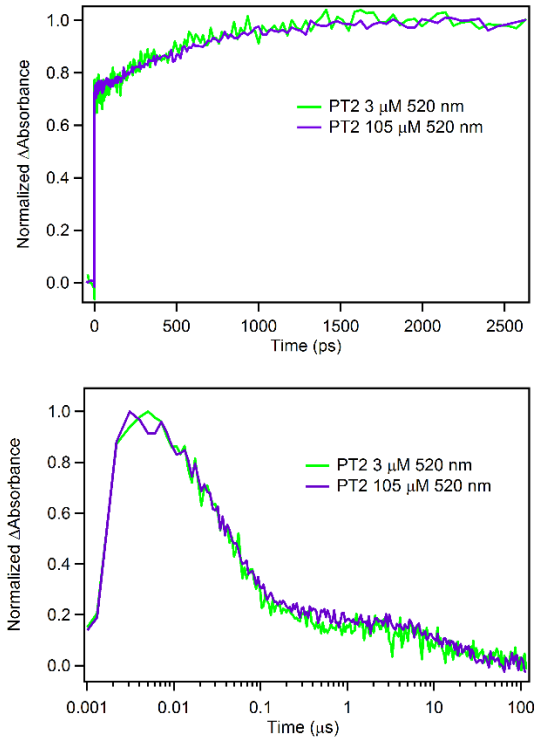

Figure 8.13. Femtosecond (top) and nanosecond (bottom) transient absorption kinetics of 3 μM (purple) and 105 μM (green) concentrations of **PT2** solutions in chloroform. The data is taken at the peak of the triplet excited state absorption signal (521 nm) but contains contributions from the singlet excited state absorption at early times. Similar behavior is observed for **PT0** and **PT1**.

All three **PTn** heterodimers were probed as dilute solutions in chloroform at three separate pump wavelengths. We pump at 545 nm to resonantly excite the tetracene monomer, as shown in the main text. We also pump at 600 nm to excite the pentacene momoner while still allowing us to observe the strongest GSB feature at 660. We finally pump at 660 and find that fission in these systems is spontaneous and does not require excess pump energy. The only difference is that, when

exciting transitions associated with the tetracene monomer, a hot exciton is first populated which cools to the equilibrium singlet.

In the case of 545 nm pump wavelength, the features associated with the tetracene monomer are photoexcited, resulting in a hot singlet exciton. This state then relaxes, over ~1 ps and ~12 ps for PT1 and PT2 respectively, to resemble the singlet exciton populated by pumping the pentacene transitions. This relaxation can be followed by the decrease in tetracene GSB and increase in pentacene GSB as the singlet relaxes. These two spectra, isolated by global analysis, are shown below.

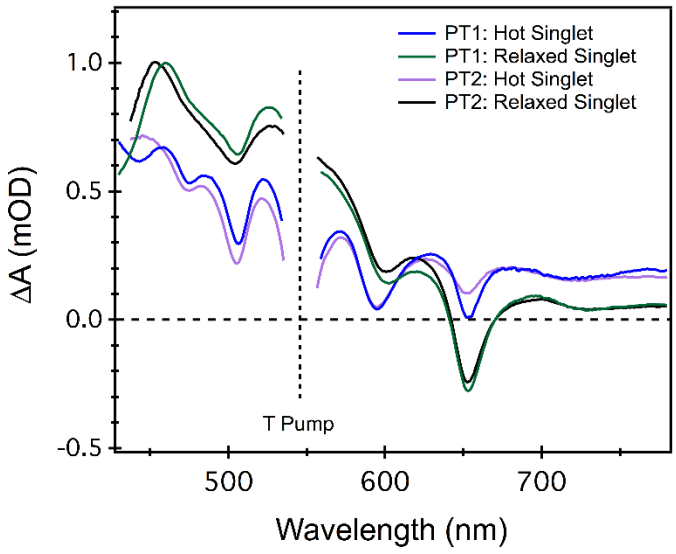

Figure 8.14. Global analysis reveals a hot singlet that is generated impulsively when resonantly exciting the tetracene at 545 nm. This hot singlet relaxes in ~1 ps and ~12 ps in PT1 and PT2, respectively, to the relaxed singlet that subsequently undergoes SF on a similar timescale to SF when we simply excite the pentacene transitions.

Because the cooling of the hot exciton is considerably faster in PT0, PT1 and PT2 than the iSF process, we do not observe a significant effect of pump wavelength on iSF rate. When exciting

transitions associated with the pentacene monomer, the equilibrium singlet is directly populated with no evidence of a hot exciton.

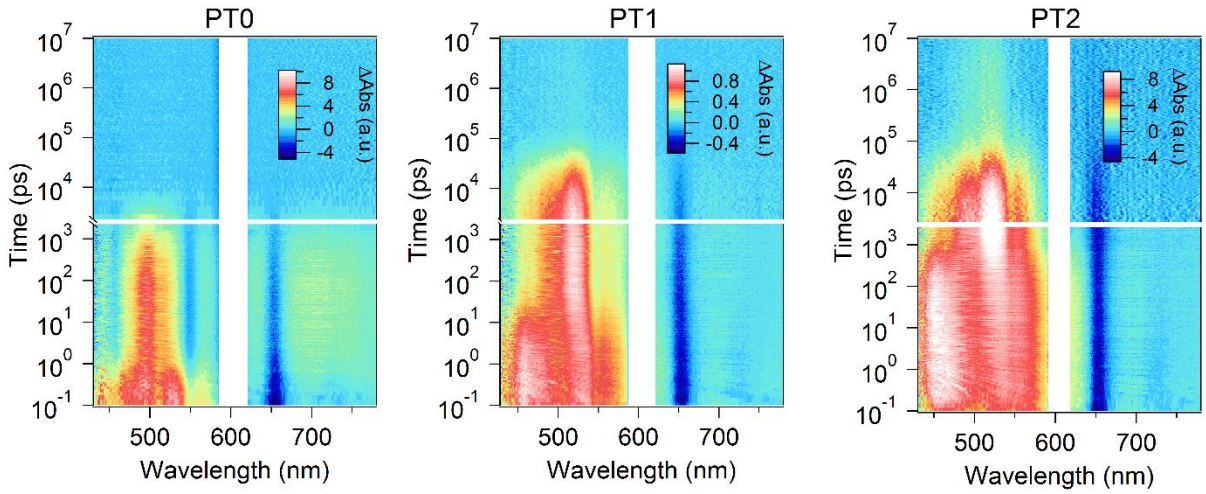

Figure 8.15. Raw data from transient absorption measurements pumping 600, a transition in the pentacene manifold. The color scales are plotted in arbitrary units. Note the different time axis for PT0 (far left) compared to PT1 (middle) and PT2 (far right).

Indistinguishable dynamics are found when pumping at 660 nm, near the pentacene absorption onset, as shown below.

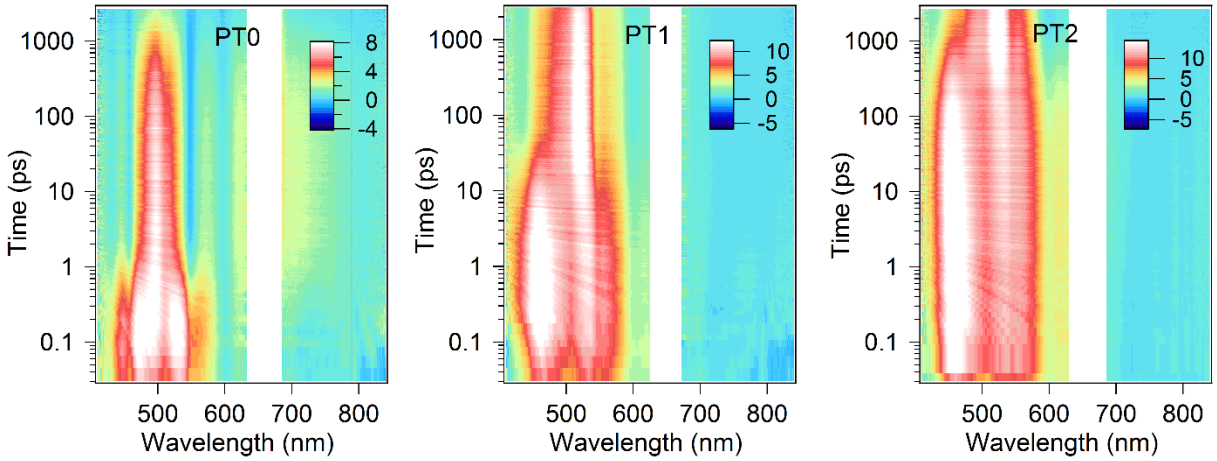

Figure 8.16. Femtosecond transient absorption data reveals identical fission dynamics when excited at 660 nm, the first vibrational peak of the S0→ S1 manifold, as compared to excitation at 600 nm shown above for PT0, PT1 and PT2 (left to right).

We note that the observed dynamics are also independent of pump fluence.

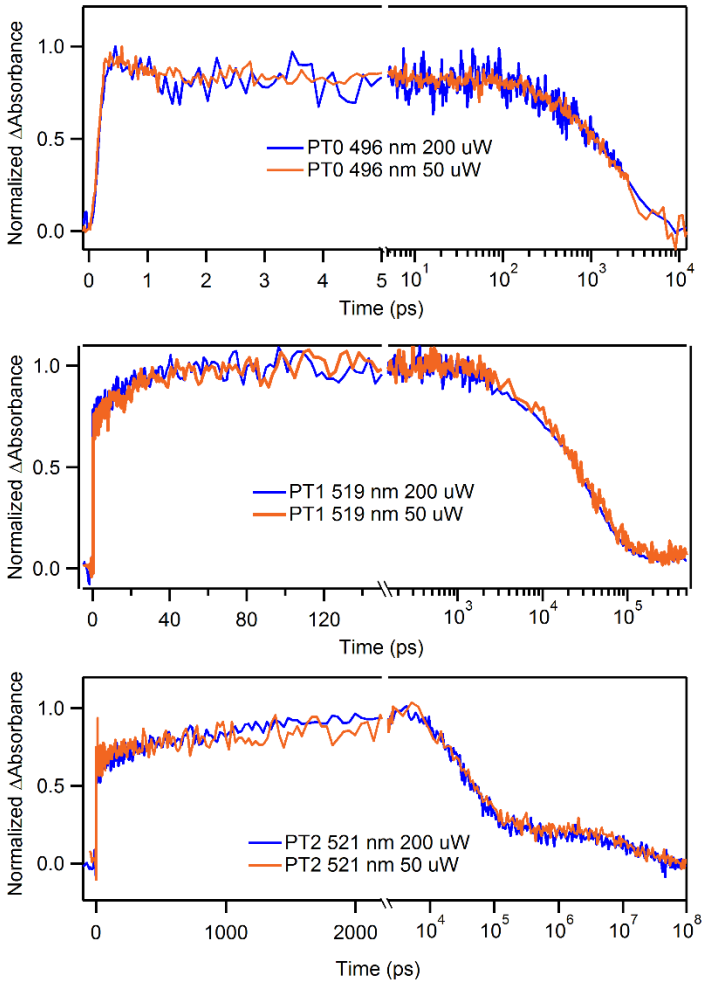

Figure 8.17. The normalized singlet fission and recombination dynamics of **PT0** (top), **PT1** (middle), and **PT2** (bottom) are identical for pump fluences of ~50 μJ/cm^2 (blue) and ~12 μJ/cm^2 (orange). Here the kinetics are shown near the peak of the triplet excited state absorption feature but also reflect the dynamics of the overlapping singlet excited state absorption features at early times.

8.14 Analysis of Delayed PL

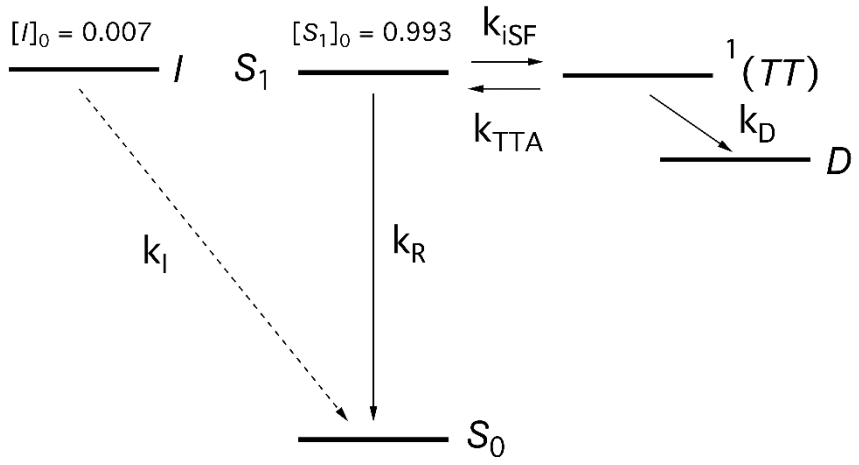

Figure 8.18. Full model used to reproduce prompt and delayed fluorescence data, where we have included a small 0.007% monomeric impurity contribution which fluoresces with rate K_1, the singlet (S_1) which emits at rate k_R, the rates of iSF shown as k_{iSF}, the rate of triplet triplet annihilation to repopulate the singlet, shown as k_{TTA}, and k_D, the rate at which the correlated $^1(\boldsymbol{TT})$ state irreversibly converts to a dark state that is no longer in equilibrium with the singlet.

Here, S_0 is a subset of the ground state that is accessible only via radiative decay of the photoexcited singlet state (S_1). The decay of the triplet pair state $^1(TT)$ is captured in the state labeled *D*, including direct non-radiative decay of triplet pairs back to the ground state as well as relaxation into uncorrelated triplets. These states are coupled by conversion processes (with associated rate constants) including photoluminescence (k_R), singlet fission (k_{iSF}), triplet pair decay (k_D), and triplet-triplet annihilation (k_{TTA}).

I is an impurity state resembling TIPS-pentacene that exists at an ~ 0.7% level and which is excited simultaneously with S_1. It decays emissively with rate constant (k_I) and is observed at long times in TRPL measurements of PT0, the only system in which the impurity lifetime is longer than triplet pair decay. Allowing this state to decay into S_0 allows us to model the total effective PL quantum yield, since differences in the emission spectra between S_1 and *I* is not resolved in our

measurement. There are likely small amounts of impurities with TIPS-tetracene emission characteristics. However, at the wavelength where the dimer emission is measured (680 nm), emission from impurities with TIPS-pentacene character dominate. The emission spectra of TIPS-tetracene and TIPS-pentacene are shown below. At 680 nm, TIPS-P emission is ~ 7.5x stronger than TIPS-T. As such, TIPS-T impurities can be ignored in our model.

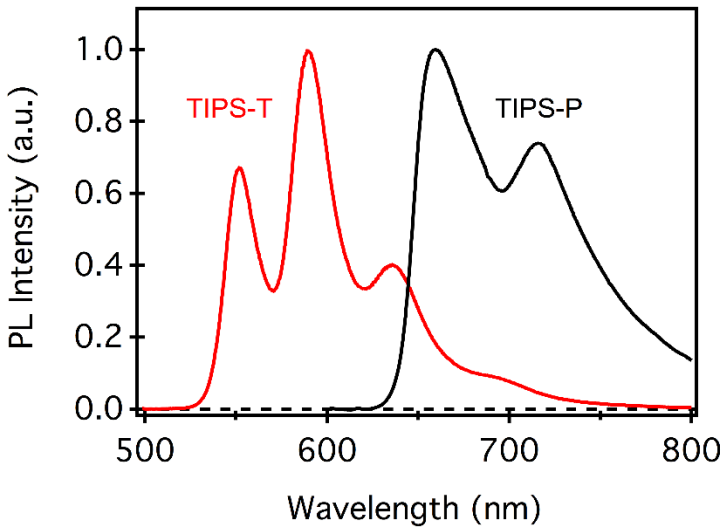

Figure 8.19. The steady-state emission spectra of TIPS-tetracene (red) excited at 514 nm and TIPS-pentacene (black) excited at 561 nm.

This state diagram results in a set of coupled differential equations, which can be solved numerically:

$$\frac{d[S_1]}{dt} = -k_{iSF}[S_1] - k_R[S_1] + k_{TTA}\left[{}^1(TT)\right] \qquad (1)$$

$$\frac{d[{}^1(TT)]}{dt} = k_{iSF}[S_1] - k_{TTA}\left[{}^1(TT)\right] - k_D\left[{}^1(TT)\right] \qquad (2)$$

$$\frac{d[S_0]}{dt} = k_R[S_1] + k_I[I] \qquad (3)$$

$$\frac{d[I]}{dt} = -k_I[I] \quad (4)$$

The rate constant for radiative decay of the singlet state (k_R) is set to the value of the emission lifetime in TIPS-pentacene and in pentacene-anthracene heterodimers (1/13 ns) and is assumed to be constant for all PTn molecules.[5] We assume a rate similar to TIPS-pentacene monomer radiative rate is a reasonable assumption based on measurements of pentacene-anthracene heterodimers we have previously reported, where dimerization is not found to have a significant effect on singlet state radiative rate.[5] The rate constant for singlet fission (k_{iSF}) is extracted from the singlet dynamics in transient absorption measurements, extracted using global analysis methods. Similarly, the triplet pair decay $[\,^1(TT)]_t$ is determined from the triplet decay component from transient absorption measurements that is coincident with the delayed fluorescence decay.

The rate constant for decay of the impurity level (k_I) matches the uncoupled TIPS-pentacene lifetime, determined from fitting the long tail in the PT0 time-resolved fluorescence data. The impurity concentration is obtained from fitting the PT0 time-resolved photoluminescence data, in which the impurity emission can be directly observed. We note that the impurity levels are too small to be seen in transient absorption measurements. Using initial conditions $[S_1]_0 = 0.993$ and $[I]_0 = 0.007$, we can solve for the overall dynamics and total PL quantum yield. The singlet contribution can then be recovered keeping the same rate constants but setting $[I]_0 = 0$.

The remaining rate constants are determined by adjusting k_{TTA} and k_D to reproduce the experimentally measured triplet pair lifetime, quantum yield, and time-resolved fluorescence data.

Following this analysis, the overall quantum yield for fluorescence can be predicted by calculating [S_0] at long times (after all dynamics have completed). Both experimental and calculated values are specified relative to TIPS-pentacene.

Table 8.2. Summary of rate constants and photoluminescence quantum yields for the PT_n series

Compound	k_{TTA} (ns^{-1})	k_D (ns^{-1})	*QY (total)*	*QY (S_1)*
TP0	100	0.44	0.021	0.015
TP1	2.08	0.025	0.112	0.106
TP2	0.11	0.02	0.248	0.242

8.15 Density Functional Theory Calculations

Density Functional Theory (DFT) and Time Dependent DFT (TDDFT) calculations (using the B3LYP functional and with the 6-31G** basis sets) were performed using Jaguar (version 8.4, Schrodinger Inc., New York, NY, 2013). The singlet ground state geometries of all the molecules were optimized; for computational simplicity the TIPS groups were abbreviated to trimethylsilyl groups.

For each molecule examined the excited singlet and triplet states at the vertical geometry, i.e., at the geometries that were optimized for the ground state. TDDFT gave the excited singlet states, and restricted open shell density functional theory (RODFT) gave the lowest-energy triplet state. TDDFT also gave descriptions of higher-lying triple states, using the lowest-energy triplet as the basis for the excited triplet calculations.

In the lowest-energy triplet state the two, singly-occupied orbitals containing the triplet-coupled electrons are localized primarily on the pentacene; in the higher-energy triplet state the corresponding two orbitals are localized on the tetracene. This localization is a consequence of exchange interactions which tend to localize triplets. The physical separation between the triplet orbitals in the "tetracene triplet" and those of the "pentacene triplet" results in static triplets which are unable to undergo Dexter triplet transfer, which requires overlap of the initial and final wavefunctions.[6]

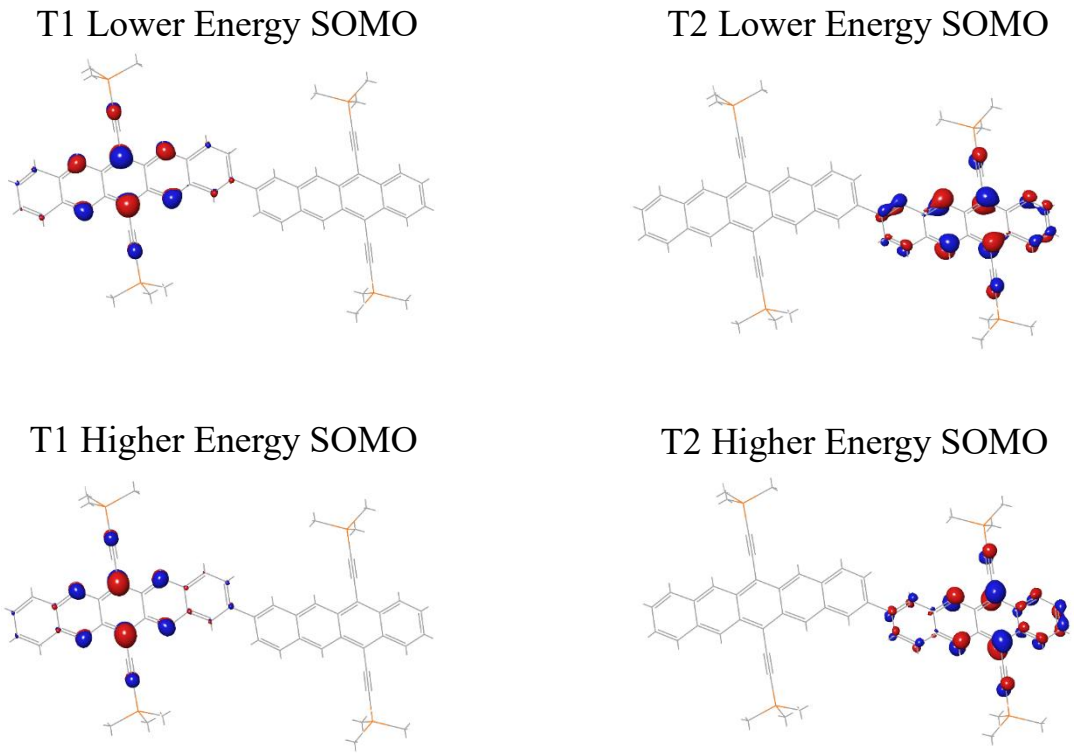

Figure 8.20. Low and high energy SOMO's for T1 and T2 reveal a triplet highly localized on the center of the pentacene, or a triplet highly localized on the center of tetracene, with no observable wavefunction overlap between these two states.

In order to compare to the experimental spectroscopic data, we used TDDFT to calculate the absorption spectra of PT0, PT1, and PT2. In each case the lowest-energy allowed optical

absorption corresponds to the promotion of an electron from the HOMO to the LUMO, and in each case the two orbitals are localized primarily on the pentacene fragment of the molecule. Nevertheless we find there is noticable delocalization of the two orbitals onto the tetracene fragment in PT0. This leakage out of the pentacene is less in PT1 and still less again in PT2. The extent of delocalization manifests itself in the TA data, where we see impulsive bleach of tetracene even when pumping pentacene transitions, but with the largest relative contribution in PT0 and decreasing from PT1 to PT2. It should be stressed that this result is unique to the heterodimer system, where two subunits with *different* singlet energies are covalently linked. In our previous work on bipentacenes, we observe a very delocalized singlet exciton both in DFT calculations and in spectral measurements of the GSB before and after fission.[2]

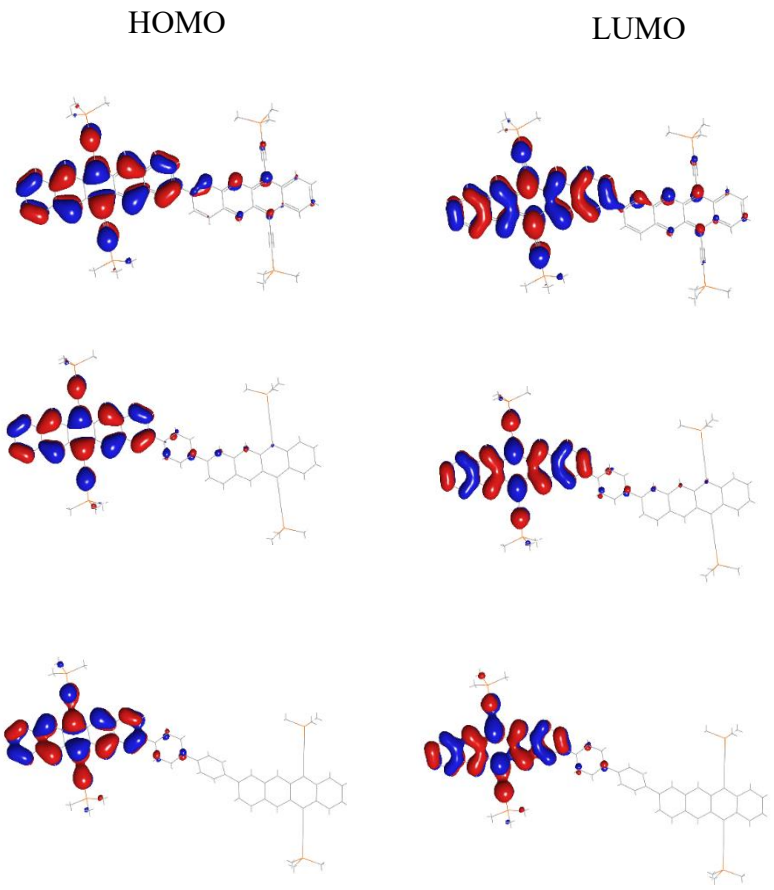

Figure 8.21. HOMO and LUMO levels for PTn reveal a relatively delocalized singlet HOMO in PT0, with the majority of density on the pentacene subunit, that becomes progressively more localized as the bridge length is increased.

Shown below, the HOMO-1 and LUMO+1 are primarily localized on the tetracene. Similar to the HOMO and LUMO, the most delocalization is observed in PT0, then PT1 and the least in PT2.

HOMO -1 LUMO+1

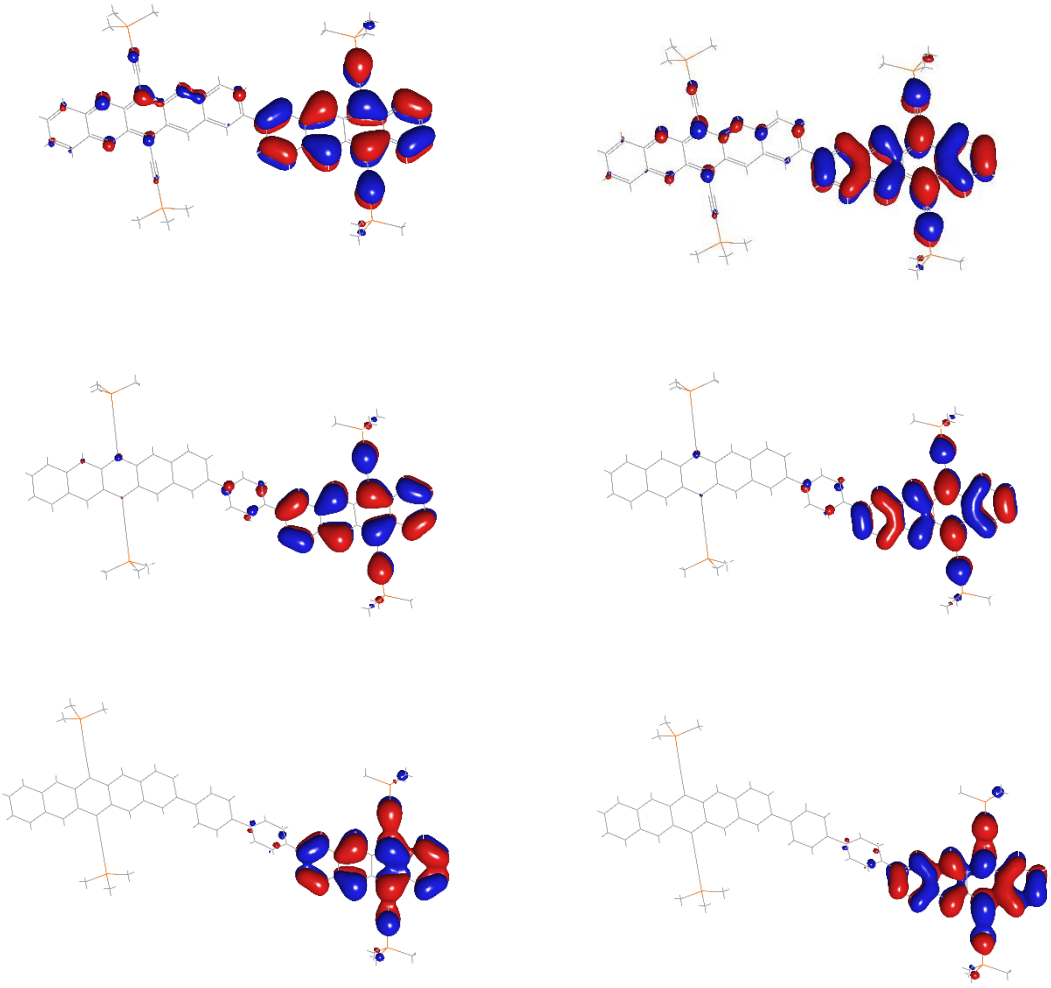

Figure 8.22. The HOMO-1 and LUMO+1 are primarily on the tetracene subunit, but with some delocalization to the pentacene which decreases with increasing bridge length.

8.16 Optimized Geometries

The optimized ground state geometries for the PT0, PT1 and PT2 are shown below. The TIPS groups have been abbreviated to trimethylsilyl groups for computational simplicity. The coordinates for the atoms are given at the end of this section.

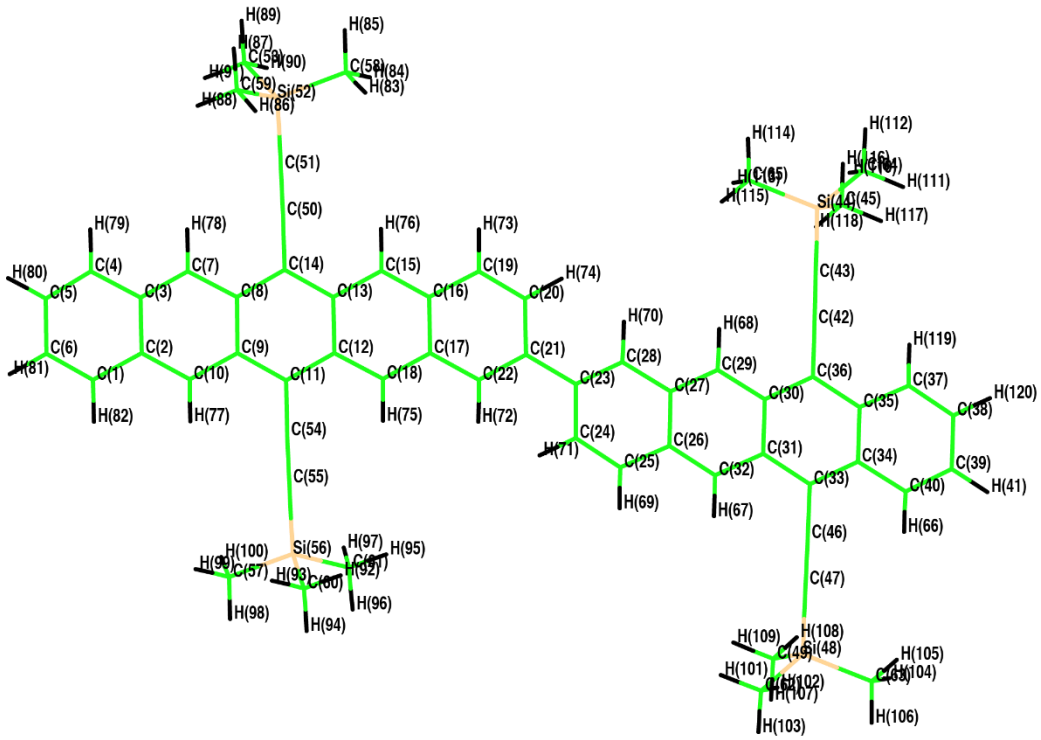

Figure 8.23. PT0 optimized ground state geometry with labeled atoms.

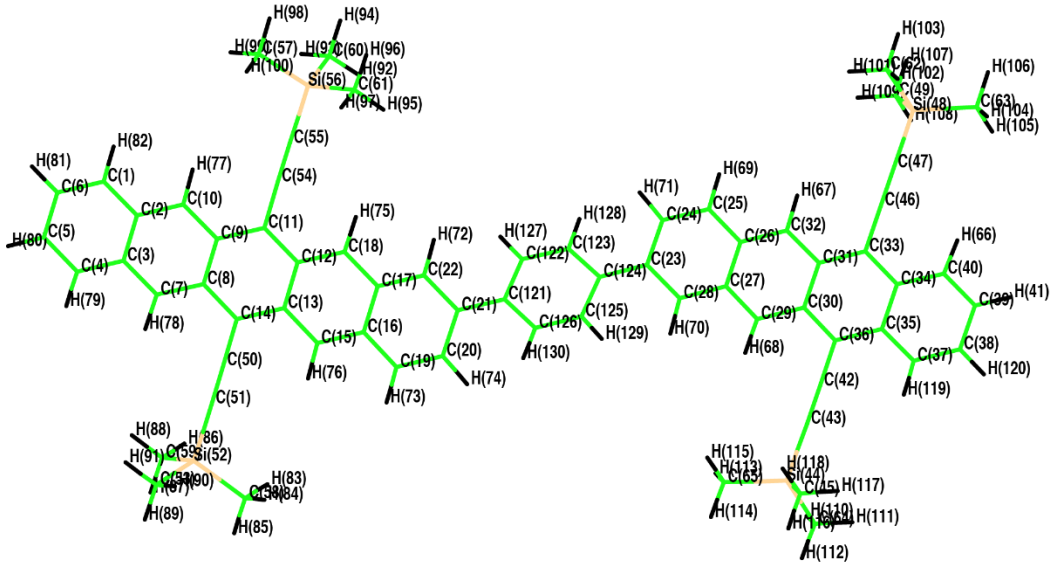

Figure 8.24. PT1 optimized ground state geometry with labeled atoms.

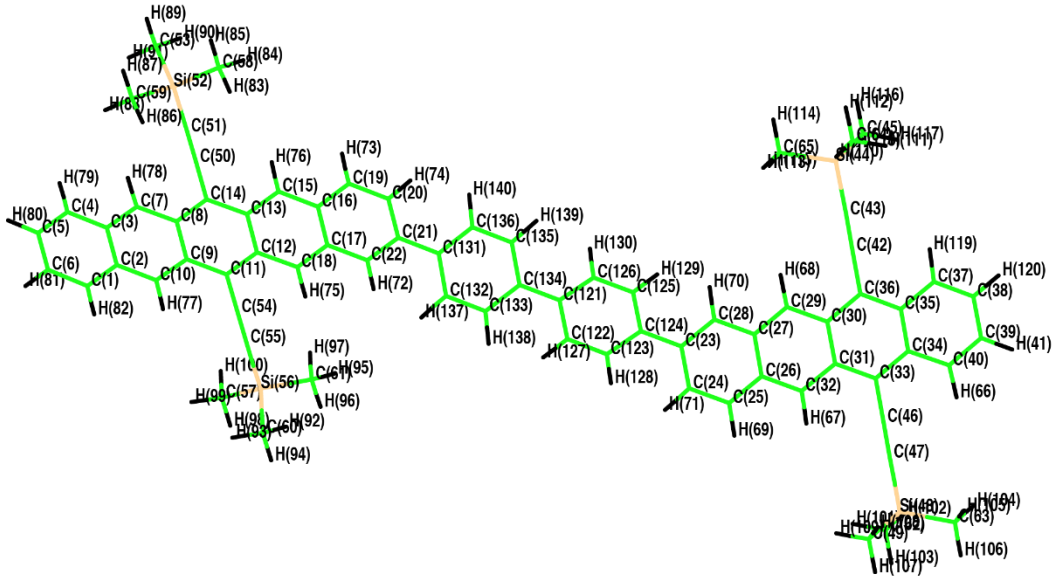

Figure 8.25. PT2 optimized ground state geometry with labeled atoms.

PT0:

Final total energy: -3478.24015 hartrees

8.17 Synthesis

General Methods

All commercially obtained reagents/solvents were used as received; chemicals were purchased from Alfa Aesar®, Sigma-Aldrich®, Acros organics®, TCI America®, Mallinckrodt®, and Oakwood® Products, and were used as received without further purification. Unless stated otherwise, reactions were conducted in oven-dried glassware under argon atmosphere. ^{1}H-NMR and ^{13}C-NMR spectra were recorded on Bruker 400 MHz (100 MHz for ^{13}C) and on 500 MHz (125 MHz for ^{13}C) spectrometers. Data from the ^{1}H-NMR and ^{13}C spectroscopy are reported as chemical shift (δ ppm) with the corresponding integration values. Coupling constants (*J*) are reported in hertz (Hz). Standard abbreviations indicating multiplicity were used as follows: s (singlet), b (broad), d (doublet), t (triplet), q (quartet), m (multiplet) and virt (virtual).

The mass spectral data for the compounds were obtained from XEVO G2-XS Waters® equipped with a QTOF detector with multiple inlet and ionization capabilities including electrospray ionization (ESI), atmospheric pressure chemical ionization (APCI), and atmospheric solids analysis probe (ASAP). The base peaks were usually obtained as $[M]^{+}$ or $[M+H]^{+}$ ions.

Absorption spectra were obtained on a Shimadzu UV 1800 UV-Vis spectrophotometer. Anhydrous solvents were obtained from a Schlenk manifold with purification columns packed with activated alumina and supported copper catalyst (Glass Contour, Irvine, CA). All reactions were carried out under argon unless otherwise noted.

General Protocol for the synthesis of Heterodimers:

Synthesis of tetracene-pentacene derivatives PT0, PT1 and PT2:

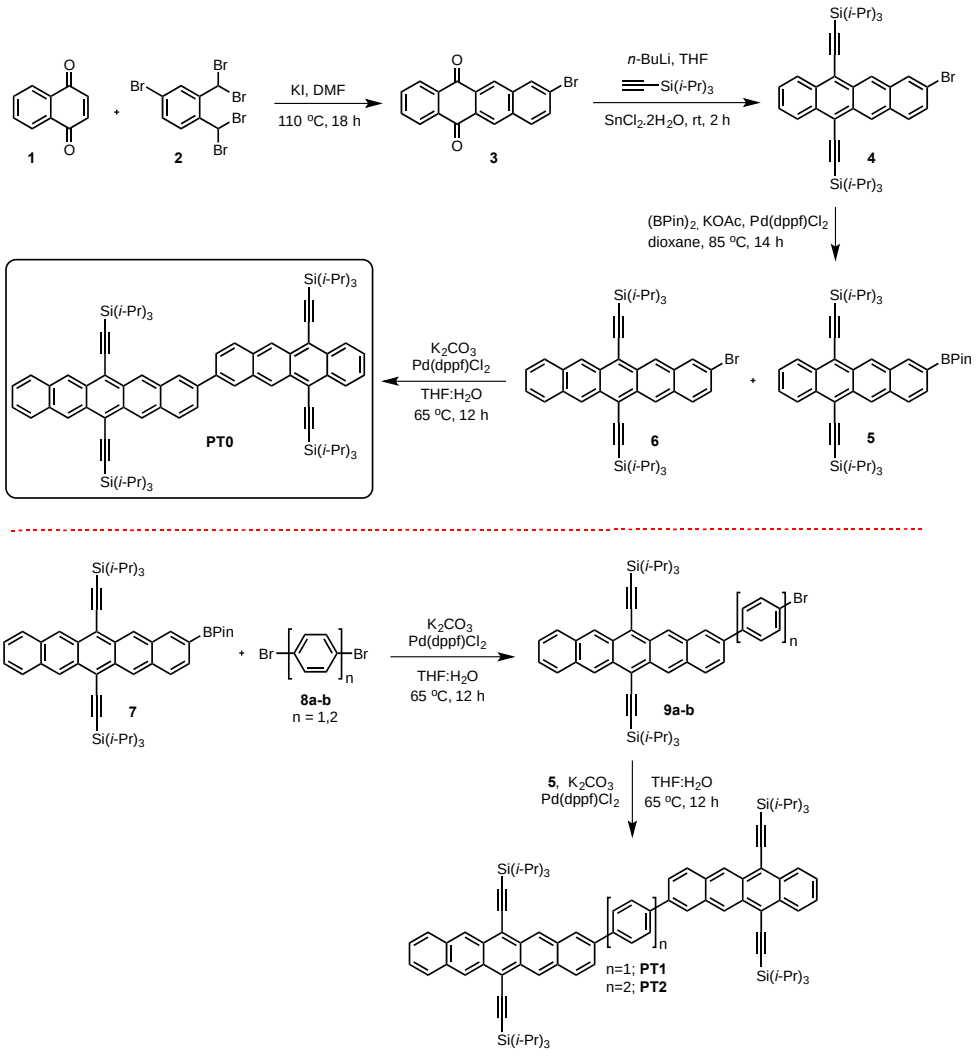

The bromo and Bpin pentacene derivatives **6** and **7** were synthesized according to a procedure reported in the literature.[2] The bromo-tetracene, Bpin tetracene derivatives and PT0 were synthesized according to a similar literature procedure.[5]

Synthesis of bromo-phenylene-pentacene derivative **9a-b**:

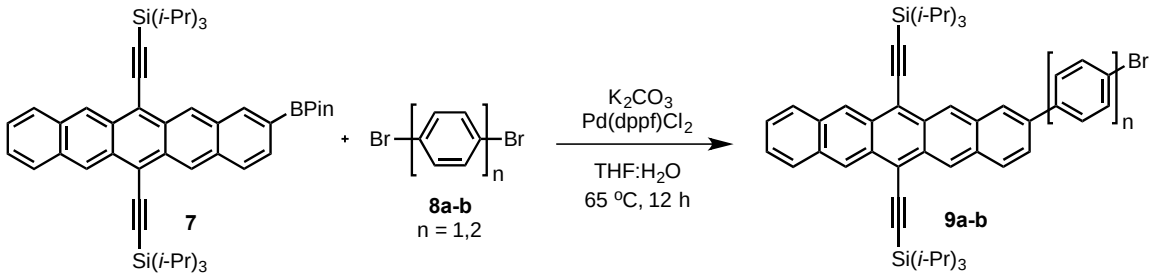

Procedure: To a dry flask, **7** (300 mg, 1.0 *equiv.*), Dibromo-phenylene derivative **8a-b** (3.0 *equiv.*), $Pd(dppf)Cl_2$ (0.1 *equiv.*) and K_2CO_3 (5.0 *equiv.*) were added. The mixture was subjected to sequential vacuum and argon to remove oxygen followed by the addition of dry, degassed $THF:H_2O$ (9:1, 60 mL) mixture. The reaction mixture was heated to 65 °C and maintained for 12 h in the dark. After the reaction, the solvent was evaporated and the crude mixture was purified in a silica column chromatography using hexanes:chloroform mixture as eluent.

9a = 56% yield

^{1}H-NMR (500 MHz, $CDCl_3$, δ ppm): 9.34-9.33 (m, 4H), 8.12-8.11 (m, 1H), 8.08-8.06 (m, 1H), 8.01-7.99 (m, 2H), 7.69-7.66 (m, 5H), 7.46-7.44 (m, 2H) and 1.46-1.39 (m, 42H)

^{13}C-NMR (125 MHz, $CDCl_3$, δ ppm): 139.7, 137.1, 132.4, 132.3, 132.2, 132.1, 131.4, 130.9, 130.8, 130.7, 129.6, 128.8, 128.7, 126.7, 126.4, 126.2, 126.1, 125.9, 125.8, 121.9, 118.5, 118.3, 107.4, 107.3, 104.7, 104.6, 19.0 and 11.7.

MS (ESI): Calculated: 792.3182; Observed: 792.3199.

9b = 61% yield

^{1}H-NMR (500 MHz, $CDCl_3$, δ ppm): 9.36-9.33 (m, 4H), 81.6 (m, 1H), 8.10-8.08 (m, 1H), 8.02-7.99 (m, 2H), 7.87-7.84 (m, 2H), 7.76-7.74 (m, 1H), 7.71-7.69 (m, 2H), 7.62-7.59 (m, 2H), 7.54-7.52 (m, 2H), 7.46-7.44 (m, 2H), 1.47-1.41 (m, 42H)

^{13}C-NMR (125 MHz, $CDCl_3$, δ ppm): 139.95, 139.45, 139.1, 137.5, 132.4, 132.3, 131.95, 131.5, 130.9,130.8, 130.6, 129.4, 128.7, 128.6, 128.5, 127.6, 127.4, 126.7, 126.3, 126.2, 126.1, 126.0, 125.8, 121.7, 118.5, 118.3, 107.3, 107.2, 104.7, 19.05, 19.04 and 11.7.

MS (ESI): Calculated: 869.3573; Observed: 869.3574.

Synthesis of phenylene spaced heterodimers PT1 and PT2:

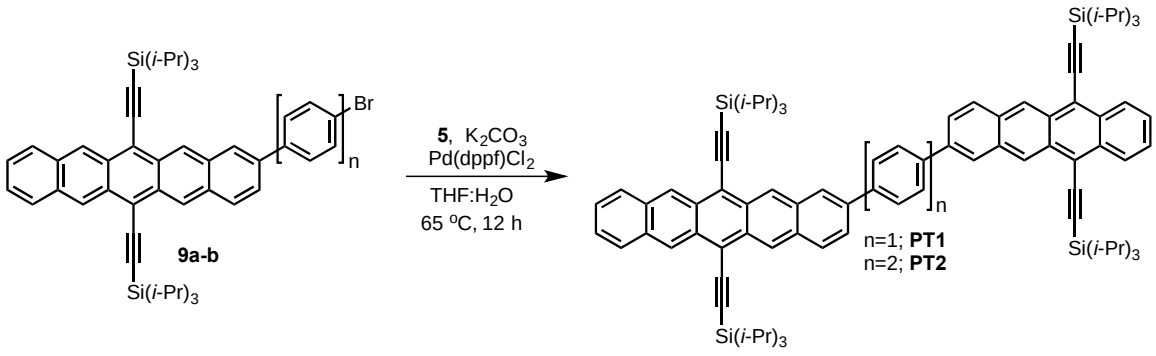

Procedure: To a dry round bottomed flask was added bromo-phenylene pentacene derivative **9a-b** (300 mg, 1.0 *equiv.*), BPin tetracene derivative **5** (1.2 *equiv*) K_2CO_3 (5 *equiv.*) and $Pd(dppf)Cl_2 \cdot DCM$ (0.1 *equiv.*). Sequential vacuum and argon were used to degas the mixture followed by the addition of degassed THF and H_2O (9:1 ratio, 100 mL). The mixture was heated to reflux and maintained for 24 h in the dark. After the reaction, the mixture was cooled to rt and the solvent was removed under reduced pressure. The crude was purified by silica chromatography using mixtures of hexanes/chloroform as an eluent to obtain the product as a reddish brown solid.

PT1 yield: 51%

^{1}H-NMR (500 MHz, $CDCl_3$, δ ppm): 9.41-9.34 (m, 6H), 8.69-8.66 (m, 2H), 8.31-8.27 (m, 2H), 8.18-8.12 (m, 2H), 8.01-8.00 (m, 6H), 7.89-7.87 (m, 1H), 7.85-7.82 (m, 1H), 7.59-7.58 (m, 2H), 7.46-7.44 (m, 2H) and 1.43-1.37 (m, 84H).

^{13}C NMR not provided due to limited solubility of the product

MS (ESI): Calculated: 1300.7528; Observed: 1300.7528.

PT2 yield: 23%

^{1}H-NMR (500 MHz, $CDCl_3$, 50 °C δ ppm): 9.42-9.35 (m, 6H), 8.69-8.67 (m, 2H), 8.29-8.25 (m, 2H), 8.17-8.11 (m, 2H), 8.01-7.81 (m, 12H), 7.59-7.57 (m, 2H), 7.45-7.43 (m, 2H) and 1.44-1.38 (m, 84H).

^{13}C NMR not provided due to limited solubility of the product

MS (ESI): Calculated: 1376.7841; Observed: 1376.7839.

MS (ESI): Calculated: 792.3182; Observed: 792.3199.

^{1}H-NMR (500 MHz, $CDCl_3$, δ ppm): 9.34-9.33 (m, 4H), 8.12-8.11 (m, 1H), 8.08-8.06 (m, 1H), 8.01-7.99 (m, 2H), 7.69-7.66 (m, 5H), 7.46-7.44 (m, 2H) and 1.46-1.39 (m, 42H)

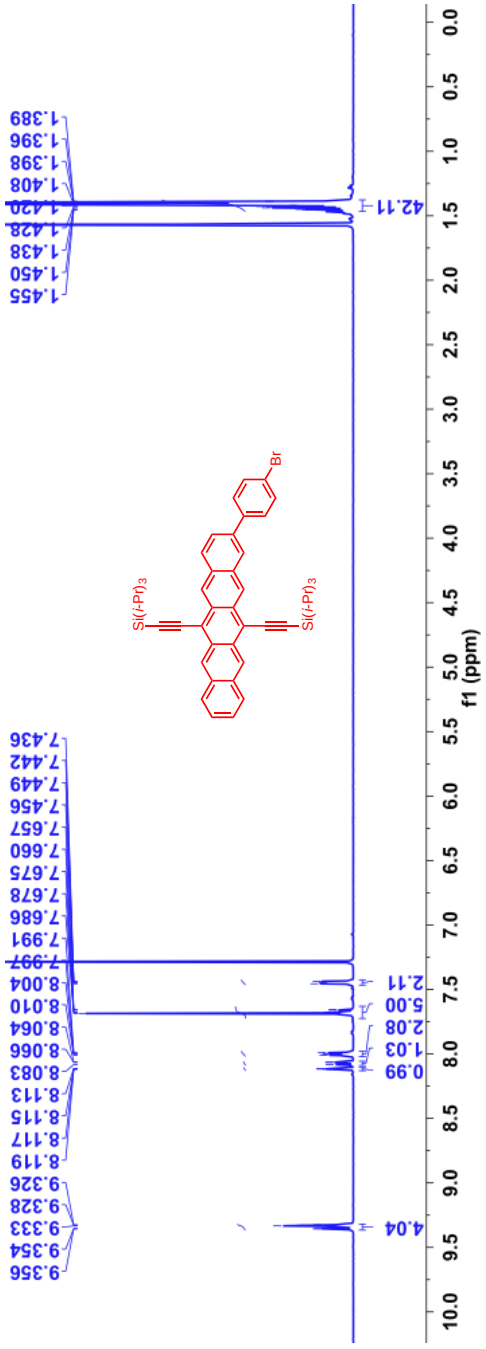

^{13}C-NMR (125 MHz, $CDCl_3$, δ ppm): 139.7, 137.1, 132.4, 132.3, 132.2, 132.1, 131.4, 130.9, 130.8, 130.7, 129.6, 128.8, 128.7, 126.7, 126.4, 126.2, 126.1, 125.9, 125.8, 121.9, 118.5, 118.3, 107.4, 107.3, 104.7, 104.6, 19.0 and 11.7.

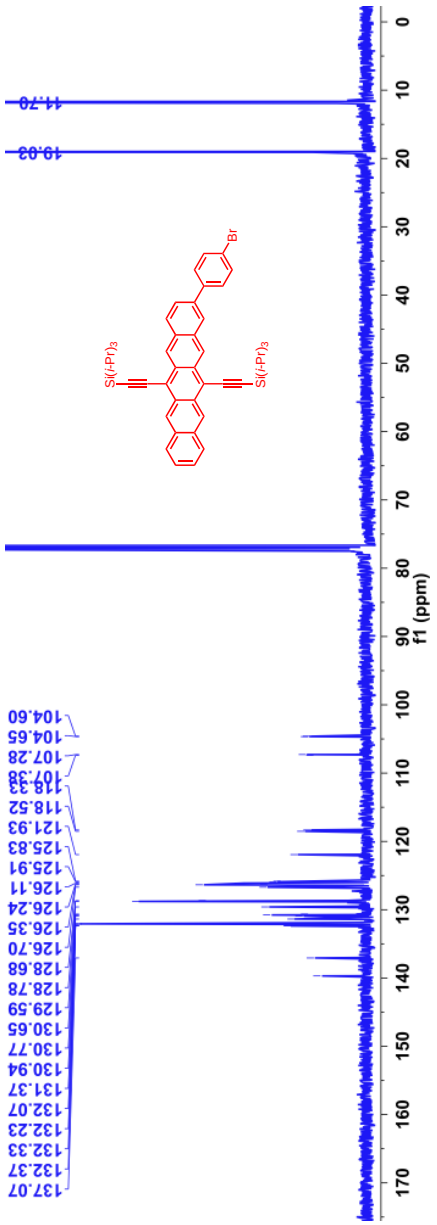

^{1}H-NMR (500 MHz, $CDCl_3$, δ ppm): 9.36-9.33 (m, 4H), 81.6 (m, 1H), 8.10-8.08 (m, 1H), 8.02-7.99 (m, 2H), 7.87-7.84 (m, 2H), 7.76-7.74 (m, 1H), 7.71-7.69 (m, 2H), 7.62-7.59 (m, 2H), 7.54-7.52 (m, 2H), 7.46-7.44 (m, 2H), 1.47-1.41 (m, 42H)

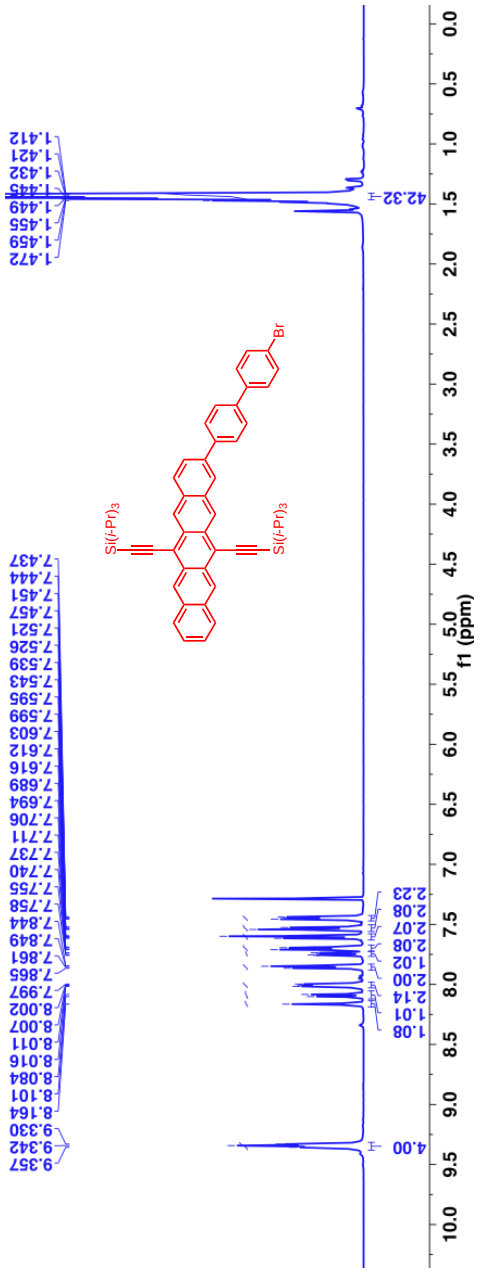

^{13}C-NMR (125 MHz, $CDCl_3$, δ ppm): 139.95, 139.45, 139.1, 137.5, 132.4, 132.3, 131.95, 131.5, 130.9,130.8, 130.6, 129.4, 128.7, 128.6, 128.5, 127.6, 127.4, 126.7, 126.3, 126.2, 126.1, 126.0, 125.8, 121.7, 118.5, 118.3, 107.3, 107.2, 104.7, 19.05, 19.04 and 11.7.

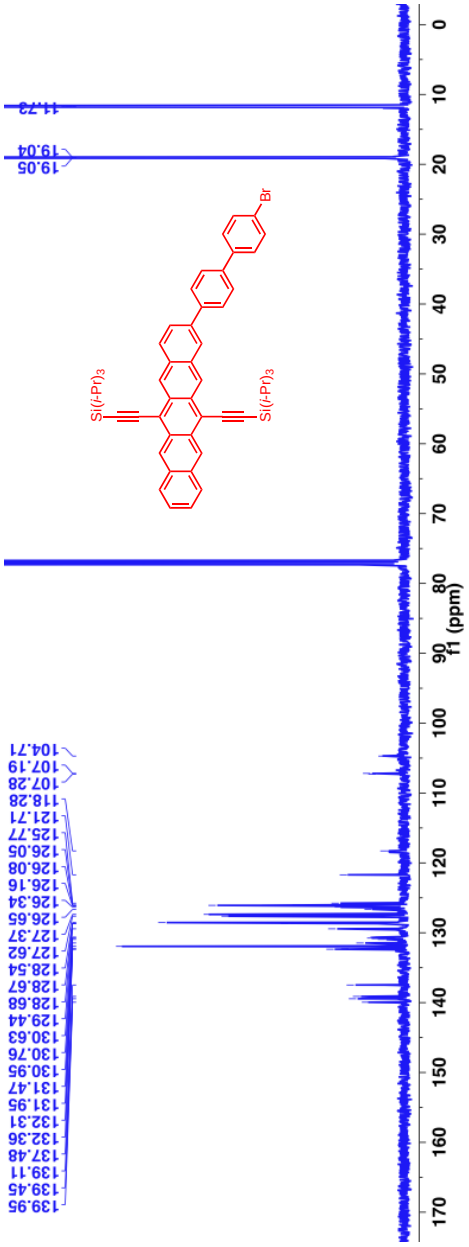

MS (ESI): Calculated: 1300.7528; Observed: 1300.7528.

^{1}H-NMR (500 MHz, $CDCl_3$, δ ppm): 9.41-9.34 (m, 6H), 8.69-8.66 (m, 2H), 8.31-8.27 (m, 2H), 8.18-8.12 (m, 2H), 8.01-8.00 (m, 6H), 7.89-7.87 (m, 1H), 7.85-7.82 (m, 1H), 7.59-7.58 (m, 2H), 7.46-7.44 (m, 2H) and 1.43-1.37 (m, 84H).

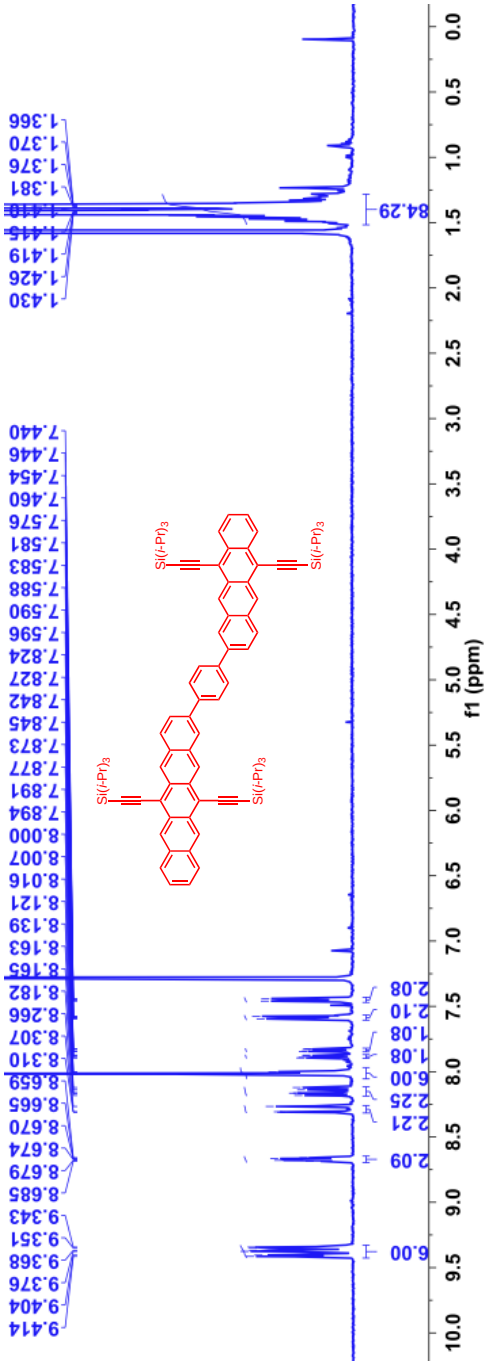

MS (ESI): Calculated: 1376.7841; Observed: 1376.7839.

^{1}H-NMR (500 MHz, $CDCl_3$, 50 °C δ ppm): 9.42-9.35 (m, 6H), 8.69-8.67 (m, 2H), 8.29-8.25 (m, 2H), 8.17-8.11 (m, 2H), 8.01-7.81 (m, 12H), 7.59-7.57 (m, 2H), 7.45-7.43 (m, 2H) and 1.44-1.38 (m, 84H).

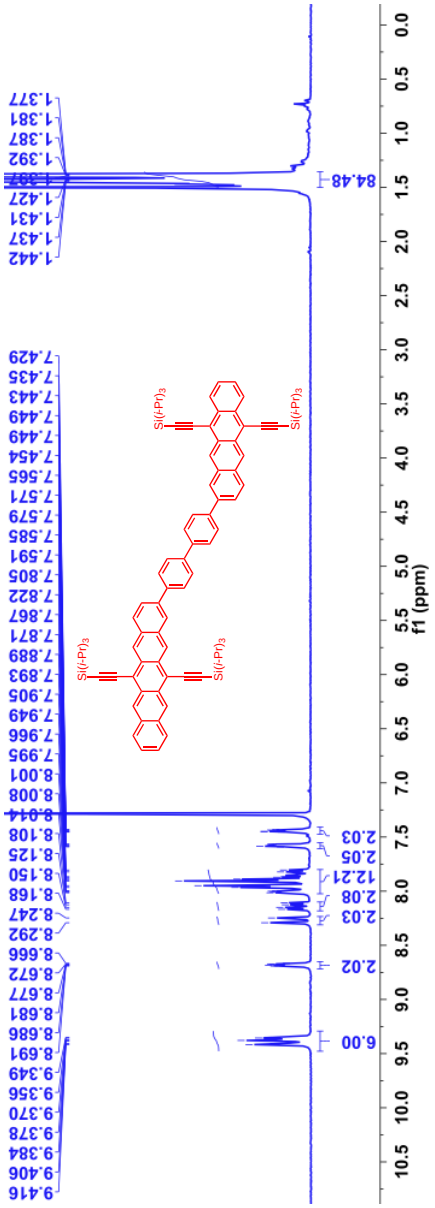

8.18 References

(1) Hanna, M. C.; Nozik, A. J. *J. Appl. Phys.* **2006**, *100*, 074510.

(2) Congreve, D. N.; Lee, J.; Thompson, N. J.; Hontz, E.; Yost, S. R.; Reusswig, P. D.; Bahlke, M. E.; Reineke, S.; Van Voorhis, T.; Baldo, M. A. *Science* **2013**, *340*, 334.

(3) Lee, J.; Jadhav, P.; Baldo, M. A. *Appl. Phys. Lett.* **2009**, *95*, 033301.

(4) Smith, M. B.; Michl, J. *Annu. Rev. Phys. Chem.* **2013**, *64*, 361.

(5) Smith, M. B.; Michl, J. *Chem. Rev.* **2010**, *110*, 6891.

(6) Tayebjee, M. J. Y.; McCamey, D. R.; Schmidt, T. W. *J. Phys. Chem. Lett.* **2015**, *6*, 2367.

(7) Tayebjee, M. J. Y.; Gray-Weale, A. A.; Schmidt, T. W. *J. Phys. Chem. Lett.* **2012**, *3*, 2749.

(8) Tayebjee, M. J. Y.; Hirst, L. C.; Ekins-Daukes, N. J.; Schmidt, T. W. *J. Appl. Phys.* **2010**, *108*, 124506.

(9) Low, J. Z.; Sanders, S. N.; Campos, L. M. *Chem. Mater.* **2015**, *27*, 5453.

(10) Monahan, N.; Zhu, X.-Y. *Annu. Rev. Phys. Chem.* **2015**, *66*, 601.

(11) Zhu, X. *Acc. Chem. Res.* **2013**, *46*, 1239.

(12) Chan, W.-L.; Berkelbach, T. C.; Provorse, M. R.; Monahan, N. R.; Tritsch, J. R.; Hybertsen, M. S.; Reichman, D. R.; Gao, J.; Zhu, X.-Y. *Acc. Chem. Res.* **2013**, *46*, 1321.

(13) Chan, W.-L.; Ligges, M.; Zhu, X. Y. *Nat Chem* **2012**, *4*, 840.

(14) Chan, W.-L.; Ligges, M.; Jailaubekov, A.; Kaake, L.; Miaja-Avila, L.; Zhu, X.-Y. *Science* **2011**, *334*, 1541.

(15) Zeng, T.; Hoffmann, R.; Ananth, N. *J. Am. Chem. Soc.* **2014**, *136*, 5755.

(16) Zeng, T.; Ananth, N.; Hoffmann, R. *J. Am. Chem. Soc.* **2014**, *136*, 12638.

(17) Miyata, K.; Tanaka, S.; Sugimoto, T.; Watanabe, K.; Uemura, T.; Takeya, J.; Matsumoto, Y. In *Ultrafast Phenomena XIX*; Yamanouchi, K., Cundiff, S., de Vivie-Riedle, R., Kuwata-Gonokami, M., DiMauro, L., Eds.; Springer International Publishing: 2015; Vol. 162, p 218.

(18) Bakulin, A. A.; Morgan, S. E.; Kehoe, T. B.; Wilson, M. W. B.; Chin, A. W.; Zigmantas, D.; Egorova, D.; Rao, A. *Nature Chemistry* **2015**, *8*, 16.

(19) Musser, A. J.; Liebel, M.; Schnedermann, C.; Wende, T.; Kehoe, T. B.; Rao, A.; Kukura, P. *Nat Phys* **2015**, *11*, 352.

(20) Busby, E.; Berkelbach, T. C.; Kumar, B.; Chernikov, A.; Zhong, Y.; Hlaing, H.; Zhu, X. Y.; Heinz, T. F.; Hybertsen, M. S.; Sfeir, M. Y.; Reichman, D. R.; Nuckolls, C.; Yaffe, O. *J. Am. Chem. Soc.* **2014**, *136*, 10654.

(21) Berkelbach, T. C.; Hybertsen, M. S.; Reichman, D. R. *J. Chem. Phys.* **2013**, *138*, 114102.

(22) Tayebjee, M. J. Y.; Clady, R. G. C. R.; Schmidt, T. W. *PCCP* **2013**, *15*, 14797.

(23) Yost, S. R.; Lee, J.; Wilson, M. W. B.; Wu, T.; McMahon, D. P.; Parkhurst, R. R.; Thompson, N. J.; Congreve, D. N.; Rao, A.; Johnson, K.; Sfeir, M. Y.; Bawendi, M. G.; Swager, T. M.; Friend, R. H.; Baldo, M. A.; Van Voorhis, T. *Nat. Chem.* **2014**, *6*, 492.

(24) Dillon, R. J.; Piland, G. B.; Bardeen, C. J. *J. Am. Chem. Soc.* **2013**, *135*, 17278.

(25) Ryerson, J. L.; Schrauben, J. N.; Ferguson, A. J.; Sahoo, S. C.; Naumov, P.; Havlas, Z.; Michl, J.; Nozik, A. J.; Johnson, J. C. *J. Phys. Chem. C* **2014**, *118*, 12121.

(26) Sharifzadeh, S.; Darancet, P.; Kronik, L.; Neaton, J. B. *J. Phys. Chem. Lett.* **2013**, *4*, 2197.

(27) Bayliss, S. L.; Chepelianskii, A. D.; Sepe, A.; Walker, B. J.; Ehrler, B.; Bruzek, M. J.; Anthony, J. E.; Greenham, N. C. *Phys. Rev. Lett.* **2014**, *112*, 238701.

(28) Sternlicht, H.; Nieman, G. C.; Robinson, G. W. *J. Chem. Phys.* **1963**, *38*, 1326.

(29) Burdett, J. J.; Bardeen, C. J. *J. Am. Chem. Soc.* **2012**, *134*, 8597.

(30) Chan, W.-L.; Tritsch, J. R.; Zhu, X. Y. *J. Am. Chem. Soc.* **2012**, *134*, 18295.

(31) Wilson, M. W. B.; Rao, A.; Johnson, K.; Gélinas, S.; di Pietro, R.; Clark, J.; Friend, R. H. *J. Am. Chem. Soc.* **2013**, *135*, 16680.

(32) Scholes, G. D. *J. Phys. Chem. A* **2015**, *119*, 12669.

(33) Trinh, M. T.; Zhong, Y.; Chen, Q.; Schiros, T.; Jockusch, S.; Sfeir, M. Y.; Steigerwald, M.; Nuckolls, C.; Zhu, X. *J. Phys. Chem. C* **2014**, *119*, 1312.

(34) Chan, W.-L.; Ligges, M.; ZhuX-Y. *Nat Chem* **2012**, *4*, 840.

(35) Stern, H. L.; Musser, A. J.; Gelinas, S.; Parkinson, P.; Herz, L. M.; Bruzek, M. J.; Anthony, J.; Friend, R. H.; Walker, B. J. *Proc. Natl Acad. Sci.* **2015**, *112*, 7656.

(36) Charbr, M.; Williams, D. F. *Chem. Phys. Lett.* **1977**, *49*, 599.

(37) Geacintov, N. E.; Burgos, J.; Pope, M.; Strom, C. *Chem. Phys. Lett.* **1971**, *11*, 504.

(38) Busby, E.; Xia, J.; Low, J. Z.; Wu, Q.; Hoy, J.; Campos, L. M.; Sfeir, M. Y. *J. Phys. Chem. B* **2015**, *119*, 7644.

(39) Busby, E.; Xia, J.; Wu, Q.; Low, J. Z.; Rong, R.; Miller, J. R.; Zhu, X.-Y.; Campos, L. M.; Sfeir, M. Y. *Nat. Mater.* **2014**, *14*, 426.

(40) Lukman, S.; Musser, A. J.; Chen, K.; Athanasopoulos, S.; Yong, C. K.; Zeng, Z.; Ye, Q.; Chi, C.; Hodgkiss, J. M.; Wu, J.; Friend, R. H.; Greenham, N. C. *Adv. Funct. Mater.* **2015**, *25*, 5452.

(41) Sanders, S. N.; Kumarasamy, E.; Pun, A. B.; Trinh, M. T.; Choi, B.; Xia, J.; Taffet, E. J.; Low, J. Z.; Miller, J. R.; Roy, X.; Zhu, X. Y.; Steigerwald, M. L.; Sfeir, M. Y.; Campos, L. M. *J. Am. Chem. Soc.* **2015**, *137*, 8965.

(42) Zirzlmeier, J.; Lehnherr, D.; Coto, P. B.; Chernick, E. T.; Casillas, R.; Basel, B. S.; Thoss, M.; Tykwinski, R. R.; Guldi, D. M. *Proc. Natl Acad. Sci.* **2015**, *112*, 5325.

(43) Sanders, S. N.; Kumarasamy, E.; Pun, A. B.; Steigerwald, M. L.; Sfeir, M. Y.; Campos, L. M. *Angew. Chem. Int. Ed.* **2016**, *55*, 3373.

(44) Pensack, R. D.; Tilley, A. J.; Parkin, S. R.; Lee, T. S.; Payne, M. M.; Gao, D.; Jahnke, A. A.; Oblinsky, D. G.; Li, P.-F.; Anthony, J. E.; Seferos, D. S.; Scholes, G. D. *J. Am. Chem. Soc.* **2015**, *137*, 6790.

(45) Pensack, R. D.; Tilley, A. J.; Parkin, S. R.; Lee, T. S.; Payne, M. M.; Gao, D.; Jahnke, A. A.; Oblinsky, D.; Li, P.-F.; Anthony, J. E.; Seferos, D. S.; Scholes, G. D. *J. Am. Chem. Soc.* **2015**, *137*, 6790.

(46) Pauling, L. *The Nature of the Chemical Bond*; Cornell University Press: Ithaca, NY, 1972.

(47) Zimmerman, P. M.; Zhang, Z.; Musgrave, C. B. *Nat Chem* **2010**, *2*, 648.

(48) Fuemmeler, E. G.; Sanders, S. N.; Pun, A. B.; Kumarasamy, E.; Zeng, T.; Miyata, K.; Steigerwald, M. L.; Zhu, X. Y.; Sfeir, M. Y.; Campos, L. M.; Ananth, N. *ACS Cent. Sci.* **2016**, *Accepted*.

(49) Fudickar, W.; Linker, T. *J. Am. Chem. Soc.* **2012**, *134*, 15071.

(50) Anthony, J. E.; Eaton, D. L.; Parkin, S. R. *Org. Lett.* **2002**, *4*, 15.

(51) Anthony, J. E.; Brooks, J. S.; Eaton, D. L.; Parkin, S. R. *J. Am. Chem. Soc.* **2001**, *123*, 9482.

(52) Sakuma, T.; Sakai, H.; Araki, Y.; Mori, T.; Wada, T.; Tkachenko, N. V.; Hasobe, T. *J. Phys. Chem. A* **2016**, *120*, 1867.

(53) Walker, B. J.; Musser, A. J.; Beljonne, D.; Friend, R. H. *Nat. Chem.* **2013**, *5*, 1019.

(54) Snellenburg, J. J. L., S. P.; Seger, R.; Mullen, K. M.; van Stokum, I. H. M. *J. Stat. Soft.* **2012**, *49*, 1.

(55) Wilson, J. S.; Chawdhury, N.; Al-Mandhary, M. R. A.; Younus, M.; Khan, M. S.; Raithby, P. R.; Köhler, A.; Friend, R. H. *J. Am. Chem. Soc.* **2001**, *123*, 9412.

(56) Caspar, J. V.; Meyer, T. J. *J. Phys. Chem.* **1983**, *87*, 952.

(57) Englman, R.; Jortner, J. *Mol. Phys.* **1970**, *18*, 145.

(58) Dexter, D. L. *J. Chem. Phys.* **1953**, *21*, 836.